

DOCTORAL DISSERTATION

As to obtain the doctorate

Speciality: Molecular and Cellular Aspects of Biology

Prepared in *Université de Rouen Normandie*

**Study of molecular, cellular, and vascular alterations induced
by apnea of prematurity in the murine cerebellum.**

**Presented and defended by
Agalic RODRIGUEZ-DUBOC**

**PhD dissertation defended publicly on June 5th, 2023,
in front of a jury composed of**

Mme. / Anne-Karine BOUZIER-SORE	Directeur de recherche / Université de Bordeaux	Rapporteur
M. / Pascal DOURNAUD	Directeur de recherche / Université Paris Diderot	Rapporteur
Mme. / Isabelle DUSART	Directeur de recherche / Sorbonne Université	Examinateur
M. / Ludovic TELLEY	Directeur de recherche / Université de Lausanne	Examinateur
Mme. / Delphine BUREL	Maître de conférences / Université de Rouen Normandie	Directeur de thèse

Thesis directed by Delphine BUREL, INSERM U1245, Cancer and Brain Genomics

ACKNOWLEDGMENTS

Les travaux présentés dans ce manuscrit ont été réalisés au sein de l'Université de Rouen, dans le laboratoire « Différenciation et Communication Neuronale et Neuroendocrine », INSERM U1239, dirigé par le **Dr. Youssef Anouar**, puis au sein du laboratoire « Génomique du cerveau et du cancer », Inserm U1245, dirigé par le **Pr. Gaël Nicolas**. Je souhaite les remercier de m'avoir accueillie dans ces structures et d'avoir permis la réalisation de ces travaux y compris lors du changement d'unité. Merci également aux **Drs. Hervé Lefèvre et Jérôme Leprince** de m'avoir permis de continuer à travailler au CURIB jusqu'à la fin de mes expérimentations.

Je tiens à remercier les membres du jury qui ont su se rendre disponible :

Le **Dr. Anne-Karine Bouzier-Sore**, Directeur de recherche Centre de Résonance Magnétique des Systèmes Biologiques, Unité Mixte de Recherche du CNRS, affiliée à l'Université de Bordeaux, me fait l'honneur d'être rapporteur de ce travail. Je tiens à lui témoigner ma reconnaissance pour son expertise et son intérêt pour ce travail.

Le **Dr. Pascal Dournaud**, Directeur de recherche au sein du Laboratoire NeuroDiderot, Unité Mixte De Recherche INSERM UMR 1141, affiliée à l'Université Paris Diderot, a accepté la charge de rapporteur. Consciente de la faveur qu'il m'accorde, je souhaite lui exprimer toute ma gratitude pour l'évaluation de ce manuscrit.

Le **Dr. Isabelle Dusart**, Directeur de Recherche au Laboratoire Neuroscience Paris Seine dans l'unité UMR 8246 du CNRS affiliée à l'Université de la Sorbonne, a accepté d'examiner ce travail. Je souhaite lui témoigner ma gratitude pour sa présence ainsi que pour son soutien et sa bienveillance lors des CSI durant mon doctorat.

Le **Dr. Ludovic Telley**, Directeur de Recherche au Département des Neurosciences Fondamentales de l'Université de Lausanne, a bien voulu examiner ce travail. Je le prie de bien vouloir trouver ici l'expression de mes sincères remerciements pour son intérêt pour la thématique et pour sa présence.

Je tiens à remercier chaleureusement le **Dr. David Vaudry**, Chargé de Recherche à l'INSERM, de m'avoir intégrée au sein de son équipe dès le M2 au DC2N. Merci pour ton soutien, tes conseils, et pour l'accès à PRIMACEN.

De même, je souhaite remercier le **Dr. Bruno Gonzalez**, Directeur de Recherche de l'équipe « Epigénétique et physiopathologie des troubles du neurodéveloppement » dans l'unité Cancer and Brain Genomics U1245, de m'avoir accueillie dans son équipe après le changement d'unité. Merci d'avoir facilité la transition autant que possible.

Je tiens à présent à remercier le **Dr. Delphine Burel** de m'avoir encadrée pendant presque quatre ans. J'adresse une pensée particulière pour le Dr. Christophe Dubessy, qui a eu la bonne idée de te transmettre mon CV alors que tu étais en convalescence. Je n'aurai pas pu mieux tomber ! Tu m'as tellement appris, et j'emporte ces leçons avec moi car je me dis souvent « mais que ferait Delphine ? ». Tu as su m'encadrer avec le parfait mélange de soutien et d'autonomie et m'as poussé à donner le meilleur de moi-même. Merci pour ta disponibilité, ta patience, ta rigueur, ta bienveillance, ton humour et surtout pour la confiance que tu m'as accordée pour développer ce projet. Entre les nombreux déménagements, le COVID, les déboires avec la chambre d'hypoxie, on aura vécu de sacrées péripéties... Et ce n'est pas fini puisque notre collaboration va continuer car on a encore de belles choses à publier !

Un grand merci au **Dr. Magali Dugay** qui m'a appris toutes les astuces de biologie moléculaire et les joies de la PCR. Je te remercie pour tous les moments de complicité, pour ton soutien (humain et logistique) et tes magnifiques protocoles. Merci d'aimer les voies de signalisation, la PCR et les tableurs Excel autant que moi ! On a encore un bel article à écrire et j'ai hâte !

Merci aux D3 en D-tres, **Inès** et **Quentin** ; cette aventure n'aurait pas été la même sans vous. Nous avons partagé nos galères et nos succès. À force de discussions de couloir et d'échanges de memes, on aura tenu la distance. Et même si je clos ce chapitre un peu avant vous, je serais votre cheerleader jusqu'au bout ! Merci à **Sarah** pour ce beau projet que j'ai eu la chance de continuer, et pour m'avoir guidé lors de mes premiers pas au labo. **Aurélien**, merci pour ton aide en IHC, je penserais à toi chaque fois que je verrais du Mowiol ! **Camille**, je compte sur toi pour prendre le relais ! Enfin, merci et bon courage à tous les futurs docteurs du labo, avec une pensée particulière pour **Lucie** et **Omayma**. You've got this !

Je n'oublie pas **Laurence** et **Catherine** qui ont toujours été là pour arriver à ma rescousse : merci à vous deux, sans vous je serais encore en train d'errer dans les couloirs ! J'aimerais aussi remercier l'ensemble de l'équipe de **PRIMACEN** pour leur aide tout au long de ces années et les membres de l'unité **INSERM 1239**, je ne peux citer tout le monde mais merci à toutes les personnes qui ont pu m'aider à un moment ou un autre, je pense à vous ! Je tiens également à remercier l'ensemble du personnel du service de ressources biologiques, et notamment le **Dr. Arnaud Arabo** et **Julie** pour leur aide (et la boîte à outils !). Un grand merci à **Mr. François Chadelaud**, pour son aide et sa patience avec la chambre d'hypoxie sur laquelle ce projet repose.

Je tiens également à remercier le **Robot Bravo** de la plateforme PRIMACEN pour les presque 2000 heures passées ensemble. Nous avons eu nos hauts et nos bas, mais il a toujours été là pour moi durant cette grande aventure.

Marc-Aurèle, through this adventure you've been my favorite coworker in times of confinement, my physical therapist for the pain after working all day, my IT service when something went wrong, my sounding board when I was struggling to make decisions, my R personal tutor, my cheerleader when I was doubting myself... I am lacking the words to thank you. You've made my life better in so many ways, and perhaps the most romantic thing (for us) was convincing me to switch to R for my analysis, I would not have done it without you! Thank you for all the work you put into that, it has made this thesis and publications infinitely better. Thank you for our impromptu scientific discussions around coffee breaks, for our journal clubs, and all your wonderful insights. Thank you for being there through thick and thin, for making me laugh no matter what, and for being as wonderfully weird as me! I'm so looking forward to our next and very different partnership!

Mutti, merci pour tout ! Merci de m'avoir passionnée pour la science et d'avoir toujours éveillé ma curiosité. Tu as toujours été là pour moi, pour me soutenir et m'aider à accomplir mes objectifs par tous les moyens. Tu m'as toujours fait croire que tout était possible, et tu m'as encouragée quand je n'y croyais plus. Tu seras toujours ma plus grande source d'inspiration.

Papounet, gracias por motivarme desde lejos. ¡Quién habrá dicho que el latín que aprendí contigo me serviría tanto en mis estudios! Tú me diste el gusto por entender el mundo natural y la biología y aquí estoy. Espero que estarás orgulloso de mi.

Thank you, **Philippe**, for your support and friendship that have carried me through the years. You have been instrumental in this day finally coming about.

Cosima, du verstehst wahrscheinlich von allen am besten, wie diese Reise verlaufen ist. Danke, dass du trotz unserer vollen Terminkalender für mich da warst und meine Kämpfe mit mir geteilt hast.

Mi querida **Pame**, tú eres lo mejor que me ha traído la carrera de medicina, y te agradezco tu amistad cada día. ¡No hay tiempo ni distancia que nos separe!

Ma **Fofy**, une amitié qui dure autant, ça ne se trouve pas tous les jours. Merci d'être là dans les hauts et les bas malgré une vie bien remplie.

María, gracias por tu apoyo desde que nos conocimos en el labo y tras la distancia. ¡Estuviste ahí cada vez que me quería quejar y me has dado confianza cuando ya no tenía!

Finally, I want to thank the #bookstagram community. I would have lost my mind without you all! You gave me a place to be myself, to share my passion freely, to discover and learn. But most of all, you gave me a place to escape and dream when real life was wearing me down. I especially want to thank **Amy** for her unwavering support (you have no idea how grateful I am!); **Heather**, for sharing my spoonie struggles; **Ceallaigh**, for the great talks; **Marie**, for going though academia along with me; **Katie**, for the great buddy reads; **Clo** for cheering me on... You all mean the world to me!

ABSTRACT

The cerebellum is involved in diverse functions, from motor control and equilibrium to spatial learning and emotion. At birth, the human cerebellar cortex is still immature, making it vulnerable to perinatal events such as hypoxia. Apnea of prematurity (AOP) is a main cause of perinatal hypoxia, as it occurs in over 50% of preterm infants. Several relationships between cerebellar functions and the deficits observed in children having suffered from AOP have been demonstrated, but the physio-pathological mechanisms by which AoP affects the cerebellum remain poorly understood.

This work aims at shedding light on the mechanisms underlying cerebellar hypoxic injury. To this end, we developed an intermittent hypoxia (IH) protocol, consisting of repeated 2-minute cycles of hypoxia-reoxygenation (including 20 seconds at 5% O₂), applied between P2 and P12, 6 hours per day, which constitutes a valid murine model of AOP.

In a first study, we show that the cerebellum is indeed sensitive to IH, and presents a significant delay in maturation at the end of our IH protocol. In addition, hypoxia seems to induce an overexpression of genes involved in reactive oxygen species (ROS) production, which accumulate in the cerebellum. Conversely, genes coding for antioxidant enzymes are underexpressed after IH, suggesting a failure of the defense system against ROS. IH also induces long-term damage, in the form of learning and motor deficits, which are associated with the over-innervation of Purkinje cells by climbing fibers.

We followed these results with a transcriptomic study of genes involved in cell differentiation and migration. We analyzed the expression of these genes by RT-qPCR, in different developmental stages and in different cell types, using laser capture microdissection to separate cerebellar layers. This allowed us to determine that the period most vulnerable to IH is the P8 stage in mice, during which a significant number of genes are dysregulated in all cerebellar cortical layers. Moreover, it seems that all processes involved in cerebellar development are impacted, including proliferation, differentiation, synaptic connectivity, and myelination. Several compensatory and neuroprotective mechanisms are put in place during and after IH, but they do not seem to be sufficiently effective considering the persistence of deficits through adulthood.

Finally, given the established connection between hypoxia and vascularization, we tested a gene panel focused on these processes and found significant regulations of angiogenic and growth factors. In addition, preliminary imaging results suggest that IH cerebella have a looser and less voluminous vascular network, a factor that could participate in the pathophysiology of AOP. We aim to pursue this line of inquiry with additional immunohistochemical and clearing studies.

Overall, the data presented here demonstrate that the cerebellum is affected by IH, and that its injury is, at least in part, responsible for the symptoms observed in children having experienced AOP. This project provides elements to better understand AOP, by connecting behavioral and histological alterations to plausible underlying cellular and molecular mechanisms. In the long term, it could lead to the identification of novel therapeutic targets to improve the current clinical management of this highly prevalent pathology.

RESUME ETENDU

Le cervelet est une région du système nerveux central (SNC), située à l'arrière du cerveau. Malgré sa petite taille, représentant seulement 15 % de la masse totale, il contient à lui seul plus de 70 % des neurones du cerveau. Le cervelet est constitué d'un cortex de substance grise superficielle recouvrant la substance blanche dans laquelle se trouvent des noyaux cérébelleux profonds de matière grise. La substance blanche cérébelleuse est constituée de fibres nerveuses et l'on compte quarante fois plus d'afférences, majoritairement représentées par les fibres moussues et grimpantes, que d'efférences.

A la naissance, le cortex cérébelleux est composé de 4 différentes couches cellulaires : la couche granulaire externe dans laquelle prolifèrent les précurseurs des cellules en grain ; la couche moléculaire, pauvre en cellules mais riche en connections ; la couche des cellules de Purkinje ; et la couche granulaire interne dans laquelle se différencient les neurones en grain. La maturation du cortex se poursuit pendant la période postnatale au cours de laquelle la couche granulaire externe disparaît peu à peu. Ainsi, à l'adolescence, le cervelet mature n'est plus constitué que de 3 couches corticales.

Les premières fonctions attribuées au cervelet étaient liées à l'équilibre et à la posture puis des fonctions motrices ont été décrites, permettant de diviser le cortex cérébelleux en trois régions fonctionnelles :

- Le spinocervelet, qui reçoit principalement des afférences de la moelle épinière. Il traite ainsi de nombreuses informations sensorimotrices et participe à l'orchestration du mouvement.
- Le corticocervelet, qui est le composant le plus récent du cervelet sur le plan phylogénétique. Il reçoit uniquement des informations du cortex cérébral et s'occupe principalement du contrôle de la motricité.
- Le vestibulocervelet, en lien avec la rétine et l'oreille interne, qui régule l'équilibre et les mouvements oculaires.

Les fonctions non motrices du cervelet ont, quant à elles, été découvertes beaucoup plus tardivement. En effet, lors de lésions ou de pathologies cérébelleuses, celles-ci ont longtemps été masquées par les déficits moteurs. Cependant, au cours des trois dernières décennies, la contribution du cervelet dans plusieurs fonctions cognitives a été démontrée et le cervelet est aujourd'hui reconnu comme étant impliqué dans des réseaux complexes responsables de nombreuses fonctions supérieures telles que le langage, la mémoire et l'affect. Ainsi, une altération de son développement pourrait engendrer des déficits moteurs et cognitifs majeurs à plus ou moins long terme. De même, du fait de son développement essentiellement postnatal, un incident périnatal pourrait induire des conséquences comportementales substantielles chez l'enfant. Ce travail s'intéresse à l'étude des effets d'une hypoxie périnatale sur le développement postnatal du cervelet.

La période périnatale (de la 36^{ème} semaine de gestation au 8^{ème} jour postnatal) est un stade de développement particulièrement vulnérable à l'hypoxie, surtout en cas de naissance prématurée (avant la 37^{ème} semaine). L'hypoxie périnatale est considérée comme une cause importante de morbi mortalité et son impact socio-économique durable en fait une priorité clinique. En effet, les épisodes d'hypoxie-ischémie sont liés à 30 % de la mortalité néonatale et peuvent causer jusqu'à 40 % de déficits neurologiques à long terme. L'hypoxie périnatale peut avoir une étiologie ventilatoire ou circulatoire, et peut être continue ou intermittente. Mais quelles que soient ces modalités, une réponse cellulaire a été mise en évidence pour combattre le stress oxydatif induit par un apport insuffisant d'O₂. En effet, dans les cellules, l'utilisation de l'O₂ entraîne nécessairement la production d'espèces réactives de l'oxygène (ROS), et l'équilibre entre la production et la neutralisation des ROS est essentiel au bon déroulement des processus physiologiques. Cependant, une accumulation de ROS peut devenir délétère pour les cellules. C'est pourquoi un double mécanisme de défense veille à maintenir des niveaux physiologiques de ROS : une composante non enzymatique qui comprend des vitamines et autres molécules antioxydantes ; et une composante enzymatique antioxydante, impliquant des enzymes telles que la SOD, la catalase ou les GPX. En revanche, si la production de ROS finit par dépasser la capacité antioxydante des cellules, le déséquilibre qui en résulte induit un stress oxydatif (SO) cellulaire qui peut mener à la mort cellulaire.

Parmi les diagnostics les plus courants d'hypoxie périnatale se trouve l'apnée du prématuré (ADP). L'ADP est caractérisée par une hypoxie intermittente (HI) et consiste en un arrêt respiratoire survenant au moins toutes les 5 minutes et durant plus de 20 secondes. L'étiologie de l'ADP n'est pas entièrement comprise, mais il semble qu'elle résulte de l'immaturité physiologique du système respiratoire et des centres de contrôle associés lors des naissances prématurées. Actuellement, deux stratégies thérapeutiques principales sont envisagées pour l'ADP : l'utilisation de traitements pharmacologiques stimulant la respiration, tels que la caféine, ou l'assistance ventilatoire non invasive. Malheureusement, leur efficacité est variable, et des études longitudinales ont mis en évidence d'importants effets secondaires à long terme associés au traitement à la caféine. D'autres pistes sont explorées à plus petite échelle mais, à ce jour, leur bénéfice est contesté.

De plus, malgré sa prévalence, les conséquences neurologiques de cette pathologie restent méconnues car elles sont souvent masquées par les altérations inhérentes à la prématurité. Les séquelles à long terme sont encore plus difficiles à déterminer en raison du suivi des patients et du temps nécessaire pour que les déficits deviennent apparents. Cependant, à mesure que la prise en charge des prématurés s'améliore, la survie de ces enfants a permis de progresser dans la compréhension de cette pathologie. Ainsi, une corrélation a été établie entre la persistance de l'ADP chez les nourrissons et l'apparition de déficits neurodéveloppementaux chez les enfants jusqu'à 3 ans. De même, la vulnérabilité du cerveau aux épisodes d'hypoxie a été amplement décrite. Plus récemment, un lien a été établi entre les fonctions cérébelleuses et les déficits observés chez les enfants ayant souffert d'ADP. Cependant, les altérations cellulaires induites par l'ADP sont encore mal comprises.

Ce travail vise donc à mettre en lumière les mécanismes sous-jacents aux lésions hypoxiques cérébelleuses. Pour cela, nous avons développé un protocole d'hypoxie intermittente (HI), consistant en des cycles répétés de 2 minutes d'hypoxie-réoxygénération (dont 20 secondes à 5% d'O₂) durant 10 jours pendant 6 heures par jour, qui constitue un modèle murin valide d'ADP.

Les premiers objectifs de ce projet étaient les suivants :

- Comprendre les effets cellulaires de l'HI en se concentrant sur la prolifération, la mort cellulaire et le SO. Ces effets ont été évalués par : *i*) des injections de BrDU pour étudier les effets de l'HI sur la prolifération et la migration ; *ii*) des tests de production de ROS et d'activité de la caspase-3/7 ; et *iii*) une analyse RT-qPCR des gènes liés au SO et à l'apoptose à l'âge de P12.
- Déterminer, grâce à des études immunohistochimiques, les effets de l'HI sur l'histologie générale du cortex cérébelleux et les afférences cérébelleuses.
- Définir si et comment ces altérations pourraient induire des déficits comportementaux à court et à long terme.

Tout d'abord, nous avons démontré que le cervelet est effectivement sensible à l'HI et présente un retard significatif de maturation à la fin du protocole d'ADP. De plus, l'hypoxie induit une surexpression des gènes impliqués dans la production de ROS au sein de cette structure, ce qui aboutit de fait à une accumulation de ces espèces réactives. A l'inverse, les gènes codant pour les enzymes antioxydantes sont sous-exprimés lors de l'HI suggérant une défaillance du système de défense contre les ROS. Celle-ci pourrait expliquer l'altération morphologique des cellules de Purkinje et être à l'origine des déficits comportementaux observés chez les souriceaux. De plus, nos résultats montrent que l'ADP peut provoquer des dommages à long terme puisque les souris adultes présentent toujours des défauts d'apprentissage et de motricité associés à une innervation exacerbée des cellules de Purkinje par les fibres grimpantes. Ces données nous ont ensuite amenés à concevoir une série d'expériences de transcriptomique pour mieux comprendre la base moléculaire des modifications induites par l'HI.

Pour ce faire, nous avons cherché à :

- Déterminer le stade de développement le plus vulnérable à l'HI. À cette fin, nous avons mené des expériences à différents stades postnataux, à savoir P4, P8, P12, P21 et P70.
- Comprendre les voies moléculaires à la base des altérations observées. En conséquence, nous avons conçu 2 processus généraux à étudier : *i*) compte tenu des effets de l'HI sur la mort cellulaire et le stress oxydatif observés à P12, nous avons cherché à tester un panel de gènes liés au SO ; et *ii*) en raison du retard de maturation histologique induit par notre protocole d'IH, nous avons entrepris de créer un nouveau panel de gènes liés à la maturation et à la différenciation cellulaires.
- Déterminer quels types de cellules pourraient être les plus affectés par l'HI et comment. Pour cette raison, nous avons décidé d'utiliser la microdissection par capture laser et de tester l'expression des gènes sur chaque couche cérébelleuse séparément.

Cette étude nous a permis de déterminer que la période la plus vulnérable à l'HI est le stade P8 chez la souris (correspondant à environ 32 semaines de gestation chez l'Homme) avec un nombre important de gènes dérégulés dans toutes les couches corticales cérébelleuses. De plus, il semble que l'ensemble des processus intervenant dans le développement du cervelet soit impacté, incluant la

prolifération, la différenciation, la connectivité synaptique ou encore la myélinisation. Plusieurs mécanismes de compensation et de neuroprotection se mettent en place pendant et après la phase d'HI mais ceux-ci ne semblent pas suffisamment efficaces puisque des déficits persistent chez l'adulte.

Enfin, étant donné que l'hypoxie joue un rôle crucial dans l'angiogenèse au cours du développement, la dernière partie du travail est centrée sur l'exploration des effets de l'HI sur la vascularisation du cervelet.

Cette partie du projet, en cours de réalisation, comporte trois axes :

- Une étude qPCR des gènes associés à la vascularisation sur l'ensemble du cervelet pour déterminer leur régulation en fonction du stade de développement.
- Des expériences d'immunocytochimie suivie de microscopie confocale pour mieux comprendre comment la vasculogénèse est affectée par l'HI dans le contexte du développement cérébelleux.
- Un protocole de transparisation suivi de microscopie à feuille de lumière pour observer la densité et la morphologie du réseau vasculaire *in situ*.

Nos résultats préliminaires ont révélé une diminution de la longueur et du volume des vaisseaux sanguins, ainsi qu'un réseau plus lâche dans le cortex cérébelleux chez les souris P8 ayant subi l'HI. De même, une étude qPCR aux différents stades d'observation a mis en évidence que de nombreux facteurs de croissance et gènes angiogéniques subissent une dysrégulation face à l'HI. La poursuite de cette étude avec des techniques d'imagerie permettra de comprendre les conséquences histologiques de ces modifications transcriptomiques.

Dans l'ensemble, les résultats de notre étude fournissent des éléments essentiels permettant de mieux comprendre divers aspects des lésions cérébelleuses induites par l'ADP. Ils montrent ainsi que l'ADP peut entraîner des altérations moléculaires, structurelles et fonctionnelles durables dans le cervelet, qui peuvent participer, au moins en partie, aux troubles neurodéveloppementaux observés chez les enfants affectés. A long terme, l'identification des cellules cibles de l'HI, d'un large éventail de gènes impliqués dans les effets de l'HI, et de la fenêtre de vulnérabilité du cervelet qui ont été mis en évidence durant ce travail, pourrait conduire à de nouvelles perspectives de recherche.

En effet, du fait du manque de traitements satisfaisants pour l'ADP, l'identification de facteurs neurotrophiques susceptibles de protéger le cervelet des dommages induits par l'HI pourrait s'avérer précieuse. À long terme, cela pourrait conduire à l'identification de nouvelles cibles thérapeutiques pour traiter cette pathologie qui touche plus de la moitié des prématurés et à un impact significatif d'un point de vue humain et socioéconomique.

Mots clés : cervelet, développement, hypoxie intermittente, périnatal, apnée du prématuré, histologie, apoptose, stress oxydatif, transcriptome, différenciation

Keywords: cerebellum, development, intermittent hypoxia, perinatal, apnea of prematurity, histology, apoptosis, oxidative stress, transcriptome, differentiation

TABLE DES MATIÈRES

ACKNOWLEDGMENTS.....	1
LIST OF ABREVIATIONS	1
LIST OF FIGURES.....	7
LIST OF TABLES.....	9
INTRODUCTION.....	11
I. CHAPTER ONE: THE CEREBELLUM.....	11
A. ANATOMY	11
1. Overview	11
2. Divisions	12
3. Grey Matter.....	13
a. Cortex	13
b. Deep Cerebellar Nuclei	17
4. White Matter.....	19
5. Cerebellar circuitry	21
a. General organization	21
b. Regional variations	26
6. Vascularization	27
a. Arterial Supply	27
b. Venous Drainage	29
B. EMBRYOLOGY.....	31
1. Overview	31
2. Ontogenesis of the cerebellum	33
a. Regionalization	33
b. Cerebellar foliation	38
3. Cerebellar vascular development	40
a. Vasculogenesis	41
b. Angiogenesis	41

4. Cell differentiation	43
a. Purkinje cells.....	44
b. Granule cells	45
c. Interneurons	47
d. DCN neurons.....	48
e. Glia	49
C. FUNCTIONS	50
1. Overview	50
2. Motor functions.....	50
a. Spinocerebellum	50
b. Corticocerebellum.....	53
c. Vestibulocerebellum	55
3. Non-motor functions	58
a. Space and time.....	58
b. Executive functions	63
c. Emotion and affect.....	66
II. CHAPTER TWO: PERINATAL HYPOXIA	69
A. OVERVIEW	69
1. Definition of hypoxia	69
2. Etiology of perinatal hypoxia	70
a. Continuous hypoxia.....	70
b. Intermittent hypoxia	71
B. APNEA OF PREMATURITY	72
1. Physiopathology	72
c. Chemoreceptors and neurological immaturity.....	72
d. Neurotransmitters and mediators.....	75
e. Genetics and other factors	76
2. Current management.....	78

a.	Nonpharmacological strategies	78
b.	Pharmaceuticals and molecules	79
C.	PATHOLOGICAL CONSEQUENCES OF AOP	83
1.	Cellular effects	83
a.	Oxidative Stress	83
b.	Transcriptomic regulation.....	86
c.	Metabolic shift	88
2.	Cellular dysfunction	89
a.	Excitotoxicity	89
b.	Cell death.....	92
3.	Neurological implications of AOP	94
a.	Clinical presentation	94
b.	Experimental findings.....	95
	OBJECTIVES	97
	MATERIALS AND METHODS	99
I.	ANIMALS	99
A.	ANIMAL MODEL.....	99
B.	HYPOXIA PROTOCOL	99
C.	COLLECTION OF BIOLOGICAL MATERIAL	101
II.	REAL-TIME Q-PCR.....	102
A.	BIOINFORMATICS	102
B.	PRIMER DESIGN.....	103
C.	LASER CAPTURE MICRODISSECTION	104
D.	RNA EXTRACTION	105
E.	RETROTRANSCRIPTION AND QPCR	106
III.	IMMUNOHISTOCHEMISTRY	107
A.	SAMPLE PREPARATION.....	107
B.	ANTIBODY CHOICE	108

C. IMAGING.....	108
IV. CLEARING	109
A. SAMPLE PREPARATION	109
B. ANTIBODY CHOICE	110
C. IMAGING.....	110
V. BEHAVIORAL STUDIES.....	110
VI. STATISTICAL ANALYSIS	112
A. CONCEPTS	112
B. SPECIFICS.....	113
1. RT-qPCR.....	113
2. IHC	113
3. Behavioral experiments	114
4. Data availability.....	114
RESULTS	115
I. PART ONE: COMPLETED WORK.....	115
A. JOURNAL ARTICLE 1	115
1. Presentation.....	115
2. Graphical summary	142
B. JOURNAL ARTICLE 2:	143
1. Presentation.....	143
2. Graphical summary	165
II. PART TWO: EFFECTS OF IH ON CEREBELLAR VASCULARIZATION	167
A. BACKGROUND	167
B. TRANSCRIPTOMICS	167
C. IMMUNOHISTOCHEMISTRY.....	169
D. CLEARING.....	170
DISCUSSION.....	171
I. EFFECTS OF IH ON GROWTH AND BEHAVIOR.....	171

II.	ANATOMICAL AND HISTOLOGICAL EFFECTS OF IH	172
III.	EFFECTS OF IH ON PURKINJE CELLS AND CEREBELLAR CIRCUITRY	173
IV.	MOLECULAR EFFECTS OF IH.....	174
A.	IH CAUSES A STATE OF OS IN THE CEREBELLUM	174
1.	IH increases ROS production	174
2.	IH is correlated with a failure of the antioxidant system	175
3.	IH regulates different cell-death and neuroprotective pathways.....	177
B.	CEREBELLAR LAYERS ARE DIFFERENTIALLY AFFECTED BY IH.....	178
1.	IH influences the maturation rate of GCs.....	178
2.	IH modifies Purkinje cell phenotype	179
3.	IH alters synaptogenesis and cerebellar circuitry	180
4.	IH affects glial cells	181
	CONCLUSION AND PERSPECTIVES	183
	REFERENCES	185
	APPENDICES	229

LIST OF ABREVIATIONS

ACA:	anterior cerebral artery
ADHD:	attention-deficit hyperactivity disorder
AICA:	anterior inferior cerebellar artery
AIF:	apoptosis inducing factor
AMPA:	alpha-amino-3-hydroxy-5-methyl-4-isoxazolepropionic acid
AMPK:	AMP-activated protein kinase
ANGPT:	angiopoietin
AOP:	apnea of prematurity
ASCLx:	achaete-scute family BHLH transcription factor x
ATOH1:	ataonal BHLH transcription factor 1
ATP:	adenosine 5'-triphosphate
BCL2:	BCL2 apoptosis regulator
BDNF:	brain-derived neurotrophic factor
BF:	beaded fiber
BG:	Bergmann glia
BK:	big potassium
BMP:	bone morphogenetic protein
BNIP3:	B-cell lymphoma 2 interacting protein 3
Ca ²⁺ :	calcium ion
CALB2:	calbindin 2
CaMK:	Ca ²⁺ /calmodulin-dependent protein kinases
CASP3:	caspase 3
CCAS:	cerebellar cognitive affective syndrome
CCT:	cuneocerebellar tract
cDNA:	complementary deoxyribonucleic acid
CF:	climbing fiber
CH:	continuous hypoxia
CNS:	central nervous system
CO ₂ :	carbon dioxide
CPAP:	continuous positive airway pressure
CPCT:	corticopontocerebellar tract
Cq:	quantification cycle
CRL:	cerebellar rhombic lip
CRMPx:	collapsin response mediator protein x
CRST:	corticoreticulospinal tract
DAPI:	4',6'-diamidino-2-phenylindole

DBE:	dibenzylether
DCM:	dichloromethane
DCN:	deep cerebellar nuclei
DCq:	delta Cq
DLL4:	delta like canonical notch ligand 4
DMSO:	dimethyl sulfoxide
DNA:	deoxyribonucleic acid
DSCT:	dorsal spinocerebellar tract
e ⁻ :	free electron
ECN:	extracerebellar neurons
EFN:	ephrin
EGL:	external granular layer
En:	engrailed homeobox gene
ENT1:	equilibrative nucleoside transporter 1
ENx:	engrailed homeobox x
EPHA:	EPH receptor A
EPO:	erythropoietin
ERK:	see Mapk1
ETC:	electron transport chain
Ex:	embryonic development day x
Fe ²⁺ :	iron (II) or ferrous ion
Fe ³⁺ :	iron (III) or ferric ion
FGFx:	fibroblast growth factor x
fMRI:	functional magnetic resonance imaging
GABA:	gamma-aminobutyric acid
GALNT17:	polypeptide n-acetylgalactosaminyltransferase 17
GBX2:	gastrulation brain homeobox 2
GC:	granule cell
GERD:	gastroesophageal reflux disease
GL:	granular layer
GLAST-1:	glutamate aspartate transporter 1
GLI1:	GLI family zinc finger 1
GLMM:	generalized linear mixed model
GLT-1:	glutamate transporter 1
GM:	grey matter
GMT:	Guillain-Mollaret triangle
GOI:	gene of interest
GPX:	glutathione peroxidase

GSH:	reduced glutathione
GSR:	glutathione reductase
GSSG:	glutathione oxide
GSX1:	genomic screened homeobox 1
GW:	gestational week
H ⁺ :	hydrogen ion
H ₂ O:	water
H ₂ O ₂ :	hydrogen peroxide
HES1:	hes family BHLH transcription factor 1
HIF-1 α :	hypoxia-inducible factor 1 alpha
HKG:	housekeeping gene
HO ⁻ :	hydroxide anion
HO•:	hydroxyl radical
HOX:	homeobox
HRE:	hypoxia response element
HRL:	hindbrain rhombic lip
IGL:	internal granular layer
IH:	intermittent hypoxia
IHC:	immunohistochemistry
I κ B α :	nuclear factor-kappa B inhibitor alpha
IKK:	I κ B kinase complex
ILx:	interleukin x
IN:	interneuron
INVp:	intraneuronal vascular plexus
IRX3 :	iroquois homeobox 3
K ⁺ :	potassium ion
LH \times x:	LIM homeobox x
LKB1:	serine-threonine kinase liver kinase B1
LMX1B:	LIM homeobox transcription factor 1 Beta
LTD:	long-term depression
LTP:	long-term potentiation
Mb:	midbrain
MCA:	middle cerebral artery
MEIS1:	myeloid ecotropic viral integration site 1 homolog 2
MF:	mossy fiber
MgCl ₂ :	magnesium chloride
mGluR2:	metabotropic glutamate receptor 2
ML:	molecular layer

mTORC1:	mechanistic target of rapamycin complex 1
mRNA:	messenger ribonucleic acid
n:	number of biological replicates
N:	normoxic control group
Na ⁺ :	sodium ion
NADP ⁺ :	oxidized nicotinamide adenine dinucleotide phosphate
NADPH:	reduced nicotinamide adenine dinucleotide phosphate
NAVA:	neurally adjusted ventilatory assistance
NDD:	neurodevelopmental disorder
NDS:	normal donkey serum
NEURODx:	neuronal differentiation x
NF-κB:	nuclear factor-kappa B
NIPPV:	nasal intermittent positive pressure ventilation
NMDA:	N-methyl-D-aspartate
NO•:	nitrogen monoxide
NOS:	nitric oxide synthase
NOTCH :	notch receptor
NOX:	NADPH oxidase
NOX2:	pro-oxidant enzyme nitric oxide synthase 2
NTS:	nucleus tractus solitarius
O ₂ :	dioxygen
O ₂ • ⁻ :	superoxide anion
OD:	optical density
OGD:	oxygen glucose deprivation
OL:	olivary nuclei
OLIGx:	oligodendrocyte transcription factor x
OS:	oxidative stress
OSA:	obstructive sleep apnea
OST:	olivospinal tract
OTX2:	orthodenticle homeobox 2
PaCO ₂ :	partial arterial pressure of carbon dioxide
PaO ₂ :	partial arterial pressure of oxygen
P _A O ₂ :	partial alveolar pressure of oxygen
PAXx:	paired box x
PBX3:	pre-B-cell leukemia homeobox 3
PC:	Purkinje cell
PCL:	Purkinje cell layer
PCR:	polymerase chain reaction

PDGF:	platelet-derived growth factor
PDGFB:	platelet derived growth factor subunit B
PDGFRB:	platelet derived growth factor receptor beta
PF:	parallel fiber
PFA:	paraformaldehyde
PFK-2:	phosphofructokinase-2
PICA:	posterior inferior cerebellar artery
PNM:	postnatal months
PNVP:	perineural vascular plexus
PRDX:	peroxiredoxin
PROX1:	Prospero-Related Homeobox 1
PTF1 α :	pancreas associated transcription factor 1 alpha
PVP:	periventricular plexus
Px:	postnatal day x
qPCR :	quantitative polymerase chain reaction
RAPTOR:	regulatory-associated protein of mTOR
RAX:	retina and anterior neural fold homeobox
RL:	rhombic lips
RNA:	ribonucleic acid
ROBO4:	roundabout guidance receptor 4
ROR α :	retinoid-related orphan receptor alpha
ROS:	reactive oxygen species
RSCT:	rostral spinocerebellar tract
RST:	rubrospinal tract
RTqPCR:	real time quantitative PCR
SC:	stellate cell
SCA:	superior cerebellar artery
SCT:	spinocerebellar tract
SDF:	stromal cell-derived factor
SDF-1 α :	stromal cellderived factor 1 alpha
SHH:	sonic hedgehog
SLIT2:	slit guidance ligand 2
SOD:	superoxide dismutase
SOXx:	SRY-box transcription factor x
SpO ₂ :	pulse oximeter saturation
TAK1:	growth factor beta-activated kinase 1
TAZ:	Tafazzin
TBRx :	T-box brain transcription factor x

TGF- β :	transforming growth factor beta
TIE:	tyrosine kinase with immunoglobulin like and EGF like domains
TLX3:	T cell leukemia homeobox 3
TRKB:	tropomyosin receptor kinase B
TRX:	thioredoxin
TSC2:	tuberous sclerosis complex subunit 2
TXNIP:	thioredoxin interacting protein
TXNRD:	thioredoxin reductase
UBC:	unipolar brush cell
VEGF:	vascular endothelial growth factor
VHL:	von Hippel-Lindau protein
VSCT:	ventral spinocerebellar tract
VST:	vestibulospinal tract
VZ:	ventricular zone
WM:	white matter
WNTx:	wingless-type MMTV integration site family member x
YAP:	transcriptional coactivator YAP1

N.B.: all gene abbreviations pertaining to the gene panels are featured in the appendix section.

LIST OF FIGURES

Figure 1: Relations and gross anatomy of the cerebellum in humans.....	11
Figure 2: Schematic representation of the cerebellum in humans, superior view.....	12
Figure 3: General organization of a cerebellar folium, longitudinal and transverse section.....	14
Figure 4: Schematic representation of cerebellar deep nuclei in humans, horizontal section.....	18
Figure 5: Schematic representation of cerebellar neuronal circuitry and cytoarchitecture.....	22
Figure 6: Patterned molecular marker expression in the mouse cerebellar cortex, dorsal view.....	26
Figure 7: Arterial irrigation of the human cerebellum: main vessels and relations.....	28
Figure 8: Venous drainage of the human cerebellum: main vessels and relations.....	30
Figure 9: Schematic representation of the formation of the neural tube.....	32
Figure 10: Schematic representation of the primary and secondary brain vesicles.....	33
Figure 11: Neural tube regionalization and genetic regulation in mice.....	34
Figure 12: Progression of cerebellar formation, transverse cuts at the metencephalic level.....	35
Figure 13: Dorsolateral view, sagittal section, and coronal section.....	36
Figure 14: Dorsal view of the developing mesencephalon and rhombencephalon.....	37
Figure 15: Schematic representation of cerebellar development along the midsagittal plane.....	39
Figure 16: Representation of the changes occurring at the anchoring center of a folium in mice.....	40
Figure 17: Vascular development in the human CNS.....	42
Figure 18: Schematic representation of spinocerebellar pathways in humans.....	52
Figure 19: Schematic representation of corticocerebellar pathways in humans.....	54
Figure 20: Schematic representation of the main vestibulocerebellar pathways in humans.....	57
Figure 21: Depiction of the moving rubber hand illusion.....	59

Figure 22: Representation of oxygen variation during different types of hypoxias.....	69
Figure 23: Location of peripheral chemoreceptors and their CNS projections.....	73
Figure 24: Summary of known causal factors of apnea of prematurity.....	77
Figure 25: Reduction of O ₂	83
Figure 26: Neutralization of H ₂ O ₂ by peroxiredoxins.....	84
Figure 27: Production, effects, and neutralization of ROS in the cell.....	85
Figure 28: Schematic synapse representing the main neuronal death pathways induced by hypoxia...	91
Figure 29: Hypoxia chamber containing a cage.....	99
Figure 30: Schematic representation of oxygen levels in the hypoxia chamber.....	100
Figure 31: Correspondence of the human perinatal period to postnatal murine stages.....	101
Figure 32: Sample of the Cerebellar Development Transcriptome Database setup.	102
Figure 33: Sample of the parameters available on Primer express.....	103
Figure 34: Sample of the validation process for each primer pair for the RT-qPCR experiments.....	104
Figure 35: Example of a slice stained with cresyl violet.....	105
Figure 36: Example of quality assessment of a suitable RNA sample.....	106
Figure 37: Main findings presented in article 1.....	142
Figure 38: Main findings presented in article 2.....	165
Figure 39: RT-qPCR results of the vascularization panel on the whole cerebellum.....	168
Figure 40: Immunohistochemistry test staining.....	169
Figure 41: Modeling of blood vessels in the Imaris software.....	170
Figure 42: Graphical conclusion.....	184

LIST OF TABLES

Table 1: Housekeeping genes primer pair sequences and specifications.....	107
Table 2: Antibodies used for immunohistochemical experiments.....	108
Table 3: Composition of the solutions of the clearing protocol.....	109
Table 4: Antibodies used for the 3D visualization of blood vessels.....	110

INTRODUCTION

I. CHAPTER ONE: THE CEREBELLUM

A. ANATOMY

1. Overview

Among the first findings concerning the cerebellum were the observations of French anatomist Raymond Vieussens in his treatise about the central nervous system (CNS), *Neurographia universalis* in 1684 (Vieussens 1684). Since, from the contributions of Santiago Ramón y Cajal to the latest findings in functional magnetic resonance imaging (fMRI), the perception and understanding of this “little brain” is constantly evolving (Ramón y Cajal 1909; Voogd and Koehler 2018). The cerebellum is a hindbrain-derived part of the CNS and occupies the posterior cranial fossa, separated from the cerebral hemispheres by the *tentorium cerebelli* (Standring 2016). It is located dorsally to the pons and medulla, from which it is separated by the fourth ventricle. The cerebellum is connected to the brainstem by three pairs of cerebellar peduncles (Figure 1). Despite its small size, representing only 15% of total brain mass, the cerebellum alone contains over 70% of the neurons in the brain (Herculano-Houzel et al. 2006).

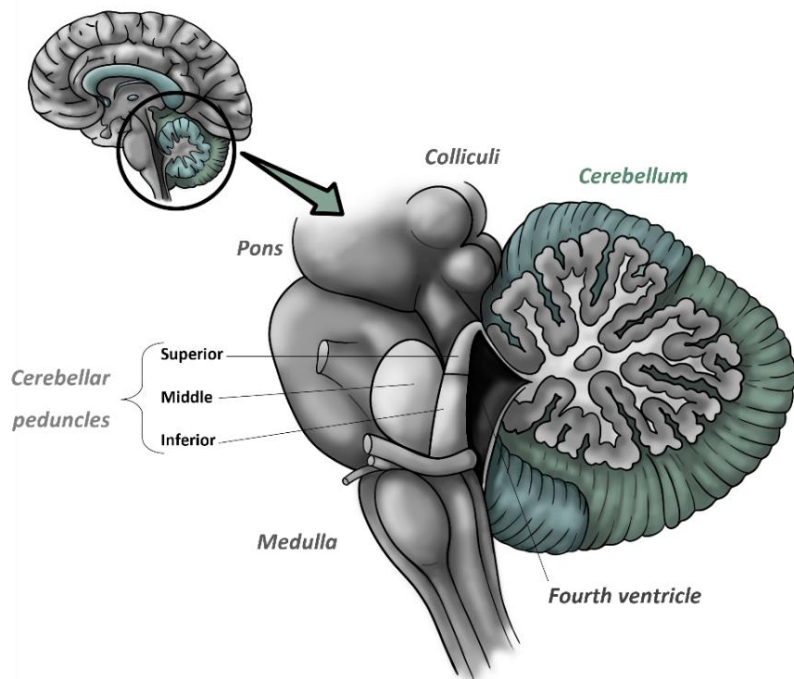


Figure 1: Relations and gross anatomy of the cerebellum in humans.

Representation of the cerebellum and its relationship with the brainstem zoomed in from a sagittal section of the brain.

2. *Divisions*

There are several approaches to describing the cerebellum: evolutionary, anatomical, functional, and histological. The evolutionary and anatomical standpoints converge to define three distinct parts (Figure 2): *i*) the archicerebellum already present early in the phylogenetic tree such as in fish, corresponding to a small primitive part of the cerebellum also called the flocculonodular lobe; *ii*) the paleocerebellum that appeared later in reptiles and birds, which is represented by the medial lobe (vermis) and intermediate lobes (paravermis), separated by two longitudinal furrows; and finally *iii*) the neocerebellum found only in mammals and embodied by the lateral portion of the cerebellum, namely the hemispheres (Larsell 1937; Kandel 2013).

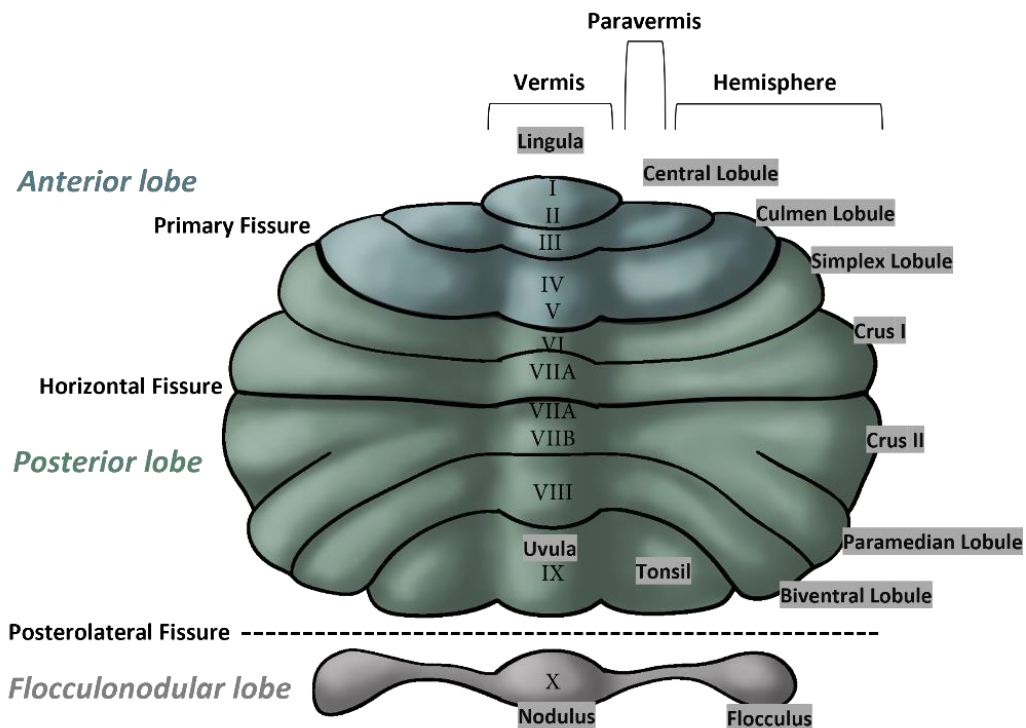


Figure 2: Schematic representation of the cerebellum in humans, superior view.

Main divisions of the cerebellum in lobes and lobules and the corresponding numerical nomenclature.

The cerebellum is further divided in tightly convoluted folds visible on its surface. From largest to smallest, these divisions are: lobes, lobules, further subdivided into folia, in turn separated by transverse fissures (Standring 2016). The anterior lobe is the most cranial and it is separated from the posterior lobe by the primary fissure. In turn, the posterior lobe is separated caudally from the flocculonodular lobe by the posterolateral fissure (Figure 2).

However, a functional afferent-based cerebellar division is more appropriate to the clinical understanding of cerebellar functions (Ito 1990). With this approach, the cerebellum is divided sagittally in: *i*) the median cerebellum which is comprised of the vermis; *ii*) the intermediate cerebellum composed of the paravermis; and *iii*) the lateral cerebellum which includes the lateral parts of the hemispheres. Additionally, the flocculonodular lobe is composed of a vermal component, the nodule, and two lateral portions, the flocculi (Vuillier et al. 2011).

Despite these divisions, the cerebellum is characterized by a stereotypical histological organization which is constant throughout. The cerebellum consists of a superficial grey matter cortex overlying a core of white matter in which are embedded grey matter deep cerebellar nuclei (DCN). Cerebellar neurons receive two major afferences in the form of mossy fibers (MFs) and climbing fibers (CFs) which arrive via the cerebellar peduncles.

3. Grey Matter

a. Cortex

The elements of the cerebellar cortex are precisely arranged in the tangential, longitudinal, and transverse planes of each folium and this organization is conserved throughout the organ and across species. Even though the layers of the cortex will vary according to the developmental stage, in adults we can distinguish three layers based on their cellular composition: granular, Purkinje and molecular layers (Figure 3).

i. The granular layer

The innermost granular layer (GL) consists, for the most part, of **granule cells** (GCs), which constitute the overall largest neuronal population in the adult human brain (Zagon et al. 1977). GCs are small glutamatergic neurons whose 5 to 8 μm -wide soma is almost entirely occupied by their nucleus (Gallo et al. 1982). They receive branches of afferent MFs from the spinal cord, brainstem, and brain. This excitatory signal arrives via 3 to 5 short dendrites, localized within a glomerulus where GCs also receive inhibitory signals from inhibitory neurons called Golgi cells (Lackey et al. 2018). The glomerular triad is surrounded by a velate astrocyte, whose role is unclear but may be involved in neuroprotection (Oliveira-Junior et al. 2019). The information is then relayed via an axon that extends toward the surface to the molecular layer (ML) where it divides into two opposed branches, thus forming parallel fibers (PFs) that synapse with Purkinje cell dendritic trees (Pichitpornchai et al. 1994).

INTRODUCTION

Scattered among the GCs, several types of inhibitory interneurons with a glycinergic/ gamma-aminobutyric acid(GABA)ergic phenotype are found in the GL: Golgi cells, Lugaro cells, and globular cells (Ottersen et al. 1988). **Golgi cells** are distributed throughout the GL and can be recognized by their large polygonal soma. They have an extensive dendritic tree that branches out in the ML. There, Golgi cells receive inhibitory inputs from other interneurons, namely, basket, stellate, and Lugaro cells (Rubenstein 2020). In the GL, they receive direct excitatory inputs from MFs and are in close contact with Sheibel collaterals from CFs although synapses between the two have not yet been evidenced (Galliano et al. 2013). **Lugaro cells** are fusiform “cigar-shaped” interneurons lying just beneath the Purkinje cell layer and can belong to three subgroups: large fusiform, triangular, and small fusiform. They receive GABAergic inputs from recurrent axon collaterals of Purkinje cells, and project glycinergic axons to the ML to innervate basket and stellate cells (Lainé and Axelrad 2002). **Globular cells**, while displaying round somata, could be a “deep” subtype of Lugaro cells as they are dispersed in the whole GL but have a similar physiology (Lainé and Axelrad 2002). Indeed, both cell types express calretinin, while Golgi cells express the metabotropic glutamate receptor 2 (mGluR2) and neurogranin (Simat et al. 2007).

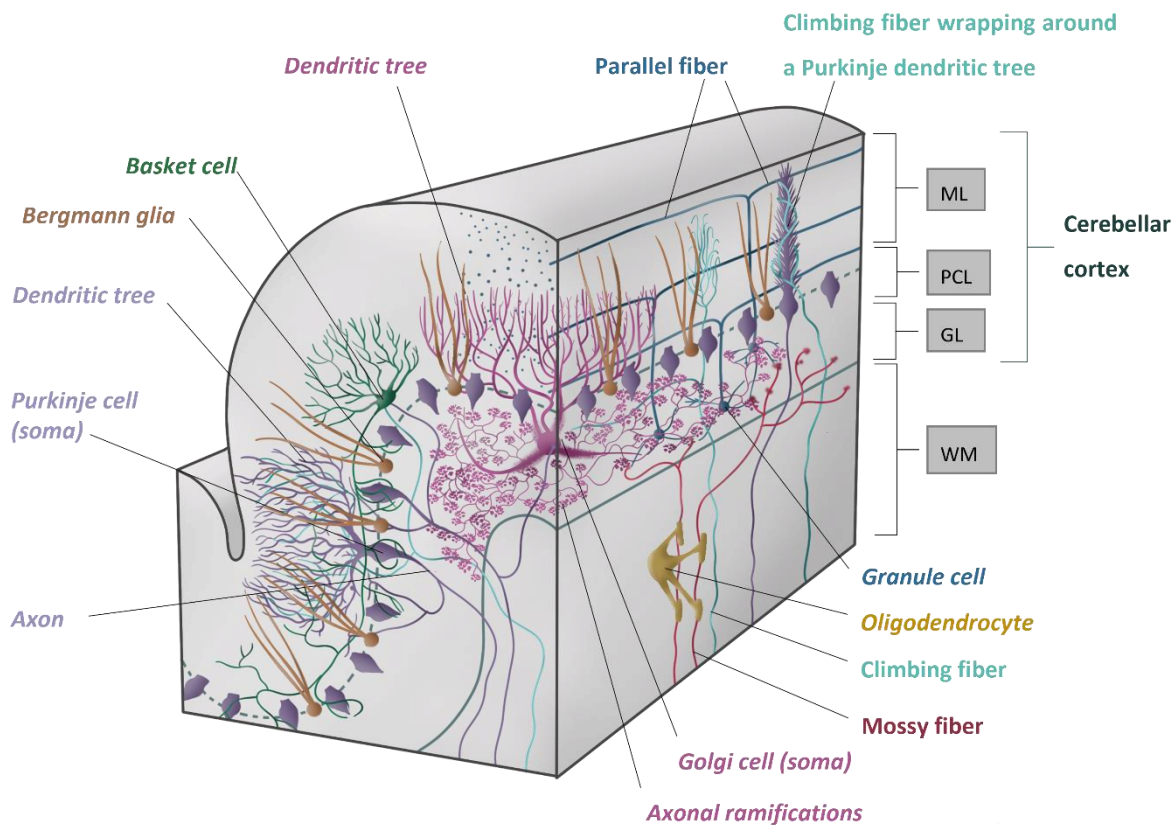


Figure 3: General organization of a cerebellar folium, longitudinal and transverse section.

GL: granular layer; ML: molecular layer; PCL: Purkinje cell layer; WM: white matter.

In addition to the different types of inhibitory interneurons, one type of excitatory interneuron has been identified in the GL. **Unipolar brush cells** (UBCs) are glutamatergic interneurons, mostly present in the vestibulocerebellum and virtually absent from the cerebellar hemispheres. Generally, high densities of UBCs coincide with the terminal regions of vestibular afferents (Barmack et al. 1992). These cells are named for their distinctive dendritic structure, which is characterized by a single, short dendrite terminating in many branches, thus resembling a brush, which engulf one or two rosettes of glutamatergic and cholinergic MFs. They innervate dendrites of other UBCs and GCs. As such, they function as an intermediate that amplifies the excitatory signals of MFs on GCs (Mugnaini and Floris 1994).

ii. The Purkinje cell layer

Overlying the GL, lies a single-cell layer of neurons with apical dendrites, called Purkinje cell layer (PCL). It contains the large, pear-shaped somata of **Purkinje cells** (PCs) which measures approximately 20 µm in diameter in mice and up to 65 µm in humans. From their basal extremity, they emit a single axon which extends to reach the cerebellar nuclei (Ito et al. 1964; Korbo and Andersen 1995). A prominent phenotypical landmark of PCs is their large dendritic tree stemming from a single apical root, called primary dendrite (Figure 3). It gives rise to secondary dendrites, which in turn branch out to form multiple tertiary dendrites. All these ramifications extend throughout the thickness of the ML to establish connections with other cells, most notably, GCs.

The PCL also contains the cell bodies of Bergmann glia, candelabrum cells, scatters of GCs, and occasional Golgi cells interspersed between PCs (Glickstein et al. 2009). **Bergmann glia** are specialized astrocytes that intercalate between PCs and emit projections towards the ML and cortical surface (Hanke and Reichenbach 1987). These cells are derived from radial glia and direct the migration of GC precursors during development (Xu et al. 2013). They are also involved in the formation of synapses and in the refinement of the mature cerebellar cortical circuit through synaptic pruning by engulfment during motor learning (Morizawa et al. 2022). Bergmann glia also oversee metabolic functions such as glucose metabolism and are involved in the reuptake of neurotransmitters via the glutamate aspartate transporter 1 (GLAST-1) and glutamate transporter 1 (GLT-1) receptors (Chaudhry et al. 1995; Tellios et al. 2022). Finally, recent findings suggest that these astrocytes may function as neural stem cells in the mature cerebellum for adult oligodendrogenesis (Alcock et al. 2007; Radecki and Samanta 2022).

Candelabrum cells represent the latest type of neurons discovered in the cerebellar cortex (Lainé and Axelrad 1994). These GABAergic inhibitory interneurons have a small piriform cell body oriented vertically between PCs and are the most abundant PCL interneuron, being ubiquitous across all cerebellar lobules (Osorno et al. 2022). One to two thick dendrites emerge from their soma and

INTRODUCTION

penetrate the ML vertically, where they emit branches that may reach the cortical surface. Smaller dendrites may also stem from the opposite pole or from the base of the main dendrites, which project in the GL while their axon travels horizontally within the PCL (Schilling et al. 2008). This axon emits a multitude of branches that ascend into the ML giving the cell its candelabrum or “menorah-like” appearance (Osorno et al. 2022).

iii. The molecular layer

The most external molecular layer (ML) is sparsely populated but is the site of many intercellular connections. In fact, the few cell bodies present in the ML are mostly those of GABAergic interneurons whose main function is to inhibit PCs, namely basket and stellate cells, as well as some GCs. Stellate cells lie more superficially, while basket cells are more closely related to the underlying PCL (Yamanaka et al. 2004). Overall, the ML is highly interconnected with basket, stellate, and Golgi cells, forming a complex network of inhibitory connections among a matrix of radial glial projections from Bergmann cells.

Basket cells have a large soma of roughly 12 µm in diameter and are in the lower third of the ML. They have sparsely branched dendrites distributed radially in the ML along a parasagittal axis and which synapse mostly with PFs. Ascending dendrites may occupy the full thickness of the ML, whereas descending dendrites are shorter and less numerous. A noteworthy feature of these cells is the presence of dendritic spines, not only along the entire length of the dendritic tree, but also occasionally on the cell body. Their axon extends along and into the PCL and emit collaterals that wrap around the somas of PCs thus forming the basket-like network, hence their name (Lemkey-Johnston and Laramendi 1968).

Stellate cells are in the upper two-thirds of the ML. The outermost ones have a diameter comprised between 5 and 9 µm and a few radial dendrites, whereas the innermost cells are larger and have a more elaborate dendritic tree. They project an axon that runs parallel to the PCL and forms synapses with PC dendritic trees. Like basket cells, they are GABAergic inhibitory neurons that receive inputs from PFs and some CFs, and send inhibitory axon collaterals to the dendrites of PCs (Lemkey-Johnston and Laramendi 1968; Llinás and Sugimori 1980).

The distinction of stellate and basket cells into two separate cell types is questioned (Ramón y Cajal 1909) and they may represent a single cell population whose morphological variations are thought to be due to their relative positioning within the ML (Sultan and Bower 1998). However, there is evidence of a timeline difference during their development, with stellate cells maturing a couple of

days after basket cells (Altman 1972). Moreover, basket cells emit prolongations which directly contact PC somata, while stellate cells exert their inhibition via contact with PC dendrites (Ito 2006).

In addition, the ML can contain some GCs, that were long believed to be ectopic. However, while it was long assumed that GCs from the ML were a minor neuronal population, it has now been shown that these are as prevalent as stellate or basket cells in the ML of the posterior cerebellum. Moreover, whole-cell patch-clamp experiments demonstrated similar action potential activity in ML-GCs as in GL-GCs, but, since their inputs differ based on their location, it is thought that both populations are involved in different cerebellar micro-circuits (Dey et al. 2022).

Aside from its cellular population, the largest volume of the ML is comprised of nerve fibers, such as dendritic trees of the underlying Purkinje and Golgi cells, numerous PFs emitted by GCs, extensions of Bergmann glial cells, and afferent CFs (Figure 3). The tertiary dendrites of PCs are covered in dendritic spines that connect to thousands of PFs, which measure approximately 5 mm in length in the rat brain, leading to more than 175,000 synaptic contacts (Herndon 1963; Harvey and Napper 1988; Napper and Harvey 1988). In addition, each PC is also connected to a single CF, which wraps around the dendritic tree, forming numerous connections (Herndon 1963). Moreover, the apical dendrites of Golgi cells ascend into the ML to connect to PFs as well as with each other (Dugué et al. 2009).

Even though most of the cerebellar grey matter is found in the cortex, an important portion lies deeper in the cerebellum. The deep cerebellar nuclei also contain a diverse neuronal population that shares some characteristics with those of the cortex.

b. Deep Cerebellar Nuclei

The deep cerebellar nuclei (DCN) are central areas of grey matter (GM) embedded within the white matter. From medial to lateral, these are: the fastigial, the two interposed (the globose posteriorly and emboliform anteriorly) and dentate nuclei (Figure 4). These neuronal clusters are connected to the cerebellar cortex via inhibitory afferences from PC axons, but they also receive excitatory afferences from mossy and climbing collaterals (Uusisaari and Knöpfel 2013).

In these central areas of GM, the extracellular matrix is organized to enwrap the neuronal somata, forming perineuronal nets. Recent findings suggest that changes these DCN structures can regulate cerebellar functions (Hirono et al. 2021). Each DCN contain three main neuron categories that differ in morphology, neurotransmitter, and connectivity (Leto et al. 2006): *i*) large glutamatergic

INTRODUCTION

neurons that project outside the cerebellum, *ii)* medium GABAergic nucleo-olivary projection neurons; and *iii)* small local GABAergic interneurons. Thus, large-somata glutamatergic neurons, which might be compared to PCs due to their wide-spanning dendritic trees, are the main efferent cells issuing from DCNs and project to various brain regions, including the red nucleus and thalamus (Uusisaari and Knöpfel 2012). DCNs are also populated by smaller GABAergic and glycinergic neurons, characteristic of the dentate and fastigial nuclei respectively. These small neurons can act either as local interneurons or project their axons to the inferior olivary nucleus (Bagnall et al. 2009; Uusisaari and Knöpfel 2012). Thus, the DCNs represent a central node of the cerebellum as the source of its output as they can be involved in inhibitory or excitatory signal transmission (Uusisaari and Knöpfel 2013).

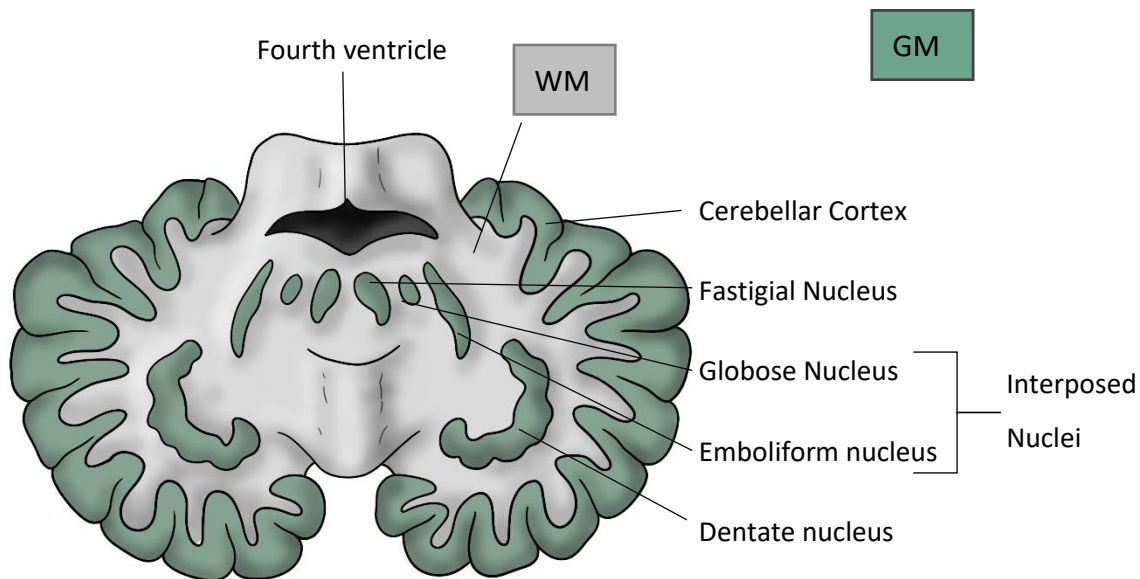


Figure 4: Schematic representation of cerebellar deep nuclei in humans, horizontal section.

GM: grey matter; WM: white matter.

The **dentate nucleus** is the largest and most recognizable in transverse section by its characteristic convoluted band, forming a crescent with a medial hilus. It contains mostly multipolar neurons with branching dendrite (Milošević et al. 2010). This DCN can be functionally divided into two areas, dorsal and ventral, which are involved in motor and non-motor functions, respectively (Küper et al. 2011). It receives inputs from the cerebral cortex via the inferior peduncle and from the ipsilateral cerebellar hemispheres, and projects outputs via the superior peduncle towards the contralateral red nucleus and the ventrolateral thalamic nucleus (Carpenter 1991; Bond et al. 2017).

Both **emboliform and globose nuclei** may be referred to conjointly as the **interposed nuclei** (anterior and posterior, respectively) and are even fused in some species. The **emboliform nucleus** is grossly wedge-shaped and is located close to the dentate hilus with which it shares a similar cell population. The **globose nucleus** is a variable group of rounded cell clusters. They are adjacent to the roof of the fourth ventricle and receive afferences issuing from the paravermis, while their efferences travel through the superior cerebellar peduncle before reaching the contralateral red nucleus (Voogd et al. 2013).

The **fastigial nucleus** is located directly above the roof of the 4th ventricle, near the midline. It is further divided in rostral and caudal fastigial nuclei based on cytological evidence, with smaller cells found in the rostral extremity (Carpenter 1991). This nucleus receives afferences from both vermic PCs and collaterals of MFs and CFs (Vuillier et al. 2011; Zhang et al. 2016). It is unique in its emission of efferent fibers through the inferior cerebellar peduncle. Most of them cross to the contralateral side within the cerebellum, and project to all levels of the brain stem (Carpenter 1991). Surrounding these clusters of neurons lies the white matter. Devoid of neuronal bodies, this area of the cerebellum is comprised of dense bundles of nerve fibers.

4. White Matter

The cerebellar white matter (WM) is located deep under the cerebellar cortex and is composed of fibers traveling to and from it. The only efference of the cerebellar cortex originates in PCs, while there are forty times more afferences in the form of climbing, mossy fibers and, to a lesser extent, beaded fibers (Carpenter 1991).

Climbing fibers (CFs) are axons that arise mainly from neurons of the contralateral inferior bulbar olfactory nucleus (Desclin 1974; Carpenter 1991). They cross the midline and enter the cerebellum via the inferior cerebellar peduncle. A minor proportion of CFs originate in the pontine nuclei and project through the middle cerebellar peduncle (Bloedel 1973). Within the cerebellum, CFs emit collateral branches to synapse with DCN interneurons, and then pursue a straight trajectory to reach the cerebellar cortex. There, they issue several tendril collaterals which join the ML where they form branches surrounding PC dendritic trees. Although a PC is innervated by only one CF, the formation of a rich plexus of fine CF terminals allows for a high number of synaptic contacts with a single PC (Palay and Chan-Palay 1974). Furthermore, a single CF connects to several PCs, which may be located in different lobules, where CFs exert an all-or-none excitatory activity mediated by glutamate and aspartate (Kimura et al. 1985; Carpenter 1991).

INTRODUCTION

Mossy fibers (MFs) originate from different brainstem nuclei, such as the pontine and vestibular nuclei, or from the spinal cord. These glutamatergic fibers enter the cerebellum via the middle and inferior cerebellar peduncles. Within the cerebellar WM, they distribute to specific lobules in the ipsi- or contralateral hemisphere depending on their origin (Sillitoe et al. 2012). Upon arrival in the GL, MFs lose their myelin sheath and form numerous bifurcations along which lobulated enlargements called “rosettes” give them their characteristic appearance (Carpenter 1991). Each rosette forms the center of a cerebellar glomerulus, a nodular structure establishing contact with about 20 GCs and multiple Golgi cell terminals (Carpenter 1991; Lackey et al. 2018).

Beaded fibers (BFs), so called due to their diffuse termination patterns, constitute a minor proportion of afferent fibers that come join the cerebellar WM (Sillitoe et al. 2012). These neuromodulatory fibers can be distinguished by their specific neurotransmitters whose targets and receptors are summarized in Figure 5.

Serotonergic fibers arise mostly from the reticular formation and, in a smaller proportion, from the raphe nuclei (Strahlendorf and Hubbard 1983; Bishop and Ho 1985). They project heterogeneously to the whole cerebellar cortex, with an increased density within lobules VII to X of the vermis (Strahlendorf and Hubbard 1983; Rahimi-Balaei et al. 2015). PCs represent the main target for these serotonergic afferents, thus having their firing activity modulated (Crivellato et al. 1992).

Noradrenergic neuromodulatory fibers originate mainly in the locus coeruleus, enter the cerebellum via the superior peduncle and project to reach the DCNs and the cortex. They thus form a sparse network that manages to reach and innervate seemingly all PCs (Bloom et al. 1971). This network also acts on other cell types, such as ML interneurons, in a nonjunctional paracrine manner, triggering an increase of their spontaneous inhibitory synaptic currents (Abbott and Sotelo 2000).

Cholinergic afferents from the pedunculopontine nucleus, the reticular formation and, to a lesser extent, the vestibular nuclei, form a diffuse web and reach the ML, GL and DCNs (Barmack et al. 1992; Jaarsma et al. 1997). Moreover, MFs also extensively innervate UBCs, some of which may rely on cholinergic input from the medial vestibular nucleus. In fact, acetyltransferase-positive MFs co-release acetylcholine and glutamate and thus, may participate in nicotinic neurotransmission in the cerebellum (Jaarsma et al. 1996).

Histaminergic fibers originating directly from the tuberomamillary nucleus of the hypothalamus connect to neurons of the ML, GL and PCL (Panula et al. 1993). There, histamine acts as an excitatory neuromodulator via its G-protein-coupled receptor on both PCs and GCs (Li et al. 2014).

Finally, *dopaminergic* afferents originate from the ventral tegmental area and travel to the cerebellar cortex (Ikai et al. 1992; Giompres and Delis 2005). Considering the localization of dopamine receptors, it is suggested that dopamine fibers act primarily on PCs to modulate cerebellar reward-based learning (Barili et al. 2000). Thus BFs and their neurotransmitters are part of a complex and tightly regulated network that is instrumental to the cerebellum's wide range of functions.

5. Cerebellar circuitry

a. General organization

i. Afferences

Most cerebellar **afferents** arrive through the inferior cerebellar peduncle. CFs and MFs are the two distinct excitatory afferents to the cerebellum (Palay and Chan-Palay 1974). Inputs issuing from the brainstem are relayed in the inferior olivary nucleus of the medulla oblongata, which then emerge as CFs to reach the contralateral cerebellum. Meanwhile, MFs originating from various extracerebellar regions, such as the spinal cord, pontine nuclei, and reticular formation reach the cerebellum where hemispheric projections decussate while those destined to the vermal cortex are bilateral. MFs issued from the motor and somatosensory areas of the cerebral cortex maintain their somatotopic organization in the cerebellum (Carpenter 1991).

CFs establish direct contact with PCs and each CF forms hundreds of synapses around proximal PC dendrites (Eccles et al. 1966). Indeed, this is facilitated by the highly convoluted shape of the cortex which enables a single inferior olive neuron to act on cerebellar output by simultaneously affecting the firing of over 100 PCs (Han et al. 2020). CF input powerfully excites PCs by triggering dendritic spikes as well as a characteristic high-frequency burst of somatic spikes known as the complex spike. A complex spike occurs at 1-2 Hz and is characterized by a fast sodium (Na^+) action potential followed by slow dendritic calcium (Ca^{2+}) spikelets (Miyakawa et al. 1992). Dendritic and complex spikes have been shown to be relatively unrelated in origin. Indeed, complex spikes are generated in the proximal part of the axon but seem to undergo some regulation by dendritic spikes. This electrical potential allows for the dual function of CF inputs which aim at triggering local plasticity as well as generating an output signal (Davie et al. 2008). Additionally, a complex spike in one PC has a local effect by ephaptic coupling on neighboring PCs that suppresses the 100 Hz Na^+ simple spikes on their axons during a few milliseconds (Han et al. 2020).

INTRODUCTION

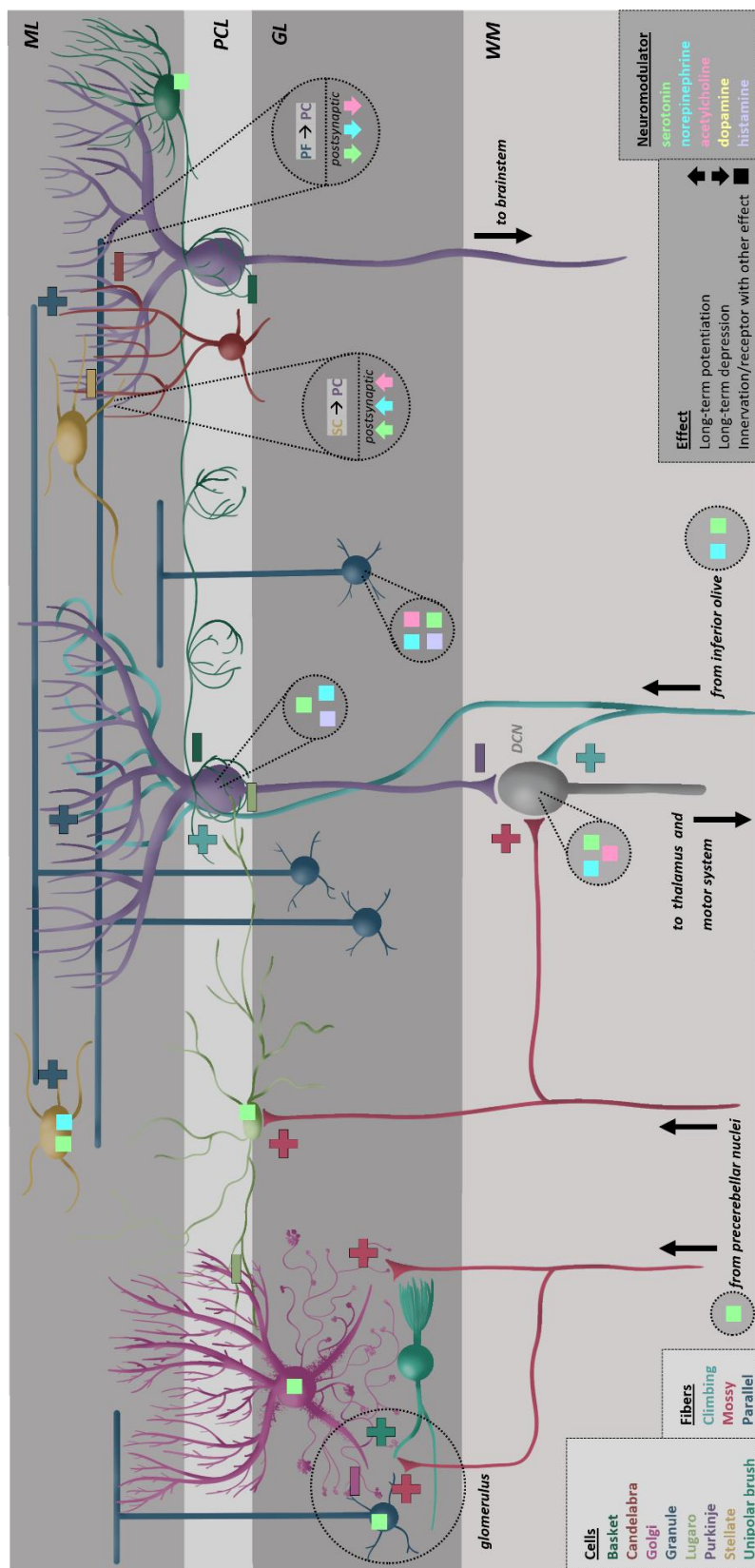


Figure 5: Schematic representation of cerebellar neuronal circuitry and cytoarchitecture.

DCN: deep cerebellar nuclei; GL: granular layer; ML: molecular layer; PC: Purkinje cell; PCL: Purkinje cell layer; SC: stellate cell; WM: white matter; +: excitation; -: inhibition.

Figure compiling information from (Schweighofer et al. 2004; Li et al. 2014; Tam et al. 2021).

While long believed to be of dichotomic nature, the complex spike's "all-or-none" character is now questioned, and it is now clear that CF signal is much more specific in order to match sensory inputs. Indeed, presynaptic CF Ca^{2+} amplitude is directly proportional to the sensory stimulus' strength, which ultimately conditions post-synaptic PC dendritic Ca^{2+} amplitude (Roh et al. 2020). In turn, PCs control the discharge of their own CF afferents and thus might participate in the regulation of cerebellar function via the olivo-cortico-nuclear network which forms a regulatory closed loop (Chaumont et al. 2013).

MFs contact GCs within a glomerulus (Figure 5), a structure that brings together GC dendrites, MF terminals and Golgi axons. GC dendrites emit 3 to 5 dendritic digits in relation with each other and which receive one or more synaptic inputs from either MF terminal or Golgi axon varicosities (Jakab and Hámori 1988). At this site, glutamate released by MFs binds to N-methyl-D-aspartate (NMDA) receptors on the postsynaptic membrane of GCs. Transmission efficacy is increased by the binding of glutamate from spillover onto alpha-amino-3-hydroxy-5-methyl-4-isoxazolepropionic acid (AMPA) receptors of the postsynaptic density (DiGregorio et al. 2002).

ii. Intracortical interactions

Within the glomerulus, GC dendrites are intermixed with UBC dendrioles, both of which receive synapses from the same one to two MF rosettes, indicating a minimal convergence of excitatory inputs. There, UBCs receive fast (AMPA) and slow (NMDA) glutamatergic signals from MFs. UBC dendrioles are also presynaptic to GC dendrites, forming dendro-dendritic contacts similar to excitatory synapses and contribute to GC excitation (Mugnaini et al. 1997). Additionally, UBCs form synaptic junctions with Golgi cell boutons, indicating that UBCs may receive an inhibitory modulation (Mugnaini et al. 1994). Likewise, communication with GCs is negatively regulated by Golgi cells which innervate GC dendrites in the cerebellar glomeruli, thus providing feedforward and feedback inhibition to GCs. Indeed, GC-secreted glutamate in the glomerulus activates mGluR2, kainate, or AMPA receptors present on Golgi cells (Bureau et al. 2000; Watanabe and Nakanishi 2003). In turn, this causes the release of GABA from Golgi cells which then binds to GABA_A receptors on GCs to exert negative feedback. Golgi cell also receive inhibitory inputs from basket, stellate, and Lugano cells. Moreover, the apical dendrites of Golgi cells ascend into the ML to connect to PFs as well as communicate with each other through electrical synapses (Dugué et al. 2009). This electrical coupling via gap junctions allow them to exert a rhythmic inhibition on GCs (Vervaeke et al. 2010). Thus, Golgi cells are thought to play a crucial role in the regulation of GC activity, which is essential for the formation of motor memories in the cerebellum (Llinás and Sugimori 1980).

INTRODUCTION

After glomerular modulation, the resulting signal ultimately ascends the axon of GCs and travels through PFs in the ML where PFs synapse with inhibitory interneurons. The diversity of expression of synapsin isoforms at GC terminals is a key component in short term plasticity that influences the recruitment of inhibitory interneurons (Dorgans et al. 2019). PFs then go on to contact the distal dendritic compartment of PCs and since each PC is innervated by approximately 175,000 PFs, excitation of a single PF only slightly depolarizes PC dendrites (Napper and Harvey 1988). Thus about 50 GCs are needed to fire in a synchronous fashion in order to generate a single Na^+ action potential or “simple spike” in the PC soma (Barbour 1993). Moreover, PC firing rate is highly sensitive to the duration of PF stimulation, which constitutes in itself a temporal regulation of signals (Grangeray-Vilmint et al. 2018).

In response to excitatory signals transmitted by PFs, basket and stellate cells release GABA and while a single interneuron may connect to several PCs, each PC receives about 1,500 inhibitory synapses from at least 10 interneurons (Korbo et al. 1993; Jaeger et al. 1997). On PCs, the binding of GABA at GABA_A receptors inhibits signal transmission, while GABAergic synapses onto basket or stellate cells creates a mutual inhibition signaling between interneurons (Briatore et al. 2010). Basket cell axons are also known to form a specialized structure around the proximal segment of PC axons called the pinceau. Although molecules involved in chemical GABAergic inhibition prevail at basket cell synapses on PC somata, the pinceau is enriched with Shaker-type potassium (K^+) channels (Laube et al. 1996; Iwakura et al. 2012). This enables basket cells to exert fast electrical inhibition via ephaptic control over the speed and stability of PC firing (Kole et al. 2015).

The action of ML interneurons is also negatively regulated by Lugano cells (Schilling et al. 2008). Indeed, Lugano cells receive GABAergic inputs from recurrent axon collaterals of PCs and project glycinergic axons to basket and stellate cells, thus indirectly providing feedback inhibition to PCs (Lainé and Axelrad 2002). Candelabrum cells primarily inhibit ML interneurons, which in turn triggers PC disinhibition and ultimately controls cerebellar output (Osorno et al. 2022). Thus, candelabrum cells, akin to basket and stellate cells, appear to also mediate PC inhibition (Schilling et al. 2008). In addition, PCs also make inhibitory GABAergic synapses with other PCs and Lugano cells via PC axon collaterals and form a cerebellar cortical microcircuit, which is driven by serotonin and noradrenaline and participates in synaptic plasticity (Hirono et al. 2021). Bergmann glia also participates in plasticity within cerebellar microdomains by extending radial extensions that form a glial sheath around ML synaptic connections (Grosche et al. 2002). The clearing of glutamate spilling over from the synaptic cleft of both CF and PF terminals is done by the glia via glutamate transporters GLAST-1 and GLT-1 (Takayasu et al. 2009).

Ultimately, the glutamatergic excitatory signals of CFs and PFs converge onto PCs, which act as an integration center. Both glutamatergic connections induce an increase in cytosolic Ca^{2+} in postsynaptic PCs via the same mechanisms. First, a rapid activation of AMPA receptors allows Na^+ entry into the Purkinje cell and leads Ca^{2+} influx through the opening of voltage-gated Ca^{2+} channels. Then, glutamate binding on mGluR1 receptors triggers two G protein-dependent pathways that results in a release of Ca^{2+} contained within the endoplasmic reticulum and the opening of a cation channel (Hartmann and Konnerth 2005; Isope et al. 2012).

The multiple sources of innervation and complex processing occurring in PCs enable plasticity mechanisms to take place. Among them, long-term depression (LTD) and long-term potentiation (LTP) are important for motor learning (Figure 5). These processes are driven by PC Ca^{2+} concentration, but the intricacies are not completely understood (Vogt and Canepari 2010). However, it is generally admitted that LTP is the default response to PF stimulation above a well-defined frequency threshold. If the Ca^{2+} signal surpasses that limit, an extracellular positive feedback loop triggers LTD instead. When full depression is reached, feedback loops are automatically inactivated and the network returns to its basal state (Gallimore et al. 2018). Besides GC input, LTP at inhibitory interneuron - PC synapses called “rebound potentiation” also participates in motor learning (Nakamura and Hirano 2016). Additionally, the short- and long-term effects of neuromodulators from BFs must be considered when examining cerebellar circuitry. It is postulated that serotonin oversees cerebellar microzone attribution and learning processes, norepinephrine regulates cortex-wide learning, dopamine enhances goal-oriented learning, and acetylcholine controls learning speed in PCs (Figure 5) (Schweighofer et al. 2004).

iii. Efferences

The integrated signal then travels through the primary PC axon, which is the only efference of the cerebellar cortex, until the distal synapse with DCN neurons. Thus, cerebellar **efferents** stem directly from PCs or via the DCNs. The largest bundle of efferent fibers originates in the emboliform, globose, and dentate nuclei, and primarily exit the cerebellum via the superior cerebellar peduncle. They reach the upper portion of the pons where they lay flush to the dorsolateral wall of the fourth ventricle, and are then dispatched to several regions to take part in specific functional loops (Rubenstein 2020).

INTRODUCTION

b. Regional variations

It was long believed that the adult cerebellar cortex presented a somewhat uniform circuitry and that differences in function were due to distinct patterns of input and output connectivity. However, anatomical, molecular, and physiological data suggest otherwise. Regional differences include changes in cell phenotype and expression of various molecular markers which define parasagittal stipes when observing PC gene expression profile. The most well-known pattern is revealed by detecting the expression of zebrin II, an antigen located on the aldolase C protein, exclusively expressed in PCs within the cerebellum (Figure 6) (Brochu et al. 1990; Cerminara et al. 2015).

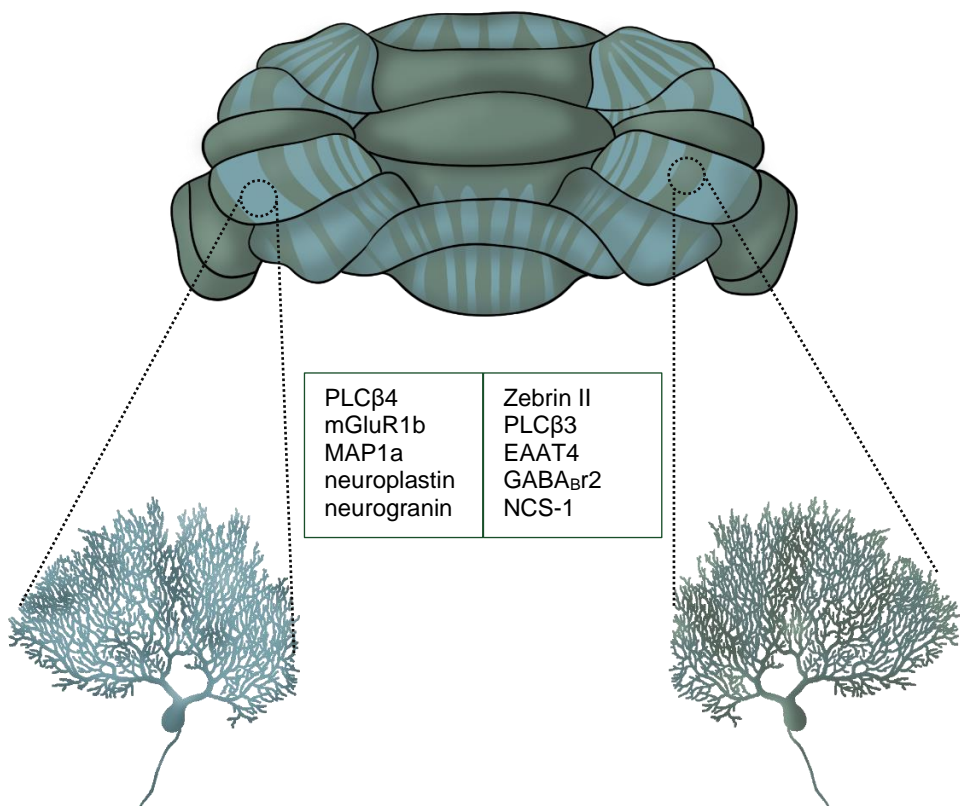


Figure 6: Patterned molecular marker expression in the mouse cerebellar cortex, dorsal view.

Colocalization of zebrin II+ Purkinje cells and zebrin II- Purkinje cells with other molecular makers. EAAT4: excitatory amino acid transporter 4; GABA_Br2: GABA-B receptor subtype 2; MAP1a: microtubule-associated protein 1a; mGluR1b: metabotropic glutamate receptor R1b; NCS-1: neuronal calcium sensor-1; PLC β 3: phospholipase C β 3; PLC β 4: phospholipase C β 4. Figure adapted from (Cerminara et al. 2015).

Cerebellar afferents are distributed along fields that are organized parasagittally which highlight how this molecular pattern is directly in service of its functions (Sillitoe and Joyner 2007). Indeed, PCs of the same longitudinal zone receive afferents from CFs of emerging from the same region of the inferior olive. Likewise, PCs from a single zone project efferents to a given set of DCN neurons. Moreover, each longitudinal area is itself divided into microzones revolving around PCs, which are composed of functional modules formed by the interactions between the different cortical cells (Ashida et al. 2018). Moreover, mouse mutant models also show that PC death follows those molecularly distinct boundaries and are related to specific functional impairments (Cerminara et al. 2015).

6. *Vascularization*

a. Arterial Supply

The cerebellum is vascularized by three arteries (Figure 7): the superior cerebellar artery (SCA), the anterior inferior cerebellar artery (AICA), and the posterior inferior cerebellar artery (PICA), all of which usually arise from the vertebrobasilar system (Delion et al. 2017). They all emit small branches that travel towards the fourth ventricle to contribute to the choroid plexus, although the PICA is the main contributor via its choroidal artery (Carpenter 1991; Delion et al. 2017).

Interindividual anatomical variations exist, but the most constant component is the **SCA** which can branch out from the first segment of the posterior cerebral artery or directly from the rostral part of the basilar artery (Carpenter 1991; Delion et al. 2017). The SCA is constituted of four segments, named for the structures it comes in contact with: anterior pontomesencephalic, lateral pontomesencephalic, cerebellomesencephalic, and cortical segments. Along the course of the first two segments, the SCA emits perforating branches to irrigate the mesencephalon and cerebellar peduncles. The cerebellomesencephalic segment emits branches that reach the cerebellar WM and DCN, while the cortical segment remains on the surface (Rodríguez-Hernández et al. 2011). After crossing the trigeminal nerve, the cerebellomesencephalic segment of the SCA divides into two branches, medial and lateral, which supply the superior areas of the vermis and cerebellar hemispheres, respectively (Naidich et al. 2009). In turn, the medial branch further subdivides *i*) medially to irrigate the mesencephalon, superior brain peduncles, colliculi and superior cerebellar cortex as well as participating to the irrigation of the DCN, and *ii*) laterally to supply the vermis and the superolateral cortex of the cerebellar hemispheres (Delion et al. 2017).

INTRODUCTION

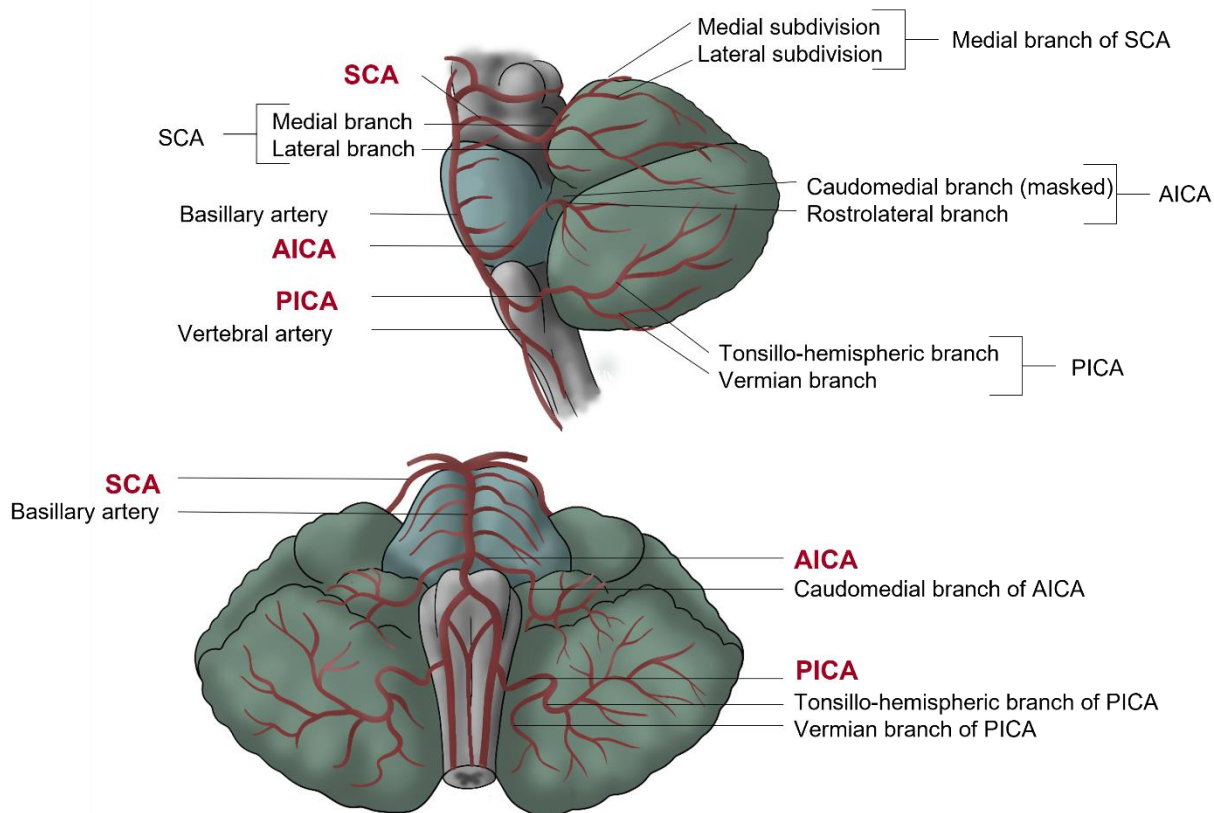


Figure 7: Arterial irrigation of the human cerebellum: main vessels and relations.

Sagittal (top) and ventral (bottom) views. AICA: anterior inferior cerebellar artery; PICA: posterior inferior cerebellar artery; SCA: superior cerebellar artery.

The **AICA** usually branches out from the proximal third of basilar artery. However, its origin, trajectory and territory are variable, and it can arise from the vertebrobasilar junction or even from a common trunk with the PICA (Delion et al. 2017). The AICA is divided into four segments: anterior pontine, lateral pontine, flocculopeduncular, and cortical segments. Along the course of the first two segments, the AICA emits branches to irrigate the pons and cranial nerves (abducens, facial and vestibulocochlear). The flocculopeduncular segment generally splits into a rostral-lateral and caudomedial branches and vascularizes the middle cerebellar peduncles, the flocculus, and the anterior hemispheric surfaces below the horizontal fissure. However, due to the AICA's variability, some of these areas may rely on blood supply from anastomoses with the SCA or even on the SCA alone (Atkinson 1949; Delion et al. 2017). Moreover, the AICA's penetrating branches irrigate part of

the dentate nucleus and the adjacent WM (Carpenter 1991). Finally, the AICA terminates superficially with the cortical portion which cover the anterior surface of the cerebellum (Rodríguez-Hernández et al. 2011).

Finally, the **PICA** arises most frequently from the vertebral artery and emits perforating branches near its origin to irrigate the lateral part of the medulla and the olivary nucleus (Delion et al. 2017). The PICA has five segments: anterior medullary, lateral medullary, tonsillomedullary, telovelotonsillar, and cortical segments. The tonsillomedullary portion gives rise to vermian and tonsillo-hemispheric branches. The vermian branch irrigates the pyramid (VIII), uvula (IX), nodule (X), and inferior part of the biventral lobule (VIII). The tonsillo-hemispheric branch supplies the superior part of the biventral lobule (VIII), the inferior part of the semilunar lobule (VIIb) and the tonsilla (IX). It also provides a secondary blood supply to the DCNs (Naidich et al. 2009; Delion et al. 2017). Finally, the telovelotonsilar segment gives rise to branches that supply the tela choroidea and choroid plexus of the fourth ventricle (Rodríguez-Hernández et al. 2011). All subsequent ramifications are cortical and terminate their transit on the cerebellar cortex where they anastomose with superficial branches of the SCA (Delion et al. 2017).

b. Venous Drainage

Cerebellar veins are described as superficial or deep veins, according to their territory (Figure 8). It is worth mentioning that veins are even more variable between individuals than arteries and are prone to forming numerous superficial anastomoses (Delion et al. 2017).

The **superficial veins** have a course somewhat similar to that of the arteries. Indeed, drainage of the cerebellum is handled by three venous systems (Naidich et al. 2009). They drain the cortical surfaces of the cerebellum and are named based on the region they correspond to. Therefore, the superior hemispheric and superior vermian veins drain the tentorial or superior surface; the inferior hemispheric and the inferior vermian veins drain the suboccipital or inferior surface; and the anterior hemispheric veins drain the petrosal or anterior surface (Matsushima et al. 1983; Rhiton 2000).

In turn, the **deep veins** are named according to their trajectory, namely the veins of the cerebellomesencephalic, cerebellomedullary, and cerebellopontine fissures as well as the veins of the superior, middle, and inferior cerebellar peduncles (Matsushima et al. 1983).

INTRODUCTION

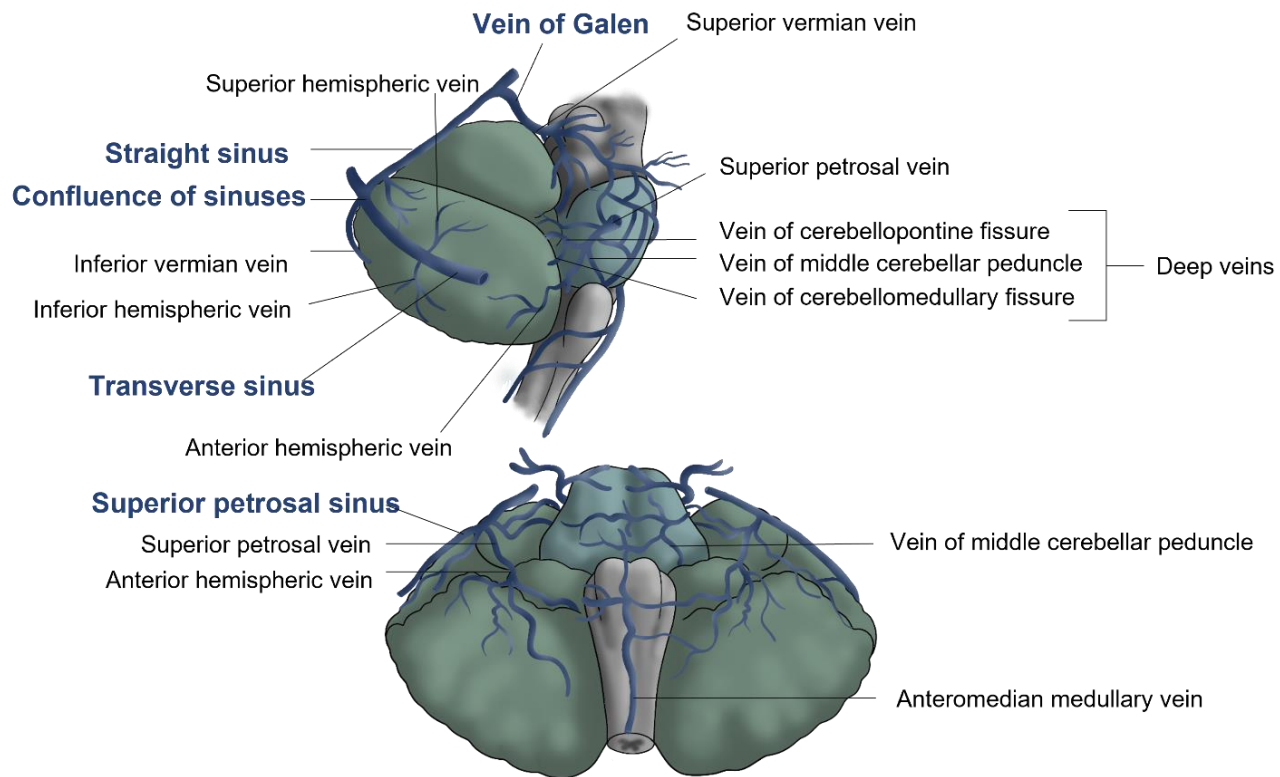


Figure 8: Venous drainage of the human cerebellum: main vessels and relations.

Sagittal (top) and ventral (bottom) views. Some deep veins are masked by the structures they drain.

All cerebellar veins terminate as **bridging veins** that cross the subarachnoid and subdural spaces to reach the venous sinuses in the dura. These are divided into three groups: galenic, petrosal and tentorial which drain respectively into the vein of Galen, petrosal sinuses, or tentorial sinuses (Matsushima et al. 1983; Rhiton 2000). Some superior hemispheric veins drain inferiorly into the transverse sinus. Others are joined by the vein of the superior cerebellar peduncle, on the superolateral side of the cerebellum and together they drain either *i)* directly into the vein of Galen or *ii)* indirectly in the vein of the cerebellomesencephalic fissure via the superior vermian veins (masked). The inferior hemispheric veins travel toward the tentorium cerebelli and usually drain into the tentorial sinus, above the cerebellum, either directly or via the inferior vermian veins. Finally, the anterior hemispheric veins drain blood to the vein of the cerebellopontine fissure which also receives the veins of the cerebellomedullary fissure and middle cerebellar peduncle, and finally converge to the superior petrosal sinus (Matsushima et al. 1983).

B. EMBRYOLOGY

1. Overview

Human CNS ontogenesis begins on day 16 of the embryonic development (E16) with gastrulation. By the end of this process, the embryo consists of three layers of cells: a dorsal ectoderm, a middle mesoderm, and a ventral endoderm. Gastrulation also defines the midline and medial/lateral axis of the body as well as the anterior/posterior and dorsal/ventral axes (Sadler 2019). The initiating event for the development of the nervous system is the formation of the notochord, a transient ridge of mesodermal cells, at the midline of the gastrulating embryo (Figure 9). The notochord invaginates and extends from a surface indentation called the primitive pit, which subsequently elongates antero-posteriorly to form the primitive streak (Purves 2018).

By the third week of development, the ectodermal germ layer has the shape of an elongated disc with a broader cephalic extremity. Neurulation begins when the notochord sends inductive signals to the overlying ectoderm which thickens into a columnar epithelium thus forming the neural plate. The plate becomes the neuroectoderm which will give rise to the entire nervous system (Sadler 2019). Between the 3rd and 4th gestational weeks (GW), the lateral margins of the neural plate fold inward, converting the neural plate into the neural tube, composed of the alar plates dorsally and basal plates ventrally (Figure 9) (Spemann and Mangold 2001; Sadler 2019).

Meanwhile, the cranial extremity of the neural tube forms three bulges that expand to become the three primary vesicles. In a cranio-caudal direction, these are called: the prosencephalon, the mesencephalon and the rhombencephalon (Figure 10). The indentation of the pontine flexure marks the formation of the five secondary vesicles by separating the rhombencephalon into metencephalon cranially and myelencephalon caudally, which will give rise to the medulla oblongata. The corresponding cavity will become the 4th ventricle during the 5th GW (Grow 2018). The mesencephalon remains unchanged at this stage. Meanwhile, the prosencephalon will divide into telencephalon cranially and diencephalon caudally (Purves 2018). Afterwards, the metencephalon will give rise to the cerebellum.

INTRODUCTION

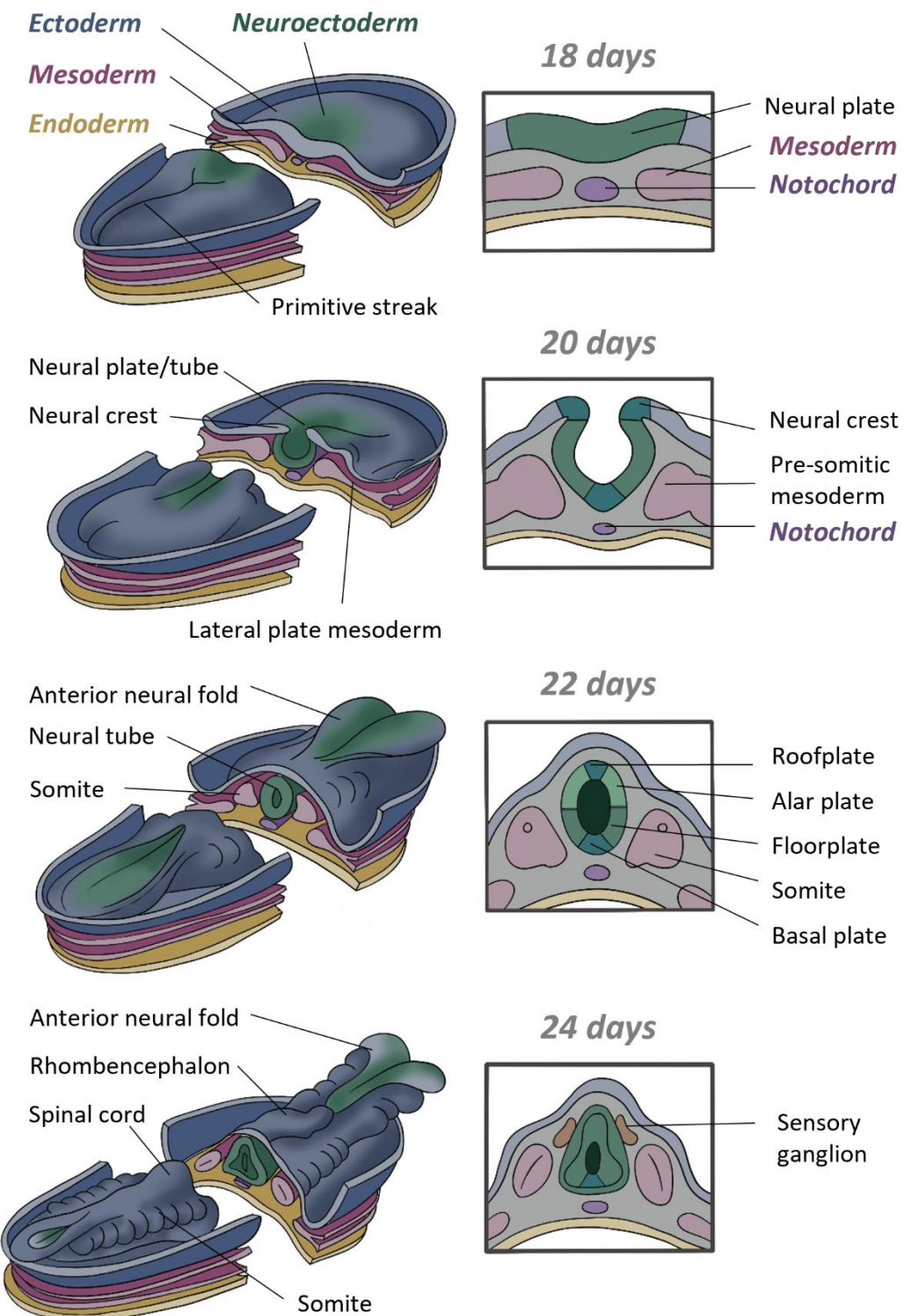


Figure 9: Schematic representation of the formation of the neural tube in humans.

Dorsolateral view of the developing embryo (left) and transversal cut (right) from day 18 to 24.

Adapted from (Purves 2018).

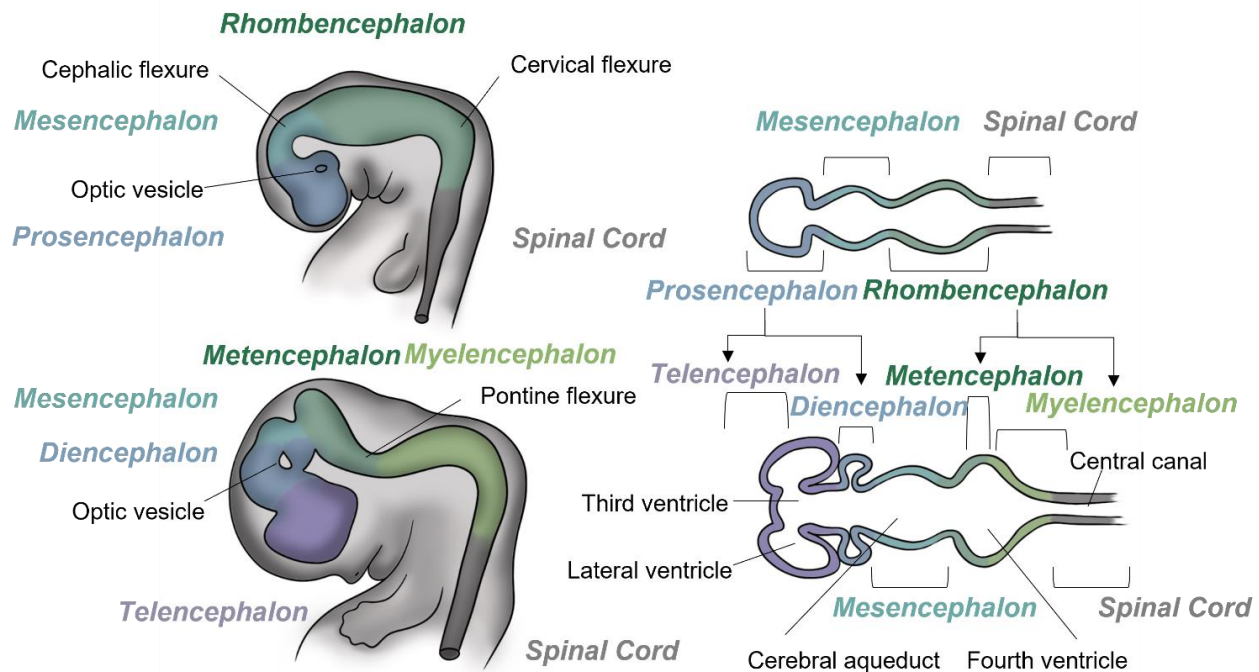


Figure 10: Schematic representation of the primary (top) and secondary (bottom) brain vesicles.
Three-dimensional view in the embryo (left) and longitudinal section of the neural tube (right).
Adapted from (Purves 2018).

2. Ontogenesis of the cerebellum

a. Regionalization

The complex formation of the brain relies on regional segmentation of the neural tube by establishing two axes. The rostro-caudal axis differentiation compartmentalizes the rhombencephalon into rhombomeres while dorso-ventral axis development separates the cerebellar primordium from the pons.

i. Rostro-caudal axis

The rostro-caudal regionalization of the neural tube during cerebellar ontogenesis follows a sequential set of events which are orchestrated by secreted factors from the isthmus, located at the boundary between the mesencephalon and the metencephalon (Nakamura et al. 2005; Hashimoto 2009).

INTRODUCTION

This isthmic organizer produces a gradient of signaling factors along the rostro-caudal axis (Figure 11). A major mediator of this process is Fgf8 (fibroblast growth factor 8), which has a polarizing activity and whose expression is promoted by En1/En2 (engrailed homeobox 1 and 2), especially after embryonic day 11 (E11) (Cheng et al. 2010). In mice, Fgf8 has 8 isoforms (Fgf8a-h) whose activity vary depending on their affinity with FGF receptors and it has been shown that specific inactivation mimicking the loss of Fgf8b results in deletion of the midbrain, isthmus, and cerebellum (Irving and Mason 2000; Guo et al. 2010). Indeed, Fgf8 restricts the expression of Otx2 (orthodenticle homeobox 2) rostrally to the isthmus while inducing the expression of Gbx2 (gastrulation brain homeobox 2) caudally. Gbx2 is crucial for the development of rhombomere 1 into the cerebellum while Otx2 prevents the expansion of cerebellar differentiation cranially and thus constitutes the rostral boundary of the cerebellar anlage. Fgf8 also induces the expression of the secreted factor Wnt1 (wingless-type MMTV integration site family member 1) expression in the isthmic organizer (Figure 11) which is essential in the regulation of isthmus inductive activity and midbrain-hindbrain regionalization (McMahon et al. 1992; Guo et al. 2007; Lowenstein et al. 2022).

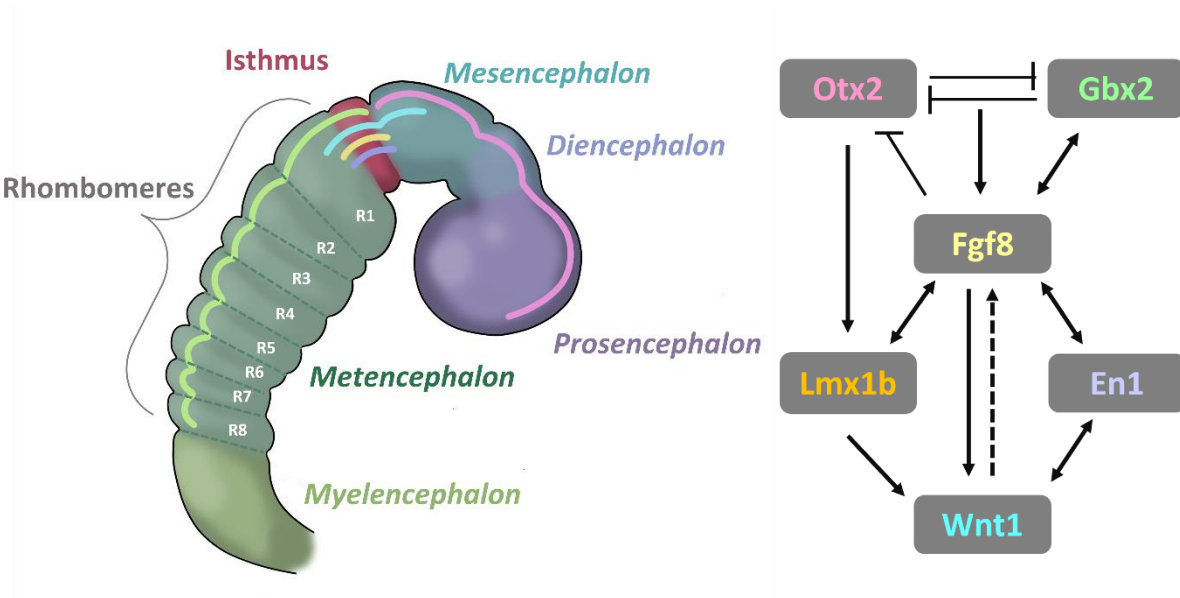


Figure 11: Neural tube regionalization and formation of the rhombomeres in a 28-day embryo (left) and genetic regulation in mice (right and color overlay in left).

En1: engrailed homeobox 1; Fgf8: fibroblast growth factor 8; Gbx2: gastrulation brain homeobox 2; Lmx1b: LIM homeobox transcription factor 1 beta; Otx2: orthodenticle homeobox 2; Rx: rhombomere x; Wnt1: Wingless-Type MMTV Integration Site Family Member 1.

Adapted from (Guo et al. 2007; Hashimoto 2009; Lowenstein et al. 2022).

The rostro-caudal differentiation is also controlled by Hox (homeobox) genes, such as Lmx1b (LIM homeobox transcription factor 1 beta), which are expressed differentially along the neural tube of the embryo (Okafuji et al. 1999; Guo et al. 2007). In turn, Lmx1b also seems to regulate the expression of Fgf8, Wnt1, Pax2 (paired box 2) and other isthmus-specific transcription factors. It is necessary to the induction activity of the isthmic organizer, and thus, to the development of the tectum and cerebellum from rhombomere 1 (Figure 11) (Guo et al. 2007). Downstream of these genetic factors, interrhombomeric boundaries are maintained by actomyosin cytoskeletal components that are enriched in these sites. These mechanical barriers are partly regulated by ephrin signaling (Calzolari et al. 2014). However, the molecular underpinnings of cerebellar development are still being established through the identification of new genes and the role of other factors has been explored.

ii. Dorsal-ventral axis

The subsequent expression and activation of several transcription factors begins to regionalize the metencephalon in the dorsal-ventral axis (Figure 12). Its alar and basal plates will differentiate to become the cerebellum and pons, respectively (Sadler 2019). In the first rhombomere, the roof plate of the fourth ventricle acts as a local organizer by secreting signaling molecules such as Wnt ligands and bone morphogenetic proteins (BMPs) which determine a dorsal destination to the adjacent portion of the neural tube (Chizhikov and Millen 2004). For example, loss of Wnt5a resulted in cerebellar hypoplasia with a particular depletion of both GABAergic and glutamatergic neurons due to decreased proliferation of radial glia and GC progenitors (Subashini et al. 2017).

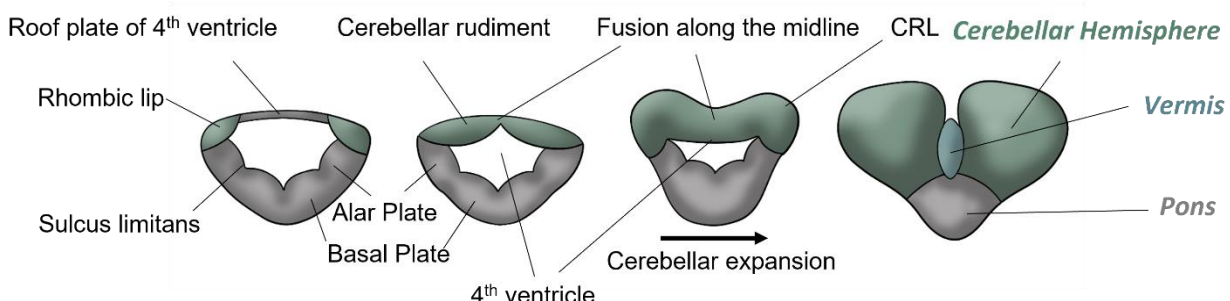


Figure 12: Progression of cerebellar formation, transverse cuts at the metencephalic level.
CRL: cerebellar rhombic lip. Adapted from (Sadler 2019).

Then, two germinal zones form: the ventricular zone (VZ) from the roof of the 4th ventricle, and the rhombic lips (RL) from the dorsolateral region (Figure 13). The VZ is a germinal zone that gives rise to cerebellar GABAergic neurons including Purkinje cells, inhibitory DCN interneurons, Golgi cells and ML interneurons. This differentiation process is under the influence of the Ptf1 α (pancreas associated transcription factor 1 alpha) produced by VZ neuronal precursors (Hoshino et al. 2005;

INTRODUCTION

Pascual et al. 2007). Additionally, the expression of Olig2/3 (oligodendrocyte transcription factor 2/3) specifies a differentiation towards PCs while Gsx1 (genomic screened homeobox 1) expression coincides with the induction of inhibitory interneurons (Figure 13) (Lowenstein et al. 2022). Moreover, Ascl1 (achaete-scute family BHLH transcription factor 1) restricts VZ progenitors from becoming RL progenitors and thus contributes to determining cell fate (Sudarov et al. 2011).

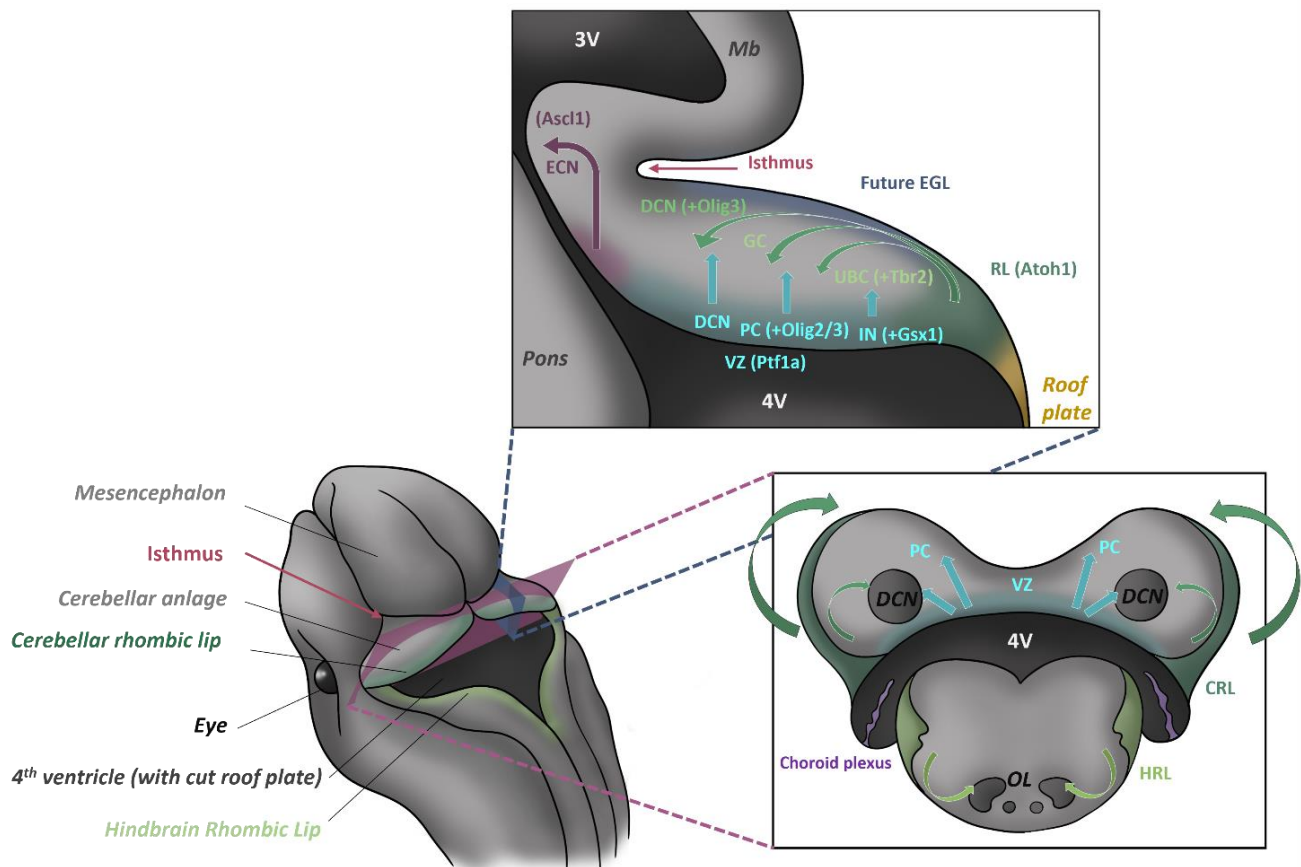


Figure 13: Dorsolateral view of a mouse embryo at E11.5, sagittal section along the blue plane, and coronal section along the pink plane.

Regionalization within the cerebellum and migration from the germinative zones. Ascl1: achaete-scute family BHLH transcription factor 1; Atoh1: atonal BHLH transcription factor 1; CRL: cerebellar rhombic lip; DCN: deep cerebellar nuclei; ECN: extracerebellar neurons; EGL: external granular layer; GC: granule cell; Gsx1: genomic screened homeo box 1; HRL: hindbrain rhombic lip; IN: interneuron; Mb: midbrain; OL: olfactory nuclei; Olig2/3: oligodendrocyte transcription factor 2/3; PC: Purkinje cell; Ptf1a: pancreas associated transcription factor 1 alpha; RL: rhombic lip; Tbr2: T-box brain protein 2; UBC: unipolar brush cell; VZ: ventricular zone; 3V: third ventricle; 4V: fourth ventricle. Figure compiling information from (Volpe 2009; Hashimoto and Hibi 2012; Millen et al. 2014; Yeung 2017; Lowenstein et al. 2022).

The RLs are the origin of glutamatergic neurons and are divided in the cerebellar RL (CRL) rostrally and the hindbrain RL caudally (HRL). The CRL produces GC precursors, UBCs, and excitatory DCN neurons, while the HRL generates the cells of the pontine and inferior olfactory nuclei (Hashimoto and

Hibi 2012). Neuronal differentiation from the CRL relies on the expression of the Atoh1 (atonal BHLH transcription factor 1). Indeed, Atoh1-deficient mice show lower cells density in the CRL as well as migration deficits of the concerned neurons (Ben-Arie et al. 1997). The co-expression of Olig3 with Atoh1 propels cells to differentiate into excitatory DCN neurons, while Tbr2 (T-box brain transcription factor 2) triggers UBC differentiation (Figure 13). The CRLs eventually form a secondary germinal zone on the surface of the cerebellar anlage called external granular layer (EGL) (Lowenstein et al. 2022).

iii. Medio-lateral axis

In parallel to the migration of neuronal precursors, the cerebellar primordium continues developing. To form the cerebellum, the dorsolateral parts of the alar plates bend medially, and the pontine flexure becomes more marked. Then, the rhombic lips compress cephalocaudally and fuse along the midline to form the cerebellar plate (Figure 14).

In a 12-week human embryo, the vermis is already visible as a small midline portion of the cerebellar plate, surrounded by the hemispheres (Sadler 2019). This mediolateral patterning of the cerebellum likely revolves around a midline organizer containing roof-plate derivatives. A scRNA-seq study identified a Fgf17⁺, Calb2⁺ (calbindin2) cell population which, in response Fgf8-mediated Wnt/β-catenin and FGF/ERK (mitogen-activated protein kinase 1) signaling, go on to form the cerebellar vermis (Wizeman et al. 2019). Additionally, knockout experiments targeting the Galnt17 (polypeptide N-acetylgalactosaminyltransferase 17) gene demonstrated that this gene is involved in the correct development of the cerebellar vermis (Chen et al. 2022).

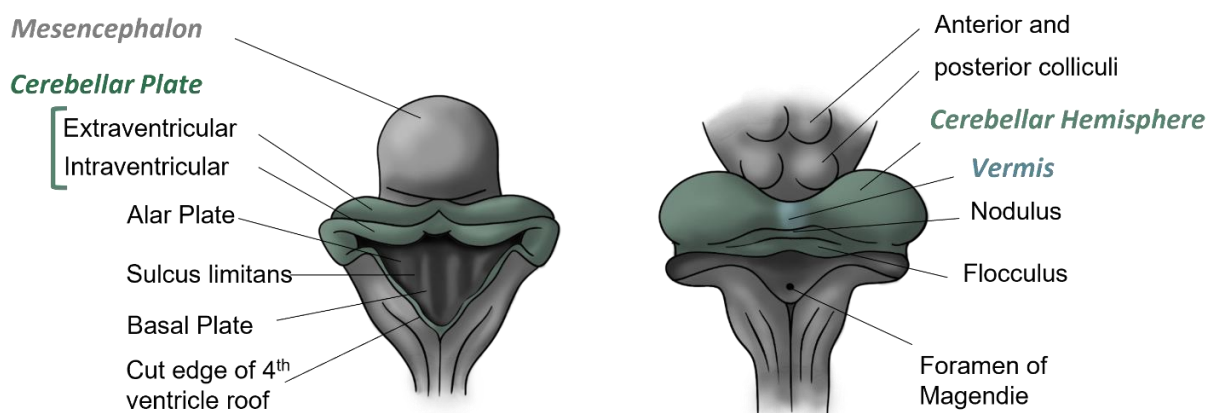


Figure 14: Dorsal view of the human developing mesencephalon and rhombencephalon.

In an 8-week embryo (left) and 4-month embryo (right); roof of the 4th ventricle removed for visibility.
Adapted from (Sadler 2019).

INTRODUCTION

Concerning hemispheric differentiation, much remains to be unveiled, but it is likely that different PC lineages condition the formation of the cerebellar hemispheres. Additionally, recent findings about the molecular regulation of the posterior transitory zone, a distinct progenitor zone anterior to the RL, highlighted new genes involved in cerebellar fate mapping, such as Notch and Hes1 (hes family BHLH transcription factor 1). These may participate in the vermis/hemisphere specification (Khouri-Farah et al. 2022). Finally, engrailed homeobox genes (En1/2) are also proposed as a class of genes involved in medio-lateral axis differentiation (Cheng et al. 2010).

b. Cerebellar foliation

The most noticeable gross morphological feature of the cerebellum is its folded appearance. This highly convoluted structure is the result of the segmentation into lobules that takes place in the 16th GW. The foliation process continues during development and is estimated to increase by a factor of 30 between the 24th GW and birth (Figure 15). As a result, the cerebellar surface area increases from 40 mm² to over 15,000 mm², while cerebellar volume increases by a factor of 4 (Rakic and Sidman 1970; Volpe 2009).

A transverse fissure appears by GW 12 and separates the nodule and flocculi from the vermis and hemispheres, respectively (Sadler 2019), while the primary fissure only appears in the 14th GW to separate the anterior and posterior lobes of the cerebellum (Liu et al. 2011). The regional differences in cerebellar fissure and folia formation are the result of precise genetic regulation, much of which remains to be elucidated. However, En1/2 have been proven essential to the timing of primary and secondary fissure formation (Orvis et al. 2012). Additionally, they have been identified as being crucial to the differentiation of the vermis and hemisphere foliation patterns. Furthermore, in mice, En differentiating activity continues beyond that of the Fgf8 isthmic organizer after embryonic day 14 making En an important class of genes that can be affected until late in cerebellar development (Cheng et al. 2010). In fact, En1/En2 gene mutants present alterations in both fissure formation and EGL layer thickness (Legué et al. 2016). Additionally, En mutant analysis shows that GCs are involved in forming the characteristic cerebellar foliation, and that GCs are differentially regulated in different lobes, notably by Tlx3 (T cell leukemia homeobox 3), Gli1 (GLI family zinc finger 1), Otx2 (Legué et al. 2016).

Indeed, the foliation process is part of the developmental interplay between cells under the surface. Thus, initiation of fissure formation is thought to be the result of a combination of cellular changes involving GCs, but also PCs and Bergmann glia. Experiments relying on genetic inducible fate mapping in mice revealed a major initiating event of foliation: the appearance of an “anchoring

center”, a cytologically distinct area that will become the root of each cerebellar fissure (Figure 16). These regions are characterized by an increase in proliferation in the EGL along with a slight invagination of the PCL. Afterwards, GC precursors elongate along the plane of the growing fissure and Bergmann glial fibers radiate towards its base. GC migration along Bergmann glial fibers then propels the outgrowth of folia (Sudarov and Joyner 2007). Recent evidence also implicates the Hippo-Yap/Taz (transcriptional coactivator YAP1 / tafazzin) pathway as part of the molecular basis of the establishment of the radial glia scaffold (Hughes et al. 2020).

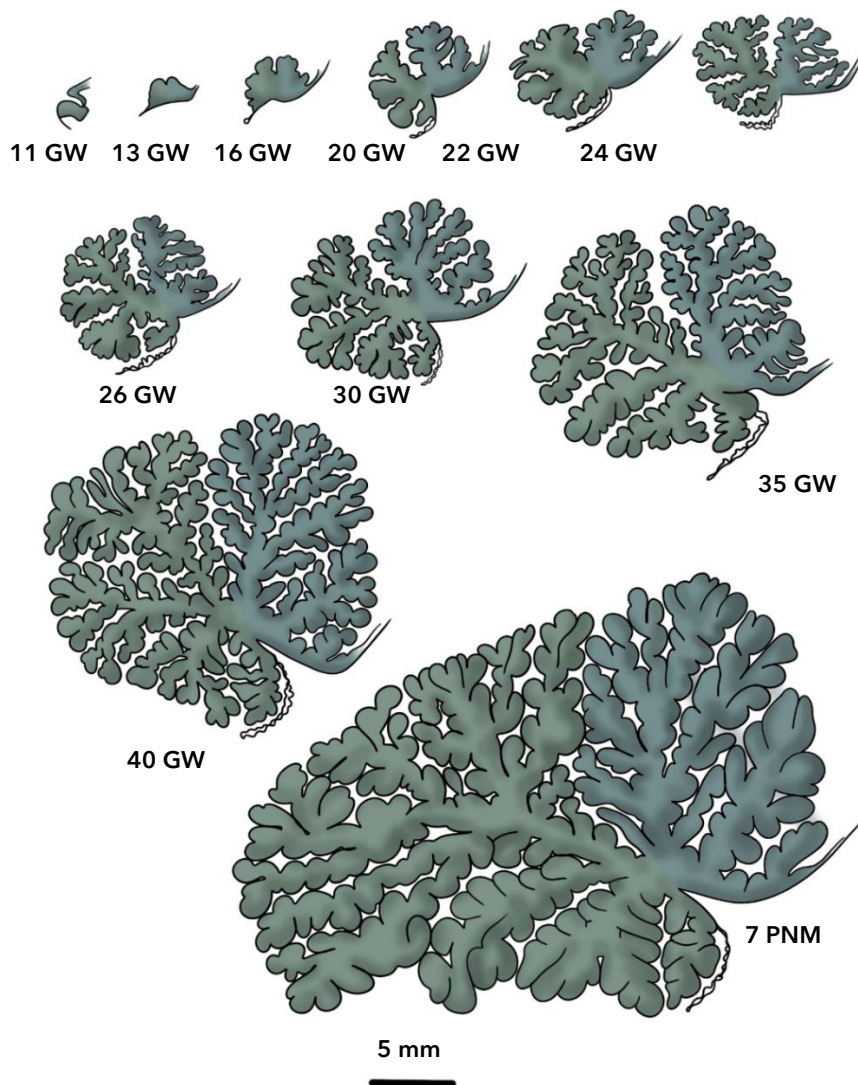


Figure 15: Schematic representation of cerebellar development along the midsagittal plane in humans from 11th gestational weeks (GW) to 7th postnatal months (PNM).

The primary fissure separates the anterior lobe (blue) from the posterior lobe (green). Adapted from (Rakic and Sidman 1970).

INTRODUCTION

The Wnt signaling pathway, which already intervenes in regionalization, also plays a critical role in tissue organization via its downstream molecule β -catenin. Deletion of β -catenin in cerebellar neuronal cells after E12.5 in mice alters the positions of where fissure formation occurs and led to improper inclusion of the meninges into the folds (Wen et al. 2013). Likewise, genetic loss of the serine-threonine Lkb1 (kinase Liver Kinase B1) in GC precursors increases cerebellar cortical size and foliation. This is likely correlated with a delayed radial migration of GCs, regardless of changes in proliferation or Hedgehog signaling (Ryan et al. 2017).

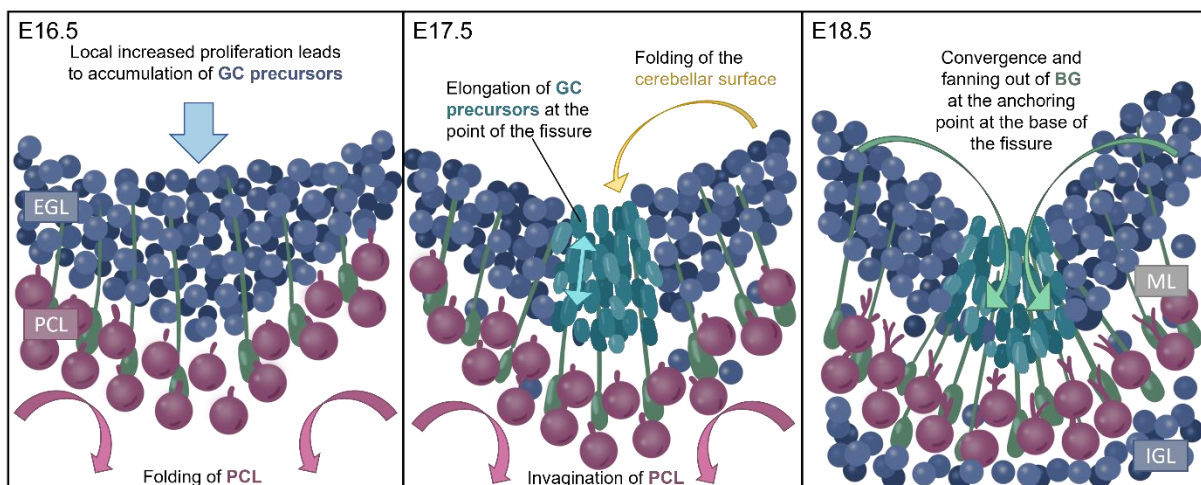


Figure 16: Representation of the changes occurring at the anchoring center of a folium in mice.

Left: E16.5. inward accumulation of GC precursors (blue) resulting from increased proliferation. Meanwhile the PCL (pink) folds inward. Middle: E17.5. GC precursors elongate and align along the fissure, as the outer cerebellar surface begins to fold inwards. Right: E18.5. Bergmann glia fibers near the anchoring centers converge on the base of the fissure. Bergmann glia fibers in the anchoring centers fan out from a narrow anchoring point. Meanwhile, Purkinje cells develop their budding dendritic tree and GCs begin migrating from EGL to IGL through the expanding ML. BG: Bergmann glia. EGL: external granular layer; GC: granule cell; IGL: internal granular layer; ML: molecular layer; PCL: Purkinje cell layer. Adapted from (Sudarov and Joyner 2007).

3. Cerebellar vascular development

Initially, the neural plate and the open neural tube are simply fed by diffusion from the amniotic fluid, but, by the middle of the 3rd GW, nutrient diffusion is no longer sufficient to fulfill the metabolic requirements of the developing embryo. Thus, two distinct mechanisms, vasculogenesis and angiogenesis, begin to take over and oversee the formation of the vascular network.

a. Vasculogenesis

Vasculogenesis begins when the notochord triggers the formation of the first blood islands in the mesoderm surrounding the wall of the yolk sac and later in the lateral plate mesoderm. To this end, notochord secretes SHH (sonic hedgehog) which induces the surrounding mesenchyme to express VEGF (vascular endothelial growth factor) (Sadler 2019). Subsequently, blood island cells activated by FGF2 (fibroblast growth factor 2) form hemangioblasts. Under the influence of mesoderm-secreted VEGF, hemangioblasts in the center of blood islands become hematopoietic stem cells, while those at the periphery differentiate into angioblasts. These angioblasts proliferate and VEGF prompts them to differentiate into endothelial cells that merge to form primitive blood vessels. This process of vasculogenesis culminates with the establishment of a primary vascular plexus including the heart, the dorsal aorta and the cardinal veins (Patan 2004; Sadler 2019). From these initial vessels, another step of vasculogenesis forms the meninx primitive which surrounds the neural tube (Raybaud 2010).

As the rostral portion of the neural tube expands into the three primary brain vesicles, the meninx primitiva further evolves into the primordial choroid plexuses to better supply the neural tissue (Raybaud 2010). This process begins with the budding of the perineural vascular plexus (PNVP) from angioblasts recruited from the pre-somitic mesoderm (Figure 17, left), which later becomes the meningeal vasculature. Then, between GW 5 and 7, the first blood vessels penetrate radially into the neural tube, as the intraneuronal vascular plexus (INVP). Once it reaches the ventricular surface, it forms the periventricular plexus (PVP). From this 2nd plexus, numerous collaterals will eventually develop to colonize the entire brain (Vogenstahl et al. 2022; Klostranec and Krings 2022).

b. Angiogenesis

The rest of the vasculature is added by angiogenesis which expands and remodels the primary network starting in the 4th GW. This process is also mediated by VEGF and is comprised of two mechanisms: endothelial sprouting and intussusceptive microvascular growth. In endothelial sprouting, VEGF stimulates endothelial cell proliferation along the existing vessels on foci that will be the root of new vessels. From these points, budding vessels sprout and grow. Alternatively, intussusception starts with a buildup of intervascular tissue in the lumen of an existing vessel which will thus be divided (Patan 2004). In the human cerebellum, the superior cerebellar artery begins to appear above the rhombencephalon around day 32 in the human embryo (Figure 17, right). From day

INTRODUCTION

35 to day 52, the basilar and vertebral arteries develop more intensely to give rise to the anteroinferior and posteroinferior cerebellar arteries (Klostranec and Krings 2022).

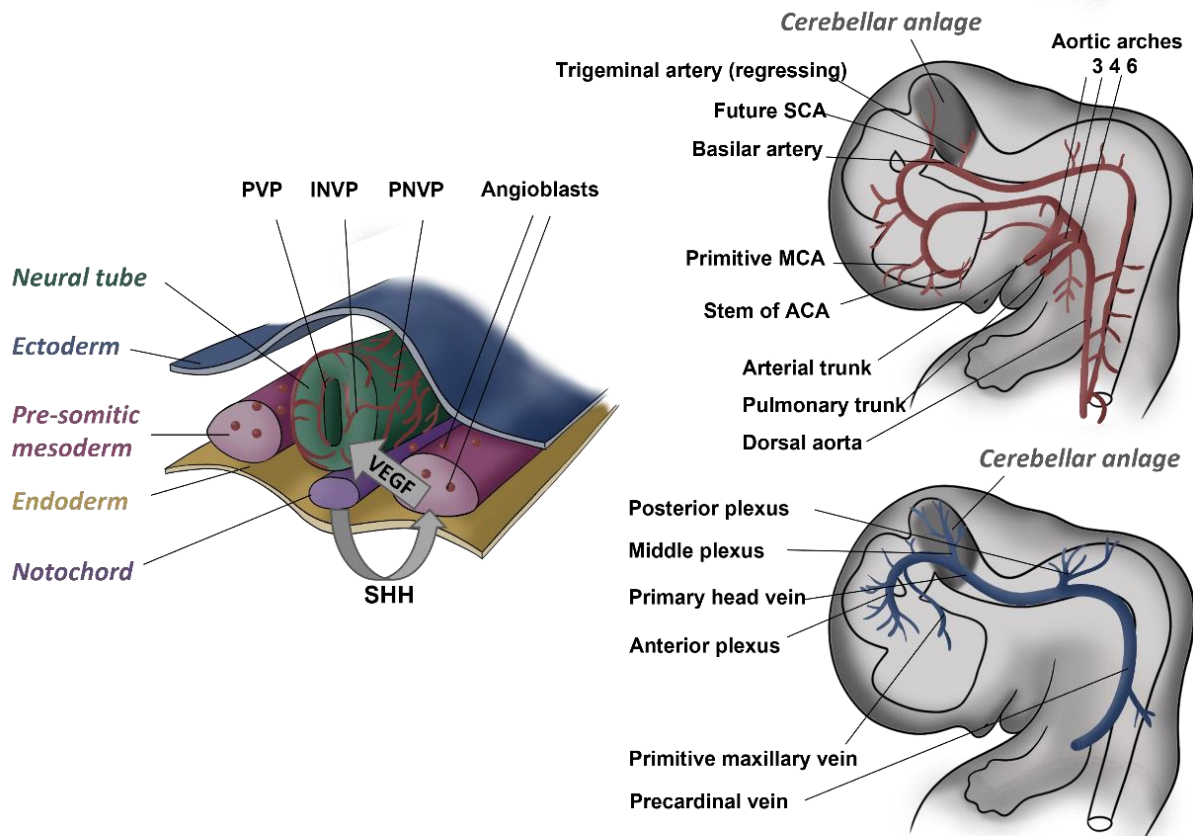


Figure 17: Vascular development in the human CNS.

Mechanisms of vascularization around the neural tube (left). Representation of the vascular system in a 32-day-old embryo (right) with the main arteries (top) and veins (bottom). ACA: anterior cerebral artery; INVP: intraneuronal vascular plexus; MCA: middle cerebral artery; PNVP: perineural vascular plexus; PVP: periventricular plexus; SCA: superior cerebellar artery; SHH: sonic hedgehog; VEGF: vascular endothelial growth factor.
Inspired by (Mullan et al. 1996; Bertulli and Robert 2021; Vogenstahl et al. 2022).

Angiogenesis is a highly regulated and coordinated process whose molecular basis is still being uncovered. Maturation and remodeling of vasculature into the definitive adult pattern are regulated by several growth factors including PDGF (platelet-derived growth factor) and TGF- β (transforming growth factor beta) (Sadler 2019). Some of the most well-known promoters of angiogenesis are VEGF and its receptors Flk1 and Flt1 (VEGF receptor 2 and 1), the EPH receptor A /EPH-B (ephrin) system, and the Angiopoietin/Tie system (Patan 2004). In the CNS, VEGF acts through the receptor VEGFR2 particularly expressed in the endothelial cells of the PNVP (Raybaud 2010), and the coreceptor

Neuropilin1. Downstream, VEGF expression induces the Notch pathway which will locally trigger: *i*) expression of EphrinB2 to stimulate arterial development while suppressing venous cell fate; *ii*) upregulation of the vein-specific EphB4; or *iii*) expression of PROX1 (prospero-related homeobox 1), a transcription factor that appears to be oversee lymphatic vessel differentiation (Sadler 2019).

Additionally, the Dll4/Notch (delta like canonical notch ligand 4/ notch receptor) and Slit2/Robo4 (slit guidance ligand 2/ roundabout guidance receptor 4) signaling pathways further regulate the density of vessels within the neural parenchyma. Meanwhile, integrins help regulate angiogenesis by maintaining endothelial cell-neuroepithelium communication. Wnt7a/b also appear to be critical in the regulation of neuroepithelial angiogenesis (Mancuso et al. 2008). There is also increasing evidence that the Hippo-YAP/TAZ pathway is involved in regulating endothelial cell proliferation, migration, and survival. Moreover, signaling cascades that regulates angiogenesis also activate YAP/TAZ to control vascular sprouting, barrier formation, and remodeling (Boopathy and Hong 2019). Blood vessels then undergo maturation, remodeling, and pruning, concomitantly with the recruitment of vascular smooth muscle cells thanks to the Pdgf β /Pdgfr β and TGF- β pathways (Mancuso et al. 2008).

Finally, the Angiopoietin/Tie2 pathway is critical for CNS angiogenesis. Indeed, deficient mice present immature vessels lacking branching (Raybaud 2010). Interestingly, this parallels the dendrite branching deficits seen in Tie2-deficient mice (Luck et al. 2021). Moreover, it has been shown that the tips of developing blood vessels respond to guidance molecules such as Slit/Robo and Semaphorin3E-PlexinD1, also involved in neuronal differentiation (Eichmann et al. 2005). Together, this highlights the parallel between neurogenic and angiogenic pathways and how these might be interconnected.

4. Cell differentiation

In the 6th GW, neuronal differentiation begins with the emergence of the GABAergic and glutamatergic neuronal precursors (Sadler 2019). Shortly after, the different progenitor lineages begin their migration from the VZ and RL, respectively (Figure 13). Their migration is facilitated by extracellular matrix molecules such as integrins which are sensed by the primary cilia and integrin receptors on the transiting cells (Pittman and Solecki 2023). Migrating cells eventually form the four layers of the immature cerebellar cortex: the external granular layer (EGL), the Purkinje cell layer (PCL), the molecular layer (ML), and the internal granular layer (IGL). As the cerebellum matures, the EGL thins and progressively disappears (Lowenstein et al. 2022).

INTRODUCTION

a. Purkinje cells

Purkinje cell precursors arise from the superior VZ during the 9th GW and migrate through the white matter along the radial glia to their final location in the PCL. Notably, three stages of PC maturation have been identified consistently across species. In humans, the first stage spans from the 12th to 16th GW; the second stage occurs during GWs 16 to 28; and the third stage continues well into the first postnatal year. In the first stage, PCs are smooth, bipolar, and distributed in a stratified layer. They then gradually organize in the second stage as a monolayer in the PCL by the end of the 28th GW. Meanwhile, PCs acquire dendritic processes and numerous somatic spines which are where the first synapses appear between GW 18 and 24 (Zecevic and Rakic 1976). The third stage is mostly dedicated to the differentiation process characterized by the formation and ramification of a large dendritic tree, which is covered with dendritic spines and whose development in the ML continues into the postnatal period. PC dendritogenesis is promoted by GC-secreted trophic factors such as brain-derived neurotrophic factor (BDNF), which binds to its receptor, tropomyosin receptor kinase B (TrkB), on PCs and stimulates branching (Sadakata et al. 2007).

The radial migration of PCs is mediated by reelin, an extracellular matrix protein produced by EGL granule cell precursors, and mice lacking this protein present a disorganized PCL (Yuasa et al. 1993). The retinoid-related orphan receptor alpha (ROR α), highly expressed by PCs, also appears essential in murine models as its mutation leads to PC degeneration and cerebellar atrophy (Hamilton et al. 1996; Sotelo and Dusart 2009). Moreover, the total loss of ROR α expression leads to cerebellar defects including a marked decrease in PC survival (Boukhtouche et al. 2006). Concurrently to PCs, glial cells develop, and since they are essential to PC migration, loss of FGF9 or reelin in mice was shown to affect both Bergmann glia's scaffold formation, as well as the survival and development of PCs and GCs (Yuasa et al. 1993; Guo et al. 2020).

Mature GCs are also potent inducers of PC differentiation and PC dendritogenesis was found to be related to GC survival and density. Indeed, MFs activate NMDA receptors expressed by GCs resulting in the activation of the BDNF-TrkB signaling pathway and promotes GC survival. In turn, this increases GC-PC synapses triggering Ca²⁺ accumulation in PCs, which has been demonstrated to promote dendritic branching (Hirai and Launey 2000). Each dendritic arbor flattens in the plane transverse to its cerebellar folium and forms an orthogonal network in relation to GC axons. This consistent phenotype has been reproduced in vitro which allowed to characterize the cytoskeletal components involved. Thus, it has been demonstrated that β III-spectrin, a protein involved in type 5 spinocerebellar ataxia, is required for the growth of dendrites, and its deficiency causes cytoskeletal disorganization, resulting in abnormal branching (Fujishima et al. 2020). In the same way, triple

knockdown of Ca^{2+} /calmodulin-dependent protein kinases (CaMKII α , II β and IV) inhibited PC branching (Horie et al. 2021) and, Wnt5a mutants also displayed phenotypically altered PCs with a shortened and less ramified dendritic arbor (Subashini et al. 2017). However, it is admittedly only part of a complex regulatory network, of which other components have yet to be identified.

Concomitantly, PC precursors establish somatic connections with climbing fibers. The refinement of CF-PC innervation has been well characterized in mice. It begins at P0 with the “creeper” stage, where CFs form transient synapses on immature PC dendrites (Chedotal and Sotelo 1993). Then, at P5, CFs densely surround and innervate PC somata during the “perisomatic nest” phase. Afterwards, at P9, CF innervation progressively moves to the apical portion of PC somata during the “capuchon” stage, and finally translocates to PC dendrites at P12 in the “dendritic” stage (Watanabe and Kano 2011). At birth, CFs from several inferior olivary neurons innervate each PC, while, in the mature cerebellum, each PC is innervated by a single CF (Crepel et al. 1976). This one-to-one relationship is achieved by the elimination of supernumerary CFs, which occurs in two phases. The early phase (from P7 to P11 in mice) relies on the strengthening of single CF inputs via voltage-dependent Ca^{2+} channels (Hashimoto and Kano 2003). The late phase (from P12 to P17) is mediated by a signaling cascade in PCs initiated at PF-PC synapses, which relies on the GluR δ 2-cerebellin1-neurexin system (Miyazaki et al. 2010; Watanabe and Kano 2011). Moreover, the elimination of excess CFs is activity-dependent and it has been shown that altered neuronal activity in either the inferior olive or PCs will result in abnormal multi-innervation of PCs by CFs (Andjus et al. 2003; Lorenzetto et al. 2009). As cerebellar lobules form postnatally, PC clusters disperse longitudinally into adult stripes and are followed by their CF terminals until they reach their final position in the PCL (Rubenstein 2020).

b. Granule cells

GC precursors appear in the superior RL from the 9th GW onwards and migrate tangentially to the surface of the cerebellum to form the EGL, guided by attractive chemokines such as stromal cell-derived factor 1 alpha (SDF-1 α) produced by pial cells (Rahimi-Balaei et al. 2015). Once in the EGL, GC precursors proliferate, induced notably by PC-secreted SHH which can initiate the cell cycle in mice and in humans (Wallace 1999; Sadler 2019; Jiao et al. 2021). Indeed, this proliferation relies on complex regulations downstream of SHH and N-myc that prevent cells from differentiating and promote the activation of cyclins to maintain the cell cycle (Knoepfle et al. 2002; Jiao et al. 2021). Additionally, SHH activity is enhanced by β 1-integrin expression from GC precursors which maintain contact with the meningeal basement membrane and recruits the laminin–SHH complex (Blaess 2004). However, due to the importance of this process, it is likely that there is a functional redundancy

INTRODUCTION

of several pathways to maintain GC precursors in a proliferative state. Indeed, $\beta 1$ -integrin expression in GCs does not seem to be essential for proliferation and is compensated (Frick et al. 2012). Interestingly, this redundancy is not present further downstream as cyclin A1 expression cannot compensate for the loss of cyclin A2 which results in severe cerebellar hypoplasia, decreased proliferation of GC progenitors and PC abnormalities (Otero et al. 2014).

After their last mitotic division, GCs undergo a transient latency in the EGL during 20 to 48 hours (Marzban et al. 2015). GCs then initiate their differentiation process by becoming bipolar and emitting two axonal expansions parallel to the cortical surface (Komuro et al. 2001). The ensuing tangential migration of post-mitotic GCs is regulated by several molecules whose functions are not yet completely understood. Among those identified, extracellular somatostatin facilitates granule cell movement near their EGL original position (Yacubova and Komuro 2002). Additionally, GCs secrete FGF9 to control the formation of the Bergmann fiber scaffold, which in turn, guides their own inward migration (Lin et al. 2009). This migration towards the ML is, at least in part, enabled by the astrotactin family of molecules (Wilson et al. 2010).

During GC migration, the EGL can temporarily be segmented into two regions, an outer zone of proliferation (oEGL), and an inner layer that the cells join before beginning their radial migration (iEGL). These two layers are populated by GCs at distinct maturation stages and expressing different markers. In fact, CRMP2 (collapsin response mediator protein 2) is highly expressed in the oEGL where GCs undergo proliferation (Ricard et al. 2001). In contrast, RAX (retina and anterior neural fold homeobox protein) is increased in the cerebellum from P4 to P9, when the GCs mainly migrate from the EGL to the IGL (Yong et al. 2015). Additionally, the Liver Kinase B1 (Lkb1) is a Hedgehog-independent migration expressed throughout the EGL, whose mutation delays radial migration of GCs (Ryan et al. 2017). Meanwhile, GC lateral extensions continue to expand, and radial migration velocity decreases.

As GCs come out of the EGL, a third orthogonal extension with a growth cone emerges and penetrates into the ML (Komuro et al. 2001). Within the ML, this neuronal extension wraps around Bergmann glial fibers and the GCs shift from tangential to radial migration. The GC soma can then move by translocation along this new axis aided by a BDNF gradient towards the IGL and D-serine released by Bergmann glia (Schell et al. 1997; Borghesani et al. 2002). Upon approaching PCs, GCs pause their migration as they get separated from the glia, regain their characteristic round shape, and complete their movement by crossing the PCL. Thus they form the IGL following contact with the underlying WM (Komuro et al. 2001) and continue their differentiation with the emission of dendrites that connect to mossy fibers already present in the cerebellum since the 16th GW, and the elongation

of the horizontal extensions within the ML forms the parallel fibers (Altman 1972; Kilpatrick et al. 2012; Rubenstein 2020). GC differentiation is facilitated by different molecules including NeuroD1 and Notch signaling (Pan et al. 2009; Adachi et al. 2021).

Postnatal cerebellar maturation is also characterized by a reduced growth rate due, in part, to selective GC apoptosis eliminating non-functional mature cells from the IGL and supernumerary pre-migratory EGL cells. There is evidence for an intervention of caspase-3 in the regulation of physiological neuronal death of post-mitotic GCs which did not establish proper synaptic connections. However, it seems that cell death at the precursor/pre-migratory stage of GC differentiation is caspase-3-independent (Lossi et al. 2018). The main contribution to this selection is most likely related to the high expression Bcl-X, a member of the Bcl-2 family of proteins, activating the intrinsic apoptotic pathway (Sohma et al. 1996). The presence of the cell death receptor Fas on GC also suggests a potential involvement of the extrinsic pathway of apoptosis upon binding of the PC-secreted Fas ligand (Nat et al. 2001; Allais et al. 2010). Thereafter, the EGL gradually thins over several months in humans, to eventually disappear, while the IGL progressively thickens into the definitive GL.

c. Interneurons

The mechanisms related to the emergence and development of interneurons are not as well studied as other cerebellar neurons. The inhibitory interneurons of the cerebellum arise from Pax-2 precursors of the VZ and migrate long distances through stereotyped migration patterns toward specific laminar positions. DCN interneurons initiate this process, followed by the interneurons of the GL (namely, Golgi and Lugano cells) and finally those of the ML (basket and stellate cells). Interestingly, genetic inducible fate mapping with an Ascl1 allele marks all VZ derivatives, but each cell type has a unique temporal profile. Thus, a timeline of origin can be inferred for each cell type. In fact, the later an interneuron expresses Ascl1, the further it will migrate towards the cortical surface. Therefore, it was concluded that candelabrum cells seem to arise from the VZ between basket and stellate cells.

Additionally, in mice, Ptf1 α expression in the VZ functions with Ascl1 in generating interneurons (Sudarov et al. 2011). Thus, Golgi and Lugano are generated from the Ptf1 α domain of the VZ after PCs, which are produced at E11.5. They migrate through the WM where they undergo “transit amplification” (i.e., continue to divide), their last mitosis occurring between E13.5 and P4. They then reach the IGL where they begin differentiation (Leto et al. 2016). Basket interneurons arise during their journey in the white matter by transit amplification between P3 and P9, while stellate cells are generated between P5 and P12 (Sudarov et al. 2011). Basket and stellate cell progenitor

INTRODUCTION

migration were found to follow four phases in an organotypic slice model: *i*) rostro-caudal tangential migration along the ML surface, *ii*) orientation change from horizontal to vertical, *iii*) radial migration toward the PCL layer, and, finally, *iv*) a second tangential migration in the ML (Cameron et al. 2009). However, it has been shown that stellate, but not basket, cells require an extra step of tangential migration along the iEGL which is facilitated by GCs (Cadilhac et al. 2021).

Meanwhile, UBCs, like GCs, originate from Atoh1-positive precursors in the CRL between E14.5 and the first postnatal days (Sekerková et al. 2004). UBCs express the transcription factor Tbr2 and complete their migration from the EGL to the GL between P0 to P10 (Englund 2006).

Concerning differentiation, it appears that GCs contribute to interneuron dendritogenesis via BDNF production (Mertz et al. 2000). Moreover, PCs also play a primary role in interneuron proliferation via SHH release (De Luca et al. 2015). PCs also secrete neurofascin and semaphorin that guide the axonal extensions of interneurons and facilitate the formation of synaptic contacts (Ciani et al. 2002; Ango et al. 2004).

d. DCN neurons

DCN neurons develop in parallel to neurons of the cerebellar cortex and are formed on days E10 to E14 (Martí-Clua 2022). These cells and their origin are also traceable via the same molecules as those of the cortex and may be inhibitory or excitatory.

Excitatory DCN neurons are produced in the CRL from Atoh1-positive precursors, also expressing Pbx3 (Pre-B-Cell Leukemia Homeobox 3), Sox4 (SRY-box transcription factor 4) and Neurod6 (neuronal differentiation) (Carter et al. 2018). They migrate rostrally in the subpial layer (future EGL) to the “nuclear transitory zone” (future DCNs) in the cerebellar WM and express transcription factors Pax6, Tbr2, and Tbr1 sequentially as they approach their destination (Fink 2006).

Inhibitory GABAergic neurons of the DCNs include nucleo-olivary projecting neurons as well as local inhibitory interneurons. The latter derive from a common pool of inhibitory interneuron progenitors of the VZ along with those of the ML and GL (Leto et al. 2006). They have been shown to emerge at E11 (Sudarov et al. 2011). The expression of the transcription factor Gsx1 in VZ progenitors seems to be responsible for shifting cell fate away from PC differentiation and towards inhibitory interneurons (Lowenstein et al. 2022). While less is known about projecting neurons, VZ progenitors begin expressing Iroquois Homeobox 3 (Irx3) and Myeloid Ecotropic Viral Integration Site 1 Homolog 2 (Meis2) at E10, which coincides with a proliferation phase. Then, the expression of LIM Homeobox

2/9 (Lhx2/9) starts at E10.25 when the first wave of postmitotic progenitors separates from the underlying VZ. These Irx3/Meis2/Lhx2/9+ cells then migrate and aggregate to form the future DCNs, where they are later joined by their excitatory counterparts (Morales and Hatten 2006).

e. Glia

Astrocytes arise from the VZ from E17 to birth, after neuronal cell types have already been generated (Altman and Bayer 1997). Indeed, neurochemical and fate mapping analysis of glia confirmed that cerebellar astrocytes originate in the VZ (Mori et al. 2006; Sudarov et al. 2011).

In contrast to other precursors, cerebellar oligodendrocytes do not arise from the VZ or CRL, but instead from the Olig2-expressing neuroepithelium in the ventral rhombomere 1. Their generation and subsequent differentiation is mediated in part by Sox9 (Hashimoto et al. 2016). In vitro, oligodendrocyte differentiation also depends on diffusing factors which are proportional to the number of PCs in the medium. Among these factors, SHH was shown to stimulate the proliferation of oligodendrocyte precursor cells while inhibiting their differentiation (much like it acts on GCs). In contrast, developmentally regulated vitronectin secretion by PCs stimulates oligodendrocyte differentiation (Bouslama-Oueghlani et al. 2012).

Finally, Bergmann precursors originate in the VZ and extend processes to the pia mater. Then they progressively retract so as to relocate their cell bodies toward the cerebellar cortex (Yuasa 1996). Bergmann glial somata migrate away from the VZ just after PCs, from E14 to P7. Indeed, current findings show that Bergman cell differentiation parallels that of neighboring PCs (Yamada and Watanabe 2002). They ultimately are guided by the Notch signaling pathway to arrange in an epithelium-like monolayer in the PCL (Komine et al. 2007). Their soma surrounds PCs and they extend three to six Bergmann fibers around the PCs' dendritic trees (Buffo and Rossi 2013). Moreover, Bergmann cells, via their role in the anchoring centers, are crucial to the establishment of the cerebellum's characteristic foliation and connectivity, and therefore to its function (Sudarov and Joyner 2007).

C. FUNCTIONS

1. Overview

The first functions attributed to the cerebellum based on case reports were related to balance and posture (Jackson 1841). Motor functions of the cerebellum were also described based on numerous animal experimentations and these findings were later confirmed in humans through clinical studies (Thomas 1898). However, a point that was raised by scientists was that, due to the length of nerve fibers in animals, feedback based on sensory signals would be delayed and result in unstable movements. Thus, biological motor control should be equipped with a compensation mechanism for this sensory delay to enable fast and stable movement. One mechanism proposed by computational neuroscience is to process a future state of the body based on a current estimate of the body and an efferent signal of motor control. This predictive computation internally models an actual movement of the body by essentially predicting body motion forward in time, thus constituting an internal forward model (Wolpert et al. 1998; McNamee and Wolpert 2019). The cerebellum was then quickly identified as the center of movement control through the processing of both sensory and motor data.

The involvement of the cerebellum in non-motor functions was only suspected in 1985 by Botez et al. (Botez et al. 1985). This relatively late discovery stems from the fact that the first and most important symptoms observed in case of cerebellar lesions or pathologies are motor in nature and may mask other deficits. Moreover, this structure being highly organized, a localized damage leads to specific deficits, making its overall function difficult to understand. Nevertheless, over the last 3 decades, the involvement of the cerebellum in several cognitive functions has been proved and its importance in non-motor functions is at the forefront of current research.

2. Motor functions

a. Spinocerebellum

The spinocerebellum, named thusly because it mostly receives spinal afferences, groups functionally the vermis and paravermis cerebellar subdivisions (Vuillier et al. 2011). It processes extensive sensorimotor input from somatosensory receptors conveying information about touch, pressure, and proprioception, thus making it a major component in the orchestration of movement.

Spinocerebellar **afferences** arise from several regions in the spinal cord and the brainstem and may be conveyed via: *i*) direct pathways that originate from interneurons in the GM of the spinal cord or *ii*) indirect pathways from the spinal cord that first relay on neurons in one of the precerebellar nuclei of the brainstem reticular formation (Nieuwenhuys et al. 2008). The main spinocerebellar inputs enter the vermis either via the cuneocerebellar and spinocerebellar tracts (Figure 18), or from the reticular substance via the reticulocerebellar tracts (Oscarsson 1965). Afferents for the hind limbs and lower trunk come mainly from the dorsal spinocerebellar tract and the ventral spinocerebellar tract. The cuneocerebellar and rostral spinocerebellar tracts are the upper extremity counterparts of the dorsal and the ventral spinocerebellar tracts, respectively (Lance and McLeod 1981).

Both pairs of tracts carry proprioceptive and cutaneous sensory information from the lower and upper parts of the body, but they are functionally different. The dorsal spinocerebellar and cuneocerebellar tracts carry information from neuromuscular spindles, tendon organs and joint receptors to provide proprioceptive feedback from a single muscle or synergistic muscle group. In contrast, the ventral and rostral spinocerebellar tracts transmit a signal from larger fields and different segments of the limbs which provides information about movement commands assembled at the spinal cord during active motion (Nieuwenhuys et al. 2008; Standring 2016). The cerebellum compares both the narrow and broad fields of inputs to potentially adjust motor commands to achieve the desired movement (Kandel 2013).

The dorsal and rostral spinocerebellar tracts enter the cerebellum through the inferior cerebellar peduncle to reach the ipsilateral spinocerebellum. They are joined by the cuneocerebellar tract after its relay in the cuneate nuclei of the medulla oblongata. Meanwhile, the ventral tract decussates twice before entering the ipsilateral cerebellum through the superior peduncle (Standring 2016). These tracts all end as MFs in the cerebellum. Individual MFs are characterized by distributing bilaterally in the cerebellum and they give off collaterals that terminate in longitudinal MF rosettes. Exteroceptive fibers terminate superficially near the apex of the folia, while proprioceptive terminate near the base (Ekerot and Larson 1972).

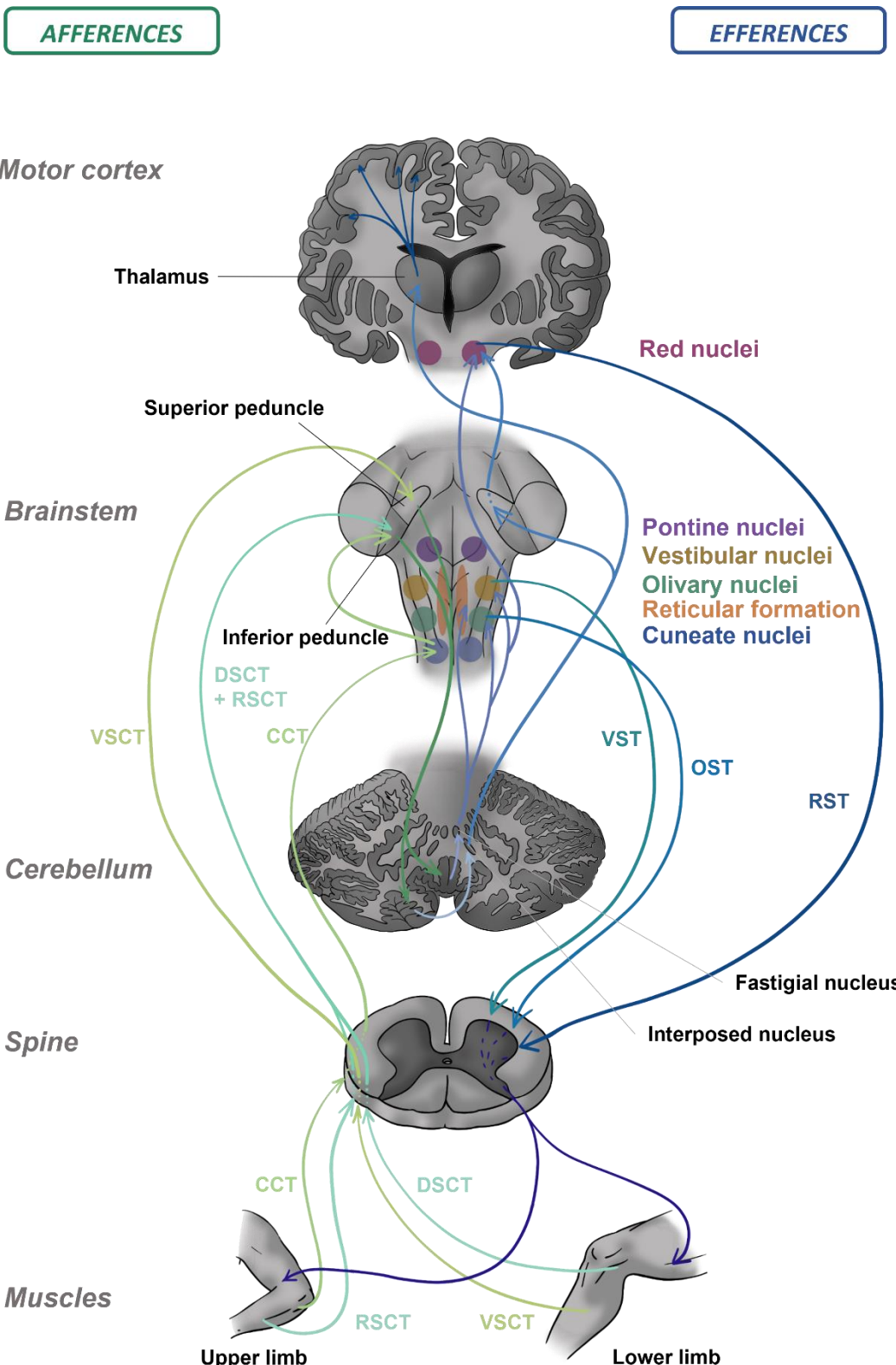


Figure 18: Schematic representation of spinocerebellar pathways in humans.

CCT: cuneocerebellar tract; DSCT: dorsal spinocerebellar tract; OST: olivospinal tract; RSCT: rostral spinocerebellar tract; RST: rubrospinal tract; VSCT: ventral spinocerebellar tract; VST: vestibulospinal tract. Afferences are depicted in shades of green and efferences in shades of blue. Arrows indicate the direction of the signal propagation.

Spinocerebellar ***efficiencies*** arise from PCs that, being the main integration center, forward this signal and project somatotopically to DCNs which control descending motor pathways. Vermal PCs of the anterior and posterior cerebellar lobes send axons to the fastigial nucleus which then projects bilaterally to the vestibular, the red and the olivary nuclei. Finally the signal proceeds to the spinal cord via the vestibulo, rubro, and olivospinal tracts respectively (Figure 18) (Vuillier et al. 2011). Additionally, the fastigial nucleus sends axons to the paramedian reticular formation, which in relays to the cranial nerve nuclei overseeing eye movements (Zhang et al. 2016). Meanwhile, PCs from the paravermis project to the interposed nuclei. From there, some axons exit through the superior cerebellar peduncle and decussate to terminate in the magnocellular portion of the red nucleus. Axons emerging from the red nucleus decussate once again and reach the spinal cord via the rubrospinal tract. Exiting axons from the interposed nucleus can also travel to the ventrolateral nucleus of the thalamus, from which neurons project to the primary motor cortex (Figure 18) (Nieuwenhuys et al. 2008; Kandel 2013).

The input relayed to the cerebellum about the dynamic state of the organism in relation to its environment enables the spinocerebellum to control posture (Ouchi et al. 1999). This processing is also critical to compare planned versus executed movement in order to modulate it in real time (Tracy et al. 2001). Thus, a spinocerebellar lesion leads to postural hypotonia and dysmetria (Hore et al. 1991; Falcon et al. 2016). Since cerebellar outputs cross the midline twice prior to reaching the spinal cord, cerebellar symptoms are ipsilateral to the lesion (Kandel 2013). Moreover, since the vermis is involved in the control of saccades and smooth-pursuit eye movements through PC in lobules V, VI, and VII, lesions of these areas cause deficits in the accuracy of eye movements (Kandel 2013).

b. Corticocerebellum

The corticocerebellum is the most recent component of the cerebellum phylogenetically and is formed by the cerebellar hemispheres. It receives input solely from the cerebral cortex and is primarily concerned with motor control (Kandel 2013).

Corticocerebellar ***afficiencies*** arise from the cortex where the information about the programmed movement is generated. It is transmitted through the corticopontocerebellar tract which has a somatotopic distribution and begins in cerebral areas involved in the planning of movements as well as the overall goal of an action. Then, pontocerebellar fibers relay at the level of the pontine nuclei, and travel through the middle cerebellar peduncle to finally terminate within the contralateral cerebellar hemisphere (Figure 19) (Ramnani 2006).

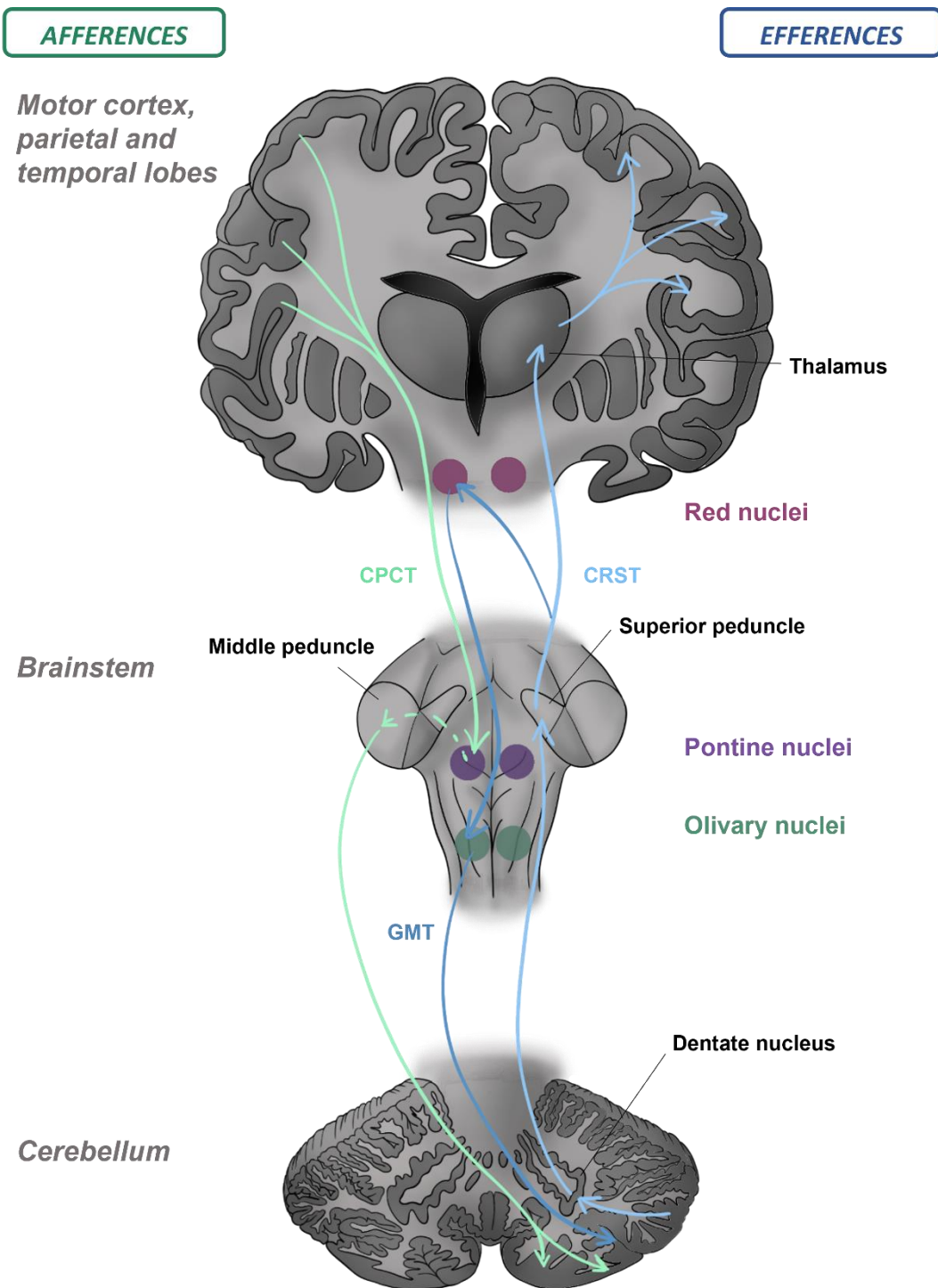


Figure 19: Schematic representation of corticocerebellar pathways in humans.

CPCT: corticopontocerebellar tract; CRST: corticoreticulospinal tract; GMT: Guillain-Mollaret triangle.
Afferences are depicted in shades of green and efferences in shades of blue. Arrows indicate the direction of the signal propagation.

Corticocerebellar ***effences*** start with the PCs of the hemispheres that integrate the signal and project to the underlying dentate nucleus (Figure 19). Dentate axons then exit the cerebellum through the superior cerebellar peduncle and follow one of two pathways: *i*) to the contralateral ventrolateral thalamus and then project to the premotor and primary motor cortex; or *ii*) to the parvocellular area of the contralateral red nucleus, whose neurons project to the inferior olivary nucleus. In turn, olivary neurons projects to the contralateral cerebellum as CFs forming a recurrent loop (Asanuma et al. 1983; Kandel 2013; Tacyildiz et al. 2021). The first pathway corresponds to the corticoreticulospinal tract in charge of regulating global voluntary movement while the second is referred to as the Guillain-Mollaret triangle and acts on the muscles of the face, the pharynx and the diaphragm (Figure 19) (Murdoch et al. 2016).

Through these two pathways, the corticocerebellum modulates the action of the motor cortex by regulating voluntary movements. It improves motor precision and plans complex movements by overseeing the corrections made by the spinocerebellum. It is also involved in motor learning processes. Therefore, a lesion in this region induces movement execution disorders with a loss of temporo-spatial organization (Ishikawa et al. 2014). Patients present delays in initiating movements and irregularities in the timing of movement components. The initiation of movement can also be delayed experimentally by inactivating the dentate nucleus (Kandel 2013). In fact, deep brain stimulation of the dentate nucleus could be a treatment option for patients presenting dystonia or dyskinesia (Nicholson et al. 2020).

c. Vestibulocerebellum

The vestibulocerebellum is composed solely of the flocculonodular lobe and regulates balance and eye movements. This region's function is closely related to the vestibular nuclei of the brainstem who possess a role similar to that of DCNs (Figure 20).

The nodulus portion of this lobe receives vestibular ***affences*** from the otolith organs within the semicircular canals of the inner ear, which sense the head's motion and relative position (Figure 20). This information travels via the ipsilateral vestibular nerve and is the only primary MF input to reach the cerebellum (Vuillier et al. 2011; Kandel 2013). Input from the inner ear also arrives via secondary cholinergic MFs that transit through the vestibular nuclei and reach the cerebellum bilaterally, or via tertiary vestibular afferents that pass through the contralateral inferior olivary nucleus and reach the cerebellum as CFs (Kaufman et al. 1996; Barmack 2003; Vuillier et al. 2011). Meanwhile, the flocculi portion of the vestibulocerebellum receives visual afferences from: *i*) pretectal

INTRODUCTION

nuclei that lie deep in the midbrain beneath the superior colliculus, *ii*) from the primary and secondary visual cortex via the pontine and pretectal nuclei, and *iii*) the retina whose output transits through the inferior olfactory nucleus and emerges as CFs that reach the cerebellum (Kandel 2013; Wylie et al. 2018).

A unique feature of vestibulocerebellar ***efferences*** is that they bypass the DCNs to directly reach the vestibular nuclei in the brainstem (Figure 20). The vestibular nuclei include four major nuclei: medial, descending, superior and lateral (Barmack 2003). The nodulus chiefly controls axial musculature via a relay in the lateral vestibular nucleus and the extrapyramidal pathway (Vuillier et al. 2011; Kandel 2013). The lateral vestibulospinal tract is organized topographically as it emerges from the lateral vestibular nucleus and remains so until it reaches the ventral horn of the spinal cord where it relays information onto motor neurons (Vuillier et al. 2011). Fibers from the dorsocaudal portion of the vestibulospinal tract are destined to the lumbosacral region while rostroventral fibers eventually reach the cervical spinal cord (Brodal 1981; Barmack 2003). Thus, the vestibulocerebellum conveys a vestibular set of coordinates to enable the adaptive guidance of movement by postural adjustment (Barmack 2003), and influences muscle tone and postural balance by controlling the motor neurons responsible for the postural muscles in charge of maintaining balance (Horak et al. 2002).

The vestibulocerebellum has also acquired vision-related functions in more recent phylogeny. As such, it is involved in the control of eye movements and in the eye-head movement coordination (Giolli et al. 1988; Bankoul and Neuhuber 1990) via the flocculi and the medial vestibular nucleus. The medial vestibulospinal tract relays signals from the flocculi to the oculomotor and accessory nerve nuclei, as well as the cervical muscles, thus mediating the vestibulo-ocular reflex that allows gaze stabilization during rapid head movements. Dynamic adaptation of this reflex to the environment relies on the integrity of the flocculus, and, a common sign following its lesions is a defect in smooth eye movement toward the side of the lesion (Broussard et al. 2011; Kandel 2013). As a whole, a lesion to the vestibulocerebellum leads to vestibulo-cerebellar ataxia which presents as the combination of balance impairment with a loss of vertical posture, walking disorders, and nystagmus (Kaufman et al. 1996; Kandel 2013).

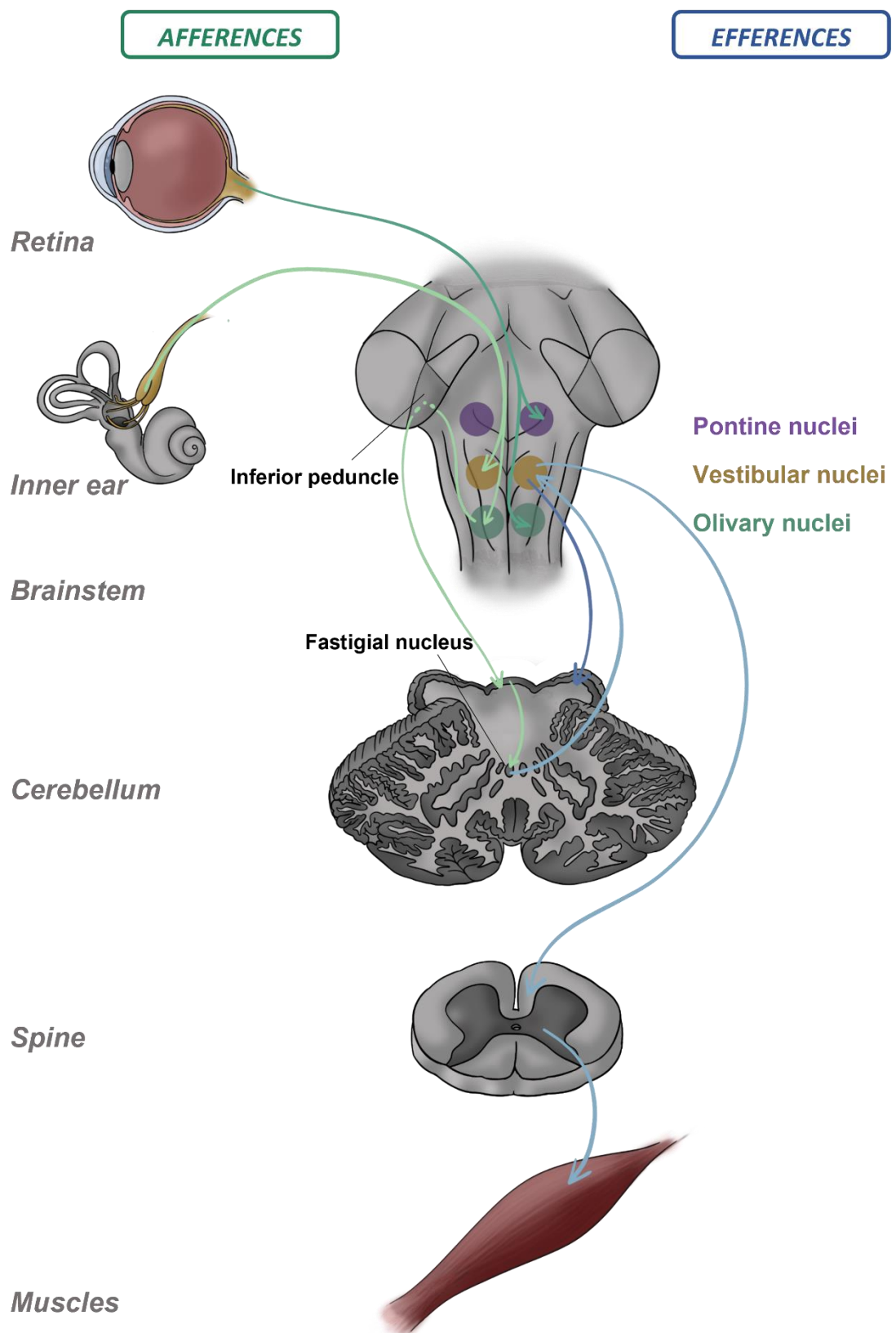


Figure 20: Schematic representation of the main vestibulocerebellar pathways in humans.
Afferences are depicted in shades of green and efferences in shades of blue. Arrows indicate the direction of the signal propagation.

3. Non-motor functions

The paradigm concerning cerebellar functions has shifted in the past few decades in light of new evidence, since several studies have found that the cerebellum is involved in higher cognitive functions. One fundamental element in this change was the characterization of the cerebellar cognitive affective syndrome (CCAS) or Schmahmann's syndrome in 1998 in which patients exhibit deficits in executive function, linguistic processing, spatial cognition and affect regulation (Schmahmann 1998). It was later evidenced that the cerebellum exchanges information with the prefrontal cortex (Middleton 2000). Moreover, the anterior and posterior lobes of the cerebellum involved in this interaction have displayed an increase in volume in the course of evolution (Balsters et al. 2010), thus supporting the notion of a cognitive cerebellar function in humans.

a. Space and time

The concept of space-time representation in the brain was redefined in 1982 by Pellionisz and Llinás using tensor network theory. This premise provides a mathematical model of the transformation of sensory space-time coordinates into motor coordinates and vice versa by cerebellar neuronal networks. The authors state the following: "(a) In order to deal with the external world, the brain embeds the external space-time continuum into a high dimensional internal space. External space-time events are represented within the CNS in overcomplete, inherently oblique, reference frames where space and time information are detected as a continuum over each coordinate axis. (b) The central nervous system may be seen as imposing a geometry on this internal hyperspace in such manner that neuronal networks transform inputs in a metric tensor-like manner. (c) In order to coordinate movements, the cerebellum acts as a predictive motor space-time metric which allows the establishment of coincidences of goal-directed movements of limbs in space-time with external targets (Pellionisz and Llinás 1982)".

Beyond these theoretical notions, recent findings support the idea that the cerebellum is critical for spatial orientation, especially due to its involvement in vestibular processing (MacNeilage and Glasauer 2018). Additionally, by analyzing the Human Connectome Project retinotopy dataset, van Es et al. were able to build a visuospatial organization map of the cerebellum. They thus demonstrated its importance in processing visuospatial information which is linked to a retinotopic organization of the cerebellum (van Es et al. 2019).

i. Space

Various clinical studies have shown that cerebellar lesions can be the cause of an alteration in visuospatial capacities, suggesting a cerebellar involvement in the mental manipulation and rotation of items in space. Yet the underpinnings of multisensory integration are not completely elucidated (Molinari et al. 2004). However, whole-brain neuroimaging while stimulating visual and vestibular senses allowed for the characterization of a self-motion network. The areas most notably involved were the cingulate sulcus, the cerebellar uvula (vermian lobule IX), and the temporo-parietal cortex. It is postulated that feedback loops involved in updating visuo-spatial and vestibular information between the cingulate sulcus and the uvula support this essential role in egomotion perception (i.e. the three-dimensional motion of the body in an environment) via multisensory integration (Ruehl et al. 2022). This concept is closely related to the feedback loops overseeing sense of agency ("experience of initiating and controlling an action") and sense of body ownership ("feeling of mineness toward one's own body parts") (Braun et al. 2018). The causal role of the premotor cortex and the cerebellum in agency and body ownership have been explored with the "moving rubber hand illusion" in which participants moved their hidden hand while watching a rubber hand (Figure 21). The reported findings suggest that the premotor cortex mainly oversees awareness of action whereas the cerebellum is involved in proprioceptive adaptation and body positioning (Marotta et al. 2021). These functions allow for an accurate feedback and control of one's actions and position in space.

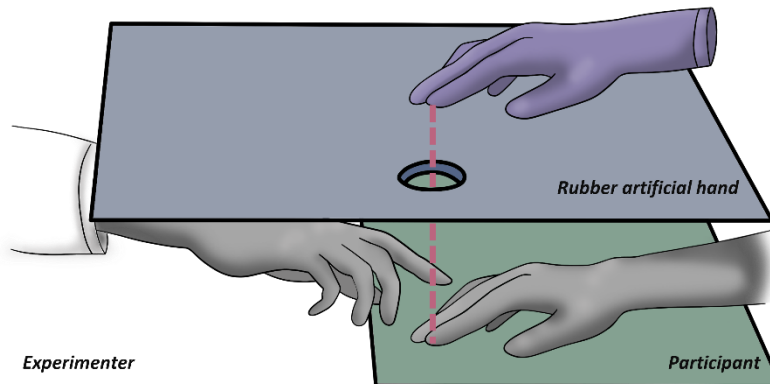


Figure 21: Depiction of the moving rubber hand illusion.

The participant's hand is hidden from them, but the rubber hand is visible. The participant's index finger and rubber index finger are connected via a rod (dashed line). Therefore, the rubber hand moves following the participant's actions. Alternatively, the rod can be moved by the experimenter, which moves the artificial hand's index finger correspondingly. This can test sense of agency and sense of ownership, respectively.

Adapted from (Braun et al. 2018).

INTRODUCTION

Interestingly, the impairments observed in patients differ according to the location of the cerebellar lesion, suggesting a likely lateralization of spatial functions. Indeed, left cerebellar lesions affect mental object rotation test with only a few errors, whereas right cerebellar lesions lead to numerous errors (Molinari et al. 2004). Another key player in visuospatial navigation and spatial representations is the hippocampus which has been proposed to collaborate with the cerebellum in visual perception. Indeed, fMRI experiments to explore the involvement of different brain structures in processing three-dimensional visual input showed activation of the left superior parietal cortex during perspective shifts (i.e., an egocentric change where the subject moves around a fixed structure), and of the right anterior hippocampus in configuration-changes in space (i.e., an allocentric change where the object is moved while the subject remains still). Interestingly, the cerebellum is able to differentiate these inputs in what seems to be a hippocampal-coupled manner. These findings highlight a cerebello-hippocampal interaction in the processing of, not only visuospatial navigation, but also perception of changes in visuospatial information (Hauser et al. 2020).

It has also been established that the cerebellum plays a critical role in sensorimotor control in space but, at this time, there is no definitive cure to movement disorders such as dysmetria, postural instability, bradykinesia, axial stiffness, and involuntary appendicular movements. However, a correlation has been established between visuo-vestibular discrepancy and symptom severity in patients presenting movement disorders suggests that exploiting the visual function represents a potential avenue for rehabilitation purposes. Indeed, testing of subjects by stimulating vestibular (moving platform) or visual (immersive virtual reality goggles) movement sensing, show that these two input processes likely involve different mechanisms (Beylgergil et al. 2022), but are directly linked with cerebellar motor functions.

Experiments in rodents have further evidenced that spatial learning is impaired following cerebellar damage. To assess spatial skills, hemispherectomized rats were subjected to the Morris pool test and showed difficulties in exploring the new environment, in the acquisition of exploration strategies and in right/left discrimination (Petrosini 1998). A study combining imaging, behavior and computational modelling, revealed that a widespread network revolving around the cerebral cortex and basal ganglia is implicated during the exploration phase, whereas connectivity centered on hippocampal and cerebellar activity oversees navigation. Moreover, it suggested a key role of the cerebello-hippocampal circuit in translating egocentric spatial information into allocentric actions (Babayan et al. 2019). It has been shown that cerebellar activity is involved in the maintenance of hippocampal egocentric movement representation and, by using mice with a PC-specific mutation, it was evidenced that potentiation of PCs contributes to stabilizing the hippocampal representation of

a familiar environment in an allocentric reference and to supporting a goal-oriented movement (Lefort et al. 2019).

ii. Time

Concerning the temporal perception of events, time-processing tasks have been linked to both prefrontal cortical and cerebellar functions, but the exact roles of each component in time perception is not yet conclusive. Psychophysical experiments have been conducted to differentiate the participation of the two structures in time perception by comparing patients with localized lesions. The results indicate that the corticocerebellum is involved in a central timing mechanism and may function as a pacemaker of the internal clock. Meanwhile, the prefrontal cortex is more likely in charge of temporal representations related to working memory and task-oriented time representation. For example, rats with prefrontal lesions expected their reward later than when it was provided during training, indicating a distortion of reference memory. The coordinated action of these regions appears to oversee a working memory system capable of discriminating timelapses extending from the millisecond to multi-second range (Mangels et al. 1998). So, while the cerebellum has been implicated in time perception in the subsecond range, it could also contribute more widely. Indeed, by analyzing behavioral data in subjects with cerebellar lesions, a regional specialization was evidenced. Lesions in the lateral superior hemispheres or the dentate nuclei resulted in increased impairment in time perception compared to lesions of other cerebellar regions. Likewise, there is a lateralization and patients with damage to the left cerebellum differed from control subjects more than those with damage to the right. Thus, it seems that damage to the middle-to-superior lobules or left hemisphere mostly alters suprasecond-range timing, most likely due to connections with the dorsolateral prefrontal cortex (Gooch et al. 2010).

The role of the prefrontal cortex and cerebellum can also be distinguished in terms of sensitivity to time perception. This is underlined when testing patients on temporal and nontemporal tasks with varying attentional loads. Participants were exposed to auditory stimuli and asked about their frequency and duration. Patients with frontal lobe lesions had significant impairments for both aspects whereas cerebellar patients struggled solely with the duration assessment. This support a stronger dependence on the attentional load for the frontal functions while the cerebellum seems to be specifically implicated in timing (Casini and Ivry 1999). Likewise, by testing patients with and without attentional cues on time-related discrimination tasks, it became apparent that the cerebellum is crucial in the process of proactive attentional modulation of perceptual sensitivity in time. Indeed, subjects with a cerebellar lesion lost the ability to discern temporal patterns among a series of stimuli (Breska and Ivry 2021). On the other hand, it has been shown that patients with damage involving the

INTRODUCTION

middle to superior cerebellar lobules presented impairments in time reproduction (maintaining a beat after cessation of the auditory stimulus) but not perception (ranking the duration between two sound stimuli). In turn, this was correlated with decreased working memory. The cerebellum was not found to be responsible for timekeeping operations but it was postulated that timing movement deficits may be related to a disruption in acquiring sensory and cognitive information germane to the task, along with an impairment in the motor output (Harrington 2003).

Therefore, the cerebellum appears to be an internal temporal evaluation system, overseeing the processing of temporally organized events and charged with the interpretation of spatiotemporal relationships between several stimuli. Further proof of the cerebellum's involvement in time-related functions appeared with the emergence of some neuroprosthetics. These are technologies that could eventually replace deficient modules in the brain and be included in the management of certain pathologies. One such device is the network-on-chip hardware architecture which effectively mimics a bio-realistic cerebellum of approximately 100,000 neurons. The simulation results confirm that this system reproduces cerebellar passage of time accurately. Additionally, this system has a stable computational speed even if the neuron number increases, which highlights the potential clinical applications of a silicon cerebellum (J. Luo et al. 2016).

This ability of the cerebellum to keep time may rely on cellular mechanisms. Just over half a century ago Bell and Grimm were the first to succeed in a simultaneous recording from multiple PCs, revealing that these neurons can fire in synchrony with a precision of the millisecond order (Bell and Grimm 1969). This was shown to be accurate for both complex spikes modulated by CF and simple spikes modulated by the MF-PF system. However, these modulating systems tend to oscillate and the basis for PC synchronicity has remained elusive while seeming to be essential in the coordination of motor behavior (De Zeeuw and Romano 2022). Indeed, by analyzing PC discharge in the oculomotor vermis in a simian model, researchers were able to show that the cerebellum can anticipate eye motion in real-time by coordinating inputs from PC synapses on DCN neurons (Herzfeld et al. 2015). According to the aforementioned theory by Llinás, the cerebellum acts as a controlling center that uses the inferior olive's rhythmic activity to synchronize PC populations for the fine-tuning of coordination (Llinás 2009). On the other hand, the Ito-Marr-Albus theory views the cerebellum as a learning computing center that heuristically refines PCs' signals based on error report stimuli from the inferior olivary nucleus (Itō 1984). Regardless, PCs seem to be the space-time integration node of the cerebellum which relies on their oscillation templates (Cheron et al. 2016).

b. Executive functions

i. Overview

As a concept, “executive function” encompasses a skillset comprised of different abilities and behaviors that are important for day-to-day life, by enabling the individual to learn and adapt to change. The scientific community has attempted to establish a unified theory of executive function and its components, but the terms coined to characterize its underlying aspects are still loosely defined (Clark et al. 2021). A generally accepted approach includes three domains: *i*) Attentional Shifting/Cognitive Flexibility, *ii*) Updating/Working Memory, and *iii*) Inhibition (Miyake et al. 2000; Diamond 2013). In a broader sense, executive functions are characterized as a set of cognitive tasks organized in such a way as to achieve a goal and the ability to constantly adjust them. They therefore require the management and coordination of afferent feedback in order to modulate output and allow the execution of simultaneous tasks (Logan 1985).

When thinking of executive function, the spotlight is usually on the prefrontal cortex, but given the abundance of connections of the cortex with the cerebellum, the latter could also participate (Middleton 2000). However, this cerebellar involvement remains controversial, and the evidence remains inconsistent across studies. Indeed, some research has demonstrated the presence of executive function impairment after cerebellar surgery where patients showed issues with abstract thinking and problem solving (Mak et al. 2016). On the contrary, other works have shown that the disorders that manifested acutely after the lesions were compensated in the long term (Schmahmann 1998; Neau et al. 2000), thus minimizing the role of the cerebellum.

Nonetheless, growing research on executive functions, behavior and clinical presentation, points toward the notion that the cerebellum might play different roles during development. Therefore, variables such as age and physio-pathological state should be taken into account when assessing and studying cerebellar executive functioning (Molinari et al. 2018). Indeed, in teens, a larger cerebellar GM volume was correlated with better executive function (Jung et al. 2019). Similarly, in adolescents and young adults suffering from congenital heart disease, cerebellar volume was found to be decreased and patients had poorer executive function. More specifically, there was a significant correlation between executive performance and posterior cerebellum involvement, which suggests a regional specialization (Semmel et al. 2018). Additionally, differences in connection strength and localization were observed between sexes, which might indicate that the adolescent cerebellum has a sex-dependent involvement in executive function (Jung et al. 2019). However, neuroimaging and clinical data show that the importance of the cerebellum’s role in human executive functions shifts from crucial in newborns to only supportive in adulthood (Beuriat et al. 2020; Beuriat et al. 2022).

INTRODUCTION

ii. Language and speech

Cerebellar injury was found to affect speech production, and while motor impairment plays a role in this effect, it does not capture the whole picture. Indeed, cerebellar disorders such as CCAS highlight the importance of the cerebellum in word recognition and sentence construction (Guell et al. 2015). This effect of cerebellar injury on speech production concerns complex processes involving the prearticulatory stage, such as subvocalizations, and also manifests as a capping of speech rate (Ackermann et al. 2007). The cerebellum is also involved in the planning of speech, the anticipation of speech rate, verbal working memory, and the creation of a predictive representation of phonation (Silveri 1998; Ackermann et al. 2007). Thus, patients with cerebellar lesions can present agrammatism, latency to speak, or aphasia (Silveri et al. 1994; Marien et al. 2000). The cerebellum can also influence the cadence and tone of speech. Indeed, one study indicates that emotional prosody activates the superior cerebellum and that cerebellar alterations cause dysprosody in patients (Pichon and Kell 2013). This was reflected in another study focused on assessing “speech naturalness” in ataxic patients, and it was found that this aspect of prosodic control was more impaired than language intelligibility (Hilger et al. 2022).

The cerebellum is also implicated in the adaptation of oral expression during conversation via the dynamic finetuning of volume, rhythmicity and tone of speech. Cerebellar degeneration has been shown to inhibit the tendency to covertly adapt to others' speech (Späth et al. 2022). These non-motor aspects of language are linked to corticocerebellar connections with the left inferior frontal gyrus (Broca's area) or the left temporal area (Wernicke's area) (Booth et al. 2007). As such, the perceptive component of language and communication subtleties may be affected in cerebellar disorders. Indeed, fMRI studies have highlighted pathways implicated in sarcasm comprehension, and the characteristic context–content incongruity effect was notable in the cerebellum (Nakamura et al. 2022). Aside from basic communication requirements, the emotional ramifications of such impairments can significantly alter quality of life (Hilger et al. 2022; Späth et al. 2022). Finally, language and speech deficits are generally associated with impaired verbal memory, indicating that the cerebellum plays a role in its encoding and reinforcement (Ravizza et al. 2006; Ackermann et al. 2007).

iii. Learning and memory

Impairments in other executive functions might appear more prominently in patients' clinical examination, but cerebellar pathologies also have major consequences on mnestic and cognitive

functions (Gottwald 2004). Indeed, the clinical presentation of patients with left cerebellar damage showcases the cerebellum's role in procedural memory. This manifested as a severe impairment in the acquisition of procedures, as assessed by the serial reaction time task (Torriero et al. 2007). In this test, a light appears at one of four locations on a screen and participants are asked to press the key directly below the light, out of a set of four keys. This is repeated a number of times and can be followed by a recall session to check if the participant memorized the sequence (Nissen and Bullemer 1987). The results of this test corroborates findings on the participation of the cerebellum in learning and conditioning mechanisms, as demonstrated in the classical eyelid closure test (McCormick et al. 1982). Eyelid closure conditioning experiments evidenced a memory defect when the interposed nuclei responsible for the connection between vermis/paravermis and thalamus were injured (Grant et al. 1960). Since these early works, progress in imaging techniques have enabled researchers to bring forward more specific findings.

Studies have demonstrated by functional neuroimaging that working memory tasks engage several posterior regions of the cerebellar hemispheres and vermis, revealing that the cerebellum acts as an important node in this circuit. Thus, when the cerebellum is affected by childhood disorders, lasting working memory deficits are commonly observed (Seese 2020). Another study showing that children treated for cerebellar medulloblastoma who presented lesions of this lobe also presented working memory impairments. Moreover, fMRI in healthy children while engaging in tasks requiring this function coincided with the activation in the left posterior cerebellar lobe, thus confirming this regional specialization (Hoang et al. 2019). More specifically, these imaging studies have led to the discovery of new evidence demonstrating the participation of cerebellar structures in the long-term storage of visual information. It was shown that cerebellar lobule VIIb/VIIa displays load-dependent activity that is proportional to the number of items held in visual working memory. These lobules have a selective activity pattern for memory storage (i.e. encoding) and this selectivity persists after the initial stimulus has been removed (i.e. maintenance) (Brissenden et al. 2021).

Another aspect to consider relies on the extensive connections between the paleocerebellum and the limbic system, notably the amygdala and the hippocampus. Thus, cerebellar involvement in fear-conditioned learning appears to be considerable. Indeed, aversive conditioning tests in rats showed that vermal lesions lead to a decrease in freezing time when presented with a fear inducing-stimulus, reflecting a defect in memory (Supple et al. 1987). The strengthening of synapses between PFs and PCs in vermal lobules V-VI after the learning phase suggests that the LTP of these cerebellar synapses may be the cellular mechanism underlying the formation of fear memory (Sacchetti et al. 2004). This high plasticity is also propitious to conditioned fear learning and, by focusing on cerebellar

INTRODUCTION

connections with the hippocampus, researchers have observed that MF terminal complexes in hippocampal and cerebellar circuits rearrange in response to learning (Ruediger et al. 2011). From a macroscopic standpoint, the evidence highlights a joint activation of both cerebellum and hippocampus. On a closer look, it appears that there is a synchronization of neuronal oscillations, and, at the cellular level, hippocampal neuronal assemblies show a cerebellar-dependent activation. This showcases the importance of looking at the bigger picture when evaluating pathologies associated with the hippocampus, as the cerebellum could also be involved (Rondi-Reig et al. 2022)..

c. Emotion and affect

The extensive anatomical connections between the cerebellum and many brain stem and forebrain structures support the cerebellum's involvement in emotional and affective behaviors (Supple et al. 1987). In fact, specific regions have been identified for each of the five primary emotions, namely: joy, sadness, fear, anger, and disgust (Baumann and Mattingley 2012). However, it seems that, while the cerebellum involved in perceiving a range of emotions, it is more concerned with negative emotions (Lupo et al. 2015). Indeed, it has been shown that both cerebellar ischemia and spinocerebellar ataxia can lead impair patients' ability to recognize negative facial expressions (Sokolovsky et al. 2010; Adamaszek et al. 2014). In CCAS, patients present a global disinhibition and heightened impulsivity, aggressiveness or irritability (Schmahmann 1998; Argyropoulos et al. 2020). This emotional response is further enhanced due to close cerebellar connections with the limbic system as well as cerebral cortical diaschisis (Bostan et al. 2018; Argyropoulos et al. 2020).

Other works have instead focused on the emotional components of social behavior, and the contributions of the cerebellum to these advanced functions. Thus, the growing corpus of evidence placing the cerebellum at the forefront of emotional processes has even led to coining the term "limbic cerebellum" to designate the cerebellar vermis (Clausi et al. 2022). Social cognition is comprised of two aspects: *i*) emotion recognition, i.e., the processing of information culminating in the accurate perception of the dispositions and intentions of others; and *ii*) mentalizing, i.e., the ability to recognize and attribute emotions, intentions, and beliefs, to others (Clausi et al. 2022). Moreover, studies have demonstrated cerebellar activation during socialization processes involving observation and imitation of facial expressions (Van Overwalle et al. 2014). Thus, the cerebellum is involved in the perception aspect of social interaction (emotion recognition and social cognitive functions) but also governs context-appropriate behavioral responses including social mirroring (Van Overwalle et al. 2020). Abnormalities in different cerebellar subregions also trigger behavioral manifestations in response to socio-emotional cues. These are related to specific cerebro-cerebellar circuits which might be crucial

to structural brain development itself. Indeed, since perinatal cerebellar lesions have been linked to impaired growth of the contralateral cerebral cortex, they could be associated with long-term alterations of behavior (Stoodley 2016). Therefore, besides emotion recognition, the cerebellum is involved in the regulation and expression of emotional states. This participates in explaining the social challenges faced by patients presenting neurodevelopmental disorders such as autism spectrum disorder or attention-deficit hyperactivity disorder (ADHD) (Sathyanesan et al. 2019).

Finally, the cerebellum's role in overseeing affective behaviors has been linked to PC function (Beckinghausen and Sillitoe 2019). Post-mortem findings have evidenced structural deficits such as cerebellar atrophy or a decrease in the number of PCs in patients on the autistic spectrum (Bailey 1998). The central role of PCs is highlighted by a study showing that PC activity in the cerebellar vermis regulates aggression (Jackman et al. 2020). Moreover, functions such as reward behavior, emotional response and social interaction, usually attributed chiefly to the limbic regions, have been shown to also involve dopamine receptors on PCs, further linking the cerebellum to social behaviors (Cutando et al. 2022).

INTRODUCTION

II. CHAPTER TWO: PERINATAL HYPOXIA

A. OVERVIEW

1. *Definition of hypoxia*

Tissues within the organism rely on the blood supply for nutrients and oxygen delivery. When the supply does not meet the oxygen (O_2) expenditure, it generates a state of hypoxia in the brain.

Four causes of hypoxia are generally recognized: *i) hypoxemic hypoxia* is by far the most common and is due to a decreased arterial partial pressure of oxygen (PaO_2) which can be caused by any ventilation to perfusion mismatch, apnea, or altitude ascent; *ii) circulatory hypoxia* is generally due to insufficient cardiac output which results in insufficient oxygenated blood supply to the tissues; *iii) anemic hypoxia* refers to a decrease in the O_2 transport capacity, whether due to erythrocytopenia or low hemoglobin binding affinity; *iv) histotoxic hypoxia* is a condition where tissues are unable to use O_2 regardless of the supply (Samuel and Franklin 2008).

Hypoxia can also be categorized based on duration, ranging from acute, if it lasts a few seconds or minutes, to chronic if it persists up to several hours or days. Aside from the permanence of the condition itself, two subtypes emerge based on the length of the low- O_2 episode. Thus, when the O_2 level remains constantly low, it is referred to as continuous hypoxia (CH), whereas if hypoxic episodes are interrupted by reoxygenation phases, the hypoxia is designated as intermittent hypoxia (IH) (Figure 22) (Prabhakar and Semenza 2012).

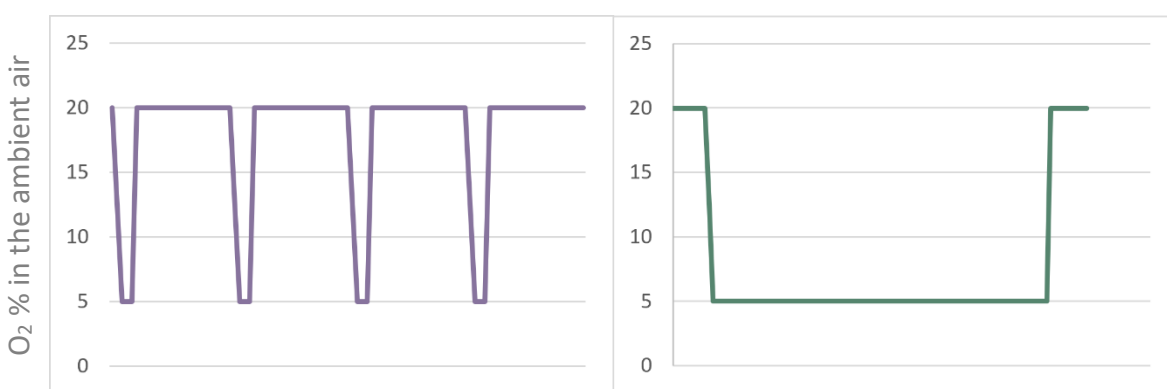


Figure 22: Representation of oxygen variation causing different types of hypoxias.

Graphs showing O_2 concentration as a function of time during intermittent hypoxia (IH; left) and continuous hypoxia (CH; right). O_2 : oxygen.

2. Etiology of perinatal hypoxia

The perinatal period (from the 36th GW to the 8th postnatal day) is a developmental stage particularly vulnerable to hypoxia, especially in case of premature birth (before the 37th GW). Perinatal hypoxia is considered to be a significant cause of morbimortality, and its long-lasting socio-economic impact makes it a clinical priority. Indeed, hypoxia-ischemia episodes are linked with 30% of newborn mortality and can cause up to 40% of long-term neurological deficits (Netto et al. 2018). Perinatal hypoxia can have a ventilatory cause, like in hypoxic hypoxia, or a circulatory etiology, and can be continuous or intermittent. Regardless of these modalities, some cellular and/or histological deficit in the CNS is always reported.

a. Continuous hypoxia

CH can often be traced back to an intrauterine origin, related to an infectious process occurring in the mother, a placental defect or umbilical cord anomalies. CH has been shown to alter synaptogenesis in the cerebral cortex and hippocampus, inducing a decrease in cortical volume and ventriculomegaly (Curristin et al. 2002). Moreover, CH alters the expression of genes involved in neuronal differentiation (e.g., downregulation of reelin), apoptosis (e.g., enhancement of caspase-3), and stress response (e.g., enhancement of HIF-1 α) (Curristin et al. 2002). CH also has histological and cytological effects on the cerebellum: it is associated with an increase in the GL and ML thicknesses, co-occurring with a decrease in cell density and a morphological alteration of the PCs. Moreover, it has been shown that these deficits persist in the long-term, suggesting important functional ramifications (Campanille et al. 2015).

CH can also be caused by ischemia or hemorrhage. In this case, the sequelae present differently according to the stage of development. For example, in humans, basal ganglia are affected in full-term infants, whereas premature infants tend to display periventricular leukomalacia (Ferriero 2001). Similarly, in rats, alterations of the WM in the cerebellar hemispheres are observable at P2, whereas at P7, the structures affected are those with a higher metabolic demand such as the basal ganglia, hippocampus, and cerebral cortex. Interestingly, at P7, hypoxia-ischemia was associated with cell death even in regions not directly affected by ischemia, such as the cerebellum, suggesting that this neurodegeneration is a result of impaired neuronal connectivity with other implicated regions (Biran et al. 2012). However, the cerebellum seems to be more sensitive to hypoxia alone as cerebellar white matter lesions and a decrease in neuronal cell density were more pronounced following hypoxia than hypoxia-ischemia (Biran et al. 2011).

b. Intermittent hypoxia

IH can be prenatal, due to maternal factors such as smoking or gestational sleep disorders, or neonatal (Mouradian et al. 2021), usually caused by apneic pathologies.

Apneas can be classified as follows: *i)* short **central** episodes account for 10-25% of cases, where the airway is clear but there is no respiratory effort or chest movements, *ii)* longer **obstructive** in 10-25% of cases, when air circulation is impeded by an upper airway obstruction/collapse, and *iii)* **mixed** or combined in the remaining 50-75% of cases (Stokowski 2005). Central apneas are due to neurological immaturity while obstructive apnea can be caused by airway secretion or collapse, and the former can lead to the latter. Indeed, prolonged central apnea may result in laryngeal closure and lead to combined apnea (Idiong et al. 1998). Treatment and clinical management vary depending on the subtype and relies both on stimulating medications as well as air cannulas (Stokowski 2005).

Nevertheless, during apnea, the organism is subjected to rapidly alternating short periods of low oxygenation followed by reoxygenation that will induce brain alterations (Prabhakar and Semenza 2012). Interestingly, while not much information is available on the effects of IH in neonates, more is known in adults. Indeed, in rat models of obstructive sleep apnea (OSA), neurons of the hippocampal CA1 area present functional and morphological abnormalities (L. Xu et al. 2022). Moreover, an O₂-dependent Purkinje and fastigial neuron damage has been reported in adult rats subjected to IH (Pae et al. 2005). Similar findings are observed in adult OSA patients with a loss of grey matter in several CNS regions, including the cerebellum (Macey et al. 2002)..

Furthermore, due to their immature respiratory system, premature newborns are particularly susceptible to apnea and a correlation has been established between the persistence of this perinatal IH, and the occurrence of neurodevelopmental deficits in children (Janvier et al. 2004). This has led to coining the term “apnea of prematurity” (AoP).

B. APNEA OF PREMATURITY

1. Physiopathology

Apnea of prematurity (AOP) is among the most common diagnoses in neonatal intensive care, but despite its prevalence, little is known about the ramifications of this phenomenon. AOP is characterized by IH and consists of breathing cessation occurring at least every 5 minutes and lasting over 20 seconds (Moriette et al. 2010). Moreover, it can be associated with bradycardia or O₂ desaturation (Eichenwald et al. 2016). The incidence of AOP is inversely proportional to gestational age and birth weight. Thus, AOP occurs in 50% of all preterm infants and nearly 100% of very preterm infants born before 28 GW. It usually subsides in 98% of cases when the corrected term is reached, but it can cause significant developmental alterations in the meantime (Henderson-Smart 1981; Pergolizzi et al. 2022a).

The etiology of AOP is not fully understood, but it is postulated that it results from physiological immaturity of the respiratory system and associated control centers in preterm births (Zhao et al. 2011). Indeed, in utero, breathing movements are intermittent and become continuous in term births. In contrast, preterm infants have an immature system where respiratory movements are irregular and can lead to apneas (Moriette et al. 2010).

c. Chemoreceptors and neurological immaturity

The major neuronal networks controlling ventilation are located within the brainstem and these are modulated by many neural inputs from the upper airway, lungs, central and peripheral chemoreceptors (Hall 2020).

Peripheral chemoreceptors are clustered into small ovoid bodies respectively localized in the carotid (carotid sinus) and aortic arch (aortic bodies). They uniquely modulate ventilation in response to oxygen availability and act as respiratory pacemakers in the early neonatal period. Both transmit impulses to the brainstem: the carotid bodies are connected to the respiratory centers while the aortic bodies are connected to the cardiovascular centers (Figure 23). Peripheral chemoreceptors sense arterial partial O₂ pressure (PaO₂) and stimulate ventilation when it falls below 50mmHg. Moreover, in utero, carotid body sensitivity is adapted to the low PaO₂. As a result, at birth, the increase in pressure leads to a transient silencing of the chemoreceptors (Hertzberg and Lagercrantz 1987). They then adjust their O₂ sensitivity during the first few days of extrauterine life (Cohen and Katz-Salamon 2005). Afterwards, initiation and maintenance of continuous breathing relies on a combination of

factors, including the decrease in peripheral body temperature and the stabilization of PaCO_2 (Kuipers et al. 1997). In addition, aortic bodies, unlike their carotid counterpart, are sensitive to carbon monoxide and anemia (Hall 2020).

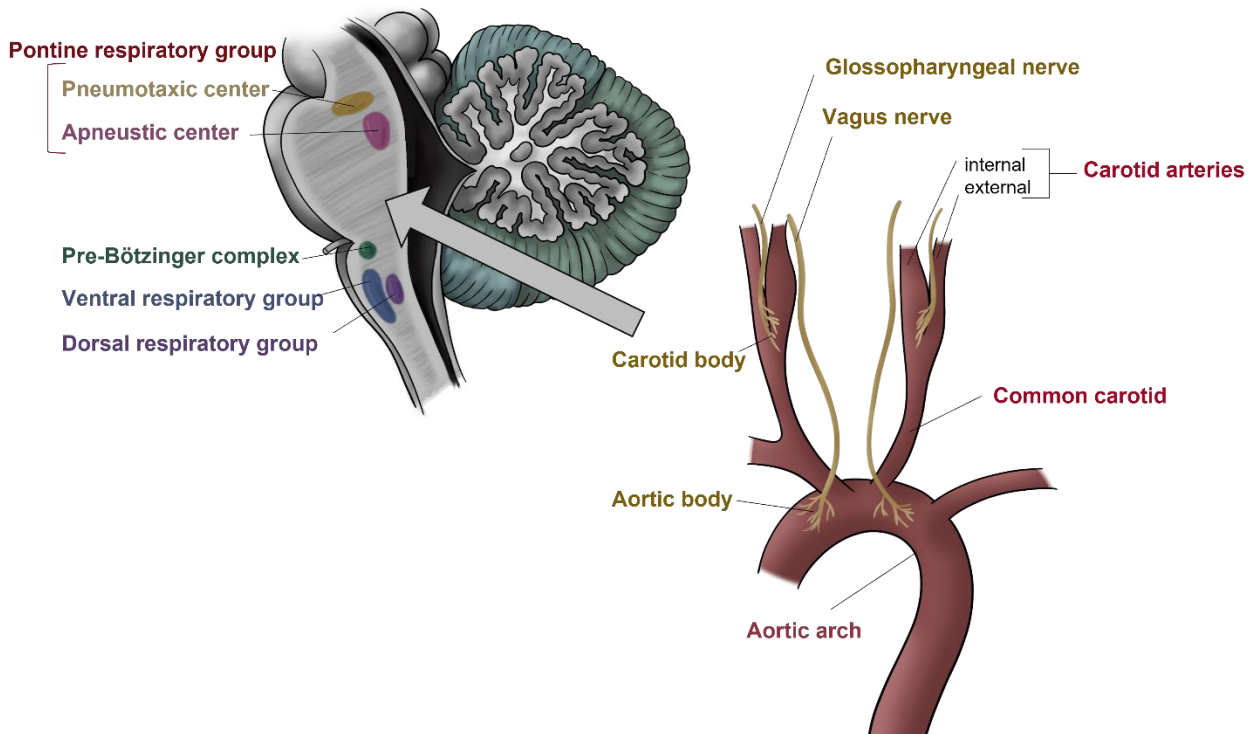


Figure 23: Location of peripheral chemoreceptors and their CNS projections.

Peripheral chemoreceptors transmit information to the brainstem's cardiovascular and respiratory centers via the glossopharyngeal and vagus nerves. CNS: central nervous system.

In parallel, autonomic control of breathing is overseen at several respiratory centers in the brainstem which gathers central and peripheral information to maintain and adjust respiratory parameters. There are three such areas (Figure 23): *i*) the dorsal respiratory group in the caudal third of the nucleus tractus solitarius (NTS) receives most input from peripheral chemoreceptors, and as such, is the first responder to hypoxia (Alheid and McCrimmon 2008); *ii*) the ventral respiratory column in the ventral medulla oblongata, containing the parafacial respiratory group and the pre-Bötzinger complex, which have been identified as the main sites of rhythmogenesis of respiration (Ikeda et al. 2017); and *iii*) the pontine respiratory group in the dorsolateral pons (Standring 2016).

INTRODUCTION

In the respiratory centers, the ventilatory response is biphasic. During hypoxia, it starts with an initial hyperpneic phase triggered by the binding of glutamate onto mostly NMDA receptors of the NTS. This is followed by a relatively hypopneic phase, mediated by inhibitory neurotransmitters or PDGF (Gozal et al. 2000). Indeed, immunoblotting experiments in rats demonstrated that early postnatal PDGF- β receptor activation during hypoxia contributes to ventilatory depression during postnatal development, and more markedly so for immature stages of development (Vlasic et al. 2001). Afterwards, and depending on the duration and type of the hypoxic episode, the pathways of respiratory control may undergo remodeling and chronic hypoxia may dysregulate them (Gozal et al. 2000).

In addition to a defective response to O₂ variations, the CO₂-related response is also altered in premature newborns. Central chemoreceptors are poorly localized clusters of monoamine neurons that are sensitive to pH and arterial partial CO₂ pressure. They are grossly situated in the brainstem, near the floor of the fourth ventricle and close to brainstem respiratory centers and seem to be composed of a diverse neuronal population. Indeed, experiments have shown that alteration in the activity of noradrenergic locus coeruleus neurons and serotonergic raphe magnus neurons can impair CO₂ response. Moreover, the redundancy of several sites involved in central chemoreception may be a safety mechanism as well as a way to allow the adjustment of the response to hypercapnia based on other signals (Nattie and Li 2009).

In fact, hypercapnia normally triggers hyperventilation with an increase in both the frequency and amplitude of respiratory movements (Hall 2020). However, in preterm neonates, the response to hypercapnia is decreased during hypoxia (Rigatto et al. 1975). Furthermore, it was observed that eupneic and apneic alveolar CO₂ partial pressure (P_ACO₂) are very close in preterm neonates. This is likely due to the compliance of their chest wall, decreased functional capacity and overall respiratory immaturity. This narrow threshold makes premature infants very susceptible to apnea, since minor oscillations in breathing may trigger irregular breathing (Khan et al. 2005). This characteristic has been exploited in clinical trials of low concentration of inhaled CO₂ to stimulate breathing in AOP (Al-Saif et al. 2001). This indicates that AOP stems from several mechanisms that are compounded into a presentation which increases in severity when occurring in less mature infants.

Moreover, in the context of preterm birth, synaptic connections between peripheral chemoreceptors and central respiratory centers are insufficient, leading to an altered ventilatory response. The immaturity of respiratory control is also related to aberrant activity of central and peripheral chemoreceptors, as well as difficulty maintaining upper airway patency due to neuromuscular underdevelopment (Martin and Wilson 2012). Indeed, autonomic activation of the

ventilatory drive via the chemoreceptor reflex is delayed in premature infants (Cohen and Katz-Salamon 2005). Additionally, since preterms rely more than term infants on peripheral chemoreceptor input to generate a ventilatory drive, a delay in that signal further exacerbates disordered breathing during prematurity (Mammel et al. 2022). Among the areas affected, hypoxic damage can alter NTS and the pre-Bötzinger complex, which further enhances hypoxia (Almado et al. 2012; Garcia et al. 2016). These elements provide some insights as to how AOP creates a downward spiral.

Finally, the persistence of AOP beyond chemoreceptors maturation suggests that other mechanisms may be involved in this pathology (Gauda et al. 2004). One such contributing factor is the laryngeal chemoreflex. Physiologically protective, this mechanism facilitates coughing and swallowing following stimulation of the laryngeal mucosa (Praud 2010). However, in premature infants, the immaturity of the upper laryngeal afferents may trigger upper airway closure instead. This may be prompted by the mucosal stimulation seen in gastroesophageal reflux disease (GERD) which may have a causal relationship with AOP. In turn, this is thought to lead to apneas, hypoxemia and even bradycardia (Thach 2008). However, extensive review of the available literature concluded that, across studies, only a minority of apneic events followed the occurrence of GERD symptoms. Current evidence is lacking to establish a clear causal link and results may be solely due to chance (Quitadamo et al. 2020).

d. Neurotransmitters and mediators

Numerous neurotransmitters and neuromodulators are also involved in respiratory regulation and may participate in the pathogenesis of AOP. Indeed, it has been shown that GABA-mediated mechanisms participate in regulating breathing rhythmicity during development. Colocalization studies in developing piglets revealed a significantly increased CO₂ reactivity in GABA-containing neurons in the medulla oblongata, notably within the Bötzinger region. Therefore, during early development, brainstem GABAergic neurons seem to be part of the CO₂ sensing network activated in response to hypercapnia (Zhang et al. 2003). Furthermore, blocking GABA_A receptors increases hyperventilation, inhibits apneas induced by laryngeal stimulation, and reduces hypoxic ventilatory depression (Miller et al. 2000; Abu-Shaweeesh and Martin 2008).

Conversely, O₂ sensing in chemoreceptors is based on the AMP/ATP ratio. When this ratio is elevated, 5'-nucleotidase enzyme activation will convert AMP to adenosine ultimately activating adenosine A_{2A} receptors. These receptors are widely distributed in the CNS and cardiovascular system. On carotid bodies, binding of adenosine triggers hypoxic cardiovascular chemoreflexes prompting an autonomic response while, in the CNS, it mediates breathing inhibition (Koos 2011). Adenosine is also involved in respiration inhibition by decreasing phrenic activity, which can be countered by blocking

INTRODUCTION

GABA_A receptors. Thus, it seems that adenosine, via A_{2A} receptors, modulates GABAergic inputs overseeing respiratory timing and drive (Wilson et al. 2004). Additionally, studies on mice deficient for the A₁ adenosine receptor or lacking the enzyme adenosine deaminase (which degrades adenosine) conclusively demonstrated its role in mediating hypoxia-induced injury. Indeed, the characteristic periventricular leukomalacia and secondary ventriculomegaly typically observed in premature newborns who suffered hypoxia was lessened in these mice. Therefore, adenosine, via A_{1A} receptors, seems to be instrumental in developing hypoxia-induced brain injury (Turner et al. 2003).

It should also be noted that glial cells could also be involved in this respiratory control since adenosine can be both of neuronal and glial origin. In the same way, blocking the release of glial glutamate has been shown to induce a decrease in respiratory rate in rats, which highlights the role of gliotransmitters in the regulation of ventilation (Young et al. 2005). However, the contribution of neurotransmitters and mediators to the pathology may be potentiated by polymorphisms in the adenosine A₁ and A_{2A} receptor genes, which have been linked to a higher risk of AOP and variable effectiveness of methylxanthine therapy as a respiratory stimulant (Kumral et al. 2012; He et al. 2021).

e. Genetics and other factors

Interestingly, a twin study to investigate the heritability of AOP showed strong arguments in favor of a genetic predisposition to this pathology. The genetic influence was even stronger in males which suggest the presence of a sex-dependent factor (Bloch-Salisbury et al. 2010). Likewise, the influence of sex chromosomes and genetic factors in CNS differentiation and development has been shown (Arnold et al. 2004; Arnold 2004).

Clinical data of premature births suggests a sex difference in hypoxia ischemia outcomes, with males exhibiting more severe cognitive/behavioral deficits relative to females. These results have been corroborated in rats, although the female advantage was only seen in some behavioral tasks (Smith et al. 2014). These findings raise the idea of a female protection via sex-specific plasticity or compensation which has been investigated, notably through the use of progesterone as a potential therapeutic strategy for hypoxia (Bairam et al. 2019). However, histopathological examination of rodent brains after hypoxia did not reveal a difference across sexes (Smith et al. 2014) and other studies do not report a statistical difference in the outcome of neonatal hypoxia between sexes, suggesting that the influence of sex may be interlinked with other confounding variables (Nagraj et al. 2021).

Finally, other factors, such as sleep state and environmental temperature influence metabolic rate inducing alterations in O₂ consumption and CO₂ release, which have a direct influence on breathing (Sawczenko and Fleming 1996). An ongoing infection can also increase the occurrence of AOP (Stock et al. 2010). As such, AOP may arise from any number of these causes (Figure 24) or a combination of them, and, in fact, seems to be the result of a “perfect storm” of adverse events culminating in a pathology that has been proven to cause significant short and long-term deficits (Di Fiore et al. 2013).

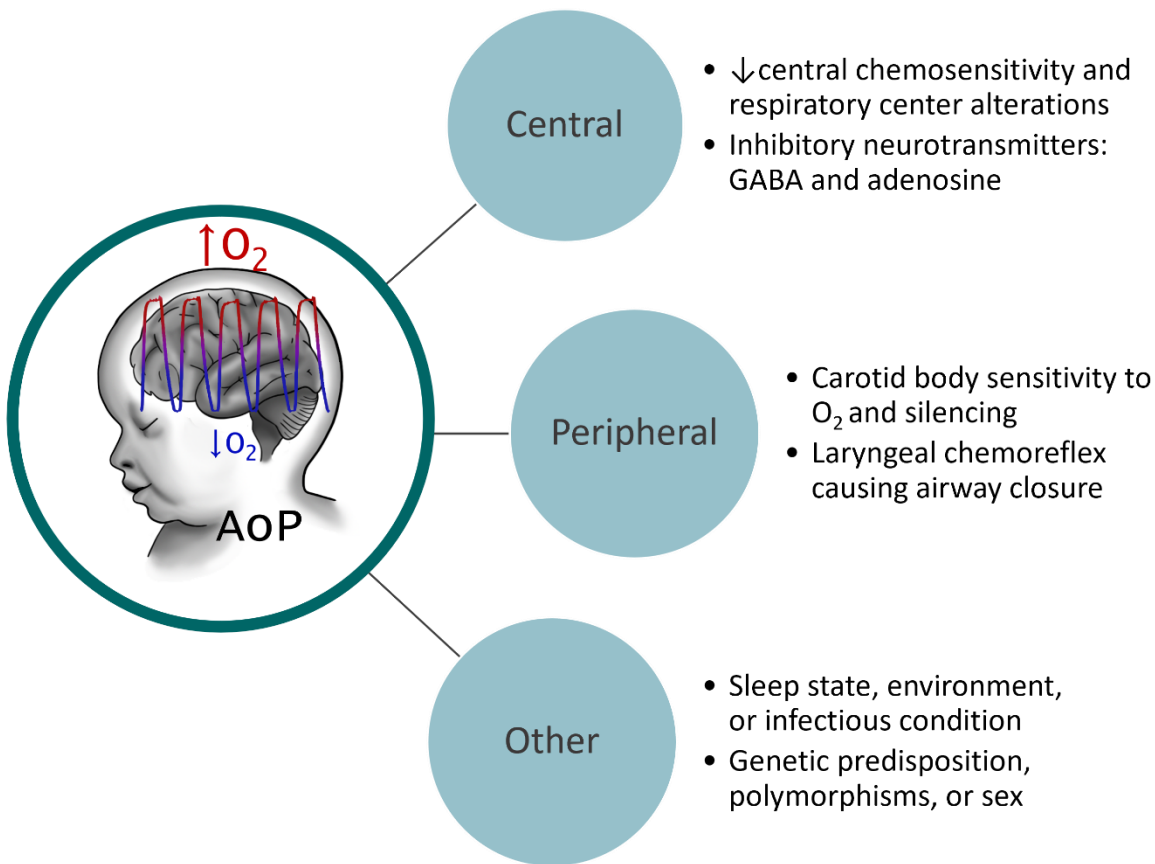


Figure 24: Summary of known causal factors of apnea of prematurity.

Central, peripheral, and other etiologies of AOP.

AOP: apnea of prematurity; GABA: gamma-aminobutyric acid; O₂: oxygen.

2. Current management

Currently, two main therapeutic strategies are considered for AOP: the use of pharmacological treatments that stimulate breathing, or noninvasive ventilatory support. Other prospective avenues are being explored on a smaller scale but, to this day, their benefit is disputed.

a. Nonpharmacological strategies

i. Ventilation

Nasal continuous positive airway pressure (CPAP) is the first line treatment and has proven effective and safe for over 35 years (Abu-Shaweeh and Martin 2008). This noninvasive ventilation technique improves airway patency by delivering a constant air pressure to the upper airway through a mask. Thus, it requires a lesser respiratory muscular effort and prevents the occurrence of soft tissue collapse causing apneas with an obstructive component. In addition, it increases functional residual capacity (Miller et al. 1985). CPAP also facilitates oxygenation and avoids the desaturation that can lead to bradycardia in case of central apneas (Di Fiore et al. 2013). It may benefit from the adjunction of an aerosolized surfactant to prevent further respiratory distress (Jardine et al. 2022). Small studies have tested heated humidified high flow nasal cannula use in AOP. This practice has shown comparable effects to CPAP with no differences in rate of AOP-related symptoms and has become more widely used (Al-Alaiyan et al. 2014). Therefore, it seems to be a viable alternative to CPAP in the treatment of AOP, but wider studies are needed to issue clinical recommendation.

Alternatively, nasal intermittent positive pressure ventilation (NIPPV) could also be considered to treat AOP (Lemyre et al. 2002). This method considers respiratory dynamics between inspiratory and expiratory pressures to improve ventilation. In addition to acting on the obstructive component of AOP, NIPPV provides a complete respiratory support and reduces central apneas (Gizzi et al. 2015). Moreover, it can be further enhanced with neurally adjusted ventilatory assistance (NAVA) which adds a synchronous rhythmic component to non-invasive ventilation. This combination seems to offer interesting benefits, since it acts centrally and seems to reduce cardiovascular compensation. Indeed, a retrospective study showed that bradycardic events were fewer and further apart when using NAVA-synchronized NIPPV. The results show a potential for application in very low birthweight infants who do not respond to pharmacological stimulation (Tabacaru et al. 2019).

ii. Alternative interventions

Several other non-pharmacological strategies have also shown some benefit, and since they present no adverse effect, it has been advocated that they could be added by default to the standard protocol.

One such therapy is sensory stimulation (tactile, proprioceptive, and kinaesthetic), which, applied with standard respiratory care (combined nasal oxygen and caffeine citrate), was shown to decrease the frequency of AOP (Abdel Mageed et al. 2022). Olfactory stimulation is also being studied in a project due to end in 2023 (Duchamp-Viret et al. 2021). This project exploits the inherent properties of several odorants to stimulate respiration. Mint and grapefruit scents trigger the main and the trigeminal olfactory pathways, whereas vanilla stimulates the main olfactory pathway. If successful, this non-invasive and cost effective method could become part of the standard regimen to treat AOP (Duchamp-Viret et al. 2021). Alternatively, skin-to-skin contact such as Kangaroo mother care has been proven effective in shortening ventilation duration, and reducing the frequency of apneas in extremely low birthweight infants (Montealegre-Pomar et al. 2020; Xie et al. 2021). Likewise propped/prone positioning of infants reduced apneic events and thus should be considered in the neonatal care unit (Richmond et al. 2023).

b. Pharmaceuticals and molecules

i. Methylxanthines

Methylxanthines are a purine-derived group of molecules whose clinical properties rely on their bronchodilatory and stimulatory effects, and have been used for over 40 years to treat AOP (Dobson and Hunt 2018). They act both centrally and peripherally to stimulate respiration via a dual mechanism of action: *i*) blockade of inhibitory A₁ receptors and *ii*) antagonism of excitatory A_{2A} receptors on GABAergic neurons (Mayer et al. 2006). They activate medullary respiratory centers and thus increase CO₂ sensitivity, bronchial dilation, and diaphragmatic function, thereby improving minute ventilation and respiratory rhythm (Herlenius et al. 2002; Dobson and Hunt 2018).

Two of these molecules, namely aminophylline and theophylline, have been shown to effectively reduce the incidence of apnea (Dobson and Hunt 2018). However, based on current evidence, caffeine is the substance of choice to treat AOP. Caffeine is a trimethylxanthine and the major metabolite of theophylline, and it demonstrates a better benefit-risk ratio than the latter. Indeed, it has a wider therapeutic index, lower toxicity, and a longer half-life that facilitates treatment

INTRODUCTION

administration (Henderson-Smart and Steer 2010). Caffeine reduces the need for mechanical ventilation and duration of intubation, and facilitates extubation (Henderson-Smart and Davis 2010). Additionally, caffeine's safety has been demonstrated in a wide study 11 years after administration and it was found to have beneficial effects on respiratory function, motor coordination, and visuospatial performance with no observed long-term side effects. However, a follow up in adulthood would be needed to draw definitive conclusions (Doyle et al. 2017; Mürner-Lavanchy et al. 2018). For extremely low birthweight infants (<1250 g), caffeine increases long-term survival without sequelae by reducing the incidence of bronchopulmonary dysplasia, patent ductus arteriosus, and the severity of retinopathy of prematurity up to 21 months of age (Schmidt et al. 2007). However, survival without disability 5 years after neonatal caffeine therapy was not found to be different compared to placebo (Schmidt 2012). This controversial benefit could be due to a partial effect of caffeine in neuronal damage. Indeed, it has been demonstrated in rat pups that caffeine can reverse perinatal hyperoxia-induced cell death but fails to restore transcriptional pathways (Giszas et al. 2022), which might then be involved in long term deficits.

Interestingly, the benefits of caffeine use for AOP are related to its administration modalities. Several studies suggest that early (before the 3rd postnatal day) intervention is paramount to observe improved outcomes and reduced ventilation time (Davis et al. 2010; Dobson and Hunt 2018). Caffeine has therefore become a widely used prophylactic strategy (Abu Jawdeh et al. 2013). However, several works highlight the presence of biases and have associated earlier initiation of caffeine therapy with significant risks (Amaro et al. 2018; Nylander Vujovic et al. 2020). Additionally, caffeine, like all methylxanthines, increases urine flow and urinary sodium excretion, which may need to be accounted for in terms of fluid management (Gillot et al. 1990). So, it appears necessary to gather more evidence about long term outcomes. Furthermore, determining the optimal duration of treatment is empirical, and neonatologists usually decide on duration based on time elapsed since the last apneic episode and general clinical status. After cessation of the treatment, infants remain under observation during elimination of the molecule for up to a week, or until 34 weeks post-menstrual age (Eichenwald et al. 2016).

In terms of posology, the standard approved protocol recommends a loading dose of 20 mg/kg followed by a daily maintenance dose of 5 mg/kg for infants between the 28th and 33rd GW. Before the 28th GW, both duration and dosing can be safely increased while providing additional benefits by reducing apnea and preventing extubation failure (Brattström et al. 2019; Puia-Dumitrescu et al. 2019). Additionally, a recent retrospective study associated a higher dosage of caffeine with improved neurodevelopmental outcomes (Ravichandran et al. 2019). Nevertheless, administration of high doses

of caffeine in fetal sheep demonstrated that the treatment induces histocytological alterations in the CNS and most notably in both cerebral and cerebellar cortices. Among them, a significant disorganization of the cortical layers was observed with pyramidal, PC and glial cell injury (Atik et al. 2019), indicating that the therapeutic dose of caffeine should be finely tuned.

Likewise, since methylxanthines are nonspecific adenosine antagonists, and adenosine receptors are ubiquitous throughout the organism, their use can also lead to secondary effects. Most notably, findings reported transient tachycardia and delayed weight gain in the caffeine treated group, but mortality, brain injury, and necrotizing enterocolitis were not significantly different between groups (Schmidt et al. 2006; Schmidt et al. 2007; Schmidt 2012). Additionally, high doses of methylxanthines (above 40 µg/mL) can cause cardiac arrhythmias, seizures, and cerebellar hemorrhages (Dobson and Hunt 2018). It has also been shown that methylxanthines induce an increase of up to 20% in metabolism and O₂ consumption, at a stage when this supply is already at risk (Gauda and Martin 2012).

Finally, genetic variations such as circadian rhythm regulators or polymorphisms in pharmacodynamics-related genes contribute to the variability in response to caffeine therapy (Long et al. 2021; Guo et al. 2022). As such, preterm infants who do not respond to the standard protocol may benefit from a customized regimen based on how they metabolize the molecule, but its effectiveness or safety are not guaranteed (Long et al. 2021).

ii. Prospective treatments

Given the mixed results of current treatments to treat such a prevalent pathology as AOP, research is ongoing to identify other therapeutic alternatives. Even though the association of AOP with gastroesophageal reflux has been called into question, gastric acid suppression is still brought forward when discussing AOP treatment. However, based on current knowledge treatment with acid inhibitors is not recommended in AOP unless gastroesophageal reflux has been independently diagnosed (Quitadamo et al. 2020).

A study in rats also assessed the efficacy of the respiratory stimulant erythropoietin (EPO) against AOP, alone or in combination with caffeine. While co-administration of both molecules did not present additional benefits, EPO was shown to prevent the oxidative imbalance/stress caused by IH in young mice of both sexes. Moreover, the study did find a sex-specific response to treatment, females being seemingly less vulnerable to IH (Laouafa et al. 2019). This gender-dependent protection could be linked to the action of progesterone, which has been studied as a treatment of AoP on rodents.

INTRODUCTION

This hormone acts directly via excitation of its receptors, and indirectly, by inhibiting GABA_A receptors, after conversion to allopregnanolone. Interestingly, the progesterone membrane receptor subtype β regulates the breathing pattern in males, while in females, the effect is mediated by the nuclear receptor (Bairam et al. 2019), which could explain the sex-dependent sensitivity to hypoxia. Moreover, progesterone's action seems to be dependent on the age of administration since in rat pups, the treatment's efficacy is increased at P12 versus P1. Together, these data suggest that further research is warranted to uncover the underlying mechanisms and to assess whether treatments should be administered distinctly between males and females.

A novel molecule, ENA-001, has also shown promising first results for the treatment of AOP. ENA-001 is a selective antagonist of large-conductance big potassium (BK) channels, which underlie the chemoreceptor function of carotid bodies. This chemical had previously been considered for the treatment of drug-induced respiratory depression, but one proof-of-principle study using premature lambs showed that ENA-001 could also be considered as adjunctive therapy for AOP (Miller et al. 2022). Likewise, another molecule, ampakine CX1739, a positive allosteric modulator of AMPA receptors present in brainstem respiratory centers was tested on rodents. Treated animals exhibit a markedly increased respiratory drive and ventilation, as well as a more regular breathing rhythm. This molecule is already undergoing human clinical trials and is an interesting prospect for therapeutic management (Ren et al. 2015).

Since erythrocytes represent the O₂-carrying component of the blood, blood transfusions have been studied as a potential treatment option. Indeed, a retrospective study showed that a low hematocrit was associated with a higher frequency of apneas, and that blood transfusions decreased their occurrence (Zagol et al. 2012; Abu Jawdeh et al. 2013). The underlying mechanism of action behind this line of treatment was identified as the increase in oxygen-carrying capacity (Kovatis et al. 2020). However, evidence in current literature does not account for many contributing factors of AOP, and further studies are needed.

As knowledge in the field expands, it appears clear that safety concerns on the long-term use on methylxanthines warrants questioning its use as a gold standard, even more so when responses are subject to interindividual variability. Given the prevalence and severity of AOP and the low efficacy of alternative molecules, the lack of consensus on a safe treatment is an issue that deserves research efforts (Pergolizzi et al. 2022b).

C. PATHOLOGICAL CONSEQUENCES OF AOP

1. Cellular effects

a. Oxidative Stress

In cells, the balance between reactive oxygen species (ROS) production and neutralization is essential to carry on physiological processes. ROS are oxygen-derived oxidizing molecules mainly produced by the electron transport chain (ETC) in the internal membrane of mitochondria (Holzerová and Prokisch 2015). They are represented by free radicals such as the superoxide anion ($O_2\bullet^-$), the hydroxyl radical ($HO\bullet$), as well as hydrogen peroxide (H_2O_2). $O_2\bullet^-$ is generated by O_2 use and represents the precursor of H_2O_2 . In turn, H_2O_2 can be transformed into $HO\bullet$ via the Fenton reaction, which relies directly on the availability of ferrous iron (Fe^{2+}) ions (Figure 25). As such, it is dependent on ferritin, a protein whose function is to maintain iron in a soluble and non-toxic state. In addition to the production of ROS by the ETC, most cells can also synthesize $O_2\bullet^-$ radicals via the activation of enzymes such as NADPH (reduced nicotinamide adenine dinucleotide phosphate) oxidase (NOX), or nitrogen monoxide ($NO\bullet$) via nitric oxide synthases (NOS) (Ferriero 2001).

It is relevant to highlight that ROS first and foremost fulfill a physiological role. Indeed, hydrogen peroxide functions partly as a signaling molecule thanks to its ability to move freely across plasma membranes, and also participates in post-translational modifications of proteins by oxidizing cysteine residues (Y. Wang et al. 2018). Moreover, free radicals are an essential component of the innate immune response through their role in the respiratory burst of phagocytes (B. Luo et al. 2016).

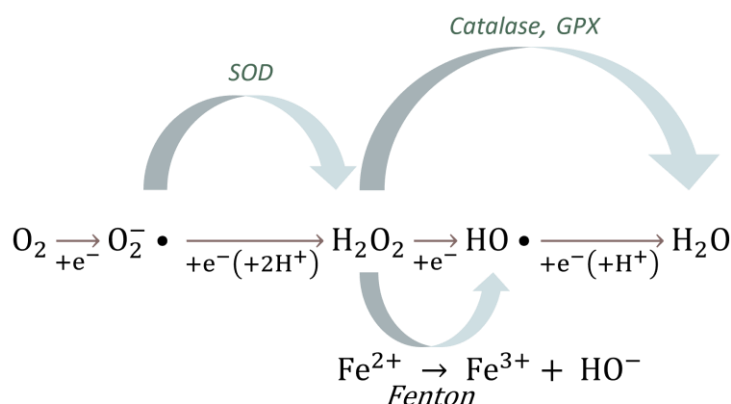


Figure 25: Reduction of O_2 .

Oxygen undergoes four chemical reactions to be neutralized into H_2O .
 e^- : free electron; Fe^{2+} : iron ion (II) or ferrous; Fe^{3+} : iron ion (III) or ferric; GPX: glutathione peroxidase; H^+ : hydrogen ion; H_2O : water; H_2O_2 : hydrogen peroxide; $HO\bullet$: hydroxyl radical; O_2 : dioxygen; $O_2\bullet^-$: superoxide anion; SOD: superoxide dismutase.

INTRODUCTION

However, despite their functional importance, ROS can become deleterious if accumulated in cells. Therefore, a double-pronged defense mechanism oversees maintaining physiological levels of ROS. The non-enzymatic component of this system includes vitamins A, C and E, among other antioxidant molecules. The enzymatic component is comprised of antioxidant enzymes such as: superoxide dismutase (SOD), catalase, or glutathione peroxidase (GPX). SOD converts $O_2\bullet^-$ in H_2O_2 , which is then neutralized either by catalase or GPX (Figure 27). GPX's ability to reduce H_2O_2 relies on the availability of reduced glutathione (GSH), whose intracellular stores are maintained by glutathione reductase (GSR), which in turn uses NADPH as a hydrogen donor (Figure 27). Alternatively, H_2O_2 can also be neutralized by peroxiredoxins (PRDX) issued from the thioredoxin (TRX) - thioredoxin reductase (TXNRD) system (Figure 26) (Birben et al. 2012).

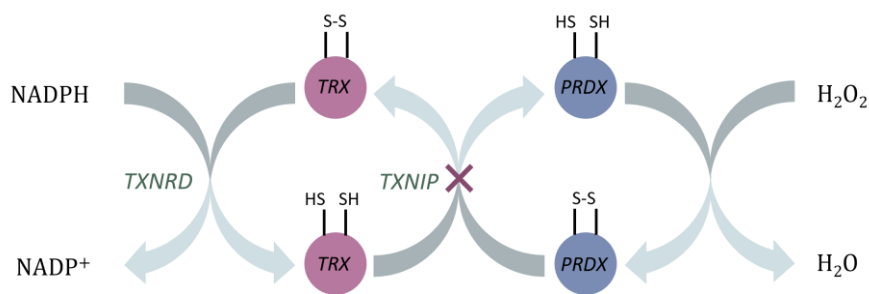


Figure 26: Neutralization of H₂O₂ by peroxiredoxins.

H: hydrogen; H₂O: water; H₂O₂: hydrogen peroxide; NADP⁺: oxidized nicotinamide adenine dinucleotide phosphate; NADPH: reduced nicotinamide adenine dinucleotide phosphate; PRDX: peroxiredoxin; TRX : thioredoxin ; TXNIP: thioredoxin interacting protein ; TXNRD: thioredoxin reductase ; S: sulfur of cysteine residues on proteins.

In the context of hypoxia, the initial decrease in O₂ availability is followed by a reoxygenation phase, which causes a sudden increase in O₂ that triggers a rise in ROS production. This increase is even more marked in the case of AOP because of the succession of hypoxia and reoxygenation cycles to which the organism is subjected. Indeed, after each cycle, ROS are generated, and their accumulation eventually surpasses the reducing capacity of the cell antioxidant defense (Figure 27). The resulting imbalance induces a cellular oxidative stress (OS) state and cell damage in the form of protein misfolding and lipid peroxidation (Birben et al. 2012). The oxidation of amino acid or peptide side chains leads to the formation of carbonylated proteins, which lose their function so are more likely to undergo degradation by the cellular machinery. Additionally, the peroxidation of polyunsaturated lipids, particularly those constituting cell membranes, alters their properties and leads to organelle and cell damage (Borst et al. 2000). In response, there is an activation of autophagic pathways, characterized by the accumulation of autophagosomes, which culminates in cell death. Concurrently, DNA damage and mitochondrial stress converge in the activation of the apoptotic pathway (Descloux et al. 2015).

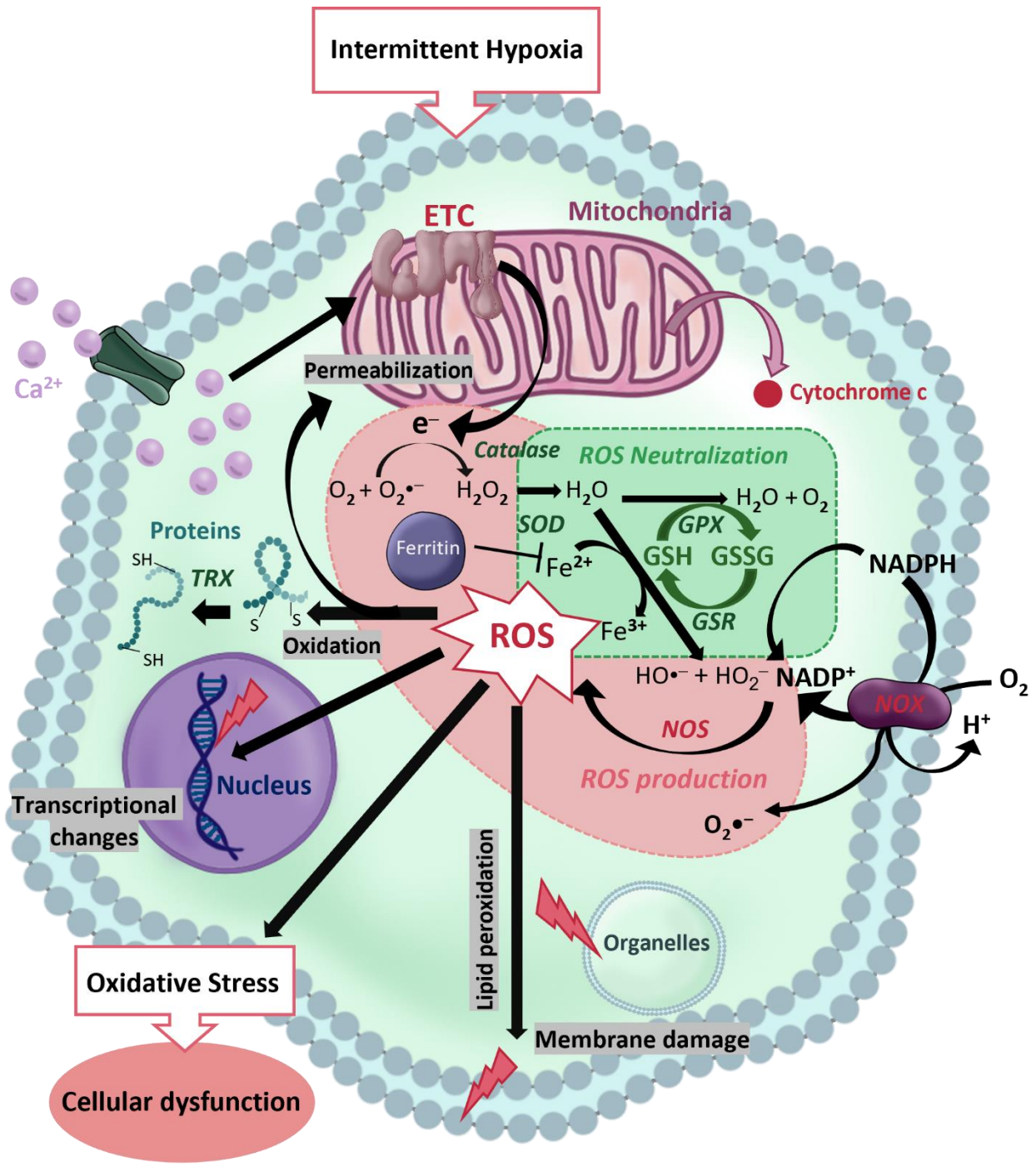


Figure 27: Production, effects, and neutralization of ROS in the cell.

Hypoxia induces the production of ROS in the cell, especially from electrons generated by the mitochondria. ROS accumulate when the enzymatic activity of neutralization is insufficient, this alters cell membranes and proteins, ultimately, leading to the activation of the apoptotic and autophagic pathways. ATP: adenosine 5'-triphosphate; Ca^{2+} : calcium ion; DNA: deoxyribonucleic acid; e^- : free electron; ETC: electron transport chain; Fe^{2+} : iron (II) or ferrous ion; Fe^{3+} : iron (III) or ferric ion; GPX: glutathione peroxidase; GSH: reduced glutathione; GSR: glutathione reductase; GSSG: oxidized glutathione; H^+ : hydrogen ion; H_2O : water; H_2O_2 : hydrogen peroxide; $HO\cdot$: hydroxyl radical; HO^- : hydroxide anion; NADP $^+$: nicotinamide adenine dinucleotide phosphate oxidized; NADPH: nicotinamide adenine dinucleotide phosphate reduced; NOS: nitric oxide synthase; NOX: NADPH oxidase; O_2 : oxygen; O_2^- : superoxide anion; ROS: reactive oxygen species; SOD: superoxide dismutase; TRX: thioredoxin.

INTRODUCTION

Additionally, this OS-generating imbalance is exacerbated by hypoxia-induced Ca^{2+} influx, which alters the membrane permeability of mitochondria. In turn, this causes an increase in ROS cytosolic concentration (Hansson et al. 2008). Eventually, this causes the release of various pro-apoptotic factors, inducing programmed cell death. ROS and H_2O_2 can also promote apoptosis through the thioredoxin system via an increase in thioredoxin interacting protein (TXNIP; Figure 26). This protein binds to and negatively regulates TRX and increases protein ubiquitination. Both of these mechanisms are likely involved in TXNIP-induced increase in GC death (Zaragoza-Campillo and Morán 2017).

b. Transcriptomic regulation

In the longer term, hypoxia triggers transcriptomic regulation mediated by hypoxia inducible factor 1 (HIF-1), a heterodimeric complex composed of two helix-loop-helix transcription factors: HIF-1 β , constitutively expressed and localized within the cell nucleus, and HIF-1 α , which is cytosolic. The latter subunit has a stable mRNA expression even though the protein subunit only has a half-life of less than 5 minutes (Huang et al. 1996). This discrepancy stems from the intervention of a degradation system via an oxygen-dependent degradation domain (Ke and Costa 2006). Indeed, in the presence of O_2 , HIF-1 α is hydroxylated by O_2 -dependent prolyl hydroxylase domain proteins, which allows the binding of the von Hippel-Lindau protein (VHL). This complex then activates an E3 ubiquitin ligase, resulting in the degradation of the whole HIF-1 by the proteasome. In contrast, hypoxia inhibits prolyl hydroxylases, thus preventing the binding of HIF-1 α to the VHL protein, and consequently increasing its half-life (Ivan et al. 2001). HIF-1 α then accumulates in the cytoplasm of the cell and translocates to the nucleus where it binds to HIF-1 β and to a CREB-binding protein (CBP)/p300 co-activator. The complex thus formed is able to recognize and bind to the hypoxia response element (HRE) DNA sequences of certain genes to modulate their expression.

In physiological conditions, HIF activity, and thus hypoxia, are developmentally important since a hypoxic environment is necessary for placental formation and later fetal development. Indeed, in mice embryos, deletion of HIF-1 α , HIF-2 α and Hif-1 β causes failure of placental formation resulting in lethality, and loss of HIF-1 α or Hif-1 β leads to arrested cardiac morphogenesis and altered neural crest cell migration. In addition, HIF-1 α is also necessary for the development of bones and chondrogenesis (Dunwoodie 2009). In hypoxia, the HIF complex is also crucial as it promotes the expression of hypoxic response genes implicated in ATP and O_2 availability. Among these, are the genes encoding EPO, the angiogenic VEGF, the vasodilator NOS2, or glycolytic enzymes and glucose transporters (Ke and Costa 2006). However, the activation of HIF-1 relies on a functional redox system,

and an excess of oxidant (e.g., H₂O₂) or antioxidant (e.g., thioredoxin) molecules may destabilize/stabilize HIF-1α, and thus decrease its response efficiency (Huang et al. 1996).

This brings back into focus AoP, where intermittent hypoxia occurs in cells with an immature redox system and thus compromises their antioxidant defense response. Indeed, in this case, HIF-1 reacts to ROS accumulation by inducing the expression of B-cell lymphoma 2 interacting protein 3 (BNIP3), which can lead to mitophagy. This effect aims to reduce the concentration of ROS, but it may also result in autophagic cell death if the OS proves to be too deleterious (Azad et al. 2008; Zhang et al. 2008). Moreover, some results suggest that IH induces the dysregulation of several HIF isoforms thus altering the transcription of genes encoding pro- and antioxidant enzymes. In fact, it has been demonstrated that IH prompts HIF-1 to upregulate the pro-oxidant enzyme nitric oxide synthase 2 (NOX2), and induces the degradation of HIF-2α leading to a lower expression of antioxidant enzymes, such as superoxide dismutase 2 (SOD2) (Prabhakar et al. 2020). Furthermore, it seems that HIF-1 and HIF-2 differ in their function depending on the brain region, cell type, cell differentiation stage, and experimental model (Schneider Gasser et al. 2021), contributing to the complexity of the physiopathology of AOP.

Alternatively, the nuclear factor-kappa B (NF-κB) may be recruited during chronic IH (Ryan et al. 2005). Under physiological conditions, this transcription factor is sequestered to the cytosol since its nuclear localization signals are masked by the inhibitor protein nuclear factor-kappa B inhibitor alpha (IκBα). NF-κB translocation is then controlled by the IκB kinase complex (IKK), which can phosphorylate and degrade IκBα. In rats submitted to IH, a downregulation of both IκBα and IKK expression was observed, indicating the recruitment of NF-κB for the response to hypoxia (Zhang et al. 2021). Indeed, when O₂ decreases, IKK is stabilized via two mechanisms: *i*) the intracellular increase in Ca²⁺ activates Ca²⁺/calmodulin-dependent protein kinase II (CaMKII) which phosphorylates TGFβ-activated kinase 1 (TAK1), which in turn stimulates IKK; *ii*) O₂ deficiency inhibits prolyl hydroxylases, which would otherwise degrade IKK in normoxia. Nuclear localization signals are then unmasked, and NF-κB is translocated within the nucleus where it can induce the expression of different protein-coding genes. These include the angiogenesis-promoting interleukin (IL) 8 and the anti-apoptotic protein B-cell lymphoma 2 (Glasgow et al. 2001; Culver et al. 2010). Finally, it has also been shown that NF-κB can counteract the inflammation and shift in energy metabolism induced by hypoxia (Rius et al. 2008).

INTRODUCTION

c. Metabolic shift

One of the first consequences of the drop in O₂ concentration is an alteration of the oxidative phosphorylation process within the mitochondrial respiratory chain. The inhibition of mitochondrial electron transport causes a deficit in ATP, which the cells try to compensate by promoting anaerobic metabolism. Neurons and glial cells in particular have developed rapid adaptation strategies to face metabolic stress and are able to switch to an anaerobic functioning in case of nutrient scarcity, while simultaneously reducing their energy-dependent processes. AMP-activated protein kinase (AMPK) is a major mediator of this metabolic adaptation. Indeed, in the absence of O₂, AMPK activates phosphofructokinase-2 (PFK-2), which catalyzes the conversion of fructose-2,6-bisphosphate to fructose-6-phosphate. The latter is an allosteric activator of phosphofructokinase-1, which is involved in the glycolytic reaction chain that will result in the net generation of two ATP molecules. However, anaerobic metabolism acidifies intracellular pH, ultimately inhibiting glycolysis and thus decreases the amount of energy produced by the cell, rendering this adaption inefficient in the long term (Peña and Ramirez 2005).

Therefore, other energy saving mechanisms are established in parallel. The γ-subunit of AMPK senses changes in the ATP-to-AMP ratio, and the binding of AMP (or ADP) to the γ-subunit stimulates AMPK activity (Herzig and Shaw 2018). This triggers a switch from ATP-consuming anabolic processes to ATP-generating catabolism thus decreasing several cellular processes, including cell growth and protein translation, which are major consumers of ATP in cells (Hardie 2000; Zhang et al. 2010). To this end, AMPK inhibits the mechanistic target of rapamycin complex 1 (mTORC1) via: *i*) the activation of the negative mTORC1 regulator tuberous sclerosis complex subunit 2 (TSC2); and *ii*) the inhibition of the mTORC1 subunit regulatory-associated protein of mTOR (RAPTOR). In turn, the inhibition of mTORC1 leads to decreased cell growth and protein synthesis. In parallel, AMPK stimulates the breakdown of macromolecules to replenish ATP stores (Herzig and Shaw 2018). Indeed, to recycle cell components, AMPK promotes autophagy both directly (via the mTORC1 pathway, for example) and indirectly (by regulating the expression of autophagy-related genes) (Fang et al. 2017; Herzig and Shaw 2018). AMPK can also promote mitophagy by translocating the autophagy machinery to damaged mitochondria (Herzig and Shaw 2018; Li and Chen 2019).

Additionally, AMPK signaling in different regions of the CNS, such as the hypothalamus, induces changes in feeding behavior and circadian rhythm in favor of long term energy management (Hardie et al. 2012). AMPK can thus phosphorylate phospholipase D1 to increase glucose uptake and TXNIP to increase translocation of glucose transporters GLUT1 and GLUT4 to the plasma membrane thereby contributing to the maintenance of neuronal function in the context of nutrient depletion

(Ashrafi et al. 2017; Muraleedharan and Dasgupta 2022). Moreover, AMPK increases glycolysis in astrocytes by promoting transcription and translocation of GLUT1 to the membrane and may contribute to neuronal energy metabolism by shuttling glucose- and glycogen-derived lactate from astrocytes to neurons (Muraleedharan and Dasgupta 2022). Altogether, AMPK induces processes that aim to preserve resources for essential functions to promote cell survival. However, these responses are insufficient when the stressor becomes chronic as in AOP, where IH leads to cellular dysfunction.

2. *Cellular dysfunction*

a. *Excitotoxicity*

As previously described, the shift from aerobic to anaerobic metabolism during hypoxia eventually decreases the amount of ATP produced and consequently causes a dysfunction of the Na^+/K^+ -ATPase pump. As this enzyme normally maintains the electric potential of the membrane essential to neuronal function, the ensuing depolarization leads to a deleterious increase in intracellular sodium (Gusarova et al. 2011). The resulting influx of water to correct this osmotic imbalance causes edema and leads to necrotic cell death (Chavez-Valdez et al. 2012).

Simultaneously, membrane depolarization causes the opening of voltage-dependent Ca^{2+} channels, leading to an intracellular buildup of Ca^{2+} . This cation influx triggers an increase in ROS and changes in the ETC, creating a state of OS. Ca^{2+} also induces the exocytosis of neurotransmitters in the synaptic cleft, notably of glutamate, which over activates the N-methyl-D-aspartate (NMDA) receptors on the post-synaptic membrane (Figure 28). In turn, this causes excitotoxicity characterized by ROS overproduction and mitochondrial membrane permeabilization, which frees the cytochrome c, thus activating the apoptotic pathway (Thornton and Hagberg 2015). To avoid this deleterious glutamate accumulation, the brain relies on rapid uptake by glutamate transporters. However, hypoxic conditions inhibit astrocytic expression of GLAST-1 (glutamate-aspartate transporter) and glutamate transporter 1 (GLT-1) transporters, further enhancing glutamate accumulation (Dallas et al. 2007).

Moreover, GLT-1 is primarily expressed by astrocytes in the mature CNS but is transiently upregulated in the immature oligodendrocytes and a few neuronal populations towards the end of gestation (Pregnolato et al. 2019). These changes in GLT-1 expression may explain the selective vulnerability of immature oligodendrocytes and neurons in the preterm brain. Furthermore, increased GLT-1 levels have been reported in human infant post-mortem brains with cystic periventricular

INTRODUCTION

leukomalacia, a known sequela of AOP (Pregnolato et al. 2019), which would suggest the establishment of a defense mechanism against excitotoxicity during IH.

In turn, the extracellular glutamate excessively stimulates NMDA receptors, which triggers a large influx of Ca^{2+} , leading to the activation of different enzymes which degrade cellular components. The Ca^{2+} influx also induces depolarization of the mitochondrial membrane, leading to altered energy metabolism, which further decreases ATP production (Jia et al. 2015). A broad analysis of neuron cultures also showed that increased extracellular Ca^{2+} sensitized neurons to glutamate-induced excitotoxicity, which potentiated apoptotic cell death (Anilkumar et al. 2017). In addition, mitochondrial stress culminates in membrane rupture, releasing pro-apoptotic factors, such as cytochrome c and apoptosis inducing factor (AIF), into the cytosol which induce programmed cell death (Andreyev et al. 2018). The loss of integrity of the mitochondrial membrane also leads to the release of ROS into the cytosol, contributing to the general OS (Zorov et al. 2014).

Finally, the CNS is able to somewhat counteract hypoxia-induced excitotoxicity by regulating adenosine. This nucleoside is released mainly by neurons, but also by glial cells, either directly or after hydrolysis of extracellular ATP (Parkinson et al. 2002). Adenosine is released into the extracellular space by nucleoside transporters, including equilibrative nucleoside transporter 1 (ENT1 or Slc29a1), which is a regulator of intra- and extracellular neurotransmitter concentrations. Binding of adenosine to A1 receptors stimulates the K^+ channels involved in stabilizing the resting potential, thus blocking the propagation of action potentials (Lüscher et al. 1997).

Despite all the evidence demonstrating the induction of excitotoxicity by hypoxia, therapeutic strategies centered on glutamate receptor antagonism have not been effective, so far. However, the approach consisting of using the brain-to-blood glutamate efflux across endothelial cells of brain capillaries has been successful in some animal studies. Blood glutamate scavengers enhance the efflux phenomenon by neutralizing glutamate in the bloodstream, thus increasing the concentration gradient across the blood brain barrier, which further increases glutamate transport from the brain to the circulation (Leibowitz et al. 2012). Therefore, this neuroprotective process may be added to therapeutic options, along with the more well understood nitric oxide inhibitors and free radical scavengers which act downstream of glutamate activation of NMDARs (Jia et al. 2015). However, this strategy relies on a normal capillary vasculature, which may not be a given in certain cases of perinatal hypoxia.

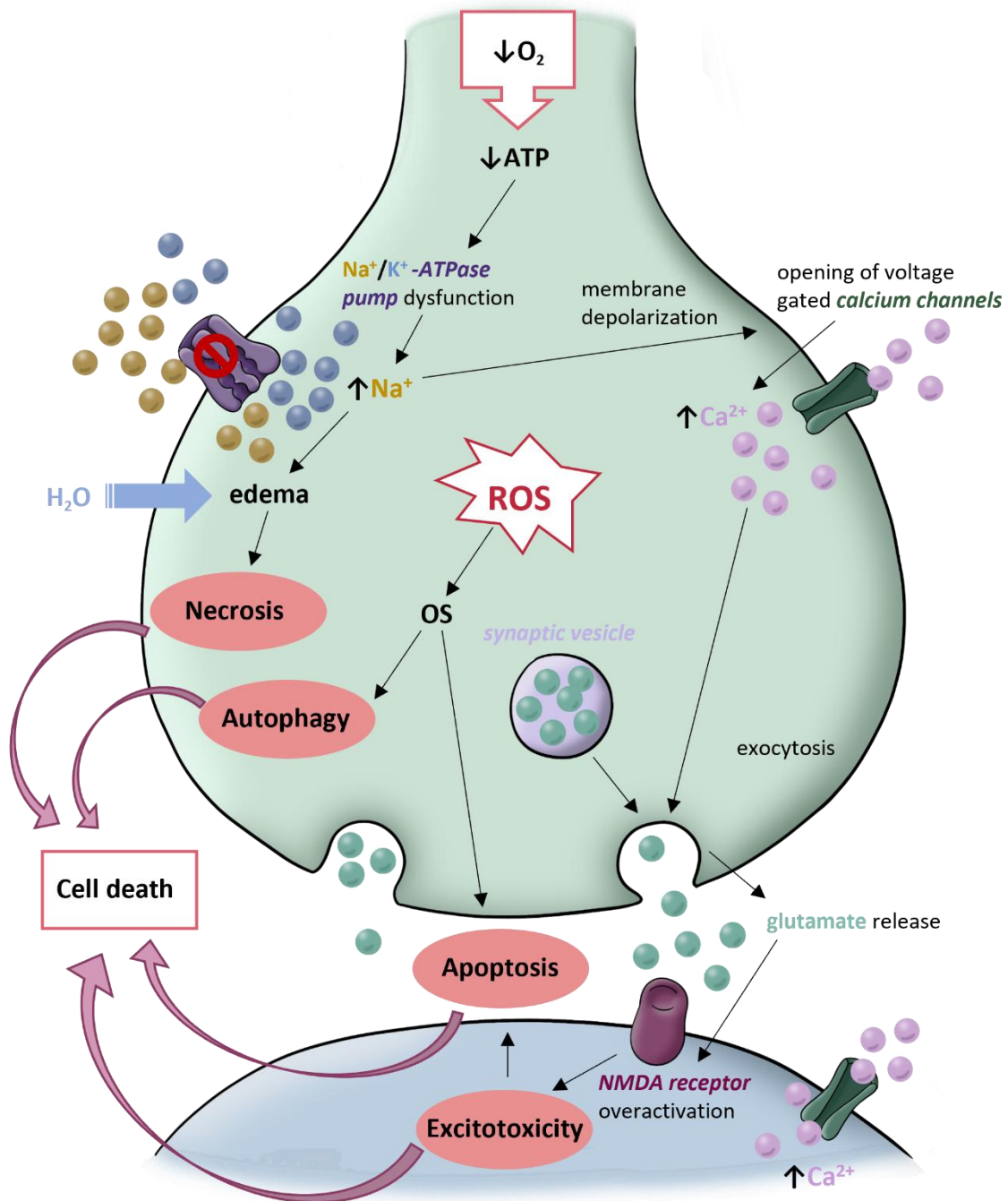


Figure 28: Schematic synapse representing the main neuronal death pathways induced by hypoxia.

O_2 deficiency induces a decrease in ATP production which leads to dysfunction of the Na^+/K^+ -ATPase pump. Na^+ accumulation causes edema which leads to necrotic cell death and membrane depolarization and allows glutamate exocytosis. The resulting excitotoxicity and oxidative stress cause activation of autophagic and apoptotic pathways that converge on cell death. ATP: adenosine 5'-triphosphate; Ca^{2+} : calcium ion; H_2O : water; K^+ : potassium ion; Na^+ : sodium ion; NMDA: N-methyl-D-aspartate; O_2 : dioxygen; OS: oxidative stress; ROS: reactive oxygen species.

INTRODUCTION

b. Cell death

As our knowledge of molecular pathways expands, so does our understanding of cell death. This has led to considerable research in the field, and the coining of numerous new terms to characterize cell death mechanisms (X. Liu et al. 2018). These processes are all morphologically distinct and are characterized by specific biochemical changes. Liu et al. postulate that there are only four types of cell death: two physiological cell death modes (apoptosis and senescent death), and two pathological modes (necrosis and stress-induced cell death). Additionally, there are processes that, in excess, may lead to cell death, but that have other physiological functions, such as autophagy (X. Liu et al. 2018). Based on the causal mechanisms, cell death can be grouped as: *i*) programmed cell death or apoptosis, *ii*) necrosis or necrosis-like cell death, *iii*) autophagy and response to metabolic stress, and *iv*) neurodegenerative cell deaths.

Apoptosis is a form of programmed cell death that affects individual cells while leaving neighboring cells intact. Programmed cell death is a physiological cell death that is essential to, and tightly regulated during development. During apoptosis, the cell shrinks, and the nuclear DNA condenses and fragments. Finally, the cell breaks down into apoptotic bodies encapsulated by a membrane, which will then be phagocytized (Elmore 2007). Apoptosis may be initiated by the extrinsic pathway, which is triggered by death receptors (e.g., FAS or TRAIL), or the intrinsic pathway, which begins in the mitochondria (via the Bcl-2 family proteins) (Green and Llambi 2015). The endoplasmic reticulum can also trigger apoptosis via molecules like IRE-1 and CHOP, as part of the stress-induced unfolded protein response (H.-F. Wang et al. 2018; Nirmala and Lopus 2020). In fact, endoplasmic reticulum stress has been implicated in IH-mediated cell death, and conversely, suppressing CHOP was found to reduce IH-driven apoptosis (Chang et al. 2019; Xu et al. 2021). These pathways all converge as the effector pathway, which is marked by the activation of caspase-3 (Elmore 2007). It was observed that chronic exposure of mice to IH induced caspase-3 activation and increased neuronal apoptosis, especially in the hippocampus (Xu et al. 2004; F. Liu et al. 2018).

Necrosis and necrosis-like cell deaths are not regulated and occur because of an injury or trauma. This can be seen as a consequence of IH-induced excitotoxicity and the resulting edema. However, a cell can initiate the necrotic cascade as a way to trigger inflammatory and/or reparative responses. Metabolic stress, such as low extracellular glucose availability, shifts cell death towards a mostly necrotic mechanism (Anilkumar et al. 2017). Cells undergoing necrosis swell, leading to membrane rupture, while organelles break down. The spill out of cellular contents to the extracellular space causes local inflammation that may induce the death of adjacent cells (Zong and Thompson 2006). In fact, membrane rupture is the chief characteristic of necrosis-like deaths such as

pyronecrosis, pyroptosis, and netosis, which are involved in the defense against infectious processes and in inflammation. Although research is still relatively scarce on these mechanisms, one study found elevated ROS and inflammatory markers in response to chronic IH in rats that culminated in pyroptosis of renal cells (Bai et al. 2022). Moreover, IH was found to aggravate neuroinflammation and pyroptosis after subarachnoid hemorrhage via HIF-1 α (J. Xu et al. 2022). Both hypoxia-reoxygenation and hypoxia-ischemia were found to induce necroptosis via the HIF-1 α or NF- κ B pathways (Yang et al. 2017; Zhu et al. 2018; Bertheloot et al. 2021). And finally, the less understood methuosis is usually associated with cancer cells and seems to involve the Bcl-2 family of molecules (Li et al. 2019; Nirmala and Lopus 2020).

Autophagy is a mechanism during which cells recycle their own organelles and macromolecular components that are non-essential, redundant, or damaged. It is an adaptive response to stressors, such as nutrient deficiency, which allows the cell to use its own metabolites as nutrients (Klionsky 2007). Beclin-1 initiates the formation of a phagophore, whose expansion will give rise to an autophagosome. This vesicle traps cytoplasmic material and fuses with a lysosome to create an autolysosome, in which cellular elements are hydrolyzed. These phenomena can, depending on the severity of hypoxia, induce autophagic death, or conversely contribute to cell survival by degrading deleterious cytosolic components thus regulating the intracellular concentration of ROS. In fact, it is postulated that autophagy is a defense mechanism against deleterious stimuli such as ROS, and may be a key component of neuronal homeostasis by being an effective compensation mechanism against acute stress (Fang et al. 2017). In IH, it was observed that cardiac cells induce autophagy to prevent apoptosis (Chang et al. 2019). However, if the exposure is repeated or prolonged, autophagy may still culminate in the activation of apoptotic pathways or in autosis. Indeed, there is a complex crosstalk between autophagy and apoptosis which, depending on the circumstances, may promote or inhibit cell death (Song et al. 2017). Alternatively, autophagy may culminate in autosis, which is characterized by dysfunction of the Na⁺/K⁺-ATPase pump and abundant autophagosomes (Liu et al. 2013). It is often seen as a result of O₂ depletion, such as in cerebral hypoxia-ischemia. In contrast, a glucose starvation triggers entosis, a form of cell cannibalism typically seen in cancer cells (Nirmala and Lopus 2020).

Finally, a few specific forms of cell deaths that have been reported in neurodegenerative diseases may be relevant to IH due to the molecular pathways they involve. Among these, ferroptosis is an iron-dependent cell death that is triggered by the presence of peroxidized lipids and is characterized by altered mitochondria. In fact, ferroptosis markers were found to be increased and associated with cognitive impairment in rats subjected to IH, suggesting the involvement of this pathway in IH-mediated neuronal death (Liu et al. 2023). Likewise, organelle dysfunction may be seen

INTRODUCTION

in lysosome-dependent cell death which involving cathepsins (Ctsb), or in parthanatos which is induced by the poly ADP-ribose polymerase (Parp) (Nirmala and Lopus 2020). Moreover, Ca²⁺ and ROS are known initiators of lysosome-dependent and mitopore cell deaths (Fricker et al. 2018). Interestingly, the endoplasmic reticulum was found to regulate parthanatos in response to OGD (H.-F. Wang et al. 2018). Thus, it is possible that this mechanism may be activated in response to oxygen deprivation alone. Due to the extensive crosstalk among all the cell death pathways discussed, it is likely that several mechanisms are responsible for the cellular consequences of IH.

3. Neurological implications of AOP

a. Clinical presentation

The brain, due to its important metabolic demand, is particularly sensitive to the damaging effects of hypoxia (Roemgens et al. 2011; Campanille et al. 2015). However, the neurological consequences of AOP are difficult to assess clinically because defects are often masked by alterations inherent to prematurity. Long-term sequelae are even more difficult to determine due to patient follow up and the time needed for the deficits to become apparent. Moreover, the vulnerability of the brain to the frequency, severity and duration of apneas is currently not well defined. Nevertheless, several studies have demonstrated a causal relationship between all these parameters and the development of neurological alterations in children.

A correlation has been established between the persistence of sleep apnea in infants, and the occurrence of neurodevelopmental deficits in children until up to 3 years of corrected age (Janvier et al. 2004). Likewise, it was found that the increased frequency and severity of apneas associated with bradycardia leads to increased mortality in infants and greater neurodevelopmental alterations at 13 months (Pillekamp et al. 2007). A broad analysis of the Canadian Oxygen Trial data, which included nearly 1,000 extremely premature infants, also reported an increased incidence of adverse neurological outcomes directly proportional with the amount of time the newborn spent with a pulse oximeter saturation (SpO₂) <80% related to AOP and disordered breathing. Indeed, the rate of occurrence of late death (after 36 weeks) or disability, the proportion of infants with cognitive or language delay, and the likelihood of developing motor deficits all increased proportionally the amount of time spent with low SpO₂ (Poets et al. 2015). Finally, the occurrence of five or more apneic events during the first two and a half months of life was associated with lower scores on the Bayley-II mental development index (Poets 2020). In older children, associations between sleep-disordered breathing, impaired cognition and academic achievements have been reported. The mechanism at the

origin of these sequalae is most likely induced by IH but a probable contribution of sleep disruption and sleep deprivation, or a cumulative effect of these three factors, should not be overlooked (Blunden and Beebe 2006; Poets 2020).

b. Experimental findings

In humans, the neonatal brain appears to be selectively vulnerable to oxidative stress, and perinatal hypoxia causes region-specific cell death depending on developmental stage (Ferriero 2001; Biran et al. 2011). Indeed, in preterm neonates, the periventricular WM is most affected while, at term, the basal ganglia are the most vulnerable (Ferriero 2001). Moreover, from an experimental standpoint, no animal model presenting with spontaneous apnea exists, and IH studies are very variable in their parameters (%O₂, frequency, duration, etc.). This makes difficult the identification of the neurological alterations due to AOP. Nevertheless, several similarities between the findings in humans and rodents have been highlighted, allowing for a better understanding of the mechanisms at play during AOP.

Thus, it has been demonstrated, that much like in humans, rodents exhibit learning, behavioral and motor deficits after IH. Indeed, a study showed that exposure to IH in rats beginning at P10 induces working memory deficits in male, associated with decreased dendritic branching in the frontal cortex, but not the hippocampus (Decker et al. 2003; Kheirandish et al. 2005). Interestingly, female rats, who did not present working memory deficits, had increased dopamine concentrations in the frontal cortex after IH (Kheirandish et al. 2005). The implication of dopamine in the physiopathology of AOP was confirmed by other findings in both rodents and humans. Thus, in rats, it has been shown that early exposure (from P7 to P11) leads to depressed dopaminergic signaling in both sexes (Decker et al. 2003). Likewise, in humans, a longitudinal study in a cohort of 9-year-old children indicates that only individuals carrying the A1 allele of the DRD2 Taq1A polymorphism related to the dopamine D2 receptor presented increased externalizing behaviors (e.g., hyperactivity, impulsivity, aggression) after a hypoxic exposure (White et al. 2019). This result also parallels the hyperlocomotive activity found in rats having experienced hypoxia (Decker et al. 2003).

From a cellular perspective, several rodent protocols have succeeded in reproducing AOP findings observed in humans (Cai et al. 2011; Cai et al. 2012). However, specific *in vitro* studies related to AOP remain very sporadic, and most use different modalities of hypoxia. Nonetheless, these works have helped us understand some cell mechanisms that could participate to the pathophysiology of AOP in the brain and the cerebellum.

INTRODUCTION

In fact, perinatal hypoxia was shown to affect several CNS structures such as the corpus callosum, striatum, frontal cortex, hippocampus, and cerebellum (Kheirandish et al. 2005; Cai et al. 2012; Darnall et al. 2017). More specifically, an IH protocol mimicking AOP was found to induce hypomyelination within both the peripheral and central nervous systems, and significant defects in oligodendrogenesis (Cai et al. 2011; Cai et al. 2012). In addition, perinatal asphyxia in rats revealed neuronal loss in the hippocampal area CA1, and morphological alterations in the cerebellar GL (Kohlhauser et al. 1999). Therefore, IH seems to alter a majority of the nervous system but the causal mechanisms are still to be determined.

In human newborns as in rat cultured GCs, NOS activation was observed after anoxia/reoxygenation, suggesting that that mechanism is a key effector of OS-induced neuronal damage (Ferriero 2001; Scorziello et al. 2004). Another mouse model sleep apnea study presented evidence that OS contributed to the pathogenesis of chronic IH-mediated neuronal apoptosis. They also demonstrated that the overexpression of SOD had neuroprotective effects in the cerebral cortex and neurocognitive dysfunction (Xu et al. 2004). Another mechanism brought forward is the induction of the endoplasmic reticulum stress response during IH, which was associated with cell death in the hippocampus and prefrontal cortex (Cai et al. 2014). The associated ROS overproduction may be due to the overactivation of NMDA receptors, which triggers the activity of oxidases (Ferriero 2001).

Regardless of the mechanism, the animal models also contributed to confirm that deficits are proportional to the number of reoxygenation episodes and thus correlated with the duration of IH. In fact, a hyperoxia model, akin to the reoxygenation phase of IH, has been shown to induce cerebellar damage with decreased proliferation of GCs, and delayed and impaired branching of PCs. These cell alterations are visible at P7 and are still present at P11 and P30, suggesting long-term damage (Scheuer et al. 2017). In fact, a single hypoxic episode during a developmentally critical time can cause lasting defects. Indeed, hypoxia in P2 rats caused cerebellar PC loss along with a proliferation deficit of in the EGL (Biran et al. 2011)

Finally, *in vitro* studies have led to understand the involvement of excitatory amino acids in hypoxic states. Indeed, glutamate, aspartate and glutamine were elevated in the hypothalamus of rats having undergone an asphyxia protocol, revealing the occurrence of an excitotoxic phenomenon, which might explain the observed behavioral deficits (Kohlhauser et al. 1999). It was also shown that IH is correlated with a deficit in LTP, which may be linked to the behavioral deficits associated with AOP, such as decreased motor coordination and impaired spatial learning (Goussakov et al. 2019). However, the molecular bases for AOP-induced alterations are still insufficiently understood, even more so when it concerns the involvement of the cerebellum.

OBJECTIVES

Despite its high incidence, AOP's impact on the CNS has not been fully explored. This is mostly due to the lack of spontaneous apnea animal model or robust reproducible protocol, which renders the comparison of the deficits observed difficult and even impossible. Indeed, the protocols found in literature are highly variable, whether in the rate of O₂ adjunction, the duration of IH cycles, or the age of the animals.

However, the protocol considered to mimic AOP the most accurately is that of Cai et al., since it reproduces the brain and behavioral alterations of AOP in humans (Cai et al., 2012). Thanks to their findings and observations, a hypoxia chamber mimicking AOP in mice was developed by our team and was used to better study the neurological effects of this pathology in a rodent model.

Furthermore, the involvement of the cerebellum in perinatal hypoxia-related sequelae has been largely overlooked. However, in humans as in rodents, cerebellar cell proliferation, migration and differentiation take place from the embryonic period until the first postnatal year (Volpe 2009), making it very vulnerable to perinatal incidents. Moreover, several neurological functions affected by AOP are, at least in part, controlled by the cerebellum, such as learning or motor coordination. These observations led us to hypothesize that perinatal IH could specifically target the immature cerebellum, altering its development and associated functions.

The results presented in **Article 1** (Leroux et al. 2022) highlight the histological and behavioral alterations resulting from our IH protocol. The goals of this project, were to:

- Understand the cellular effects of IH by focusing on proliferation, cell death, and OS. This was assessed via: *i*) BrDU injections to study the effects of IH on proliferation and migration; *ii*) ROS production and caspase-3/7 activity assays; and *iii*) RT-qPCR analysis of OS and apoptosis related genes at P12.
- Analyze the effects of IH general histology of the cerebellar cortex and cerebellar afferences. This was done via IHC experiments targeting: *i*) DAPI and calbindin; and *ii*) Gluδ2, VGlut2 and MBP.
- Determine how these alterations might affect behavior in the short and long term via a series of behavioral tests.

OBJECTIVES

These findings led us to design a series of experiments to better understand the molecular basis of the changes we observed, these results are presented as **Article 2** (Rodriguez-Duboc et al., in preparation). For our purpose, we aimed to:

- Pinpoint which developmental stage was most vulnerable to IH. To this end, we conducted experiments on key timepoints, namely P4, P8, P12, P21 and P70.
- Understand the molecular pathways at the base of the observed alterations. Accordingly, we devised 2 general processes to investigate: *i)* considering the effects of IH on cell death and oxidative stress observed at P12, we aimed to test a panel of genes related to OS (Lacaille et al. 2015); and *ii)* because of the histological delay in maturation induced by our IH protocol, we set out on creating a new panel of genes related to cell maturation and differentiation.
- Narrow down which cell types might be most impacted by IH and how. For this reason, we decided to use laser capture microdissection and test gene expression on each cerebellar layer separately.

The final and ongoing part of the work is centered on exploring possible vascular effects of IH. This part of the project is three-pronged:

- RT-qPCR testing of vascularization-associated genes on the whole cerebellum to determine their regulation by stage.
- Immunocytochemistry experiments followed by confocal microscopy to better understand how vasculogenesis is affected by IH in the context of cerebellar development.
- Clearing followed by light sheet microscopy to observe the density and morphology of the vascular network *in situ*.

This project is still underway but RT-qPCR results and preliminary imaging results are presented in this manuscript.

MATERIALS AND METHODS

I. ANIMALS

A. ANIMAL MODEL

We used wild type C57BL/6 mice born and bred in an accredited animal facility (approval number B.76-451-04) in accordance with the French Ministry of Agriculture and the European Community Council Directive 2010/63/UE of September 22nd, 2010, on the protection of animals used for scientific purposes. The integrality of animals used for this project were authorized under the APAFiS reference number 2015120915461786.

The mice were kept under a 12-hour light/dark cycle at +/- 21°C and had free access to food and water. Sex identification was done by both by anogenital distance measurement and pigment-spot localization (Wolterink-Donselaar et al. 2009). Mice were weighed every morning of the IH protocol prior to initializing the chamber.

B. HYPOXIA PROTOCOL

A hypoxia chamber was developed in the INSERM U1239 in collaboration with the Institute of Technology of the University of Rouen Normandy (Figure 29). The device is composed of a 21L (23x23x39 cm) Plexiglas enclosure, compliant with regulatory dimensions for rodent cages and allowing visual monitoring of the animals.

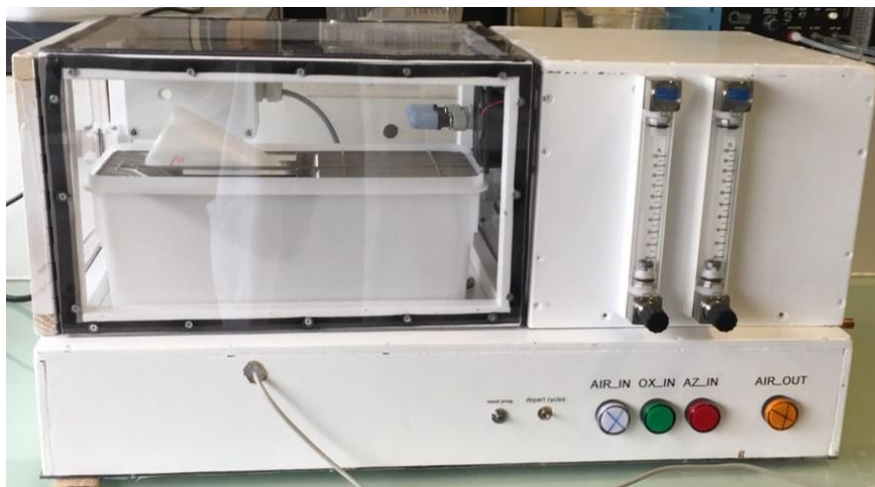


Figure 29: Hypoxia chamber containing a cage.

The transparent plexiglass allows for constant monitoring of the mice inside the chamber. Within the chamber are detectors for O₂, temperature, atmospheric pressure, and hygrometry. The front panel features the USB to connect to the controlling computer, on/off and reset button, as well as light indicators for the different gas input/output. The right-side box contains the tubing for the gas input and two flowmeters are visible for oxygen and nitrogen control.

MATERIALS AND METHODS

In addition, the chamber is equipped with several sensors that ensure the monitoring of different parameters including O₂, temperature, atmospheric pressure, and hygrometry. The induction of hypoxia is achieved by the injection of nitrogen, while the return to normoxia is done by an ambient air injection via a pump at a flow rate of 60L/min, associated with pure O₂ for a faster transition. In the chamber, a fan allows to mix the gases which reach the enclosure via copper pipes (8 mm in diameter) and PVC tubes (10 mm in diameter).

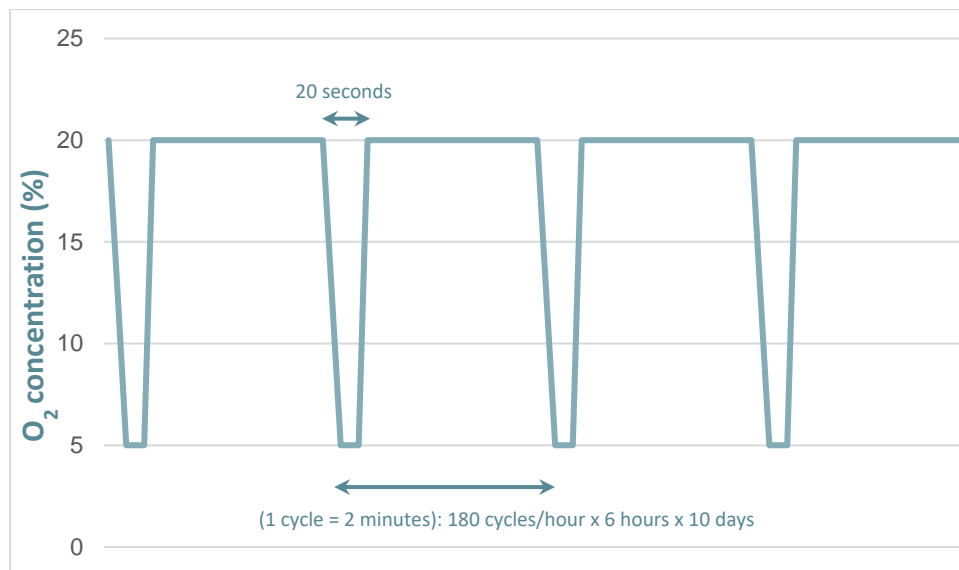


Figure 30: Schematic representation of oxygen levels in the hypoxia chamber.

Graph showing the O₂ concentration in the hypoxia chamber plotted against time during the intermittent hypoxia (IH) protocol. The hypoxia/reoxygenation cycles last 2 minutes, including 20 seconds of hypoxia at 5% O₂ and then a return to 21% O₂, repeated for 6 hours, each day for 10 days, from P2 to P12. O₂: oxygen. Px: postnatal day x.

In order to reduce the sound intensity as much as possible and to maintain comfortable warmth, 5-meter-long PVC pipes were used, with silencers installed at each gas inlet. The gas flows entering the device are controlled upstream by pressure gauges, flowmeters, and solenoid valves. The automatization of the IH cycles is done through an Arduino board connected to the valves and an oxygen sensor. The board was programmed to adjust O₂ flow based on the measured O₂ levels. The whole system is connected to a portable computer used to initiate the procedure manually. Therefore, the opening of the solenoid valves and the starting of the pump are synchronized to the protocol. The software also allows to track and record the data transmitted by the different sensors and to follow in real time the environmental parameters in the chamber.

At age P2, the IH groups were placed with the dams in the hypoxia chamber, where they experienced repeated episodes of hypoxia and reoxygenation (Figure 30). Each cycle lasts 2 minutes and consists of: *i*) a 40-second nitrogen diffusion phase to decrease the ambient O₂ level in the

chamber, *ii)* a 20-second hypoxia ($\approx 5\% O_2$) during which the chamber is a closed system, *iii)* a 20-second reoxygenation step through an influx of both ambient air and pure O_2 , and finally *iv)* a 40-second normoxia ($\approx 21\% O_2$) phase where equilibrium with ambient air is maintained. These cycles are repeated during 6 hours throughout the sleep phase of the animals (10 am - 4 pm) for 10 days maximum, or until the desired stage. The corresponding control group, designated normoxic (N), was placed with their dam in an open-air cage in contact with the hypoxia chamber. Thus, they were simultaneously exposed to the same noise, vibrations, and stress conditions to minimize environmental experimental bias.

C. COLLECTION OF BIOLOGICAL MATERIAL

This project relies on the use of a murine model, which presents the advantage of having postnatal stages corresponding the human perinatal period (Figure 31). We chose the stages: P4 (peak GC proliferation and PC monolayer), P8 (Peak GC migration and primary PC dendrite), P12 (PC dendrite branching and CF innervation), P21 (EGL absent and mature PCs), and P70 (maturity and long-term effects).

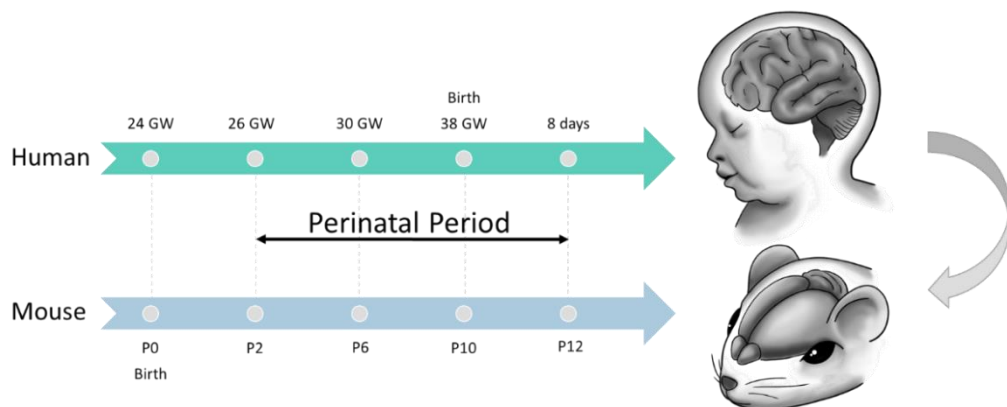


Figure 31: Correspondence of the human perinatal period to postnatal murine stages.
GW: gestational week; Px: postnatal day number “x”.

For laser-capture microdissection and real-time quantitative polymerase chain reaction (LMD/RT-qPCR) experiments, mice were sacrificed at stages P4, P8, P12, P21, and P70 by decapitation after being anesthetized by isoflurane inhalation (1000 mg/g iso-vet[®]). Whole brains were immediately harvested, rinsed in RNase-free phosphate buffer saline (PBS), and set into pure isopentane kept at -30°C. They were then stored in sterile containers at -80°C until further use.

MATERIALS AND METHODS

For **clearing and immunohistochemistry** studies, mice underwent lethal anesthesia by intraperitoneal injection of ketamine (100 mg/kg) and xylazine (10 mg/kg) and were then sacrificed by intracardiac perfusion of NaCl 9% followed by paraformaldehyde 4%. Brains were rapidly removed, fixed overnight in 4 % paraformaldehyde (PFA), and stored in PBS with sodium azide until used. In the case of bromodeoxyuridine (BrdU) testing, animals received intraperitoneal injections of BrdU (50 mg/kg) at P6 to assess the capacity of GC precursors to divide and migrate during the days following the IH protocol, and again, 4 h before euthanasia to analyze GC precursors' immediate ability to proliferate at P12.

II. REAL-TIME Q-PCR

A. BIOINFORMATICS

The bioinformatics component of this project relied on the availability of genomic databases and primer sets. The **Oxidative Stress panel (Appendix 1)** was developed in the team and was available on the Primacen platform (Lacaille et al. 2015). The **Neurodevelopment panel (Appendix 2)** was developed through my thesis work and relied on the Cerebellar Development Transcriptome Database (Figure 32; CDT-DB <http://www.cdt-db.brain.riken.jp>). This annotated experimental database includes transcriptomic data during different developmental stages on a genome-wide basis in a layer-specific manner (Sato et al. 2008). The **Vascularization panel (Appendix 3)** was constituted based on bibliographical data and enrichment. Gene annotation, pathway identification and functions were investigated and illustrated with the Cytoscape software and stringR enrichment database.

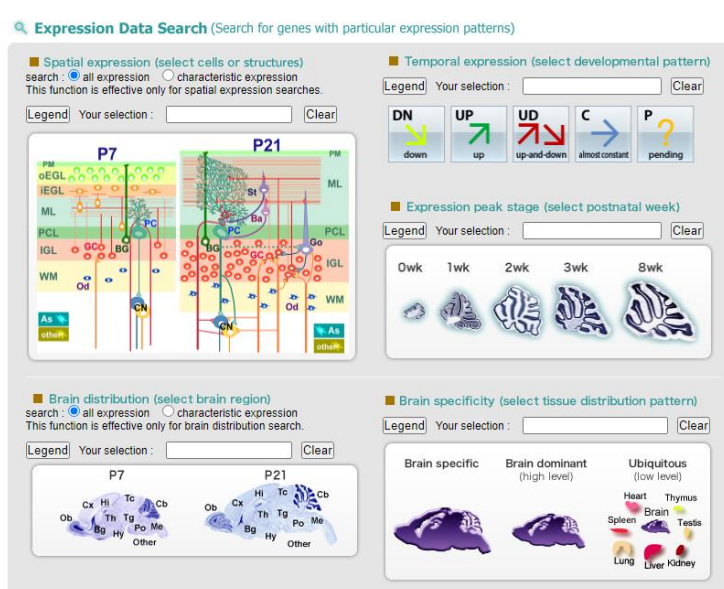


Figure 32: Sample of the Cerebellar Development Transcriptome Database setup.
This resource allows for the choosing of a developmental stage, cerebellar layer, and regulation.

B. PRIMER DESIGN

For each of the chosen genes, messenger ribonucleic acid (mRNA) and exon junction sequences were retrieved from the NCBI PubMed database using the R package {rentrez} (Winter 2017). Based on those sequences, gene primers were designed with the software Primer Express (v3.0.1; ThermoFischer Scientific) using nucleotide sequences from the NCBI Pubmed database. Primer pairs were chosen preferentially to be on exon joining sites, with the least possible hairpin and dimer formation, and with similar size, GC percentage and melting temperature for the forward and reverse primers (Figure 33). Each sequence was then blasted on Pubmed to ensure specificity. See Appendices 1-3 for primer pair sequences and specifications.

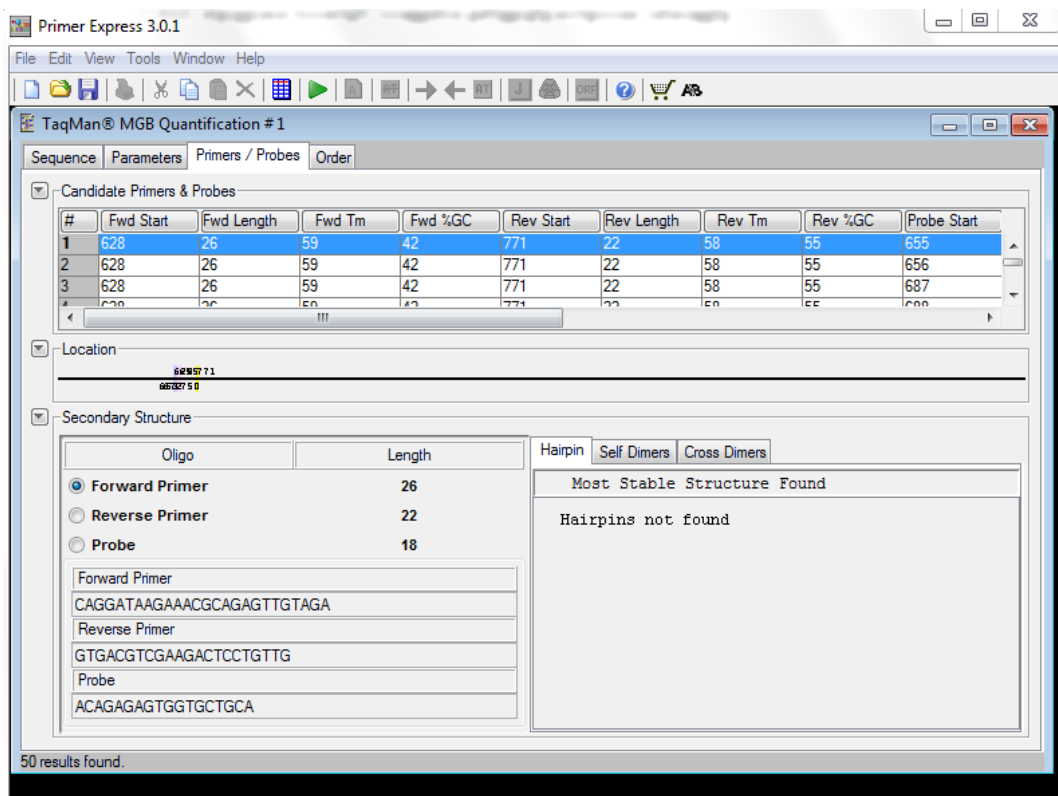


Figure 33: Sample of the parameters available on Primer express.

Primer pairs are chosen preferentially to be on exon joining sites, with the least possible hairpin and dimer formation, and with similar size, GC percentage and melting temperature for the forward and reverse primers.

Validation of each primer pair was done using serial dilutions of wild-type genetic material from whole cerebellum extract on 384 plates. A linear regression was plotted of the Cq as a function the log of the concentration to assess the validity of the primer pair to quantify nucleic acids. A slope between -3.2 and -3.5 and an $R^2 > 0.98$ were considered satisfactory (Figure 34).

MATERIALS AND METHODS

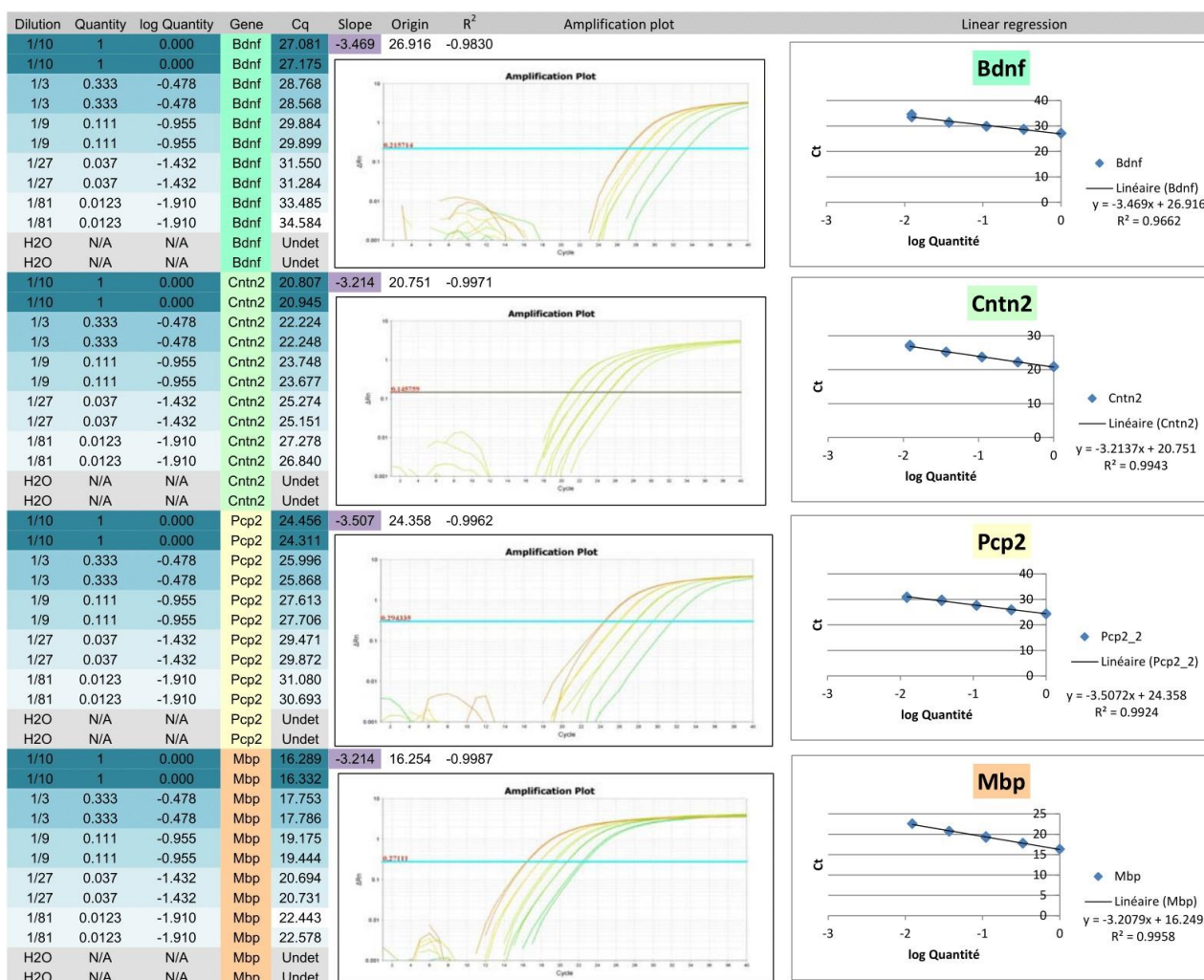


Figure 34: Sample of the validation process done for each primer pair for the RT-qPCR experiments.
 Serial dilutions of a control cDNA are distributed on the plate along with a mix of SYBRgreen, forward primer and reverse primer. A linear regression is plotted of the Cq as a function the log of the concentration to assess the validity of the primer pair to quantify nucleic acids. On the right column are screenshots of the amplification curves from the QuantStudio device.

C. LASER CAPTURE MICRODISSECTION

Frozen brains were transferred to a -20°C freezer two hours prior to use. Brains were fixed to the refrigerated support (set to -20°C) of the Cryomicrocut (Leica 3050) with cryotomy embedding medium (cat. 4583 Tissue-Tek® O.C.T. Compound, Sakura) by the frontal extremity. Cerebella were then cut into 14 micrometers-thick slices with a blade kept at -18°C. Slices were immediately placed on membrane coated slides (cat. 415190-9041-000 1.0 PEN, Carl Zeiss SAS) previously sterilized with dry heat (3 hours at 170°C). Each slide was dipped for 5 seconds in 100% ethanol at -20°C to preserve RNA and then stained with a 2.8% cresyl violet solution in 70% pure ethanol and progressively dehydrated in ethanol solutions of increasing concentrations (50%, 70%, 100%).

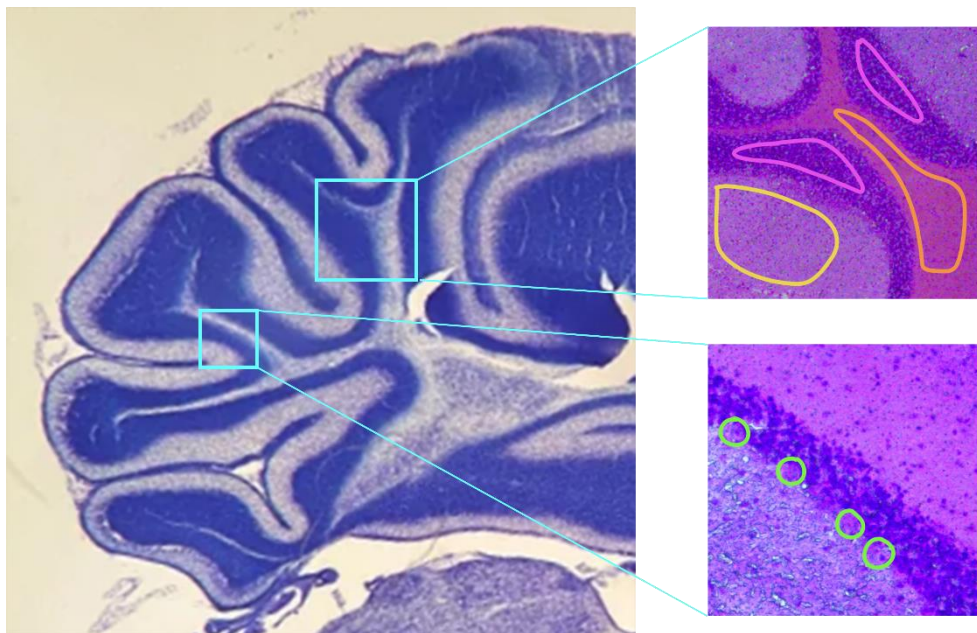


Figure 35: Example of a slice stained with cresyl violet.

Representation of surfaces that would be selected: internal granular layer (pink); molecular layer (yellow); white matter (orange); Purkinje cells (green). x5 zoom top, x20 zoom bottom.

Surfaces of $700,000 \mu\text{m}^2$ (for the EGL, IGL, ML, and WM layers) and $130,000 \mu\text{m}^2$ (for approximately 300 individual PCs) were drawn and cut with the Laser Capture Microdissection microscope and software (Figure 35; Leica Microsystems Laser Microdissection System) and kept in lysis buffer (from the RNA extraction kit mentioned below) on ice until RNA extraction.

D. RNA EXTRACTION

The mRNAs were purified on column using the Nucleospin RNA plus XS extraction kit by Macherey-Nagel (cat. 740 990 250) according to manufacturer recommendations. RNA quantity and purity are analyzed by UV spectrophotometry (Nanodrop Technologies). The optical density (OD) of RNA is read at 230, 260, and 280 nm. The ratios OD 260 nm/OD 280 nm and OD 260 nm/DO 230 nm are calculated as indicators of protein, and salt/ethanol contamination, respectively. These ratios should be between 1.6 and 2.0 for the sample to be considered acceptable.

As per the MIQE guidelines (Bustin et al. 2009), mRNA quality assessment was performed by gel electrophoresis on RNA 6000 Pico chips (cat. 5067-1513, Agilent). The analysis of the migration of RNAs in the gel allows the calculation of the RNA integrity number (RIN). RNAs are considered to be

MATERIALS AND METHODS

of good quality when these values are homogeneous and between 7 and 10 (Figure 36). The mRNAs were then stored at -80°C until the next step.

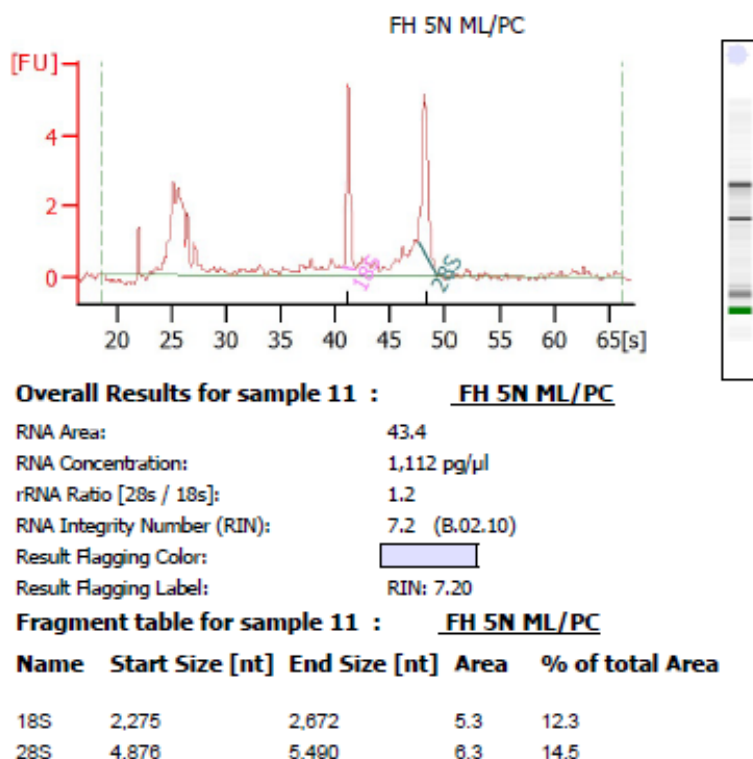


Figure 36: Example of quality assessment of a suitable RNA sample.

Results from gel electrophoresis on RNA 6000 Pico chips. RIN values above 7 are deemed adequate.

E. RETROTRANSCRIPTION AND QPCR

Total mRNAs were retrotranscribed to cDNA by reverse transcription using *i*) the Quantitect RT Kit from Qiagen (cat. 205313) for surfaces of 700,000 µm² or *ii*) amplified and retrotranscribed with the SMARTer® Pico PCR cDNA Synthesis Kit and Advantage® 2 PCR Kit (cat. 634928/7 and 639207 from Takara) for Purkinje cells.

The determination of the relative expression of genes of interest (GOIs) was done by quantitative polymerase chain reaction (qPCR) in 384-well plates (Applied Biosystems), in the presence of Fast SYBR Green PCR Mastermix (Thermofisher, cat. 4385612) and target gene-specific sense and antisense primers (Appendices 1-3). The distribution of cDNA samples and reaction mixes is performed by the Bravo 1 pipetting robot available on the Primacen platform. For each gene in the panel, the sample is measured at least in duplicate, with at least two housekeeping genes (HKGs) from Table 1.

Gene	Name	Function	NCBI reference	Primer pair sequence	
Gapdh	glyceraldehyde-3-phosphate dehydrogenase	glucose metabolism	NM_001289726.1	Forward	CATGGCCTCCGTGTTCTA
				Reverse	CCTGCTTACCACTTCTTGA
Hsp90ab1	heat shock protein 90 alpha (cytosolic), class B member 1	signal transduction	NM_008302.3	Forward	CAGAAATTGCCAGCTCATGT
				Reverse	CCGTCAAGGCTCTCATATCGAA
Ppia	peptidylprolyl isomerase A	protein folding	NM_008907.1	Forward	CCACTGTCGTTTCGCCGC
				Reverse	TGCAAACAGCTCGAAGGAGACGC
Ywhaz	tyrosine 3-monooxygenase / tryptophan 5-monooxygenase activation protein zeta	signal transduction	NM_011740.3	Forward	AGGACCTAAAGGGTCGGTCA
				Reverse	CGGGGTTTCTCCAATCACT

Table 1: Housekeeping genes primer pair sequences and specifications.

At least two were present on each plate. Values were averaged prior to $2^{(-\Delta\Delta Cq)}$ calculation.

The quantitative PCR reaction takes place in the QuantStudio Flex 12k thermal cycler (Applied Biosystems). Raw data output gives quantification cycle (Cq) values. Results are then calculated via the $2^{(-\Delta\Delta Cq)}$ method which allows relative quantification of gene expression within an experimental condition. This value is defined by the formula:

$$2^{-\Delta\Delta Cq} = 2^{(-(Cq_{GOI_{IH}} - Cq_{HKG_{IH}}) - (Cq_{GOI_N} - Cq_{HKG_N}))}$$

III. IMMUNOHISTOCHEMISTRY

A. SAMPLE PREPARATION

For this purpose, cerebella previously fixed with 4% PFA were retrieved, cut into 40 µm-thick slices with a vibratome (Leica Microsystems VT1000S), and placed in a 24-well plate. Non-specific site blocking was first performed for one hour in the presence of normal donkey serum (NDS) diluted 1:50 in an incubation solution containing 1X PBS, Triton X-100 (0.3%) and bovine serum albumin (1%). The slices are then incubated overnight at 4°C with specific primary antibodies (Table 2). Afterwards, the slices are rinsed with 1X PBS, and incubated for 2 hours at room temperature with the corresponding secondary antibodies diluted at 1:300 (Table 2). This step is followed by 3 additional PBS 1X rinses. The slices are then incubated in the presence of 4',6'-diamidino-2-phenylindole (DAPI; 1 µg/mL) for 1 minute for nuclear labeling. After a final rinse, the sections are mounted on slides using Mowiol

MATERIALS AND METHODS

B. ANTIBODY CHOICE

Primary Ab	Target	Dilution	Species	Supplier	2 nd Ab
Angpt2	Secreted molecule	1:300	Rabbit	Cell signaling technology (#2948)	DAR 488
BrdU	Migratory/proliferative cell	1:400	Sheep	Abcam (#ab1893)	DAS 633
Calbindin	Purkinje cell	1:1000	Mouse	Sigma Aldrich (#C9848)	DAM 594
Cleaved caspase-3	Apoptotic cell	1:400	Rabbit	Cell signaling technology (#9661S)	DAR 488
GFAP	Astrocyte (Bergmann glia)	1:600	Rabbit	Dako (#Z0334)	DAR 488
Gluδ2	Parallel fibers	1:500	Goat	Santa Cruz (#sc26118)	DAG-488
MBP	Myelinated fibers	1:300	Rabbit	Sigma-Aldrich (#M3821)	DAR 488
Phospho-Tie2	Endothelial cells	1:300	Rabbit	Cell signaling technology (#4221)	DAR 488
Podocalyxin	Capillaries	1:200	Goat	R&D Systems (#AF1556)	DAG 594
Tie2	Endothelial cells	1:300	Mouse	Cell signaling technology (#4224)	DAM 594
Vegf-B	Secreted molecule	1:300	Rabbit	Cell signaling technology (#2463)	DAR 488
VGlut	Climbing and mossy fibers	1:500	Guinea pig	Millipore (#AB2251)	DAGp-Cy3
α-SMA-Cy3	Arteries	1:500	Mouse	Sigma-Aldrich (#C6198)	N/A

Table 2: Antibodies used for immunohistochemical experiments.

Ab: antibody; Angpt2: angiopoietin 2; BrdU: bromodeoxyuridine; DAG: donkey anti-goat; DAGp: donkey anti-guinea pig; DAM: donkey anti-mouse; DAR: donkey anti-rabbit; DAS: donkey anti-sheep; GFAP : glial fibrillary acidic protein; Glu δ 2: glutamate receptor delta2; MBP: Myelin binding protein; α -SMA: smooth muscle actin alpha; Tie-2: tyrosine kinase with ig and egf homology domains-2; Vglut2: vesicular glutamate transporter 2; Vegf-B: vascular endothelial growth factor.

C. IMAGING

The study of the thickness of the cortical layers of the cerebellum was performed using an Eclipse 600D upright microscope (Nikon). The acquisition of the cleaved caspase-3 was performed under a widefield microscope (PRIMACEN, Thunder 3D, Leica). These data were analyzed with the ImageJ software, version 1.46 (Schindelin et al. 2012). Proliferation, migration, and dendritic arborization of PCs were observed on the TCS SP8 MP confocal microscope (Leica Microsystems). Quantification was done using the ImageJ software for proliferation/migration images and with Imaris software for VGlut, Glu δ 2, MBP, and co-localization images (BitPlane, South Windsor, CT, USA).

IV. CLEARING

A. SAMPLE PREPARATION

For this part of the project, cerebella previously fixed with 4% PFA were retrieved underwent a clearing protocol (Table 3). The samples are dehydrated by being submerged in increasing concentrations of methanol (MeOH; 20%, 40%, 60%, 80% and 100%). Dehydrated samples then undergo a bleaching phase by being transferred to a solution composed of 5% H₂O₂ (hydrogen peroxide) and 95% MeOH for 24 hours in order to decrease tissue autofluorescence. The samples are then rehydrated by a decreasing solution of MeOH (80%, 60%, 40% and 20%), washed in a rinsing solution PTx.2 (Table 3), and then permeabilized for one day at 37 °C under agitation with a solution containing 1X PBS, 0.2% TritonX-100, 20% dimethyl sulfoxide (DMSO), glycine (23 mg/mL) and thimerosal at 0.1 g/L (antifungal). The non-specific binding sites are, subsequently, blocked with a 1X PBS solution containing 0.2% Triton-X100, 10% DMSO, 6% NDS and thimerosal for one day at 37 °C with agitation.

Thereafter, the brains are incubated with the desired primary antibodies (Table 4) diluted in PTwP solution, containing 5% DMSO and 3% NDS at 37 °C under agitation for 6 days. After 6 rinses with PTwH at room temperature, the samples are incubated for 5 days with the secondary antibodies (Table 4) diluted in PTwH containing 3% NDS at 37°C under agitation. The brains are then rinsed several times with PTwH at room temperature under agitation, followed by dehydration in MeOH baths of increasing concentration (20%, 40% and concentration (20%, 40%, 60%, 80% and 100%). A delipidation of the brains is then performed by incubation in a solution containing 66% dichloromethane (DCM) and 33% MeOH for one night under agitation and then in DCM for 30 minutes. These last two steps allow to homogenize the refractive indexes of the cellular structures and to induce their transparency once placed in dibenzylether (DBE).

Solution	Reagents
PTx.2 (1 L)	100 mL PBS 10X + 2 mL TritonX-100 + Q.S. distilled water
PTwH (1 L)	100 mL PBS 10X + 200 µL Heparin (50 mg/mL) + Q.S. distilled water
Permeabilization solution (500 mL)	400 mL PTx.2 + 100 mL DMSO + 11,5 g glycine
Blocking solution (50 mL)	42 mL PTx.2 + 5 mL DMSO + 3 mL NDS
Primary Ab incubation solution (50 mL)	2.5 mL DMSO + 1.5 mL NDS + Q.S. PTwH
Secondary Ab incubation solution (50 mL)	1.5 mL NDS + Q.S. PTwH

Table 3: Composition of the solutions of the clearing protocol.

Ab: antibody; DMSO: dimethyl sulfoxide; NDS: normal donkey serum; PBS: phosphate buffer saline.

MATERIALS AND METHODS

B. ANTIBODY CHOICE

Primary Ab	Target	Dilution	Species	Supplier	2 ^{ry} Ab	Dilution
Calbindin	Purkinje cell	1:1000	Mouse	Sigma Aldrich (#C9848)	DAM 488	1:300
Podocalyxin	Capillaries	1:200	Goat	R&D Systems (#AF1556)	DAG 594	1:200
α-SMA-Cy3	Arteries	1:500	Mouse	Sigma-Aldrich (#C6198)	N/A	N/A
PECAM1	Arterioles	1:200	Rat	Millipore (#CBL1337)	DARt 594	1:400

Table 4: Antibodies used for the 3D visualization of blood vessels.

Ab: antibody; DAG: donkey anti-goat; DAM: donkey anti-mouse; DARb: donkey anti-rabbit; DARt: donkey anti-rat; GalC: galactocerebrosidase; α-SMA: smooth muscle actin alpha; PECAM1: platelet endothelial cell adhesion molecule 1.

C. IMAGING

The 3D acquisitions of the transparent cerebella were performed by Dr. David GODEFROY (INSERM U1239) on the Ultramicroscope II (LaVision BioTec, Bielefeld, Germany) using the software InspectorPro (LaVision BioTec, Bielefeld Germany). Quantification and image analysis was done using the Imaris software with the help of Camille Racine, M2 student.

V. BEHAVIORAL STUDIES

The behavioral studies were conducted by Dr. Sarah LEROUX and Dr Arnaud ARABO in the animal facility, and I contributed with the statistical analysis of the results. They are featured here to facilitate the interpretation of results.

The **righting reflex test** assesses the pups' locomotor coordination by placing them in a supine position and measuring the time needed to recover a completely prone position. Two daily consecutive trials were performed on each pup from P2 to P11 with a 60-second cut-off period.

The **grasping reflex** test determines the pups' forepaw strength and motor skills. The pups were set hanging by their forepaws on a stretched string and the latency to fall was measured. Two daily consecutive trials were performed on each pup from P2 to P11 with a 60-second cut-off period.

A ***muscular strength test*** was conducted by having the mice held by the tail and allowed to grasp a string with their forepaws. Then, they were progressively pulled backward by the tail. The maximal force was recorded by a dynamometer linked to the grip-strength apparatus. Four trials were performed on each mouse at P21.

The ***actimetry test*** was used to observe spontaneous behavior in P63 mice by placing them in the middle of a 45x45x30 box and recording their spontaneous locomotor activity during 10 minutes with the video tracking software Any-MAZE. Various parameters, such as distance traveled, mean speed, grooming time, and the number of rearing were measured and logged.

The ***elevated plus maze*** is designed to evaluate anxiety in mice by using their innate preference for dark and enclosed spaces. P64 mice were placed at the intersection of a maze consisting of 2 opposed closed arms intersecting 2 opposed open arms. The movements of the animals were tracked for 5 min with the Any-MAZE software. The time spent and the number of entries in each arm were recorded.

The ***horizontal beam test*** was conducted to check the mice's motor coordination. They were placed on a wooden beam (1 m length, 0.5 cm diameter), and the time needed to cross the beam and number of missteps were recorded. Three trials were performed on each mouse at P53.

The ***Morris water-maze test*** evaluates spatial learning and memory. It requires a round pool of 120 cm in diameter, surrounded with visual clues and filled with water mixed with an opaque white dye. Each mouse aged P53 was given 60 seconds to habituate to the pool. Then, a cue session was performed at P56 and during 5 consecutive days, corresponding to the acquisition and consolidation phases. An invisible platform was placed in the northwest quadrant and submerged approximately 1 cm below the water surface. Each animal was placed in the pool and had 60 seconds to find the platform and to stay on it for 5 seconds. If mice did not find the platform, they were gently guided to it and stayed there for 20 seconds. Four trials with different starting positions were performed each day. On the last day, a probe session was conducted, referring to the retrieval phase. The platform was removed from the pool and each mouse was placed in the center of the pool. Mice were given 60 seconds to explore the environment. Their behavior, trajectory, and different parameters such as freezing time or distance traveled, were recorded via the video tracking software Any-MAZE.

MATERIALS AND METHODS

VI. STATISTICAL ANALYSIS

A. CONCEPTS

Statistical analysis was performed on R version 4.2 (R Core team, 2022). All data types (RT-qPCR, IHC and behavioral) were modeled through the generalized linear mixed model (GLMM) framework, using the {glmmTMB} package (Brooks et al. 2017).

GLMM (also called multilevel models or hierarchical models) are a class of statistical models extending the standard linear models (which include t-tests and ANOVA as special cases). It allows modeling of a wider variety of phenomena by relaxing the linear models' main assumptions, namely the assumptions of normality of the residuals, of linearity, of homogeneity of variance (aka homoscedasticity), and of independence of the observations.

GLMM can model non-Gaussian conditional distributions, which often arise from biological processes. For example, strictly positive and continuous variables such as weights, areas, or lengths, are usually best modeled with a Gamma distribution, whereas variables with a theoretical lower and upper bound, like proportions, would be best represented by a binomial or a Beta distribution. Those non-Gaussian distributions have the additional property of having a non-constant mean-variance relationship, meaning that expected mean of a group will systematically affect its expected variance or shape, which allows them to naturally account for heteroscedasticity.

The linearity assumption is relaxed by modeling an arbitrary function of the response variable instead of the response itself. The transformed response is the one assumed to vary linearly with the predictors, and the function used for this transformation is called the *link function*, while the transformed response is said to vary on the *link scale*. This allows the modeling of many physical phenomena for which the linearity assumption is unrealistic.

Finally, GLMM can model non-independent observations by including a combination of fixed and random effects as predictors. Fixed effects are our predictors of interest (i.e. our treatments and relevant covariates), while random effects are parameters allowing us to explicitly account for the non-independence of samples that are temporally or hierarchically related (e.g. like pseudo-replicates taken from the same mouse) (Harrison et al. 2018; Zimmerman et al. 2021). Random effects define specific variance-covariance matrices that will, if they appropriately model the structure of the data, account for the parts of the response's variance that are not explained by the fixed effects. Random effects can range from simple random intercepts for independent clusters containing exchangeable measures, to more complex combinations of random intercepts and slopes for longitudinal measurements on the same individual (e.g., evolution of a measure across time). Compared to

ignoring or simply averaging pseudo-replicates, explicitly including the appropriate random grouping structure helps improve power and generalizability, lower the rate of false positives, and lead to better inferences about fixed effects (Barr et al. 2013; Aarts et al. 2015; Brauer and Curtin 2018).

The fitness of each of our models was evaluated through both visual checks (e.g., posterior predictive checks, QQ plots, residuals vs predicted values) and quantitative indices of model fit (e.g., AIC: Aikake information criterion). When several competing models were possible a priori, we selected the most plausible one primarily based on our theoretical understanding of the response properties and its causal relationship to our predictors of interest, and, to a lesser extent, to minimize AIC and favor model parsimony (Bates et al. 2015). For example, even if a Gaussian likelihood had the best fit on a given sample of data, a Gamma likelihood would still be favored for a response known to be continuous and strictly positive, in order to get better out-of-sample generalization, and thus more valid inferences. Those checks were made using the {DHARMA} (Hartig 2022) and {performance} (Lüdecke et al. 2021) packages.

Contrasts and p-values for relevant hypotheses were obtained using the {emmeans} package (Lenth 2022). They were computed on the link scale, using Wald t-tests, without any multiplicity adjustments. For all analyses, $p < 0.05$ was considered significant.

B. SPECIFICS

1. RT-qPCR

For RT-qPCR data, a Gaussian likelihood with an identity link function was used to model the distribution of the delta Cq (DCq) for each gene of interest. When samples for one gene were split over multiple plates, a random intercept was added to account for intra-plate correlations.

2. IHC

Immunohistochemistry data consisted of many types of measures, which required different likelihood families. Count data (e.g., cell counts) were modeled using Generalized Poisson likelihoods to account for potential over or under-dispersion. Measures bound at 0 (e.g., cell density, areas, and volumes) were modeled using a Gamma likelihood, and proportions (e.g., ratios of areas) with a Beta likelihood. When multiple measures were taken from the same mouse, a mouse random intercept was added.

MATERIALS AND METHODS

3. Behavioral experiments

Similarly, behavioral measures were varied and required the use of various types of distributional families (i.e., Gamma likelihoods for durations and weights). When multiple measures were taken from the same mouse in the same condition, a random intercept per mouse was added. The temporal dependency of measures such as changes in weight over time, or the evolution of mice's performance in Morris water maze over developmental stages, was accounted for using an autoregressive factor of order one.

4. Data availability

The data and R code for the analyses of the article "Intermittent hypoxia in a mouse model of apnea of prematurity leads to a retardation of cerebellar development and long-term functional deficits" were open-sourced on GitHub and archived through Zenodo (Rivière and Rodriguez-Duboc 2022). A website documenting those analyses was generated using the {Quarto} scientific publishing system (Allaire 2022), to allow interested readers to explore our models' outputs without having to run the code themselves. It is available at <https://ma-riviere.github.io/LT-AOP-22/>. The same process will be followed for the journal article currently in preparation.

RESULTS

I. PART ONE: COMPLETED WORK

A. JOURNAL ARTICLE 1

1. Presentation

Intermittent hypoxia in a mouse model of apnea of prematurity leads to a retardation of cerebellar development and long-term functional deficits.

S. Leroux, A. Rodriguez-Duboc, A. Arabo, M. Basille-Dugay, D. Vaudry and D. Burel.

Published September 6th, 2022, in Cell and Bioscience.

My contributions to this work consisted in:

- Part of the IH protocols
- BRDU injections
- GluRδ2 image acquisition
- Vglut image acquisition
- RT-qPCR experiments
- Statistical analyses
- Part of the writing

Our main findings, as summarized in figure 37 (c.f. page 142):

- P12 mice present OS and delayed maturation of the cerebellar cortex after IH.
- IH mice present with growth retardation and motor disorders at P12.
- A compensatory mechanism takes place to reestablish an unaltered organization at P21.
- Purkinje cells abnormalities such as the dendritic densification, the increase in afferent innervation, and axon hypomyelination persist in the long term.
- Adult mice still present an impairment and significant disorders in spatial learning.

RESEARCH

Open Access



Intermittent hypoxia in a mouse model of apnea of prematurity leads to a retardation of cerebellar development and long-term functional deficits

S. Leroux¹, A. Rodriguez-Duboc^{1,2}, A. Arabo³, M. Basille-Dugay¹, D. Vaudry^{1,2,4*} and D. Burel^{1,2,4*}

Abstract

Background: Apnea of prematurity (AOP) is caused by respiratory control immaturity and affects nearly 50% of premature newborns. This pathology induces perinatal intermittent hypoxia (IH), which leads to neurodevelopmental disorders. The impact on the brain has been well investigated. However, despite its functional importance and immaturity at birth, the involvement of the cerebellum remains poorly understood. Therefore, this study aims to identify the effects of IH on cerebellar development using a mouse model of AOP consisting of repeated 2-min cycles of hypoxia and reoxygenation over 6 h and for 10 days starting on postnatal day 2 (P2).

Results: At P12, IH-mice cerebella present higher oxidative stress associated with delayed maturation of the cerebellar cortex and decreased dendritic arborization of Purkinje cells. Moreover, mice present with growth retardation and motor disorders. In response to hypoxia, the developing cerebellum triggers compensatory mechanisms resulting in the unaltered organization of the cortical layers from P21 onwards. Nevertheless, some abnormalities remain in adult Purkinje cells, such as the dendritic densification, the increase in afferent innervation, and axon hypomyelination. Moreover, this compensation seems insufficient to allow locomotor recovery because adult mice still show motor impairment and significant disorders in spatial learning.

Conclusions: All these findings indicate that the cerebellum is a target of intermittent hypoxia through alterations of developmental mechanisms leading to long-term functional deficits. Thus, the cerebellum could contribute, like other brain structures, to explaining the pathophysiology of AOP.

Keywords: Apnea of prematurity, Intermittent hypoxia, Cerebellum, Purkinje cells

Background

Apnea of prematurity (AOP) is a developmental disorder characterized by a sudden cessation of breathing, lasting at least 20 s and/or associated with bradycardia or oxygen desaturation [1]. This condition affects at least 50%

of premature infants and nearly 100% of extremely preterm neonates, born before 29 weeks of gestation [2]. Although it has been shown that apneas are mostly due to a physiological immaturity of respiratory control, the pathogenesis and neurological consequences of this disease remain unclear [3].

Nonetheless, as improvements in healthcare have helped reduce mortality in recent years, long-term deficits following AOP are now noticeable. Indeed, it has been shown that AOP was associated with an increased risk of periventricular leukomalacia [4, 5]. Moreover, a

*Correspondence: delphine.burel@univ-rouen.fr

¹ Laboratory of Neuronal and Neuroendocrine Communication and Differentiation, Institute for Research and Innovation in Biomedicine (IRIB), Normandie Univ, UNIROUEN, INSERM U1239, 76000 Rouen, France
 Full list of author information is available at the end of the article



© The Author(s) 2022. **Open Access** This article is licensed under a Creative Commons Attribution 4.0 International License, which permits use, sharing, adaptation, distribution and reproduction in any medium or format, as long as you give appropriate credit to the original author(s) and the source, provide a link to the Creative Commons licence, and indicate if changes were made. The images or other third party material in this article are included in the article's Creative Commons licence, unless indicated otherwise in a credit line to the material. If material is not included in the article's Creative Commons licence and your intended use is not permitted by statutory regulation or exceeds the permitted use, you will need to obtain permission directly from the copyright holder. To view a copy of this licence, visit <http://creativecommons.org/licenses/by/4.0/>. The Creative Commons Public Domain Dedication waiver (<http://creativecommons.org/publicdomain/zero/1.0/>) applies to the data made available in this article, unless otherwise stated in a credit line to the data.

correlation has been established between apnea duration and neurodevelopmental disorders, including language, cognitive, and motor impairments [6]. These deficits appear to reflect the severity of the apnea, with short respiratory arrests being inconsequential and longer ones deleterious [7].

Several animal models of intermittent hypoxia (IH) have been developed to better understand the pathogenesis and outcomes of AOP in humans [8–10]. The repeated cycles of hypoxia and reoxygenation that characterize this pathology have been shown to induce cellular damage and oxidative stress, leading to central nervous system injuries. Indeed, Cai et al. [11] demonstrated oligodendrocyte and synaptic alterations in the striatum and corpus callosum following perinatal IH. Moreover, decreased long-term potentiation and memory disorders have also been observed [9, 10].

However, despite the increasing number of studies trying to assess the effects of AOP on the brain, very few investigate its impact on the rest of the nervous system, notably the cerebellum which is particularly vulnerable. Indeed, the cerebellar cortex is immature at birth [12] and consists of 4 layers that undergo an important maturation process from the last trimester of pregnancy and well into the postnatal period. In humans, the granular cell precursors (GCP) first proliferate in the external granular layer (EGL), which reaches its peak thickness between the 20th and 30th weeks of gestation. These neuron precursors then migrate through the molecular layer (ML) thanks to the Bergmann glia, cross the Purkinje cell layer (PL), and differentiate to form the internal granular layer (IGL) [13]. In the meantime, Purkinje cells develop their dendritic arborization. This allows for the establishment of synaptic contacts with ascending granule cell axons, called parallel fibers, and for the enlargement of the ML. As a result, these neurons receive indirect information from mossy fibers and integrate it along with data directly supplied by the climbing fibers from the olfactory nucleus.

Thus, the cerebellum controls various motor behaviors such as equilibrium or motor coordination, but also higher functions such as language, learning, or spatial orientation [14–16]. It appears that most of these processes are altered in children affected by AOP [6, 7]. In fact, Sathyanesan et al. [17] demonstrated that chronic perinatal hypoxia induces persistent motor coordination disorders and learning deficits. These data suggest that perinatal incidents such as apnea could affect cerebellar development and lead to behavioral impairments. Based on this hypothesis, it has been shown that IH in rodents causes Purkinje cell alterations, hypomyelination, and oxidative stress [8, 11, 18, 19].

In this work, we decided to analyze cerebellar histology during development, as well as the behavior of young and adult mice in a model of AOP. We first determined the effect of intermittent hypoxia on oxidative stress, proliferation, apoptosis, and cortical layer organization. On a functional level, we investigated short and long-term motor and learning aptitudes to determine whether cellular defects were associated with behavioral disorders. Altogether, our results aim to correlate cerebellar alterations with the long-term deleterious consequences observed in preterm children having experienced AOP.

Results

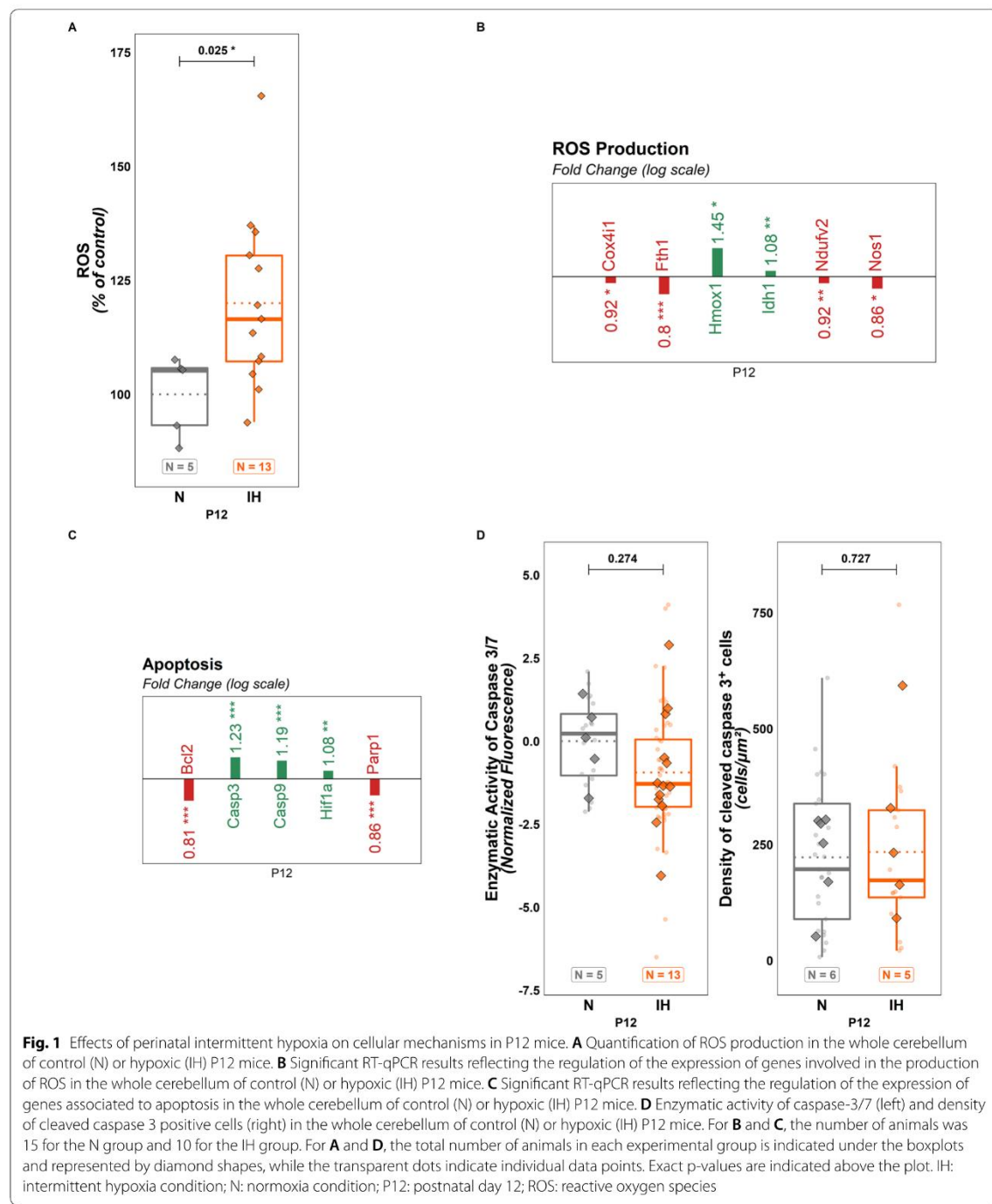
Effects of perinatal intermittent hypoxia on cellular mechanisms of development

In order to mimic apnea of prematurity, neonatal mice were exposed to cycles of hypoxia and reoxygenation (2 min/cycle, 6 h/day for 10 days, starting at the postnatal day 2 (P2)). To evaluate the oxidative stress induced by hypoxia in the cerebellum, the concentration of reactive oxygen species (ROS) produced in mice cerebella at the end of the apnea protocol was measured. We observed that IH induces an increase in ROS production in the whole cerebellum ($t(17) = -2.454; p = 0.025$; $Ratio = 0.833$; $CI_{95} = [0.713, 0.975]$; Fig. 1A). Moreover, our qPCR analysis shows that, of the 9 genes tested from the "ROS production" panel, 6 are differentially expressed at P12 after IH. More precisely, Cox4i1 and Ndufv2 are slightly under-expressed, Nos1 and Fth1 are more markedly under-expressed, and Hmox1 and Idh1 are over-expressed (Fig. 1B; see statistics in Additional file 1: Table S1).

Concerning the "Apoptosis" panel, the expression of Casp3, Casp9, Hif1 α was up-regulated while Bcl2 and Parp1 are under-expressed after IH at P12 (Fig. 1C, see statistics in Additional file 1: Table S1). However, this result is not reflected in terms of the enzymatic activity of caspases-3/7 or the density of cleaved caspase-3 positive cells (Fig. 1D). Similarly, DAPI labeling in the different cortical layers at P12 revealed no difference concerning the density of cells (spots per volume) (EGL: $t(120) = -0.076; p = 0.939$; $Ratio = 0.995$; $CI_{95} = [0.868, 1.14]$; ML: $t(120) = 0.237; p = 0.813$; $Ratio = 1.017$; $CI_{95} = [0.887, 1.166]$; IGL: $t(120) = 0.745; p = 0.458$; $Ratio = 1.053$; $CI_{95} = [0.918, 1.207]$; Fig. 2A) or in the average distance between cells (EGL: $t(120) = 0.775; p = 0.440$; $Ratio = 1.012$; $CI_{95} = [0.981, 1.044]$; ML: $t(120) = -0.589; p = 0.557$; $Ratio = 0.991$; $CI_{95} = [0.961, 1.022]$; IGL: $t(120) = -1.364; p = 0.175$; $Ratio = 0.979$; $CI_{95} = [0.949, 1.01]$; Fig. 2A).

Additionally, the effect of IH on the expression of genes implicated in the antioxidant response was studied. While some genes involved in redox homeostasis,

RESULTS



such as Gpx4, Gsk1, Prdx1, Sod1 and Srxn1, are under-expressed after IH, thus reflecting cellular distress, other antioxidant genes like Sod 2, Sod 3, Txnrd3 and Gstm1 are over-expressed indicating the establishment of a defense system (Fig. 2B; see statistics in Additional file 1: Table S1). The impact of IH on GCP proliferation and migration was also analyzed by counting bromodeoxyuridine (BrDU)-positive cells (N group = 2 males and 2 females; IH group = 3 males and 2 females). P6 injection of BrDU helped us estimate the capacity of GCP to divide and then migrate to the IGL until P12. P12 administration revealed the immediate proliferation at the end of the IH protocol. Our results indicate that hypoxia did not change the number of BrDU-positive cells in the IGL, indicating no deficit of neuronal migration (Fig. 2C), but did increase BRDU-labeled precursors in the EGL ($t(31) = -3.295; p = 0.002; Ratio = 0.443; CI_{95} = [0.268, 0.734]$; Fig. 2C), demonstrating a higher proliferative activity.

Effects of perinatal intermittent hypoxia on the structural organization of the developing cerebellum

Immunohistochemical studies were performed using DAPI and calbindin labeling at the end of the protocol (P12; N group = 3 males; IH group = 3 males and 1 female) or 9 days later (P21; N group = 1 male and 2 females; IH group = 2 males-1 female) to analyze the short and long-term effects of IH on cerebellar histology.

At P12, immunofluorescent imaging revealed a disorganization of the cerebellar cortex in IH-treated mice compared to controls (Fig. 3A–C). The measurement of cerebellar cortex thickness at P12 showed a global reduction in IH mice ($t(1112) = 4.099; p = < 0.001; Ratio = 1.503; CI_{95} = [1.237, 1.827]$; Fig. 3A, B). This alteration is associated with a decrease in the IGL and ML thicknesses (respectively, $t(1112) = 6.06; p = < 0.001; Ratio = 1.673; CI_{95} = [1.416, 1.976]$; and $t(1112) = 3.789; p = < 0.001; Ratio = 1.781; CI_{95} = [1.321, 2.402]$; Fig. 3A, B) and an increase in EGL thickness ($t(1112) = -2.108; p = 0.035; Ratio = 0.816; CI_{95} = [0.676, 0.986]$; Fig. 3A, B), which further supports the delay in development. The immunochemical observation also revealed that the dendritic tree of Purkinje cells is visibly affected (Fig. 3B). The quantitative analysis of calbindin labeling confirmed the decrease of dendritic arborization volume per Purkinje cell body

($t(147) = 2.26; p = 0.025; Ratio = 1.257; CI_{95} = [1.029, 1.535]$; Fig. 3C). The difference is more pronounced in the anterior part (Ant) of the cerebellum than in the medium (Med) or posterior (Post) part (Ant: $t(147) = 2.209; p = 0.029; Ratio = 1.382; CI_{95} = [1.035, 1.847]$; Med: $t(147) = 1.494; p = 0.137; Ratio = 1.235; CI_{95} = [0.934, 1.632]$; Post: $t(147) = 1.219; p = 0.225; Ratio = 1.164; CI_{95} = [0.91, 1.488]$; Fig. 3C).

At P21, the thinning of the cortical layers is no longer significant (Fig. 4A, B). Moreover, the quantitative analysis of calbindin labeling demonstrated that the volume of the dendritic tree of Purkinje cells is increased in IH animals ($t(74) = -2.249; p = 0.027; Ratio = 0.832; CI_{95} = [0.708, 0.979]$; Fig. 4C). This effect is mostly accounted for by the posterior part of the cerebellum (Ant: $t(74) = -0.787; p = 0.434; Ratio = 0.891; CI_{95} = [0.666, 1.192]$; Med: $t(74) = -0.853; p = 0.396; Ratio = 0.908; CI_{95} = [0.724, 1.138]$; Post: $t(74) = -2.207; p = 0.030; Ratio = 0.713; CI_{95} = [0.525, 0.968]$; Fig. 4C). However, neither P12 nor P21 stages showed a significant difference in Purkinje cell count (Figs. 3C, 4C).

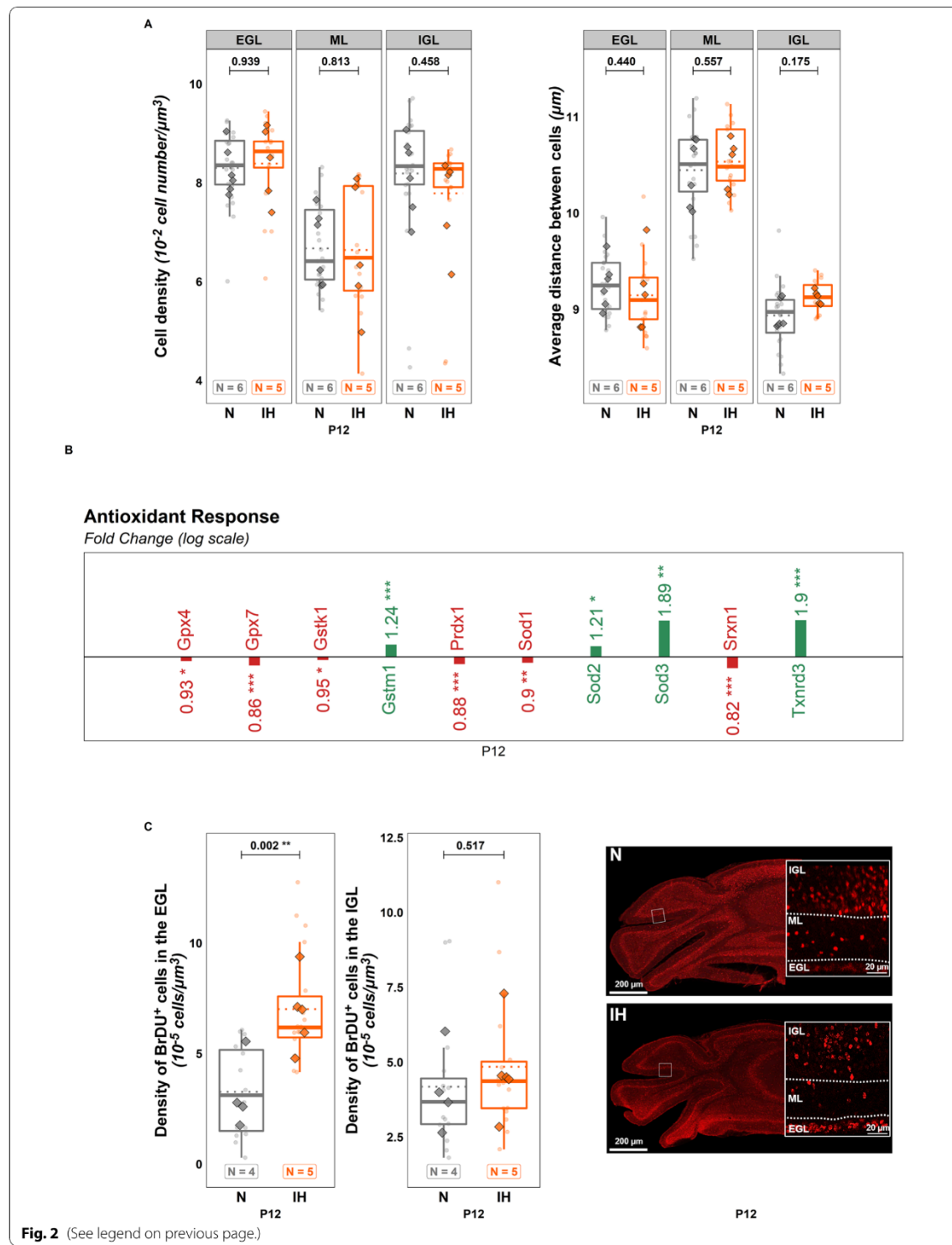
Effects of perinatal intermittent hypoxia on physical and behavioral development

Two different tests were performed to determine whether perinatal IH could alter behavioral development in pups (N group = 11 males and 7 females; IH group = 7 males and 8 females). Firstly, we found that, in the righting reflex test, hypoxic mice take longer to turn at P6 and P7 compared to the control group (respectively $+26.56 \pm 6.266$ s and $+32.79 \pm 6.45$ s; $t(327) = -3.711; p = < 0.001; Estimate = -7.931; CI_{95} = [-12.136, -3.727]$; Fig. 5A). Our data also revealed that, in the grasping reflex test, the hanging time of hypoxic mice is shorter than that of the control pups from P9 to P11 (respectively -2.92 ± 0.63 s; 6.52 ± 0.897 s; -10.29 ± 0.45 s; $t(327) = 5.569; p = < 0.001; Estimate = 2.226; CI_{95} = [1.44, 3.013]$; Fig. 5B). Moreover, IH induces a growth delay in IH mice. Thus, while the mean weight of pups (nest weight/number of pups per nest) is similar at P0 ($t(3) = -0.107; p = 0.921; Estimate = -0.003; CI_{95} = [-0.091, 0.085]$; Fig. 5C, top left inset), animals display a lower daily weight gain from P2 to the end of the protocol ($t(331) = 13.971; p = < 0.001; Ratio = 2.007; CI_{95} = [1.819, 2.213]$; Fig. 5C). No significant difference was found in weight

(See figure on next page.)

Fig. 2 Cellular defense against oxidative stress during perinatal intermittent hypoxia in P12 mice. **A** Cell density (left) and average distance between cells (right) measured on DAPI-stained cerebellar slices of control (N) or hypoxic (IH) P12 mice. **B** Significant RT-qPCR results reflecting the regulation of the expression of genes involved in the antioxidant response to oxidative stress in the whole cerebellum of control (N) or hypoxic (IH) P12 mice. **C** Density of BrdU-immunoreactive cells in the EGL (left) and IGL (middle) and confocal images (right) illustrating the distribution of BrdU-positive cells in the cerebellar cortex in control (N) or hypoxic (IH) mice. For **B**, the number of animals was 15 for the N group and 10 for the IH group. For **A** and **C**, the total number of animals in each experimental group is indicated under the boxplots and represented by diamond shapes, while the transparent dots indicate individual data points. Exact p-values are indicated above the plot. BrdU: bromodeoxyuridine; EGL: external granular layer; IGL: internal granular layer; IH: intermittent hypoxia condition; N: normoxia condition; P12: postnatal day 12; ROS: reactive oxygen species

RESULTS



gain by sex ($t(603) = 1.334; p = 0.183; Ratio = 1.048; CI_{95} = [0.978, 1.122]$; data not shown). This lower weight gain is associated with a significant effect on the muscular strength of mice at P21 ($t(19) = 2.369; p = 0.029; Ratio = 1.34; CI_{95} = [1.035, 1.735]$; Fig. 5D). It even seems that an overcompensation occurs after weaning, since IH mice exhibit a significantly higher weight at P49 before stabilizing at the same level as controls at P53 (Fig. 6A).

Long term effects of perinatal intermittent hypoxia on locomotor activity and motor coordination

To examine whether motor impairments due to perinatal IH in young mice could lead to long-term deficits in spontaneous locomotor activity and motor coordination, adult mice were subjected to actimetry and horizontal beam tests. Our results do not reveal any effect of IH on mean speed or on distance traveled (Fig. 6B). Similarly, IH animals spend the same time walking through the horizontal beam as control mice (Fig. 6C). However, hypoxic mice make more miss steps on their path than controls at P53 ($+229.17 \pm 23.245\% ; t(23) = -3.188; p = 0.004; Estimate = -2.019; CI_{95} = [-3.329, -0.709]$; Fig. 6C).

Long term effects of perinatal intermittent hypoxia on spatial learning

As the cerebellum is now well known to participate in cognitive functions such as spatial navigation [20], we determined the impact of perinatal IH on adult mice performances in the Morris water maze test. We showed that IH mice are able to learn since their results improve over the 5 cue session days. However, they displayed an increased latency to find the platform and a prolonged freezing time (respectively, $t(117) = -3.607; p = < 0.001; Ratio = 0.704; CI_{95} = [0.581, 0.854]$; and $t(117) = -3.331; p = 0.001; Ratio = 0.399; CI_{95} = [0.232, 0.689]$; Fig. 7A, B), and presented an altered path efficiency ($t(117) = 2.116; p = 0.036; Odds.ratio = 1.415; CI_{95} = [1.023, 1.959]$; Fig. 7C). Moreover, in the probe test, IH-treated mice spent less time ($-25.13 \pm 9.51\%; t(23) = 2.176; p = 0.040; Odds.ratio = 1.696; CI_{95} = [1.026, 2.801]$) and traveled a shorter distance in the platform quadrant

($-23.24 \pm 8.712\%; t(23) = 2.359; p = 0.027; Odds.ratio = 1.655; CI_{95} = [1.064, 2.574]$) compared to control mice (Fig. 7D, E).

Long-term effects of perinatal intermittent hypoxia on anxiety

The effect of perinatal IH on anxiety was investigated in adult mice to check if the behavioral disorders observed in adults were due to distress. As shown in Additional file 2: Figure S1, the number of rearings and the grooming time, as well as the percentage of time spent in the center (data not shown) are similar in both groups of animals in the actimetry device. Moreover, in the elevated plus maze test, the time and number of entries in both closed and open arms are not significantly different for IH-treated and control mice (see Additional file 2: Figure S1). This indicates that IH mice do not display a more stressed or anxious behavior than the control animals.

Long term effects of perinatal intermittent hypoxia on the functional organization of the cerebellum

To determine if the behavioral deficits observed in IH adult mice are due to a persistence of histological alterations in the cerebellum, we studied the structure of the cortical layers with a focus on Purkinje cells and their afferences.

Our results showed that there was no longer a difference in the thickness of the ML and in the Purkinje cell count between conditions in adulthood (Fig. 8A, B). In contrast, like at P21, the volume of Purkinje cell dendrites was significantly higher in the hypoxic group compared to the control animals ($t(215) = -6.795; p = < 0.001; Ratio = 0.663; CI_{95} = [0.589, 0.747]$; Fig. 8B) and this can be observed in the entire cerebellum (Ant: $t(215) = -4.498; p = < 0.001; Ratio = 0.634; CI_{95} = [0.52, 0.774]$; Med: $t(215) = -2.826; p = 0.005; Ratio = 0.746; CI_{95} = [0.608, 0.915]$; Post: $t(215) = -4.438; p = < 0.001; Ratio = 0.617; CI_{95} = [0.498, 0.764]$; Fig. 8C).

In parallel, a double staining with calbindin and glutamate receptor delta2 (Glu82) or vesicular glutamate transporter 2 (Vglut2) was performed to analyze the connections between the Purkinje cell dendrites and parallel or climbing fibers, respectively. Although we did not see any difference in Glu82 labeling (Fig. 9A), our results show an increase of Vglut2-labeled fibers in IH mice

(See figure on next page.)

Fig. 3 Effects of perinatal intermittent hypoxia on the organization of the developing cerebellum in P12 mice. **A** Measurement of the thickness of the cerebellar cortex and each cerebellar layer in control (N) or hypoxic (IH) P12 mice. **B** Low and high magnification confocal images illustrating the thickness of the cerebellar cortex layers in control (N) or hypoxic (IH) P12 mice. The Purkinje cells were labeled by antibodies against calbindin (red) and nuclei were counterstained with DAPI (blue). **C** Measurement of the number of Purkinje cell bodies per frame of $413 \times 10^3 \mu\text{m}^3$ (left) and of the volume of the calbindin-labeled Purkinje dendrites in the molecular layer of control (N) or hypoxic (IH) P12 mice, in the whole cerebellum (middle) and per cerebellar region (right). The total number of animals in each experimental group is indicated under the boxplots and represented by diamond shapes, while the transparent dots indicate individual data points. Exact p-values are indicated above the plot. EGL: external granular layer; IGL: internal granular layer; IH: intermittent hypoxia condition; N: normoxia condition; ML: molecular layer; P12: postnatal day 12; PL: Purkinje cell layer

RESULTS

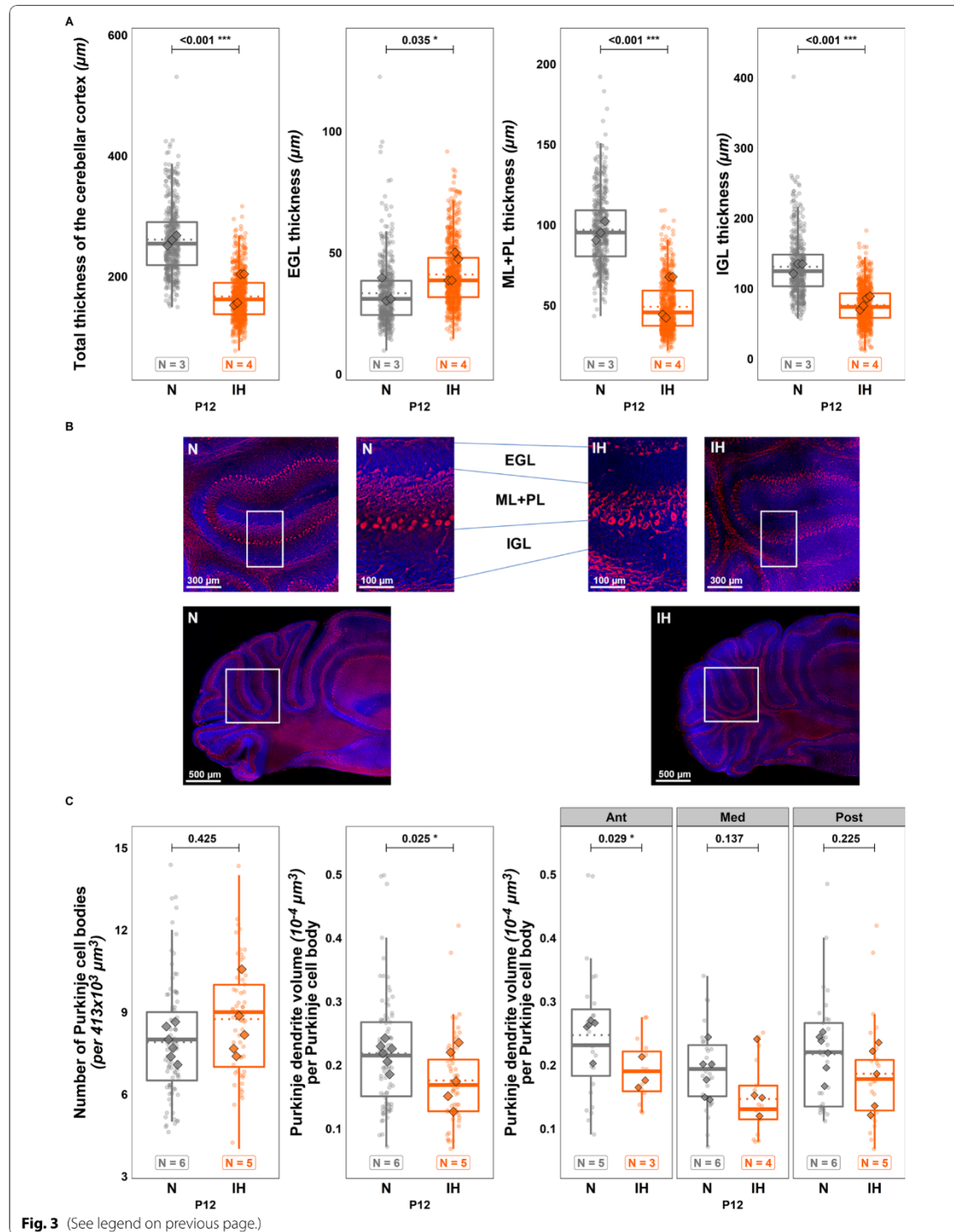


Fig. 3 (See legend on previous page.)

$t(207) = -4.507; p = < 0.001; \text{Ratio} = 0.431; CI_{95} = [0.298, 0.623]$; Fig. 9A). Vglut2 labeling, which is specific to mossy fibers in the adult granule cell layer, enabled us to demonstrate that IH increases the density of mossy afferences in adult animals ($t(208) = -4.448; p = < 0.001; \text{Ratio} = 0.837; CI_{95} = [0.774, 0.906]$; Fig. 9B).

Since hypomyelination is one of the major alteration observable in humans, we performed a staining for MBP and analyzed labeled fibers in the IGL. Interestingly, the difference in fiber length was not significant (Fig. 9C) but a significantly lower fiber volume was found in the hypoxic group ($t(238) = 2.529; p = 0.012; \text{Ratio} = 1.249; CI_{95} = [1.05, 1.485]$; Fig. 9C).

Discussion

The development of the cerebellum begins during the embryonic stage but continues well into the postnatal period [12]. Indeed, this structure is immature at birth and thus particularly vulnerable to several perinatal incidents. As a result, it has been shown that it is affected in premature newborns who suffer, among other things, from cerebellar atrophy [21, 22]. However, the consequences of apnea of prematurity, a common pathology affecting over 50% of premature newborns, have not been studied on the cerebellum, even though the behavioral deficits observed in children suffering from this pathology are correlated with cerebellar functions [6, 7]. Based on these data, we undertook to investigate the effects of IH on cerebellar development in a murine model of AOP based on the works of Cai et al. [8]. While our protocol does not induce any mortality, we showed that it leads to growth retardation in mice. The effect of IH on the body weight of pups is well known [23–25]. It has been demonstrated that it is not due to an impact on the mothers, since perinatal IH causes a weight decrease in pups, regardless of the presence of hypoxic dams in the litter [23]. Moreover, we did not observe any weight difference, stress or behavioral changes in mothers during our hypoxia protocol (data not shown). We cannot exclude that IH may cause a lower quality in the dams' milk production or coordination problems affecting pup suckling during lactation, although no data have been

published about this hypothesis in the literature. Moreover, the fact that the difference in weight gain tended to decrease between IH and N animals from P16 onwards is in favour of IH-related fatigue or general stress, inducing a decrease in milk intake, which would then fade at the end of the protocol.

Concerning neurodevelopment, perinatal hypoxia is known to affect various brain regions such as the corpus callosum, striatum, frontal cortex, hippocampus, and cerebellum [11, 26, 27]. We confirm here that the cerebellum is a major target of perinatal IH since we observed signs of oxidative stress in this structure at P12.

Indeed, our IH protocol induces an overproduction of ROS supported by the overexpression of the genes Hmox1, Idh1 and Hif1 α , known to be sensors of oxidative stress [28–30]. We also observed a decrease of Cox4i1 and Fth1 expression, which could contribute to ROS accumulation [31, 32]. Similarly, several antioxidant enzymes are less expressed at P12, such as the glutathione peroxidases, the superoxide dismutase 1, the peroxiredoxin 1, the sulfiredoxin 1 and the glutathione-S-transferase kappa 1 [33–36], indicating that cerebellar cells have suffered from the hypoxia. This oxidative stress is accompanied by an overall decrease in the thickness of the cerebellum that affects all cortical layers. This thinning could be due to an increase of apoptosis as qPCR experiments show that the genes for numerous pro-apoptotic enzymes, including caspases 3 and 9 are upregulated and the anti-apoptotic factor Bcl2 is under-expressed after IH at P12. However, we do not see any changes in cleaved caspase-3/7 activity and in the number of cleaved caspase-3 immunoreactive cells, suggesting that apoptosis is not or no longer exacerbated at the end of the protocol. One explanation for this discrepancy could be the establishment of a protective system against oxidative stress. Indeed, IH decreases the expression of the pro-oxidant genes Ndufv2 and Nos1 [33, 37], while significantly increasing the expression of antioxidant enzymes' genes for superoxide dismutases 2 and 3, glutathione-S-transferase mu and thioredoxin reductase 3 [36, 38, 39]. This compensatory mechanism could balance the increased apoptotic cell death as suggested by the decrease in Parp1 expression [19], leading to the same cell density in all cerebellar layers at the end of the IH protocol. Therefore, the

(See figure on next page.)

Fig. 4 Effects of perinatal intermittent hypoxia on the organization of the developing cerebellum in P21 mice. **A** Measurement of the thickness of the cerebellar cortex and each cerebellar layer in control (N) or hypoxic (IH) P21 mice. **B** Low and high magnification confocal images illustrating the thickness of the cerebellar cortex layers in control (N) or hypoxic (IH) P21 mice. The Purkinje cells were labeled by antibodies against calbindin (red) and nuclei were counterstained with DAPI (blue). **C** Measurement of the number of Purkinje cell bodies per frame of $413 \times 10^3 \mu\text{m}^3$ (left) and of the volume of the calbindin-labeled Purkinje dendrites in the molecular layer of control (N) or hypoxic (IH) P21 mice, in the whole cerebellum (middle) and per cerebellar region (right). The total number of animals in each experimental group is indicated under the boxplots and represented by diamond shapes, while the transparent dots indicate individual data points. Exact p-values are indicated above the plot. GL: granular layer; IH: intermittent hypoxia condition; N: normoxia condition; ML: molecular layer; P21: postnatal day 21; PL: Purkinje cell layer

RESULTS

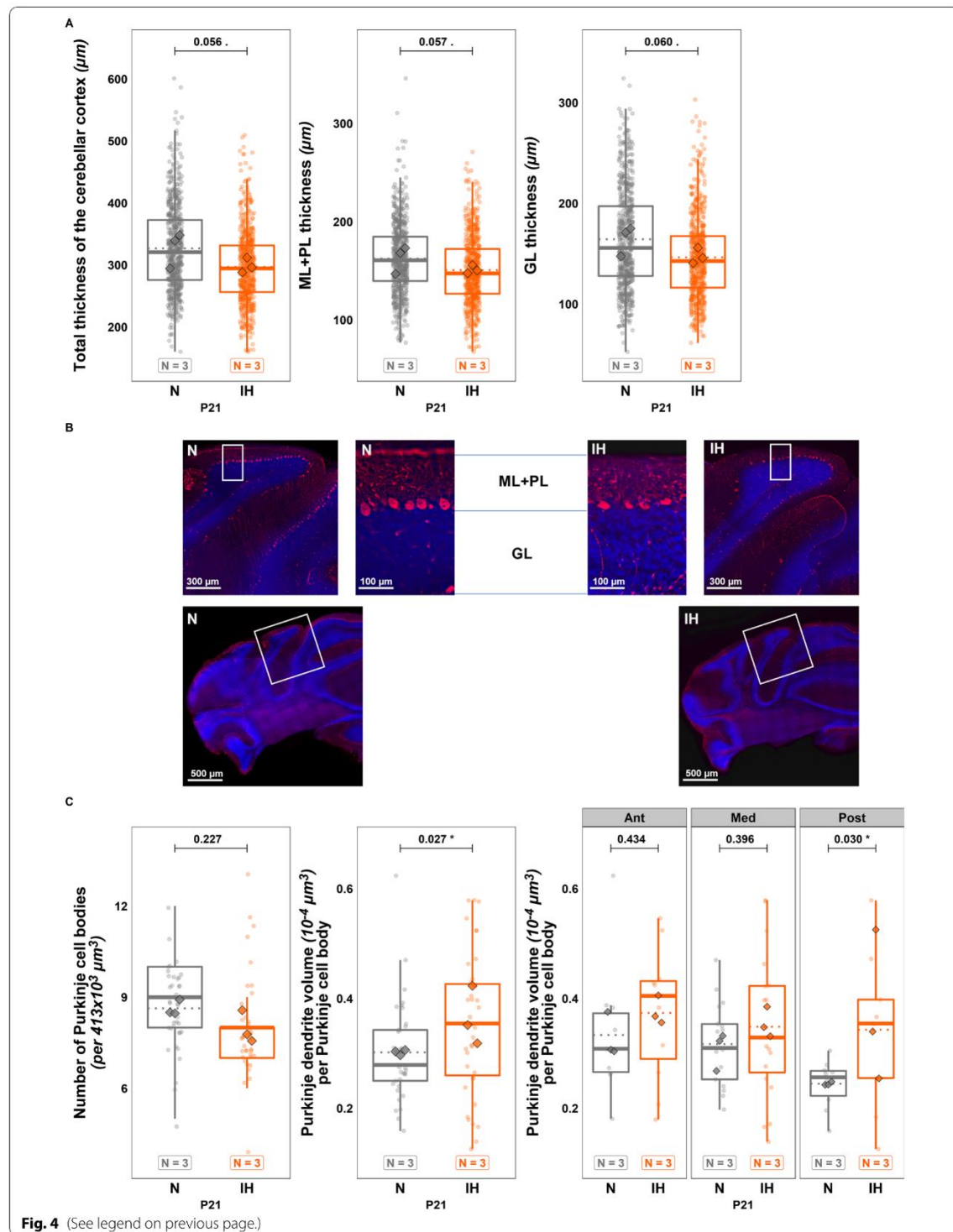


Fig. 4 (See legend on previous page.)

thickness decrease could instead be imputable to a general delay in cerebellar maturation consistent with the global growth retardation. This hypothesis is supported by our immunohistochemical analysis showing that, in IH mice, the proportional thickness of each cortical layer is close to that of a P6 cerebellum with a thicker EGL and thinner ML and IGL. We also revealed that hypoxia increases the number of BrDU-positive cells in the EGL, indicating that IH maintains a high proliferative activity of GCP at P12 much like that of an immature cerebellum. In contrast, no difference in the number of BrDU-positive cells was seen in the IGL. This result shows that precursors that proliferated between P6 and P12 did not have difficulty reaching the IGL despite of IH, suggesting that hypoxia does not affect GCP migration. Moreover, IH does not modify the cell density in the ML and IGL, which respectively contain stellate and basket cells; and granule, Golgi and Lugano interneurons, suggesting that these neurons are not (or no longer) significantly affected by IH at P12. The weak impact of IH on granule cells is confirmed by our Glu82 immunohistochemical analysis in adult mice, which shows no difference in the parallel fiber innervation of Purkinje cells.

However, by focusing on Purkinje cells, we determined that, while the number of cell bodies is equivalent in both groups, the volume of their dendritic tree is lower at P12 post IH. These data revealed that hypoxia induces a delay in Purkinje cell differentiation that mainly occurs in the anterior part of the cerebellum. This differential sensitivity to hypoxia has already been shown in rodents as well as in humans and demonstrates that the anterior part of the cerebellum is usually more affected by a perinatal deprivation of oxygen [40, 41]. It could be explained by the developmental timing of the cerebellum, which begins with lobules I-III and ends with the separation of lobules IV-V [42, 43]. Thus, the posterior regions were already mature at P2 when we started the IH protocol, while the foliation of the anterior part was still ongoing until P5. Similarly, it has been demonstrated that Purkinje cells located in the anterior cerebellum become mature later than in the posterior region [43], suggesting that this region-specific immaturity could make Purkinje cells more sensitive to perinatal hypoxia.

Since Purkinje cells represent the cerebellum's information integration center, we performed behavioral tests to

determine if IH could lead to functional deficits in addition to structural alterations. Indeed, between P2 and P12, IH-treated pups show locomotor deficits, such as a delayed righting reflex and diminished grasping reflex. While these differences could be due, in part, to a gross morphological underdevelopment and lower weight, they are also consistent with a dysfunction of the anterior part of the cerebellum known to be implicated in sensorimotor control [44].

At P21, although mice still display a significantly lower body weight and reduced muscular strength, the difference in the histological organization of the cortical layers is no longer observed, indicating that a compensatory mechanism occurred since the end of the IH protocol. This process was also effective on Purkinje cells since these neurons no longer present a decrease of their dendritic tree volume. Indeed, they exhibit a denser arborization that mainly appears in the posterior part of the cerebellum. This result suggests that the compensatory mechanism takes place throughout the cerebellum and allows the IH neurons to catch up with the cells of control animals in the anterior and medium parts. However, this compensation induces an overdevelopment of the Purkinje dendritic tree in the posterior region, which was not altered by hypoxia at P12. These data led us to study the long-term effects of perinatal IH in adulthood.

Starting at P49, the body weight of IH mice caught up with and even transiently surpassed the controls. Likewise, the ML is similar in both conditions. However, we showed that functional impairments, such as the motor coordination deficits assessed by the horizontal beam test, are still present in adult mice that have experienced perinatal hypoxia. Moreover, these animals have lower performances in both cue and probe sessions of the Morris water-maze test. The increased freezing time could suggest a potentiated stress behavior but the results obtained in the actimetry and elevated plus maze tests do not reveal any anxiety in IH-treated mice (see Additional file 2). Thus, our results indicate that perinatal IH induces long-term motor function deficits associated with learning and/or even orientation impairments in adulthood. Such a deficit in spatial memory after hypoxia has already been demonstrated but it has been mainly attributed to decreased synaptic plasticity in hippocampal neurons [10]. However, the role of the interaction between

(See figure on next page.)

Fig. 5 Effects of perinatal intermittent hypoxia on weight and behavioral development in young mice. **A, B** Measurement of the latency to turn in the righting reflex test (**A**) and to fall in the grasping reflex test (**B**) between P2 and P11 in 18 control (N) and 15 hypoxic (IH) mice. **C** Measurement of the weight gain of control (N) and hypoxic (IH) mice between P2 and P21 ($N=22$, $IH=18$ from P2 to P11— $N=4$, $IH=3$ from P12 to P21). Top-left insert: baseline control of P0 weight averaged from the total litter weight. **D** Measurement of the muscular strength using the forelimb grip strength test in control (N) and hypoxic (IH) P21 mice (3 technical replicates per animal). The total number of animals in each experimental group is indicated under the boxplots and represented by diamond shapes, while the transparent dots indicate individual data points. Exact p-values are indicated above the plot. IH: intermittent hypoxia condition; N: normoxia condition; Px: postnatal day x

RESULTS

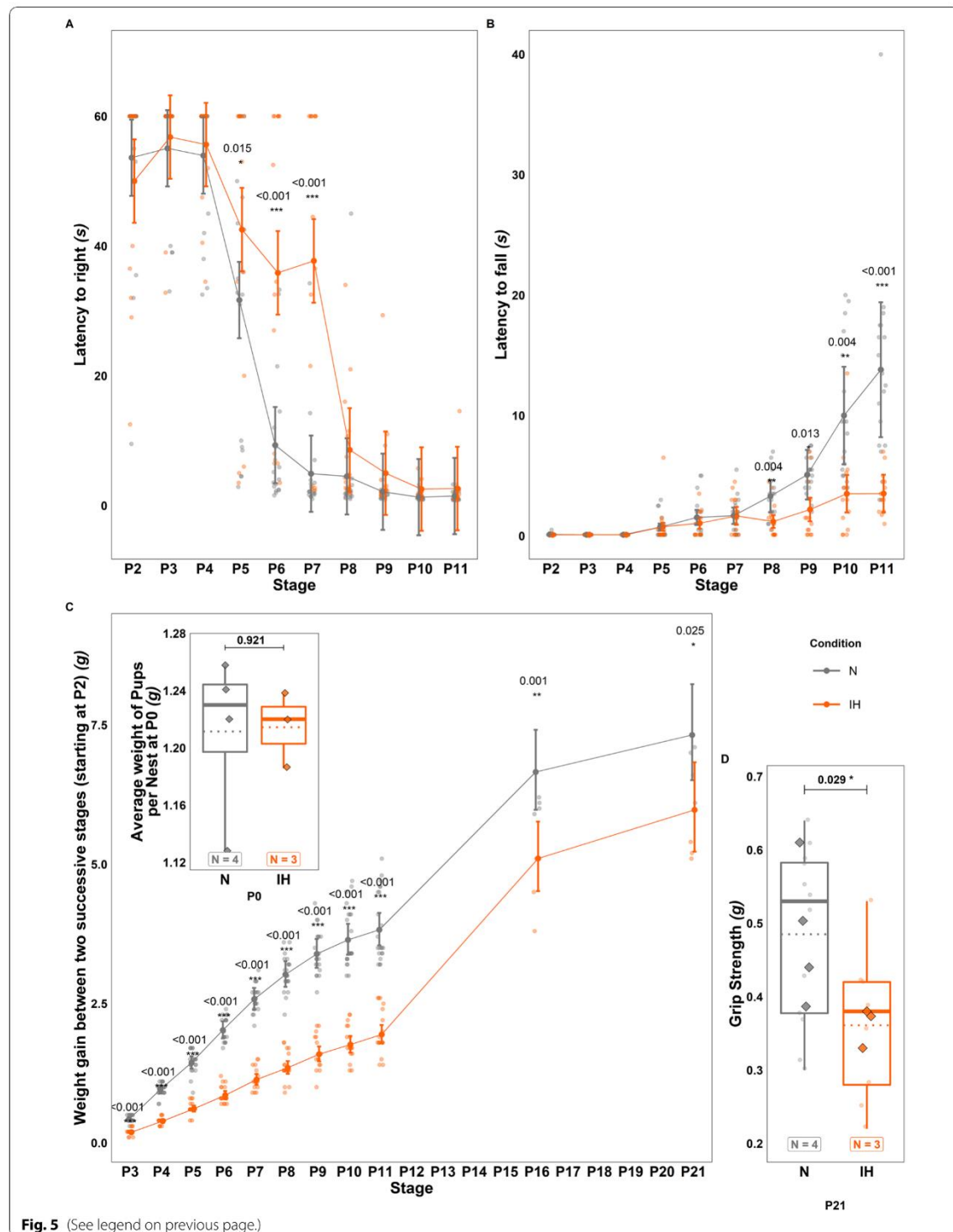


Fig. 5 (See legend on previous page.)

cerebellum and hippocampus in the control of spatial navigation is now well known [45, 46], indicating that the perinatal IH-induced alteration of the cerebellum could also be responsible for this behavioral deficit.

Since, in the hippocampus, IH decreases synaptic plasticity and long-term potentiation [10], we examined the morphology of Purkinje cells and studied cerebellar afferences. We found that, in adult IH mice, Purkinje dendrites are denser, not only in the posterior part as in P21, but throughout the cerebellum. Thus, the locomotor and spatial learning deficits could be linked to the alteration of the anterior and the posterior parts of the cerebellum, respectively [44, 47, 48].

Concerning afferences, a high Vglut2 labeling was detected in the ML of IH mice, suggesting that cerebellar innervation by climbing fibers is also affected by hypoxia. During development, Purkinje neurons receive inputs from multiple climbing fibers, but they are progressively eliminated during the first two postnatal weeks and only one afference per Purkinje cell will persist in adulthood [49]. Two selection steps occur in physiological conditions: a granule cell-independent phase between P6 and P12 and a later phase, between P12 and P17, which relies on the activity of parallel fibers [50]. Since our IH protocol was applied before P12, we can hypothesize that hypoxia mostly altered the early selection phase leading to the over-innervation of Purkinje cells by climbing fibers. This hypothesis is further reinforced by the Glu δ 2 immunolabeling that showed no difference in the parallel fiber innervation of Purkinje dendrites.

Similarly, an increase in Vglut2 labeling was seen in the IGL, indicating that mossy fibers may also be impacted by perinatal IH. These afferences originate from various central nervous regions, such as the spinal cord or brainstem nuclei, enter the cerebellum at birth and make contacts with granule cells in the mature cerebellum. Several studies have shown that granule neuron activity is important for an appropriate innervation during the first postnatal week [50], and we found here that the marker of Purkinje cell-parallel fiber synapses Glu δ 2 reveals no difference in adult mice. However, it is known that mossy fibers first connect Purkinje cells before moving on to mature granule cells as the IGL appears [50, 51]. Therefore, we can hypothesize that the delay in IGL formation after hypoxia allows a high late mossy fiber innervation that persists in adulthood. In fact, this differential mossy input according to the maturation degree of granule cells has already been

suggested [52, 53]. Alternatively, the reduction of the Purkinje dendritic tree density at P12 in IH mice could also increase the switch to contact with granule cells and later could induce an over-innervation in adulthood.

Finally, we show that the volume (but not the length) of myelin sheaths is decreased in adult mice after a perinatal IH, which is consistent with numerous studies [10, 11, 54]. However, although most of these works analyzed cerebellar white matter, we focused on the granule cell layer. Since mossy and climbing fibers mostly lose their myelin sheaths when entering the cerebellar cortex, our results demonstrate that the myelination defect mainly concerned Purkinje axons.

Conclusion

We have investigated the effects of a model of apnea of prematurity on cerebellar development in mice. Here, we demonstrated that perinatal IH induces modifications of cellular mechanisms such as oxidative stress, leading to a delay in cerebellar cortex maturation. This developmental retardation seems to be compensated by mechanisms such as an increased proliferation, allowing the cerebellar cortex to achieve its development. However, some structural modifications, including denser dendritic arborization of Purkinje cells, over-innervation by cortical afferences and axon hypomyelination, persist after IH and induce short and long-term impairments affecting motor coordination, learning and/or orientation. Such a link between Purkinje cell development failure, afferent innervation and long-term behavioral deficits has already been proven in another pathological context [55] and suggests that apnea of prematurity can lead to structural and functional alterations within the cerebellum, that may participate, at least in part, in the observed neurodevelopmental disorders.

Methods

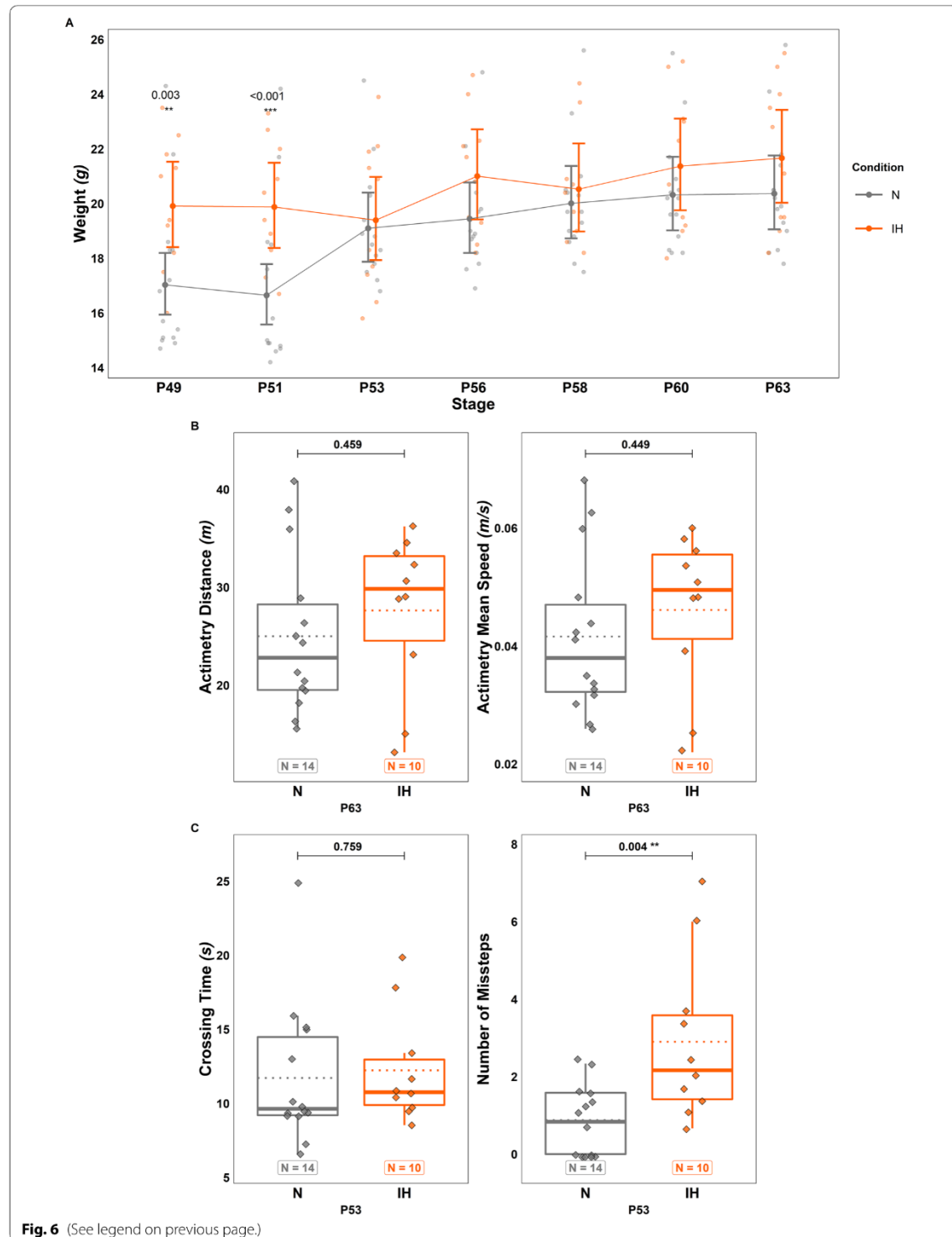
Animals

Animals used in this study were wild type C57/Bl6J mice born and bred in an accredited animal facility (approval B.76-451-04) in accordance with the French Ministry of Agriculture and the European Community Council Directive 2010/63/UE of September 22nd, 2010, on the protection of animals used for scientific purposes. The mice were kept under a 12-h light/dark cycle and had free access to food and water. Due to the age of mice at the beginning of the hypoxia protocol (P2), it was not feasible

(See figure on next page.)

Fig. 6 Long-term effects of perinatal intermittent hypoxia on locomotor activity and motor coordination in adult mice. **A** Measurement of the body weight in control (N) and hypoxic (IH) mice between P49 and P63. **B** Measurement of the distance travelled (left) and mean speed (right) in P63 control (N) and hypoxic (IH) mice during the actimetry test. **C** Measurement of the crossing time (left) and the number of missteps (right) in P53 control (N) and hypoxic (IH) mice during the horizontal beam test. The total number of animals in each experimental group is indicated under the boxplots in **B** and **C**, and exact p-values are indicated above. IH: intermittent hypoxia condition; N: normoxia condition; Px: postnatal day x

RESULTS



to manage the sex ratio. However, the sex of animals was determined at P12 at the end of the protocol. For immunolabeling, enzyme activity and behavioral tests, 18 N (11 males-7 females) and 15 IH (12 males-3 females) pups have been used at P12, 4 N (3 males-1 female) and 3 IH (2 males-1 female) juvenile animals at P21, and 14 N (5 males-9 females) and 10 IH (6 males-4 females) mice in adulthood. For qRT-PCR, 15 N (7 males-8 females) and 10 IH (7 males-3 females) have been used at P12. For all experiments, no sex dimorphism was observed (data not shown). Each animal was weighed at 9:00 each day before the beginning of the IH protocol. To avoid handling animals individually before P2 because of the stress-induced cannibalism of the mother, the whole nests were weighed at P0 when the pups were counted. Then, from P2, animals were identified and their weight gain was measured individually until P12 (or P21). There was no blinding in this study and sample size determination was done empirically based on bibliographic data.

Intermittent hypoxia protocol

The model of IH is based on the paradigm developed by Cai et al. [8] and consisted of 2-min cycles of hypoxia (5% O₂; 20 s/cycle) and reoxygenation for 6 h per day. The protocol was initiated in neonatal P2 C57Bl6/J pups (IH group) and continued for 10 consecutive days. Oxygen concentration, temperature, hygrometry, and atmospheric pressure in the hypoxic chamber were continuously monitored. Control normoxia pups (N group) were placed in another chamber in the same environment but in normoxic conditions. Upon completion of an IH course, some mice were used for enzymatic and oxidative assays. For histological studies, P12 or P21 mice were lethally anesthetized by intraperitoneal injection of ketamine (100 mg/kg) and xylazine (10 mg/kg) and then sacrificed by intracardiac perfusion of NaCl 9% and paraformaldehyde 4%. Brains were rapidly removed, fixed overnight in 4% paraformaldehyde and then stored in phosphate buffer saline (PBS) prior to section. The remaining mice were raised until P64 for behavioral assessments.

Reactive oxygen species (ROS) production assay

100 µL of homogenized cerebellum were incubated with 2 µL of 2,7'-dichlorofluorescein diacetate (Sigma-Aldrich). In the presence of ROS, this probe is converted to fluorescent 2,7'-dichlorofluorescein. The fluorescence intensity was measured at an excitation wavelength of 485 nm and an emission wavelength of 530 nm every 15 min over 45 min with an Infinite 200 microplate reader (Tecan). Data were standardized after protein quantification of each sample with a Bradford assay.

Expression of genes involved in oxidative stress and apoptosis

Sample gathering

Mice were sacrificed by decapitation after completion of the IH protocol at P12. Cerebella were immediately harvested and set into isopentane kept at -30 °C. They were then stored in sterile containers at -80 °C until further use.

Primer design

Gene primers were designed with the software Primer Express (v3.0.1; ThermoFischer Scientific) using nucleotide sequences from the NCBI Pubmed database. They were classified into 3 panels according to the functional enrichment in the GO database: ROS production (9 genes), antioxidant response (23 genes) and apoptosis (6 genes). Primer pairs were ordered from Integrated DNA Technologies and validated by linear regression of serial dilution data. The list of primer pair sequences is available in Additional file 3: Table S2.

RNA Extraction

The mRNAs were purified on column using the Nucleospin RNA extract II extraction kit by Macherey-Nagel (cat.740955250) according to manufacturer recommendations. mRNA concentration and purity were controlled by UV spectrophotometry on the NanoDrop One (ThermoFisher Scientific) and quality assessment was performed by gel electrophoresis on RNA 6000 Pico chips (cat. 5067-1513, Agilent). The mRNAs were then stored at -80 °C until the next step.

(See figure on next page.)

Fig. 7 Long-term effects of perinatal intermittent hypoxia on spatial learning in adult mice. **A–C**, Measurement of the latency to find the platform (**A**), of the freezing time (**B**), and of the path efficiency (**C**) during the cue sessions of the Morris water-maze test performed in 14 control (N) and 10 hypoxic (IH) mice between P56 and P60. **D** Measurement of the time spent (left) and distance travelled (right) in the target quadrant during the probe session of the Morris water-maze test, performed on control (N) and hypoxic (IH) P60 mice. **E** Representative pattern of the time spent in the target quadrant during the probe session of the Morris water-maze test for one control mouse (N) and one hypoxic mouse (IH) at P60. Red and yellow regions represent areas of high occupancy; green and blue represent areas of low occupancy. The total number of animals in each experimental group is indicated under the boxplots in **D** and exact p-values are indicated above. IH: intermittent hypoxia condition; N: normoxia condition; Px: postnatal day x

RESULTS

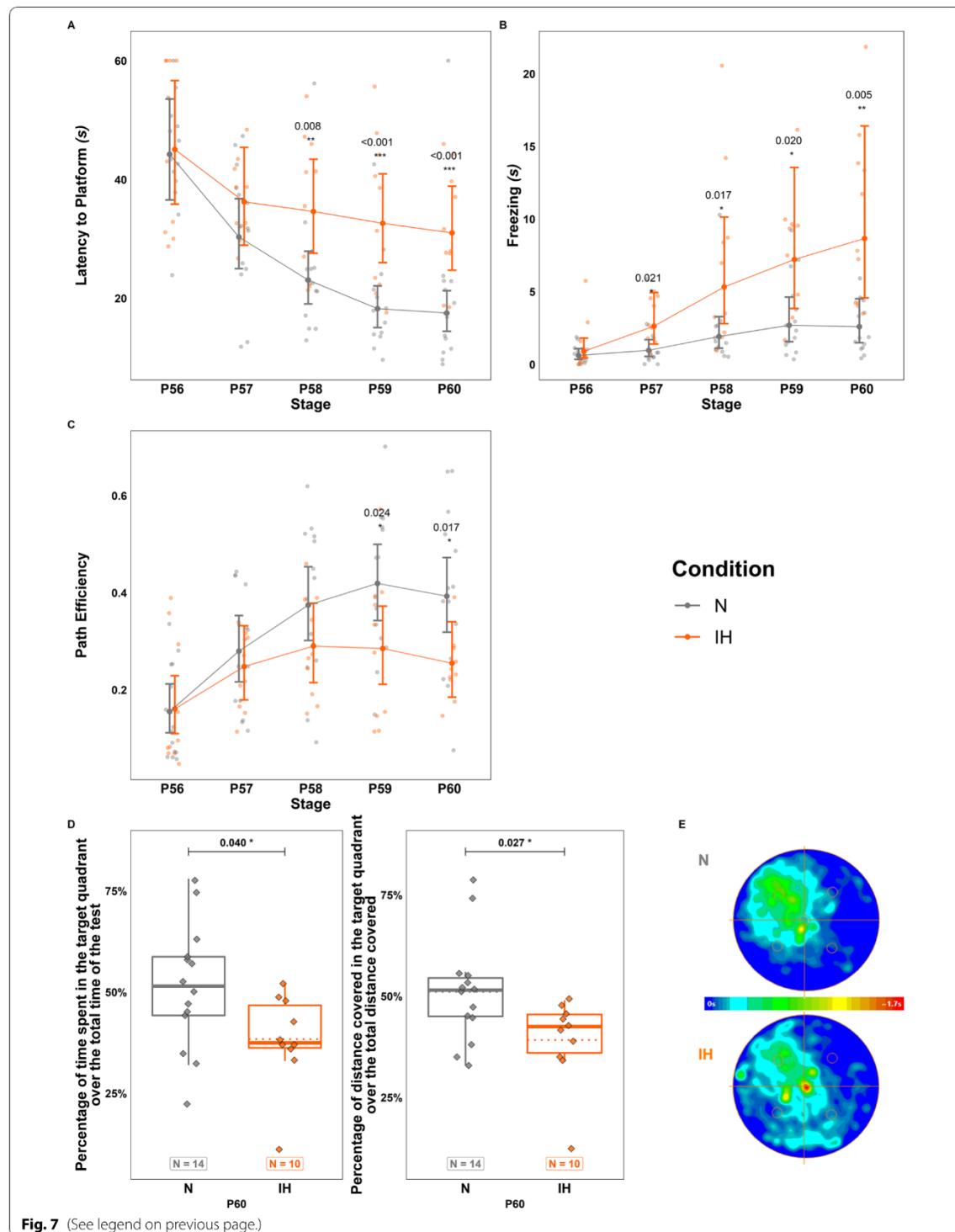


Fig. 7 (See legend on previous page.)

qRT-PCR

The determination of the expression level of genes was done by quantitative PCR in 384-well plates with a 5 μ L reaction volume in the presence of Fast SYBR Green PCR Mastermix (Thermofisher, cat. 4,385,612). The distribution of cDNA samples and reaction mixes was performed by the Bravo 1 Automated Liquid Handling Platform (Agilent). The quantitative PCR reaction took place in the QuantStudio Flex 12 k thermal cycler (Applied Biosystems). Two technical replicates per animal and per gene of interest (GOI) were averaged prior to DCq calculation. The average Cq value of three housekeeping genes (HKG) was used to calculate DCq. Efficiency for all primer pairs was above 95% and as such, the $2^{(-\Delta\Delta Cq)}$ method can be applied confidently. This method provides a relative quantification of the expression of a gene within an experimental condition and makes it possible to compute fold change for the graphic representation. This value is defined by the formula

$$2^{-\Delta\Delta Cq} = 2^{(-(Cq_{GOIH}-Cq_{HKGH})-(Cq_{GOIN}-Cq_{HKGN}))}$$

Caspases-3/7 activity assay

The enzymatic activity of caspases-3/7 in the cerebellum was evaluated with the Apo-ONE® Homogeneous Caspase-3/7 Assay (Promega). 100 μ L of homogenized cerebellum were incubated at 37 °C with 100 μ L of caspase assay buffer containing the Z-DEVD-aminoluciferin substrate. The fluorescence intensity was measured at an excitation wavelength of 485 nm and an emission wavelength of 530 nm every 6 min over 3 h with an Infinite 200 microplate reader. Data were standardized after protein quantification of each sample with a Bradford assay.

Bromodeoxyuridine (BrDU) injections

Animals received intraperitoneal administration of BrdU (50 mg/kg) at P6 to assess the capacity of GCP to divide and migrate, and then, at P12, 4 h before euthanasia, to analyze immediate proliferation of GCP.

Immunolabeling

For immunohistochemical studies, fixed brains were cut into frontal 80- μ m thick slices with a vibratome (VT1000S, Leica Microsystems). Slices were then blocked 30–60 min at room temperature with normal

donkey serum diluted at 1:50 in a buffer containing 0.3% Triton X-100. Then, the slices were incubated at 4 °C with primary antibodies diluted in the same buffer (Table 1). For BrDU labeling, a step of DNA denaturation consisting in a 15-min incubation in an HCl 1 N solution at 45 °C was done before adding BrDU antibodies. After three 10-min washes in PBS, they were incubated at room temperature for 2 h with the corresponding secondary antibodies diluted at 1:250 (Table 1). The slices were rinsed three times for 10 min in PBS and labeled for 1 min with 4',6-diamidino-2-phenylindole (DAPI; 2 μ g/mL) for nucleus counterstaining before the last wash in PBS. Finally, they were mounted with Mowiol before image acquisition.

Image analysis

Frontal sections were chosen to acquire symmetric images from as many lobules as possible on a minimum of slices and thus obtain a large panel of data. For each animal, 8 slices were harvested in the whole cerebellum and assigned to one of three groups according to Bregma coordinates, namely, the posterior (from -8.5 to -7.5 mm), the medium (from -7.5 to -7.0 mm) and the anterior parts (from -7.0 to -6.0 mm) (see Additional file 4).

For the measurement of layer thickness, image acquisition was done with a conventional Eclipse 600D microscope (Nikon) using a $\times 20$ objective. Mosaics were manually reconstructed prior to whole-slice measurements on the Fiji software [56, 57].

For the cell density measurement and the counting of BrDU and caspase-3-positive cells, images were acquired with a confocal microscope (TCS SP8 MP, Leica Microsystems). Each image corresponds to a 20- μ m thick section with 4- μ m step z-stacks (2048 \times 2048 focal planes) acquired using a $\times 20$ objective. Analysis was done on the Imaris software (Bitplane, Zurich, Switzerland) and all three-dimensional reconstructions were done with the same threshold.

For the study of calbindin, Gluδ2, Vglut2 and myelin binding protein (MBP) immunolabeling, image acquisition was completed on a confocal microscope (TCS SP8 MP, Leica Microsystems). Each image corresponds to a 10- μ m thick section with 1- μ m step z-stacks (2048 \times 2048 focal planes) acquired using a $\times 40$ objective. Analysis was done using the Imaris software (Bitplane, Zurich,

(See figure on next page.)

Fig. 8 Effects of perinatal intermittent hypoxia on the structural organization of adult mouse cerebellum. **A** Measurement of the thickness of the molecular layer in control (N) and hypoxic (IH) P60 mice. **B, C**, Measurement of the number of Purkinje cell bodies (**B**, left) and of the volume of the calbindin-labeled Purkinje dendrites in the molecular layer of control (N) and hypoxic (IH) P60 mice, in the whole cerebellum (**B**, right) and per cerebellar region (**C**). The total number of animals in each experimental group is indicated under the boxplots and represented by diamond shapes, while the transparent dots indicate individual data points. Exact p-values are indicated above the plot. IH: intermittent hypoxia condition; N: normoxia condition; P60: postnatal day 60

RESULTS

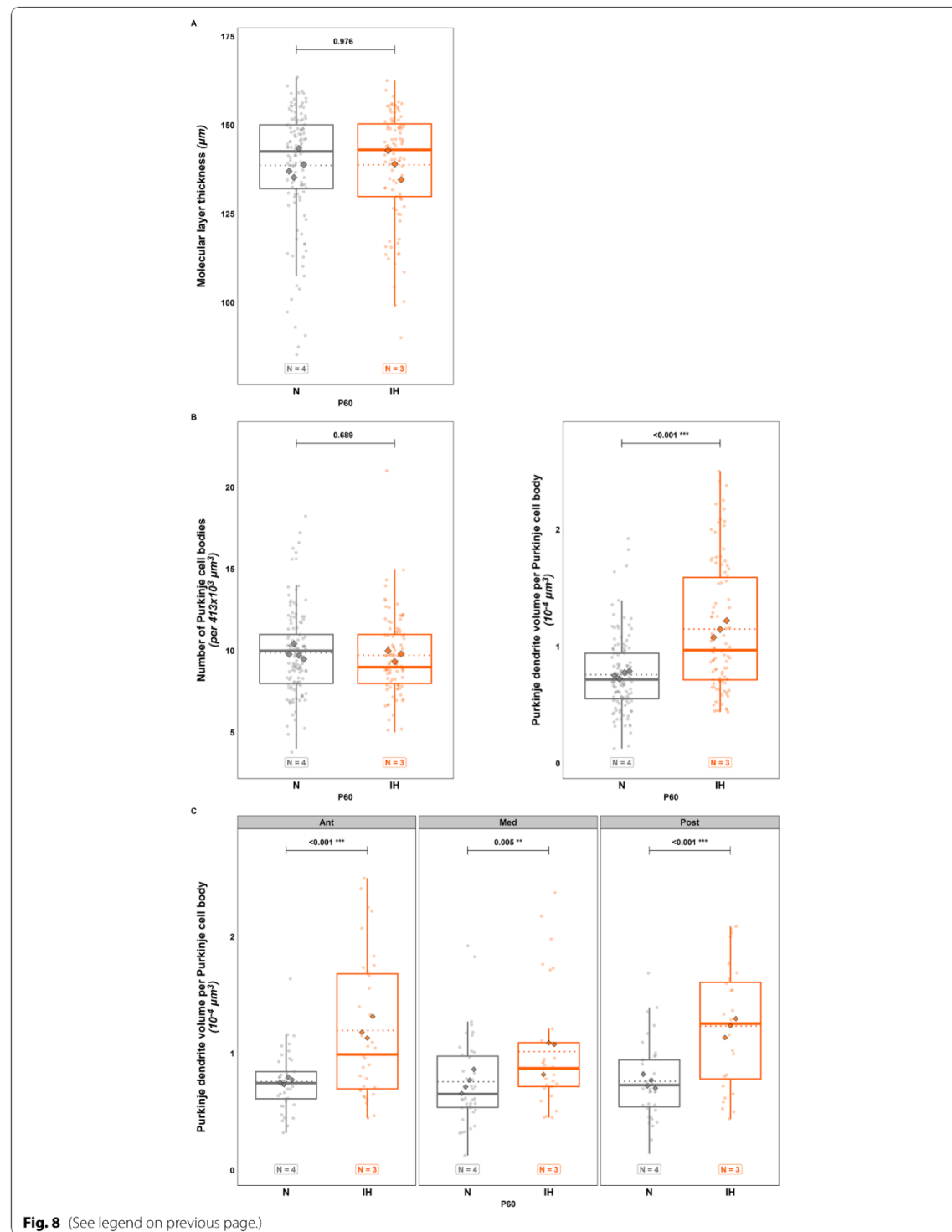


Fig. 8 (See legend on previous page.)

Switzerland) and all three-dimensional reconstructions were done with the same threshold.

Behavioral studies

Behavioral assessments were performed in blind condition between 10:00 a.m. and 5:00 p.m. At least one hour before the beginning of each test, animals were familiarized with the testing room. The apparatus were cleaned with an alcohol solution (10% ethanol) and dried before testing each animal.

Righting reflex test

This test evaluates the activity of the vestibular, articular, and muscular structures as well as movement completion. Pups were placed in a supine position and the time needed to recover a completely prone position was measured. Two daily consecutive trials were performed on each pup from P2 to P11 with a 60-s cut-off period.

Grasping reflex test

This experiment appraises the animal's grasping reflex and motor coordination. Pups were hanged by their forepaws on a stretched string and the latency to fall was measured. Two daily consecutive trials were performed for each pup from P2 to P11 with a 60-s cut-off period.

Muscular strength test

This test, which monitors the muscle strength of animals, can only be performed from P21 onwards. Mice were held by the tail and allowed to grasp a string with their forepaws. Then, they were progressively pulled backward by the tail. The maximal force was recorded by a dynamometer linked to the grip-strength apparatus. Three trials were performed on each mouse at P21.

Actimetry test

This test evaluates the spontaneous locomotor activity of animals in a new environment. In this session, P63 mice were placed in the middle of a $45 \times 45 \times 30$ cm box, and

their spontaneous locomotor activity was recorded for 10 min with the video tracking software Any-MAZE. Various parameters, such as the distance traveled and mean speed were measured, and the grooming time as well as the number of rearings were logged (see Additional file 2).

Elevated plus maze

This test estimates the anxiety state of the animals. P64 mice were placed at the intersection of a maze consisting of 2 opposed closed arms crossing 2 opposed open arms. The movements of the animals were tracked for 5 min with the Any-MAZE software. The time spent and the number of entries in each arm were recorded (see Additional file 2).

Horizontal beam test

This test assesses anxious behavior in mice. Mice were placed on a wooden beam (1 m in length, 0.5 cm in diameter), and the time needed to cross the beam was measured, as well as the number of missteps. Three trials were performed for each mouse at P53.

Morris water-maze test

This test studies spatial learning and memory. It requires a round pool of 120 cm in diameter, surrounded with visual clues and filled with water mixed with an opaque white dye. Each mouse aged P53 was given 60 s to habituate to the pool. Then, a cue session was performed at P56 and during 5 consecutive days, corresponding to the acquisition and consolidation phases. An invisible platform was placed in the northwest quadrant and submerged approximately 1 cm below the water surface. Each animal was placed in the pool and had 60 s to find the platform and to stay on it for 5 s. If mice did not find the platform, they were gently guided to it and stayed there for 20 s. Four trials with different starting positions were performed each day. On the last day, a probe session was conducted, referring to the retrieval phase. The

(See figure on next page.)

Fig. 9 Long-term effects of perinatal intermittent hypoxia on the functional organization of adult mouse cerebellum. **A** Analysis of the Glu δ 2-labeled parallel fiber area (left), and of the Vglut2-labeled climbing fiber area (middle) in the molecular layer of control (N) and hypoxic (IH) mice at P60. Measurements were done from confocal images as illustrated on the right. On Glu δ 2 images, parallel fibers appear in green and calbindin-labeled Purkinje dendrites in red. On Vglut2 images, climbing fibers appear in red and calbindin-labeled Purkinje dendrites in green. The white labeling indicates the connection points between fibers and Purkinje dendrites. **B** Analysis of the Vglut2-labeled mossy fiber area in the granule cell layer (left) of control (N) and hypoxic (IH) mice at P60. Measurements were done from confocal images as illustrated on the right. Red labeling represents mossy fiber rosettes in the granule layer delimited by calbindin-labeled Purkinje cell bodies in green. **C** Measurement of the length (left) and the volume (right) of myelin binding protein (MBP)-labeled fibers in the granule cell layer in control (N) and hypoxic (IH) mice at P60. Measurements were done from confocal images as illustrated on the right. MBP-labeling (green) indicates that myelin sheaths are mainly located in the granule layer identified by a high DAPI-labeled nucleus density. Each box-plot represents the analysis of 2000 Purkinje cells from four different animals (Calbindin), 750 Purkinje cells from three different animals (Glu δ 2), 1230 Purkinje cells from four different animals (Vglut2) and 120 confocal stack images of 10- μ m thickness and 370- μ m 2 surface from four different animals (MBP). The total number of animals in each experimental group is indicated under the boxplots and represented by diamond shapes, while the transparent dots indicate individual data points. Exact p-values are indicated above the plot. IH: intermittent hypoxia condition; N: normoxia condition; P60: postnatal day 60

RESULTS

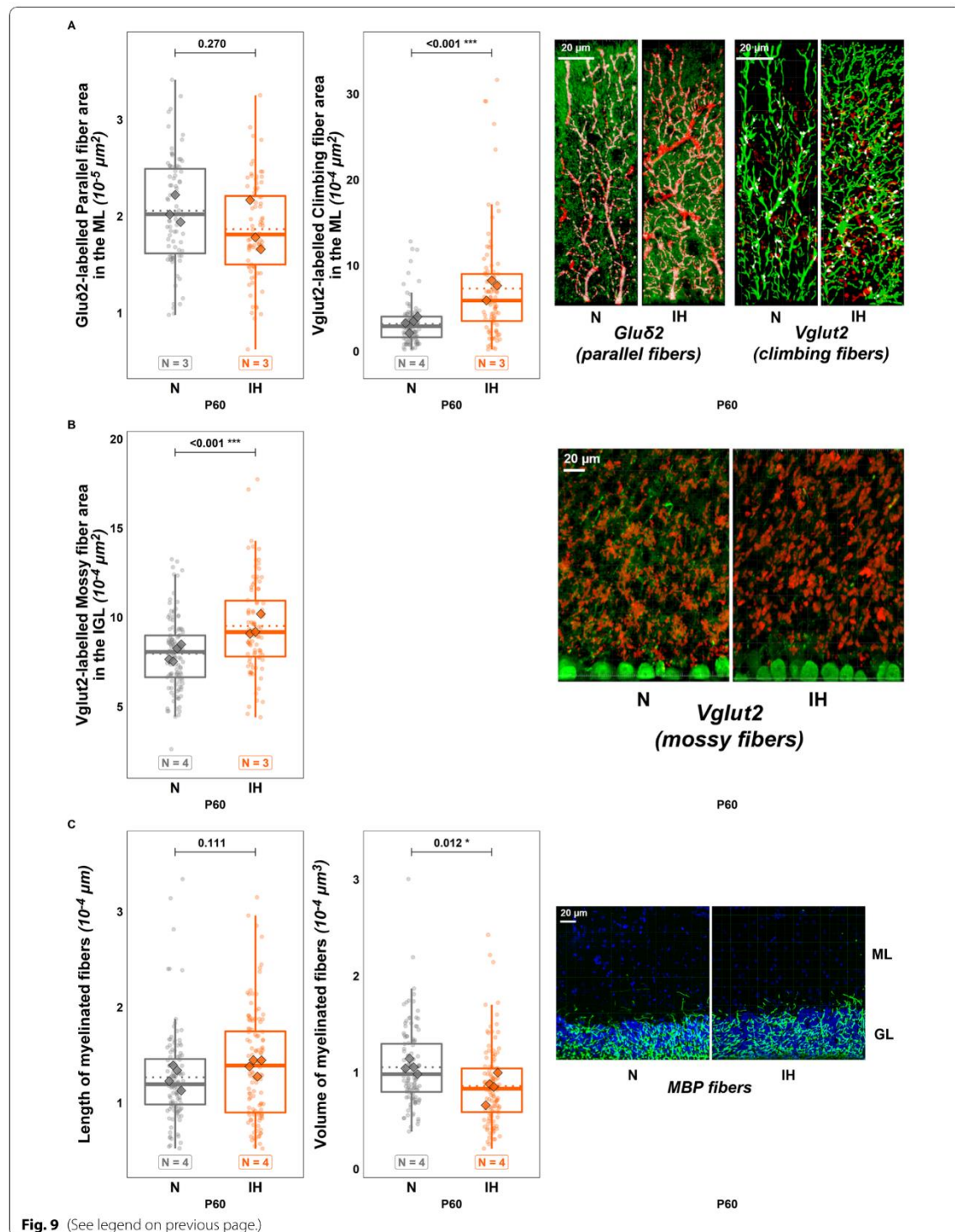


Table 1 Summary table of immunohistochemical markers used in this study

Primary antibody	Marker	Dilution	Species	Provider	Secondary antibody	Incubation time
BrdU	Proliferating cells	1/400	Sheep	Abcam (#ab1893)	DAS-633	O/N at 4 °C
Calbindin	Purkinje cells	1/1000	Mouse	Sigma-Aldrich (#C9848)	DAM-594	O/N (or 72 h with Gluδ2 and Vglut2) at 4 °C
Cleaved-caspase-3	Apoptotic cells	1/400	Rabbit	Cell Signaling Technology (#9661S)	DAR-488	O/N at 4 °C
Gluδ2	Parallel fibers	1/500	Goat	Santa Cruz (#sc26118)	DAG-488	72 h at 4 °C
MBP	Myelinated fibers	1/300	Rabbit	Sigma-Aldrich (#M3821)	DAR-488	O/N at 4 °C
Vglut2	Climbing fibers + Mossy fibers	1/500	Guinea pig	Millipore (#AB2251)	DAGp-Cy3	72 h at 4 °C

BrdU bromodeoxyuridine, DAG donkey anti-goat, DAGp donkey anti-guinea pig, DAM donkey anti-mouse, DAR donkey anti-rabbit, DAS donkey anti-sheep, Gluδ2 glutamate receptor delta2, MBP Myelin binding protein, O/N overnight, Vglut2: vesicular glutamate transporter 2

platform was removed from the pool and each mouse was placed in the center of the pool. Mice were given 60 s to explore the environment. Their behavior and different parameters such as the freezing time or distance traveled were analyzed with the video tracking software Any-MAZE.

Statistical analysis

Statistical analyses were performed within the R statistical computing environment (version 4.1.3) [58]. Model fitting was done using the "glmmTMB" package [59], and model diagnostics were done using the "DHARMa" [60] & "performance" [61] packages. Expected marginal means and contrasts were computed with the "emmeans" package [62]. P-values for the relevant contrasts were computed on the link scale, using Wald t-tests, without any adjustments. For all analyses, $p < 0.05$ was considered significant.

Data from image acquisition following immunolabeling were modeled within the Generalized Linear Mixed Model (GLMM) framework, with a random intercept per mouse to account for the correlation between pseudo-replicates taken from the same mouse [63]. Temporal data (i.e. weight changes, righting and gripping reflexes, and Morris water maze) was analyzed within the Generalized Linear Model (GLM) framework, using an autoregressive factor of order one (AR1) to account for the dependencies between the repeated measures.

For RT-qPCR data model fitting and subsequent statistical testing was done on DCq values. We used a linear mixed effect model with a random effect by plate to account for fluorescence variability between experiments.

For each response variable, the optimal likelihood families were selected based on our theoretical understanding of each variable's properties and based on Aikake's Information Criterion (AIC). Count data (e.g., cell counts, number of maze entries, ...) were modeled using

a Generalized Poisson likelihood family, measures bound at 0 (e.g., cell density, volumes, weights, ...) were modeled using a Gamma likelihood, and proportions (e.g., ratios of areas) with a Beta likelihood family. The only exception was the righting reflex measures, which were modeled using a Gaussian due to the censored nature of the data resulting in unrealistic expected values with other more theoretically appropriate distributional families.

Abbreviations

AOP: Apnea of prematurity; Ant: Anterior part of the cerebellum; BrDU: Bromodeoxyuridine; EGL: External granular layer; GCP: Granular cell precursors; Gluδ2: Glutamate receptor delta2; IGL: Internal granular layer; IH: Intermittent hypoxia; MBP: Myelin binding protein; Med: Medium part of the cerebellum; ML: Molecular layer; N: Normoxia; PL: Purkinje cell layer; Px: Postnatal day x; Post: Posterior part of the cerebellum; ROS: Reactive oxygen species; VGlut2: Vesicular glutamate transporter 2.

Supplementary Information

The online version contains supplementary material available at <https://doi.org/10.1186/s13578-022-00869-5>.

Additional file 1: Table S1. Full statistical summary of RT-qPCR data.

Additional file 2: Figure S1. Long-term effects of potential intermittent hypoxia on anxiety in adult mice.

Additional file 3: Table S2. List of primers used for RT-qPCR experiments and their corresponding sequences.

Additional file 4: Figure S2. Cerebellar frontal illustrations indicating the allocation of the slices used for immunohistochemical analyses and their assignment to one of three groups according to Bregma coordinates.

Acknowledgements

We also thank Attilio Pavan, François Chadelaud and Franck Bernard from the Electrical Engineering and Industrial Computing Department of Rouen University for their assistance in the development of the hypoxia chamber. We are grateful to Alexis Lebon for his help regarding the Imaris software and to Marc-Aurèle Rivière for his contribution to the statistical analysis and software development.

Author contributions

SL and ARD equally contributed to this work. DB, DV, AA, SL participated in the study conception and design. DB, AA, DV and SL contributed to study design

and interpretation. SL and AA performed the behavioral experiments on mice. DB, ARD and SL contributed to the immunohistochemical experiments and their quantitative analysis. ARD and MB contributed to the RT-qPCR experiments. SL and MB contributed to the biochemical assays. All authors read and approved the final manuscript.

Funding

SL and ARD were recipients of doctoral fellowships from Normandy Region and The Ministère de l'Enseignement Supérieur, de la Recherche et de l'Innovation, respectively. This work was supported by INSERM (U1239), Rouen University, Normandy Region and European Union. Europe gets involved in Normandie with European Regional Development Fund (ERDF).

Availability of data and materials

The datasets supporting the conclusions of this article are available in the following GitHub repository at <https://github.com/ma-riviere/LT-AoP-22>, also referenced on Zenodo under: <https://doi.org/10.5281/zenodo.6480947>.

Declaration

Ethic approval and consent to participate

All animal experiments were performed according to the protocols approved by the French Ministry of Agriculture and the European Community Council Directive.

Consent for publication

Not applicable.

Competing interests

The authors declare that they have no competing interests.

Author details

¹Laboratory of Neuronal and Neuroendocrine Communication and Differentiation, Institute for Research and Innovation in Biomedicine (IRIB), Normandie Univ, UNIROUEN, INSERM U1239, 76000 Rouen, France. ²Cancer and brain genomics, Institute for Research and Innovation in Biomedicine (IRIB), Normandie Univ, UNIROUEN, INSERM U1245, 76000 Rouen, France. ³Faculty of Sciences, Experimental Investigation - Service Ressources Biologiques (SRB), Institute for Research and Innovation in Biomedicine (IRIB), Normandie University, UNIROUEN, 76000 Rouen, France. ⁴Regional Platform for Cell Imaging of Normandy (PRIMACEN), Normandie University, UNIROUEN, 76000 Rouen, France.

Received: 10 May 2022 Accepted: 2 August 2022

Published online: 06 September 2022

References

- Eichenwald EC, Watterberg KL, Aucott S, Benitz WE, Cummings JJ, et al. Apnea of prematurity. *Pediatrics*. 2016;137(1):e20153757.
- Zhao J, Gonzalez F, Mu D. Apnea of prematurity: from cause to treatment. *Eur J Pediatr*. 2011;170(9):1097–105.
- Abu-Shawesh JM, Martin RJ. Neonatal apnea: what's new? *Pediatr Pulmonol*. 2008;43(10):937–44.
- Kakita H, Hussein MH, Yamada Y, Henmi H, Kato S, Kobayashi S, et al. High postnatal oxidative stress in neonatal cystic periventricular leukomalacia. *Brain Develop*. 2009;31(9):641–8.
- Huang J, Zhang L, Kang B, Zhu T, Li Y, Zhao F, et al. Association between perinatal hypoxic-ischemia and periventricular leukomalacia in preterm infants: a systematic review and meta-analysis. *PLoS ONE*. 2017;12(9):e0184993.
- Janvier A, Khairy M, Kokkotis A, Cormier C, Messmer D, Barrington KJ. Apnea is associated with neurodevelopmental impairment in very low birth weight infants. *J Perinatol*. 2004;24(12):763–8.
- Pillekamp F, Hermann C, Keller T, von Gontard A, Kribs A, Roth B. Factors influencing apnea and bradycardia of prematurity—implications for neurodevelopment. *Neonatology*. 2007;91(3):155–61.
- Cai J, Tuong CM, Gozal D. A neonatal mouse model of intermittent hypoxia associated with features of apnea in premature infants. *Respir Physiol Neurobiol*. 2011;178(2):210–7.
- Oorschot DE, Voss L, Covey MV, Goddard L, Huang W, Birchall P, et al. Spectrum of short- and long-term brain pathology and long-term behavioral deficits in male repeated hypoxic rats closely resembling human extreme prematurity. *J Neurosci*. 2013;33(29):11863–77.
- Goussakov I, Synowiec S, Yarnykh V, Drobyshevsky A. Immediate and delayed decrease of long term potentiation and memory deficits after neonatal intermittent hypoxia. *Int J Dev Neurosci*. 2019;74(1):27–37.
- Cai J, Tuong CM, Zhang Y, Shields CB, Guo G, Fu H, et al. Mouse intermittent hypoxia mimicking apnoea of prematurity: effects on myelinogenesis and axonal maturation: Intermittent hypoxia and white matter in the neonatal period. *J Pathol*. 2012;226(3):495–508.
- Volpe JJ. Cerebellum of the premature infant: rapidly developing, vulnerable, clinically important. *J Child Neurol*. 2009;24(9):1085–104.
- Rahimi-Balaei M, Bergen H, Kong J, Marzban H. Neuronal migration during development of the cerebellum. *Front Cell Neurosci*. 2018;12:484.
- Petrosini L. The cerebellum in the spatial problem solving: a co-star or a guest star? *Prog Neurobiol*. 1998;56(2):191–210.
- Lavond DG. Role of the nuclei in eyeblink conditioning. *Annals NY Acad Sci*. 2002;978:93–105.
- Guell X, Hoche F, Schmahmann JD. Metalinguistic deficits in patients with cerebellar dysfunction: empirical support for the dysmetria of thought theory. *Cerebellum*. 2015;14(1):50–8.
- Sathyanesan A, Kundu S, Abbah J, Gallo V. Neonatal brain injury causes cerebellar learning deficits and Purkinje cell dysfunction. *Nat Commun*. 2018;9(1):3235.
- Biran V, Heine VM, Verney C, Sheldon RA, Spadafora R, Vexler ZS, et al. Cerebellar abnormalities following hypoxia alone compared to hypoxic-ischemic forebrain injury in the developing rat brain. *Neurobiol Dis*. 2011;41(1):138–46.
- Chiu SC, Huang SY, Tsai YC, Chen SP, Pang CY, Lien CF, et al. Poly (ADP-ribose) polymerase plays an important role in intermittent hypoxia-induced cell death in rat cerebellar granule cells. *J Biomed Sci*. 2012;19(1):29.
- Rochefort C, Arabo A, André M, Poucet B, Save E, Rondi-Reig L. Cerebellum shapes hippocampal spatial code. *Science*. 2011;334(6054):385–9.
- Srinivasan L, Allsop J, Counsell SJ, Boardman JP, Edwards AD, Rutherford M. Smaller cerebellar volumes in very preterm infants at term-equivalent age are associated with the presence of supratentorial lesions. *AJNR Am J Neuroradiol*. 2006;27(3):573–9.
- Steggerda SJ, Leijser LM, Wiggers-de Bruine FT, van der Grond J, Walther FJ, van Wezel-Meijler G. Cerebellar injury in preterm infants: incidence and findings on US and MR images. *Radiology*. 2009;252(1):190–9.
- Farahani R, Kanaan A, Gavrialov O, Brunnert S, Douglas RM, Morcillo P, et al. Differential effects of chronic intermittent and chronic constant hypoxia on postnatal growth and development. *Pediatr Pulmonol*. 2008;43(1):20–8.
- Pozo ME, Cave A, Körögöl ÖA, Litvin DG, Martin RJ, Di Fiore J, et al. Effect of postnatal intermittent hypoxia on growth and cardiovascular regulation of rat pups. *Neuroatology*. 2012;102(2):107–13.
- Morken TS, Nyman AKG, Sandvig I, Torp SH, Skranes J, Goa PE, et al. Brain development after neonatal intermittent hyperoxia-hypoxia in the rat studied by longitudinal MRI and immunohistochemistry. *PLoS ONE*. 2013;8(12):e84109.
- Kheirandish L, Gozal D, Pequignot JM, Pequignot J, Row BW. Intermittent hypoxia during development induces long-term alterations in spatial working memory, monoamines, and dendritic branching in rat frontal cortex. *Pediatr Res*. 2005;58(3):594–9.
- Darnall RA, Chen X, Nemani KV, Sirieix CM, Gimé B, Knoblauch S, et al. Early postnatal exposure to intermittent hypoxia in rodents is proinflammatory, impairs white matter integrity, and alters brain metabolism. *Pediatr Res*. 2017;82(1):164–72.
- Dunn LL, Midwinter RG, Ni J, Hamid HA, Parish CR, Stocker R. New Insights into intracellular locations and functions of heme oxygenase-1. *Antioxid Redox Signal*. 2014;20(11):1723–42.
- Nedden S, Tomaselli B, Baier-Bitterlich G. HIF-1 alpha is an essential effector for purine nucleoside-mediated neuroprotection against hypoxia in PC12 cells and primary cerebellar granule neurons. *J Neurochem*. 2008;105(5):1901–14.

30. Wahl DR, Dresser J, Wilder-Romans K, Parsels JD, Zhao SG, Davis M, et al. Glioblastoma therapy can be augmented by targeting IDH1-mediated NADPH biosynthesis. *Can Res*. 2017;77(4):960–70.
31. Bourens M, Fontanesi F, Soto IC, Liu J, Barrientos A. Redox and reactive oxygen species regulation of mitochondrial cytochrome c oxidase biogenesis. *Antioxid Redox Signal*. 2013;19(16):1940–52.
32. Scaramuzzino L, Lucchino V, Scalise S, Lo Conte M, Zannino C, Sacco A, et al. Uncovering the metabolic and stress responses of human embryonic stem cells to FTH1 gene silencing. *Cells*. 2021;10(9):2431.
33. Curristin SM, Cao A, Stewart WB, Zhang H, Madri JA, Morrow JS, et al. Disrupted synaptic development in the hypoxic newborn brain. *Proc Natl Acad Sci USA*. 2002;99(24):15729–34.
34. Wu J, Chen Y, Yu S, Li L, Zhao X, Li Q, et al. Neuroprotective effects of sulfiredoxin-1 during cerebral ischemia/reperfusion oxidative stress injury in rats. *Brain Res Bull*. 2017;132:99–108.
35. Coimbra-Costa D, Alva N, Duran M, Carbonell T, Rama R. Oxidative stress and apoptosis after acute respiratory hypoxia and reoxygenation in rat brain. *Redox Biol*. 2017;12:216–25.
36. Raza H. Dual localization of glutathione S-transferase in the cytosol and mitochondria: implications in oxidative stress, toxicity and disease: dual localization of glutathione transferase. *FEBS J*. 2011;278(22):4243–51.
37. Lv Y, Lin Z, Li D, Han S, Zhang N, Zhang H, Li J. cPKC beta II is significant to hypoxic preconditioning in mice cerebrum. *Front Biosci*. 2020;25(4):683–98.
38. Zaghoul N, Patel H, Codipilly C, Marambaud P, Dewey S, Frattini S, et al. Overexpression of extracellular superoxide dismutase protects against brain injury induced by chronic hypoxia. *PLoS ONE*. 2014;9(9):e108168.
39. Machnicka S, Walendzik K, Kopcewicz M, Wisniewska J, Rokka A, Pääkkönen M, et al. Hypoxia reveals a new function of Foxn1 in the keratinocyte antioxidant defense system. *The FASEB J*. 2022. <https://doi.org/10.1096/fj.202200249RR>.
40. Connolly DJA, Widjaja E, Griffiths PD. Involvement of the anterior lobe of the cerebellar vermis in perinatal profound hypoxia. *AJNR Am J Neuroradiol*. 2007;28(1):16–9.
41. Biran V, Verney C, Ferriero DM. Perinatal cerebellar injury in human and animal models. *Neuro Res Int*. 2012;2012:1–9.
42. Sudarov A, Joyner AL. Cerebellum morphogenesis: the foliation pattern is orchestrated by multi-cellular anchoring centers. *Neural Dev*. 2007;2(1):26.
43. Beekhof GC, Osório C, White JJ, van Zoomeren S, van der Stok H, Xiong B, et al. Differential spatiotemporal development of Purkinje cell populations and cerebellum-dependent sensorimotor behaviors. *eLife*. 2021;10:e63668.
44. Stoodley CJ, Schmahmann JD. Functional topography of the human cerebellum. *The Cerebellum: from embryology to diagnostic investigations*. Amsterdam: Elsevier; 2018. p. 59–70.
45. Rochefort C, Lefort J, Rondi-Reig L. The cerebellum: a new key structure in the navigation system. *Front Neural Circuits*. 2013. <https://doi.org/10.3389/fncir.2013.00035>.
46. Yu W, Krook-Magnuson E. Cognitive collaborations: bidirectional functional connectivity between the cerebellum and the hippocampus. *Front Syst Neurosci*. 2015;22:9.
47. Yakusheva TA, Shaikh AG, Green AM, Blazquez PM, Dickman JD, Angelaki DE. Purkinje cells in posterior cerebellar vermis encode motion in an inertial reference frame. *Neuron*. 2007;54(6):973–85.
48. Hernández RG, De Zeeuw CI, Zhang R, Yakusheva TA, Blazquez PM. Translation information processing is regulated by protein kinase C-dependent mechanism in Purkinje cells in murine posterior vermis. *Proc Natl Acad Sci USA*. 2020;117(29):17348–58.
49. Kano M, Watanabe T, Yesaka N, Watanabe M. Multiple phases of climbing fiber synapse elimination in the developing cerebellum. *Cerebellum*. 2018;17(6):722–34.
50. Park H, Yamamoto Y, Tanaka-Yamamoto K. Refinement of cerebellar network organization by extracellular signaling during development. *Neuroscience*. 2021;462:44–55.
51. Kalinovsky A, Boukhtouche F, Blazeski R, Bornmann C, Suzuki N, Mason CA, et al. Development of axon-target specificity of ponto-cerebellar afferents. *PLoS Biol*. 2011;9(2):e1001013.
52. Zhang Q, Mason CA. Developmental regulation of mossy fiber afferent interactions with target granule cells. *Dev Biol*. 1998;195(1):75–87.
53. Hall AC, Lucas FR, Salinas PC. Axonal remodeling and synaptic differentiation in the cerebellum is regulated by WNT-7a signaling. *Cell*. 2000;100(5):525–35.
54. Juliano C, Sosunov S, Niatsetskaya Z, Isler JA, Utkina-Sosunova I, Jang I, et al. Mild intermittent hypoxemia in neonatal mice causes permanent neurofunctional deficit and white matter hypomyelination. *Exp Neurol*. 2015;264:33–42.
55. Hamza MM, Rey SA, Hilber P, Arabo A, Collin T, Vaudry D, et al. Early disruption of extracellular pleiotrophin distribution alters cerebellar neuronal circuit development and function. *Mol Neurobiol*. 2016;53(8):5203–16.
56. Schindelin J, Arganda-Carreras I, Frise E, Kaynig V, Longair M, Pietzsch T, et al. Fiji: an open-source platform for biological-image analysis. *Nat Methods*. 2012;9(7):676–82.
57. Schneider CA, Rasband WS, Eliceiri KW. NIH Image to ImageJ: 25 years of image analysis. *Nat Methods*. 2012;9(7):671–5.
58. R Core Team. R: A language and environment for statistical computing [Internet]. Vienna, Austria; 2022. <https://www.R-project.org/>. Accessed Apr 2022.
59. Brooks ME, Kristensen K, Bentham KJ, Magnusson A, Berg CW, Nielsen A, et al. glmmTMB balances speed and flexibility among packages for zero-inflated generalized linear mixed modeling. *The R Journal*. 2017;9(2):378.
60. Hartig F. DHARMa: Residual diagnostics for hierarchical (multi-level / mixed) regression models. 2022. <https://CRAN.R-project.org/package=DHARMa>. Accessed Apr 2022.
61. Lüdecke D, Ben-Shachar M, Patil I, Waggoner P, Makowski D. Performance: an R package for assessment, comparison and testing of statistical models. *JOSS*. 2021;6(60):3139.
62. Lenth RV. emmeans: Estimated marginal means, aka least-squares means [Internet]. 2022. <https://CRAN.R-project.org/package=emmeans>. Accessed Apr 2022.
63. Zimmerman KD, Espeland MA, Langefeld CD. A practical solution to pseudoreplication bias in single-cell studies. *Nat Commun*. 2021;12(1):738.
64. Paxinos G, Franklin KBJ, Franklin KBJ. The mouse brain in stereotaxic coordinates. 2nd ed. San Diego: Academic Press; 2001.

Publisher's Note

Springer Nature remains neutral with regard to jurisdictional claims in published maps and institutional affiliations.

Ready to submit your research? Choose BMC and benefit from:

- fast, convenient online submission
- thorough peer review by experienced researchers in your field
- rapid publication on acceptance
- support for research data, including large and complex data types
- gold Open Access which fosters wider collaboration and increased citations
- maximum visibility for your research: over 100M website views per year

At BMC, research is always in progress.

Learn more biomedcentral.com/submissions



RESULTS

Gene	Fold Change	Mean DCq N	Mean DCq IH	Difference	CI 95	t	Hedge g	p Value
Bax	1.073375864	5.054340496	5.035602139	0.088264285	[<0.049, 0.23]	1.34069274	0.091756692	0.194
Bcl2	0.813401016	6.905553367	7.186905812	-0.28967436	[-0.37, -0.21]	-7.83876947	-2.597825303	<0.001 ***
Casp3	1.227772125	5.160683025	4.87044249	0.290338752	[0.18, 0.4]	5.65278443	2.012341332	<0.001 ***
Casp9	1.19077743	8.567307924	8.349436329	0.248081341	[0.13, 0.37]	4.31806231	0.769238237	<0.001 ***
Cat	0.956480377	5.003649146	5.113754033	-0.076221338	[<0.17, 0.017]	-1.68895065	-0.859118513	0.104
Cox4i1	0.918959058	1.221241639	1.356367444	-0.135449162	[<0.26, -0.008]	-2.20944076	-0.838161711	0.038 *
Fth1	0.795027307	0.885491946	1.237648751	-0.34126045	[-0.45, -0.23]	-6.66941984	-2.240126687	<0.001 ***
Gpx1	0.943156154	4.231170533	4.333988904	-0.094148522	[<0.19, 0.0054]	-1.96698414	-0.765679412	0.063
Gpx3	1.042421308	6.319821809	6.302708767	0.051174178	[<0.066, 0.17]	0.90892046	0.080019892	0.374
Gpx4	0.927511168	4.280015062	4.39421687	-0.114201809	[-0.22, -0.098]	-2.23287873	-0.817357508	0.035 *
Gpx7	0.859932249	7.080293789	7.319214963	-0.220812757	[-0.3, -0.14]	-5.68848621	-1.254742874	<0.001 ***
Gpx8	0.945226228	7.161568203	7.297933339	-0.098038695	[<0.21, 0.018]	-1.75933826	-0.678314187	0.093
Gsr	0.928008246	4.902904262	5.02961933	-0.118051506	[<0.27, 0.033]	-1.632939086	-0.618977237	0.118
Gss	1.054673927	7.831836071	7.784705113	0.053467933	[<0.089, 0.2]	0.78171228	0.199406357	0.443
Gstk1	0.94722059	7.970946382	8.084911299	-0.113544922	[-0.21, -0.017]	-2.4442897	-0.936663645	0.023 *
Gstm1	1.239027344	4.837695463	4.517984723	0.319711741	[0.21, 0.43]	6.2323724	-2.359844659	<0.001 ***
Hadh	1.051150377	6.105565757	6.105938862	0.062270747	[<0.023, 0.15]	1.51921105	-0.002144386	0.144
Hif1a	1.07954192	4.788985212	4.740251492	0.105097599	[0.037, 0.17]	3.2188656	0.264951672	0.004 **
Hmox1	1.4449373017	7.866616573	7.338318394	0.528288179	[0.098, 0.96]	2.55150135	0.392309076	0.019 *
Idh1	1.076292279	3.495304062	3.366418408	0.110536107	[0.044, 0.18]	3.48087495	1.107746846	0.002 **
Ndufv2	0.916589123	1.717166271	1.8892093609	-0.149004267	[<0.26, -0.04]	-2.8444403	-1.282430717	0.010 **
Nos1	0.855651816	6.621599967	6.809994464	-0.205929901	[-0.37, -0.038]	-2.54461902	-0.809964216	0.019 *
Nqo1	0.9992977	9.003167095	8.994080685	0.00908641	[<0.15, 0.17]	0.11955384	0.047193945	0.906
Parp1	0.856514073	5.799363749	6.081332921	-0.23291455	[-0.33, -0.13]	-4.88369494	-1.631458778	<0.001 ***
Por	1.013099808	5.075462475	5.06525503	0.01693935	[<0.11, 0.14]	0.28155383	0.044664301	0.781
Prdx1	0.880579973	1.937549443	2.147491406	-0.189605261	[-0.27, -0.1]	-4.9895532	-1.84117525	<0.001 ***
Prdx2	0.970208002	2.842361711	2.918415021	-0.056043339	[<0.13, 0.017]	-1.60484975	-0.800311068	0.123
Prdx3	0.965858205	5.155521526	5.270882557	-0.060140847	[<0.14, 0.024]	-1.4897351	-0.777692151	0.151
Prdx4	1.068857575	5.56208306	5.467628621	0.093253199	[<0.012, 0.2]	1.83476927	0.514319493	0.081
Prdx5	0.927347222	3.195616283	3.351262921	-0.139197767	[<0.29, 0.095]	-1.94721249	-0.803815341	0.065
Prdx6	1.005072792	4.149100501	4.186116932	-0.007108567	[<0.12, 0.11]	-0.15634461	-0.186007056	0.901
Sod1	0.901691884	1.902865607	1.824410199	-0.149531093	[-0.24, -0.059]	-3.4413664	0.061911477	0.002 **
Sod2	1.207819919	3.617966534	3.289964055	0.255499925	[0.034, 0.481]	2.3950507	0.330793948	0.026 *
Sod3	1.889785622	5.323452757	3.869291377	0.770766111	[0.24, 1.3]	3.04419683	0.347067498	0.006 **
Srxn1	0.819579439	5.171401602	5.373212002	-0.288052655	[-0.38, -0.19]	-6.19069043	-0.214769087	<0.001 ***
Txnip	0.978655031	4.864162706	4.711002682	-0.075026972	[<0.41, 0.26]	-0.47189974	0.149759844	0.642
Txnrd1	1.055447021	4.887084967	4.611986302	0.076317094	[<0.0097, 0.16]	1.84546982	0.251331266	0.079
Txnrd3	1.904100738	7.398833171	6.359954213	0.83982495	[0.49, 1.2]	5.04212011	0.756234142	<0.001 ***

Table S1. Full statistical summary of RT-qPCR data.

Alphabetical list of all the genes tested. All tests were performed on DCq values of which the means of normoxic (N) and hypoxic (IH) and differences between both are indicated here. Test statistics (t), confidence intervals (CI 95), effect size (Hedge g) and p values were computed and are summarized in the table. Fold change is the result of the $2^{-\Delta\Delta C_t}$ calculation. Bold text represents statistically significant results, which are discussed in the text.

Panel	Gene	Gene name	NCBI reference	Forward primer	Reverse primer
Apoptosis	Bax	BCl2-associated X protein	NM_007527.3	GTTGAGCGGCCTGTCTTGTCT	GTCCTGGAAAGTAGGAGGAGGA
Apoptosis	Bcl2	B-cell CLL/lymphoma 2	NM_009741.4	GTACCTGAACGGGATCTG	GGGGCATATAGTTCACAA
Apoptosis	Casp3	caspase 3, apoptosis-related cysteine peptidase	NM_001284409.1	GAGGGCTGACTTCCGTATGCTT	AACCAGAACCGGCTCTTT
Apoptosis	Casp9	caspase 9, apoptosis-related cysteine peptidase	NM_001277932.1	TGCACTGGAGGAAGTTAAA	GCTTTCTGGAGGAAGTTAAA
Apoptosis	Hif1a	hypoxia inducible factor 1, alpha subunit	NM_010431.2	GTGACCCCTAACAGGGGG	CGTGAGTAAGCACCTCCA
Apoptosis	Parp1	poly (ADP-ribose) polymerase 1	NM_007415.2	CTATAGTCTCTCAGGGGTG	TCTCTGCTAACCCACCTTAAT
ROS Production	Cox4i1	cytochrome c oxidase subunit IV isoform 1	NM_009941.2	TGTCCTTCGAGCACATGGAG	GGCAAGGGGTAGTTCACGCCG
ROS Production	Fth1	feritin, heavy polypeptide 1	NM_010239.2	ACCGTGTCCCAGGGGTGTGCTT	ACCGTGTCCCAGGGGTGTGCTT
ROS Production	Hadh	hydroxacyt-CoA dehydrogenase	NM_0082212.4	AGGGTACAGGAGGAGCGA	ACGGACCCATGGGATAACCCAGC
ROS Production	Hmox1	heme oxygenases (decycling) 1	NM_010442.2	TCGAGCATAGGCCGAGCCT	AATCTCTGGGATGCTGTGCG
ROS Production	Idh1	isocitrate dehydrogenase 1 (NADP+), soluble	NM_00111320.1	CATTCTGGTGGCACTGTCTT	TATGCAATGTCGCCAATGAA
ROS Production	Ndufv2	NADH dehydrogenase (ubiquinone) flavoprotein 2	NM_001278415.1	GCTATGAAACAAGGGCTGCAA	TCCCCACTGGTTTCGATTAA
ROS Production	Nos1	nitric oxide synthase 1	NM_008712.2	CCTGAAAGGATGGAAAGAACG	CAGGCTGCTTGGAGCAAAA
ROS Production	Nqo1	NAD(P)H dehydrogenase, quinone 1	NM_008706.5	TCCAGGTTGCCAACATTCGA	TCCAGGCAAGGGACTATGGTC
ROS Production	Por	P450 (cytochrome) oxidoreductase	NM_008838.1	GGCCCCAACAGGTCTATGTC	TCTTGGCCATATTGGAGC
Antioxidant Response	Cat	catalase	NM_009804.2	GGAGGGGGAAACCAAAT	CAAAGTGTAAAAATTGGGCTGAA
Antioxidant Response	Gpx1	glutathione peroxidase 1	NM_008160.6	ACACCGGGAAATGCAAGAA	TTCTGCTGGCTCTGTT
Antioxidant Response	Gpx3	glutathione peroxidase 3	NM_008161.3	TCAAAGAACTGAATGGCACTACAGAA	TCGCGGGATGCAACATGGT
Antioxidant Response	Gpx4	glutathione peroxidase 4	NM_001037741.3	GGGGGTCTGAGCGCTTAC	TGCTCTGTTAATACGGGCTT
Antioxidant Response	Gpx7	glutathione peroxidase 7	NM_024198.3	GCCTTCAGTACCAACCCAGAC	GTTCTCTGGCTTCAGGAATT
Antioxidant Response	Gpx8	glutathione peroxidase 8	NM_027127.2	AGATATTGCACTTGTCTCTATGG	AATGCAACACCACTTTCTT
Antioxidant Response	Gsr	glutathione reductase	NM_010344.4	GCCTTACCCCGATGATCA	GGCAGTCCCCTGCTGGGGT
Antioxidant Response	Gss	glutathione synthetase	NM_00129111.1	CAGCTGACCCGACAGTCTT	AAGAACAGCGAACAAACCA
Antioxidant Response	Gstk1	glutathione S-transferase kappa 1	NM_029555.2	GGTCAGTCTCTGTAAGGCAGTT	GGATGGGGTGTGTCAGTCGC
Antioxidant Response	Gstm1	glutathione S-transferase mu 1	NM_010358.5	GTGAGACACTGTTGGTCGAC	TGTCCATCTGGCATAACAGC
Antioxidant Response	Prdx1	peroxiredoxin 1	NM_011034.4	GGCTTACGGCTCAAGCAGT	GAAGGACCATCCACAC
Antioxidant Response	Prdx2	peroxiredoxin 2	NM_011563.5	CTTAAAGCACCAGTTCTCTTCCA	GACTGAGCTCTTGAACCTCCATT
Antioxidant Response	Prdx3	peroxiredoxin 3	NM_007452.2	GACCAAGACACTGGTTGG	GCAGACTCTCCATGCTGTC
Antioxidant Response	Prdx4	peroxiredoxin 4	NM_016764.4	CGAGTCCTGGGCTGQAAA	CACACTCCAAACCTGCTCTT
Antioxidant Response	Prdx5	peroxiredoxin 5	NM_012021.2	CCACCCACGGGCAAGGA	GGGAACATACATCACGCTCTT
Antioxidant Response	Prdx6	peroxiredoxin 6	NM_007453.3	AAGGGGTGACCCGGAGGA	CTGGCATGGTACAGCTTGTGTA
Antioxidant Response	Sod1	superoxide dismutase 1	NM_011434.1	GGCTGGGAGCACACATTA	GTTGGGGTTGAGATTGTTCA
Antioxidant Response	Sod2	superoxide dismutase 2	NM_013671.3	GGGGAGGCAACTCAGAG	TGGCTGAGGTCTCTGAC
Antioxidant Response	Sod3	superoxide dismutase 3	NM_011435.3	AGGGGTTCTGCAAACCTA	TGGCATAGTACTCTACGTCT
Antioxidant Response	Srxn1	sulfiredoxin 1	NM_029688.5	NM_00109935.2	CCTTGATCCACAGGACCTT
Antioxidant Response	Tnrip	thioredoxin interacting protein	NM_001042513.1	GTGGCCGGACGGGTTAATGT	GATGTCACCGATGGGTAGAT
Antioxidant Response	Tnrd1	thioredoxin reductase 1	NM_001178058.1	ACCGTGGGGCTGAAGATAAA	TTGGCTTACCTGCTGGTTATA
Antioxidant Response	Tnrd3	thioredoxin reductase 3	NM_008302.3	GTGAAACATGGCCGATTCATGT	CGTCAAGCTCTCATATCGAA
Housekeeping Genes	Hsp90ab1	heat shock protein 90 alpha, class B member 1	NM_008907.1	CCATGTCGCTTTGGCGC	TGCAAACAGCTCGAAGGAGACGC
Housekeeping Genes	Pia	peptidylprolyl isomerase A	NM_011740.3	AGGAACTAAAGGGTGGGTCA	CGGGGTTCTCCAAATCACT
Housekeeping Genes	Ywhaz	Tyrosine 3-Monoxygenase/Tryptophan 5-Monooxygenase Activation Protein Zeta			

Table S2. List of primers used for RT-qPCR experiments and their corresponding sequences. Table providing the list of genes tested, its full name and National Center for Biotechnology Information reference number. Genes are divided into three panels, namely "Apoptosis", "ROS production" and "Antioxidant response". Primer sequences indicated were designed on the Primer Express software and ordered from Integrated DNA Technologies.

RESULTS

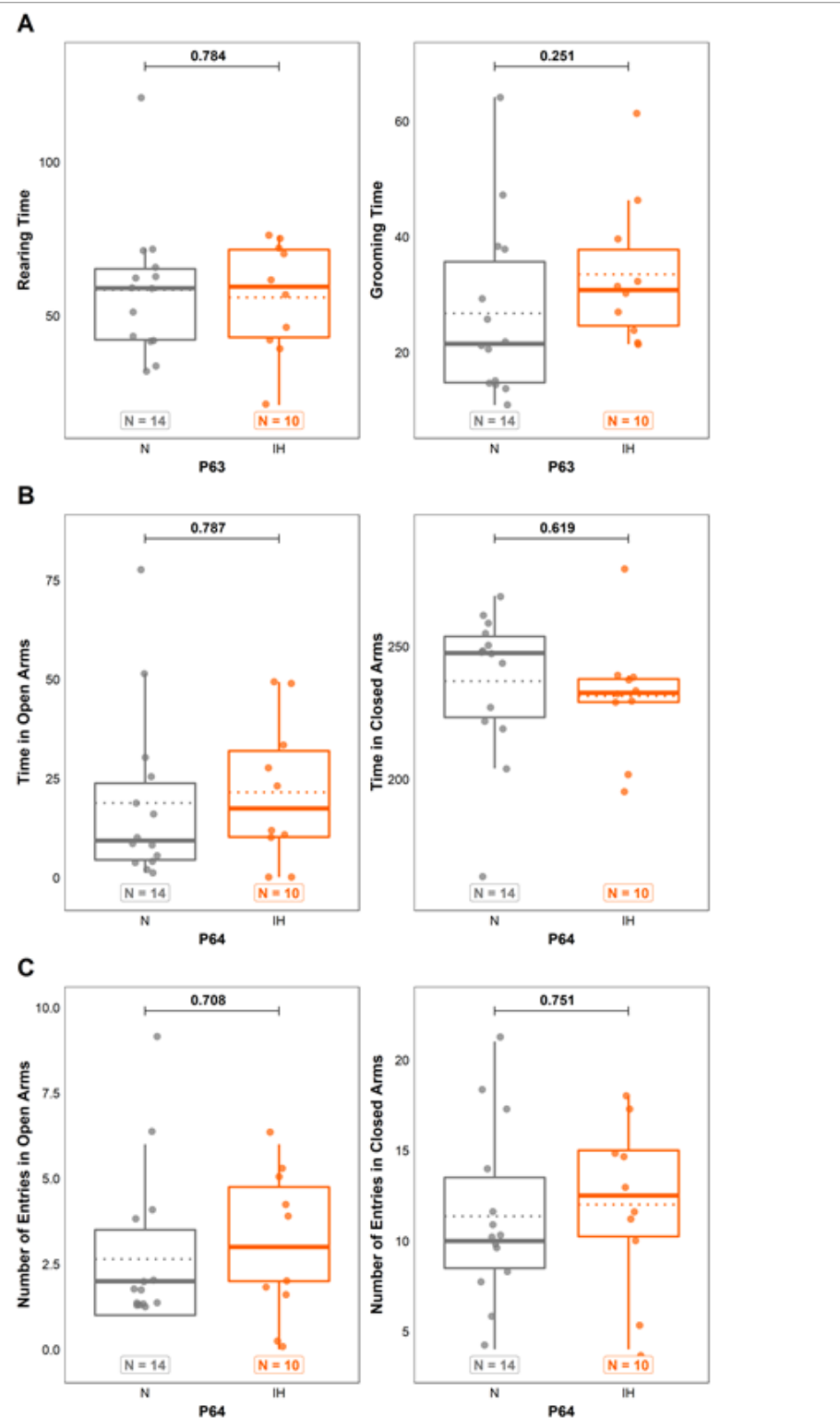


Figure S1. Long-term effects of perinatal intermittent hypoxia on anxiety in adult mice.

A. Measurement of the rearing (left) and grooming (right) times in control (N) and hypoxic (IH) P63 mice during the actimetry test. **B-C.** Measurement of the time spent (B) in open (left) and closed (right) arms, as well as the number of entries (C) in the open (bottom left) and closed (bottom right) arms of the elevated plus maze for control (N) and hypoxic (IH) P64 mice. The total number of animals in each experimental group is indicated under the boxplots and exact p-values are indicated above. IH: intermittent hypoxia condition; N: normoxia condition.

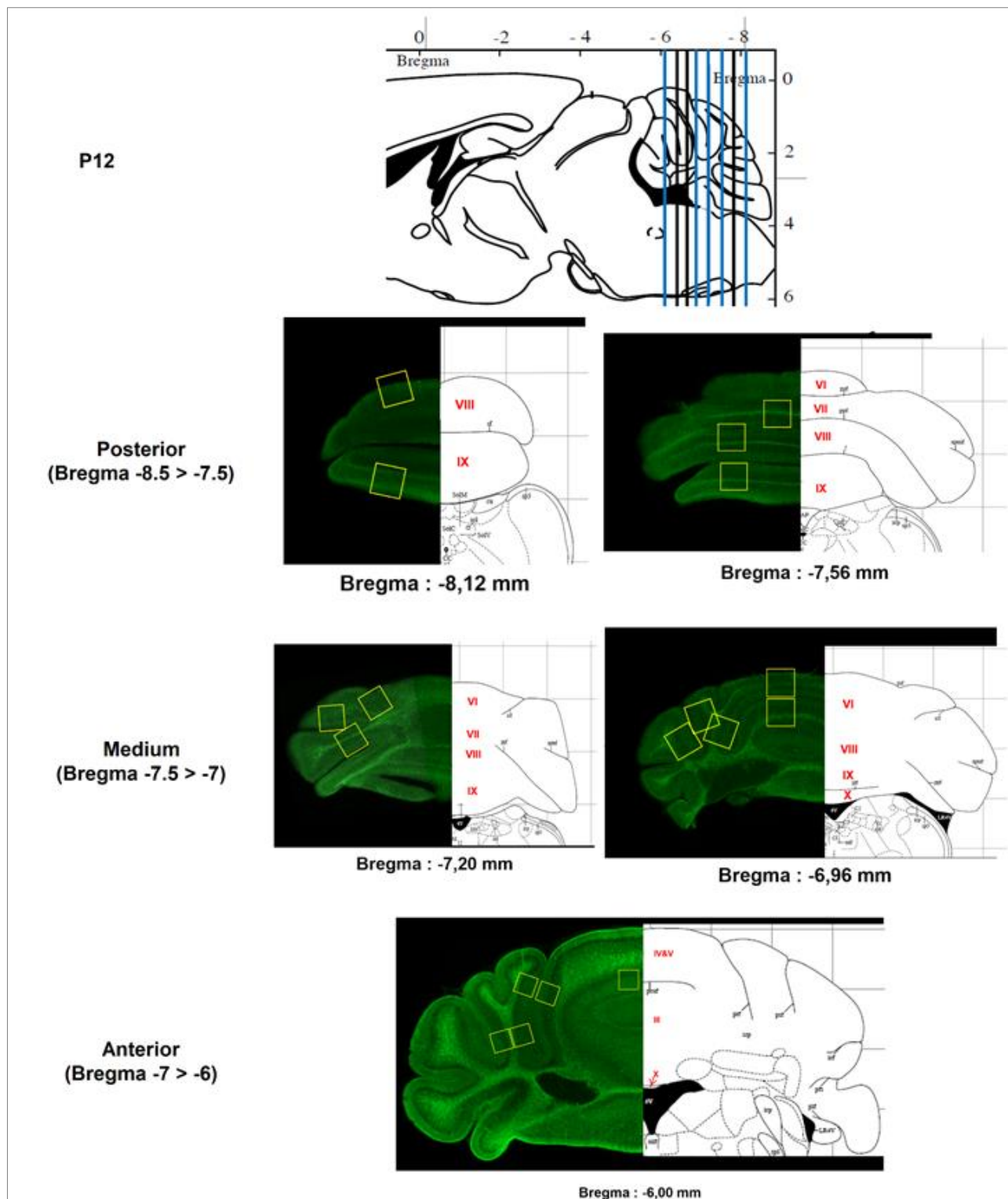


Figure S2. Cerebellar frontal illustrations indicating the allocation of the slices used for immunohistochemical analyses and their assignment to one of three groups according to Bregma coordinates.

Diagrams come from an adult mouse brain atlas [64] and the cerebellum images were acquired in a P12 mouse following a GFAP labeling. Yellow squares indicate the regions we focused on for acquisition. The black grid on the diagrams represents 1-mm squares. GFAP: glial fibrillary acidic protein; P12: postnatal day 12.

2. Graphical summary

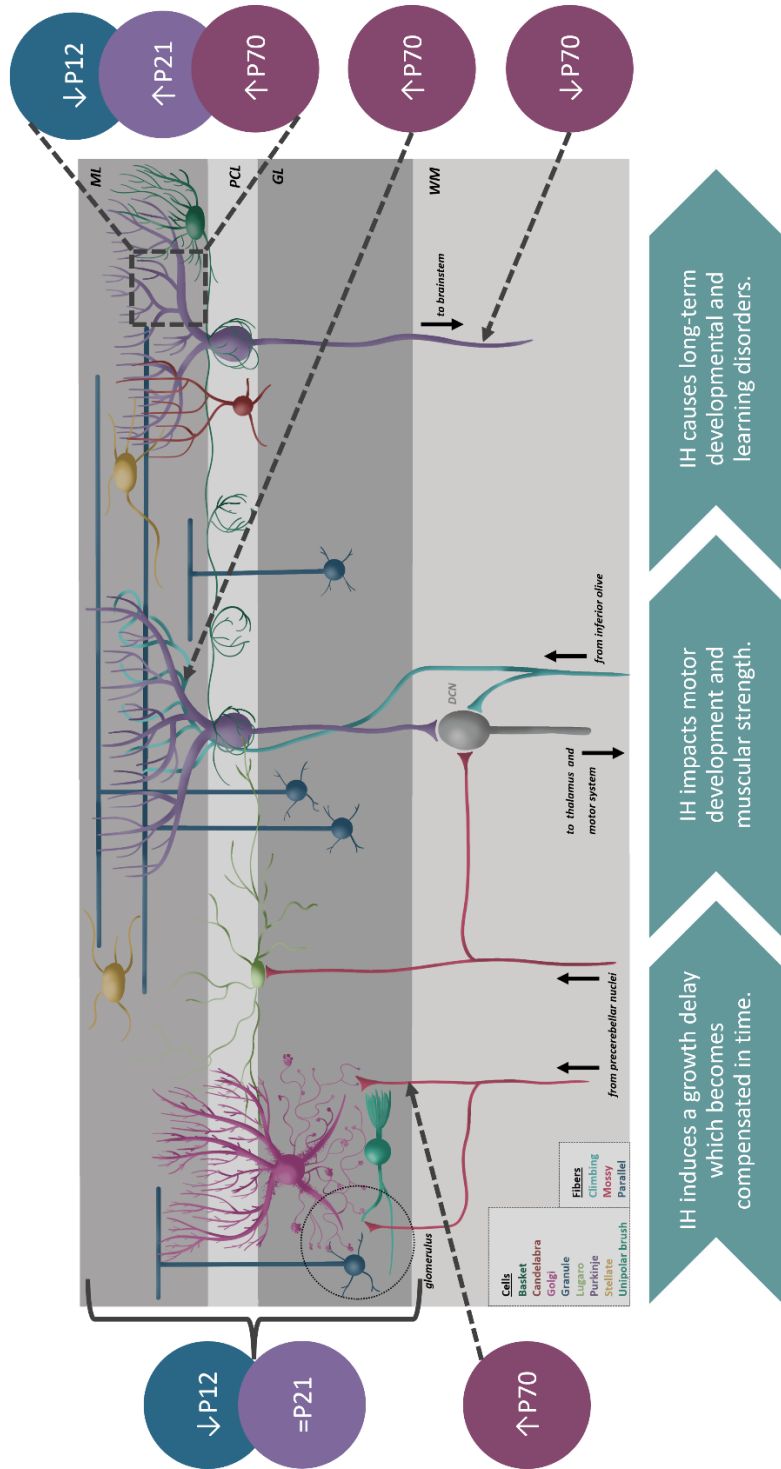


Figure 37: Main findings presented in article 1.

Concerning the cerebellar cortex, we found delayed maturation and thickness at P12 after IH which was later compensated at P21. Purkinje cells abnormalities present initially as a less dense dendritic tree at P12 in IH, then as a dendritic densification at P21 and in adulthood. Additionally, the increase in afferent innervation and axon hypomyelination persist in the long term. In addition to the observed histological deficits, our IH protocol induces short term growth delay and motor deficits as well as significant disorders in spatial learning that persist in adulthood. DCN: deep cerebellar nuclei; GL: granular layer; ML: molecular layer; PCL: Purkinje cell layer; Px: postnatal day x; WM: white matter.

B. JOURNAL ARTICLE 2:

1. Presentation***Apnea of prematurity induces oxidative stress-mediated transcriptional changes in the murine cerebellum*****A. Rodriguez-Duboc, M. Basille-Dugay, A. Debonne, D. Vaudry and D. Burel.***In submission.***My contributions to this work consisted in:**

- IH protocols
- IHC protocols
- Primer design and validation
- Laser capture microdissection
- RT-qPCR experiments
- Statistical analyses
- Writing

Our main findings, as summarized in figure 38 (c.f. page 165):

- Our IH protocol causes OS as shown by the increase in ROS.
- In response there was the establishment of an antioxidant defense.
- We did not find an increased marking of cleaved caspase-3 at P4 or P8.
- OS elicits cellular adaptative responses and triggers different cell death pathways.
- P4 pups having undergone IH present a delay in proliferation that is later compensated.
- Overall, P8 seems to be the stage most sensitive to IH-induced gene regulation.
- The migration of GCs is affected.
- Purkinje cells and the cerebellar circuit are impacted by IH.

RESEARCH

Apnea of Prematurity induces short and long-term development-related transcriptional changes in the murine cerebellum.

Agalie Rodriguez-Duboc¹, Magali Basille-Dugay², Aurélien Debonne^{1,3}, Marc-Aurèle Rivière⁴, David Vaudry^{1,3} and Daphné Burel^{1,3*}

Abstract

Apnea of prematurity (AOP) affects more than 50% of preterm infants and leads to perinatal intermittent hypoxia (IH) which is a major cause of morbimortality worldwide. At birth, the human cerebellar cortex is still immature, making it vulnerable to perinatal events. Additionally, studies have shown a correlation between cerebellar functions and the deficits observed in children who have experienced AOP. Yet, the cerebellar alterations underpinning this link remain poorly understood. To gain insight into the involvement of the cerebellum in perinatal hypoxia-related consequences, we developed a mouse model of AOP. Our previous research has revealed that IH induces oxidative stress in the developing cerebellum, as evidenced by the overexpression of genes involved in reactive oxygen species production and the under-expression of genes encoding antioxidant enzymes. These changes suggest a failure of the defense system against oxidative stress and could be responsible for neuronal death in the cerebellum.

Building upon these findings, we conducted a transcriptomic study of the genes involved in the processes that occur during cerebellar development. Using real-time PCR, we analyzed the expression of these genes at different developmental stages and in various cell types. This enabled us to pinpoint a timeframe of vulnerability at P8, which represents the age with the highest number of downregulated genes in the cerebellum. Furthermore, we discovered that our IH protocol affects several molecular pathways, including proliferation, migration, and differentiation. This indicates that IH can impact the development of different cell types, potentially contributing to the histological and behavioral deficits observed in this model.

Overall, our data strongly suggest that the cerebellum is highly sensitive to IH, and provide valuable insights into the cellular and molecular mechanisms underlying AOP. In the long term, these findings may contribute to the identification of novel therapeutic targets for improving the clinical management of this prevalent pathology.

Keywords: Apnea of prematurity; Intermittent hypoxia; Transcriptome; Cerebellum; Development

1 Introduction

Apnea of prematurity (AOP) is particularly common in premature newborns due to their immature respiratory system (Moriette *et al.*, 2010). This condition affects 50% of all preterm infants and nearly 100% of very preterm infants (i.e., born before 28 gestational weeks). AOP is characterized by breathing cessation episodes occurring at least every 5 minutes, and lasting over 20 seconds, which can be associated with bradycardia or O_2 desaturation (Eichenwald *et al.*, 2016).

AOP thus induces intermittent hypoxia (IH), which typically subsides in 98% of cases by the time the corrected term is reached. However, numerous studies have shown a correlation between the duration of AOP and the occurrence of developmental abnormalities (Henderson-Smart, 1981; Pergolizzi *et al.*, 2022; Poets, 2020).

Due to its high metabolic requirements, the central nervous system (CNS) is particularly sensitive to O_2 availability, and the consequences of AOP appear to be essentially neurological. The impact of hypoxic brain injuries has been well investigated, and several studies have shown that IH affects various CNS regions such as the periventricular white matter (WM), frontal cor-

*Correspondence: delphine.burel@univ-rouen.fr

¹Normandie Univ, UNIROUEN, INSERM, U1245, Cancer and brain genomics, Institute for Research and Innovation in Biomedicine (IRIB), 76000, Rouen, France

Full list of author information is available at the end of the article

tex, corpus callosum, and brainstem (Cai *et al.*, 2012; Darnall *et al.*, 2017; Ferriero, 2001; Kheirandish *et al.*, 2005). In contrast, the involvement of the cerebellum in perinatal hypoxia-related sequelae has been largely overlooked. However, both in rodents and humans, the cerebellum's immaturity at birth renders it particularly vulnerable to perinatal events, and several neurological functions affected by AOP, such as learning and motor coordination, are partially controlled by the cerebellum (Volpe, 2009).

Using a mouse model of AOP, we have recently demonstrated that the cerebellum is indeed impacted by IH, leading to short- and long-term behavioral disorders, such as motor impairments and significant deficits in spatial learning (Leroux *et al.*, 2022). These alterations are associated with a delay in cerebellar cortex differentiation, a density change in Purkinje cell arborization, a decrease of the volume of myelin sheaths, and an increase of afferent innervations (Cai *et al.*, 2012; Leroux *et al.*, 2022; Scheuer *et al.*, 2017). However, the molecular mechanisms underlying IH-induced impairments have yet to be fully elucidated.

During episodes of hypoxia, O_2 deprivation is always followed by a reoxygenation phase (Prabhakar and Semenza, 2012). This causes both metabolic and oxidative stresses, which results in an increase of reactive oxygen species (ROS). Normally, cells can compensate for this increase by adjusting their energy metabolism and activating antioxidant mechanisms (Birben *et al.*, 2012; Hardie *et al.*, 2012). However, in the case of AOP, the chronic nature of IH leads to repeated reoxygenation phases. This cycle results in an overproduction of ROS, which ends up surpassing the reducing capacity of antioxidant enzymes, causing oxidative stress (OS), and leading to neuronal defects (Cai *et al.*, 2012; Leroux *et al.*, 2022).

In this project, our aim was to determine whether there is a specific timeframe or cell type that is more vulnerable to IH during cerebellar development, and to uncover the molecular bases underlying short- and long-term deficits observed after AOP. We initially examined a specific panel of OS-related genes in the whole cerebellum at different postnatal stages, from P4 to adulthood. Subsequently, we performed a transcriptomic analysis of genes involved in different developmental processes such as proliferation, cell differentiation, and migration, on each cerebellar layer. As Purkinje cells represent the cerebellum's integration center and seem to be the most affected during AOP (Leroux *et al.*, 2022), we also narrowed our focus to study these neurons. Altogether, our goal is to provide elements to correlate cerebellar transcriptomic regulations with both existing histological findings and

long-term impairments observed in children having experienced AOP. Through these efforts, we aim to enhance our understanding of the cellular and molecular mechanisms underlying the pathophysiology of AOP.

2 Materials and methods

2.1 Animals

This study used wild-type C57Bl6/J mice born and bred in an accredited animal facility (approval number B.76-451-04), in accordance with the French Ministry of Agriculture and the European Community Council Directive 2010/63/UE of September 22nd, 2010, on the protection of animals used for scientific purposes. The mice were kept under a 12-hour light/dark cycle and had free access to food and water. Sex identification was done both by anogenital distance measurement and pigment-spot localization before sacrifice (Wolterink-Donselaar *et al.*, 2009). Starting at P2, mice were assigned a unique identifier before initializing the protocol. There was no blinding in this study, and sample size was chosen based on power determination from our preliminary studies.

2.2 Intermittent hypoxia protocol

Our IH model relies on an in-house hypoxia chamber, which is based on the protocol developed by Cai *et al.*, and has been validated to mimic AOP (Cai *et al.*, 2012; Leroux *et al.*, 2022). The IH sequence consisted of 2-min cycles of hypoxia (5% O_2 ; 20 s/cycle) and re-oxygenation, for 6 hours per day, throughout the sleep phase of the animals (10 am - 4 pm). The protocol was initiated on neonatal P2 C57Bl6/J pups (IH group) and continued for 10 consecutive days maximum, or until the desired stage. During experiments, oxygen concentration, hygrometry, temperature, and atmospheric pressure were constantly monitored within the chamber. The control group (N) was placed in another chamber, which mimics the hypoxia chamber's environment, to control for external stressors.

2.3 Sample gathering

For real-time PCR experiments, mice were sacrificed at stages P4, P8, P12, P21, and P70 by decapitation after anesthesia by isoflurane inhalation (Iso-VET). Whole brains were immediately harvested and put in pure isopentane at -30°C. They were then stored in sterile containers at -80°C until further use. Sample size for real-time PCR were: 13 for P4 (7N + 6IH), 16 for P8 (6N + 10IH), 25 for P12 (15N + 10IH), 17 for P21 (9N + 8IH), and 8 for P70 (5N + 3IH).

For immunohistochemistry, P8 mice were lethally anesthetized by intraperitoneal injection of ketamine (100 mg/kg) and xylazine (10 mg/kg), and then sacrificed by intracardiac perfusion of NaCl 9% and

paraformaldehyde 4%, before removing the brains. Due to their diminutive size, brains from P4 mice were directly harvested and fixed by immersion. Brains were then submerged overnight in 4% paraformaldehyde, and then stored in phosphate buffer saline (PBS) prior to slicing. Sample size for IHC were: 13 for P4 (8N + 5IH), and 12 for P8 (6N + 6IH).

2.4 Panels and primer design

This project relies on 2 panels of genes of interest (GOI). The **oxidative stress panel** was developed by Lacaille et al. to specifically study OS, ROS increase mechanisms, and the cellular response to OS (Lacaille et al., 2015). Gene annotation, pathway identification and functions were investigated and illustrated with the Cytoscape software and the stringR enrichment database (Fig. 1). The **neurodevelopment panel** was built based on the cerebellar development transcriptome database (CDT-DB; <http://www.cdtb.brain.riken.jp>). This annotated experimental database includes layer-specific genome-wide transcriptomic data for different developmental stages (Sato et al., 2008). The panel was further expanded based on bibliographical data and the Cytoscape software, and by enrichment with stringR and GO.

Gene primers were designed with the Primer Express software (v3.0.1; ThermoFischer Scientific) using nucleotide sequences from the NCBI Pubmed database. Primer pairs were supplied by Integrated DNA Technologies and validated by linear regression of serial dilution data. Primer pairs were chosen preferentially to be on exon joining sites, with the least possible hairpin and dimer formation, and with similar size, GC percentage, and melting temperature for forward and reverse primers. Each sequence was blasted on Pubmed to ensure specificity. See Appendices A and B for primer pair sequences and specifications.

2.5 Laser capture microdissection

Frozen brains were transferred to a -20°C freezer two hours prior to use. Brains were fixed to the refrigerated support (set to -20°C) of the Cryomicrocut (Leica 3050) with Tissue-Tek by the frontal extremity. Cerebella were then cut into 14 micrometers-thick slices with a blade kept at -18°C. Slices were immediately placed on membrane-coated slides (cat. 415190-9041-000 1.0 PEN, Carl Zeiss SAS) previously sterilized with dry heat (3 hours at 170°C). Each slide was stained with 2.8% cresyl violet solution and progressively dehydrated in ethanol solutions. Surfaces of 700,000 μm^2 (for each cerebellar layer) and 130,000 μm^2 (for approximately 300 individual Purkinje cells) were drawn and cut with the LCM microscope and software (Leica) and then kept in lysis buffer

(LB1+LB2 from the Nucleospin RNA plus XS extraction kit by Macherey-Nagel) until extraction.

2.6 RNA Extraction

The samples issued from microdissection were purified on column using the Nucleospin RNA plus XS extraction kit from Macherey-Nagel (cat. 740 990 250). Samples for the whole cerebellum study were homogenized in 1 ml of Trizol (ThermoFisher), and mRNAs were further purified on column using the Nucleospin RNA extract II from Macherey-Nagel (cat. 740 955 250) according to manufacturer recommendations. RNA quantity and purity were analyzed by UV spectrophotometry (Nanodrop Technologies) and mRNA quality assessment was performed by a bioanalyzer gel electrophoresis on RNA 6000 Pico chips (cat. 5067-1513, Agilent). The mRNAs were then stored at 80°C until the next step.

2.7 Real-time qPCR

Total mRNAs were retrotranscribed to cDNA by reverse transcription using either i) the Quantitect RT Kit (cat. 205313, Qiagen) for surfaces of 700,000 μm^2 ; ii) amplified and retrotranscribed with the SMARTer® Pico PCR cDNA Synthesis Kit and Advantage® 2 PCR Kit (cat. 634928/7 and 639207, Takara) for surfaces of 130,000 μm^2 ; or iii) retrotranscribed with the Prime Script RT reagent kit (cat. RR037A, Takara) for whole cerebella. The determination of the expression level of genes was done by real-time PCR in 384-well plates. The reaction volume was 5 μL including: 2.5 μL 2X Fast SYBR Green PCR Mastermix (cat. 4385612, ThermoFisher), target gene-specific sense and antisense primers (0.15 μL of each, 100 nM final concentration), 1 μL PCR-grade water, and 1.2 μL of sample solution. The distribution of cDNA samples and reaction mixes was performed by the Bravo 1 liquid handling platform (Agilent). The real-time PCR reaction took place in a QuantStudio Flex 12k thermal cycler (Applied Biosystems). For each gene of the panel, sample measurements were conducted at least in duplicate, with at least two house-keeping genes (HKG) from Table 1. Raw data output was calculated via the $2(-\Delta\Delta\text{Cq})$ method where:

$$2^{-\Delta\Delta\text{Cq}} = 2^{(-(Cq_{GOI_{IH}} - Cq_{HKG_{IH}}) - (Cq_{GOI_N} - Cq_{HKG_N}))}$$

2.8 Immunohistochemistry

Fixed cerebella were cut in 40 μm -thick slices with a vibratome (Leica Microsystems VT1000S), and then placed in a 24-well plate in 1mL 1X PBS. Non-specific site blocking was first performed for one hour in the presence of normal donkey serum diluted at 1:50 in an incubation solution containing 1X PBS, Triton X-100 (0.3%), and bovine serum albumin (1%). The slices

were then incubated overnight at 4°C with specific primary antibodies: i) rabbit cleaved caspase-3 (Cell signaling technology #9661S at a 1:400 dilution) to mark apoptotic cells; and ii) mouse calbindin (Sigma Aldrich #C9848 at a 1:1000 dilution) to target Purkinje cells. Afterward, the slices were rinsed with 1X PBS and incubated for 2 hours at room temperature, with donkey anti-rabbit Alexa488 and donkey anti-rabbit Alexa594 diluted at 1:300, respectively. This step was followed by 3 further 1X PBS rinses. The slices were then incubated in the presence of 4',6'-diamidino-2-phenylindole (DAPI; 1 µg/mL) for 1 minute for nuclear labeling. After a final rinse, the sections were mounted on slides using Mowiol.

2.9 Statistical analysis

Statistical analyses were performed within the R statistical computing environment (version 4.3). Both real-time PCR and IHC data were modeled through the Generalized Linear Mixed Model (GLMM) framework, using the {glmmTMB} package (Brooks et al., 2017).

For real-time PCR data, a Gaussian likelihood with an identity link function was used to model the distribution of the DCq samples for each gene of interest. When DCq samples for one gene were split over multiple plates, a random intercept was added to account for intra-plate correlations. Immunohistochemistry data consisted of many types of variables, which required different likelihood families. Count data (e.g., cell counts) were modeled using Generalized Poisson likelihoods, to account for potential over or under-dispersion. Measures bound at 0 (e.g., cell density, areas, and volumes) were modeled using a Gamma likelihood, and proportions (e.g., ratios of areas) with a Beta likelihood. When multiple measures were taken from the same mouse, a mouse random intercept was added to account for the correlation between technical replicates (Zimmerman et al., 2021).

Model diagnostics were done using the {DHARMA} (Hartig, 2022) and {performance} (Lüdecke et al., 2021) packages. The fitness of each model was assessed through both visual checks (e.g., posterior predictive checks, QQ plots, residuals vs predicted values) and quantitative indices of model fit (e.g., AIC: Akaike Information Criterion). When several competing models were possible a priori, we selected the most plausible one primarily based on our theoretical understanding of the response's properties, and, to a lesser extent, to minimize AIC and favor model parsimony.

Contrasts and p-values for relevant hypotheses were obtained using the {emmeans} package (Lenth, 2022). They were computed on the link scale, using Wald t-tests, without any multiplicity adjustments. For all analyses, $p \leq 0.05$ was considered significant.

3 Results

In addition to the results mentioned below, all real-time PCR results are featured in Appendices C, D and E.

3.1 IH induces OS and triggers different cellular response mechanisms

3.1.1 All stages are sensitive to IH but P8 is more vulnerable

Among the 37 OS-related genes tested, 31 show differential expression between normoxia and IH at P4, P8, P12, P21, and/or P70 (Fig. 2). Cerebellar cells start responding to hypoxia at P4, with the maximum number of regulated genes observed at P12. However, this regulation is mainly a positive defense reaction with a high upregulation of antioxidant enzymes, such as Txnrd3 and Sod3. In contrast, the most deleterious regulation is found at P8, with the downregulation of 5 antioxidant enzymes (Txnrd1, Sod3, Prdx6, Prdx5 and Cat), and only a few beneficial regulations. After the end of the protocol, some genes remain differentially regulated or become so (Fig. 2). Two such genes are Idh1 and Txnrd3, which are upregulated at P12 and P21 but become downregulated at P70, or Ccs and Gpx3 whose expression is only increased in adulthood.

3.1.2 IH induces the regulation of various cell death and survival pathways

Our immunohistochemical analysis indicated that the cleaved caspase-3 positive cells are mainly localized in the IGL and the WM (Fig. 3A). The comparison of the density of these cells between hypoxic and normoxic mice revealed a higher number of apoptotic cells after IH at P4 ($t(32) = -2.58; p = 0.015; Ratio = 0.454; CI_{95} = [0.243, 0.847]$) but no statistically difference between both conditions at P8 ($t(30) = -1.532; p = 0.136; Ratio = 0.591; CI_{95} = [0.293, 1.192]$) (Fig. 3B).

In contrast, real-time PCR results indicated that cell death/protection pathways are activated during IH. Indeed, after a slight regulation as early as P4, the response to IH is most prominent at P8 and P12, with 10 and 9 regulated genes, respectively. It is interesting to note that, at P8, there is a downregulation of genes expected to exert a protective effect on cellular components, such as the transcription factor Sp1. Meanwhile, there is an equilibrium between pro- and anti-apoptotic mechanisms at P8. However, the response is shifted towards an overall upregulation of the apoptotic pathway at P12 (Fig. 4), with the upregulation of both caspase-3 and -9 genes and downregulation of the anti-apoptotic gene Bcl2.

3.1.3 IH activates various cellular response pathways during cerebellar development

OS also triggers the activation of various cellular pathways, such as inflammation and autophagy. Indeed, 29 genes belonging to these intracellular pathways were tested on the whole cerebella of P4, P8, P12, P21, and P70 mice. 19 of these are differentially regulated by IH during cerebellar development (Fig. 4). At P4, IH induces a moderate pro-inflammatory (3 regulated genes) effect, while an opposite regulation is observed at P8, with 9 anti-inflammatory regulations. These expression modifications are somewhat maintained at P12, while Mt1 and Mt2 become markedly underexpressed at P21. Concerning autophagy and mitochondrial adaptation, the effect of IH is less clear since Kif9 and Hspa5, but also Jun and Parp1 are downregulated between P4 to P21. Finally, at P70, only a few genes are still dysregulated (Fig. 4).

3.2 The effect of IH on the cerebellum varies by stage and layer

A panel of 54 genes in total was tested in the different cerebellar layers, microdissected at P4, P8, P12, P21, and P70. A graphical representation provides an overview of the molecular pathways altered by IH, grouped by developmental stage and cerebellar layer (Fig. 5), and sorted according to the major mechanisms implicated in cerebellar development i.e., proliferation and repair, cellular differentiation, migration and response, and cell communication. The impact of IH on each of these mechanisms is described below, but overall, the stage which presents the most transcriptomic regulations is P8 (Fig. 5).

3.2.1 IH affects the EGL and cellular proliferation

By using DAPI labelling, we have demonstrated that the area of the EGL is significantly smaller in IH mice at P4 ($t(32) = 2.903; p = 0.007; Ratio = 1.47; CI_{95} = [1.122, 1.927]$) but this difference is no longer present at P8 ($t(30) = 0.671; p = 0.507; Ratio = 1.083; CI_{95} = [0.85, 1.38]$) (Fig. 6A).

Of the 29 tested genes, 7 are regulated by IH at P4, 11 and 18, respectively, in the outer proliferative EGL and the inner premigratory EGL at P8, and 11 in the whole EGL at P12. Interestingly we mainly observed an underexpression of these genes with the most significant effect of IH visible in the inner EGL at P8. Of note, cyclin Ccnd1 is downregulated at P4 and P8 in the proliferative outer EGL of IH mice, while the guidance-related gene Robo1 is downregulated in the whole EGL. In contrast, at P12, some genes specifically implicated in synapse formation, such as Calb2 and Homer2, or in migration, such as Cdh8, are upregulated (Fig. 6B).

3.2.2 IH alters neuronal migration and Purkinje cell development

No statistically significant difference in the area of the ML (including Purkinje cells) was found between IH and N mice at P4 ($t(32) = 0.113; p = 0.911; Ratio = 1.012; CI_{95} = [0.815, 1.257]$) nor P8 ($t(30) = 0.588; p = 0.561; Ratio = 1.051; CI_{95} = [0.884, 1.249]$) (Fig. 7A). At P4 and P8, the ML is too narrow to be microdissected, but the results obtained by testing 29 genes at P12 indicate that the IH protocol is associated with a downregulation of migration-associated genes, namely L1cam and Astn2, as well as some genes involved in cell differentiation or communication, such as Tln1 (talin 1), and Gabra1 or Grin1, respectively. At P21, only Nav3 is upregulated, and no gene expression modification is seen at P70 (Fig. 7B).

Focusing on PCs, we showed that their phenotype is not visibly altered by our IH protocol at P8 (Fig. 8A). However, out of 33 OS-panel genes tested, 8 are downregulated at P8, notably the 6 antioxidant-coding genes Gpx4, Gsr, and Prdx2, 3, 5, 6 (Fig. 8B). This phenomenon is accompanied by a decrease in the expression of the cytoskeletal proteins Tln1 and Nefl (neurofilament light polypeptide), and of the maturation-indicating genes Calb1, Slc17a7, and Syn2, including the Purkinje-specific gene Pcp2 (Fig. 8C). At P12, an equilibrium in positive and negative cell responses occurs with a downregulation of Gss and Prdx5, balanced by Parp1 and Rheb (Fig. 8B). In addition, Rac1, which is not affected by IH at P8, becomes upregulated at P12 (Fig. 8C), as well as Calb and Slc17a6 in the ML (Fig. 7B). In the longer term (i.e., post-IH protocol), IH seems to modify the expression of only a few genes, such as Txrnd3, Gabra1, and Syn1 (Fig. 8B, C).

3.2.3 IH affects major differentiation processes in the IGL

A slight decrease in the area of IGL in IH mice was observed at P4 ($t(32) = 2.464; p = 0.019; Ratio = 1.176; CI_{95} = [1.029, 1.345]$), but this difference is no longer significant at P8 ($t(30) = -1.625; p = 0.115; Ratio = 0.915; CI_{95} = [0.819, 1.023]$) (Fig. 9A).

However, at P8, IH downregulates 18 genes out of the 30 tested, including 12 genes associated with synaptogenesis and neuronal maturation (Fig. 9B). Among them, we find Homer1/2, Syn2, and Syp. Interestingly, the cerebellum-specific Nrnx1 and/or its ligand Nxph4 are both downregulated during the whole IH protocol period. At P21, a mild upregulation of the cytoskeletal gene Stmn1 is observed, whereas it is previously found downregulated at P12. In contrast, the synapse-associated Cadps2 is downregulated at P8 and P12 but becomes upregulated at P70 (Fig. 9B).

3.2.4 Effect of IH on the WM

No statistically significant difference in the area of the WM was found between IH and N mice at P4 ($t(32) = -1.998; p = 0.054$; $Ratio = 0.609$; $CI_{95} = [0.368, 1.01]$) nor P8 ($t(30) = -0.853; p = 0.400$; $Ratio = 0.862$; $CI_{95} = [0.604, 1.23]$) (Fig. 10A). The expression of the 30 genes tested is decreased in the WM of P8 and P12 IH mice, except for *Akt1* and *Grm3*. (Fig. 10B). Interestingly, among these genes, those implicated in the formation of the myelin sheath are simultaneously and strongly downregulated by IH at P12. Moreover, other genes such as *Tln1* and *Stmn1* present a biphasic expression, with an upregulation at P4 and P70, and a downregulation between P8 and P12 (Fig. 10B).

4 Discussion

In humans, the cerebellum undergoes development from the embryonic stage to beyond the first year of life, rendering it vulnerable to early injury (Volpe, 2009). This vulnerability is particularly pronounced in the case of premature births, where systemic immaturity compounds the risk to the nervous system. Therefore, a participation of the cerebellum in the sequelae observed during AOP cannot be excluded (Eichenwald et al., 2016; Steggerda et al., 2009). To investigate this hypothesis, we developed a murine model of AOP, based on the IH protocol of Cai et al. (Cai et al., 2012). Using this protocol, we showed that IH leads to growth retardation in mice, associated with short and long-term behavioral, and histological alterations (Leroux et al., 2022). To gain a better understanding of the molecular mechanisms underlying these findings, we analyzed the expression of a set of genes related to oxidative stress, cell death, inflammation, and differentiation pathways using real-time PCR. Due to the exploratory nature of this work, we chose to present and discuss all statistically significant results, even if the associated fold changes were small. Indeed, we aim to provide the basis for further proteomic studies, and whether these changes are effectively translated remains to be determined.

We initially confirmed that the cerebellum is sensitive to IH during postnatal development, with evidence of oxidative stress at P4, P8, and P12. Furthermore, we identified P8 as a critical period of vulnerability to IH, where the cerebellar cells' defense against oxidative stress is the most affected. Indeed, we observed the downregulation of genes coding for major antioxidant enzymes, namely, *Txnrd1*, *Sod3*, *Prdx6*, *Prdx5* and *Cat*, which are all involved in neutralizing ROS (Birben et al., 2012). Cerebellar cells appear to initiate compensation mechanisms, beginning at P12, by significantly upregulating *Txnrd3* and *Sod3*. The expression of *Hmox1* (heme oxygenase 1), a stress response protein known to respond to hypoxia and exert

neuroprotective effects (David et al., 2006; Jazwa and Cuadrado, 2010), was also increased by our IH protocol. However, this antioxidant process seems insufficient since an accumulation of ROS is still present in cultured granule cells and cerebellar explants at P12 post-IH (Chiu et al., 2012; Leroux et al., 2022). The protective mechanism appears to continue at P21, with activation of the *Txnrd* and *Gpx* pathways, along with increased expression of *Idh1*. This gene encodes the isocitrate dehydrogenase-1 metabolic enzyme, which produces NADPH (Itsumi et al., 2015), which in turn participates in ROS elimination via reduction reactions. In contrast, *Idh1*, as well as several other redox enzymes, are downregulated at P70, indicating that the OS state of the cerebellum persists after the end of the protocol, and that IH could induce long-term alterations. Interestingly, the most marked upregulation in adulthood is *Ccs*, the gene coding for the copper chaperone of the superoxide dismutase enzyme SOD1 (Furukawa et al., 2004). Thus, a pattern emerges where short-term regulations primarily involve immediate actors in redox reactions, while long-term regulations involve upstream molecules.

Given that several studies have demonstrated that chronic exposure of mice to IH induced caspase-3 activation and increased neuronal apoptosis (Liu et al., 2018; Xu et al., 2004), we analyzed caspase-dependent cell death. At P4, the expression of caspase-3 is not increased, or even detected in IH mice. However, cleaved caspase-3 immunoreactive cells are more abundant in the IGL and the WM of the P4 cerebellum, supporting numerous observations of IH-induced alterations of myelin (Cai et al., 2012; Ferriero, 2001). At P8 and P12, there is no longer a difference in the density of apoptotic cells, despite an increased expression of caspase-3 in IH mice at P12. This belated caspase-3 expression has already been observed in the mouse brain after a continuous perinatal hypoxia (Curristin et al., 2002). However, we did not see any difference in caspase-3 activity at P12 (Leroux et al., 2022), suggesting that this pro-apoptotic process could be compensated by anti-apoptotic factors. One candidate could be *Adcyap1* (also known as PACAP, or pituitary adenylate cyclase-activating peptide), which is known to play a neuroprotective role in the cerebellum via the inhibition of caspase-3 activity (Lacaille et al., 2015). Nevertheless, previous works have shown that hypoxia eventually induces a decrease in the volume of the cerebellum in mice at P12, as well as in humans (Leroux et al., 2022; Volpe, 2009). Thus, the loss of cells could be due to a caspase-3-independent apoptosis. For example, the under-expression of *Bcl2* at P4, P8 and P12 during IH remains in favor of an increase in apoptotic cell death, via the poly ADP-ribose polymerase (PARP) pathway instead. Indeed,

it has been shown that in hypoxic granule cells, DNA damage caused by ROS accumulation induces PARP activation, which results in the induction of caspase-independent apoptosis (Chiu et al., 2012). As Bcl2 can inhibit PARP1, and thus cell death (Dutta et al., 2012), its under-expression could, reciprocally, lead to cell death. Moreover, the decrease of Parp1 expression at P8 and P12 observed in our IH condition might represent a compensatory mechanism in response to the failure of Bcl2 to control the PARP pathway. These results match those of Chiu et al. showing that IH-induced cell death is caspase-independent (Chiu et al., 2012). The decrease in the number of granule cells could also be due to a failure in cytoprotection. In fact, there is an overall downregulation, albeit slight, of genes expected to exert a protective effect on cellular components in IH mice at P8. Among them, Sp1 is known to be specifically activated by OS and acts as a transcription factor to promote neuronal survival (Ryu et al., 2003). Another example is Ercc2, which codes for an ATP-dependent DNA helicase, to repair OS-mediated DNA damage. Whether this is part of the metabolic response to save energy after IH or not, the end result is likely an accumulation of DNA damage (Zhao et al., 2021). Thus, several compartments of the cell lack protection when faced with IH-induced OS.

In light of our results, we also hypothesized that cell death could be related to a necrotic phenomenon induced by hypoxia. Indeed, it has been shown that the extracellular spill out of cellular contents after necrosis causes a local inflammation, which could be exacerbated by IH (Xu et al., 2022; Zong and Thompson, 2006). In fact, we observed a strong activation of the anti-inflammatory pathway at P8, which is mostly maintained at P12, suggesting that the cerebellum tries to counteract the pro-inflammatory effect initiated at P4. Indeed, IH induces a downregulation of NfkB at P8 and a subsequent upregulation of NfkBIB at P12, modifying the expression of two factors known to control inflammation (Dong et al., 2022; Palazzo et al., 2023). Most notably, we highlighted the upregulation of Mt1/2 at P8 and P12, which code for metallothioneins, whose potent anti-inflammatory role may have a cytoprotective effect (Dai et al., 2021; Zhou et al., 2017). Interestingly, the expression of these two genes is significantly decreased at P21, indicating that inflammatory pathways are still implicated after the IH protocol.

A well-known parallel response to IH is a metabolic adaptation, meant to counteract the decrease of mitochondrial production of ATP due to a diminished O_2 availability (Herzig and Shaw, 2018; Peña and Ramirez, 2005). The activation of this mechanism is

illustrated by an under-expression of several genes involved in the autophagy/mitophagy pathway, in which dynamin 2, encoded by Dnm2, plays a key role. Indeed, this cytoskeletal protein participates in the mitochondrial fission machinery (Lee et al., 2016), so its down-regulation throughout all stages could represent a dual defense mechanism, first by limiting high energy processes in a context of energetic scarcity, while at the same time limiting the ROS-producing mitochondrial pathway.

To determine if some cerebellar cells or processes are more sensitive to IH, we further studied specific molecular pathways, for each developmental stage and cerebellar layer. We showed a downregulation of Zic1, Ccnd1, and Pax6 in the outer EGL at P4, indicating that IH affects the proliferation of GC precursors (Aruga and Millen, 2018; Miyashita et al., 2021; Yeuung et al., 2016). This defect results in a significantly smaller EGL in IH mice at P4. Although the under-expression of the proliferative genes is still noticeable at P8, there were no associated histological differences at this stage. Furthermore, our previous results reported an increase in EGL thickness at P12 in IH animals (Leroux et al., 2022). In this latter stage, the proliferation-associated genes are no longer downregulated, and BrDU positive cells are more numerous (Leroux et al., 2022), which could explain how the EGL of IH mice caught up with that of controls at P21. In addition, the downregulation of the guidance-related gene Robo1 at P8 and the upregulation of cadherin 8 at P12 suggest that the thickening of the EGL could be accentuated by a delay in GC migration (Gruner et al., 2019; Taniguchi et al., 2006). However, the most important IH effect on the EGL is visible in the inner premigratory EGL, with marked downregulation of numerous synapse-related genes at P8, such as Grin1, Homer1/2, Slc17a6/7 (Vglut1/2), Syn1, and Syp (Chin et al., 1995; Kao et al., 2017; Parenti et al., 2022). We also found an under-expression of Homer2, which is involved in GC synaptic densities (Shiraishi et al., 2003). In contrast, at P12, some of these genes become upregulated in IH animals, including the GC-enriched calretinin (Calb2) and Homer2, suggesting a delay in the maturation of GC precursors in hypoxic mice (Bearzatto et al., 2006).

As for the molecular layer, since it was too difficult to microdissect without risking contamination by other cells, we did not perform real-time PCR at P4 and P8. However, through our immunohistochemical analyses, we found no difference in ML surface area at P4 nor P8. In contrast, we have previously reported that the thickness of the ML (including Purkinje cells) was significantly lower in hypoxic mice at P12 (Leroux et al., 2022). This decrease is associated with the downregulation of migration-associated genes such as Astn2,

which should be highly expressed in migrating granule neurons, given the role of astrotactin 2 in glial-guided neuronal migration (Wilson et al., 2010). Likewise, the L1 cell adhesion molecule (L1cam), important for axonal growth and migration (Thelen et al., 2002), is downregulated by our protocol. Similarly, talin 1, which is responsible for neurite outgrowth (Wang et al., 2019), was also downregulated. These dysregulations could imply a deficit in neurite development of ML interneurons and/or Purkinje cells. Interestingly, we also observed changes in several genes implicated in Purkinje cells connectivity, such as Camk4, Grin1, Slc17a6 and Gabra1 (Arsović et al., 2020; Kono et al., 2019; Miyazaki et al., 2003; Nietz et al., 2020). These data suggest that Purkinje innervation by parallel fibers, climbing fibers, and GABAergic interneurons is affected by IH as early as P12, which could explain the locomotor deficits observed after IH during the first postnatal weeks (Leroux et al., 2022). After the end of the protocol, only Nav3, involved in migration, neurite growth, and axon guidance (Powers et al., 2023), is upregulated, suggesting that this molecule may have participated in the compensatory process that allowed the ML thickness of IH mice to catch up to that of controls at P21 (Leroux et al., 2022), and the transcriptomic profile to become similar to control mice by adulthood.

We then focused on Purkinje cells, since they are considered as the integration center of the cerebellum. Although no difference is observed in the phenotype of PCs at P8, our real-time PCR results showed that these neurons are particularly sensitive to IH at this stage, with a downregulation of both hydrogen peroxide neutralizing enzymes Prdx2, 3, 5, 6, and of the glutathione reducing enzymes, Gpx4 and Gsr (Birben et al., 2012). This defect in the defense against OS is accompanied by a decrease in the expression of genes implicated in the connectivity of Purkinje cells, such as Calb1, Calb2, and Syn2. These downregulations also include VGlut1 (Slc17a7), which represents the hallmark of GC-PC synapses after the first postnatal week. Interestingly, a deficit in these synapses has been shown to impair the correct pruning of CF-PC synapses (van der Heijden et al., 2021). Therefore, the downregulation of Vglut1 at P8 could trigger a compensatory Vglut2 upregulation at P12 in the ML, which could be the premise of the over-innervation of PCs by CFs in adulthood (Leroux et al., 2022). At P8, PCs also show significant downregulation of the PC-specific Pcp2, suggesting an alteration in PC differentiation (Guan et al., 2005). The expression of Cadps2, which codes for the calcium-dependent activator protein for secretion 2, is decreased at this stage too. Interestingly, this factor is the only one to be still reg-

ulated in the IGL at P70. Since Cadps2 has been recently shown to participate in the physiopathology of attention-deficit hyperactivity disorder (ADHD) and spatial memory (Duan et al., 2023), it brings to mind the memory deficits found in behavioral experiments in adult mice after IH (Leroux et al., 2022). Finally, the under-expression of Tln1 at P8 may be associated with our previous finding of a lower volume of PC dendritic trees post-IH (Leroux et al., 2022; Wang et al., 2019). At P12, it seems that PCs try to counteract the deleterious effect of IH through a downregulation of the death-promoting Parp1 and Rheb genes (Chiu et al., 2012). Despite this, several mechanisms are triggered in favor of the reported histological abnormalities. Indeed, we observed an increase in the expression of Rac1, which is known to cause defects in cerebellar foliation, ectopic GCs, and altered Bergmann glia morphology (Mulherkar et al., 2014). In addition, the morphogenesis of PCs starts to present some defects, with the upregulation of the neurofilament light chain gene (Nefl). Neurofilaments are cytoskeletal components enriched at PC axonal “torpedoes” or focal swellings, and, while their function is poorly understood, they seem to be a developmental characteristic that peaks at P11 (Ljungberg et al., 2016). This could signify that, during IH, PCs modify their phenotype, and later, their connection profile. However, in the longer term, IH only modifies the expression of a few genes such as Txrnd3, Gabra1, and Syn1 in PCs. As Syn1 is a crucial effector of synaptic plasticity and axonal elongation, whose alteration is a hallmark of neurodevelopmental disorders such as autism and epilepsy (Chin et al., 1995; Kao et al., 2017; Parenti et al., 2022), we can postulate that this regulation is a compensatory mechanism to counteract the early deficits.

Regarding the IGL, we observed a slight decrease in the area between IH and control mice at P4, but no difference at P8. However, at P8, we found an overall downregulation of genes associated with critical neuronal functions, such as the synaptogenic Homer1/2, Syn2, and Syp. Notably, Nrxn1 and/or its ligand Nxph4 were consistently downregulated during the entire IH protocol period. The alteration of this pathway is associated with impaired inhibitory neurotransmission, and a reduced synapse number, which is implicated in motor learning and coordination deficits (Meng et al., 2019). Thus, the dysregulation of this pathway during the IH protocol may condition the behavioral deficits we evidenced in IH mice (Leroux et al., 2022). At P12, most downregulated genes are involved in the synaptic network such as Grin1, Cadps2, and Syn2, indicating that mature GC functions have been impaired by IH. Moreover, we also found a decrease

in the expression of factors such as Stathmin (Stmn1) and Robo1, which are implicated in cell motility and guidance (Giampietro et al., 2005; Gruner et al., 2019). This suggests that mature GCs have difficulties finding their proper localization into the IGL, and then fail to establish synapses. The ectopic cells may eventually be eliminated, explaining the thinner IGL observed at P12 (Leroux et al., 2022).

Finally, despite being less studied than the neuronal population, WM and glial cells are conclusively implicated in the physiopathology of AOP. Indeed, periventricular leukomalacia is a common finding in AOP, while the demyelination of both the peripheral and central nervous systems has been associated with IH (Cai et al., 2012; Ferriero, 2001). Interestingly, in the WM, the major differentiation genes implicated in the formation of the myelin sheath, namely Mbp, Mobp, Mog, and Plp1, are simultaneously and strongly downregulated by IH at P12. Although a compensatory increase in the expression of some of these genes appeared in adulthood (Stmn1 and Plp1), the volume of myelin sheaths of Purkinje axons was decreased in adult mice after perinatal IH in the cerebellar cortex (Leroux et al., 2022). Moreover, our transcriptomic results indicate that such a defect could also concern mossy and climbing fibers. Finally, the expression of glutamate metabotropic receptor 3 (Grm3), a hallmark of neuroinflammation, was upregulated in the WM, indicating the presence of fibrous astrocytes and suggesting a post-injury reaction after IH that persists into adulthood and could contribute to the behavioral and cognitive impairments observed (Egan et al., 2004; Zinni et al., 2021).

5 Conclusion

In conclusion, our transcriptomic analysis sheds light on the molecular effects of neonatal oxygen deprivation and perinatal intermittent hypoxia on cerebellar development in mice. The cerebellum is shown to be sensitive to neonatal oxygen deprivation, with P8 being the most sensitive stage. The deleterious effects of IH involve a dual mechanism of increased reactive oxygen species production and a failure of the antioxidant defense system. This culminates in the activation of several cell death mechanisms, associated with an alteration in cellular developmental processes, such as proliferation, migration, neurite outgrowth, synaptogenesis, and myelin sheath formation. These molecular dysregulations correlate with histological and behavioral defects observed in AOP, including motor coordination, learning, and behavior impairments. Despite the presence of compensatory mechanisms, the structural modifications caused by IH persist into adulthood, resulting in impaired cerebellar functions.

Ethic approval

All animal experiments were performed according to the protocols approved by the French Ministry of Agriculture and the European Community Council Directive.

Availability of data and materials

The datasets, analyses and code supporting the conclusions of this article are available in the following GitHub repository at <https://github.com/ma-riviere/DE-AoP-23>, also referenced on Zenodo under: <https://doi.org/10.5281/zenodo.8139284>.

Competing interests

The authors declare that they have no known competing financial interests or personal relationships that could have appeared to influence the work reported in this paper.

Funding

Agalie Rodriguez-Duboc was the recipient of a doctoral fellowship from The Ministère de l'Enseignement Supérieur, de la Recherche et de l'Innovation. This work was supported by INSERM U1239 and U1245, Rouen University, the Normandy Region and the European Union.

CRediT author statement

Agalie Rodriguez-Duboc: Investigation, Methodology, Project administration, Data Curation, Formal analysis, Visualization, Illustration, Validation, Writing - Original Draft, Writing - Review and Editing. **Magali Basille-Dugay:** Supervision, Investigation, Resources, Writing - Review and Editing. **Aurélie Debonne:** Investigation, Writing - Review and Editing. **Marc-Aurèle Rivière:** Methodology, Software, Data Curation, Formal analysis, Visualization, Validation, Writing - Review and Editing. **David Vaudry:** Funding acquisition, Resources, Conceptualization, Writing - Review and Editing. **Delphine Burel:** Conceptualization, Methodology, Funding acquisition, Project administration, Supervision, Resources, Writing - Original Draft, Writing - Review and Editing.

Acknowledgements

We would like to thank François Chadelaud and Dr. Sarah Leroux from Rouen University for the development of the hypoxia chamber. We are grateful to Dr. Hélène Lacaille for the development of the oxidative stress panel during her PhD.

Author details

¹Normandie Univ, UNIROUEN, INSERM, U1245, Cancer and brain genomics, Institute for Research and Innovation in Biomedicine (IRIB), 76000, Rouen, France. ²Normandie Univ, UNIROUEN, INSERM, U1239, Neuroendocrine, Endocrine and Germinal Differentiation Communication, Institute for Research and Innovation in Biomedicine (IRIB), 76000, Rouen, France. ³Normandie Univ, UNIROUEN, USS1, Regional Platform for Cell Imaging of Normandy (PRIMACEN), 76000, Rouen, France. ⁴Laboratoire d'Informatique, du Traitement de l'Information et des Systèmes (LITIS), Normandie Univ, UNIROUEN, 76000, Rouen, France.

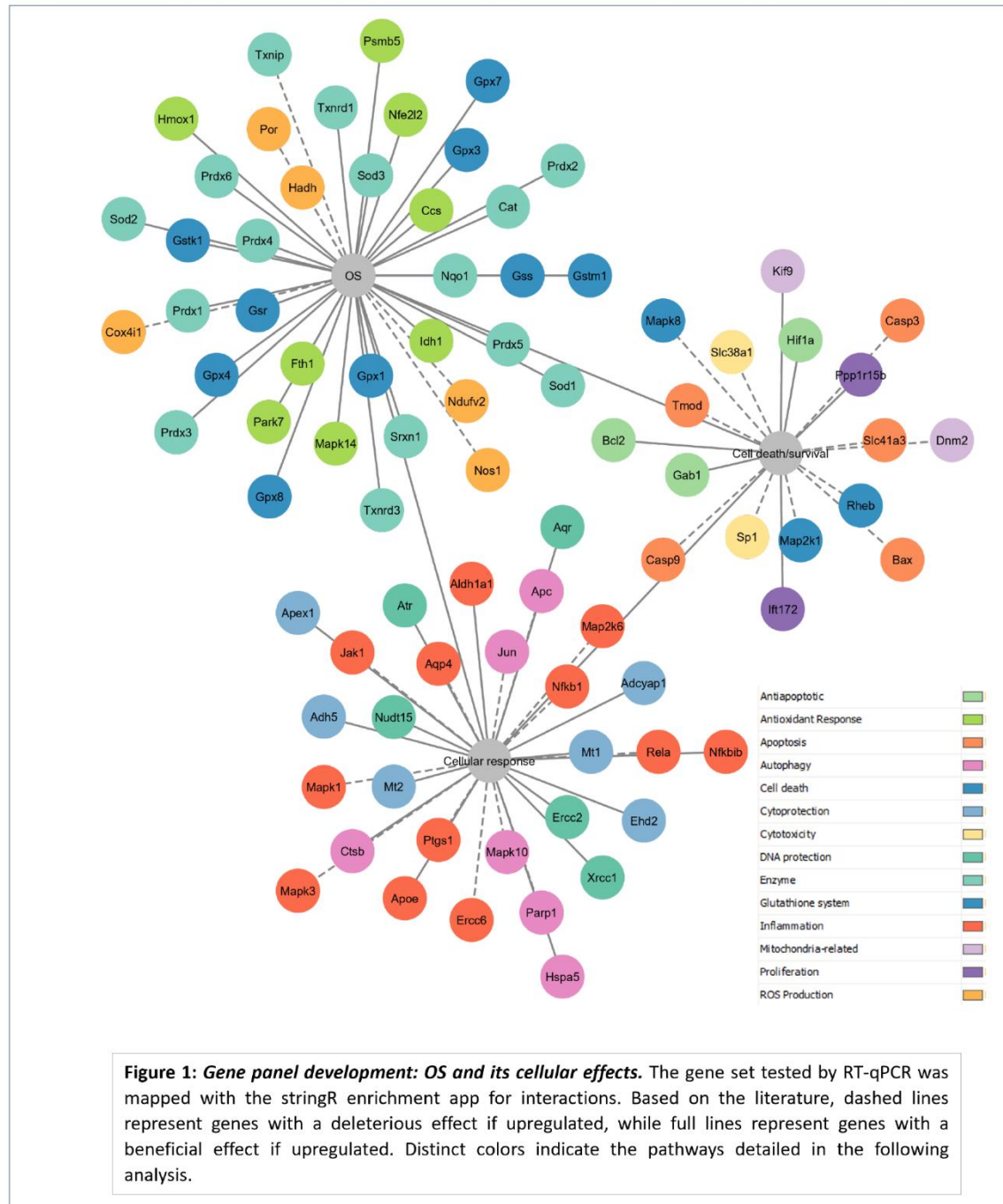
References

- Arsović et al., 2020. Arsović, A., Halbach, M. V., Canet-Pons, J., Esen-Sehir, D., Döring, C., Freudenberg, F., Czechowska, N., Seidel, K., Baader, S. L., Gispert, S., Sen, N.-E., & Auburger, G. (2020). Mouse ataxin-2 expansion downregulates camkii and other calcium signaling factors, impairing granule—purkinje neuron synaptic strength. *International Journal of Molecular Sciences*, 21(18), 6673.
- Aruga & Millen, 2018. Aruga, J. & Millen, K. J. (2018). Zic1 function in normal cerebellar development and human developmental pathology. In J. Aruga (Ed.), *Zic family*, volume 1046 (pp. 249–268). Singapore: Springer Singapore. collection-title: Advances in Experimental Medicine and Biology.
- Bearzatto et al., 2006. Bearzatto, B., Servais, L., Roussel, C., Gall, D., Baba-Aïssa, F., Schurmans, S., de Kerchove d'Exaerde, A., Cheron, G., & Schiffmann, S. N. (2006). Targeted calretinin expression in granule cells of calretinin^{-/-} mice restores normal cerebellar functions. *The FASEB Journal*, 20(2), 380–382.
- Birben et al., 2012. Birben, E., Sahiner, U. M., Sackesen, C., Erzurum, S., & Kalayci, O. (2012). Oxidative stress and antioxidant defense. *World Allergy Organization Journal*, 5(1), 9–19.
- Brooks et al., 2017. Brooks, E., M., Kristensen, K., Bentham, J., v. K., Magnusson, A., Berg, W., C., Nielsen, A., Skaug, J., H., Mächler, M., &

- Bolker, M., B. (2017). glmmTMB balances speed and flexibility among packages for zero-inflated generalized linear mixed modeling. *The R Journal*, 9(2), 378.
- Cai et al., 2012. Cai, J., Tuong, C. M., Zhang, Y., Shields, C. B., Guo, G., Fu, H., & Gozal, D. (2012). Mouse intermittent hypoxia mimicking apnoea of prematurity: effects on myelinogenesis and axonal maturation. *The Journal of Pathology*, 226(3), 495–508.
- Chin et al., 1995. Chin, L. S., Li, L., Ferreira, A., Kosik, K. S., & Greengard, P. (1995). Impairment of axonal development and of synaptogenesis in hippocampal neurons of synapsin I-deficient mice. *Proceedings of the National Academy of Sciences*, 92(20), 9230–9234.
- Chiu et al., 2012. Chiu, S.-C., Huang, S.-Y., Tsai, Y.-C., Chen, S.-P., Pang, C.-Y., Lien, C.-F., Lin, Y.-J., & Yang, K.-T. (2012). Poly (adp-ribose) polymerase plays an important role in intermittent hypoxia-induced cell death in rat cerebellar granule cells. *Journal of Biomedical Science*, 19(1), 29.
- Curristin et al., 2002. Curristin, S. M., Cao, A., Stewart, W. B., Zhang, H., Madri, J. A., Morrow, J. S., & Ment, L. R. (2002). Disrupted synaptic development in the hypoxic newborn brain. *Proceedings of the National Academy of Sciences*, 99(24), 15729–15734.
- Dai et al., 2021. Dai, H., Wang, L., Li, L., Huang, Z., & Ye, L. (2021). Metallothionein 1: A new spotlight on inflammatory diseases. *Frontiers in Immunology*, 12, 739918.
- Darnall et al., 2017. Darnall, R. A., Chen, X., Nemanic, K. V., Sirieix, C. M., Gimí, B., Knoblauch, S., McEntire, B. L., & Hunt, C. E. (2017). Early postnatal exposure to intermittent hypoxia in rodents is proinflammatory, impairs white matter integrity, and alters brain metabolism. *Pediatric Research*, 82(1), 164–172.
- David et al., 2006. David, J., Boelens, W. C., & Grongnet, J. (2006). Up-regulation of heat shock protein hsp 20 in the hippocampus as an early response to hypoxia of the newborn. *Journal of Neurochemistry*, 99(2), 570–581.
- Dong et al., 2022. Dong, J., Liao, Y., & Wu, B. (2022). Tak-242 ameliorates epileptic symptoms in mice by inhibiting the tlr4/nf- κ b signaling pathway. *Annals of Translational Medicine*, 10(14), 795–795.
- Duan et al., 2023. Duan, K., Chen, J., Calhoun, V. D., Jiang, W., Rootes-Murdy, K., Schoenmacker, G., Silva, R. F., Franke, B., Buitelaar, J. K., Hoogman, M., Oosterlaan, J., Hoekstra, P. J., Heslenfeld, D., Hartman, C. A., Sprooten, E., Arias-Vasquez, A., Turner, J. A., & Liu, J. (2023). Genomic patterns linked to gray matter alterations underlying working memory deficits in adults and adolescents with attention-deficit/hyperactivity disorder. *Translational Psychiatry*, 13(1), 50.
- Dutta et al., 2012. Dutta, C., Day, T., Kopp, N., van Bodegom, D., Davids, M. S., Ryan, J., Bird, L., Kommajosyula, N., Weigert, O., Yoda, A., Fung, H., Brown, J. R., Shapiro, G. I., Letai, A., & Weinstock, D. M. (2012). Bcl2 suppresses parp1 function and nonapoptotic cell death. *Cancer Research*, 72(16), 4193–4203.
- Egan et al., 2004. Egan, M. F., Straub, R. E., Goldberg, T. E., Yakub, I., Callicott, J. H., Hariri, A. R., Mattay, V. S., Bertolino, A., Hyde, T. M., Shannon-Weickert, C., Akil, M., Crook, J., Vakkalanka, R. K., Balkissoon, R., Gibbs, R. A., Kleinman, J. E., & Weinberger, D. R. (2004). Variation in GRM3 affects cognition, prefrontal glutamate, and risk for schizophrenia. *Proceedings of the National Academy of Sciences*, 101(34), 12604–12609.
- Eichenwald et al., 2016. Eichenwald, E. C., FETUS, C. O., NEWBORN, Watterberg, K. L., Autcott, S., Benitz, W. E., Cummings, J. J., Goldsmith, J., Poindexter, B. B., Puopolo, K., Stewart, D. L., & Wang, K. S. (2016). Apnea of prematurity. *Pediatrics*, 137(1), e20153757.
- Ferriero, 2001. Ferriero, D. M. (2001). Oxidant mechanisms in neonatal hypoxia-ischemia. *Developmental Neuroscience*, 23(3), 198–202.
- Furukawa et al., 2004. Furukawa, Y., Torres, A. S., & O'Halloran, T. V. (2004). Oxygen-induced maturation of sod1: a key role for disulfide formation by the copper chaperone ccs. *The EMBO Journal*, 23(14), 2872–2881.
- Giampietro et al., 2005. Giampietro, C., Luzzati, F., Gambarotta, G., Giacobini, P., Boda, E., Fasolo, A., & Perroteau, I. (2005). Stathmin expression modulates migratory properties of gn-11 neurons in vitro. *Endocrinology*, 146(4), 1825–1834.
- Gruner et al., 2019. Gruner, H. N., Kim, M., & Mastick, G. S. (2019). Robo1 and 2 repellent receptors cooperate to guide facial neuron cell migration and axon projections in the embryonic mouse hindbrain. *Neuroscience*, 402, 116–129.
- Guan et al., 2005. Guan, J., Luo, Y., & Denker, B. (2005). Purkinje cell protein-2 (pcp2) stimulates differentiation in pc12 cells by g β γ -mediated activation of ras and p38 mapk. *Biochemical Journal*, 392(2), 389–397.
- Hardie et al., 2012. Hardie, D. G., Ross, F. A., & Hawley, S. A. (2012). Ampk: a nutrient and energy sensor that maintains energy homeostasis. *Nature Reviews Molecular Cell Biology*, 13(4), 251–262.
- Hartig, 2022. Hartig, F. (2022). DHARMA: Residual diagnostics for hierarchical (multi-level / mixed) regression models. Technical report.
- Henderson-Smart, 1981. Henderson-Smart, D. (1981). The effect of gestational age on the incidence and duration of recurrent apnoea in newborn babies. *Journal of Paediatrics and Child Health*, 17(4), 273–276.
- Herzig & Shaw, 2018. Herzig, S. & Shaw, R. J. (2018). Ampk: guardian of metabolism and mitochondrial homeostasis. *Nature Reviews Molecular Cell Biology*, 19(2), 121–135.
- Itsumi et al., 2015. Itsumi, M., Inoue, S., Elia, A. J., Murakami, K., Sasaki, M., Lind, E. F., Brenner, D., Harris, I. S., Chio, I. I. C., Afzal, S., Cairns, R. A., Cescon, D. W., Elford, A. R., Ye, J., Lang, P. A., Li, W. Y., Wakeham, A., Duncan, G. S., Haight, J., You-Ten, A., Snow, B., Yamamoto, K., Ohashi, P. S., & Mak, T. W. (2015). Idh1 protects murine hepatocytes from endotoxin-induced oxidative stress by regulating the intracellular nadp+/nadph ratio. *Cell Death & Differentiation*, 22(11), 1837–1845.
- Jazwa & Cuadrado, 2010. Jazwa, A. & Cuadrado, A. (2010). Targeting heme oxygenase-1 for neuroprotection and neuroinflammation in neurodegenerative diseases. *Current Drug Targets*, 11(12), 1517–1531.
- Kao et al., 2017. Kao, H., Ryoo, K., Lin, A., Janoschka, S. R., Augustine, G. J., & Porton, B. (2017). Synapsins regulate brain-derived neurotrophic factor-mediated synaptic potentiation and axon elongation by acting on membrane rafts. *European Journal of Neuroscience*, 45(8), 1085–1101.
- Kheirandish et al., 2005. Kheirandish, L., Gozal, D., Pequignot, J.-M., Pequignot, J., & Row, B. W. (2005). Intermittent hypoxia during development induces long-term alterations in spatial working memory, monoamines, and dendritic branching in rat frontal cortex. *Pediatric Research*, 58(3), 594–599.
- Kono et al., 2019. Kono, M., Kakegawa, W., Yoshida, K., & Yuzaki, M. (2019). Interneuronal nmda receptors regulate long-term depression and motor learning in the cerebellum. *The Journal of Physiology*, 597(3), 903–920.
- Lacaille et al., 2015. Lacaille, H., Duterte-Boucher, D., Liot, D., Vaudry, H., Naassila, M., & Vaudry, D. (2015). Comparison of the deleterious effects of binge drinking-like alcohol exposure in adolescent and adult mice. *Journal of Neurochemistry*, 132(6), 629–641.
- Lee et al., 2016. Lee, J. E., Westrate, L. M., Wu, H., Page, C., & Voeltz, G. K. (2016). Multiple dynamin family members collaborate to drive mitochondrial division. *Nature*, 540(7631), 139–143.
- Lenth, 2022. Lenth, R. V. (2022). emmeans: Estimated marginal means, aka least-squares means. Technical report.
- Leroux et al., 2022. Leroux, S., Rodriguez-Duboc, A., Arabo, A., Basille-Dugay, M., Vaudry, D., & Burel, D. (2022). Intermittent hypoxia in a mouse model of apnea of prematurity leads to a retardation of cerebellar development and long-term functional deficits. *Cell & Bioscience*, 12(1), 148.
- Liu et al., 2018. Liu, F., Liu, T.-W., & Kang, J. (2018). The role of nf- κ b-mediated jnk pathway in cognitive impairment in a rat model of sleep apnea. *Journal of Thoracic Disease*, 10(12), 6921–6931.
- Ljungberg et al., 2016. Ljungberg, L., Lang-Ouellette, D., Yang, A., Jayabal, S., Quilez, S., & Watt, A. J. (2016). Transient developmental purkinje cell axonal torpedoes in healthy and ataxic mouse cerebellum. *Frontiers in Cellular Neuroscience*, 10. [Online; accessed 2023-04-14].
- Lüdecke et al., 2021. Lüdecke, D., Ben-Shachar, M., Patil, I., Waggoner, P., & Makowski, D. (2021). performance: An r package for assessment, comparison and testing of statistical models. *Journal of Open Source Software*, 6(60), 3139.
- Meng et al., 2019. Meng, X., McGraw, C. M., Wang, W., Jing, J., Yeh, S.-Y., Wang, L., Lopez, J., Brown, A. M., Lin, T., Chen, W., Xue, M., Sillitoe, R. V., Jiang, X., & Zoghbi, H. Y. (2019). Neurexophilin4 is a selectively expressed α -neurexin ligand that modulates specific cerebellar synapses and motor functions. *eLife*, 8, e46773.
- Miyashita et al., 2021. Miyashita, S., Owa, T., Seto, Y., Yamashita, M.,

RESULTS

- Aida, S., Sone, M., Ichijo, K., Nishioka, T., Kaibuchi, K., Kawaguchi, Y., Taya, S., & Hoshino, M. (2021). Cyclin d1 controls development of cerebellar granule cell progenitors through phosphorylation and stabilization of atoh1. *The EMBO Journal*, 40(14). [Online; accessed 2023-04-14].
- Miyazaki et al., 2003. Miyazaki, T., Fukaya, M., Shimizu, H., & Watanabe, M. (2003). Subtype switching of vesicular glutamate transporters at parallel fibre-purkinje cell synapses in developing mouse cerebellum: Developmental switching of vglut in parallel fibre. *European Journal of Neuroscience*, 17(12), 2563–2572.
- Moriette et al., 2010. Moriette, G., Lescure, S., El Ayoubi, M., & Lopez, E. (2010). Apnées du prématuré : données récentes. *Archives de Pédiatrie*, 17(2), 186–190.
- Mulherkar et al., 2014. Mulherkar, S., Uddin, M. D., Couvillon, A. D., Sillitoe, R. V., & Tolias, K. F. (2014). The small gtpases rhoa and rac1 regulate cerebellar development by controlling cell morphogenesis, migration and foliation. *Developmental Biology*, 394(1), 39–53.
- Nietz et al., 2020. Nietz, A., Krook-Magnuson, C., Gutierrez, H., Klein, J., Sauve, C., Hoff, I., Christenson Wick, Z., & Krook-Magnuson, E. (2020). Selective loss of the gaba α_1 subunit from purkinje cells is sufficient to induce a tremor phenotype. *Journal of Neurophysiology*, 124(4), 1183–1197.
- Palazzo et al., 2023. Palazzo, I., Kelly, L., Koenig, L., & Fischer, A. J. (2023). Patterns of nfkb activation resulting from damage, reactive microglia, cytokines, and growth factors in the mouse retina. *Experimental Neurology*, 359, 114233.
- Parenti et al., 2022. Parenti, I., Leitão, E., Kuechler, A., Villard, L., Goizet, C., Courdier, C., Bayat, A., Rossi, A., Julia, S., Bruel, A.-L., Tran Mau-Them, F., Nambot, S., Lehalle, D., Willems, M., Lespinasse, J., Ghoumid, J., Caumes, R., Smol, T., El Chehadeh, S., Schaefer, E., Abi-Warde, M.-T., Keren, B., Afenjar, A., Tabet, A.-C., Levy, J., Maruani, A., Aledo-Serrano, A., Garming, W., Milleret-Pignot, C., Chassevent, A., Koopmans, M., Verbeek, N. E., Person, R., Belles, R., Bellus, G., Salbert, B. A., Kaiser, F. J., Mazzola, L., Convers, P., Perrin, L., Piton, A., Wiegand, G., Accogli, A., Brancati, F., Benfenati, F., Chatron, N., Lewis-Smith, D., Thomas, R. H., Zara, F., Striano, P., Lesca, G., & Depienne, C. (2022). The different clinical facets of syn1-related neurodevelopmental disorders. *Frontiers in Cell and Developmental Biology*, 10, 1019715.
- Pergolizzi et al., 2022. Pergolizzi, J. V., Fort, P., Miller, T. L., LeQuang, J. A., & Raffa, R. B. (2022). The epidemiology of apnoea of prematurity. *Journal of Clinical Pharmacy and Therapeutics*, 47(5), 685–693.
- Peña & Ramirez, 2005. Peña, F., & Ramirez, J.-M. (2005). Hypoxia-induced changes in neuronal network properties. *Molecular Neurobiology*, 32(3), 251–284.
- Poets, 2020. Poets, C. F. (2020). Intermittent hypoxia and long-term neurological outcome: How are they related? *Seminars in Fetal and Neonatal Medicine*, 25(2), 101072.
- Powers et al., 2023. Powers, R. M., Hevner, R. F., & Halpain, S. (2023). The neuron navigators: Structure, function, and evolutionary history. *Frontiers in Molecular Neuroscience*, 15, 1099554.
- Prabhakar & Semenza, 2012. Prabhakar, N. R., & Semenza, G. L. (2012). Adaptive and maladaptive cardiorespiratory responses to continuous and intermittent hypoxia mediated by hypoxia-inducible factors 1 and 2. *Physiological Reviews*, 92(3), 967–1003.
- Ryu et al., 2003. Ryu, H., Lee, J., Zaman, K., Kubilis, J., Ferrante, R. J., Ross, B. D., Neve, R., & Ratan, R. R. (2003). Sp1 and sp3 are oxidative stress-inducible, antideath transcription factors in cortical neurons. *The Journal of Neuroscience*, 23(9), 3597–3606.
- Sato et al., 2008. Sato, A., Sekine, Y., Saruta, C., Nishibe, H., Morita, N., Sato, Y., Sadakata, T., Shinoda, Y., Kojima, T., & Furuichi, T. (2008). Cerebellar development transcriptome database (cdt-db): Profiling of spatio-temporal gene expression during the postnatal development of mouse cerebellum. *Neural Networks*, 21(8), 1056–1069.
- Scheuer et al., 2017. Scheuer, T., Sharkovska, Y., Tarabykin, V., Marggraf, K., Brockmöller, V., Bührer, C., Endesfelder, S., & Schmitz, T. (2017). Neonatal hyperoxia perturbs neuronal development in the cerebellum. *Molecular Neurobiology*. [Online; accessed 2023-02-03].
- Shiraishi et al., 2003. Shiraishi, Y., Mizutani, A., Yuasa, S., Mikoshiba, K., & Furuichi, T. (2003). Glutamate-induced declustering of post-synaptic adaptor protein cupidin (homer 2/vesl-2) in cultured cerebellar granule cells: Glutamate-induced declustering of cupidin/homer. *Journal of Neurochemistry*, 87(2), 364–376.
- Steggerda et al., 2009. Steggerda, S. J., Leijser, L. M., Wiggers-de Bruïne, F. T., van der Grond, J., Walther, F. J., & van Wezel-Meijler, G. (2009). Cerebellar injury in preterm infants: Incidence and findings on us and mr images. *Radiology*, 252(1), 190–199.
- Taniguchi et al., 2006. Taniguchi, H., Kawauchi, D., Nishida, K., & Murakami, F. (2006). Clasic cadherins regulate tangential migration of precerebellar neurons in the caudal hindbrain. *Development*, 133(10), 1923–1931.
- Thelen et al., 2002. Thelen, K., Kedar, V., Panicker, A. K., Schmid, R.-S., Midkiff, B. R., & Maness, P. F. (2002). The neural cell adhesion molecule 1 potentiates integrin-dependent cell migration to extracellular matrix proteins. *The Journal of Neuroscience*, 22(12), 4918–4931.
- van der Heijden et al., 2021. van der Heijden, M. E., Lackey, E. P., Perez, R., İşleyen, F. S., Brown, A. M., Donofrio, S. G., Lin, T., Zoghbi, H. Y., & Sillitoe, R. V. (2021). Maturation of purkinje cell firing properties relies on neurogenesis of excitatory neurons. *eLife*, 10, e68045.
- Volpe, 2009. Volpe, J. J. (2009). Cerebellum of the premature infant: Rapidly developing, vulnerable, clinically important. *Journal of Child Neurology*, 24(9), 1085–1104.
- Wang et al., 2019. Wang, Y., Zhang, X., Tian, J., Shan, J., Hu, Y., Zhai, Y., & Guo, J. (2019). Talin promotes integrin activation accompanied by generation of tension in talin and an increase in osmotic pressure in neurite outgrowth. *The FASEB Journal*, 33(5), 6311–6326.
- Wilson et al., 2010. Wilson, P. M., Fryer, R. H., Fang, Y., & Hatten, M. E. (2010). Asn2, a novel member of the astrotactin gene family, regulates the trafficking of astn1 during glial-guided neuronal migration. *Journal of Neuroscience*, 30(25), 8529–8540.
- Wolterink-Donselaar et al., 2009. Wolterink-Donselaar, I. G., Meerdink, J. M., & Fernandes, C. (2009). A method for gender determination in newborn dark pigmented mice. *Lab Animal*, 38(1), 35–38.
- Xu et al., 2022. Xu, J., Li, Q., Xu, C.-Y., Mao, S., Jin, J.-J., Gu, W., Shi, Y., Zou, C.-F., & Ye, L. (2022). Obstructive sleep apnea aggravates neuroinflammation and pyroptosis in early brain injury following subarachnoid hemorrhage via asc/hif-1 α pathway. *Neural Regeneration Research*, 17(11), 2537.
- Xu et al., 2004. Xu, W., Chi, L., Row, B., Xu, R., Ke, Y., Xu, B., Luo, C., Kheirandish, L., Gozal, D., & Liu, R. (2004). Increased oxidative stress is associated with chronic intermittent hypoxia-mediated brain cortical neuronal cell apoptosis in a mouse model of sleep apnea. *Neuroscience*, 126(2), 313–323.
- Yeung et al., 2016. Yeung, J., Ha, T. J., Swanson, D. J., & Goldowitz, D. (2016). A novel and multivalent role of pax6 in cerebellar development. *Journal of Neuroscience*, 36(35), 9057–9069.
- Zhao et al., 2021. Zhao, W., Liu, Z., Luo, J., Ma, C., Lai, L., Xia, Z., & Xu, S. (2021). The roles of parp-1 and xpd and their potential interplay in repairing bupivacaine-induced neuron oxidative dna damage. *Aging*, 13(3), 4274–4290.
- Zhou et al., 2017. Zhou, S., Yin, X., Jin, J., Tan, Y., Conklin, D. J., Xin, Y., Zhang, Z., Sun, W., Cui, T., Cai, J., Zheng, Y., & Cai, L. (2017). Intermittent hypoxia-induced cardiomyopathy and its prevention by nrf2 and metallothionein. *Free Radical Biology and Medicine*, 112, 224–239.
- Zimmerman et al., 2021. Zimmerman, K. D., Espeland, M. A., & Langefeld, C. D. (2021). A practical solution to pseudoreplication bias in single-cell studies. *Nature Communications*, 12(1), 738.
- Zinni et al., 2021. Zinni, M., Mairesse, J., Pansiot, J., Fazio, F., Iacovelli, L., Antenucci, N., Orlando, R., Nicoletti, F., Vaiman, D., & Baud, O. (2021). mglu3 receptor regulates microglial cell reactivity in neonatal rats. *Journal of Neuroinflammation*, 18(1), 13.
- Zong & Thompson, 2006. Zong, W.-X., & Thompson, C. B. (2006). Necrotic death as a cell fate. *Genes & Development*, 20(1), 1–15.



RESULTS

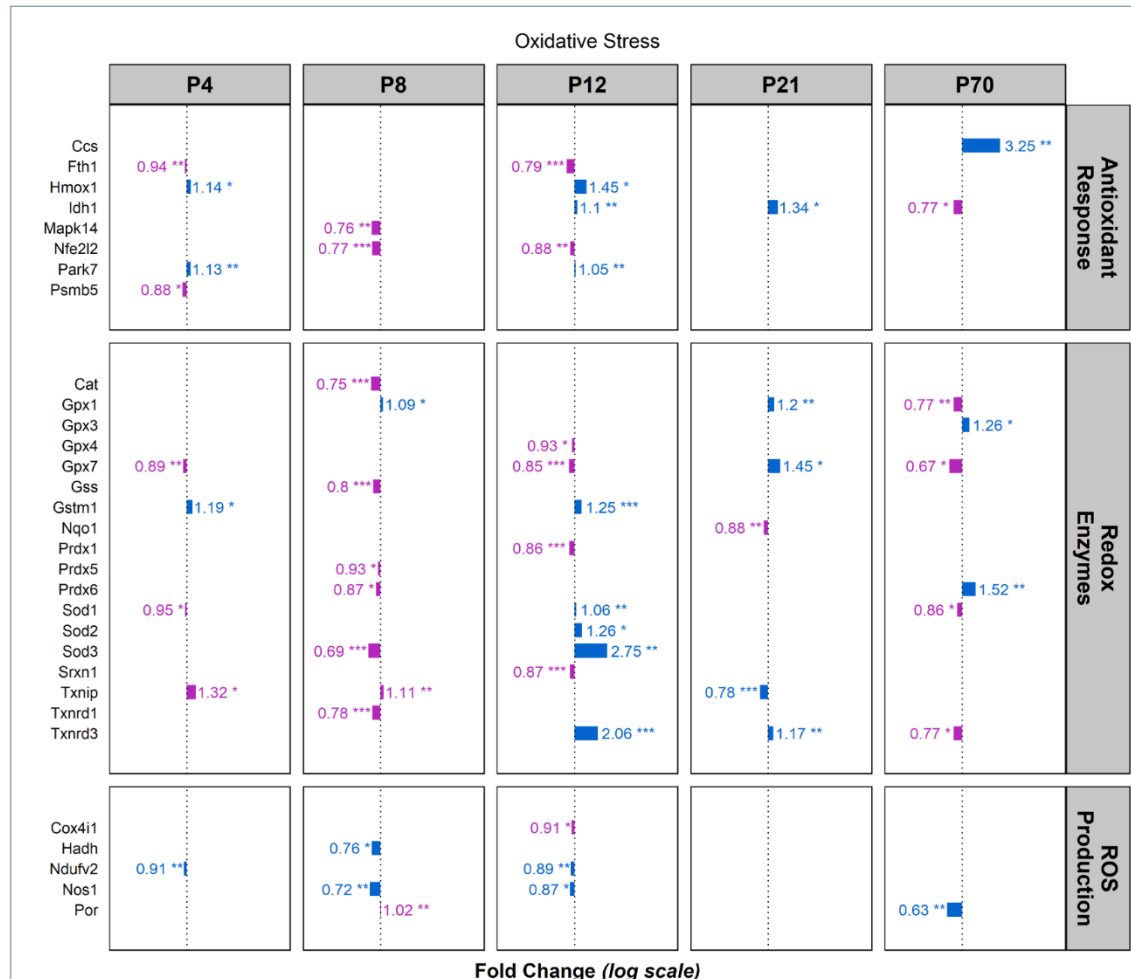
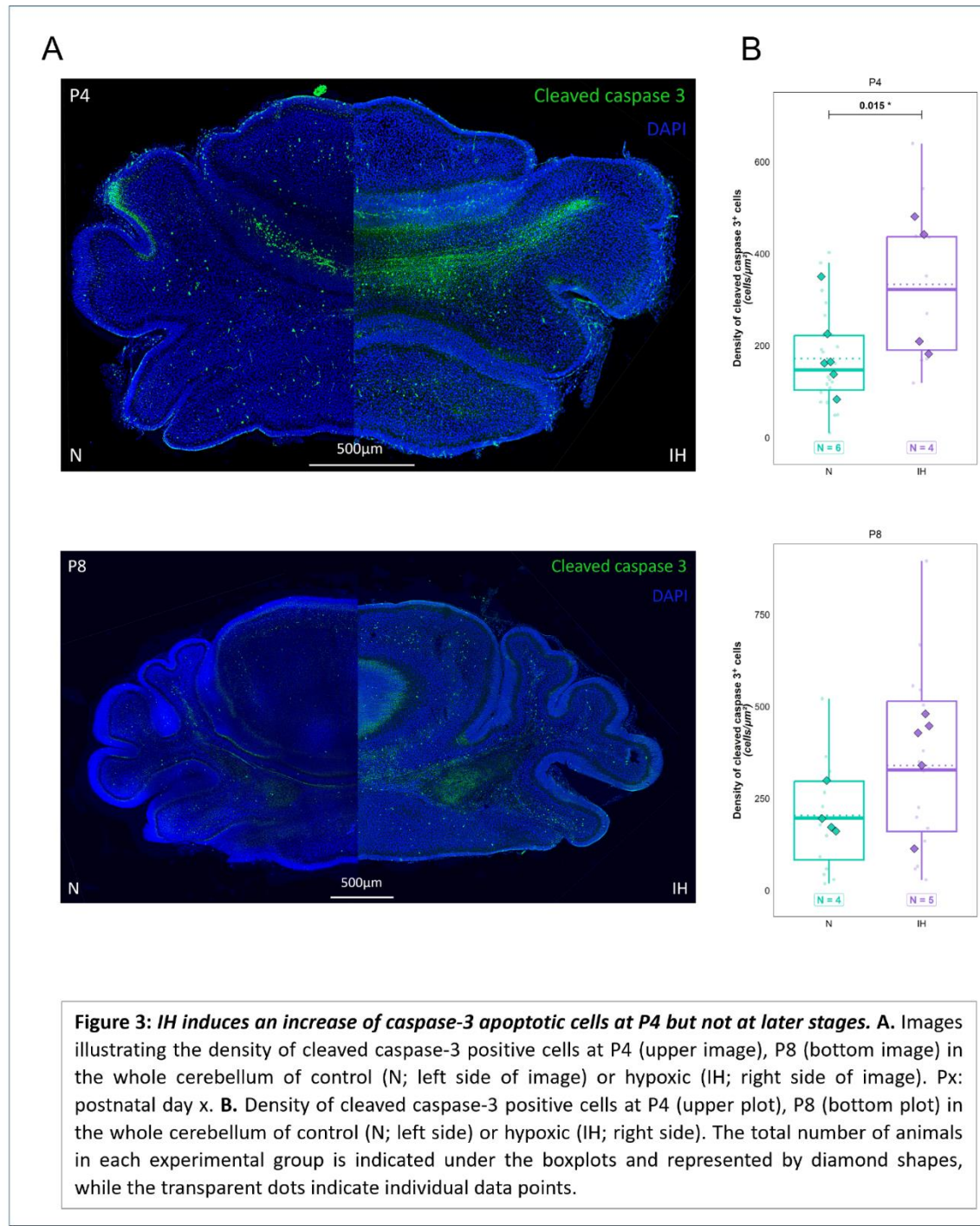
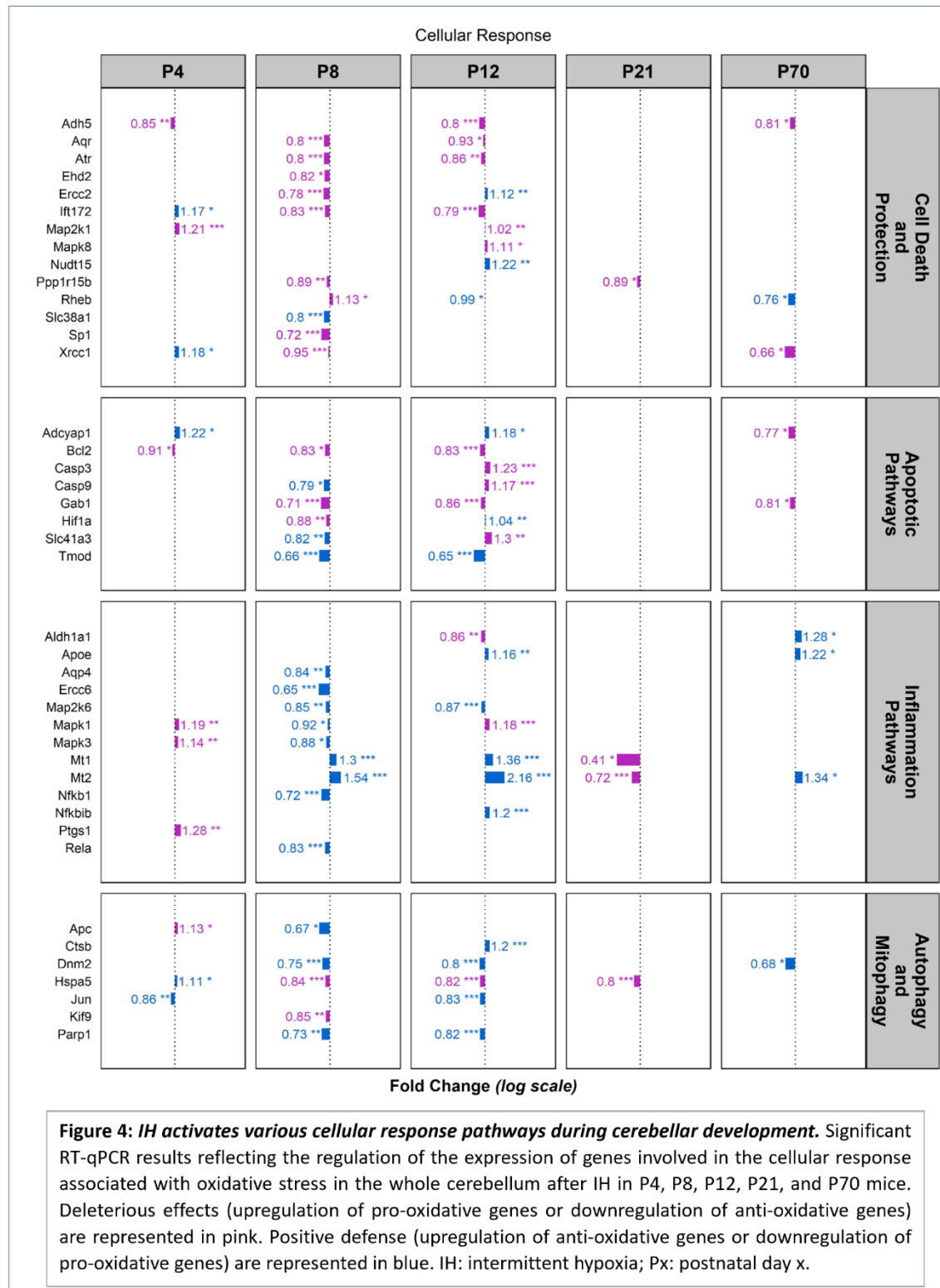
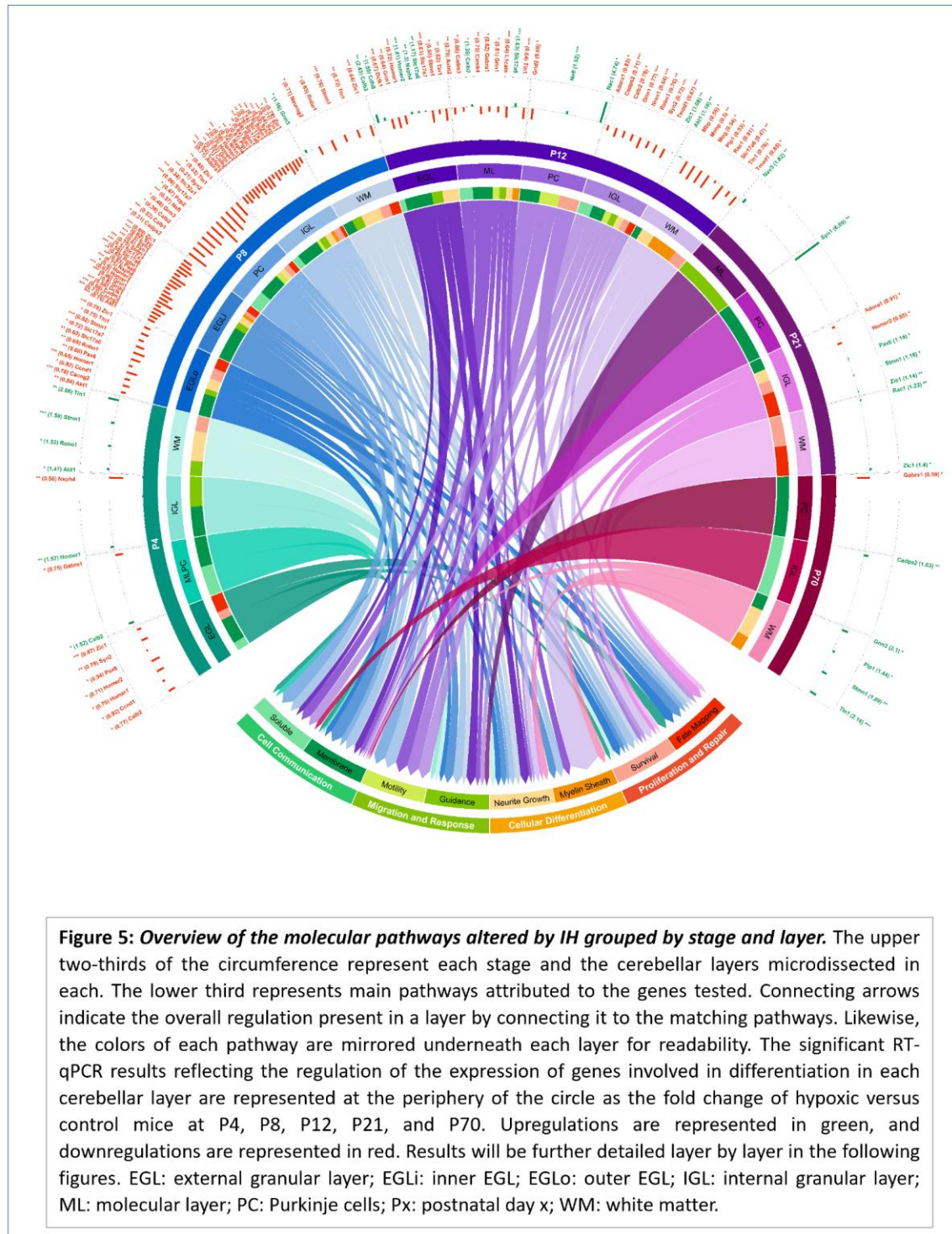


Figure 2: All stages are sensitive to IH but P8 is more vulnerable. Significant RT-qPCR results reflecting the regulation of the expression of genes involved in oxidative stress after IH in the whole cerebellum of P4, P8, P12, P21, and P70 mice. Deleterious effects (upregulation of pro-oxidative genes or downregulation of anti-oxidative genes) are represented in pink. Positive defense (upregulation of anti-oxidative genes or downregulation of pro-oxidative genes) are represented in blue. IH: intermittent hypoxia; Px: postnatal day x.

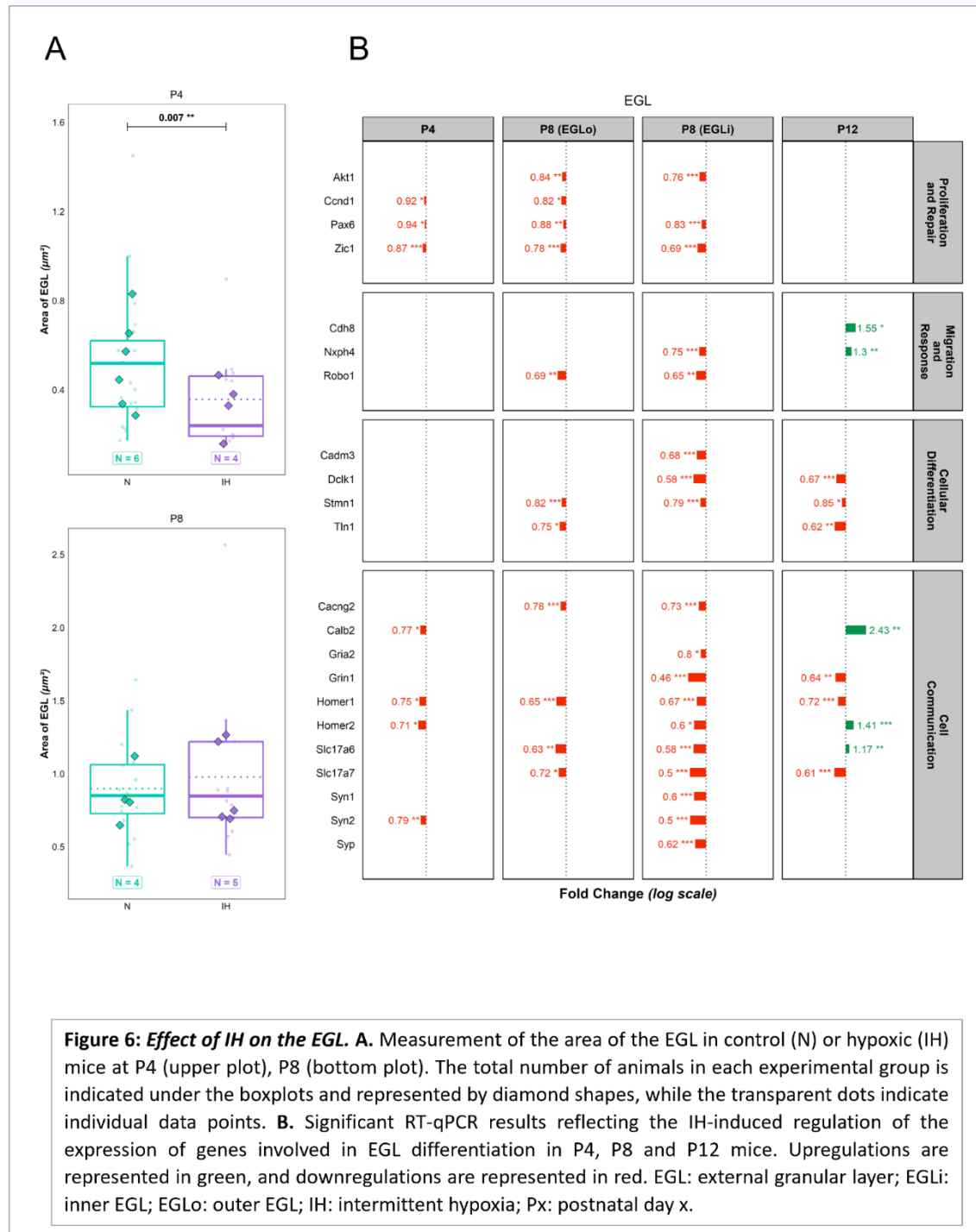


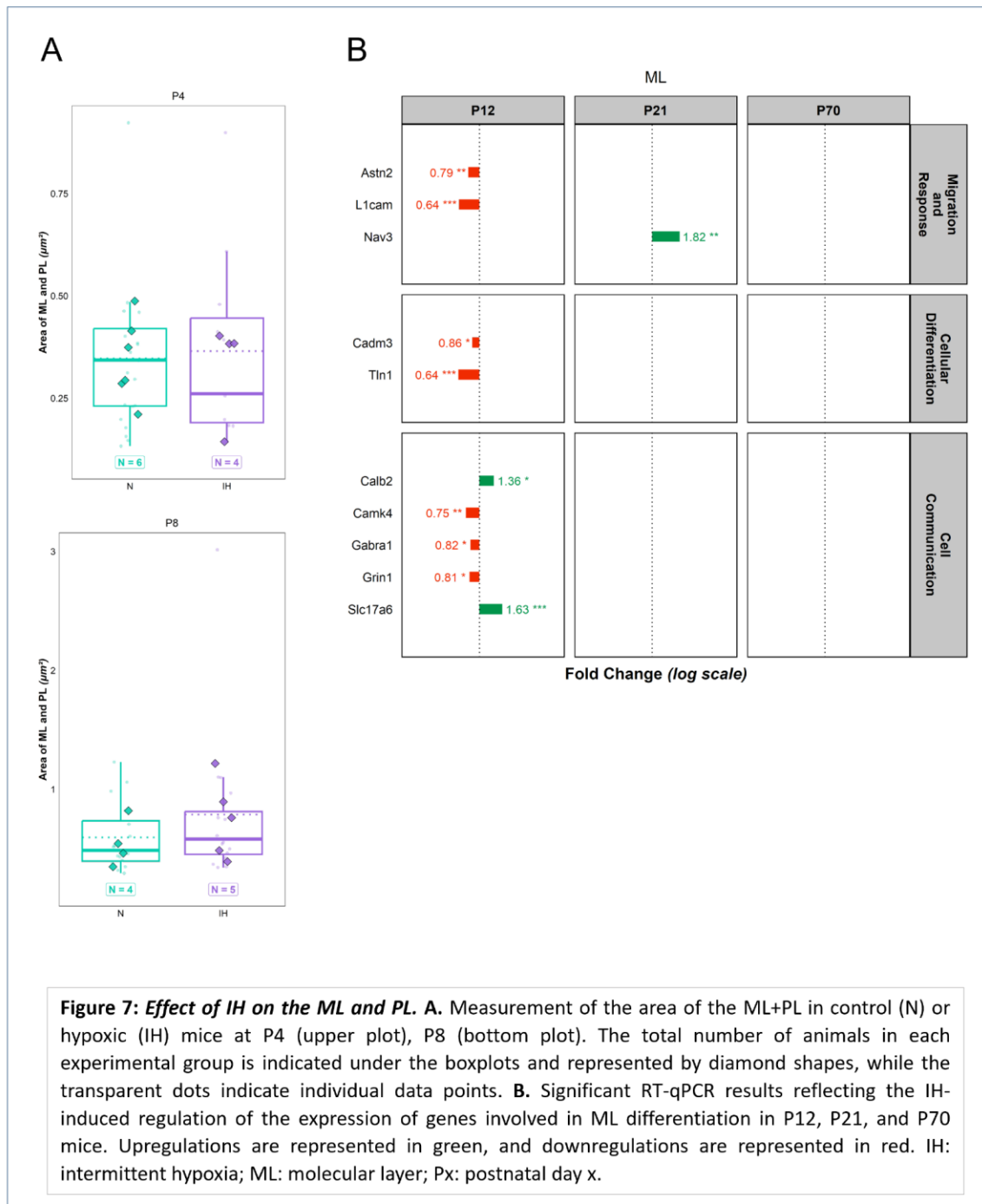
RESULTS

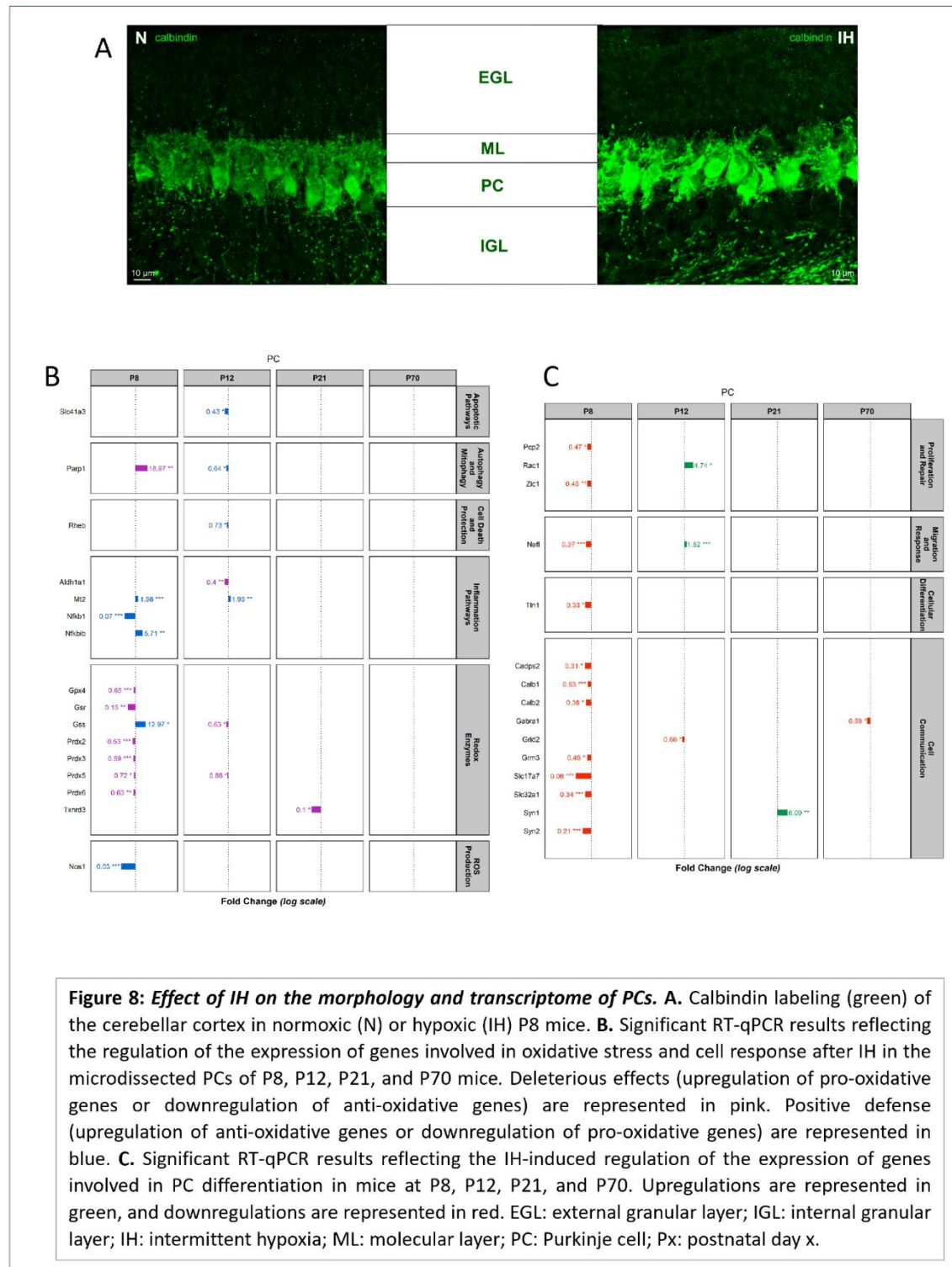


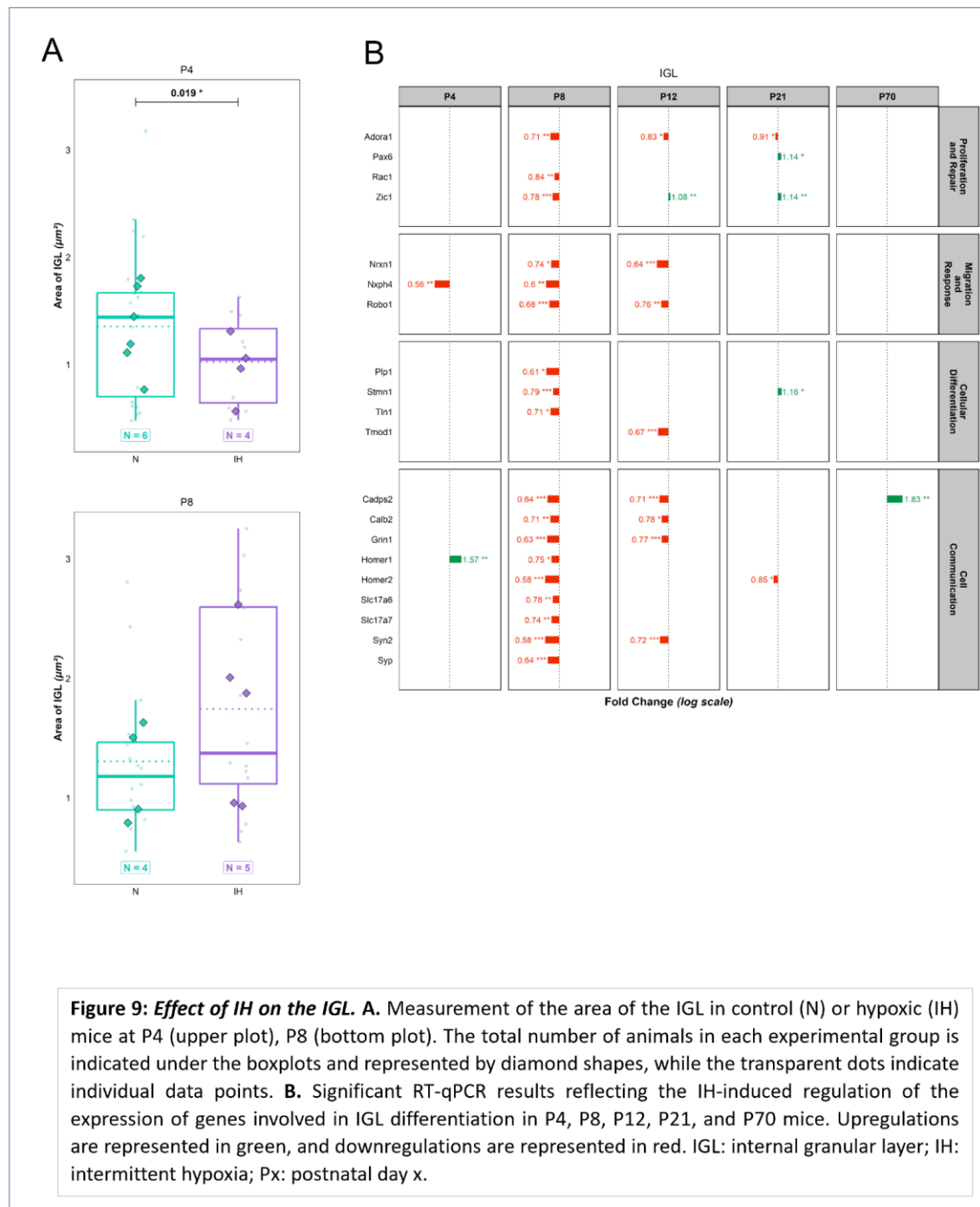


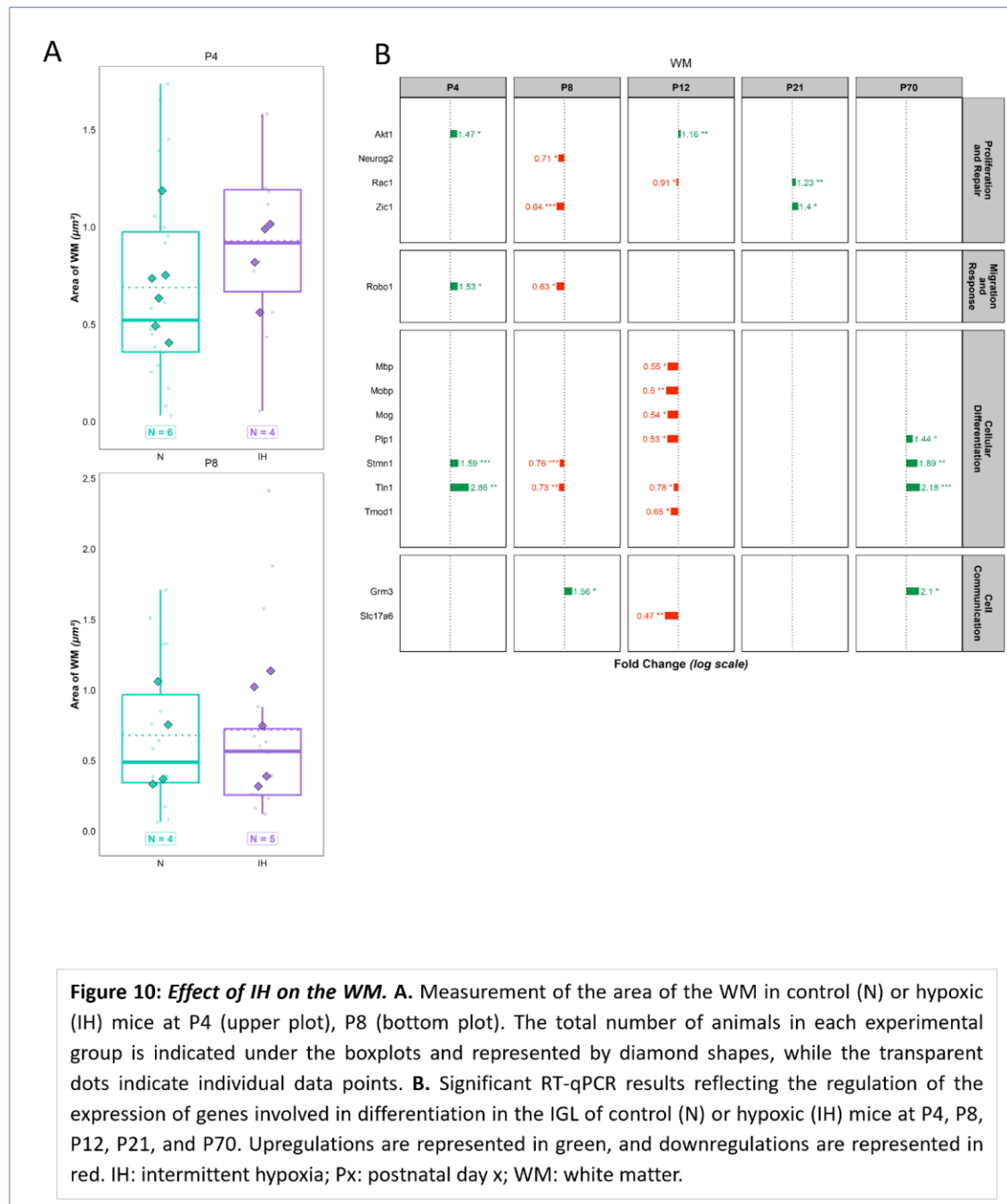
RESULTS











2. Graphical summary

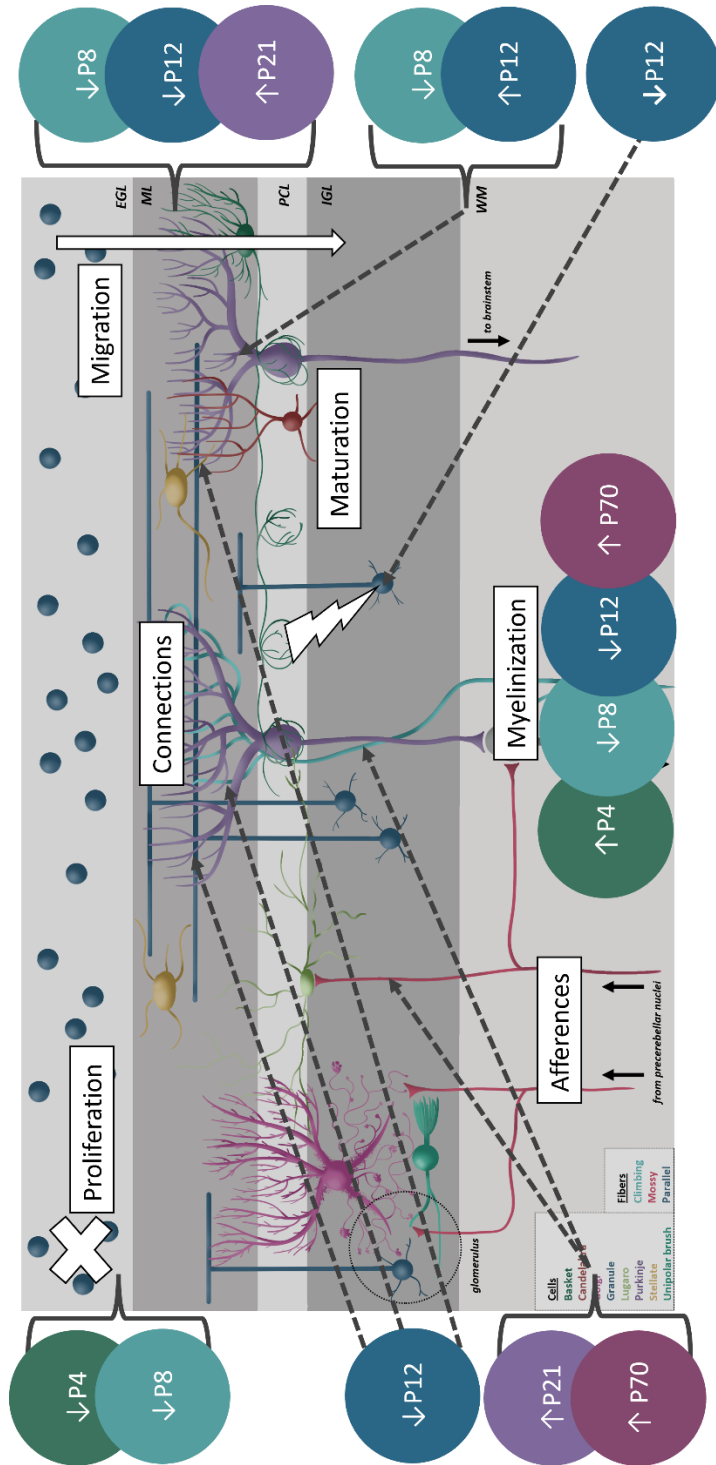


Figure 38: Main findings presented in article 2.

Our IH protocol induces a general state of oxidative stress associated with transcriptomic changes. P8 is highlighted as a critically vulnerable stage. Gene regulations suggest decreased proliferation at P4 and P8, delayed migration at P8 and P12, which later increases at P21. In addition, differentiation of granule and Purkinje cells is affected at P8 and P12. Markers of Purkinje connectivity with inhibitory interneurons and climbing and parallel fibers are underexpressed at P12 while indicators of cerebellar afferences are upregulated at P21 and P70. The myelination process is affected at all stages. DCN: deep cerebellar nuclei; EGL: external granular layer; IGL: internal granular layer; ML: molecular layer; PCL: Purkinje cell layer; Px: postnatal day x; WM: white matter.

RESULTS

II. PART TWO: EFFECTS OF IH ON CEREBELLAR VASCULARIZATION

A. BACKGROUND

We have seen that, in early embryonic development, the establishment of the neural tube precedes vascularization. However, the evidence shows that there is an interplay between the nervous and the vascular systems as they develop. In fact, several neural-derived signals that initiate and regulate CNS development may also be involved in vascularization signaling (Vogenstahl et al. 2022).

Thus, neurogenesis and angiogenesis go hand in hand during development (Carmeliet and Tessier-Lavigne 2005). As an example, angiopoietins 1 and 2 are expressed in both cerebellar neural and endothelial cells, and reciprocally, the receptor Tie2 is expressed in blood vessels as well as PCs. This pathway regulates angiogenic remodeling as well as dendritogenesis, thus indicating a connection between neural and vascular developmental pathways in the cerebellum (Luck et al. 2021). Likewise, metalloproteases associated with angiogenesis have also been shown to promote the migration of neural progenitors (Wang et al. 2006).

Moreover, we have shown that the regulation of factors such as HIF-1 α , which stimulates the transcription of vascular endothelial growth factor (VEGF) to induce neovascularization (Forsythe et al. 1996), is also associated to histological and cellular alterations in response to our IH protocol (Leroux et al. 2022). Finally, hypoxia is a prominent driving force of angiogenesis, which affects initial sprouting, proliferation, and maturation stages (Guan et al. 2022).

Considering these findings, we hypothesized that our IH protocol could induce vascular changes. We therefore devised a series of experiments to explore this idea, including a transcriptomic study and imaging techniques.

B. TRANSCRIPTOMICS

In addition to the RT-qPCR results presented in published work, an analysis of 23 genes related to vascularization was conducted to explore the effects of IH on vascularization (Figure 39). The testing was done on whole cerebella at different stages: 13 for P4 (7N + 6IH), 16 for P8 (6N + 10IH), 25 for P12 (15N + 10IH), 17 for P21 (9N + 8IH), and 8 for P70 (5N + 3IH). A full statistical summary is presented in Appendix 7.

At stage P4 we found 30.4% regulation (7/23 genes), all of which were upregulated, indicating an overall increase in transcription of angiogenic factors. Interestingly, the pro-coagulation tissue factor (F3) and the endothelial adhesion molecule thrombospondin 1 (Thsb1) are upregulated,

RESULTS

indicating a clotting susceptibility (Phelan et al. 1998; Bhagat et al. 2020). Most notably, this stage sees the most upregulation of growth factors: transforming growth factor, beta 1 (*Tgfb1*), vascular endothelial growth factor a (*Vegfa*), and two *Vegf* receptors, *Flkt* and *Flt1*.

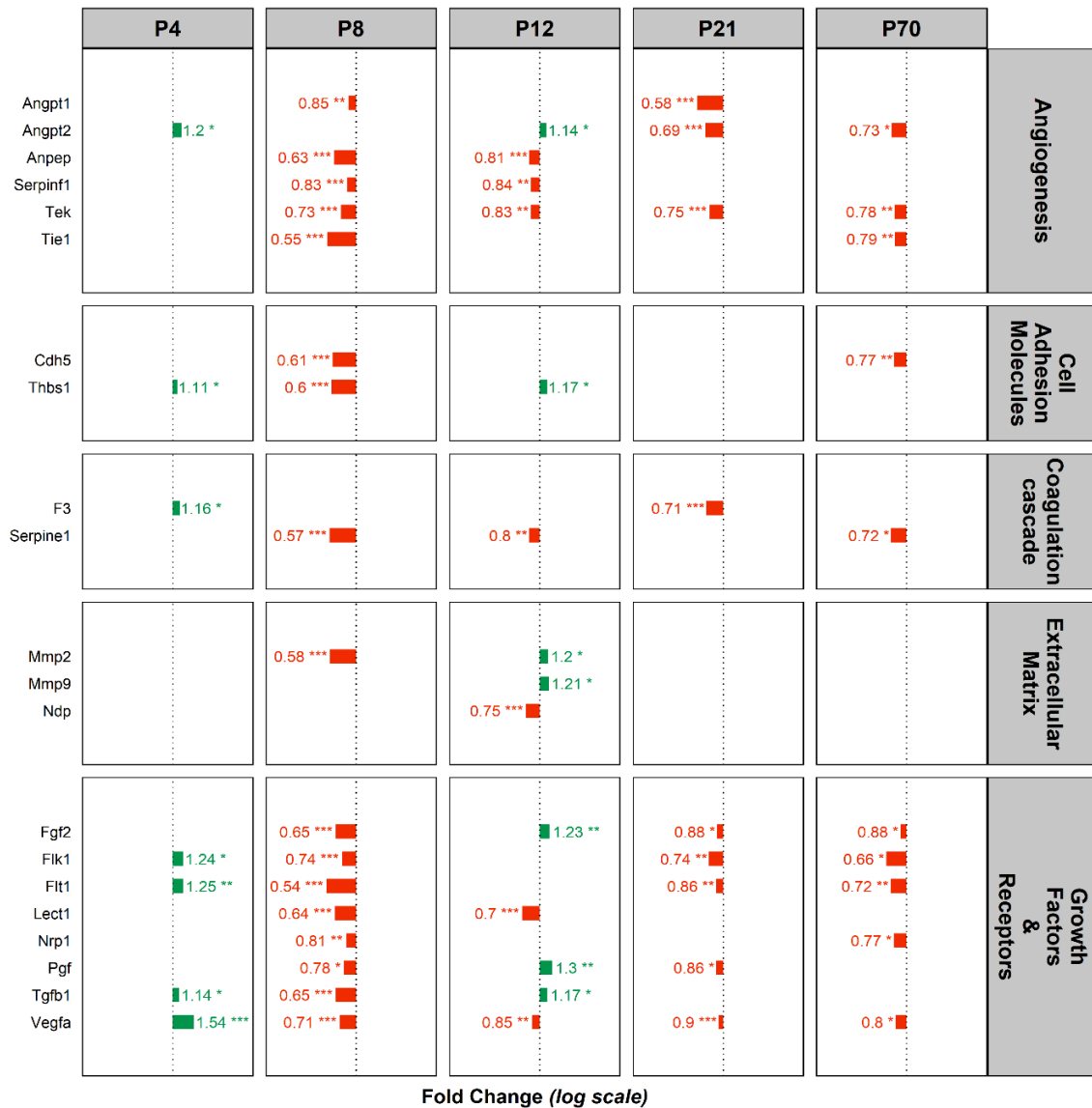


Figure 39: RT-qPCR results of the vascularization panel on the whole cerebellum.
Genes are grouped by stage and pathway. Red indicates a downregulation and green indicates an upregulation.

In contrast, P8 was the most regulated stage overall with 73.9% (17/23) differentially expressed genes, but all were downregulated. This includes the previously upregulated growth factors as well as the angiogenic receptor Tek, its ligand angiopoietin1 (Angpt1) and regulator Tie1. Then, P12 had 60.9% (14/23) of regulated genes with a partial switch to upregulation of certain genes such as the platelet growth factor (Pgf), fibroblast growth factor2 (Fgf2) and Tgfb1. Most notably, we see

regulations suggestive of a loosening of the extracellular matrix with the downregulation of norrin (Ndp) and the upregulation of matrix metalloprotease 2 and 9. Although the latter two can also be involved in neuronal migration (Wang et al. 2006).

At P21 we observed a differential expression of 39.1% (9/23) genes, predominantly growth and angiogenic factors. Indeed, Pgf, Fgf2, Tgfb1, Flk1 and Flt1 were once again downregulated. Finally, at P70, 43.5% (10/23) were still regulated suggesting that the vascular response to hypoxia is long lasting on a transcriptomic level. We also highlight the downregulation of SerpinE1 at P70 but also P12 and P8. Indeed, this protein's expression has been shown to increase after hypoxia-induced ROS accumulation. It is also involved in the HIF-1 α -SERPINE1 signaling pathway, which may be deleterious in the long term by exacerbating OS injury (Zhang et al. 2023).

Interestingly, angiopoietin 2 (Angpt2) was regulated in all stages save P8. Given our findings on the alterations of PC morphogenesis after IH, this cements the hypothesis that there may be a parallel alteration of neurogenesis and angiogenesis during IH (Luck et al. 2021). Thus, we aim to continue the exploration of the vascularization pathway via imaging studies.

C. IMMUNOHISTOCHEMISTRY

Samples have been harvested and prepared: 8 for P4 (4N + 4IH), 9 for P8 (4N + 5 IH), 8 for P12 (4N + 4IH), 6 for P21 (3N + 3IH), and 6 for P70 (3N + 3IH). Several IHC tests were performed to find a suitable marker for blood vessels (Figure 40). Once tests are finalized, IHC will be performed to correlate these data with the RT-qPCR results.

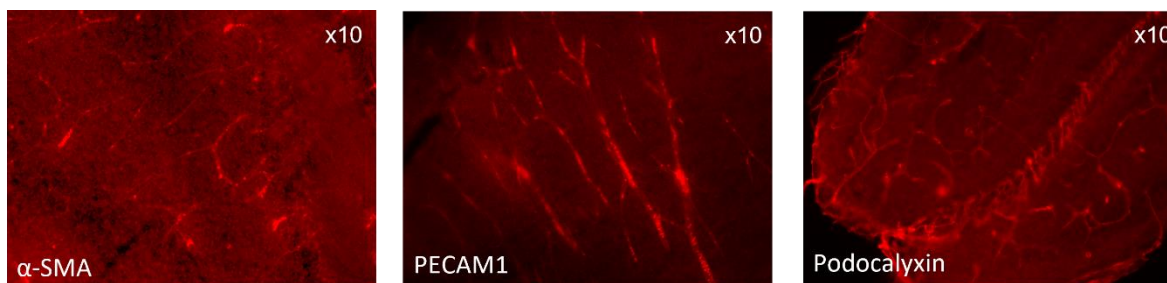


Figure 40: Immunohistochemistry test staining.

α-SMA: smooth muscle actin alpha; PECAM1: Platelet endothelial cell adhesion molecule 1. Slices (50 μ m) of a P8 cerebellum were cut with a vibratome and incubated overnight at 4°C, x10 zoom.

For the imaging studies, we initially tested several antibodies based on our transcriptomic findings, namely Tie2, phosphorylated Tie2, Vegf-B and Angpt2 (Table 2). We tested several

RESULTS

combinations with the addition of calbindin to identify PCs, and a marker for blood vessels. Phosphorylated Tie2 and Angpt2 shown promising results but the association of PECAM1 was unsuccessful in marking vessels during our test. These incubations were done on 40 µm slice of adult cerebellum so new tests were later conducted to find a suitable vessel marker.

Tests at P8 on thicker slicer have been started, and the rest of this area of focus will be continued within the team. We will then be able to correlate the findings with both our previous histological results and the transcriptomic regulations of the vascular network.

D. CLEARING

Samples have been harvested and prepared with the clearing technique: 9 for P4 (4N + 5IH), 11 for P8 (5N + 6 IH), 8 for P12 (4N + 4IH), 8 for P21 (4N + 4IH), and 8 for P70 (4N + 4IH). Once acquisition is finalized, analysis will be performed on Imaris (Figure 41). Anterior (lobules I-V) and posterior (lobules VI-X) cerebellar areas have been defined.

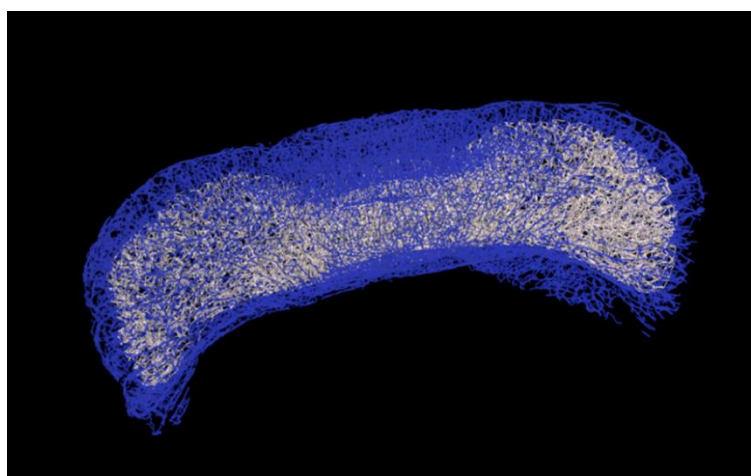


Figure 41: Modeling of blood vessels in the Imaris software.

Surfaces defined in a P21 whole cerebellum.

Through the IHC images, we will be able to study the cerebellar vascular network at the level of the lobule and cell-cell interactions, but we are also interested in seeing the three-dimensional organization of the vascular web *in situ* at the organ level. This will be done via the clearing technique associated with vascular immunolabeling. The image stacks have been acquired for P4, P8, and P21 so far with the iDISCO technology. Image analysis is underway by a new member of the team who uses the Imaris software to mark total vascular surfaces. Thus, we will obtain data on the total volume, density and branching parameters of the cerebellar vascular network, and be able to analyze the influence of IH on these variables at different stages.

DISCUSSION

The development of the cerebellum begins during the embryonic stage, but continues well into the postnatal period, making it particularly vulnerable to perinatal incidents (Volpe 2009). AOP is one of the most common of those pathologies, affecting over 50 % of premature newborns. It subjects the organism to IH from premature birth until the corrected term, and has been shown to be associated with long lasting deficits in children. The most commonly observed impairments are motor, behavioral, or learning issues, which are commonly associated with the cerebellum. However, the consequences of AOP on the cerebellum are still largely unknown at present (Janvier et al. 2004; Pillekamp et al. 2007). Therefore, we aimed to investigate the effects of a perinatal IH on cerebellar development in a murine model of AOP.

I. EFFECTS OF IH ON GROWTH AND BEHAVIOR

Our IH protocol, which is based onthe work of Cai et al. (Cai et al. 2012) does not induce any mortality, but still leads to significant growth retardation in mice. This effect of hypoxia on body weight is well known (Farahani et al. 2008; Pozo et al. 2012), but our results also showed that animals that underwent IH present a delay in the acquisition of the righting reflex, and fail the grasping test. Although this delay could be due, in part, to the pups' morphological underdevelopment, it is also consistent with a dysfunction of the anterior part of the cerebellum implicated in sensori-motor control (Stoodley and Schmahmann 2018). This theory is further supported by the finding of a lower response in the grip strength test at P21 even though the difference in weight between IH and N animals gradually decreases and disappears by adulthood. Taken together, those results suggest that the behavioral deficits we observed cannot be fully accounted for by gross physical development delay.

Similarly, many behavioral deficits persist in adulthood, despite that the weight difference has been fully compensated. Our Morris pool tests revealed that the different phases of spatial learning are impaired in hypoxic mice. Usually, spatial memory functions are attributed to the hippocampus (Goussakov et al. 2019), but the interplay between cerebellum and hippocampus in the control of spatial navigation is now recognized (Rochefort et al. 2013). Furthermore, during the retention phase, mice subjected to hypoxia spent less time and covered less distance in the target quadrant where the platform was located, indicating short-term memory deficits. Moreover, a poor performance in the

DISCUSSION

water maze has been linked to cerebellar impairments (Lalonde and Strazielle 2003), indicating that a cerebellar alteration could contribute to the behavioral deficit induced by our IH protocol.

In addition, adult IH mice had a higher number of stumbles in the horizontal beam test while having a similar crossing time to control animals, indicating a motor coordination deficit unrelated to motivation. We also controlled for a potentiated stress behavior or a locomotor disorder by conducting the actimetry and elevated cross maze tests, which revealed no difference. Altogether, our results indicate that our AOP-mimicking IH protocol induces long-term motor and non-motor deficits. We therefore undertook to investigate if these deficits might be related to histological alterations.

II. ANATOMICAL AND HISTOLOGICAL EFFECTS OF IH

It is known that perinatal incidents can lead to histological injury of the cerebellum since premature newborns present, among other things, with cerebellar atrophy (Allin et al. 2001; Srinivasan et al. 2006). Moreover, several studies conducted in mice have shown that a perinatal hypoxia induces histological alterations in various brain regions, including the cerebellum (Kheirandish et al. 2005; Cai et al. 2012; Darnall et al. 2017). Our findings confirm that the cerebellum is indeed a major target of perinatal IH, and presents observable histological defects.

The immunohistological analyses revealed an alteration in the developmental timing of the cerebellar cortex in IH mice. At P4, we observed a difference in the EGL, which is markedly decreased in hypoxic animals, suggesting an impact of IH on the proliferation of GC precursors. In contrast, none of the cerebellar layers showed a default at P8, which suggests that the proliferative processes were merely delayed, and a compensatory mechanism occurred to catch up. However, at P12, the thickness of the entire cerebellar cortex is decreased in IH mice, and resembles that of a P8 normoxic cerebellum, with a thicker EGL, and thinner ML and IGL. Additionally, BrDU marking enabled us to highlight that GCs *i)* maintain a high proliferative activity in the EGL of P12 IH mice (akin to a less mature cerebellum, *ii)* are able to migrate towards the IGL from P6 to P12, despite the IH protocol. These results suggest that the decrease of the cerebellar cortical thickness observed at P12 could be due either to the delay in global growth, or an increase in cell death throughout the IH protocol, which the cerebellum then tries to compensate with an increase in proliferation. This led us to study the effect of IH on the number of caspase-3 positive cells and the pro-apoptotic activity within the different cerebellar layers. No difference was observed in term of labelled cell density at P4, P8 and

P12, nor in enzyme activity at P12, suggesting that no major apoptotic process occurs during the IH protocol. The thickness decrease could thus be imputable to a caspase-independent apoptotic death (Chiu et al. 2012), or to cell death by necrosis or autophagy (Song et al. 2017). Similarly to body weight, we observed that histological defects in the cerebellar cortex are no longer visible at P21, suggesting that those defects are a mere consequence of growth retardation.

Finally, given that hypoxia plays a crucial role in angiogenesis during development, we aimed to explore the effects of our IH protocol of the development of the vascular network (Fajersztajn and Veras 2017). Our preliminary findings revealed a decrease in blood vessel length and volume, as well as a looser network in the cerebellar cortex in P8 IH mice. Therefore, applying IHC and clearing techniques on different developmental stages seems like a promising avenue to further study the impact of IH on cerebellar vascular organization.

III. EFFECTS OF IH ON PURKINJE CELLS AND CEREBELLAR CIRCUITRY

Our behavioral and histological results demonstrate that the motor and learning impairments induced by our IH protocol are associated with a significant delay in cerebellar cortex maturation. Moreover, it has been shown that IH decreases synaptic plasticity and long-term potentiation in several CNS areas such as the hippocampus (Goussakov et al. 2019). These data suggest that Purkinje cells, being considered as the cerebellum's integration center, are a likely target.

To test this hypothesis, we focused on the morphology and the afferences of Purkinje cells. We found that IH does not affect the number of PC somata, but decreases the volume of their dendritic tree at P12, with a stronger effect in the anterior cortex. Our results highlight a regional cerebellar sensibility to hypoxia, which is congruent with previous findings demonstrating that the anterior part of the cerebellum is usually more affected by a perinatal O₂ deprivation (Connolly et al. 2007; Biran et al. 2012). Surprisingly, at P21, Purkinje dendrites become denser in the posterior part of the cerebellum and throughout the cerebellum in adults. This shows that PCs, after the end of the IH protocol, try to compensate their under-arborization with an intensification of dendrite development, which ends up exceeding the normoxic volume of the dendritic trees. These long-term cellular alterations could explain the locomotor and spatial learning deficits observed (Yakusheva et al. 2007; Stoodley and Schmahmann 2018). In addition, we found that the volume of myelin sheaths is decreased in adult mice having experienced a perinatal IH. As our imaging focused on the GC layer where MFs and CFs are unmyelinated, our results show that this myelination defect mainly concerns

DISCUSSION

PC axons. This finding aligns with the current evidence on the effects of IH on myelination (Cai et al. 2012; Juliano et al. 2015).

As PC development conditions cerebellar afferences, we further studied Vglut2 and Glu δ 2 immunoreactivities in adult mice to determine if mossy (MF), climbing (CF) and/or parallel (PF) fibers are affected by our IH protocol. Our findings show a higher colocalization between Vglut2 and calbindin in the ML of IH mice, thus confirming that perinatal hypoxia alters the early CF selection phase and leads to the over-innervation of Purkinje cells by CFs (Park et al. 2021). Likewise, the increase in Vglut2 labeling seen in the IGL indicates that MFs may also be impacted by IH. In contrast, Glu δ 2 immunolabelling showed no difference in the PF innervation of PC dendrites. Taken together, our IHC results highlight how the cerebellar cortical network is affected by IH, and suggest that these changes in connectivity may be at the root of the behavioral deficits. However, to go further and unveil molecules able to counteract the deleterious effects of IH, it is necessary to understand the cellular pathways involved in the response to hypoxia.

IV. MOLECULAR EFFECTS OF IH

A. IH CAUSES A STATE OF OS IN THE CEREBELLUM

1. *IH increases ROS production*

Since the most deleterious effect of hypoxia is the induction of a state of OS, we firstly confirmed that our IH protocol does lead to an overproduction of ROS in the cerebellar cortex at P12. Then, RT-qPCR results helped us determine how this ROS increase came to be.

One of the main signs of the heightened OS state in the cerebellum following our IH protocol is the overexpression of the genes Hmox1 and Idh1, and downregulation of Fth1 at P12, which are associated to ROS production (Dunn et al. 2014; Wahl et al. 2017; Mukherjee et al. 2020). Moreover, at P8, we observed an overexpression of Rheb, which might contribute to the overall vulnerability of the cerebellum to hypoxia. Indeed, Rheb encodes a pentameric protein associated with membrane lipids whose activation is associated with neuronal degeneration and sensitivity to OS (Patel and Tamanoi 2006; Potheraveedu et al. 2017).

During OS, there are different pathways leading to ROS production (see p.78). One of them takes place via the mitochondria by involving the cytochrome c oxidase enzyme (Holzerová and Prokisch 2015). This enzyme is the last of the mitochondrial electron transport chain, and its subunit

IV has 2 isoforms, respectively encoded by the genes Cox4i1 and Cox4i2. The ratio of isoform 1 to isoform 2 of this oxidase has been shown to be directly correlated with ROS production in astrocytes (Roemgens et al. 2011). Thus, the decrease in Cox4i1 expression observed after our IH protocol could cause a reduction in this ratio, and generate an increase in ROS within the cerebellum (Bourens et al. 2013; Scaramuzzino et al. 2021). Another ROS production pathway is related to iron availability. At P4 and P12, we observed a decrease in the expression of Fth1, which encodes the large subunit of ferritin. This could imply a greater availability of intracellular Fe^{2+} , which would then contribute to an increase in the amount of ROS produced via the Fenton reaction (Birben et al. 2012).

In parallel, the activation of mechanisms that take place to reduce ROS production can also attest to the presence of OS. Indeed, we observed a decrease in Nos1 (nitric oxide synthase 1) expression at P8 and P12, which encodes NOS. This enzyme produces nitric oxide and reactive nitrogen species as byproducts which, as free radicals, also contribute to OS (Spandou et al. 1999). Indeed, NOS inhibitors have been shown to have neuroprotective effects, indicating that oxidative species produced by NOS contribute to OS-induced alterations (Ferriero 2001). In addition, in the presence of oxygen, such as in the reoxygenation phase of our IH protocol, NADPH oxidase is activated and produces $\text{O}_2\bullet^-$, which leads to the production of NADP^+ , which becomes available for NOS. Interestingly, our IH protocol also induces the upregulation of Idh1 (isocitrate dehydrogenase-1) at P8, which becomes even more marked at P21. Idh1 is a metabolic enzyme that produces NADPH (Itsumi et al. 2015), which is a substrate for reduction reactions. These redox reactions enable the replenishment of reduced glutathione (GSH), which in turn is necessary for the conversion of H_2O_2 to H_2O by glutathione peroxidases (Birben et al. 2012). This result indicates that the cerebellum is still trying to counteract the ROS accumulation several days after the end of the protocol.

In conclusion, the transcriptomic landscape indicates that the cerebellum enters an OS state after our IH protocol. We showed that ROS accumulation mainly occurs via the mitochondrial, NADPH, and ferritin pathways, and that a contribution of nitrogen-derived free radicals should not be excluded.

2. IH is correlated with a failure of the antioxidant system

To counter the deleterious regulations causing OS, the cell can activate several defense mechanisms. One central effector of this defense is the system revolving around glutathione (GSH), which we found to be regulated during our IH protocol.

DISCUSSION

GSH serves as a substrate for glutathione S-transferases that conjugate GSH to reactive chemical species (e.g., peroxidized lipids) to promote their removal (Birben et al. 2012). The mu1 subunit of this enzyme, encoded by the *Gstm1* gene, is upregulated at P4 and P12 in the cerebellum, much like the evidence found by Curristin et al., who demonstrated significant overexpression of other subunits in the CNS following their hypoxia protocol (Curristin et al. 2002). It thus seems that this detoxification process via GSH is involved in the elimination of cellular components denatured by OS.

In parallel, GSH also serves as a substrate for the glutathione peroxidases (encoded by *Gpx* genes) to reduce H₂O₂ and limit the production of HO[•] radicals in the cell. Moreover, cellular stores of GSH are limited and must be maintained by glutathione synthetase, encoded by the *Gss* gene (Birben et al. 2012). Here, our data show that, in IH mice, the expression of *Gss* is specifically decreased at P8. Meanwhile, *Gpx* expression varies differently depending on the isoforms and the stage, but is overall decreased from P4 to P12, with the exception of *Gpx1* at P8. Altogether, our data indicates that IH induces a failure of this protective system. However, the significant overexpression of *Gpx 1* and *7* at P21 suggests that this component of the defense is later re-activated, despite a new downregulation at P70.

Other possibilities to fight ROS is the reduction of O₂^{•-} or H₂O₂ by superoxide dismutases (SOD) or peroxyredoxins (PRDX), respectively. However, once again, we found a significantly decreased expression of several isoforms of both enzymes at P8, suggesting that this defense mechanism is also affected by hypoxia. Additionally, PRDX activity is directly linked to the thioredoxin (TRX) antioxidant system, which undergoes regulation during our IH protocol. Indeed, *Txnip* (encoding a thioredoxin inhibitory protein) is upregulated at P4 and P8, and *Txnrd1* (encoding thioredoxin reductase which allows thioredoxin turnover) is downregulated at P8.

In contrast, at P12, a compensation seems to occur with an upregulation of *Sods* and *Txnrd3* expression, but this compensation is only partially effective due to the downregulation of sulfiredoxin 1 (encoded by *Srxn1*), which results in a failure to activate PRDX and TRX (Wu et al. 2017; Li et al. 2018). Interestingly, the most marked regulation observed at P70 was the upregulation of *Ccs*, encoding for a copper chaperone of SOD1 (Furukawa et al. 2004). Given the essential role of *Ccs* in SOD1 functionality, this regulation might be a long-lasting adaptation to an early exposure to hypoxia.

Despite this adaptation process and attempt at compensation, the antioxidant defense systems seem to be overwhelmed by the repeated cycles of IH and fail to neutralize OS. Eventually, it leads to cell death, we thus tested genes associated with different cell death mechanisms to better understand the repercussions of OS.

3. IH regulates different cell-death and neuroprotective pathways

Since caspase-dependent apoptosis is considered the main physiological process to control cellular population, our first focus was to assess the regulation of the pro-apoptotic enzyme caspase-3. In our IH condition, the expression of the corresponding gene Casp3 is not increased, or even detected at P4 and P8, which is in accordance with our immunohistochemical study. However, it is significantly more expressed at P12 in hypoxic animals. This belated caspase-3 expression has already been observed in the mouse brain after a continuous perinatal hypoxia (Curristin et al. 2002). Moreover, we did not see any difference in caspase-3 activity at P12, suggesting that this pro-apoptotic process could be compensated by the overexpression of the anti-apoptotic Adcyap1 (also known as PACAP or pituitary adenylate cyclase-activating peptide), which is known to play a neuroprotective role in the cerebellum via an inhibition of caspase-3 activity (Lacaille et al. 2015).

However, the underexpression of Bcl2 at P4, P8 and P12 during IH remains in favor of an increase in apoptotic cell death, which could be due to the poly ADP-ribose polymerase (PARP) pathway instead. Indeed, it has been shown that, in GCs under hypoxic conditions, DNA damage caused by ROS accumulation induces PARP activation which results in the production of poly (ADP-ribose) polymers. These polymers activate mitochondrial calpain, leading to the translocation of the apoptosis inducing-factor (AIF) into the nucleus, which results in the induction of caspase-independent apoptosis (Chiu et al. 2012). As Bcl2 can inhibit PARP1, and thus cell death (Dutta et al. 2012), its underexpression could reciprocally lead to cell death. Moreover, the decrease of Parp1 expression at P8 and P12 observed in our IH condition might represent a compensatory mechanism in response to the failure of Bcl2 to control of the PARP pathway. These results match those of Chiu et al. showing that IH-induced cell death is caspase-independent (Chiu et al. 2012).

Finally, adenosine normally protects neurons from hypoxia by inhibiting excitatory neurotransmission through activation of ADORA1, thus attenuating cell loss and degeneration. This activation, during reoxygenation, is mediated by extracellular endogenous adenosine, and plays a role in cell survival (Logan and Sweeney 1997; Duarte et al. 2016). However, in the IGL, we observed a significant downregulation of Adora1 at P8, which persisted at P12 and P21. This could predispose IH-mice to neuronal degeneration, an effect that would be exacerbated by immaturity and lower available adenosine concentrations. Indeed, low basal concentration of extracellular adenosine metabolites is detected in immature cerebellar slices (Atterbury and Wall 2009). In addition, several studies have demonstrated the neuroprotective effect of Akt and its downstream pathways in cultured GCs in response to stressors, including hypoxia (Dudek et al. 1997; Kumari et al. 2001; Heaton et al. 2004). However, we found that Akt was downregulated at P8 in the whole EGL, thus affecting

DISCUSSION

both proliferating and pre-migratory GCs (Dudek et al. 1997; Kumari et al. 2001; Heaton et al. 2004). Therefore, this could be one of the pathways that places P8 as a particularly vulnerable stage to IH damage.

Overall, our transcriptomic data point toward a twofold sensitization of the cerebellum, as there is both an activation of cell death pathways and a reduction of the neuroprotective environment. We thus further investigated the effects of IH on specific pathways in different cerebellar layers.

B. CEREBELLAR LAYERS ARE DIFFERENTIALLY AFFECTED BY IH

1. IH influences the maturation rate of GCs

In the cerebellar cortex, GCs undergo sequential proliferation, migration, and synaptogenesis. Within the EGL, we found that IH induces the downregulation of several genes related to proliferation at P4 and P8, including Zic1, Ccnd1 and Pax6 (Yeung et al. 2016; Aruga and Millen 2018; Miyashita et al. 2021). As an example, Zic1 belongs to the zinc finger proteins (Zic) that are strongly expressed in the cerebellum, especially in GC progenitors. Thus, this downregulation suggests that GCs may be less responsive to SHH (sonic hedgehog) signals from the underlying PCs (Aruga and Millen 2018). We also observed a downregulation of stathmin in P8 and P12 pups who had undergone the IH protocol. To our knowledge, no information about this genetic regulation is available regarding granule cells in the EGL but, in GnRH neurons, stathmin expression is directly proportional to both motility and proliferation (Giampietro et al. 2005). Thus, this suggests that IH alters the motile/proliferative profile of GC precursors during early postnatal development. However, at P12, the proliferation associated genes are no longer downregulated, which could partially explain that, at the end of our IH protocol, there is an increase of BrDU-positive cells in the EGL of IH mice, which have caught up with the controls.

Another way our IH protocol could affect the migration of GC precursors is by the way of a decrease in guidance, cell adhesion, or cytoskeletal molecules. Indeed, we observed a downregulation of the guidance-related gene Robo1, indicating that some trophic signals will miss their mark during migration in the inner premigratory EGL of IH P8 mice (Gruner et al. 2019). Similarly, the genes Dclk1 (doublecortin-like kinase 1), talin 1, and cadherin 8 are dysregulated in the GC, suggesting that IH may decrease the ability of cells to remodel their cytoskeleton in order to initiate migration (Taniguchi et al. 2006; Shin et al. 2013; Wang et al. 2019). Moreover, we found that the cell adherence molecules L1cam (L1 cell adhesion molecule) and astrotactin 2 are under-expressed at P12 (Thelen et al. 2002;

Wilson et al. 2010). Thus, the late migratory process through the ML may also be impacted by IH. Moreover, we cannot exclude that the under-expression of astrotactin could also affect the postsynaptic activity of PCs (Behesti et al. 2018).

However, the most important overall regulation in GCs is a marked dysregulation of genes involved in cell communication. Indeed, we found a decrease in homer 2 expression, suggesting an impairment in GC synaptic densities (Shiraishi et al. 2003). In contrast, the expression of calretinin is increased by IH, as it usually is in the mature cerebellum, and particularly in GCs, UBCs, mossy and climbing fibers (Bearzatto et al. 2006). This indicates that IH induces an alteration of the maturation of GC precursors in the ML and this defect persists in the IGL. Indeed, Nrnx1 and/or its ligand, Nxph4, are both downregulated in the IGL during the whole IH protocol period. The alteration of this pathway is associated with impaired inhibitory neurotransmission and a decrease in synapse number, which are both implicated in motor learning and coordination deficits (Meng et al. 2019). Similarly, regulation of the synapse-associated Cadps2, which persists in the long term, may contribute to the spatial memory deficits in adult mice after IH (Duan et al. 2023). Alternatively, Calb2 upregulation at P12 could serve as a defense against excitotoxicity by sequestering Ca^{2+} (Bearzatto et al. 2006).

2. IH modifies Purkinje cell phenotype

Aside from GCs, we also aimed to understand the molecular basis for the morphological changes we observed in PCs. We first focused on cytoskeleton-related genes such as Tln1, which promotes integrin activation and is essential for neurite outgrowth (Wang et al. 2019). The underexpression of Tln1 in PCs at P8 could likely reflect the incipient dendritic tree, while the marked downregulation in the ML at P12 may correspond to later branching. Both findings indicate less neurite outgrowth in the PC dendritic tree, suggesting a delay in arborization, which corroborates our immunohistochemical finding of a lower volume of PC dendritic tree at P12 post-IH (Leroux et al. 2022).

Similarly, Nefl (neurofilament light chain gene), which was downregulated at P8, becomes upregulated at P12. Neurofilaments are cytoskeletal components enriched at PC axonal “torpedoes”, or focal swellings. While their function is poorly understood, they seem to be a developmental characteristic which peaks at P11 (Ljungberg et al. 2016). This could signify that, during IH, PCs modify their phenotype and, later, their connection profile.

DISCUSSION

In addition, Rac1 becomes upregulated at P12, which may point to an abnormal morphogenesis. Indeed, elevated Rac1 activity has been shown to cause defects in cerebellar foliation, ectopic GCs, and altered Bergmann glia morphology (Mulherkar et al. 2014). In contrast, at P21, only the migration, neurite growth, and axon guidance molecule Nav3 is upregulated (McNeill et al. 2011; Powers et al. 2023). This could point towards the establishment of a compensation mechanism, which would explain the observed lack of thickness difference in the molecular and Purkinje layers at P21.

3. IH alters synaptogenesis and cerebellar circuitry

Given the role of PCs as the cerebellum's integration center, alterations in their structure should have repercussions on the cortical circuit, and could explain behavioral deficits due to IH. Being highly specific to PCs, the downregulation of Pcp2 (Purkinje cell protein 2) at P8 could be a good candidate to investigate. However, it has been shown that a loss of Pcp2 in mice is associated with only moderate cerebellar hypoplasia and increased motor learning (Guan et al. 2005; Iscru et al. 2009), which raises questions as to its role in the cerebellar circuit. Conversely, we found a downregulation of genes specific to synaptic function such as Cadps2, which codes for the calcium-dependent activator protein for secretion 2. This molecule is implicated in the physiopathology of ADHD (Duan et al. 2023), which brings to mind the memory deficits found in behavioral experiments in adult mice after IH.

IH is also accompanied by a marked downregulation in VGlut1 expression (Slc17a7) in PCs at P8. Vglut1 is a hallmark of GC-PC synapses, and a deficit in these synapses has been shown to impair the correct pruning of CF-PC synapses (van der Heijden et al. 2021). In parallel, the upregulation of VGlut2 (Slc17a6) has been observed in the ML of P12 IH mice. Together, these findings could, at least partly, explain the observed over-innervation of Purkinje cells by CFs in adulthood. In contrast, no difference in the expression of Cacng2 is observed after IH, suggesting that the connection between GCs and ML interneurons is not affected by our protocol (Shevtsova and Leitch 2012; Rigby et al. 2015). However, the significant under expression of Astn2 at P12 in the ML may signify that IH decreases PC postsynaptic activity.

In the longer term, IH seems to only affect the expression of a few genes such as Gabra1 and Syn1. As Syn1 (Synapsin 1) is a crucial effector of synaptic plasticity and axonal elongation, whose alteration is a hallmark of neurodevelopmental disorders such as autism and epilepsy (Chin et al. 1995; Kao et al. 2017; Parenti et al. 2022), we can theorize that this regulation is a compensatory mechanism at P21, meant to counteract the early deficits. However, GABAergic neurotransmission (tested with Gabra1) seems to stay altered even at P70.

4. IH affects glial cells

Finally, despite being less studied than the neuronal population, white matter and glial cells are conclusively impacted by our IH protocol. Indeed, in the WM layer, the major differentiation genes involved in the formation of the myelin sheath, namely Mbp, Mbp, Mog, and Plp1, are simultaneously, and strongly, downregulated by IH at P12. A compensatory increase of the expression of some of them occurs in adulthood, but it seems inefficient since the volume of myelin sheaths of Purkinje axons is lower in adult mice after a perinatal IH.

Since stathmin participates in the proper myelination of neurons (Richter-Landsberg 2008), its upregulation in the P4 and P21 WM could indicate a myelination defect, or glial immaturity. Interestingly, the neuroprotective Akt1 (Dudek et al. 1997; Kumari et al. 2001; Heaton et al. 2004) was upregulated P4 and P12 in the WM, which could be part of a glial defense mechanism.

Finally, one long term upregulation we highlighted in the WM relates to Grm3 (glutamate metabotropic receptor 3) at P70. This molecule is a hallmark of neuroinflammation and indicates the presence of fibrous astrocytes (Egan et al. 2004; Zinni et al. 2021). Thus, our findings may indicate a post-injury reaction to IH, which persists in time, and could be involved in behavioral alterations and cognitive impairment (Egan et al. 2004).

DISCUSSION

CONCLUSION AND PERSPECTIVES

The information obtained in the course of this project, and presented in this manuscript, contributes to the understanding of the impact of AOP on cerebellar development. By using our in-house hypoxia chamber, we were able to induce reproducible IH protocols mimicking the human pathology of AOP.

Overall, our results confirm that the cerebellum is sensitive to neonatal oxygen deprivation. The combination of experimental protocols enabled us to establish correlations between several levels of alteration: behavioral, histological, cellular, and molecular. Moreover, our preliminary results on the vascular impact of AOP in the cerebellum are the basis of ongoing experiments, which will further help understand the pathology. Recent advances in image analysis software will allow us to assess the impact of AOP on both the density of blood vessels and their branching patterns.

The most substantial part of this PhD work was an exploratory transcriptomic study. The study of oxidative stress-related genes on the whole cerebellum revealed a dual mechanism: an increase in genes associated with ROS production, and a failure of the antioxidant defense system, which culminates in the activation of several cell death mechanisms. We were then able to single out P8 as a critical timepoint in terms of OS vulnerability.

We also demonstrated that IH alters numerous cerebellar developmental processes, including proliferation, migration, neurite growth, synaptogenesis, and myelin sheath formation, thus explaining, at least in part, the histological and behavioral deficits observed in IH pups. Thus, our compilation of data is instrumental in understanding and interpreting the long-term learning and motor coordination deficits that persist through adulthood. Indeed, we showed that several genes, mainly involved in the cerebellar circuit, are still altered at P70, and participate to hyper-dendritic and over-innervated Purkinje cells.

Altogether, these results provide elements to better understand the diverse aspects of AOP-induced cerebellar injury. They show that AOP can lead to lasting molecular, structural, and functional alterations within the cerebellum, which may, at least in part, participate in the neurodevelopmental disorders observed in affected children (Figure 42). The identification of such a wide array of implicated genes, their window of vulnerability, as well as target cells could lead to new research prospects, especially in terms of protein expression.

CONCLUSION

Due to the paucity of satisfactory treatments for AOP, identifying neurotrophic factors likely to protect the cerebellum from IH-induced damage could prove very valuable. In the long term, it could lead to the identification of novel therapeutic targets to address this socially and economically impactful health issue.

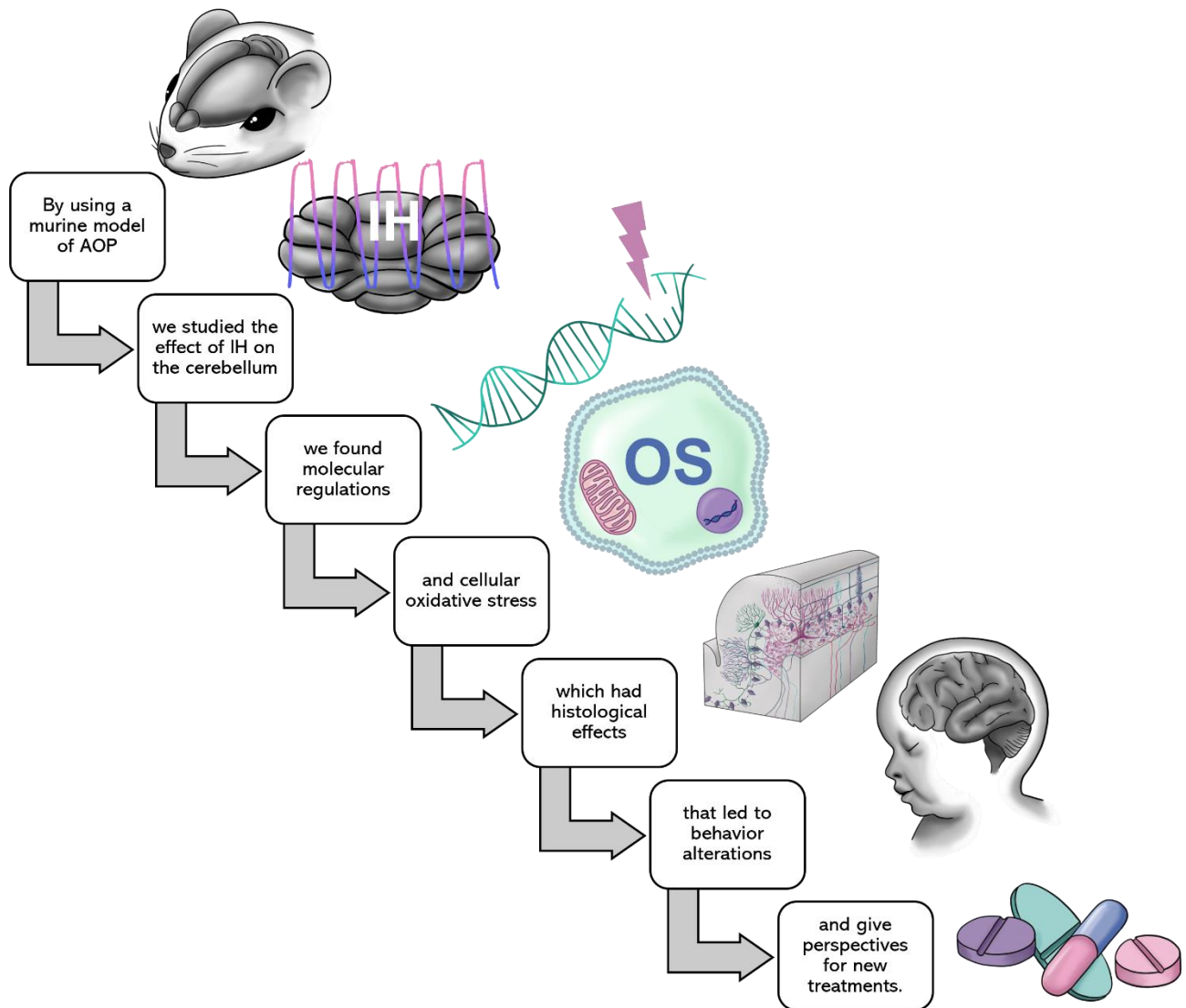


Figure 42: Graphical conclusion.

AOP: apnea of prematurity; IH: intermittent hypoxia; OS: oxidative stress.

REFERENCES

- Aarts E, Dolan CV, Verhage M, van der Sluis S. 2015. Multilevel analysis quantifies variation in the experimental effect while optimizing power and preventing false positives. *BMC Neurosci.* 16(1):94. <https://doi.org/10.1186/s12868-015-0228-5>
- Abbott LC, Sotelo C. 2000. Ultrastructural analysis of catecholaminergic innervation in weaver and normal mouse cerebellar cortices. *J Comp Neurol.* 426(2):316–329.
- Abdel Mageed ASA, Olama KA, Abdel Rahman SA, El-Gazzar HE. 2022. The effect of sensory stimulation on apnea of prematurity. *J Taibah Univ Med Sci.* 17(2):311–319. <https://doi.org/10.1016/j.jtumed.2021.10.016>
- Abu Jawdeh EG, O’Riordan M, Limrungskul A, Bandyopadhyay A, Argus BM, Nakad PE, Supapannachart S, Yunis KA, Davis PG, Martin RJ. 2013. Methylxanthine use for apnea of prematurity among an international cohort of neonatologists. *J Neonatal-Perinat Med.* 6(3):251–256. <https://doi.org/10.3233/NPM-1371013>
- Abu-Shaweeh JM, Martin RJ. 2008. Neonatal Apnea: What’s New? *Pediatr Pulmonol.* 43(10):937–944. <https://doi.org/10.1002/ppul.20832>
- Ackermann H, Mathiak K, Riecker A. 2007. The contribution of the cerebellum to speech production and speech perception: Clinical and functional imaging data. *The Cerebellum.* 6(3):202–213. <https://doi.org/10.1080/14734220701266742>
- Adachi T, Miyashita S, Yamashita M, Shimoda M, Okonechnikov K, Chavez L, Kool M, Pfister SM, Inoue T, Kawauchi D, Hoshino M. 2021. Notch Signaling between Cerebellar Granule Cell Progenitors. *eneuro.* 8(3):ENEURO.0468-20.2021. <https://doi.org/10.1523/ENEURO.0468-20.2021>
- Adamaszek M, D’Agata F, Kirkby KC, Trenner MU, Sehm B, Steele CJ, Berneiser J, Strecker K. 2014. Impairment of Emotional Facial Expression and Prosody Discrimination Due to Ischemic Cerebellar Lesions. *The Cerebellum.* 13(3):338–345. <https://doi.org/10.1007/s12311-013-0537-0>
- Al-Alaiyan S, Dawoud M, Al-Hazzani F. 2014. Positive distending pressure produced by heated, humidified high flow nasal cannula as compared to nasal continuous positive airway pressure in premature infants. *J Neonatal-Perinat Med.* 7(2):119–124. <https://doi.org/10.3233/NPM-1474113>
- Alcock J, Scotting P, Sottile V. 2007. Bergmann glia as putative stem cells of the mature cerebellum. *Med Hypotheses.* 69(2):341–345. <https://doi.org/10.1016/j.mehy.2007.01.006>
- Alheid GF, McCrimmon DR. 2008. The chemical neuroanatomy of breathing. *Respir Physiol Neurobiol.* 164(1–2):3–11. <https://doi.org/10.1016/j.resp.2008.07.014>
- Allaire JJ. 2022. quarto: R Interface to “Quarto” Markdown Publishing System [Internet]. [place unknown]. <https://CRAN.R-project.org/package=quarto>
- Allais A, Burel D, Roy V, Arthaud S, Galas L, Isaac ER, Desfeux A, Parent B, Fournier A, Chapillon P, et al. 2010. Balanced effect of PACAP and FasL on granule cell death during cerebellar development: a morphological, functional and behavioural characterization. *J Neurochem.* 113(2):329–340. <https://doi.org/10.1111/j.1471-4159.2009.06555.x>

REFERENCES

- Allin M, Matsumoto H, Santhouse AM, Nosarti C, AlAsady MHS, Stewart AL, Rifkin L, Murray RM. 2001. Cognitive and motor function and the size of the cerebellum in adolescents born very pre-term. *Brain.* 124(1):60–66. <https://doi.org/10.1093/brain/124.1.60>
- Almado CEL, Machado BH, Leao RM. 2012. Chronic Intermittent Hypoxia Depresses Afferent Neurotransmission in NTS Neurons by a Reduction in the Number of Active Synapses. *J Neurosci.* 32(47):16736–16746. <https://doi.org/10.1523/JNEUROSCI.2654-12.2012>
- Al-Saif S, Alvaro R, Manfreda J, Kwiatkowski K, Cates D, Rigatto H. 2001. Inhalation of low (0.5%–1.5%) CO₂ as a potential treatment for apnea of prematurity. *Semin Perinatol.* 25(2):100–106. <https://doi.org/10.1053/sper.2001.23199>
- Altman J. 1972. Postnatal development of the cerebellar cortex in the rat. I. The external germinal layer and the transitional molecular layer. *J Comp Neurol.* 145(3):353–397. <https://doi.org/10.1002/cne.901450305>
- Altman J, Bayer SA. 1997. Development of the cerebellar system: in relation to its evolution, structure, and functions. Boca Raton: CRC Press.
- Amaro CM, Bello JA, Jain D, Ramnath A, D'Ugard C, Vanbuskirk S, Bancalari E, Claure N. 2018. Early Caffeine and Weaning from Mechanical Ventilation in Preterm Infants: A Randomized, Placebo-Controlled Trial. *J Pediatr.* 196:52–57. <https://doi.org/10.1016/j.jpeds.2018.01.010>
- Andjus PR, Zhu L, Cesa R, Carulli D, Strata P. 2003. A change in the pattern of activity affects the developmental regression of the purkinje cell polyinnervation by climbing fibers in the rat cerebellum. *Neuroscience.* 121(3):563–572. [https://doi.org/10.1016/S0306-4522\(03\)00556-6](https://doi.org/10.1016/S0306-4522(03)00556-6)
- Andreyev A, Tamrakar P, Rosenthal RE, Fiskum G. 2018. Calcium uptake and cytochrome c release from normal and ischemic brain mitochondria. *Neurochem Int.* 117:15–22. <https://doi.org/10.1016/j.neuint.2017.10.003>
- Ango F, di Cristo G, Higashiyama H, Bennett V, Wu P, Huang ZJ. 2004. Ankyrin-Based Subcellular Gradient of Neurofascin, an Immunoglobulin Family Protein, Directs GABAergic Innervation at Purkinje Axon Initial Segment. *Cell.* 119(2):257–272. <https://doi.org/10.1016/j.cell.2004.10.004>
- Anilkumar U, Weisova P, Schmid J, Bernas T, Huber HJ, Düssmann H, Connolly NMC, Prehn JHM. 2017. Defining external factors that determine neuronal survival, apoptosis and necrosis during excitotoxic injury using a high content screening imaging platform. Ceña V, editor. *PLOS ONE.* 12(11):e0188343. <https://doi.org/10.1371/journal.pone.0188343>
- Argyropoulos GPD, van Dun K, Adamaszek M, Leggio M, Manto M, Masciullo M, Molinari M, Stoodley CJ, Van Overwalle F, Ivry RB, Schmahmann JD. 2020. The Cerebellar Cognitive Affective/Schmahmann Syndrome: a Task Force Paper. *The Cerebellum.* 19(1):102–125. <https://doi.org/10.1007/s12311-019-01068-8>
- Arnold AP. 2004. Sex chromosomes and brain gender. *Nat Rev Neurosci.* 5(9):701–708. <https://doi.org/10.1038/nrn1494>
- Arnold AP, Xu J, Grisham W, Chen X, Kim Y-H, Itoh Y. 2004. Minireview: Sex Chromosomes and Brain Sexual Differentiation. *Endocrinology.* 145(3):1057–1062. <https://doi.org/10.1210/en.2003-1491>

- Aruga J, Millen KJ. 2018. ZIC1 Function in Normal Cerebellar Development and Human Developmental Pathology. In: Aruga J, editor. *Zic Fam* [Internet]. Vol. 1046. Singapore: Springer Singapore; [accessed 2023 Mar 22]; p. 249–268. https://doi.org/10.1007/978-981-10-7311-3_13
- Asanuma C, Thach WT, Jones EG. 1983. Distribution of cerebellar terminations and their relation to other afferent terminations in the ventral lateral thalamic region of the monkey. *Brain Res Rev.* 5(3):237–265. [https://doi.org/10.1016/0165-0173\(83\)90015-2](https://doi.org/10.1016/0165-0173(83)90015-2)
- Ashida R, Cerminara NL, Brooks J, Apps R. 2018. Principles of organization of the human cerebellum: macro- and microanatomy. In: *Handb Clin Neurol* [Internet]. Vol. 154. [place unknown]: Elsevier; [accessed 2023 Jan 19]; p. 45–58. <https://doi.org/10.1016/B978-0-444-63956-1.00003-5>
- Ashrafi G, Wu Z, Farrell RJ, Ryan TA. 2017. GLUT4 Mobilization Supports Energetic Demands of Active Synapses. *Neuron.* 93(3):606-615.e3. <https://doi.org/10.1016/j.neuron.2016.12.020>
- Atik A, De Matteo R, Boomgardt M, Rees S, Harding R, Cheong J, Rana S, Crossley K, Tolcos M. 2019. Impact of High-Dose Caffeine on the Preterm Ovine Cerebrum and Cerebellum. *Front Physiol.* 10:990. <https://doi.org/10.3389/fphys.2019.00990>
- Atkinson WJ. 1949. THE ANTERIOR INFERIOR CEREBELLAR ARTERY: ITS VARIATIONS, PONTINE DISTRIBUTION, AND SIGNIFICANCE IN THE SURGERY OF CEREBELLO-PONTINE ANGLE TUMOURS. *J Neurol Neurosurg Psychiatry.* 12(2):137–151. <https://doi.org/10.1136/jnnp.12.2.137>
- Atterbury A, Wall MJ. 2009. Adenosine signalling at immature parallel fibre-Purkinje cell synapses in rat cerebellum: Development of adenosine signalling. *J Physiol.* 587(18):4497–4508. <https://doi.org/10.1113/jphysiol.2009.176420>
- Azad MB, Chen Y, Henson ES, Cizeau J, McMillan-Ward E, Israels SJ, Gibson SB. 2008. Hypoxia induces autophagic cell death in apoptosis-competent cells through a mechanism involving BNIP3. *Autophagy.* 4(2):195–204. <https://doi.org/10.4161/auto.5278>
- Babayan BM, Watilliaux A, Viejo G, Paradis A-L, Girard B, Rondi-Reig L. 2019. Author Correction: A hippocampo-cerebellar centred network for the learning and execution of sequence-based navigation. *Sci Rep.* 9(1):19904. <https://doi.org/10.1038/s41598-019-56345-7>
- Bagnall MW, Zingg B, Sakatos A, Moghadam SH, Zeilhofer HU, Lac S d. 2009. Glycinergic Projection Neurons of the Cerebellum. *J Neurosci.* 29(32):10104–10110. <https://doi.org/10.1523/JNEUROSCI.2087-09.2009>
- Bai C, Zhu Y, Dong Q, Zhang Y. 2022. Chronic intermittent hypoxia induces the pyroptosis of renal tubular epithelial cells by activating the NLRP3 inflammasome. *Bioengineered.* 13(3):7528–7540. <https://doi.org/10.1080/21655979.2022.2047394>
- Bailey A. 1998. A clinicopathological study of autism. *Brain.* 121(5):889–905. <https://doi.org/10.1093/brain/121.5.889>
- Bairam A, Boukari R, Joseph V. 2019. Targeting progesterone receptors in newborn males and females: From the animal model to a new perspective for the treatment of apnea of prematurity? *Respir Physiol Neurobiol.* 263:55–61. <https://doi.org/10.1016/j.resp.2019.03.004>
- Balsters JH, Cussans E, Diedrichsen J, Phillips KA, Preuss TM, Rilling JK, Ramnani N. 2010. Evolution of the cerebellar cortex: The selective expansion of prefrontal-projecting cerebellar lobules. *NeuroImage.* 49(3):2045–2052. <https://doi.org/10.1016/j.neuroimage.2009.10.045>

REFERENCES

- Bankoul S, Neuhuber WL. 1990. A cervical primary afferent input to vestibular nuclei as demonstrated by retrograde transport of wheat germ agglutinin-horseradish peroxidase in the rat. *Exp Brain Res.* 79(2):405–411. <https://doi.org/10.1007/BF00608252>
- Barbour B. 1993. Synaptic currents evoked in purkinje cells by stimulating individual granule cells. *Neuron.* 11(4):759–769. [https://doi.org/10.1016/0896-6273\(93\)90085-6](https://doi.org/10.1016/0896-6273(93)90085-6)
- Barili P, Bronzetti E, Ricci A, Zaccheo D, Amenta F. 2000. Microanatomical localization of dopamine receptor protein immunoreactivity in the rat cerebellar cortex. *Brain Res.* 854(1–2):130–138. [https://doi.org/10.1016/S0006-8993\(99\)02306-9](https://doi.org/10.1016/S0006-8993(99)02306-9)
- Barmack NH. 2003. Central vestibular system: vestibular nuclei and posterior cerebellum. *Brain Res Bull.* 60(5–6):511–541. [https://doi.org/10.1016/S0361-9230\(03\)00055-8](https://doi.org/10.1016/S0361-9230(03)00055-8)
- Barmack NH, Baughman RW, Eckenstein FP. 1992. Cholinergic Innervation of the Cerebellum of the Rat by Secondary Vestibular Afferents. *Ann N Y Acad Sci.* 656(1 Sensing and C):566–579. <https://doi.org/10.1111/j.1749-6632.1992.tb25236.x>
- Barr DJ, Levy R, Scheepers C, Tily HJ. 2013. Random effects structure for confirmatory hypothesis testing: Keep it maximal. *J Mem Lang.* 68(3):255–278. <https://doi.org/10.1016/j.jml.2012.11.001>
- Bates D, Kliegl R, Vasishth S, Baayen H. 2015. Parsimonious mixed models.
- Baumann O, Mattingley JB. 2012. Functional topography of primary emotion processing in the human cerebellum. *NeuroImage.* 61(4):805–811. <https://doi.org/10.1016/j.neuroimage.2012.03.044>
- Bearzatto B, Servais L, Roussel C, Gall D, Baba-Aïssa F, Schurmans S, de Kerchove d'Exaerde A, Cheron G, Schiffmann SN. 2006. Targeted calretinin expression in granule cells of calretininnull mice restores normal cerebellar functions. *FASEB J.* 20(2):380–382. <https://doi.org/10.1096/fj.05-3785fje>
- Beckinghausen J, Sillitoe RV. 2019. Insights into cerebellar development and connectivity. *Neurosci Lett.* 688:2–13. <https://doi.org/10.1016/j.neulet.2018.05.013>
- Behesti H, Fore TR, Wu P, Horn Z, Leppert M, Hull C, Hatten ME. 2018. ASTN2 modulates synaptic strength by trafficking and degradation of surface proteins. *Proc Natl Acad Sci [Internet].* [accessed 2023 Mar 22] 115(41). <https://doi.org/10.1073/pnas.1809382115>
- Bell CC, Grimm RJ. 1969. Discharge properties of Purkinje cells recorded on single and double microelectrodes. *J Neurophysiol.* 32(6):1044–1055. <https://doi.org/10.1152/jn.1969.32.6.1044>
- Ben-Arie N, Bellen HJ, Armstrong DL, McCall AE, Gordadze PR, Guo Q, Matzuk MM, Zoghbi HY. 1997. Math1 is essential for genesis of cerebellar granule neurons. *Nature.* 390(6656):169–172. <https://doi.org/10.1038/36579>
- Bertheloot D, Latz E, Franklin BS. 2021. Necroptosis, pyroptosis and apoptosis: an intricate game of cell death. *Cell Mol Immunol.* 18(5):1106–1121. <https://doi.org/10.1038/s41423-020-00630-3>
- Bertulli L, Robert T. 2021. Embryological development of the human crano-facial arterial system: a pictorial review. *Surg Radiol Anat.* 43(6):961–973. <https://doi.org/10.1007/s00276-021-02684-y>
- Beuriat P-A, Cohen-Zimerman S, Smith GNL, Krueger F, Gordon B, Grafman J. 2020. A New Insight on the Role of the Cerebellum for Executive Functions and Emotion Processing in Adults. *Front Neurol.* 11:593490. <https://doi.org/10.3389/fneur.2020.593490>

- Beuriat P-A, Cristofori I, Gordon B, Grafman J. 2022. The shifting role of the cerebellum in executive, emotional and social processing across the lifespan. *Behav Brain Funct.* 18(1):6. <https://doi.org/10.1186/s12993-022-00193-5>
- Beylergil SB, Gupta P, ElKasaby M, Kilbane C, Shaikh AG. 2022. Does visuospatial motion perception correlate with coexisting movement disorders in Parkinson's disease? *J Neurol.* 269(4):2179–2192. <https://doi.org/10.1007/s00415-021-10804-2>
- Bhagat S, Biswas I, Ahmed R, Khan GA. 2020. Hypoxia induced up-regulation of tissue factor is mediated through extracellular RNA activated Toll-like receptor 3-activated protein 1 signalling. *Blood Cells Mol Dis.* 84:102459. <https://doi.org/10.1016/j.bcmd.2020.102459>
- Biran V, Heine VM, Verney C, Sheldon RA, Spadafora R, Vexler ZS, Rowitch DH, Ferriero DM. 2011. Cerebellar abnormalities following hypoxia alone compared to hypoxic-ischemic forebrain injury in the developing rat brain. *Neurobiol Dis.* 41(1):138–146. <https://doi.org/10.1016/j.nbd.2010.09.001>
- Biran V, Verney C, Ferriero DM. 2012. Perinatal Cerebellar Injury in Human and Animal Models. *Neurol Res Int.* 2012:1–9. <https://doi.org/10.1155/2012/858929>
- Birben E, Sahiner UM, Sackesen C, Erzurum S, Kalayci O. 2012. Oxidative Stress and Antioxidant Defense: *World Allergy Organ J.* 5(1):9–19. <https://doi.org/10.1097/WOX.0b013e3182439613>
- Bishop GA, Ho RH. 1985. The distribution and origin of serotonin immunoreactivity in the rat cerebellum. *Brain Res.* 331(2):195–207. [https://doi.org/10.1016/0006-8993\(85\)91545-8](https://doi.org/10.1016/0006-8993(85)91545-8)
- Blaess S. 2004. 1-Integrins Are Critical for Cerebellar Granule Cell Precursor Proliferation. *J Neurosci.* 24(13):3402–3412. <https://doi.org/10.1523/JNEUROSCI.5241-03.2004>
- Bloch-Salisbury E, Hall MH, Sharma P, Boyd T, Bednarek F, Paydarfar D. 2010. Heritability of Apnea of Prematurity: A Retrospective Twin Study. *Pediatrics.* 126(4):e779–e787. <https://doi.org/10.1542/peds.2010-0084>
- Bloedel JR. 1973. Cerebellar afferent systems: A review. *Prog Neurobiol.* 2:3–68. [https://doi.org/10.1016/0301-0082\(73\)90006-3](https://doi.org/10.1016/0301-0082(73)90006-3)
- Bloom FE, Hoffer BJ, Siggins GR. 1971. Studies on norepinephrine-containing afferents to Purkinje cells of rat cerebellum. I. Localization of the fibers and their synapses. *Brain Res.* 25(3):501–521. [https://doi.org/10.1016/0006-8993\(71\)90457-4](https://doi.org/10.1016/0006-8993(71)90457-4)
- Blunden SL, Beebe DW. 2006. The contribution of intermittent hypoxia, sleep debt and sleep disruption to daytime performance deficits in children: Consideration of respiratory and non-respiratory sleep disorders. *Sleep Med Rev.* 10(2):109–118. <https://doi.org/10.1016/j.smrv.2005.11.003>
- Bond KM, Brinjikji W, Eckel LJ, Kallmes DF, McDonald RJ, Carr CM. 2017. Dentate Update: Imaging Features of Entities That Affect the Dentate Nucleus. *Am J Neuroradiol.* 38(8):1467–1474. <https://doi.org/10.3174/ajnr.A5138>
- Boopathy GTK, Hong W. 2019. Role of Hippo Pathway-YAP/TAZ Signaling in Angiogenesis. *Front Cell Dev Biol.* 7:49. <https://doi.org/10.3389/fcell.2019.00049>
- Booth JR, Wood L, Lu D, Houk JC, Bitan T. 2007. The role of the basal ganglia and cerebellum in language processing. *Brain Res.* 1133:136–144. <https://doi.org/10.1016/j.brainres.2006.11.074>

REFERENCES

- Borghesani PR, Peyrin JM, Klein R, Rubin J, Carter AR, Schwartz PM, Luster A, Corfas G, Segal RA. 2002. BDNF stimulates migration of cerebellar granule cells. *Development.* 129(6):1435–1442. <https://doi.org/10.1242/dev.129.6.1435>
- Borst JW, Visser NV, Koupstova O, Visser AJWG. 2000. Oxidation of unsaturated phospholipids in membrane bilayer mixtures is accompanied by membrane fluidity changes. *Biochim Biophys Acta BBA - Mol Cell Biol Lipids.* 1487(1):61–73. [https://doi.org/10.1016/S1388-1981\(00\)00084-6](https://doi.org/10.1016/S1388-1981(00)00084-6)
- Bostan AC, Dum RP, Strick PL. 2018. Functional Anatomy of Basal Ganglia Circuits with the Cerebral Cortex and the Cerebellum. In: Niranjan A, Lunsford LD, Richardson RM, editors. *Prog Neurol Surg [Internet].* Vol. 33. [place unknown]: S. Karger AG; [accessed 2022 Nov 9]; p. 50–61. <https://doi.org/10.1159/000480748>
- Botez MI, Gravel J, Attig E, Vezina J-L. 1985. Reversible chronic cerebellar ataxia after phenytoin intoxication: Possible role of cerebellum in cognitive thought. *Neurology.* 35(8):1152–1152. <https://doi.org/10.1212/WNL.35.8.1152>
- Boukhtouche F, Doulazmi M, Frederic F, Dusart I, Brugg B, Mariani J. 2006. Rora, a pivotal nuclear receptor for Purkinje neuron survival and differentiation: From development to ageing. *The Cerebellum.* 5(2):97. <https://doi.org/10.1080/14734220600750184>
- Bourens M, Fontanesi F, Soto IC, Liu J, Barrientos A. 2013. Redox and Reactive Oxygen Species Regulation of Mitochondrial Cytochrome c Oxidase Biogenesis. *Antioxid Redox Signal.* 19(16):1940–1952. <https://doi.org/10.1089/ars.2012.4847>
- Bouslama-Oueghlani L, Wehrlé R, Doulazmi M, Chen XR, Jaudon F, Lemaigre-Dubreuil Y, Rivals I, Sotelo C, Dusart I. 2012. Purkinje Cell Maturation Participates in the Control of Oligodendrocyte Differentiation: Role of Sonic Hedgehog and Vitronectin.Tang Y-P, editor. *PLoS ONE.* 7(11):e49015. <https://doi.org/10.1371/journal.pone.0049015>
- Brattström P, Russo C, Ley D, Bruschettini M. 2019. High-versus low-dose caffeine in preterm infants: a systematic review and meta-analysis. *Acta Paediatr.* 108(3):401–410. <https://doi.org/10.1111/apa.14586>
- Brauer M, Curtin JJ. 2018. Linear mixed-effects models and the analysis of nonindependent data: A unified framework to analyze categorical and continuous independent variables that vary within-subjects and/or within-items. *Psychol Methods.* 23(3):389–411. <https://doi.org/10.1037/met0000159>
- Braun N, Debener S, Spychala N, Bongartz E, Sörös P, Müller HHO, Philipsen A. 2018. The Senses of Agency and Ownership: A Review. *Front Psychol.* 9:535. <https://doi.org/10.3389/fpsyg.2018.00535>
- Breska A, Ivry RB. 2021. The human cerebellum is essential for modulating perceptual sensitivity based on temporal expectations. *eLife.* 10:e66743. <https://doi.org/10.7554/eLife.66743>
- Briatore F, Patrizi A, Viltno L, Sassoè-Pognetto M, Wulff P. 2010. Quantitative Organization of GABAergic Synapses in the Molecular Layer of the Mouse Cerebellar Cortex.Tell F, editor. *PLoS ONE.* 5(8):e12119. <https://doi.org/10.1371/journal.pone.0012119>
- Brissenden JA, Tobyne SM, Halko MA, Somers DC. 2021. Stimulus-Specific Visual Working Memory Representations in Human Cerebellar Lobule VIIb/VIIla. *J Neurosci.* 41(5):1033–1045. <https://doi.org/10.1523/JNEUROSCI.1253-20.2020>

- Brochu G, Maler L, Hawkes R. 1990. Zebrin II: A polypeptide antigen expressed selectively by purkinje cells reveals compartments in rat and fish cerebellum. *J Comp Neurol.* 291(4):538–552. <https://doi.org/10.1002/cne.902910405>
- Brodal A. 1981. Neurological anatomy in relation to clinical medicine. 3d ed. New York: Oxford University Press.
- Brooks M E, Kristensen K, Bentham K J ,van, Magnusson A, Berg C W, Nielsen A, Skaug H J, Mächler M, Bolker B M. 2017. glmmTMB Balances Speed and Flexibility Among Packages for Zero-inflated Generalized Linear Mixed Modeling. *R J.* 9(2):378. <https://doi.org/10.32614/RJ-2017-066>
- Broussard DM, Titley HK, Antflick J, Hampson DR. 2011. Motor learning in the VOR: the cerebellar component. *Exp Brain Res.* 210(3–4):451–463. <https://doi.org/10.1007/s00221-011-2589-z>
- Buffo A, Rossi F. 2013. Origin, lineage and function of cerebellar glia. *Prog Neurobiol.* 109:42–63. <https://doi.org/10.1016/j.pneurobio.2013.08.001>
- Bureau I, Dieudonné S, Coussen F, Mulle C. 2000. Kainate receptor-mediated synaptic currents in cerebellar Golgi cells are not shaped by diffusion of glutamate. *Proc Natl Acad Sci.* 97(12):6838–6843. <https://doi.org/10.1073/pnas.97.12.6838>
- Bustin SA, Benes V, Garson JA, Hellemans J, Huggett J, Kubista M, Mueller R, Nolan T, Pfaffl MW, Shipley GL, et al. 2009. The MIQE Guidelines: Minimum Information for Publication of Quantitative Real-Time PCR Experiments. *Clin Chem.* 55(4):611–622. <https://doi.org/10.1373/clinchem.2008.112797>
- Cadilhac C, Bachy I, Forget A, Hodson DJ, Jahannault-Talignani C, Furley AJ, Ayrault O, Mollard P, Sotelo C, Ango F. 2021. Excitatory granule neuron precursors orchestrate laminar localization and differentiation of cerebellar inhibitory interneuron subtypes. *Cell Rep.* 34(13):108904. <https://doi.org/10.1016/j.celrep.2021.108904>
- Cai J, Tuong CM, Gozal D. 2011. A neonatal mouse model of intermittent hypoxia associated with features of apnea in premature infants. *Respir Physiol Neurobiol.* 178(2):210–217. <https://doi.org/10.1016/j.resp.2011.06.003>
- Cai J, Tuong CM, Zhang Y, Shields CB, Guo G, Fu H, Gozal D. 2012. Mouse intermittent hypoxia mimicking apnoea of prematurity: effects on myelinogenesis and axonal maturation. *J Pathol.* 226(3):495–508. <https://doi.org/10.1002/path.2980>
- Cai X-H, Li X-C, Jin S-W, Liang D-S, Wen Z-W, Cao H-C, Mei H-F, Wu Y, Lin Z-D, Wang L-X. 2014. Endoplasmic reticulum stress plays critical role in brain damage after chronic intermittent hypoxia in growing rats. *Exp Neurol.* 257:148–156. <https://doi.org/10.1016/j.expneurol.2014.04.029>
- Calzolari S, Terriente J, Pujades C. 2014. Cell segregation in the vertebrate hindbrain relies on actomyosin cables located at the interhombomeric boundaries. *EMBO J.* 33(7):686–701. <https://doi.org/10.1002/embj.201386003>
- Cameron DB, Kasai K, Jiang Y, Hu T, Saeki Y, Komuro H. 2009. Four distinct phases of basket/stellate cell migration after entering their final destination (the molecular layer) in the developing cerebellum. *Dev Biol.* 332(2):309–324. <https://doi.org/10.1016/j.ydbio.2009.05.575>

REFERENCES

- Campanille V, Saraceno GE, Rivière S, Logica T, Kölliker R, Capani F, Castilla R. 2015. Long lasting cerebellar alterations after perinatal asphyxia in rats. *Brain Res Bull.* 116:57–66. <https://doi.org/10.1016/j.brainresbull.2015.06.003>
- Carmeliet P, Tessier-Lavigne M. 2005. Common mechanisms of nerve and blood vessel wiring. *Nature.* 436(7048):193–200. <https://doi.org/10.1038/nature03875>
- Carpenter MB. 1991. Core text of neuroanatomy. 4th ed. Baltimore: Williams & Wilkins.
- Carter RA, Bihannic L, Rosencrance C, Hadley JL, Tong Y, Phoenix TN, Natarajan S, Easton J, Northcott PA, Gawad C. 2018. A Single-Cell Transcriptional Atlas of the Developing Murine Cerebellum. *Curr Biol.* 28(18):2910-2920.e2. <https://doi.org/10.1016/j.cub.2018.07.062>
- Casini L, Ivry RB. 1999. Effects of divided attention on temporal processing in patients with lesions of the cerebellum or frontal lobe. *Neuropsychology.* 13(1):10–21. <https://doi.org/10.1037/0894-4105.13.1.10>
- Cerminara NL, Lang EJ, Sillitoe RV, Apps R. 2015. Redefining the cerebellar cortex as an assembly of non-uniform Purkinje cell microcircuits. *Nat Rev Neurosci.* 16(2):79–93. <https://doi.org/10.1038/nrn3886>
- Chang J-C, Hu W-F, Lee W-S, Lin J-H, Ting P-C, Chang H-R, Shieh K-R, Chen T-I, Yang K-T. 2019. Intermittent Hypoxia Induces Autophagy to Protect Cardiomyocytes From Endoplasmic Reticulum Stress and Apoptosis. *Front Physiol.* 10:995. <https://doi.org/10.3389/fphys.2019.00995>
- Chaudhry FA, Lehre KP, Lookeren Campagne M van, Ottersen OP, Danbolt NC, Storm-Mathisen J. 1995. Glutamate transporters in glial plasma membranes: Highly differentiated localizations revealed by quantitative ultrastructural immunocytochemistry. *Neuron.* 15(3):711–720. [https://doi.org/10.1016/0896-6273\(95\)90158-2](https://doi.org/10.1016/0896-6273(95)90158-2)
- Chaumont J, Guyon N, Valera AM, Dugué GP, Popa D, Marcaggi P, Gautheron V, Reibel-Foisset S, Dieudonné S, Stephan A, et al. 2013. Clusters of cerebellar Purkinje cells control their afferent climbing fiber discharge. *Proc Natl Acad Sci.* 110(40):16223–16228. <https://doi.org/10.1073/pnas.1302310110>
- Chavez-Valdez R, Martin LJ, Northington FJ. 2012. Programmed Necrosis: A Prominent Mechanism of Cell Death following Neonatal Brain Injury. *Neurol Res Int.* 2012:1–12. <https://doi.org/10.1155/2012/257563>
- Chedotal A, Sotelo C. 1993. The ‘creep’ stage’ in cerebellar climbing fiber synaptogenesis precedes the ‘pericellular nest’ - ultrastructural evidence with parvalbumin immunocytochemistry. *Dev Brain Res.* 76(2):207–220. [https://doi.org/10.1016/0165-3806\(93\)90209-S](https://doi.org/10.1016/0165-3806(93)90209-S)
- Chen C-Y, Seward CH, Song Y, Inamdar M, Leddy AM, Zhang H, Yoo J, Kao W-C, Pawlowski H, Stubbs LJ. 2022. Galnt17 loss-of-function leads to developmental delay and abnormal coordination, activity, and social interactions with cerebellar vermis pathology. *Dev Biol.* 490:155–171. <https://doi.org/10.1016/j.ydbio.2022.08.002>
- Cheng Y, Sudarov A, Szulc KU, Sgaier SK, Stephen D, Turnbull DH, Joyner AL. 2010. The Engrailed homeobox genes determine the different foliation patterns in the vermis and hemispheres of the mammalian cerebellum. *Development.* 137(3):519–529. <https://doi.org/10.1242/dev.027045>
- Cheron G, Márquez-Ruiz J, Dan B. 2016. Oscillations, Timing, Plasticity, and Learning in the Cerebellum. *The Cerebellum.* 15(2):122–138. <https://doi.org/10.1007/s12311-015-0665-9>

- Chin LS, Li L, Ferreira A, Kosik KS, Greengard P. 1995. Impairment of axonal development and of synaptogenesis in hippocampal neurons of synapsin I-deficient mice. *Proc Natl Acad Sci.* 92(20):9230–9234. <https://doi.org/10.1073/pnas.92.20.9230>
- Chiu S-C, Huang S-Y, Tsai Y-C, Chen S-P, Pang C-Y, Lien C-F, Lin Y-J, Yang K-T. 2012. Poly (ADP-ribose) polymerase plays an important role in intermittent hypoxia-induced cell death in rat cerebellar granule cells. *J Biomed Sci.* 19(1):29. <https://doi.org/10.1186/1423-0127-19-29>
- Chizhikov VV, Millen KJ. 2004. Mechanisms of roof plate formation in the vertebrate CNS. *Nat Rev Neurosci.* 5(10):808–812. <https://doi.org/10.1038/nrn1520>
- Ciani E, Virgili M, Contestabile A. 2002. Akt pathway mediates a cGMP-dependent survival role of nitric oxide in cerebellar granule neurones: Akt role in nitric oxide-mediated survival. *J Neurochem.* 81(2):218–228. <https://doi.org/10.1046/j.1471-4159.2002.00857.x>
- Clark SV, Semmel ES, Aleksonis HA, Steinberg SN, King TZ. 2021. Cerebellar-Subcortical-Cortical Systems as Modulators of Cognitive Functions. *Neuropsychol Rev.* 31(3):422–446. <https://doi.org/10.1007/s11065-020-09465-1>
- Clausi S, Siciliano L, Olivito G, Leggio M. 2022. Cerebellum and Emotion in Social Behavior. In: Adamaszek M, Manto M, Schutter DJLG, editors. *Emot Cerebellum [Internet]*. Vol. 1378. Cham: Springer International Publishing; [accessed 2022 Nov 9]; p. 235–253. https://doi.org/10.1007/978-3-030-99550-8_15
- Cohen G, Katz-Salamon M. 2005. Development of chemoreceptor responses in infants. *Respir Physiol Neurobiol.* 149(1–3):233–242. <https://doi.org/10.1016/j.resp.2005.02.013>
- Connolly DJA, Widjaja E, Griffiths PD. 2007. Involvement of the anterior lobe of the cerebellar vermis in perinatal profound hypoxia. *AJNR Am J Neuroradiol.* 28(1):16–19.
- Crepel F, Mariani J, Delhaye-Bouchaud N. 1976. Evidence for a multiple innervation of purkinje cells by climbing fibers in the immature rat cerebellum. *J Neurobiol.* 7(6):567–578. <https://doi.org/10.1002/neu.480070609>
- Crivellato E, Damiani D, Travani L, Marcon G, Fusaroli PF, Mallardi F. 1992. Serotonergic fibres form dense synaptic contacts with Purkinje cells in the mouse cerebellar cortex — An immunohistochemical study. *Acta Histochem.* 92(1):54–60. [https://doi.org/10.1016/S0065-1281\(11\)80141-8](https://doi.org/10.1016/S0065-1281(11)80141-8)
- Culver C, Sundqvist A, Mudie S, Melvin A, Xirodimas D, Rocha S. 2010. Mechanism of Hypoxia-Induced NF-κB. *Mol Cell Biol.* 30(20):4901–4921. <https://doi.org/10.1128/MCB.00409-10>
- Curristin SM, Cao A, Stewart WB, Zhang H, Madri JA, Morrow JS, Ment LR. 2002. Disrupted synaptic development in the hypoxic newborn brain. *Proc Natl Acad Sci.* 99(24):15729–15734. <https://doi.org/10.1073/pnas.232568799>
- Cutando L, Puighermanal E, Castell L, Tarot P, Belle M, Bertaso F, Arango-Lievano M, Ango F, Rubinstein M, Quintana A, et al. 2022. Cerebellar dopamine D2 receptors regulate social behaviors. *Nat Neurosci.* 25(7):900–911. <https://doi.org/10.1038/s41593-022-01092-8>
- Dallas M, Boycott HE, Atkinson L, Miller A, Boyle JP, Pearson HA, Peers C. 2007. Hypoxia Suppresses Glutamate Transport in Astrocytes. *J Neurosci.* 27(15):3946–3955. <https://doi.org/10.1523/JNEUROSCI.5030-06.2007>

REFERENCES

- Darnall RA, Chen X, Nemanic KV, Sirieix CM, Gimi B, Knoblauch S, McEntire BL, Hunt CE. 2017. Early postnatal exposure to intermittent hypoxia in rodents is proinflammatory, impairs white matter integrity, and alters brain metabolism. *Pediatr Res.* 82(1):164–172. <https://doi.org/10.1038/pr.2017.102>
- Davie JT, Clark BA, Haussler M. 2008. The Origin of the Complex Spike in Cerebellar Purkinje Cells. *J Neurosci.* 28(30):7599–7609. <https://doi.org/10.1523/JNEUROSCI.0559-08.2008>
- Davis PG, Schmidt B, Roberts RS, Doyle LW, Asztalos E, Haslam R, Sinha S, Tin W. 2010. Caffeine for Apnea of Prematurity Trial: Benefits May Vary in Subgroups. *J Pediatr.* 156(3):382-387.e3. <https://doi.org/10.1016/j.jpeds.2009.09.069>
- De Luca A, Parmigiani E, Tosatto G, Martire S, Hoshino M, Buffo A, Leto K, Rossi F. 2015. Exogenous Sonic Hedgehog Modulates the Pool of GABAergic Interneurons During Cerebellar Development. *The Cerebellum.* 14(2):72–85. <https://doi.org/10.1007/s12311-014-0596-x>
- De Zeeuw CI, Romano V. 2022. Time and tide of cerebellar synchrony. *Proc Natl Acad Sci.* 119(17):e2204155119. <https://doi.org/10.1073/pnas.2204155119>
- Decker MJ, Hue GE, Caudle WM, Miller GW, Keating GL, Rye DB. 2003. Episodic neonatal hypoxia evokes executive dysfunction and regionally specific alterations in markers of dopamine signaling. *Neuroscience.* 117(2):417–425. [https://doi.org/10.1016/S0306-4522\(02\)00805-9](https://doi.org/10.1016/S0306-4522(02)00805-9)
- Delion M, Dinomais M, Mercier P. 2017. Arteries and Veins of the Cerebellum. *The Cerebellum.* 16(5–6):880–912. <https://doi.org/10.1007/s12311-016-0828-3>
- Desclin JC. 1974. Histological evidence supporting the inferior olive as the major source of cerebellar climbing fibers in the rat. *Brain Res.* 77(3):365–384. [https://doi.org/10.1016/0006-8993\(74\)90628-3](https://doi.org/10.1016/0006-8993(74)90628-3)
- Descloux C, Ginet V, Clarke PGH, Puyal J, Truttmann AC. 2015. Neuronal death after perinatal cerebral hypoxia-ischemia: Focus on autophagy-mediated cell death. *Int J Dev Neurosci.* 45:75–85. <https://doi.org/10.1016/j.ijdevneu.2015.06.008>
- Dey MR, Reddy K, Yoshida H, Nishiyama N, Zemelman BV, Nishiyama H. 2022. Granule Cells Constitute One of the Major Neuronal Subtypes in the Molecular Layer of the Posterior Cerebellum. *eneuro.* 9(3):ENEURO.0289-21.2022. <https://doi.org/10.1523/ENEURO.0289-21.2022>
- Di Fiore JM, Martin RJ, Gaudia EB. 2013. Apnea of prematurity – Perfect storm. *Respir Physiol Neurobiol.* 189(2):213–222. <https://doi.org/10.1016/j.resp.2013.05.026>
- Diamond A. 2013. Executive Functions. *Annu Rev Psychol.* 64(1):135–168. <https://doi.org/10.1146/annurev-psych-113011-143750>
- DiGregorio DA, Nusser Z, Silver RA. 2002. Spillover of Glutamate onto Synaptic AMPA Receptors Enhances Fast Transmission at a Cerebellar Synapse. *Neuron.* 35(3):521–533. [https://doi.org/10.1016/S0896-6273\(02\)00787-0](https://doi.org/10.1016/S0896-6273(02)00787-0)
- Dobson NR, Hunt CE. 2018. Caffeine: an evidence-based success story in VLBW pharmacotherapy. *Pediatr Res.* 84(3):333–340. <https://doi.org/10.1038/s41390-018-0089-6>
- Dorgans K, Demais V, Bailly Y, Poulain B, Isopé P, Doussau F. 2019. Short-term plasticity at cerebellar granule cell to molecular layer interneuron synapses expands information processing. *eLife.* 8:e41586. <https://doi.org/10.7554/eLife.41586>

- Doyle LW, Ranganathan S, Cheong JLY. 2017. Neonatal Caffeine Treatment and Respiratory Function at 11 Years in Children under 1,251 g at Birth. *Am J Respir Crit Care Med.* 196(10):1318–1324. <https://doi.org/10.1164/rccm.201704-0767OC>
- Duan K, Chen J, Calhoun VD, Jiang W, Rootes-Murdy K, Schoenmacker G, Silva RF, Franke B, Buitelaar JK, Hoogman M, et al. 2023. Genomic patterns linked to gray matter alterations underlying working memory deficits in adults and adolescents with attention-deficit/hyperactivity disorder. *Transl Psychiatry.* 13(1):50. <https://doi.org/10.1038/s41398-023-02349-x>
- Duarte JMN, Cunha RA, Carvalho RA. 2016. Adenosine A₁ receptors control the metabolic recovery after hypoxia in rat hippocampal slices. *J Neurochem.* 136(5):947–957. <https://doi.org/10.1111/jnc.13512>
- Duchamp-Viret P, Nguyen HK, Maucort-Boulch D, Remontet L, Guyon A, Franco P, Cividjian A, Thevenet M, Iwaz J, Galletti S, et al. 2021. Protocol of controlled odorant stimulation for reducing apnoeic episodes in premature newborns: a randomised open-label Latin-square study with independent evaluation of the main endpoint (PREMODEUR). *BMJ Open.* 11(9):e047141. <https://doi.org/10.1136/bmjopen-2020-047141>
- Dudek H, Datta SR, Franke TF, Birnbaum MJ, Yao R, Cooper GM, Segal RA, Kaplan DR, Greenberg ME. 1997. Regulation of Neuronal Survival by the Serine-Threonine Protein Kinase Akt. *Science.* 275(5300):661–665. <https://doi.org/10.1126/science.275.5300.661>
- Dugué GP, Brunel N, Hakim V, Schwartz E, Chat M, Lévesque M, Courtemanche R, Léna C, Dieudonné S. 2009. Electrical Coupling Mediates Tunable Low-Frequency Oscillations and Resonance in the Cerebellar Golgi Cell Network. *Neuron.* 61(1):126–139. <https://doi.org/10.1016/j.neuron.2008.11.028>
- Dunn LL, Midwinter RG, Ni J, Hamid HA, Parish CR, Stocker R. 2014. New Insights into Intracellular Locations and Functions of Heme Oxygenase-1. *Antioxid Redox Signal.* 20(11):1723–1742. <https://doi.org/10.1089/ars.2013.5675>
- Dunwoodie SL. 2009. The Role of Hypoxia in Development of the Mammalian Embryo. *Dev Cell.* 17(6):755–773. <https://doi.org/10.1016/j.devcel.2009.11.008>
- Dutta C, Day T, Kopp N, van Bodegom D, Davids MS, Ryan J, Bird L, Kommajosyula N, Weigert O, Yoda A, et al. 2012. BCL2 Suppresses PARP1 Function and Nonapoptotic Cell Death. *Cancer Res.* 72(16):4193–4203. <https://doi.org/10.1158/0008-5472.CAN-11-4204>
- Eccles JC, Llinás R, Sasaki K. 1966. The excitatory synaptic action of climbing fibres on the Purkinje cells of the cerebellum. *J Physiol.* 182(2):268–296. <https://doi.org/10.1113/jphysiol.1966.sp007824>
- Egan MF, Straub RE, Goldberg TE, Yakub I, Callicott JH, Hariri AR, Mattay VS, Bertolino A, Hyde TM, Shannon-Weickert C, et al. 2004. Variation in GRM3 affects cognition, prefrontal glutamate, and risk for schizophrenia. *Proc Natl Acad Sci.* 101(34):12604–12609. <https://doi.org/10.1073/pnas.0405077101>
- Eichenwald EC, COMMITTEE ON FETUS AND NEWBORN, Watterberg KL, Aucott S, Benitz WE, Cummings JJ, Goldsmith J, Poindexter BB, Puopolo K, Stewart DL, Wang KS. 2016. Apnea of Prematurity. *Pediatrics.* 137(1):e20153757. <https://doi.org/10.1542/peds.2015-3757>
- Eichmann A, Makinen T, Alitalo K. 2005. Neural guidance molecules regulate vascular remodeling and vessel navigation. *Genes Dev.* 19(9):1013–1021. <https://doi.org/10.1101/gad.1305405>

REFERENCES

- Ekerot CF, Larson B. 1972. Differential termination of the exteroceptive and proprioceptive components of the cuneocerebellar tract. *Brain Res.* 36(2):420–424. [https://doi.org/10.1016/0006-8993\(72\)90748-2](https://doi.org/10.1016/0006-8993(72)90748-2)
- Elmore S. 2007. Apoptosis: A Review of Programmed Cell Death. *Toxicol Pathol.* 35(4):495–516. <https://doi.org/10.1080/01926230701320337>
- Englund C. 2006. Unipolar Brush Cells of the Cerebellum Are Produced in the Rhombic Lip and Migrate through Developing White Matter. *J Neurosci.* 26(36):9184–9195. <https://doi.org/10.1523/JNEUROSCI.1610-06.2006>
- van Es DM, van der Zwaag W, Knapen T. 2019. Topographic Maps of Visual Space in the Human Cerebellum. *Curr Biol.* 29(10):1689–1694.e3. <https://doi.org/10.1016/j.cub.2019.04.012>
- Fajersztajn L, Veras MM. 2017. Hypoxia: From Placental Development to Fetal Programming: Influence of Hypoxia on Development. *Birth Defects Res.* 109(17):1377–1385. <https://doi.org/10.1002/bdr2.1142>
- Falcon MI, Gomez CM, Chen EE, Shereen A, Solodkin A. 2016. Early Cerebellar Network Shifting in Spinocerebellar Ataxia Type 6. *Cereb Cortex.* 26(7):3205–3218. <https://doi.org/10.1093/cercor/bhv154>
- Fang C, Gu L, Smerin D, Mao S, Xiong X. 2017. The Interrelation between Reactive Oxygen Species and Autophagy in Neurological Disorders. *Oxid Med Cell Longev.* 2017:1–16. <https://doi.org/10.1155/2017/8495160>
- Farahani R, Kanaan A, Gavrialov O, Brunnert S, Douglas RM, Morcillo P, Haddad GG. 2008. Differential effects of chronic intermittent and chronic constant hypoxia on postnatal growth and development. *Pediatr Pulmonol.* 43(1):20–28. <https://doi.org/10.1002/ppul.20729>
- Ferriero DM. 2001. Oxidant Mechanisms in Neonatal Hypoxia-Ischemia. *Dev Neurosci.* 23(3):198–202. <https://doi.org/10.1159/000046143>
- Fink AJ. 2006. Development of the Deep Cerebellar Nuclei: Transcription Factors and Cell Migration from the Rhombic Lip. *J Neurosci.* 26(11):3066–3076. <https://doi.org/10.1523/JNEUROSCI.5203-05.2006>
- Forsythe JA, Jiang B-H, Iyer NV, Agani F, Leung SW, Koos RD, Semenza GL. 1996. Activation of Vascular Endothelial Growth Factor Gene Transcription by Hypoxia-Inducible Factor 1. *Mol Cell Biol.* 16(9):4604–4613. <https://doi.org/10.1128/MCB.16.9.4604>
- Frick A, Grammel D, Schmidt F, Pöschl J, Priller M, Pagella P, von Bueren AO, Peraud A, Tonn J-C, Herms J, et al. 2012. Proper cerebellar development requires expression of $\beta 1$ -integrin in Bergmann glia, but not in granule neurons. *Glia.* 60(5):820–832. <https://doi.org/10.1002/glia.22314>
- Fricker M, Tolokovsky AM, Borutaite V, Coleman M, Brown GC. 2018. Neuronal Cell Death. *Physiol Rev.* 98(2):813–880. <https://doi.org/10.1152/physrev.00011.2017>
- Fujishima K, Kurisu J, Yamada M, Kengaku M. 2020. β III spectrin controls the planarity of Purkinje cell dendrites by modulating perpendicular axon-dendrite interactions. *Development.* 147(24):dev194530. <https://doi.org/10.1242/dev.194530>

- Furukawa Y, Torres AS, O'Halloran TV. 2004. Oxygen-induced maturation of SOD1: a key role for disulfide formation by the copper chaperone CCS. *EMBO J.* 23(14):2872–2881. <https://doi.org/10.1038/sj.emboj.7600276>
- Galliano E, Baratella M, Sgritta M, Ruigrok TJH, Haasdijk ED, Hoebeek FE, D'Angelo E, Jaarsma D, De Zeeuw CI. 2013. Anatomical investigation of potential contacts between climbing fibers and cerebellar Golgi cells in the mouse. *Front Neural Circuits* [Internet]. [accessed 2022 Dec 4] 7. <https://doi.org/10.3389/fncir.2013.00059>
- Gallimore AR, Kim T, Tanaka-Yamamoto K, De Schutter E. 2018. Switching On Depression and Potentiation in the Cerebellum. *Cell Rep.* 22(3):722–733. <https://doi.org/10.1016/j.celrep.2017.12.084>
- Gallo V, Ciotti MT, Coletti A, Aloisi F, Levi G. 1982. Selective release of glutamate from cerebellar granule cells differentiating in culture. *Proc Natl Acad Sci.* 79(24):7919–7923. <https://doi.org/10.1073/pnas.79.24.7919>
- Garcia AJ, Zanella S, Dashevskiy T, Khan SA, Khuu MA, Prabhakar NR, Ramirez J-M. 2016. Chronic Intermittent Hypoxia Alters Local Respiratory Circuit Function at the Level of the preBötziinger Complex. *Front Neurosci* [Internet]. [accessed 2019 Sep 11] 10. <https://doi.org/10.3389/fnins.2016.00004>
- Gauda EB, Martin RJ. 2012. Control of Breathing. In: Avery's Dis Newborn [Internet]. [place unknown]: Elsevier; [accessed 2023 Feb 21]; p. 584–597. <https://doi.org/10.1016/B978-1-4377-0134-0.10043-5>
- Gauda EB, McLemore GL, Tolosa J, Marston-Nelson J, Kwak D. 2004. Maturation of peripheral arterial chemoreceptors in relation to neonatal apnoea. *Semin Neonatol.* 9(3):181–194. <https://doi.org/10.1016/j.siny.2003.11.002>
- Giampietro C, Luzzati F, Gambarotta G, Giacobini P, Boda E, Fasolo A, Perroteau I. 2005. Stathmin Expression Modulates Migratory Properties of GN-11 Neurons in Vitro. *Endocrinology.* 146(4):1825–1834. <https://doi.org/10.1210/en.2004-0972>
- Gillot I, Gouyon JB, Guignard JP. 1990. Renal Effects of Caffeine in Preterm Infants. *Neonatology.* 58(3):133–136. <https://doi.org/10.1159/000243252>
- Giolli RA, Torigoe Y, Blanks RHI, Mark McDonald H. 1988. Projections of the dorsal and lateral terminal accessory optic nuclei and of the interstitial nucleus of the superior fasciculus (posterior fibers) in the rabbit and rat. *J Comp Neurol.* 277(4):608–620. <https://doi.org/10.1002/cne.902770412>
- Giompres P, Delis F. 2005. Dopamine transporters in the cerebellum of mutant mice. *The Cerebellum.* 4(2):105–111. <https://doi.org/10.1080/14734220510007851>
- Giszas V, Strauß E, Bührer C, Endesfelder S. 2022. The Conflicting Role of Caffeine Supplementation on Hyperoxia-Induced Injury on the Cerebellar Granular Cell Neurogenesis of Newborn Rats. Ciobica A, editor. *Oxid Med Cell Longev.* 2022:1–21. <https://doi.org/10.1155/2022/5769784>
- Gizzi C, Montecchia F, Panetta V, Castellano C, Mariani C, Campelli M, Papoff P, Moretti C, Agostino R. 2015. Is synchronised NIPPV more effective than NIPPV and NCPAP in treating apnoea of prematurity (AOP)? A randomised cross-over trial. *Arch Dis Child - Fetal Neonatal Ed.* 100(1):F17–F23. <https://doi.org/10.1136/archdischild-2013-305892>

REFERENCES

- Glasgow JN, Qiu J, Rassin D, Grafe M, Wood T, Perez-Polo JR. 2001. Transcriptional Regulation of the BCL-X Gene by NF- κ B Is an Element of Hypoxic Responses in the Rat Brain. *Neurochem Res.* 26(6):647–659. <https://doi.org/10.1023/A:1010987220034>
- Glickstein M, Strata P, Voogd J. 2009. Cerebellum: history. *Neuroscience.* 162(3):549–559. <https://doi.org/10.1016/j.neuroscience.2009.02.054>
- Gooch CM, Wiener M, Wencel EB, Coslett HB. 2010. Interval timing disruptions in subjects with cerebellar lesions. *Neuropsychologia.* 48(4):1022–1031. <https://doi.org/10.1016/j.neuropsychologia.2009.11.028>
- Gottwald B. 2004. Evidence for distinct cognitive deficits after focal cerebellar lesions. *J Neurol Neurosurg Psychiatry.* 75(11):1524–1531. <https://doi.org/10.1136/jnnp.2003.018093>
- Goussakov I, Synowiec S, Yarnykh V, Drobyshevsky A. 2019. Immediate and delayed decrease of long term potentiation and memory deficits after neonatal intermittent hypoxia. *Int J Dev Neurosci.* 74:27–37. <https://doi.org/10.1016/j.ijdevneu.2019.03.001>
- Gozal D, Gozal E, Simakajornboon N. 2000. Signaling pathways of the acute hypoxic ventilatory response in the nucleus tractus solitarius. *Respir Physiol.* 121(2–3):209–221. [https://doi.org/10.1016/S0034-5687\(00\)00129-8](https://doi.org/10.1016/S0034-5687(00)00129-8)
- Grangeray-Vilmint A, Valera AM, Kumar A, Isope P. 2018. Short-Term Plasticity Combines with Excitation–Inhibition Balance to Expand Cerebellar Purkinje Cell Dynamic Range. *J Neurosci.* 38(22):5153–5167. <https://doi.org/10.1523/JNEUROSCI.3270-17.2018>
- Grant DA, McFarling C, Gormezano I. 1960. Temporal Conditioning and the Effect of Interpolated UCS Presentations in Eyelid Conditioning. *J Gen Psychol.* 63(2):249–257. <https://doi.org/10.1080/00221309.1960.9711822>
- Green DR, Llambi F. 2015. Cell Death Signaling. *Cold Spring Harb Perspect Biol.* 7(12):a006080. <https://doi.org/10.1101/cshperspect.a006080>
- Grosche J, Kettenmann H, Reichenbach A. 2002. Bergmann glial cells form distinct morphological structures to interact with cerebellar neurons. *J Neurosci Res.* 68(2):138–149. <https://doi.org/10.1002/jnr.10197>
- Grow WA. 2018. Development of the Nervous System. In: Fundam Neurosci Basic Clin Appl [Internet]. [place unknown]: Elsevier; [accessed 2023 Apr 7]; p. 72-90.e1. <https://doi.org/10.1016/B978-0-323-39632-5.00005-0>
- Gruner HN, Kim M, Mastick GS. 2019. Robo1 and 2 Repellent Receptors Cooperate to Guide Facial Neuron Cell Migration and Axon Projections in the Embryonic Mouse Hindbrain. *Neuroscience.* 402:116–129. <https://doi.org/10.1016/j.neuroscience.2019.01.017>
- Guan J, Luo Y, Denker BM. 2005. Purkinje cell protein-2 (Pcp2) stimulates differentiation in PC12 cells by G β γ -mediated activation of Ras and p38 MAPK. *Biochem J.* 392(2):389–397. <https://doi.org/10.1042/BJ20042102>
- Guan Y, Liu J, Gu Y, Ji X. 2022. Effects of Hypoxia on Cerebral Microvascular Angiogenesis: Benefits or Damages? *Aging Dis.*:0. <https://doi.org/10.14336/AD.2022.0902>

- Guell X, Hoche F, Schmahmann JD. 2015. Metalinguistic Deficits in Patients with Cerebellar Dysfunction: Empirical Support for the Dysmetria of Thought Theory. *The Cerebellum*. 14(1):50–58. <https://doi.org/10.1007/s12311-014-0630-z>
- Guo C, Qiu H-Y, Huang Y, Chen H, Yang R-Q, Chen S-D, Johnson RL, Chen Z-F, Ding Y-Q. 2007. *Lmx1b* is essential for *Fgf8* and *Wnt1* expression in the isthmic organizer during tectum and cerebellum development in mice. *Development*. 134(2):317–325. <https://doi.org/10.1242/dev.02745>
- Guo H-L, Long J-Y, Hu Y-H, Liu Y, He X, Li L, Xia Y, Ding X-S, Chen F, Xu J, Cheng R. 2022. Caffeine Therapy for Apnea of Prematurity: Role of the Circadian CLOCK Gene Polymorphism. *Front Pharmacol*. 12:724145. <https://doi.org/10.3389/fphar.2021.724145>
- Guo M, Chen H, Duan W, Li Z, Li Y, Ma Y, Xu X, Yi L, Bi Y, Liu Y, et al. 2020. FGF9 knockout in GABAergic neurons induces apoptosis and inflammation via the Fas/caspase-3 pathway in the cerebellum of mice. *Brain Res Bull*. 154:91–101. <https://doi.org/10.1016/j.brainresbull.2019.10.012>
- Guo Q, Li K, Sunmonu NA, Li JYH. 2010. *Fgf8b*-containing spliceforms, but not *Fgf8a*, are essential for *Fgf8* function during development of the midbrain and cerebellum. *Dev Biol*. 338(2):183–192. <https://doi.org/10.1016/j.ydbio.2009.11.034>
- Gusarov GA, Trejo HE, Dada LA, Briva A, Welch LC, Hamanaka RB, Mutlu GM, Chandel NS, Prakriya M, Sznajder JI. 2011. Hypoxia Leads to Na,K-ATPase Downregulation via Ca²⁺ Release-Activated Ca²⁺ Channels and AMPK Activation. *Mol Cell Biol*. 31(17):3546–3556. <https://doi.org/10.1128/MCB.05114-11>
- Hall JE. 2020. Guyton and hall textbook of medical physiology. 14th ed. Philadelphia: Elsevier.
- Hamilton BA, Frankel WN, Kerrebrock AW, Hawkins TL, FitzHugh W, Kusumi K, Russell LB, Mueller KL, van Berkel V, Birren BW, et al. 1996. Disruption of the nuclear hormone receptor ROR α in staggerer mice. *Nature*. 379(6567):736–739. <https://doi.org/10.1038/379736a0>
- Han K-S, Chen CH, Khan MM, Guo C, Regehr WG. 2020. Climbing fiber synapses rapidly and transiently inhibit neighboring Purkinje cells via ephaptic coupling. *Nat Neurosci*. 23(11):1399–1409. <https://doi.org/10.1038/s41593-020-0701-z>
- Hanke S, Reichenbach A. 1987. Quantitative-morphometric aspects of bergmann glial (Golgi epithelial) cell development in rats: A golgi study. *Anat Embryol (Berl)*. 177(2):183–188. <https://doi.org/10.1007/BF00572543>
- Hansson MJ, Måansson R, Morota S, Uchino H, Kallur T, Sumi T, Ishii N, Shimazu M, Keep MF, Jegorov A, Elmér E. 2008. Calcium-induced generation of reactive oxygen species in brain mitochondria is mediated by permeability transition. *Free Radic Biol Med*. 45(3):284–294. <https://doi.org/10.1016/j.freeradbiomed.2008.04.021>
- Hardie DG. 2000. Metabolic control: A new solution to an old problem. *Curr Biol*. 10(20):R757–R759. [https://doi.org/10.1016/S0960-9822\(00\)00744-2](https://doi.org/10.1016/S0960-9822(00)00744-2)
- Hardie DG, Ross FA, Hawley SA. 2012. AMPK: a nutrient and energy sensor that maintains energy homeostasis. *Nat Rev Mol Cell Biol*. 13(4):251–262. <https://doi.org/10.1038/nrm3311>
- Harrington DL. 2003. Does the representation of time depend on the cerebellum?: Effect of cerebellar stroke. *Brain*. 127(3):561–574. <https://doi.org/10.1093/brain/awh065>

REFERENCES

- Harrison XA, Donaldson L, Correa-Cano ME, Evans J, Fisher DN, Goodwin CED, Robinson BS, Hodgson DJ, Inger R. 2018. A brief introduction to mixed effects modelling and multi-model inference in ecology. *PeerJ*. 6:e4794. <https://doi.org/10.7717/peerj.4794>
- Hartig F. 2022. DHARMA: Residual diagnostics for hierarchical (multi-level / mixed) regression models [Internet]. [place unknown]. <https://CRAN.R-project.org/package=DHARMA>
- Hartmann J, Konnerth A. 2005. Determinants of postsynaptic Ca²⁺ signaling in Purkinje neurons. *Cell Calcium*. 37(5):459–466. <https://doi.org/10.1016/j.ceca.2005.01.014>
- Harvey RJ, Napper RMA. 1988. Quantitative study of granule and Purkinje cells in the cerebellar cortex of the rat. *J Comp Neurol*. 274(2):151–157. <https://doi.org/10.1002/cne.902740202>
- Hashimoto K, Kano M. 2003. Functional Differentiation of Multiple Climbing Fiber Inputs during Synapse Elimination in the Developing Cerebellum. *Neuron*. 38(5):785–796. [https://doi.org/10.1016/S0896-6273\(03\)00298-8](https://doi.org/10.1016/S0896-6273(03)00298-8)
- Hashimoto M. 2009. Development of the Cerebellum. In: Lajtha A, Mikoshiba K, editors. *Handb Neurochem Mol Neurobiol* [Internet]. Boston, MA: Springer US; [accessed 2023 Jan 25]; p. 15–25. https://doi.org/10.1007/978-0-387-30370-3_2
- Hashimoto M, Hibi M. 2012. Development and evolution of cerebellar neural circuits. *Dev Growth Differ*. 54(3):373–389. <https://doi.org/10.1111/j.1440-169X.2012.01348.x>
- Hashimoto R, Hori K, Owa T, Miyashita S, Dewa K, Masuyama N, Sakai K, Hayase Y, Seto Y, Inoue YU, et al. 2016. Origins of oligodendrocytes in the cerebellum, whose development is controlled by the transcription factor, Sox9. *Mech Dev*. 140:25–40. <https://doi.org/10.1016/j.mod.2016.02.004>
- Hauser MFA, Heba S, Schmidt-Wilcke T, Tegenthoff M, Manahan-Vaughan D. 2020. Cerebellar-hippocampal processing in passive perception of visuospatial change: An ego- and allocentric axis? *Hum Brain Mapp*. 41(5):1153–1166. <https://doi.org/10.1002/hbm.24865>
- He X, Qiu J-C, Lu K-Y, Guo H-L, Li L, Jia W-W, Ni M-M, Liu Y, Xu J, Chen F, Cheng R. 2021. Therapy for Apnoea of Prematurity: A Retrospective Study on Effects of Standard Dose and Genetic Variability on Clinical Response to Caffeine Citrate in Chinese Preterm Infants. *Adv Ther*. 38(1):607–626. <https://doi.org/10.1007/s12325-020-01544-2>
- Heaton MB, Madorsky I, Paiva M, Siler-Marsiglio KI. 2004. Vitamin E amelioration of ethanol neurotoxicity involves modulation of apoptosis-related protein levels in neonatal rat cerebellar granule cells. *Dev Brain Res*. 150(2):117–124. <https://doi.org/10.1016/j.devbrainres.2004.03.010>
- van der Heijden ME, Lackey EP, Perez R, İslleyen FS, Brown AM, Donofrio SG, Lin T, Zoghbi HY, Sillitoe RV. 2021. Maturation of Purkinje cell firing properties relies on neurogenesis of excitatory neurons. *eLife*. 10:e68045. <https://doi.org/10.7554/eLife.68045>
- Henderson-Smart DJ. 1981. The effect of gestational age on the incidence and duration of recurrent apnoea in newborn babies. *J Paediatr Child Health*. 17(4):273–276. <https://doi.org/10.1111/j.1440-1754.1981.tb01957.x>
- Henderson-Smart DJ, Davis PG. 2010. Prophylactic methylxanthines for endotracheal extubation in preterm infants. *Cochrane Neonatal Group*, editor. *Cochrane Database Syst Rev* [Internet]. [accessed 2023 Feb 21]. <https://doi.org/10.1002/14651858.CD000139.pub2>

- Henderson-Smart DJ, Steer PA. 2010. Caffeine versus theophylline for apnea in preterm infants. Cochrane Neonatal Group, editor. Cochrane Database Syst Rev [Internet]. [accessed 2023 Feb 15]. <https://doi.org/10.1002/14651858.CD000273.pub2>
- Herculano-Houzel S, Mota B, Lent R. 2006. Cellular scaling rules for rodent brains. *Proc Natl Acad Sci.* 103(32):12138–12143. <https://doi.org/10.1073/pnas.0604911103>
- Herlenius E, Ådén U, Tang LQ, Lagercrantz H. 2002. Perinatal Respiratory Control and Its Modulation by Adenosine and Caffeine in the Rat. *Pediatr Res.* 51(1):4–12. <https://doi.org/10.1203/00006450-200201000-00004>
- Herndon RM. 1963. The Fine Structure of the Purkinje Cell. *J Cell Biol.* 18(1):167–180.
- Hertzberg T, Lagercrantz H. 1987. Postnatal sensitivity of the peripheral chemoreceptors in newborn infants. *Arch Dis Child.* 62(12):1238–1241. <https://doi.org/10.1136/adc.62.12.1238>
- Herzfeld DJ, Kojima Y, Soetedjo R, Shadmehr R. 2015. Encoding of action by the Purkinje cells of the cerebellum. *Nature.* 526(7573):439–442. <https://doi.org/10.1038/nature15693>
- Herzig S, Shaw RJ. 2018. AMPK: guardian of metabolism and mitochondrial homeostasis. *Nat Rev Mol Cell Biol.* 19(2):121–135. <https://doi.org/10.1038/nrm.2017.95>
- Hilger A, Cloud C, Fahey T. 2022. Speech Impairment in Cerebellar Ataxia Affects Naturalness More Than Intelligibility. *The Cerebellum* [Internet]. [accessed 2022 Nov 8]. <https://doi.org/10.1007/s12311-022-01427-y>
- Hirai H, Launey T. 2000. The Regulatory Connection between the Activity of Granule Cell NMDA Receptors and Dendritic Differentiation of Cerebellar Purkinje Cells. *J Neurosci.* 20(14):5217–5224. <https://doi.org/10.1523/JNEUROSCI.20-14-05217.2000>
- Hirono M, Karube F, Yanagawa Y. 2021. Modulatory Effects of Monoamines and Perineuronal Nets on Output of Cerebellar Purkinje Cells. *Front Neural Circuits.* 15:661899. <https://doi.org/10.3389/fncir.2021.661899>
- Hoang DH, Pagnier A, Cousin E, Guichardet K, Schiff I, Iché C, Dilharreguy B, Grill J, Frappaz D, Berger C, et al. 2019. Anatomical-functional study of the cerebellum in working memory in children treated for medulloblastoma. *J Neuroradiol.* 46(3):207–213. <https://doi.org/10.1016/j.neurad.2019.01.093>
- Holzerová E, Prokisch H. 2015. Mitochondria: Much ado about nothing? How dangerous is reactive oxygen species production? *Int J Biochem Cell Biol.* 63:16–20. <https://doi.org/10.1016/j.biocel.2015.01.021>
- Horak FB, Buchanan J, Creath R, Jeka J. 2002. Vestibulospinal Control of Posture. In: Gandevia SC, Proske U, Stuart DG, editors. *Sensorimotor Control Mov Posture* [Internet]. Vol. 508. Boston, MA: Springer US; [accessed 2022 Nov 29]; p. 139–145. https://doi.org/10.1007/978-1-4615-0713-0_17
- Hore J, Wild B, Diener HC. 1991. Cerebellar dysmetria at the elbow, wrist, and fingers. *J Neurophysiol.* 65(3):563–571. <https://doi.org/10.1152/jn.1991.65.3.563>
- Horie Y, Arame T, Hirashima N, Tanaka M. 2021. Promotion of Dendritic Differentiation of Cerebellar Purkinje Cells by Ca²⁺/calmodulin-dependent Protein Kinase II α , II β and IV and Possible Involvement of CREB Phosphorylation. *Neuroscience.* 458:87–98. <https://doi.org/10.1016/j.neuroscience.2021.01.024>

REFERENCES

- Hoshino M, Nakamura S, Mori K, Kawauchi T, Terao M, Nishimura YV, Fukuda A, Fuse T, Matsuo N, Sone M, et al. 2005. Ptf1a, a bHLH Transcriptional Gene, Defines GABAergic Neuronal Fates in Cerebellum. *Neuron*. 47(2):201–213. <https://doi.org/10.1016/j.neuron.2005.06.007>
- Huang LE, Arany Z, Livingston DM, Bunn HF. 1996. Activation of Hypoxia-inducible Transcription Factor Depends Primarily upon Redox-sensitive Stabilization of Its α Subunit. *J Biol Chem*. 271(50):32253–32259. <https://doi.org/10.1074/jbc.271.50.32253>
- Hughes LJ, Park R, Lee MJ, Terry BK, Lee DJ, Kim H, Cho S-H, Kim S. 2020. Yap/Taz are required for establishing the cerebellar radial glia scaffold and proper foliation. *Dev Biol*. 457(1):150–162. <https://doi.org/10.1016/j.ydbio.2019.10.002>
- Idiong N, Lemke RP, Lin Y-J, Kwiatkowski K, Cates DB, Rigatto H. 1998. Airway closure during mixed apneas in preterm infants: Is respiratory effort necessary? *J Pediatr*. 133(4):509–512. [https://doi.org/10.1016/S0022-3476\(98\)70058-7](https://doi.org/10.1016/S0022-3476(98)70058-7)
- Ikai Y, Takada M, Shinonaga Y, Mizuno N. 1992. Dopaminergic and non-dopaminergic neurons in the ventral tegmental area of the rat project, respectively, to the cerebellar cortex and deep cerebellar nuclei. *Neuroscience*. 51(3):719–728. [https://doi.org/10.1016/0306-4522\(92\)90310-X](https://doi.org/10.1016/0306-4522(92)90310-X)
- Ikeda K, Kawakami K, Onimaru H, Okada Y, Yokota S, Koshiya N, Oku Y, Iizuka M, Koizumi H. 2017. The respiratory control mechanisms in the brainstem and spinal cord: integrative views of the neuroanatomy and neurophysiology. *J Physiol Sci*. 67(1):45–62. <https://doi.org/10.1007/s12576-016-0475-y>
- Irving C, Mason I. 2000. Signalling by FGF8 from the isthmus patterns anterior hindbrain and establishes the anterior limit of Hox gene expression. *Development*. 127(1):177–186. <https://doi.org/10.1242/dev.127.1.177>
- Iscru E, Serinagaoglu Y, Schilling K, Tian J, Bowers-Kidder SL, Zhang R, Morgan JI, DeVries AC, Nelson RJ, Zhu MX, Oberdick J. 2009. Sensorimotor enhancement in mouse mutants lacking the Purkinje cell-specific Gi/o modulator, Pcp2(L7). *Mol Cell Neurosci*. 40(1):62–75. <https://doi.org/10.1016/j.mcn.2008.09.002>
- Ishikawa T, Tomatsu S, Tsunoda Y, Lee J, Hoffman DS, Kakei S. 2014. Releasing Dentate Nucleus Cells from Purkinje Cell Inhibition Generates Output from the Cerebrocerebellum. Aumann TD, editor. *PLoS ONE*. 9(10):e108774. <https://doi.org/10.1371/journal.pone.0108774>
- Isope P, Hildebrand ME, Snutch TP. 2012. Contributions of T-Type Voltage-Gated Calcium Channels to Postsynaptic Calcium Signaling within Purkinje Neurons. *The Cerebellum*. 11(3):651–665. <https://doi.org/10.1007/s12311-010-0195-4>
- Itō M. 1984. The cerebellum and neural control. New York: Raven Press.
- Ito M. 1990. A new physiological concept on cerebellum. *Rev Neurol (Paris)*. 146(10):564–569.
- Ito M. 2006. Cerebellar circuitry as a neuronal machine. *Prog Neurobiol*. 78(3–5):272–303. <https://doi.org/10.1016/j.pneurobio.2006.02.006>
- Ito M, Yoshida M, Obata K. 1964. Monosynaptic inhibition of the intracerebellar nuclei induced from the cerebellar cortex. *Experientia*. 20(10):575–576. <https://doi.org/10.1007/BF02150304>

- Itsumi M, Inoue S, Elia AJ, Murakami K, Sasaki M, Lind EF, Brenner D, Harris IS, Chio IIC, Afzal S, et al. 2015. Idh1 protects murine hepatocytes from endotoxin-induced oxidative stress by regulating the intracellular NADP+/NADPH ratio. *Cell Death Differ.* 22(11):1837–1845. <https://doi.org/10.1038/cdd.2015.38>
- Ivan M, Kondo K, Yang H, Kim W, Valiando J, Ohh M, Salic A, Asara JM, Lane WS, Kaelin Jr. WG. 2001. HIF α Targeted for VHL-Mediated Destruction by Proline Hydroxylation: Implications for O $_2$ Sensing. *Science.* 292(5516):464–468. <https://doi.org/10.1126/science.1059817>
- Iwakura A, Uchigashima M, Miyazaki T, Yamasaki M, Watanabe M. 2012. Lack of Molecular-Anatomical Evidence for GABAergic Influence on Axon Initial Segment of Cerebellar Purkinje Cells by the Pinceau Formation. *J Neurosci.* 32(27):9438–9448. <https://doi.org/10.1523/JNEUROSCI.1651-12.2012>
- Jaarsma D, Diño MR, Cozzari C, Mugnaini E. 1996. Cerebellar choline acetyltransferase positive mossy fibres and their granule and unipolar brush cell targets: a model for central cholinergic nicotinic neurotransmission. *J Neurocytol.* 25(1):829–842. <https://doi.org/10.1007/BF02284845>
- Jaarsma D, Ruigrok TJH, Caffé R, Cozzari C, Levey AI, Mugnaini E, Voogd J. 1997. Chapter 5 Cholinergic innervation and receptors in the cerebellum. In: *Prog Brain Res [Internet].* Vol. 114. [place unknown]: Elsevier; [accessed 2022 Sep 26]; p. 67–96. [https://doi.org/10.1016/S0079-6123\(08\)63359-2](https://doi.org/10.1016/S0079-6123(08)63359-2)
- Jackman SL, Chen CH, Offermann HL, Drew IR, Harrison BM, Bowman AM, Flick KM, Flaquer I, Regehr WG. 2020. Cerebellar Purkinje cell activity modulates aggressive behavior. *eLife.* 9:e53229. <https://doi.org/10.7554/eLife.53229>
- Jackson W. 1841. Cases of Diseases of the Cerebellum: Read before the Sheffield Medical Society. *BMJ.* s1-3(13):251–254. <https://doi.org/10.1136/bmj.s1-3.13.251>
- Jaeger D, De Schutter E, Bower JM. 1997. The Role of Synaptic and Voltage-Gated Currents in the Control of Purkinje Cell Spiking: A Modeling Study. *J Neurosci.* 17(1):91–106. <https://doi.org/10.1523/JNEUROSCI.17-01-00091.1997>
- Jakab RL, Hámori J. 1988. Quantitative morphology and synaptology of cerebellar glomeruli in the rat. *Anat Embryol (Berl).* 179(1):81–88. <https://doi.org/10.1007/BF00305102>
- Janvier A, Khairy M, Kokkotis A, Cormier C, Messmer D, Barrington KJ. 2004. Apnea Is Associated with Neurodevelopmental Impairment in Very Low Birth Weight Infants. *J Perinatol.* 24(12):763–768. <https://doi.org/10.1038/sj.jp.7211182>
- Jardine L, Lui K, Liley HG, Schindler T, Fink J, Asselin J, Durand D. 2022. Trial of aerosolised surfactant for preterm infants with respiratory distress syndrome. *Arch Dis Child - Fetal Neonatal Ed.* 107(1):51–55. <https://doi.org/10.1136/archdischild-2021-321645>
- Jia M, Njapo SAN, Rastogi V, Hedna VS. 2015. Taming Glutamate Excitotoxicity: Strategic Pathway Modulation for Neuroprotection. *CNS Drugs.* 29(2):153–162. <https://doi.org/10.1007/s40263-015-0225-3>
- Jiao X, Rahimi Balaei M, Abu-El-Rub E, Casoni F, Pezeshgi Modarres H, Dhingra S, Kong J, Consalez GG, Marzban H. 2021. Reduced Granule Cell Proliferation and Molecular Dysregulation in the Cerebellum of Lysosomal Acid Phosphatase 2 (ACP2) Mutant Mice. *Int J Mol Sci.* 22(6):2994. <https://doi.org/10.3390/ijms22062994>

REFERENCES

- Juliano C, Sosunov S, Niatsetskaya Z, Isler JA, Utkina-Sosunova I, Jang I, Ratner V, Ten V. 2015. Mild intermittent hypoxemia in neonatal mice causes permanent neurofunctional deficit and white matter hypomyelination. *Exp Neurol.* 264:33–42. <https://doi.org/10.1016/j.expneurol.2014.11.010>
- Jung K-I, Park M-H, Park B, Kim S-Y, Kim YO, Kim B-N, Park S, Song C-H. 2019. Cerebellar Gray Matter Volume, Executive Function, and Insomnia: Gender Differences in Adolescents. *Sci Rep.* 9(1):855. <https://doi.org/10.1038/s41598-018-37154-w>
- Kandel ER, editor. 2013. *Principles of neural science.* 5th ed. New York: McGraw-Hill.
- Kao H, Ryoo K, Lin A, Janoschka SR, Augustine GJ, Porton B. 2017. Synapsins regulate brain-derived neurotrophic factor-mediated synaptic potentiation and axon elongation by acting on membrane rafts. Kano M, editor. *Eur J Neurosci.* 45(8):1085–1101. <https://doi.org/10.1111/ejn.13552>
- Kaufman GD, Mustari MJ, Miselis RR, Perachio AA. 1996. Transneuronal pathways to the vestibulocerebellum. *J Comp Neurol.* 370(4):501–523. [https://doi.org/10.1002/\(SICI\)1096-9861\(19960708\)370:4<501::AID-CNE7>3.0.CO;2-8](https://doi.org/10.1002/(SICI)1096-9861(19960708)370:4<501::AID-CNE7>3.0.CO;2-8)
- Ke Q, Costa M. 2006. Hypoxia-Inducible Factor-1 (HIF-1). *Mol Pharmacol.* 70(5):1469–1480. <https://doi.org/10.1124/mol.106.027029>
- Khan A, Qurashi M, Kwiatkowski K, Cates D, Rigatto H. 2005. Measurement of the CO₂ apneic threshold in newborn infants: possible relevance for periodic breathing and apnea. *J Appl Physiol.* 98(4):1171–1176. <https://doi.org/10.1152/japplphysiol.00574.2003>
- Kheirandish L, Gozal D, Pequignot J-M, Pequignot J, Row BW. 2005. Intermittent Hypoxia during Development Induces Long-Term Alterations in Spatial Working Memory, Monoamines, and Dendritic Branching in Rat Frontal Cortex. *Pediatr Res.* 58(3):594–599. <https://doi.org/10.1203/01.pdr.0000176915.19287.e2>
- Khouri-Farah N, Guo Q, Morgan K, Shin J, Li JYH. 2022. Integrated single-cell transcriptomic and epigenetic study of cell state transition and lineage commitment in embryonic mouse cerebellum. *Sci Adv.* 8(13):eabl9156. <https://doi.org/10.1126/sciadv.abl9156>
- Kilpatrick DL, Wang W, Gronostajski R, Litwack ED. 2012. Nuclear Factor I and Cerebellar Granule Neuron Development: An Intrinsic–Extrinsic Interplay. *The Cerebellum.* 11(1):41–49. <https://doi.org/10.1007/s12311-010-0227-0>
- Kimura H, Okamoto K, Sakai Y. 1985. Pharmacological evidence for L-aspartate as the neurotransmitter of cerebellar climbing fibres in the guinea-pig. *J Physiol.* 365(1):103–119. <https://doi.org/10.1113/jphysiol.1985.sp015761>
- Klionsky DJ. 2007. Autophagy: from phenomenology to molecular understanding in less than a decade. *Nat Rev Mol Cell Biol.* 8(11):931–937. <https://doi.org/10.1038/nrm2245>
- Klostranec JM, Krings T. 2022. Cerebral neurovascular embryology, anatomic variations, and congenital brain arteriovenous lesions. *J NeuroInterventional Surg.* 14(9):910–919. <https://doi.org/10.1136/neurintsurg-2021-018607>
- Knoepfler PS, Cheng PF, Eisenman RN. 2002. N- myc is essential during neurogenesis for the rapid expansion of progenitor cell populations and the inhibition of neuronal differentiation. *Genes Dev.* 16(20):2699–2712. <https://doi.org/10.1101/gad.1021202>

- Kohlhauser C, Kaehler S, Mosgoeller W, Singewald N, Kouvelas D, Prast H, Hoeger H, Lubec B. 1999. Histological changes and neurotransmitter levels three months following perinatal asphyxia in the rat. *Life Sci.* 64(23):2109–2124. [https://doi.org/10.1016/S0024-3205\(99\)00160-5](https://doi.org/10.1016/S0024-3205(99)00160-5)
- Kole MJ, Qian J, Waase MP, Klassen TL, Chen TT, Augustine GJ, Noebels JL. 2015. Selective Loss of Presynaptic Potassium Channel Clusters at the Cerebellar Basket Cell Terminal Pinceau in Adam11 Mutants Reveals Their Role in Ephaptic Control of Purkinje Cell Firing. *J Neurosci.* 35(32):11433–11444. <https://doi.org/10.1523/JNEUROSCI.1346-15.2015>
- Komite O, Nagaoka M, Watase K, Gutmann DH, Tanigaki K, Honjo T, Radtke F, Saito T, Chiba S, Tanaka K. 2007. The monolayer formation of Bergmann glial cells is regulated by Notch/RBP-J signaling. *Dev Biol.* 311(1):238–250. <https://doi.org/10.1016/j.ydbio.2007.08.042>
- Komuro H, Yacubova Ellada, Yacubova Elina, Rakic P. 2001. Mode and Tempo of Tangential Cell Migration in the Cerebellar External Granular Layer. *J Neurosci.* 21(2):527–540. <https://doi.org/10.1523/JNEUROSCI.21-02-00527.2001>
- Koos BJ. 2011. Adenosine A_{2a} receptors and O₂ sensing in development. *Am J Physiol-Regul Integr Comp Physiol.* 301(3):R601–R622. <https://doi.org/10.1152/ajpregu.00664.2010>
- Korbo L, Andersen BB. 1995. The distributions of Purkinje cell perikaryon and nuclear volume in human and rat cerebellum with the nucleator method. *Neuroscience.* 69(1):151–158. [https://doi.org/10.1016/0306-4522\(95\)00223-6](https://doi.org/10.1016/0306-4522(95)00223-6)
- Korbo L, Andersen BB, Ladefoged O, Møller A. 1993. Total numbers of various cell types in rat cerebellar cortex estimated using an unbiased stereological method. *Brain Res.* 609(1–2):262–268. [https://doi.org/10.1016/0006-8993\(93\)90881-M](https://doi.org/10.1016/0006-8993(93)90881-M)
- Kovatis KZ, Di Fiore JM, Martin RJ, Abbasi S, Chaundhary AS, Hoover S, Zhang Z, Kirpalani H. 2020. Effect of Blood Transfusions on Intermittent Hypoxic Episodes in a Prospective Study of Very Low Birth Weight Infants. *J Pediatr.* 222:65–70. <https://doi.org/10.1016/j.jpeds.2020.03.015>
- Kuipers IM, Maertzdorf WJ, De Jong DS, Hanson MA, Blanco CE. 1997. Initiation and Maintenance of Continuous Breathing at Birth. *Pediatr Res.* 42(2):163–168. <https://doi.org/10.1203/00006450-199708000-00006>
- Kumari S, Liu X, Nguyen T, Zhang X, D'Mello SR. 2001. Distinct phosphorylation patterns underlie Akt activation by different survival factors in neurons. *Mol Brain Res.* 96(1–2):157–162. [https://doi.org/10.1016/S0006-8993\(01\)03045-1](https://doi.org/10.1016/S0006-8993(01)03045-1)
- Kumral A, Tuzun F, Yesilirmak DC, Duman N, Ozkan H. 2012. Genetic basis of apnoea of prematurity and caffeine treatment response: role of adenosine receptor polymorphisms: Genetic basis of apnoea of prematurity. *Acta Paediatr.* 101(7):e299–e303. <https://doi.org/10.1111/j.1651-2227.2012.02664.x>
- Küper M, Dimitrova A, Thürling M, Maderwald S, Roths J, Elles HG, Gizewski ER, Ladd ME, Diedrichsen J, Timmann D. 2011. Evidence for a motor and a non-motor domain in the human dentate nucleus — An fMRI study. *NeuroImage.* 54(4):2612–2622. <https://doi.org/10.1016/j.neuroimage.2010.11.028>
- Lacaille H, Duterte-Boucher D, Liot D, Vaudry H, Naassila M, Vaudry D. 2015. Comparison of the deleterious effects of binge drinking-like alcohol exposure in adolescent and adult mice. *J Neurochem.* 132(6):629–641. <https://doi.org/10.1111/jnc.13020>

REFERENCES

- Lackey EP, Heck DH, Sillitoe RV. 2018. Recent advances in understanding the mechanisms of cerebellar granule cell development and function and their contribution to behavior. *F1000Research*. 7:1142. <https://doi.org/10.12688/f1000research.15021.1>
- Lainé J, Axelrad H. 1994. The candelabrum cell: A new interneuron in the cerebellar cortex: CEREBELLAR CORTEX CANDELABRUM INTERNEURON. *J Comp Neurol*. 339(2):159–173. <https://doi.org/10.1002/cne.903390202>
- Lainé J, Axelrad H. 2002. Extending the cerebellar Lugano cell class. *Neuroscience*. 115(2):363–374. [https://doi.org/10.1016/S0306-4522\(02\)00421-9](https://doi.org/10.1016/S0306-4522(02)00421-9)
- Lalonde R, Strazielle C. 2003. The effects of cerebellar damage on maze learning in animals. *The Cerebellum*. 2(4):300–309. <https://doi.org/10.1080/14734220310017456>
- Lance JW, McLeod JG. 1981. The cerebellum and its disorders. In: *Physiol Approach Clin Neurol* [Internet]. [place unknown]: Elsevier; [accessed 2023 Jan 17]; p. 191–218. <https://doi.org/10.1016/B978-0-407-00196-1.50014-0>
- Laouafa S, Iturri P, Arias-Reyes C, Marcouiller F, Gonzales M, Joseph V, Bairam A, Soliz J. 2019. Erythropoietin and caffeine exert similar protective impact against neonatal intermittent hypoxia: Apnea of prematurity and sex dimorphism. *Exp Neurol*. 320:112985. <https://doi.org/10.1016/j.expneurol.2019.112985>
- Larsell O. 1937. THE CEREBELLUM: A REVIEW AND INTERPRETATION. *Arch Neurol Psychiatry*. 38(3):580. <https://doi.org/10.1001/archneurpsyc.1937.02260210146011>
- Laube G, Röper J, Christian Pitt J, Sewing S, Kistner U, Garner CC, Pongs O, Veh RW. 1996. Ultrastructural localization of Shaker-related potassium channel subunits and synapse-associated protein 90 to septate-like junctions in rat cerebellar Pinceaux. *Mol Brain Res*. 42(1):51–61. [https://doi.org/10.1016/S0169-328X\(96\)00120-9](https://doi.org/10.1016/S0169-328X(96)00120-9)
- Lefort JM, Vincent J, Tallot L, Jarlier F, De Zeeuw Cl, Rondi-Reig L, Rochefort C. 2019. Impaired cerebellar Purkinje cell potentiation generates unstable spatial map orientation and inaccurate navigation. *Nat Commun*. 10(1):2251. <https://doi.org/10.1038/s41467-019-09958-5>
- Legué E, Gottshall JL, Jaumouillé E, Roselló-Díez A, Shi W, Barraza LH, Washington S, Grant RL, Joyner AL. 2016. Differential timing of granule cell production during cerebellum development underlies generation of the foliation pattern. *Neural Develop*. 11(1):17. <https://doi.org/10.1186/s13064-016-0072-z>
- Leibowitz A, Boyko M, Shapira Y, Zlotnik A. 2012. Blood Glutamate Scavenging: Insight into Neuroprotection. *Int J Mol Sci*. 13(8):10041–10066. <https://doi.org/10.3390/ijms130810041>
- Lemkey-Johnston N, Larramendi LMH. 1968. Types and distribution of synapses upon basket and stellate cells of the mouse cerebellum: An electron microscopic study. *J Comp Neurol*. 134(1):73–111. <https://doi.org/10.1002/cne.901340106>
- Lemyre B, Davis PG, De Paoli AG. 2002. Nasal intermittent positive pressure ventilation (NIPPV) versus nasal continuous positive airway pressure (NCPAP) for apnea of prematurity. *Cochrane Neonatal Group*, editor. *Cochrane Database Syst Rev* [Internet]. [accessed 2023 Feb 21]. <https://doi.org/10.1002/14651858.CD002272>

- Lenth RV. 2022. emmeans: Estimated marginal means, aka least-squares means [Internet]. [place unknown]. <https://CRAN.R-project.org/package=emmeans>
- Leroux S, Rodriguez-Duboc A, Arabo A, Basille-Dugay M, Vaudry D, Burel D. 2022. Intermittent hypoxia in a mouse model of apnea of prematurity leads to a retardation of cerebellar development and long-term functional deficits. *Cell Biosci.* 12(1):148. <https://doi.org/10.1186/s13578-022-00869-5>
- Leto K, Arancillo M, Becker EBE, Buffo A, Chiang C, Ding B, Dobyns WB, Dusart I, Halldipur P, Hatten ME, et al. 2016. Consensus Paper: Cerebellar Development. *The Cerebellum.* 15(6):789–828. <https://doi.org/10.1007/s12311-015-0724-2>
- Leto K, Carletti B, Williams IM, Magrassi L, Rossi F. 2006. Different Types of Cerebellar GABAergic Interneurons Originate from a Common Pool of Multipotent Progenitor Cells. *J Neurosci.* 26(45):11682–11694. <https://doi.org/10.1523/JNEUROSCI.3656-06.2006>
- Li B, Zhu J-N, Wang J-J. 2014. Histaminergic afferent system in the cerebellum: structure and function. *Cerebellum Ataxias.* 1(1):5. <https://doi.org/10.1186/2053-8871-1-5>
- Li X, He P, Wang X-L, Zhang S, Devejian N, Bennett E, Cai C. 2018. Sulfiredoxin-1 enhances cardiac progenitor cell survival against oxidative stress via the upregulation of the ERK/NRF2 signal pathway. *Free Radic Biol Med.* 123:8–19. <https://doi.org/10.1016/j.freeradbiomed.2018.05.060>
- Li Y, Chen Y. 2019. AMPK and Autophagy. In: Qin Z-H, editor. *Autophagy Biol Dis* [Internet]. Vol. 1206. Singapore: Springer Singapore; [accessed 2023 Mar 21]; p. 85–108. https://doi.org/10.1007/978-981-15-0602-4_4
- Li Z, Mbah NE, Overmeyer JH, Sarver JG, George S, Trabbi CJ, Erhardt PW, Maltese WA. 2019. The JNK signaling pathway plays a key role in methuosis (non-apoptotic cell death) induced by MOMIPP in glioblastoma. *BMC Cancer.* 19(1):77. <https://doi.org/10.1186/s12885-019-5288-y>
- Lin Y, Chen L, Lin C, Luo Y, Tsai RYL, Wang F. 2009. Neuron-derived FGF9 is essential for scaffold formation of Bergmann radial fibers and migration of granule neurons in the cerebellum. *Dev Biol.* 329(1):44–54. <https://doi.org/10.1016/j.ydbio.2009.02.011>
- Liu F, Liu T-W, Kang J. 2018. The role of NF-κB-mediated JNK pathway in cognitive impairment in a rat model of sleep apnea. *J Thorac Dis.* 10(12):6921–6931. <https://doi.org/10.21037/jtd.2018.12.05>
- Liu F, Zhang Z, Lin X, Teng G, Meng H, Yu T, Fang F, Zang F, Li Z, Liu S. 2011. Development of the human fetal cerebellum in the second trimester: a post mortem magnetic resonance imaging evaluation: Development of the human fetal cerebellum in the second trimester. *J Anat.* 219(5):582–588. <https://doi.org/10.1111/j.1469-7580.2011.01418.x>
- Liu X, Yang W, Guan Z, Yu W, Fan B, Xu N, Liao DJ. 2018. There are only four basic modes of cell death, although there are many ad-hoc variants adapted to different situations. *Cell Biosci.* 8(1):6. <https://doi.org/10.1186/s13578-018-0206-6>
- Liu Y, Shoji-Kawata S, Sumpter RM, Wei Y, Ginet V, Zhang L, Posner B, Tran KA, Green DR, Xavier RJ, et al. 2013. Autosis is a Na^+, K^+ -ATPase-regulated form of cell death triggered by autophagy-inducing peptides, starvation, and hypoxia-ischemia. *Proc Natl Acad Sci.* 110(51):20364–20371. <https://doi.org/10.1073/pnas.1319661110>

REFERENCES

- Liu Z, Huang Y, Wang X, He Y, Li J, Li B. 2023. The role of ferroptosis in chronic intermittent hypoxia-induced cognitive impairment. *Sleep Breath* [Internet]. [accessed 2023 Apr 2]. <https://doi.org/10.1007/s11325-022-02760-6>
- Ljungberg L, Lang-Ouellette D, Yang A, Jayabal S, Quilez S, Watt AJ. 2016. Transient Developmental Purkinje Cell Axonal Torpedoes in Healthy and Ataxic Mouse Cerebellum. *Front Cell Neurosci* [Internet]. [accessed 2023 Apr 14] 10. <https://doi.org/10.3389/fncel.2016.00248>
- Llinás R. 2009. Inferior olive oscillation as the temporal basis for motricity and oscillatory reset as the basis for motor error correction. *Neuroscience*. 162(3):797–804. <https://doi.org/10.1016/j.neuroscience.2009.04.045>
- Llinás R, Sugimori M. 1980. Electrophysiological properties of in vitro Purkinje cell dendrites in mammalian cerebellar slices. *J Physiol*. 305(1):197–213. <https://doi.org/10.1113/jphysiol.1980.sp013358>
- Logan GD. 1985. Executive control of thought and action. *Acta Psychol (Amst)*. 60(2–3):193–210. [https://doi.org/10.1016/0001-6918\(85\)90055-1](https://doi.org/10.1016/0001-6918(85)90055-1)
- Logan M, Sweeney MI. 1997. Adenosine A₁ receptor activation preferentially protects cultured cerebellar neurons versus astrocytes against hypoxia-induced death. *Mol Chem Neuropathol*. 31(2):119–133. <https://doi.org/10.1007/BF02815237>
- Long J-Y, Guo H-L, He X, Hu Y-H, Xia Y, Cheng R, Ding X-S, Chen F, Xu J. 2021. Caffeine for the Pharmacological Treatment of Apnea of Prematurity in the NICU: Dose Selection Conundrum, Therapeutic Drug Monitoring and Genetic Factors. *Front Pharmacol*. 12:681842. <https://doi.org/10.3389/fphar.2021.681842>
- Lorenzetto E, Caselli L, Feng G, Yuan W, Nerbonne JM, Sanes JR, Buffelli M. 2009. Genetic perturbation of postsynaptic activity regulates synapse elimination in developing cerebellum. *Proc Natl Acad Sci*. 106(38):16475–16480. <https://doi.org/10.1073/pnas.0907298106>
- Lossi L, Castagna C, Merighi A. 2018. Caspase-3 Mediated Cell Death in the Normal Development of the Mammalian Cerebellum. *Int J Mol Sci*. 19(12):3999. <https://doi.org/10.3390/ijms19123999>
- Lowenstein ED, Cui K, Hernandez-Miranda LR. 2022. Regulation of early cerebellar development. *FEBS J*.febs.16426. <https://doi.org/10.1111/febs.16426>
- Luck R, Karakatsani A, Shah B, Schermann G, Adler H, Kupke J, Tisch N, Jeong H-W, Back MK, Hetsch F, et al. 2021. The angiopoietin-Tie2 pathway regulates Purkinje cell dendritic morphogenesis in a cell-autonomous manner. *Cell Rep*. 36(7):109522. <https://doi.org/10.1016/j.celrep.2021.109522>
- Lüdecke D, Ben-Shachar M, Patil I, Waggoner P, Makowski D. 2021. performance: An R Package for Assessment, Comparison and Testing of Statistical Models. *J Open Source Softw*. 6(60):3139. <https://doi.org/10.21105/joss.03139>
- Luo B, Wang J, Liu Z, Shen Z, Shi R, Liu Y-Q, Liu Y, Jiang M, Wu Y, Zhang Z. 2016. Phagocyte respiratory burst activates macrophage erythropoietin signalling to promote acute inflammation resolution. *Nat Commun*. 7(1):12177. <https://doi.org/10.1038/ncomms12177>
- Luo J, Coapes G, Mak T, Yamazaki T, Tin C, Degenaar P. 2016. Real-Time Simulation of Passage-of-Time Encoding in Cerebellum Using a Scalable FPGA-Based System. *IEEE Trans Biomed Circuits Syst*. 10(3):742–753. <https://doi.org/10.1109/TBCAS.2015.2460232>

- Lupo M, Troisi E, Chiricozzi FR, Clausi S, Molinari M, Leggio M. 2015. Inability to Process Negative Emotions in Cerebellar Damage: a Functional Transcranial Doppler Sonographic Study. *The Cerebellum*. 14(6):663–669. <https://doi.org/10.1007/s12311-015-0662-z>
- Lüscher C, Jan LY, Stoffel M, Malenka RC, Nicoll RA. 1997. G Protein-Coupled Inwardly Rectifying K⁺ Channels (GIRKs) Mediate Postsynaptic but Not Presynaptic Transmitter Actions in Hippocampal Neurons. *Neuron*. 19(3):687–695. [https://doi.org/10.1016/S0896-6273\(00\)80381-5](https://doi.org/10.1016/S0896-6273(00)80381-5)
- Macey PM, Henderson LA, Macey KE, Alger JR, Frysinger RC, Woo MA, Harper RK, Yan-Go FL, Harper RM. 2002. Brain Morphology Associated with Obstructive Sleep Apnea. *Am J Respir Crit Care Med*. 166(10):1382–1387. <https://doi.org/10.1164/rccm.200201-050OC>
- MacNeilage PR, Glasauer S. 2018. Gravity Perception: The Role of the Cerebellum. *Curr Biol*. 28(22):R1296–R1298. <https://doi.org/10.1016/j.cub.2018.09.053>
- Mak M, Tyburski E, Madany Ł, Sokołowski A, Samochowiec A. 2016. Executive Function Deficits in Patients after Cerebellar Neurosurgery. *J Int Neuropsychol Soc*. 22(1):47–57. <https://doi.org/10.1017/S1355617715001174>
- Mammel DM, Carroll JL, Warner BB, Edwards BA, Mann DL, Wallendorf MJ, Hoffmann JA, Conklin CM, Pyles H, Kemp JS. 2022. Quantitative and Qualitative Changes in Peripheral Chemoreceptor Activity in Preterm Infants. *Am J Respir Crit Care Med*.:rccm.202206-1033OC. <https://doi.org/10.1164/rccm.202206-1033OC>
- Mancuso MR, Kuhnert F, Kuo CJ. 2008. Developmental Angiogenesis of the Central Nervous System. *Lymphat Res Biol*. 6(3–4):173–180. <https://doi.org/10.1089/lrb.2008.1014>
- Mangels JA, Ivry RB, Shimizu N. 1998. Dissociable contributions of the prefrontal and neocerebellar cortex to time perception. *Cogn Brain Res*. 7(1):15–39. [https://doi.org/10.1016/S0926-6410\(98\)00005-6](https://doi.org/10.1016/S0926-6410(98)00005-6)
- Marien P, Engelborghs S, Pickut BA, De Deyn PP. 2000. Aphasia following cerebellar damage: fact or fallacy? *J Neurolinguistics*. 13(2–3):145–171. [https://doi.org/10.1016/S0911-6044\(00\)00009-9](https://doi.org/10.1016/S0911-6044(00)00009-9)
- Marotta A, Re A, Zampini M, Fiorio M. 2021. Bodily self-perception during voluntary actions: The causal contribution of premotor cortex and cerebellum. *Cortex*. 142:1–14. <https://doi.org/10.1016/j.cortex.2021.05.012>
- Martí-Clua J. 2022. Times of neuron origin and neurogenetic gradients in mice Purkinje cells and deep cerebellar nuclei neurons during the development of the cerebellum. A review. *Tissue Cell*. 78:101897. <https://doi.org/10.1016/j.tice.2022.101897>
- Martin RJ, Wilson CG. 2012. Apnea of Prematurity. In: Terjung R, editor. *Compr Physiol [Internet]*. 1st ed. [place unknown]: Wiley; [accessed 2023 Feb 13]; p. 2923–2931. <https://doi.org/10.1002/cphy.c100021>
- Marzban H, Del Bigio MR, Alizadeh J, Ghavami S, Zachariah RM, Rastegar M. 2015. Cellular commitment in the developing cerebellum. *Front Cell Neurosci [Internet]*. [accessed 2023 Jan 2] 8. <https://doi.org/10.3389/fncel.2014.00450>
- Matsushima T, Rhoton AL, Oliveira E de, Peace D. 1983. Microsurgical anatomy of the veins of the posterior fossa. *J Neurosurg*. 59(1):63–105. <https://doi.org/10.3171/jns.1983.59.1.0063>

REFERENCES

- Mayer CA, Haxhiu MA, Martin RJ, Wilson CG. 2006. Adenosine A_{2A} receptors mediate GABAergic inhibition of respiration in immature rats. *J Appl Physiol.* 100(1):91–97. <https://doi.org/10.1152/japplphysiol.00459.2005>
- McCormick DA, Clark GA, Lavond DG, Thompson RF. 1982. Initial localization of the memory trace for a basic form of learning. *Proc Natl Acad Sci.* 79(8):2731–2735. <https://doi.org/10.1073/pnas.79.8.2731>
- McMahon AP, Joyner AL, Bradley A, McMahon JA. 1992. The midbrain-hindbrain phenotype of Wnt-1-Wnt-1- mice results from stepwise deletion of engrailed-expressing cells by 9.5 days postcoitum. *Cell.* 69(4):581–595. [https://doi.org/10.1016/0092-8674\(92\)90222-X](https://doi.org/10.1016/0092-8674(92)90222-X)
- McNamee D, Wolpert DM. 2019. Internal Models in Biological Control. *Annu Rev Control Robot Auton Syst.* 2(1):339–364. <https://doi.org/10.1146/annurev-control-060117-105206>
- McNeill EM, Klöckner-Bormann M, Roesler EC, Talton LE, Moechars D, Clagett-Dame M. 2011. Nav2 hypomorphic mutant mice are ataxic and exhibit abnormalities in cerebellar development. *Dev Biol.* 353(2):331–343. <https://doi.org/10.1016/j.ydbio.2011.03.008>
- Meng X, McGraw CM, Wang W, Jing J, Yeh S-Y, Wang L, Lopez J, Brown AM, Lin T, Chen W, et al. 2019. Neurexophilin4 is a selectively expressed α -neurexin ligand that modulates specific cerebellar synapses and motor functions. *eLife.* 8:e46773. <https://doi.org/10.7554/eLife.46773>
- Mertz K, Koscheck T, Schilling K. 2000. Brain-derived neurotrophic factor modulates dendritic morphology of cerebellar basket and stellate cells: an in vitro study. *Neuroscience.* 97(2):303–310. [https://doi.org/10.1016/S0306-4522\(99\)00585-0](https://doi.org/10.1016/S0306-4522(99)00585-0)
- Middleton F. 2000. Basal ganglia and cerebellar loops: motor and cognitive circuits. *Brain Res Rev.* 31(2–3):236–250. [https://doi.org/10.1016/S0165-0173\(99\)00040-5](https://doi.org/10.1016/S0165-0173(99)00040-5)
- Millen KJ, Steshina EY, Iskusnykh IY, Chizhikov VV. 2014. Transformation of the cerebellum into more ventral brainstem fates causes cerebellar agenesis in the absence of *Ptf1a* function. *Proc Natl Acad Sci [Internet].* [accessed 2023 Jan 24] 111(17). <https://doi.org/10.1073/pnas.1315024111>
- Miller MJ, Carlo WA, Martin RJ. 1985. Continuous positive airway pressure selectively reduces obstructive apnea in preterm infants. *J Pediatr.* 106(1):91–94. [https://doi.org/10.1016/S0022-3476\(85\)80475-3](https://doi.org/10.1016/S0022-3476(85)80475-3)
- Miller MJ, Haxhiu MA, Haxhiu-Poskurica B, Dreshaj IA, DiFiore JM, Martin RJ. 2000. Recurrent hypoxic exposure and reflex responses during development in the piglet. *Respir Physiol.* 123(1–2):51–61. [https://doi.org/10.1016/S0034-5687\(00\)00149-3](https://doi.org/10.1016/S0034-5687(00)00149-3)
- Miller TL, Raab LM, Shaffer TH, Schweikert A, Diana F, Fort P, Frum AS, Pergolizzi J, Raffa RB. 2022. A Novel Agnostic Respiratory Stimulant as a Treatment for Apnea of Prematurity: A Proof-of-Concept Study. *Cureus [Internet].* [accessed 2023 Feb 26]. <https://doi.org/10.7759/cureus.28900>
- Milošević NT, Ristanović D, Marić DL, Rajković K. 2010. Morphology and cell classification of large neurons in the adult human dentate nucleus: A quantitative study. *Neurosci Lett.* 468(1):59–63. <https://doi.org/10.1016/j.neulet.2009.10.063>
- Miyakawa H, Lev-Ram V, Lasser-Ross N, Ross WN. 1992. Calcium transients evoked by climbing fiber and parallel fiber synaptic inputs in guinea pig cerebellar Purkinje neurons. *J Neurophysiol.* 68(4):1178–1189. <https://doi.org/10.1152/jn.1992.68.4.1178>

- Miyake A, Friedman NP, Emerson MJ, Witzki AH, Howerter A, Wager TD. 2000. The Unity and Diversity of Executive Functions and Their Contributions to Complex “Frontal Lobe” Tasks: A Latent Variable Analysis. *Cognit Psychol.* 41(1):49–100. <https://doi.org/10.1006/cogp.1999.0734>
- Miyashita S, Owa T, Seto Y, Yamashita M, Aida S, Sone M, Ichijo K, Nishioka T, Kaibuchi K, Kawaguchi Y, et al. 2021. Cyclin D1 controls development of cerebellar granule cell progenitors through phosphorylation and stabilization of ATOH1. *EMBO J* [Internet]. [accessed 2023 Apr 14] 40(14). <https://doi.org/10.1525/embj.2020105712>
- Miyazaki T, Yamasaki M, Takeuchi T, Sakimura K, Mishina M, Watanabe M. 2010. Ablation of Glutamate Receptor GluR 2 in Adult Purkinje Cells Causes Multiple Innervation of Climbing Fibers by Inducing Aberrant Invasion to Parallel Fiber Innervation Territory. *J Neurosci.* 30(45):15196–15209. <https://doi.org/10.1523/JNEUROSCI.0934-10.2010>
- Molinari M, Masciullo M, Bulgheroni S, D’Arrigo S, Riva D. 2018. Cognitive aspects: sequencing, behavior, and executive functions. In: *Handb Clin Neurol* [Internet]. Vol. 154. [place unknown]: Elsevier; [accessed 2022 Nov 9]; p. 167–180. <https://doi.org/10.1016/B978-0-444-63956-1.00010-2>
- Molinari M, Petrosini L, Misciagna S, Leggio MG. 2004. Visuospatial abilities in cerebellar disorders. *J Neurol Neurosurg Psychiatry.* 75(2):235–240.
- Montealegre-Pomar A, Bohorquez A, Charpak N. 2020. Systematic review and meta-analysis suggest that Kangaroo position protects against apnoea of prematurity. *Acta Paediatr.* 109(7):1310–1316. <https://doi.org/10.1111/apa.15161>
- Morales D, Hatten ME. 2006. Molecular Markers of Neuronal Progenitors in the Embryonic Cerebellar Anlage. *J Neurosci.* 26(47):12226–12236. <https://doi.org/10.1523/JNEUROSCI.3493-06.2006>
- Mori T, Tanaka K, Buffo A, Wurst W, Kühn R, Götz M. 2006. Inducible gene deletion in astroglia and radial glia-A valuable tool for functional and lineage analysis. *Glia.* 54(1):21–34. <https://doi.org/10.1002/glia.20350>
- Moriette G, Lescure S, El Ayoubi M, Lopez E. 2010. Apnées du prématuré : données récentes. *Arch Pédiatrie.* 17(2):186–190. <https://doi.org/10.1016/j.arcped.2009.09.016>
- Morizawa YM, Matsumoto M, Nakashima Y, Endo N, Aida T, Ishikane H, Beppu K, Moritoh S, Inada H, Osumi N, et al. 2022. Synaptic pruning through glial synapse engulfment upon motor learning. *Nat Neurosci.* 25(11):1458–1469. <https://doi.org/10.1038/s41593-022-01184-5>
- Mouradian GC, Lakshminrusimha S, Konduri GG. 2021. Perinatal Hypoxemia and Oxygen Sensing. In: Terjung R, editor. *Compr Physiol* [Internet]. 1st ed. [place unknown]: Wiley; [accessed 2023 Mar 25]; p. 1653–1677. <https://doi.org/10.1002/cphy.c190046>
- Mugnaini E, Diño MR, Jaarsma D. 1997. Chapter 8 The unipolar brush cells of the mammalian cerebellum and cochlear nucleus: cytology and microcircuitry. In: *Prog Brain Res* [Internet]. Vol. 114. [place unknown]: Elsevier; [accessed 2023 Jan 23]; p. 131–150. [https://doi.org/10.1016/S0079-6123\(08\)63362-2](https://doi.org/10.1016/S0079-6123(08)63362-2)
- Mugnaini E, Floris A. 1994. The unipolar brush cell: A neglected neuron of the mammalian cerebellar cortex. *J Comp Neurol.* 339(2):174–180. <https://doi.org/10.1002/cne.903390203>

REFERENCES

- Mugnaini E, Floris A, Wright-Goss M. 1994. Extraordinary synapses of the unipolar brush cell: An electron microscopic study in the rat cerebellum. *Synapse.* 16(4):284–311. <https://doi.org/10.1002/syn.890160406>
- Mukherjee C, Kling T, Russo B, Miebach K, Kess E, Schifferer M, Pedro LD, Weikert U, Fard MK, Kannaiyan N, et al. 2020. Oligodendrocytes Provide Antioxidant Defense Function for Neurons by Secreting Ferritin Heavy Chain. *Cell Metab.* 32(2):259-272.e10. <https://doi.org/10.1016/j.cmet.2020.05.019>
- Mulherkar S, Uddin MD, Couvillon AD, Sillitoe RV, Tolias KF. 2014. The small GTPases RhoA and Rac1 regulate cerebellar development by controlling cell morphogenesis, migration and foliation. *Dev Biol.* 394(1):39–53. <https://doi.org/10.1016/j.ydbio.2014.08.004>
- Mullan S, Mojtahedi S, Johnson DL, Macdonald RL. 1996. Embryological basis of some aspects of cerebral vascular fistulas and malformations. *J Neurosurg.* 85(1):1–8. <https://doi.org/10.3171/jns.1996.85.1.0001>
- Muraleedharan R, Dasgupta B. 2022. AMPK in the brain: its roles in glucose and neural metabolism. *FEBS J.* 289(8):2247–2262. <https://doi.org/10.1111/febs.16151>
- Murdoch S, Shah P, Jampana R. 2016. The Guillain–Mollaret triangle in action. *Pract Neurol.* 16(3):243–246. <https://doi.org/10.1136/practneurol-2015-001142>
- Mürner-Lavanchy IM, Doyle LW, Schmidt B, Roberts RS, Asztalos EV, Costantini L, Davis PG, Dewey D, D’Ilario J, Grunau RE, et al. 2018. Neurobehavioral Outcomes 11 Years After Neonatal Caffeine Therapy for Apnea of Prematurity. *Pediatrics.* 141(5):e20174047. <https://doi.org/10.1542/peds.2017-4047>
- Nagraj VP, Lake DE, Kuhn L, Moorman JR, Fairchild KD. 2021. Central Apnea of Prematurity: Does Sex Matter? *Am J Perinatol.* 38(13):1428–1434. <https://doi.org/10.1055/s-0040-1713405>
- Naidich TP, Haacke EM, Kollias SS, Sorensen AG, Duvernoy HM, Delman BN. 2009. Duvernoy’s Atlas of the Human Brain Stem and Cerebellum: High-Field MRI: Surface Anatomy, Internal Structure, Vascularization and 3D Sectional Anatomy. Vienna: Springer Vienna Springer e-books.
- Nakamura H, Katahira T, Matsunaga E, Sato T. 2005. Isthmus organizer for midbrain and hindbrain development. *Brain Res Rev.* 49(2):120–126. <https://doi.org/10.1016/j.brainresrev.2004.10.005>
- Nakamura T, Matsui T, Utsumi A, Sumiya M, Nakagawa E, Sadato N. 2022. Context-prosody interaction in sarcasm comprehension: A functional magnetic resonance imaging study. *Neuropsychologia.* 170:108213. <https://doi.org/10.1016/j.neuropsychologia.2022.108213>
- Nakamura Y, Hirano T. 2016. Intracellular Ca²⁺ thresholds for induction of excitatory long-term depression and inhibitory long-term potentiation in a cerebellar Purkinje neuron. *Biochem Biophys Res Commun.* 469(4):803–808. <https://doi.org/10.1016/j.bbrc.2015.12.065>
- Napper RMA, Harvey RJ. 1988. Number of parallel fiber synapses on an individual Purkinje cell in the cerebellum of the rat. *J Comp Neurol.* 274(2):168–177. <https://doi.org/10.1002/cne.902740204>
- Nat R, Voiculescu B, Stanciu C, Vidulescu C, Cergan R, Badiu C, Popescu LM. 2001. Apoptosis in human embryo development: 2. Cerebellum. *J Cell Mol Med.* 5(2):179–187. <https://doi.org/10.1111/j.1582-4934.2001.tb00151.x>

- Nattie E, Li A. 2009. Central chemoreception is a complex system function that involves multiple brain stem sites. *J Appl Physiol.* 106(4):1464–1466. <https://doi.org/10.1152/japplphysiol.00112.2008>
- Neau J-Ph, Anlo EA, Bonnaud V, Ingrand P, Gil R. 2000. Neuropsychological disturbances in cerebellar infarcts: Neuropsychological disturbances in cerebellar infarcts. *Acta Neurol Scand.* 102(6):363–370. <https://doi.org/10.1034/j.1600-0404.2000.102006363.x>
- Netto CA, Sanches EF, Odorcyk F, Duran-Carabali LE, Sizonenko SV. 2018. Pregnancy as a valuable period for preventing hypoxia-ischemia brain damage. *Int J Dev Neurosci.* 70:12–24. <https://doi.org/10.1016/j.ijdevneu.2018.06.004>
- Nicholson CL, Coubes P, Poulen G. 2020. Dentate nucleus as target for deep brain stimulation in dystono-dyskinetic syndromes. *Neurochirurgie.* 66(4):258–265. <https://doi.org/10.1016/j.neuchi.2020.04.132>
- Nieuwenhuys R, Voogd J, Huijzen C van. 2008. The human central nervous system. 4th ed. New York: Springer.
- Nirmala JG, Lopus M. 2020. Cell death mechanisms in eukaryotes. *Cell Biol Toxicol.* 36(2):145–164. <https://doi.org/10.1007/s10565-019-09496-2>
- Nissen MJ, Bullemer P. 1987. Attentional requirements of learning: Evidence from performance measures. *Cognit Psychol.* 19(1):1–32. [https://doi.org/10.1016/0010-0285\(87\)90002-8](https://doi.org/10.1016/0010-0285(87)90002-8)
- Nylander Vujovic S, Nava C, Johansson M, Bruschettini M. 2020. Confounding biases in studies on early- versus late-caffeine in preterm infants: a systematic review. *Pediatr Res.* 88(3):357–364. <https://doi.org/10.1038/s41390-020-0757-1>
- Okafuji T, Funahashi J, Nakamura H. 1999. Roles of Pax-2 in initiation of the chick tectal development. *Dev Brain Res.* 116(1):41–49. [https://doi.org/10.1016/S0165-3806\(99\)00073-5](https://doi.org/10.1016/S0165-3806(99)00073-5)
- Oliveira-Junior MS, Pereira EP, de Amorim VCM, Reis LTC, do Nascimento RP, da Silva VDA, Costa SL. 2019. Lupeol inhibits LPS-induced neuroinflammation in cerebellar cultures and induces neuroprotection associated to the modulation of astrocyte response and expression of neurotrophic and inflammatory factors. *Int Immunopharmacol.* 70:302–312. <https://doi.org/10.1016/j.intimp.2019.02.055>
- Orvis GD, Hartzell AL, Smith JB, Barraza LH, Wilson SL, Szulc KU, Turnbull DH, Joyner AL. 2012. The engrailed homeobox genes are required in multiple cell lineages to coordinate sequential formation of fissures and growth of the cerebellum. *Dev Biol.* 367(1):25–39. <https://doi.org/10.1016/j.ydbio.2012.04.018>
- Oscarsson O. 1965. Functional Organization of the Spino- and Cuneocerebellar Tracts. *Physiol Rev.* 45(3):495–522. <https://doi.org/10.1152/physrev.1965.45.3.495>
- Osorno T, Rudolph S, Nguyen T, Kozareva V, Nadaf NM, Norton A, Macosko EZ, Lee W-CA, Regehr WG. 2022. Candelabrum cells are ubiquitous cerebellar cortex interneurons with specialized circuit properties. *Nat Neurosci.* 25(6):702–713. <https://doi.org/10.1038/s41593-022-01057-x>
- Otero JJ, Kalaszczynska I, Michowski W, Wong M, Gyigli PE, Gokozan HN, Griveau A, Odajima J, Czeisler C, Catacutan FP, et al. 2014. Cerebellar cortical lamination and foliation require cyclin A2. *Dev Biol.* 385(2):328–339. <https://doi.org/10.1016/j.ydbio.2013.10.019>

REFERENCES

- Ottersen OP, Storm-Mathisen J, Somogyi P. 1988. Colocalization of glycine-like and GABA-like immunoreactivities in Golgi cell terminals in the rat cerebellum: a postembedding light and electron microscopic study. *Brain Res.* 450(1–2):342–353. [https://doi.org/10.1016/0006-8993\(88\)91573-9](https://doi.org/10.1016/0006-8993(88)91573-9)
- Ouchi Y, Okada H, Yoshikawa E, Nobezawa S, Futatsubashi M. 1999. Brain activation during maintenance of standing postures in humans. *Brain.* 122(2):329–338. <https://doi.org/10.1093/brain/122.2.329>
- Pae E-K, Chien P, Harper RM. 2005. Intermittent hypoxia damages cerebellar cortex and deep nuclei. *Neurosci Lett.* 375(2):123–128. <https://doi.org/10.1016/j.neulet.2004.10.091>
- Palay SL, Chan-Palay V. 1974. Cerebellar Cortex [Internet]. Berlin, Heidelberg: Springer Berlin Heidelberg; [accessed 2022 Sep 26]. <https://doi.org/10.1007/978-3-642-65581-4>
- Pan N, Jahan I, Lee JE, Fritzsch B. 2009. Defects in the cerebella of conditional Neurod1 null mice correlate with effective Tg(Atoh1-cre) recombination and granule cell requirements for Neurod1 for differentiation. *Cell Tissue Res.* 337(3):407–428. <https://doi.org/10.1007/s00441-009-0826-6>
- Panula P, Takagi H, Inagaki N, Yamatodani A, Tohyama M, Wada H, Kotilainen E. 1993. Histamine-containing nerve fibers innervate human cerebellum. *Neurosci Lett.* 160(1):53–56. [https://doi.org/10.1016/0304-3940\(93\)90915-8](https://doi.org/10.1016/0304-3940(93)90915-8)
- Parenti I, Leitão E, Kuechler A, Villard L, Goizet C, Courdier C, Bayat A, Rossi A, Julia S, Bruel A-L, et al. 2022. The different clinical facets of SYN1-related neurodevelopmental disorders. *Front Cell Dev Biol.* 10:1019715. <https://doi.org/10.3389/fcell.2022.1019715>
- Park H, Yamamoto Y, Tanaka-Yamamoto K. 2021. Refinement of Cerebellar Network Organization by Extracellular Signaling During Development. *Neuroscience.* 462:44–55. <https://doi.org/10.1016/j.neuroscience.2020.05.036>
- Parkinson FE, Sinclair CJD, Othman T, Haughey NJ, Geiger JD. 2002. Differences between rat primary cortical neurons and astrocytes in purine release evoked by ischemic conditions. *Neuropharmacology.* 43(5):836–846. [https://doi.org/10.1016/S0028-3908\(02\)00083-7](https://doi.org/10.1016/S0028-3908(02)00083-7)
- Pascual M, Abasolo I, Mingorance-Le Meur A, Martínez A, Del Rio JA, Wright CVE, Real FX, Soriano E. 2007. Cerebellar GABAergic progenitors adopt an external granule cell-like phenotype in the absence of Ptf1a transcription factor expression. *Proc Natl Acad Sci.* 104(12):5193–5198. <https://doi.org/10.1073/pnas.0605699104>
- Patan S. 2004. Vasculogenesis and Angiogenesis. In: Kirsch M, Black PMcL, editors. *Angiogenesis Brain Tumors* [Internet]. Vol. 117. Boston, MA: Springer US; [accessed 2023 Jan 29]; p. 3–32. https://doi.org/10.1007/978-1-4419-8871-3_1
- Patel PH, Tamanoi F. 2006. Increased Rheb-TOR signaling enhances sensitivity of the whole organism to oxidative stress. *J Cell Sci.* 119(20):4285–4292. <https://doi.org/10.1242/jcs.03199>
- Pellionisz A, Llinás R. 1982. Space-time representation in the brain. The cerebellum as a predictive space-time metric tensor. *Neuroscience.* 7(12):2949–2970. [https://doi.org/10.1016/0306-4522\(82\)90224-X](https://doi.org/10.1016/0306-4522(82)90224-X)
- Peña F, Ramirez J-M. 2005. Hypoxia-Induced Changes in Neuronal Network Properties. *Mol Neurobiol.* 32(3):251–284. <https://doi.org/10.1385/MN:32:3:251>

- Pergolizzi JV, Fort P, Miller TL, LeQuang JA, Raffa RB. 2022a. The epidemiology of apnoea of prematurity. *J Clin Pharm Ther.* 47(5):685–693. <https://doi.org/10.1111/jcpt.13587>
- Pergolizzi JV, Fort P, Miller TL, LeQuang JA, Raffa RB. 2022b. The limited management options for apnoea of prematurity. *J Clin Pharm Ther.* 47(3):396–401. <https://doi.org/10.1111/jcpt.13547>
- Petrosini L. 1998. The cerebellum in the spatial problem solving: a co-star or a guest star? *Prog Neurobiol.* 56(2):191–210. [https://doi.org/10.1016/S0301-0082\(98\)00036-7](https://doi.org/10.1016/S0301-0082(98)00036-7)
- Phelan MW, Forman LW, Perrine SP, Faller DV. 1998. Hypoxia increases thrombospondin-1 transcript and protein in cultured endothelial cells. *J Lab Clin Med.* 132(6):519–529. [https://doi.org/10.1016/S0022-2143\(98\)90131-7](https://doi.org/10.1016/S0022-2143(98)90131-7)
- Pichitpornchai C, Rawson JA, Rees S. 1994. Morphology of parallel fibres in the cerebellar cortex of the rat: An experimental light and electron microscopic study with biocytin. *J Comp Neurol.* 342(2):206–220. <https://doi.org/10.1002/cne.903420205>
- Pichon S, Kell CA. 2013. Affective and Sensorimotor Components of Emotional Prosody Generation. *J Neurosci.* 33(4):1640–1650. <https://doi.org/10.1523/JNEUROSCI.3530-12.2013>
- Pillekamp F, Hermann C, Keller T, von Gontard A, Kribs A, Roth B. 2007. Factors Influencing Apnea and Bradycardia of Prematurity – Implications for Neurodevelopment. *Neonatology.* 91(3):155–161. <https://doi.org/10.1159/000097446>
- Pittman AE, Solecki DJ. 2023. Cooperation between primary cilia signaling and integrin receptor extracellular matrix engagement regulates progenitor proliferation and neuronal differentiation in the developing cerebellum. *Front Cell Dev Biol.* 11:1127638. <https://doi.org/10.3389/fcell.2023.1127638>
- Poets CF. 2020. Intermittent hypoxia and long-term neurological outcome: How are they related? *Semin Fetal Neonatal Med.* 25(2):101072. <https://doi.org/10.1016/j.siny.2019.101072>
- Poets CF, Roberts RS, Schmidt B, Whyte RK, Asztalos EV, Bader D, Bairam A, Moddemann D, Peliowski A, Rabi Y, et al. 2015. Association Between Intermittent Hypoxemia or Bradycardia and Late Death or Disability in Extremely Preterm Infants. *JAMA.* 314(6):595. <https://doi.org/10.1001/jama.2015.8841>
- Potheraveedu VN, Schöpel M, Stoll R, Heumann R. 2017. Rheb in neuronal degeneration, regeneration, and connectivity. *Biol Chem.* 398(5–6):589–606. <https://doi.org/10.1515/hsz-2016-0312>
- Powers RM, Hevner RF, Halpain S. 2023. The Neuron Navigators: Structure, function, and evolutionary history. *Front Mol Neurosci.* 15:1099554. <https://doi.org/10.3389/fnmol.2022.1099554>
- Pozo ME, Cave A, Köroğlu ÖA, Litvin DG, Martin RJ, Di Fiore J, Kc P. 2012. Effect of Postnatal Intermittent Hypoxia on Growth and Cardiovascular Regulation of Rat Pups. *Neonatology.* 102(2):107–113. <https://doi.org/10.1159/000338096>
- Prabhakar NR, Peng Y-J, Nanduri J. 2020. Hypoxia-inducible factors and obstructive sleep apnea. *J Clin Invest.* 130(10):5042–5051. <https://doi.org/10.1172/JCI137560>
- Prabhakar NR, Semenza GL. 2012. Adaptive and Maladaptive Cardiorespiratory Responses to Continuous and Intermittent Hypoxia Mediated by Hypoxia-Inducible Factors 1 and 2. *Physiol Rev.* 92(3):967–1003. <https://doi.org/10.1152/physrev.00030.2011>

REFERENCES

- Praud J-P. 2010. Upper airway reflexes in response to gastric reflux. *Paediatr Respir Rev.* 11(4):208–212. <https://doi.org/10.1016/j.prrv.2010.07.001>
- Pregnolato S, Chakkrapani E, Isles AR, Luyt K. 2019. Glutamate Transport and Preterm Brain Injury. *Front Physiol.* 10:417. <https://doi.org/10.3389/fphys.2019.00417>
- Puia-Dumitrescu M, Smith PB, Zhao J, Soriano A, Payne EH, Harper B, Bendel-Stenzel E, Moya F, Chhabra R, Ku L, et al. 2019. Dosing and Safety of Off-label Use of Caffeine Citrate in Premature Infants. *J Pediatr.* 211:27-32.e1. <https://doi.org/10.1016/j.jpeds.2019.04.028>
- Purves D, editor. 2018. Neuroscience. Sixth edition. New York: Oxford University Press.
- Quitadamo P, Giorgio V, Zenzeri L, Baldassarre M, Cresi F, Borrelli O, Salvatore S. 2020. Apnea in preterm neonates: what's the role of gastroesophageal reflux? A systematic review. *Dig Liver Dis.* 52(7):723–729. <https://doi.org/10.1016/j.dld.2020.03.032>
- Radecki DZ, Samanta J. 2022. Endogenous Neural Stem Cell Mediated Oligodendrogenesis in the Adult Mammalian Brain. *Cells.* 11(13):2101. <https://doi.org/10.3390/cells11132101>
- Rahimi-Balaei M, Afsharinezhad P, Bailey K, Buchok M, Yeganeh B, Marzban H. 2015. Embryonic stages in cerebellar afferent development. *Cerebellum Ataxias.* 2(1):7. <https://doi.org/10.1186/s40673-015-0026-y>
- Rakic P, Sidman RL. 1970. Histogenesis of cortical layers in human cerebellum, particularly the lamina dissecans. *J Comp Neurol.* 139(4):473–500. <https://doi.org/10.1002/cne.901390407>
- Ramnani N. 2006. The primate cortico-cerebellar system: anatomy and function. *Nat Rev Neurosci.* 7(7):511–522. <https://doi.org/10.1038/nrn1953>
- Ramón y Cajal S. 1909. Histologie du système nerveux de l'homme & des vertébrés [Internet]. Paris: Maloine; [accessed 2022 Sep 23]. <https://doi.org/10.5962/bhl.title.48637>
- Ravichandran S, Chouthai NS, Patel B, Sharma A, Gupte A, Ma MM, Mamilla D, Lulic-Botica M, Thomas R, Kamat D. 2019. Higher daily doses of caffeine lowered the incidence of moderate to severe neurodevelopmental disabilities in very low birth weight infants. *Acta Paediatr.* 108(3):430–435. <https://doi.org/10.1111/apa.14465>
- Ravizza SM, McCormick CA, Schlerf JE, Justus T, Ivry RB, Fiez JA. 2006. Cerebellar damage produces selective deficits in verbal working memory. *Brain.* 129(2):306–320. <https://doi.org/10.1093/brain/awh685>
- Raybaud C. 2010. Normal and Abnormal Embryology and Development of the Intracranial Vascular System. *Neurosurg Clin N Am.* 21(3):399–426. <https://doi.org/10.1016/j.nec.2010.03.011>
- Ren J, Ding X, Greer JJ. 2015. Ampakines Enhance Weak Endogenous Respiratory Drive and Alleviate Apnea in Perinatal Rats. *Am J Respir Crit Care Med.* 191(6):704–710. <https://doi.org/10.1164/rccm.201410-1898OC>
- Rhoton AL. 2000. The Posterior Fossa Veins. *Neurosurgery.* 47(suppl_3):S69–S92. <https://doi.org/10.1097/00006123-200009001-00012>
- Ricard D, Rogemond V, Charrier E, Aguera M, Bagnard D, Belin M-F, Thomasset N, Honnorat J. 2001. Isolation and Expression Pattern of Human Unc-33-Like Phosphoprotein 6/Collapsin Response

Mediator Protein 5 (Ulip6/CRMP5): Coexistence with Ulip2/CRMP2 in Sema3A- Sensitive Oligodendrocytes. *J Neurosci.* 21(18):7203–7214. <https://doi.org/10.1523/JNEUROSCI.21-18-07203.2001>

Richmond CM, Ring F, Richmond L, Rossouw E, Ballard E, Birch P. 2023. ‘Propped and prone’ positioning reduces respiratory events in spontaneously breathing preterm infants: A randomised triple crossover study. *J Paediatr Child Health.* 59(1):81–88. <https://doi.org/10.1111/jpc.16241>

Richter-Landsberg C. 2008. The Cytoskeleton in Oligodendrocytes: Microtubule Dynamics in Health and Disease. *J Mol Neurosci.* 35(1):55–63. <https://doi.org/10.1007/s12031-007-9017-7>

Rigatto H, De La Torre Verduzco R, Gates DB. 1975. Effects of O₂ on the ventilatory response to CO₂ in preterm infants. *J Appl Physiol.* 39(6):896–899. <https://doi.org/10.1152/jappl.1975.39.6.896>

Rigby M, Cull-Candy SG, Farrant M. 2015. Transmembrane AMPAR Regulatory Protein γ-2 Is Required for the Modulation of GABA Release by Presynaptic AMPARs. *J Neurosci.* 35(10):4203–4214. <https://doi.org/10.1523/JNEUROSCI.4075-14.2015>

Rius J, Guma M, Schachtrup C, Akassoglou K, Zinkernagel AS, Nizet V, Johnson RS, Haddad GG, Karin M. 2008. NF-κB links innate immunity to the hypoxic response through transcriptional regulation of HIF-1α. *Nature.* 453(7196):807–811. <https://doi.org/10.1038/nature06905>

Rivière M-A, Rodriguez-Duboc A. 2022. ma-riviere/LT-AoP-22: Final release [Internet]. [accessed 2023 Feb 19]. <https://doi.org/10.5281/ZENODO.6480947>

Rochefort C, Lefort J, Rondi-Reig L. 2013. The cerebellum: a new key structure in the navigation system. *Front Neural Circuits* [Internet]. [accessed 2022 Apr 29] 7. <https://doi.org/10.3389/fncir.2013.00035>

Rodríguez-Hernández A, Rhoton AL, Lawton MT. 2011. Segmental anatomy of cerebellar arteries: a proposed nomenclature: Laboratory investigation. *J Neurosurg.* 115(2):387–397. <https://doi.org/10.3171/2011.3.JNS101413>

Roemgens A, Singh S, Beyer C, Arnold S. 2011. Inducers of Chemical Hypoxia Act in a Gender- and Brain Region-Specific Manner on Primary Astrocyte Viability and Cytochrome c Oxidase. *Neurotox Res.* 20(1):1–14. <https://doi.org/10.1007/s12640-010-9213-z>

Roh S-E, Kim SH, Ryu C, Kim C-E, Kim YG, Worley PF, Kim SK, Kim SJ. 2020. Direct translation of climbing fiber burst-mediated sensory coding into post-synaptic Purkinje cell dendritic calcium. *eLife.* 9:e61593. <https://doi.org/10.7554/eLife.61593>

Rondi-Reig L, Paradis A-L, Fallahnezhad M. 2022. A Liaison Brought to Light: Cerebellum-Hippocampus, Partners for Spatial Cognition. *The Cerebellum.* 21(5):826–837. <https://doi.org/10.1007/s12311-022-01422-3>

Rubenstein JLR, editor. 2020. Neural circuit and cognitive development: comprehensive developmental neuroscience. Second edition. London ; San Diego, CA: Academic Press, imprint Elsevier Ltd.

Ruediger S, Vittori C, Bednarek E, Genoud C, Strata P, Sacchetti B, Caroni P. 2011. Learning-related feedforward inhibitory connectivity growth required for memory precision. *Nature.* 473(7348):514–518. <https://doi.org/10.1038/nature09946>

REFERENCES

- Ruehl RM, Flanigin VL, Ophey L, Raiser TM, Seiderer K, Ertl M, Conrad J, zu Eulenburg P. 2022. The human egomotion network. *NeuroImage*. 264:119715. <https://doi.org/10.1016/j.neuroimage.2022.119715>
- Ryan KE, Kim PS, Fleming JT, Brignola E, Cheng FY, Litingtung Y, Chiang C. 2017. Lkb1 regulates granule cell migration and cortical folding of the cerebellar cortex. *Dev Biol*. 432(1):165–177. <https://doi.org/10.1016/j.ydbio.2017.09.036>
- Ryan S, Taylor CT, McNicholas WT. 2005. Selective Activation of Inflammatory Pathways by Intermittent Hypoxia in Obstructive Sleep Apnea Syndrome. *Circulation*. 112(17):2660–2667. <https://doi.org/10.1161/CIRCULATIONAHA.105.556746>
- Sacchetti B, Scelfo B, Tempia F, Strata P. 2004. Long-Term Synaptic Changes Induced in the Cerebellar Cortex by Fear Conditioning. *Neuron*. 42(6):973–982. <https://doi.org/10.1016/j.neuron.2004.05.012>
- Sadakata T, Kakegawa W, Mizoguchi A, Washida M, Katoh-Semba R, Shutoh F, Okamoto T, Nakashima H, Kimura K, Tanaka M, et al. 2007. Impaired Cerebellar Development and Function in Mice Lacking CAPS2, a Protein Involved in Neurotrophin Release. *J Neurosci*. 27(10):2472–2482. <https://doi.org/10.1523/JNEUROSCI.2279-06.2007>
- Sadler TW. 2019. Langman's medical embryology. Fourteenth edition. Philadelphia: Wolters Kluwer.
- Samuel J, Franklin C. 2008. Hypoxemia and Hypoxia. In: Myers JA, Millikan KW, Saclarides TJ, editors. *Common Surg Dis* [Internet]. New York, NY: Springer New York; [accessed 2023 Feb 7]; p. 391–394. https://doi.org/10.1007/978-0-387-75246-4_97
- Sathyanesan A, Zhou J, Scafidi J, Heck DH, Sillitoe RV, Gallo V. 2019. Emerging connections between cerebellar development, behaviour and complex brain disorders. *Nat Rev Neurosci*. 20(5):298–313. <https://doi.org/10.1038/s41583-019-0152-2>
- Sato A, Sekine Y, Saruta C, Nishibe H, Morita N, Sato Y, Sadakata T, Shinoda Y, Kojima T, Furuichi T. 2008. Cerebellar development transcriptome database (CDT-DB): Profiling of spatio-temporal gene expression during the postnatal development of mouse cerebellum. *Neural Netw*. 21(8):1056–1069. <https://doi.org/10.1016/j.neunet.2008.05.004>
- Sawczenko A, Fleming PJ. 1996. Thermal stress, sleeping position, and the sudden infant death syndrome. *Sleep*. 19(10 Suppl):S267-270.
- Scaramuzzino L, Lucchino V, Scalise S, Lo Conte M, Zannino C, Sacco A, Biamonte F, Parrotta EI, Costanzo FS, Cuda G. 2021. Uncovering the Metabolic and Stress Responses of Human Embryonic Stem Cells to FTH1 Gene Silencing. *Cells*. 10(9):2431. <https://doi.org/10.3390/cells10092431>
- Schell MJ, Brady Jr. RO, Molliver ME, Snyder SH. 1997. d-Serine as a Neuromodulator: Regional and Developmental Localizations in Rat Brain Glia Resemble NMDA Receptors. *J Neurosci*. 17(5):1604–1615. <https://doi.org/10.1523/JNEUROSCI.17-05-01604.1997>
- Scheuer T, Sharkovska Y, Tarabykin V, Marggraf K, Brockmöller V, Bührer C, Endesfelder S, Schmitz T. 2017. Neonatal Hyperoxia Perturbs Neuronal Development in the Cerebellum. *Mol Neurobiol* [Internet]. [accessed 2023 Feb 3]. <https://doi.org/10.1007/s12035-017-0612-5>
- Schilling K, Oberdick J, Rossi F, Baader SL. 2008. Besides Purkinje cells and granule neurons: an appraisal of the cell biology of the interneurons of the cerebellar cortex. *Histochem Cell Biol*. 130(4):601–615. <https://doi.org/10.1007/s00418-008-0483-y>

- Schindelin J, Arganda-Carreras I, Frise E, Kaynig V, Longair M, Pietzsch T, Preibisch S, Rueden C, Saalfeld S, Schmid B, et al. 2012. Fiji: an open-source platform for biological-image analysis. *Nat Methods*. 9(7):676–682. <https://doi.org/10.1038/nmeth.2019>
- Schmahmann J. 1998. The cerebellar cognitive affective syndrome. *Brain*. 121(4):561–579. <https://doi.org/10.1093/brain/121.4.561>
- Schmidt B. 2012. Survival Without Disability to Age 5 Years After Neonatal Caffeine Therapy for Apnea of Prematurity. *JAMA*. 307(3):275. <https://doi.org/10.1001/jama.2011.2024>
- Schmidt B, Roberts RS, Davis P, Doyle LW, Barrington KJ, Ohlsson A, Solimano A, Tin W. 2006. Caffeine Therapy for Apnea of Prematurity. *N Engl J Med*. 354(20):2112–2121. <https://doi.org/10.1056/NEJMoa054065>
- Schmidt B, Roberts RS, Davis P, Doyle LW, Barrington KJ, Ohlsson A, Solimano A, Tin W. 2007. Long-Term Effects of Caffeine Therapy for Apnea of Prematurity. *N Engl J Med*. 357(19):1893–1902. <https://doi.org/10.1056/NEJMoa073679>
- Schneider Gasser EM, Gassmann M, Thiersch M. 2021. HIF-2: an important player in neuronal response to ischemia. *Pflüg Arch - Eur J Physiol*. 473(8):1175–1176. <https://doi.org/10.1007/s00424-021-02601-7>
- Schweighofer N, Doya K, Kuroda S. 2004. Cerebellar aminergic neuromodulation: towards a functional understanding. *Brain Res Rev*. 44(2–3):103–116. <https://doi.org/10.1016/j.brainresrev.2003.10.004>
- Scorziello A, Pellegrini C, Secondo A, Sirabella R, Formisano L, Sibaud L, Amoroso S, Canzoniero LMT, Annunziato L, Di Renzo GF. 2004. Neuronal NOS activation during oxygen and glucose deprivation triggers cerebellar granule cell death in the later reoxygenation phase. *J Neurosci Res*. 76(6):812–821. <https://doi.org/10.1002/jnr.20096>
- Seese RR. 2020. Working Memory Impairments in Cerebellar Disorders of Childhood. *Pediatr Neurol*. 107:16–23. <https://doi.org/10.1016/j.pediatrneurol.2020.02.005>
- Sekerková G, Ilijic E, Mugnaini E. 2004. Time of origin of unipolar brush cells in the rat cerebellum as observed by prenatal bromodeoxyuridine labeling. *Neuroscience*. 127(4):845–858. <https://doi.org/10.1016/j.neuroscience.2004.05.050>
- Semmel ES, Dotson VM, Burns TG, Mahle WT, King TZ. 2018. Posterior Cerebellar Volume and Executive Function in Young Adults With Congenital Heart Disease. *J Int Neuropsychol Soc*. 24(9):939–948. <https://doi.org/10.1017/S1355617718000310>
- Shevtsova O, Leitch B. 2012. Selective loss of AMPA receptor subunits at inhibitory neuron synapses in the cerebellum of the ataxic stargazer mouse. *Brain Res*. 1427:54–64. <https://doi.org/10.1016/j.brainres.2011.10.022>
- Shin E, Kashiwagi Y, Kuriu T, Iwasaki H, Tanaka T, Koizumi H, Gleeson JG, Okabe S. 2013. Doublecortin-like kinase enhances dendritic remodelling and negatively regulates synapse maturation. *Nat Commun*. 4(1):1440. <https://doi.org/10.1038/ncomms2443>
- Shiraishi Y, Mizutani A, Yuasa S, Mikoshiba K, Furuichi T. 2003. Glutamate-induced declustering of post-synaptic adaptor protein Cupidin (Homer 2/vesl-2) in cultured cerebellar granule cells: Glutamate-induced declustering of Cupidin/Homer. *J Neurochem*. 87(2):364–376. <https://doi.org/10.1046/j.1471-4159.2003.02003.x>

REFERENCES

- Sillitoe RV, Fu Y, Watson C. 2012. Cerebellum. In: Mouse Nerv Syst [Internet]. [place unknown]: Elsevier; [accessed 2022 Sep 26]; p. 360–397. <https://doi.org/10.1016/B978-0-12-369497-3.10011-1>
- Sillitoe RV, Joyner AL. 2007. Morphology, Molecular Codes, and Circuitry Produce the Three-Dimensional Complexity of the Cerebellum. *Annu Rev Cell Dev Biol.* 23(1):549–577. <https://doi.org/10.1146/annurev.cellbio.23.090506.123237>
- Silveri M. 1998. Verbal short-term store-rehearsal system and the cerebellum. Evidence from a patient with a right cerebellar lesion. *Brain.* 121(11):2175–2187. <https://doi.org/10.1093/brain/121.11.2175>
- Silveri MC, Leggio MG, Molinari M. 1994. The cerebellum contributes to linguistic production: A case of agrammatic speech following a right cerebellar lesion. *Neurology.* 44(11):2047–2047. <https://doi.org/10.1212/WNL.44.11.2047>
- Simat M, Parpan F, Fritschy J-M. 2007. Heterogeneity of glycinergic and gabaergic interneurons in the granule cell layer of mouse cerebellum. *J Comp Neurol.* 500(1):71–83. <https://doi.org/10.1002/cne.21142>
- Smith AL, Alexander M, Rosenkrantz TS, Sadek ML, Fitch RH. 2014. Sex differences in behavioral outcome following neonatal hypoxia ischemia: Insights from a clinical meta-analysis and a rodent model of induced hypoxic ischemic brain injury. *Exp Neurol.* 254:54–67. <https://doi.org/10.1016/j.expneurol.2014.01.003>
- Sohma O, Mizuguchi M, Takashima S, Yamada M, Ikeda K, Ohta S. 1996. High expression of Bcl-x protein in the developing human cerebellar cortex. *J Neurosci Res.* 43(2):175–182. [https://doi.org/10.1002/\(SICI\)1097-4547\(19960115\)43:2<175::AID-JNR5>3.0.CO;2-D](https://doi.org/10.1002/(SICI)1097-4547(19960115)43:2<175::AID-JNR5>3.0.CO;2-D)
- Sokolovsky N, Cook A, Hunt H, Giunti P, Cipolotti L. 2010. A Preliminary Characterisation of Cognition and Social Cognition in Spinocerebellar Ataxia Types 2, 1, and 7. *Behav Neurol.* 23(1–2):17–29. <https://doi.org/10.1155/2010/395045>
- Song S, Tan J, Miao Y, Li M, Zhang Q. 2017. Crosstalk of autophagy and apoptosis: Involvement of the dual role of autophagy under ER stress. *J Cell Physiol.* 232(11):2977–2984. <https://doi.org/10.1002/jcp.25785>
- Sotelo C, Dusart I. 2009. Intrinsic versus extrinsic determinants during the development of Purkinje cell dendrites. *Neuroscience.* 162(3):589–600. <https://doi.org/10.1016/j.neuroscience.2008.12.035>
- Spandou E, Zanelli S, Taylor ML, Legido A, Mishra OP, Delivoria-Papadopoulos M, Katsetos CD. 1999. Effect of Hypoxia on the Expression of Inducible Nitric Oxide Synthase (iNOS) in the Brain of Term Fetal Guinea Pig. *Pediatr Res.* 45(4, Part 2 of 2):70A-70A. <https://doi.org/10.1203/00006450-199904020-00420>
- Späth M, Aichert I, Timmann D, Ceballos-Baumann AO, Wagner-Sonntag E, Ziegler W. 2022. The role of the basal ganglia and cerebellum in adaptation to others' speech rate and rhythm: A study of patients with Parkinson's disease and cerebellar degeneration. *Cortex.* 157:81–98. <https://doi.org/10.1016/j.cortex.2022.08.012>
- Spemann H, Mangold H. 2001. Induction of embryonic primordia by implantation of organizers from a different species. 1923. *Int J Dev Biol.* 45(1):13–38.

- Srinivasan L, Allsop J, Counsell SJ, Boardman JP, Edwards AD, Rutherford M. 2006. Smaller cerebellar volumes in very preterm infants at term-equivalent age are associated with the presence of supratentorial lesions. *AJNR Am J Neuroradiol.* 27(3):573–579.
- Standring S, editor. 2016. Gray's anatomy: the anatomical basis of clinical practice. Forty-first edition. New York: Elsevier Limited.
- Stock C, Teyssier G, Pichot V, Goffaux P, Barthelemy J-C, Patural H. 2010. Autonomic dysfunction with early respiratory syncytial virus-related infection. *Auton Neurosci.* 156(1–2):90–95. <https://doi.org/10.1016/j.autneu.2010.03.012>
- Stokowski LA. 2005. A PRIMER ON APNEA OF PREMATURITY. *Adv Neonatal Care.* 5(3):155–170. <https://doi.org/10.1016/j.adnc.2005.02.010>
- Stoodley CJ. 2016. The Cerebellum and Neurodevelopmental Disorders. *The Cerebellum.* 15(1):34–37. <https://doi.org/10.1007/s12311-015-0715-3>
- Stoodley CJ, Schmahmann JD. 2018. Functional topography of the human cerebellum. In: *Handb Clin Neurol [Internet].* Vol. 154. [place unknown]: Elsevier; [accessed 2022 Apr 29]; p. 59–70. <https://doi.org/10.1016/B978-0-444-63956-1.00004-7>
- Strahlendorf JC, Hubbard GD. 1983. Serotonergic interactions with rat cerebellar Purkinje cells. *Brain Res Bull.* 11(2):265–269. [https://doi.org/10.1016/0361-9230\(83\)90202-2](https://doi.org/10.1016/0361-9230(83)90202-2)
- Subashini C, Dhanesh SB, Chen C-M, Riya PA, Meera V, Divya TS, Kuruvilla R, Buttler K, James J. 2017. Wnt5a is a crucial regulator of neurogenesis during cerebellum development. *Sci Rep.* 7(1):42523. <https://doi.org/10.1038/srep42523>
- Sudarov A, Joyner AL. 2007. Cerebellum morphogenesis: the foliation pattern is orchestrated by multi-cellular anchoring centers. *Neural Develop.* 2(1):26. <https://doi.org/10.1186/1749-8104-2-26>
- Sudarov A, Turnbull RK, Kim EJ, Lebel-Potter M, Guillemot F, Joyner AL. 2011. Ascl1 Genetics Reveals Insights into Cerebellum Local Circuit Assembly. *J Neurosci.* 31(30):11055–11069. <https://doi.org/10.1523/JNEUROSCI.0479-11.2011>
- Sultan F, Bower JM. 1998. Quantitative Golgi study of the rat cerebellar molecular layer interneurons using principal component analysis. *J Comp Neurol.* 393(3):353–373. [https://doi.org/10.1002/\(SICI\)1096-9861\(19980413\)393:3<353::AID-CNE7>3.0.CO;2-0](https://doi.org/10.1002/(SICI)1096-9861(19980413)393:3<353::AID-CNE7>3.0.CO;2-0)
- Supple WF, Leaton RN, Fanselow MS. 1987. Effects of cerebellar vermal lesions on species-specific fear responses, neophobia, and taste-aversion learning in rats. *Physiol Behav.* 39(5):579–586. [https://doi.org/10.1016/0031-9384\(87\)90156-9](https://doi.org/10.1016/0031-9384(87)90156-9)
- Tabacaru CR, Moores RR, Khoury J, Rozycki HJ. 2019. NAVA—synchronized compared to nonsynchronized noninvasive ventilation for apnea, bradycardia, and desaturation events in VLBW infants. *Pediatr Pulmonol.* 54(11):1742–1746. <https://doi.org/10.1002/ppul.24464>
- Tacyildiz AE, Bilgin B, Gungor A, Ucer M, Karadag A, Tanriover N. 2021. Dentate Nucleus: Connectivity-Based Anatomic Parcellation Based on Superior Cerebellar Peduncle Projections. *World Neurosurg.* 152:e408–e428. <https://doi.org/10.1016/j.wneu.2021.05.102>

REFERENCES

- Takayasu Y, Iino M, Takatsuru Y, Tanaka K, Ozawa S. 2009. Functions of glutamate transporters in cerebellar Purkinje cell synapses. *Acta Physiol.* 197(1):1–12. <https://doi.org/10.1111/j.1748-1716.2009.02019.x>
- Tam WY, Wang X, Cheng ASK, Cheung K-K. 2021. In Search of Molecular Markers for Cerebellar Neurons. *Int J Mol Sci.* 22(4):1850. <https://doi.org/10.3390/ijms22041850>
- Taniguchi H, Kawauchi D, Nishida K, Murakami F. 2006. Classic cadherins regulate tangential migration of precerebellar neurons in the caudal hindbrain. *Development.* 133(10):1923–1931. <https://doi.org/10.1242/dev.02354>
- Tellios V, Maksoud MJE, Lu W. 2022. The expression and function of glutamate aspartate transporters in Bergmann glia are decreased in neuronal nitric oxide SYNTHASE-KNOCKOUT mice during postnatal development. *Glia.* 70(5):858–874. <https://doi.org/10.1002/glia.24143>
- Thach BT. 2008. Some aspects of clinical relevance in the maturation of respiratory control in infants. *J Appl Physiol.* 104(6):1828–1834. <https://doi.org/10.1152/japplphysiol.01288.2007>
- Thelen K, Kedar V, Panicker AK, Schmid R-S, Midkiff BR, Maness PF. 2002. The Neural Cell Adhesion Molecule L1 Potentiates Integrin-Dependent Cell Migration to Extracellular Matrix Proteins. *J Neurosci.* 22(12):4918–4931. <https://doi.org/10.1523/JNEUROSCI.22-12-04918.2002>
- Thomas A. 1898. Le Cervelet: Étude anatomique, clinique, et physiologique. Par le Dr. André Thomas, Ancien Interne des Hôpitaux de Paris. (Travail du Laboratoire du Dr. Déjerine Hospice de la Salpêtrière.) Paris: G. Steinheil, Éditeur, 1897, pp. 356. Price 14 fr. *J Ment Sci.* 44(186):578–581. <https://doi.org/10.1192/bj.p.44.186.578>
- Thornton C, Hagberg H. 2015. Role of mitochondria in apoptotic and necroptotic cell death in the developing brain. *Clin Chim Acta.* 451:35–38. <https://doi.org/10.1016/j.cca.2015.01.026>
- Torriero S, Oliveri M, Koch G, Gerfo EL, Salerno S, Petrosini L, Caltagirone C. 2007. Cortical networks of procedural learning: Evidence from cerebellar damage. *Neuropsychologia.* 45(6):1208–1214. <https://doi.org/10.1016/j.neuropsychologia.2006.10.007>
- Tracy JL, Faro SS, Mohammed FB, Pinus AB, Madi SM, Laskas JW. 2001. Cerebellar mediation of the complexity of bimanual compared to unimanual movements. *Neurology.* 57(10):1862–1869. <https://doi.org/10.1212/WNL.57.10.1862>
- Turner CP, Seli M, Ment L, Stewart W, Yan H, Johansson B, Fredholm BB, Blackburn M, Rivkees SA. 2003. A₁ adenosine receptors mediate hypoxia-induced ventriculomegaly. *Proc Natl Acad Sci.* 100(20):11718–11722. <https://doi.org/10.1073/pnas.1931975100>
- Uusisaari MY, Knöpfel T. 2012. Diversity of Neuronal Elements and Circuitry in the Cerebellar Nuclei. *The Cerebellum.* 11(2):420–421. <https://doi.org/10.1007/s12311-011-0350-6>
- Uusisaari MY, Knöpfel T. 2013. Neurons of the Deep Cerebellar Nuclei. In: Manto M, Schmahmann JD, Rossi F, Gruol DL, Koibuchi N, editors. *Handb Cerebellum Cerebellar Disord [Internet].* Dordrecht: Springer Netherlands; [accessed 2022 Sep 26]; p. 1101–1110. https://doi.org/10.1007/978-94-007-1333-8_46
- Van Overwalle F, Baetens K, Mariën P, Vandekerckhove M. 2014. Social cognition and the cerebellum: A meta-analysis of over 350 fMRI studies. *NeuroImage.* 86:554–572. <https://doi.org/10.1016/j.neuroimage.2013.09.033>

- Van Overwalle F, Manto M, Cattaneo Z, Clausi S, Ferrari C, Gabrieli JDE, Guell X, Heleven E, Lupo M, Ma Q, et al. 2020. Consensus Paper: Cerebellum and Social Cognition. *The Cerebellum*. 19(6):833–868. <https://doi.org/10.1007/s12311-020-01155-1>
- Vervaeke K, Lőrincz A, Gleeson P, Farinella M, Nusser Z, Silver RA. 2010. Rapid Desynchronization of an Electrically Coupled Interneuron Network with Sparse Excitatory Synaptic Input. *Neuron*. 67(3):435–451. <https://doi.org/10.1016/j.neuron.2010.06.028>
- Vieussens R. 1684. *Neurographia universalis: Hoc est, omnium corporis humani nervorum, simul & cerebri, medullaeque spinalis descriptio anatomica ...* [Internet]. [place unknown]: Certe. <https://books.google.fr/books?id=8N1fAAAAcAAJ>
- Vlasic V, Simakajornboon N, Gozal E, Gozal D. 2001. PDGF- β Receptor Expression in the Dorsocaudal Brainstem Parallels Hypoxic Ventilatory Depression in the Developing Rat. *Pediatr Res*. 50(2):236–241. <https://doi.org/10.1203/00006450-200108000-00012>
- Vogenstahl J, Parrilla M, Acker-Palmer A, Segarra M. 2022. Vascular Regulation of Developmental Neurogenesis. *Front Cell Dev Biol*. 10:890852. <https://doi.org/10.3389/fcell.2022.890852>
- Vogt KE, Canepari M. 2010. On the Induction of Postsynaptic Granule Cell–Purkinje Neuron LTP and LTD. *The Cerebellum*. 9(3):284–290. <https://doi.org/10.1007/s12311-010-0174-9>
- Volpe JJ. 2009. Cerebellum of the Premature Infant: Rapidly Developing, Vulnerable, Clinically Important. *J Child Neurol*. 24(9):1085–1104. <https://doi.org/10.1177/0883073809338067>
- Voogd J, Koehler PJ. 2018. Historic notes on anatomic, physiologic, and clinical research on the cerebellum. In: *Handb Clin Neurol* [Internet]. Vol. 154. [place unknown]: Elsevier; [accessed 2022 Sep 23]; p. 3–26. <https://doi.org/10.1016/B978-0-444-63956-1.00001-1>
- Voogd J, Shinoda Y, Ruigrok TJH, Sugihara I. 2013. Cerebellar Nuclei and the Inferior Olivary Nuclei: Organization and Connections. In: Manto M, Schmahmann JD, Rossi F, Gruol DL, Koibuchi N, editors. *Handb Cerebellum Cerebellar Disord* [Internet]. Dordrecht: Springer Netherlands; [accessed 2022 Sep 26]; p. 377–436. https://doi.org/10.1007/978-94-007-1333-8_19
- Vuillier F, Medeiros de Bustos É, Tatu L. 2011. Organisation fonctionnelle du cervelet : approche neuro-anatomique. *Rev Neurol (Paris)*. 167(5):361–369. <https://doi.org/10.1016/j.neurol.2010.07.045>
- Wahl DR, Dresser J, Wilder-Romans K, Parsels JD, Zhao SG, Davis M, Zhao L, Kachman M, Wernisch S, Burant CF, et al. 2017. Glioblastoma Therapy Can Be Augmented by Targeting IDH1-Mediated NADPH Biosynthesis. *Cancer Res*. 77(4):960–970. <https://doi.org/10.1158/0008-5472.CAN-16-2008>
- Wallace VA. 1999. Purkinje-cell-derived Sonic hedgehog regulates granule neuron precursor cell proliferation in the developing mouse cerebellum. *Curr Biol*. 9(8):445–448. [https://doi.org/10.1016/S0960-9822\(99\)80195-X](https://doi.org/10.1016/S0960-9822(99)80195-X)
- Wang H-F, Wang Z-Q, Ding Y, Piao M-H, Feng C-S, Chi G-F, Luo Y-N, Ge P-F. 2018. Endoplasmic reticulum stress regulates oxygen-glucose deprivation-induced parthanatos in human SH-SY5Y cells via improvement of intracellular ROS. *CNS Neurosci Ther*. 24(1):29–38. <https://doi.org/10.1111/cns.12771>
- Wang L, Zhang ZG, Zhang RL, Gregg SR, Hozeska-Solgot A, LeTourneau Y, Wang Y, Chopp M. 2006. Matrix Metalloproteinase 2 (MMP2) and MMP9 Secreted by Erythropoietin-Activated Endothelial

REFERENCES

- Cells Promote Neural Progenitor Cell Migration. *J Neurosci.* 26(22):5996–6003. <https://doi.org/10.1523/JNEUROSCI.5380-05.2006>
- Wang Y, Branicky R, Noë A, Hekimi S. 2018. Superoxide dismutases: Dual roles in controlling ROS damage and regulating ROS signaling. *J Cell Biol.* 217(6):1915–1928. <https://doi.org/10.1083/jcb.201708007>
- Wang Y, Zhang X, Tian J, Shan J, Hu Y, Zhai Y, Guo J. 2019. Talin promotes integrin activation accompanied by generation of tension in talin and an increase in osmotic pressure in neurite outgrowth. *FASEB J.* 33(5):6311–6326. <https://doi.org/10.1096/fj.201801949RR>
- Watanabe D, Nakanishi S. 2003. mGluR2 Postsynaptically Senses Granule Cell Inputs at Golgi Cell Synapses. *Neuron.* 39(5):821–829. [https://doi.org/10.1016/S0896-6273\(03\)00530-0](https://doi.org/10.1016/S0896-6273(03)00530-0)
- Watanabe M, Kano M. 2011. Climbing fiber synapse elimination in cerebellar Purkinje cells: Climbing fiber synapse elimination. *Eur J Neurosci.* 34(10):1697–1710. <https://doi.org/10.1111/j.1460-9568.2011.07894.x>
- Wen J, Yang H-B, Zhou B, Lou H-F, Duan S. 2013. β -Catenin Is Critical for Cerebellar Foliation and Lamination. Sugihara I, editor. *PLoS ONE.* 8(5):e64451. <https://doi.org/10.1371/journal.pone.0064451>
- White R, Gatzke-Kopp LM, Ryan PJ, Lydon-Staley DM. 2019. The association between perinatal hypoxia exposure and externalizing symptoms and children's decision making in conditions of uncertainty is moderated by DRD2 genotype. *Dev Psychobiol.* 61(1):56–68. <https://doi.org/10.1002/dev.21785>
- Wilson CG, Martin RJ, Jaber M, Abu-Shaweesh J, Jafri A, Haxhiu MA, Zaidi S. 2004. Adenosine A2A receptors interact with GABAergic pathways to modulate respiration in neonatal piglets. *Respir Physiol Neurobiol.* 141(2):201–211. <https://doi.org/10.1016/j.resp.2004.04.012>
- Wilson PM, Fryer RH, Fang Y, Hatten ME. 2010. *Astn2*, A Novel Member of the Astrotactin Gene Family, Regulates the Trafficking of *ASTN1* during Glial-Guided Neuronal Migration. *J Neurosci.* 30(25):8529–8540. <https://doi.org/10.1523/JNEUROSCI.0032-10.2010>
- Winter DJ. 2017. *rentrez*: An R package for the NCBI eUtils API. 9.
- Wizeman JW, Guo Q, Wilion EM, Li JY. 2019. Specification of diverse cell types during early neurogenesis of the mouse cerebellum. *eLife.* 8:e42388. <https://doi.org/10.7554/eLife.42388>
- Wolpert DM, Miall RC, Kawato M. 1998. Internal models in the cerebellum. *Trends Cogn Sci.* 2(9):338–347. [https://doi.org/10.1016/S1364-6613\(98\)01221-2](https://doi.org/10.1016/S1364-6613(98)01221-2)
- Wolterink-Donselaar IG, Meerding JM, Fernandes C. 2009. A method for gender determination in newborn dark pigmented mice. *Lab Anim.* 38(1):35–38. <https://doi.org/10.1038/laban0109-35>
- Wu J, Chen Y, Yu S, Li L, Zhao X, Li Q, Zhao J, Zhao Y. 2017. Neuroprotective effects of sulfiredoxin-1 during cerebral ischemia/reperfusion oxidative stress injury in rats. *Brain Res Bull.* 132:99–108. <https://doi.org/10.1016/j.brainresbull.2017.05.012>
- Wylie DR, Gutiérrez-Ibáñez C, Gaede AH, Altshuler DL, Iwaniuk AN. 2018. Visual-Cerebellar Pathways and Their Roles in the Control of Avian Flight. *Front Neurosci.* 12:223. <https://doi.org/10.3389/fnins.2018.00223>

- Xie X, Chen X, Sun P, Cao A, Zhuang Y, Xiong X, Yang C. 2021. Kangaroo Mother Care Reduces Noninvasive Ventilation and Total Oxygen Support Duration in Extremely Low Birth Weight Infants. *Am J Perinatol.* 38(08):791–795. <https://doi.org/10.1055/s-0039-3402717>
- Xu H, Yang Y, Tang X, Zhao M, Liang F, Xu P, Hou B, Xing Y, Bao X, Fan X. 2013. Bergmann Glia Function in Granule Cell Migration During Cerebellum Development. *Mol Neurobiol.* 47(2):833–844. <https://doi.org/10.1007/s12035-013-8405-y>
- Xu J, Li Q, Xu C-Y, Mao S, Jin J-J, Gu W, Shi Y, Zou C-F, Ye L. 2022. Obstructive sleep apnea aggravates neuroinflammation and pyroptosis in early brain injury following subarachnoid hemorrhage via ASC/HIF-1 α pathway. *Neural Regen Res.* 17(11):2537. <https://doi.org/10.4103/1673-5374.339000>
- Xu L, Bi Y, Xu Y, Wu Y, Du X, Mou Y, Chen J. 2021. Suppression of CHOP Reduces Neuronal Apoptosis and Rescues Cognitive Impairment Induced by Intermittent Hypoxia by Inhibiting Bax and Bak Activation. Peña-Ortega F, editor. *Neural Plast.* 2021:1–14. <https://doi.org/10.1155/2021/4090441>
- Xu L, Li Q, Ke Y, Yung W-H. 2022. Chronic Intermittent Hypoxia-Induced Aberrant Neural Activities in the Hippocampus of Male Rats Revealed by Long-Term *in vivo* Recording. *Front Cell Neurosci.* 15:784045. <https://doi.org/10.3389/fncel.2021.784045>
- Xu W, Chi L, Row BW, Xu R, Ke Y, Xu B, Luo C, Kheirandish L, Gozal D, Liu R. 2004. Increased oxidative stress is associated with chronic intermittent hypoxia-mediated brain cortical neuronal cell apoptosis in a mouse model of sleep apnea. *Neuroscience.* 126(2):313–323. <https://doi.org/10.1016/j.neuroscience.2004.03.055>
- Yacubova E, Komuro H. 2002. Cellular and Molecular Mechanisms of Cerebellar Granule Cell Migration. *Cell Biochem Biophys.* 37(3):213–234. <https://doi.org/10.1385/CBB:37:3:213>
- Yakusheva TA, Shaikh AG, Green AM, Blazquez PM, Dickman JD, Angelaki DE. 2007. Purkinje Cells in Posterior Cerebellar Vermis Encode Motion in an Inertial Reference Frame. *Neuron.* 54(6):973–985. <https://doi.org/10.1016/j.neuron.2007.06.003>
- Yamada K, Watanabe M. 2002. Cytodifferentiation of Bergmann glia and its relationship with Purkinje cells. *Anat Sci Int.* 77(2):94–108. <https://doi.org/10.1046/j.0022-7722.2002.00021.x>
- Yamanaka H, Yanagawa Y, Obata K. 2004. Development of stellate and basket cells and their apoptosis in mouse cerebellar cortex. *Neurosci Res.* 50(1):13–22. <https://doi.org/10.1016/j.neures.2004.06.008>
- Yang X-S, Yi T-L, Zhang S, Xu Z-W, Yu Z-Q, Sun H-T, Yang C, Tu Y, Cheng S-X. 2017. Hypoxia-inducible factor-1 alpha is involved in RIP-induced necroptosis caused by *in vitro* and *in vivo* ischemic brain injury. *Sci Rep.* 7(1):5818. <https://doi.org/10.1038/s41598-017-06088-0>
- Yeung J. 2017. The role of Pax6 and WIs in rhombic lip compartmentation and cerebellar development [Internet]. [accessed 2023 Jan 24]. <https://doi.org/10.14288/1.0340490>
- Yeung J, Ha TJ, Swanson DJ, Goldowitz D. 2016. A Novel and Multivalent Role of Pax6 in Cerebellar Development. *J Neurosci.* 36(35):9057–9069. <https://doi.org/10.1523/JNEUROSCI.4385-15.2016>
- Yong Y, Meng Y, Ding H, Fan Z, Tang Y, Zhou C, Luo J, Ke Z-J. 2015. PACT/RAX Regulates the Migration of Cerebellar Granule Neurons in the Developing Cerebellum. *Sci Rep.* 5(1):7961. <https://doi.org/10.1038/srep07961>

REFERENCES

- Young JK, Dreshaj IA, Wilson CG, Martin RJ, Zaidi SIA, Haxhiu MA. 2005. An astrocyte toxin influences the pattern of breathing and the ventilatory response to hypercapnia in neonatal rats. *Respir Physiol Neurobiol.* 147(1):19–30. <https://doi.org/10.1016/j.resp.2005.01.009>
- Yuasa S. 1996. Bergmann glial development in the mouse cerebellum as revealed by tenascin expression. *Anat Embryol (Berl)* [Internet]. [accessed 2023 Feb 2] 194(3). <https://doi.org/10.1007/BF00187133>
- Yuasa S, Kitoh J, Oda S, Kawamura K. 1993. Obstructed migration of Purkinje cells in the developing cerebellum of the reeler mutant mouse. *Anat Embryol (Berl)* [Internet]. [accessed 2023 Jan 1] 188(4). <https://doi.org/10.1007/BF00185941>
- Zagol K, Lake DE, Vergales B, Moorman ME, Paget-Brown A, Lee H, Rusin CG, Delos JB, Clark MT, Moorman JR, Kattwinkel J. 2012. Anemia, Apnea of Prematurity, and Blood Transfusions. *J Pediatr.* 161(3):417-421.e1. <https://doi.org/10.1016/j.jpeds.2012.02.044>
- Zagon IS, McLaughlin PJ, Smith S. 1977. Neural populations in the human cerebellum: estimations from isolated cell nuclei. *Brain Res.* 127(2):279–282. [https://doi.org/10.1016/0006-8993\(77\)90541-8](https://doi.org/10.1016/0006-8993(77)90541-8)
- Zaragoza-Campillo MA, Morán J. 2017. Reactive Oxygen Species Evoked by Potassium Deprivation and Staurosporine Inactivate Akt and Induce the Expression of TXNIP in Cerebellar Granule Neurons. *Oxid Med Cell Longev.* 2017:1–13. <https://doi.org/10.1155/2017/8930406>
- Zecevic N, Rakic P. 1976. Differentiation of Purkinje cells and their relationship to other components of developing cerebellar cortex in man. *J Comp Neurol.* 167(1):27–47. <https://doi.org/10.1002/cne.901670103>
- Zhang C-Q, Yi S, Chen B-B, Cui P-P, Wang Y, Li Y-Z. 2021. mTOR/NF- κ B signaling pathway protects hippocampal neurons from injury induced by intermittent hypoxia in rats. *Int J Neurosci.* 131(10):994–1003. <https://doi.org/10.1080/00207454.2020.1766460>
- Zhang H, Bosch-Marce M, Shimoda LA, Tan YS, Baek JH, Wesley JB, Gonzalez FJ, Semenza GL. 2008. Mitochondrial Autophagy Is an HIF-1-dependent Adaptive Metabolic Response to Hypoxia. *J Biol Chem.* 283(16):10892–10903. <https://doi.org/10.1074/jbc.M800102200>
- Zhang L, Cao Y, Guo X, Wang X, Han X, Kanwore K, Hong X, Zhou H, Gao D. 2023. Hypoxia-induced ROS aggravate tumor progression through HIF-1 α -SERPINE1 signaling in glioblastoma. *J Zhejiang Univ-Sci B.* 24(1):32–49. <https://doi.org/10.1631/jzus.B2200269>
- Zhang L, Wilson CG, Liu S, Haxhiu MA, Martin RJ. 2003. Hypercapnia-induced activation of brainstem GABAergic neurons during early development. *Respir Physiol Neurobiol.* 136(1):25–37. [https://doi.org/10.1016/S1569-9048\(03\)00041-7](https://doi.org/10.1016/S1569-9048(03)00041-7)
- Zhang X, Gao R, Li Juan, Qi Y, Song X, Zhao L, Wang H, Pu Y, Xu K, Li Jinhua. 2010. A Pharmacological Activator of AMP-Activated Protein Kinase Protects Hypoxic Neurons in a Concentration-Dependent Manner. *Neurochem Res.* 35(8):1281–1289. <https://doi.org/10.1007/s11064-010-0186-3>
- Zhang X-Y, Wang J-J, Zhu J-N. 2016. Cerebellar fastigial nucleus: from anatomic construction to physiological functions. *Cerebellum Ataxias.* 3(1):9. <https://doi.org/10.1186/s40673-016-0047-1>
- Zhao J, Gonzalez F, Mu D. 2011. Apnea of prematurity: from cause to treatment. *Eur J Pediatr.* 170(9):1097–1105. <https://doi.org/10.1007/s00431-011-1409-6>

- Zhu C, Liu Y, Guan Z, Zhou Y, Liu F, Zhang T. 2018. Hypoxia-reoxygenation induced necroptosis in cultured rat renal tubular epithelial cell line. *Iran J Basic Med Sci* [Internet]. [accessed 2023 Apr 11] (Online First). <https://doi.org/10.22038/ijbms.2018.26276.6444>
- Zimmerman KD, Espeland MA, Langefeld CD. 2021. A practical solution to pseudoreplication bias in single-cell studies. *Nat Commun.* 12(1):738. <https://doi.org/10.1038/s41467-021-21038-1>
- Zinni M, Mairesse J, Pansiot J, Fazio F, Iacovelli L, Antenucci N, Orlando R, Nicoletti F, Vaiman D, Baud O. 2021. mGlu3 receptor regulates microglial cell reactivity in neonatal rats. *J Neuroinflammation.* 18(1):13. <https://doi.org/10.1186/s12974-020-02049-z>
- Zong W-X, Thompson CB. 2006. Necrotic death as a cell fate. *Genes Dev.* 20(1):1–15. <https://doi.org/10.1101/gad.1376506>
- Zorov DB, Juhaszova M, Sollott SJ. 2014. Mitochondrial Reactive Oxygen Species (ROS) and ROS-Induced ROS Release. *Physiol Rev.* 94(3):909–950. <https://doi.org/10.1152/physrev.00026.2013>

REFERENCES

APPENDICES

Appendix 1: Oxidative Stress panel

Appendix 2: Neurodevelopment panel

Appendix 3: Vascularization panel

Appendix 4: Statistical results of the OS panel on the whole cerebellum

Appendix 5: Statistical results of the OS panel on Purkinje cells

Appendix 6: Statistical results of the neurodevelopment panel on cerebellar layer

Appendix 7: Statistical results of the vascularization panel on the whole cerebellum

Gene	Gene name	Putative function	NCBI reference	Forward primer	Reverse primer
Antioxidant Response					
Ccs	copper chaperone for superoxide dismutase	Cu delivery	NM_016892.3	TCAAGGGTATGGGCAGTAGC	CACAGCCCTCCAGAAATGG
Fth1	ferritin, heavy polypeptide 1	iron storage	NM_010239.2	ACCGTGTCCCAGGGTGTGCTT	ACCGTGTCCCAGGGTGTGCTT
Hmox1	heme oxygenase (decycling) 1	heme reduction	NM_010442.2	TCGAGCATAGCCGGAGCCT	AATCCTGGGCATGCTGTCGG
Idh1	isocitrate dehydrogenase 1 (NADP+), soluble	NADPH regeneration	NM_001111320 .1	CATTCTGGTGGACTGTCTT	TATGCATGTCGGCCAATGA
Mapk14	mitogen-activated protein kinase 14	cell signalling	NM_001168508 .1	GTTGGAACCCCAGGGGCTGAG	GTCGACAGCCAGGGGATTGGC
Nfe2l2	nuclear factor, erythroid 2-like 2	transcription factor	NM_010902.3	TTTCGACTACGCAGTGACGG	GAGCGTGGAGGTGGATGATG
Park7	parkinson protein 7	redox-sensitive chaperone	NM_020569.3	TGGGTACACGTCGGGTGCGA	TTAAAGACTGCAGCCGCGCCTC
Psmb5	proteasome subunit, beta type, 5	protein degradation	NM_011186.1	GCTCGGCAGTGTCAATCTAT	GCCCCATGCCTTGACTGA
Apoptotic Pathways					
Adcyap1	adenylate cyclase activating polypeptide 1	adenylate cyclase ativation	NM_009625.2	GATGCTTCTGGGTTGTGAT	GGTCATTGGTGTCTAGGAAAGG
Bax	BCL2-associated X protein	apoptosis	NM_007527.3	GTGAGCGGCTGCTTGCT	GGTCCCGAAGTAGGAGAGGA
Bcl2	B-cell CLL/lymphoma 2	apoptosis blockage	NM_009741.4	GTACCTGAACCGGCATCTG	GGGGCCATATAAGTCCACAA
Casp3	caspase 3, apoptosis-related cysteine peptidase	apoptosis	NM_001284409 .1	GAGGCTGACTTCCTGTATGCTT	AACCACGACCCGTCTTT
Casp9	caspase 9, apoptosis-related cysteine peptidase	apoptosis	NM_001277932 .1	TGCAGTCCCTCCTTCTAG	GCTTTTCCGGAGGAAGTTAAA
Gab1	GRB2-associated binding protein 1	tubulogenesis	NM_021356.2	CACGCCACCACGGAAGCAAAAG	CTGCCTCCCATCCGTCCAAGC
Hif1a	hypoxia inducible factor 1, alpha subunit	hypoxia response	NM_010431.2	GTGCACCTAACAAAGCCGGGG	CCGTGCAGTGAAGCACCTCCA
Slc41a3	solute carrier family 41, member 3	amino acid transporter	NM_001037493 .2	TGTTAAAGACCTGATGACGTTGGT	GTCATCGATTGCCAGTGTT
Tmod	tropomodulin 1	actin binding	NM_021883.2	ACAGCCTCACACAATGTCCTACAGA	GCAGGGAGCAGTGCATTATCAGGG
Autophagy and Mitophagy					
Apc	adenomatous polyposis coli	cell signalling	NM_007462.3	GGAGTGGCAGAAAGCAACAC	CCACACGTGTAGCTGGACTC
Ctsb	cathepsin B	protein degradation	NM_007798.3	GTGTCTGCTGAAGACCTGCTT	GGGATAGCCACCATTACAGC
Dnm2	dynamin 2	endocytosis	NM_001039520 .2	TGGCAGCCGAGAGGAAATT	TCAGTTGCTGGTCAGGGTTTT
Hspa5	heat shock 70kDa protein 5	ER assembly	NM_001163434 .1	AGCGACAAGCAACCAAAGAT	CAGCTGCTGTAGGCTATTG

Gene	Gene name	Putative function	NCBI reference	Forward primer	Reverse primer
Jun	jun proto-oncogene	transcription factor	NM_010591.2	CCAGAAGATGGTGTGGTGT	CTGACCCTCTCCCCTTC
Kif9	kinesin family member 9	ATP binding	NM_001163569.1	GCCTCCCAGGACTGGTTAT	TCTCCGTTGCCCTGTCA
Mapk10	mitogen-activated protein kinase 10	cell signalling	NM_001081567.1	TCGCCTTCAGGTGCAGCAGTG	AACAACCCAACGGTCCGCC
Parp1	poly (ADP-ribose) polymerase 1	DNA damages	NM_007415.2	CTATAGTCTTCAGGGGTG	TCTCTGTCAACCACCTTAAT
Cell Death and Protection					
Adh5	alcohol dehydrogenase 5	alcohol metabolism	NM_001288578.1	AATTGTGACCGGAATCTC	CAGTCGAATGCTGTCTCC
Apex1	APEX nuclease (multifunctional DNA repair enzyme) 1	DNA base excision repair	NM_009687.2	ACAGCCTATGTTCCAATGC	CCCCACATAGCACTAGAGGC
Aqr	aquarius intron-binding spliceosomal factor	RNA splicing	NM_001290788.1	ACAGAGAACGAGATGACCACGAT	CCACATTGGAGAGGGCAAAG
Atr	ataxia telangiectasia and Rad3 related	DNA damages repair	NM_019864.1	GGAGAGTCACGACTTGCTGA	ACAATAAGCGCTGGTGAAC
Ehd2	EH-Domain Containing 2	membrane reorganization	NM_153068.3	GAGACTTCCTGACTGGAGA	TAGCGAGTGGAACTTGGTTGA
Ercc2	excision repair cross-complementing 2	nucleotide excision repair	NM_007949.4	GACCAGTTCCAGATCCGAGAGA	TCAGCAAAGACCATGAGTCATA
Ift172	intraflagellar transport 172 homolog	cell signalling	NM_026298.5	AGCAGTGGCTGATGGAG	GAGGCAGGAACTTGATGGAC
Map2k1	mitogen-activated protein kinase kinase 1	cell signalling	NM_008927.3	GCGCGCTCCCTGCTGAGTTG	AGGCCTCCAGGTTGGTCTCGG
Mapk8	mitogen-activated protein kinase 8	cell signalling	NM_016700.4	GGCAGCCGTCTCCTTAGCACAG	TGACAGACGGCGAAGACGATGGA
Nudt15	nudix (nucleoside diphosphate linked moiety X)-type motif 15	8-oxo-dGTP degradation	NM_172527.2	CCGAGGAATATGGAGCCTGAA	TGGGTCTAACCTGCTTTTGA
Ppp1r15b	protein phosphatase 1, regulatory subunit 15B	dephosphorylation	NM_133819.3	TGCTGGAGAAAGATAACACCCATA	AATTCTCCATGGTCCTTG
Rheb	Ras homolog enriched in brain	cell cycle progression	NM_053075.3	ACCTGCATATGGAAAGGGTG	AAAAAGCTGCATTCCAAGATT
Slc38a1	solute carrier family 38, member 1	amino acid transporter	NM_001166456.1	GGCGTGTGAATGGGTCTCAGGC	GCTCCGTTAGCTCGAGGCCACT
Sp1	specific protein 1	transcription factor	NM_013672.2	GCTGCCACCATGAGCGACCAA	CACCGCCACCATTGCCGCTA
Xrcc1	X-ray repair complementing defective repair in Chinese hamster cells 1	DNA single break repair	NM_009532.4	TACATCTCAGAAGGTGACAGT	CTGATGACGTCTGTTGATA

Gene	Gene name	Putative function	NCBI reference	Forward primer	Reverse primer
Inflammation Pathways					
Aldh1a1	aldehyde dehydrogenase 1 family	alcohol metabolism	NM_013467.3	TATGATGTTGTAGGCCAGTG	CCATGTTCACCCAGTTCTCTT
Apoe	apolipoprotein E	inflammatory process	NM_009696.3	GCTCAGACCCCTGGAGGCTAA	CTCGGCTAGGCATCCTGTCA
Aqp4	aquaporin 4	water channel	NM_009700.2	AGCAATTGGATTTCCGTTG	AATATATCCAGTGGTTGCCA
Ercc6	excision repair cross-complementing 6	nucleotide excision repair	NM_001081221.1	ATGCCAGCCTAGAGGAGGA	GCATGAGCATACTGCCAAGA
Jak1	janus kinase 1	interferron signaling	NM_146145.2	GTGAGCACCTGGCAGAGGCAC	AGAAGGCCAGAGAGATGTCCC GGT
Map2k6	mitogen-activated protein kinase kinase 6	cell signalling	NM_011943.2	GCTGGGACGAGGTGCGTACG	GCCCCGTATCCGCTTCACTGCC
Mapk1	mitogen-activated protein kinase 1	cell signalling	NM_001038663.1	TTGGTCAGGACAAGGGCTCAGAGA	GCTGAGACGGGCTGAAGACAGG
Mapk3	mitogen-activated protein kinase 3	cell signalling	NM_011952.2	AGATGAGCCAGTGGCGAGGAG	CTGGCTGGAAGCGGGCTGTCT
Mt1	metallothionein 1	heavy metal binding	NM_013602.3	CACCTCCTGCAAGAACAGAGCTGCTG	CAGCACGTGCACTTGTCCGC
Mt2	metallothionein 2	heavy metal binding	NM_008630.2	CTGTGCCCTCGATGGATCCTGCT	AGCCCTGGGAGCACTTCGCA
Nfkbia	nuclear factor of kappa light polypeptide gene enhancer in B-cells 1)	transcription factor	NM_008689.2	GGCTACGTCACTGAGGATGGGAA	GCAGGGCTGTTGGCTAGGT
Nfkbb	nuclear factor of kappa light polypeptide gene enhancer in B-cells inhibitor, beta	transcription factor	NM_010908.4	CATCAGGCACCCAAGTT	CAGCAGCATGTTGGACACA
Ptgs1	prostaglandin-endoperoxide synthase 1	anti-inflammatory process	NM_008969.4	TGCCCTCACAGTCATCC	GTAGCCCGTGCAGTACAATC
Rela	v-rel avian reticuloendotheliosis viral oncogene homolog A	transcription factor	NM_009045.4	GCCAGACACAGATGATGCC	GAGTTCGGGTAGGCACAGC
ROS Production					
Cox4i1	cytochrome c oxidase subunit IV isoform 1	mitochondrial chain	NM_009941.2	TGTGCCTCGAGCACATGGGAG	GGCAAGGGTAGTCACGCCG
Hadhd	hydroxyacyl-CoA dehydrogenase	beta oxydation	NM_008212.4	AGGCTACAGAGCGAGGCGA	ACGGACCCATGGATACCCAGC
Ndufv2	NADH dehydrogenase (ubiquinone) flavoprotein 2	mitochondrial chain	NM_001278415.1	GCTATGAACAAGGTGGCTGAA	TCCCAACTGGTTTCGATTA
Nos1	nitric oxide synthase 1	NO metabolism	NM_008712.2	CCTGGAAGGATGGAAGAACG	CAGGCTGCTTGGAGCAAAA
Por	P450 (cytochrome) oxidoreductase	electron tranfert	NM_008898.1	GGCCCAAGGTCTATGTC	TCTTGGCCATATTCGAGC

Gene	Gene name	Putative function	NCBI reference	Forward primer	Reverse primer
Redox Enzymes					
Cat	catalase	H ₂ O ₂ conversion	NM_009804.2	GGAGGCCGGAAACCCAATA	CAAAGTGTGCCATCTCGTCAGT
Gpx1	glutathione peroxidase 1	H ₂ O ₂ detoxification	NM_008160.6	ACACCAGGAGAATGGCAAGAA	AACAATGAAAATTGGGCTGA A
Gpx3	glutathione peroxidase 3	H ₂ O ₂ detoxification	NM_008161.3	TCAAAGAACTGAATGCACTACAA GAA	TTCTCGCTGGCTCCTGTT
Gpx4	glutathione peroxidase 4	H ₂ O ₂ detoxification	NM_001037741 .3	GGGCCGTCTGAGCCGCTTAC	TCGCAGGATGCACACATGGT
Gpx7	glutathione peroxidase 7	DNA damage protection	NM_024198.3	GCCTTCAAGTACCTAACCCAGAC	TGCTCTGTAATACGGGGCTT
Gpx8	glutathione peroxidase 8	H ₂ O ₂ detoxification	NM_027127.2	AGATATTGAGTTTGCTCTCTA TGG	GGTTCTGGCTTCAGGAATT
Gsr	glutathione reductase	gluthation metabolism	NM_010344.4	GCCTTACCCGATGTATCA	AATGCCAACCACCTTCCT
Gss	glutathione synthetase	gluthation metabolism	NM_001291111 .1	CAGCTGTGCACCGACACGTTCT	GGCCAGTCCCTGCTGGGGT
Gstk1	glutathione S-transferase kappa 1	gluthation metabolism	NM_029555.2	AAGACAGCGGAAACCAACCA	AAGAACTGCTTCAGGAGAGGA ATC
Gstm1	glutathione S-transferase mu 1	gluthation metabolism	NM_010358.5	GGTCAGTCCTGCTGAAGCCAGTT	GGATCGGGTGTGTCAGCCGC
Nqo1	NAD(P)H dehydrogenase, quinone 1	detoxification	NM_008706.5	TCCCAGGTTGCCACATTCCA	TCCAGGGCAAGCGACTCATGGT C
Prdx1	peroxiredoxin 1	H ₂ O ₂ conversion	NM_011034.4	GTGAGACCTGTGGCTCGAC	TGTCCATCTGGCATAACAGC
Prdx2	peroxiredoxin 2	H ₂ O ₂ conversion	NM_011563.5	GGCTCTTGCTCACGCAGT	GAAGGCACCATCCACCCAC
Prdx3	peroxiredoxin 3	H ₂ O ₂ conversion	NM_007452.2	CTTTAGCACCAAGTTCTCTTCCA	GAECTCAGCTTTGAACCTCTCCA TT
Prdx4	peroxiredoxin 4	H ₂ O ₂ conversion	NM_016764.4	GACGAGACACTGCGTTGG	GCAGACTTCTCATGCTTGTC
Prdx5	peroxiredoxin 5	H ₂ O ₂ conversion	NM_012021.2	CGAGTCCTGGGCTGCAA	CACACTCCAACCTGCTTCTTT
Prdx6	peroxiredoxin 6	H ₂ O ₂ conversion	NM_007453.3	CCACCACGGGCAGGAA	GGGAACATACCATCACGCTCT
Sod1	superoxide dismutase 1	superoxide conversion	NM_011434.1	AAGCGGTGAACCAGTTGTGTT	CTGCACTGGTACAGCCTGTGT A
Sod2	superoxide dismutase 2	superoxide conversion	NM_013671.3	GCGCTGGAGCCACACATTA	GGTGGCGTTGAGATTGTTCA
Sod3	superoxide dismutase 3	superoxide conversion	NM_011435.3	GGGGAGGCAACTCAGAGG	TGGCTGAGGTTCTCTGCAC
Srxn1	sulfiredoxin 1	peroxiredoxin reduction	NM_029688.5	AGGGGCTCTGCAAACCTA	TGGCATAGCTACCTCACTGCT
Txnip	thioredoxin interacting protein	thioredoxin inhibition	NM_001009935 .2	GTGGCCGGACGGTAATAGT	CCTTGCATCCACAGGACCTT
Txnrd1	thioredoxin reductase 1	thioredoxin reduction	NM_001042513 .1	ACCGTGGCGTGAAAGATAAA	GATGTCACCGATGGCGTAGAT
Txnrd3	thioredoxin reductase 3	thioredoxin reduction	NM_001178058 .1	GTGAACGTAGGCTGTATTCCAAA GA	TTGTGCTTCACCTGCTGGTTATA

Gene	Gene name	Putative function	NCBI reference	Forward primer	Reverse primer
Fate Mapping					
Ascl1	Achaete-Scute Family BHLH Transcription Factor 1	DNA-binding transcription factor; chromatin binding; and sequence-specific DNA binding activity.	NM_008553.5	GTCCTCCCTTGATCGTGCTT	GAGTAGGACGAGACCGGAGA
Atoh2	neurogenic differentiation 6, Math2	DNA-binding transcription activator activity, RNA polymerase II-specific.	NM_009717.2	GATCTGCTCACGTTCGTCCA	CCAATTACGCAGCCCACAAG
Neurod 1	neurogenic differentiation 1	DNA-binding transcription activator activity, RNA polymerase II-specific.	NM_010894.3	CGCAGAAGGCAAGGTGTC	TTTGGTCATGTTCCACTTCC
Pax6	paired box gene 6, differentiation - sensitif	Regulator of transcription.	NM_001244198 .2	ATGTGATCGAGAGAGGAAATTGT G	AGTGCTTCTAACGCCATTCT
Zic1	zinc finger protein of the cerebellum 1	DNA-binding transcription activator activity, RNA polymerase II-specific.	NM_001376941 .1	CTACCTTGCAAGATGTGCGATAA	AGGACTCATGGACCTTCATGTGT
Guidance					
Cdh8	cadherin 8	Mediates cell adhesion and regulates many morphogenetic events during development.	NM_001285913	CGTGCAATGTTGAAGCTTATGTC	CAATGACGAGCAGCAAATGA
L1cam	L1 cell adhesion molecule	Identical protein; integrin binding activity; and sialic acid binding activity.	NM_008478	CCTGCTGACTTGGGATCGA	GTAGCGGGTGGTAAGAAAGAGA CT
Nav3	neuron navigator 3	Microtubule binding activity.	NM_001081035	TTTCCTCCCTCATGTTATCTT	CCAGATCAGCGCTCTTAATG
Nxph4	neurexophilin 4	Predicted to enable signaling receptor binding activity.	NM_183297.2	CCGAGCCAAGAAGATTTCG	TCACCAACAGCGAGAACTTGA
Robo1	roundabout guidance receptor 1	Axon guidance receptor activity.	NM_001415010 .1	TGGCTTCAGCATCTGGCTTAC	GATAAGTTACTGTTGGCGTGAAG GT
Robo2	roundabout guidance receptor 2	Predicted to enable identical protein binding activity.	NM_001358490 .2	CAGCCATTGCTCTGTAGTAATAG G	AACTTCGTTACGTCCCCAATTAT

Gene	Gene name	Putative function	NCBI reference	Forward primer	Reverse primer
Sema6a	sema domain, transmembrane domain (TM), and cytoplasmic domain, (semaphorin) 6A	Transmembrane signaling receptor activity.	NM_001311097 .1	AGGACATTGAGCGTGGCAATACG	CCATTCACTGCCACGAAGGAATTG
Membrane					
Cacng2	calcium channel, voltage-dependent, gamma subunit 2	Enables voltage-gated calcium channel activity.	NM_007583	CGGCGAGCGAGTTCTACAA	ACTAAGACCTGCAGACACGAAGAAG
Gabra1	gamma-aminobutyric acid (GABA) A receptor, subunit alpha 1	Regulation of postsynaptic membrane potential.	NM_001359035 .1	TTGGGAGAGCGTGTAACTGAAG	ATACTCCATATCGTGGTCTGAAA CTG
Gabrg2	gamma-aminobutyric acid (GABA) A receptor, subunit gamma 2	GABA-A receptor subunit.	NM_177408	TGCTTGCTAACATGTTTACCTTACTTTG	TACAAGGCCTCACAGTCAGTAGA
Gria2	glutamate receptor, ionotropic, AMPA2 (alpha 2)	Glutamate receptors.	NM_001357924	CACCAAGCTTCCAACAGATG	TGCGAACTTATCCATTGGTAGT
Grid2	glutamate receptor, ionotropic, delta 2	Enables domain and scaffold protein binding activity.	NM_001370966 .1	TCAACCGAAGCAATGGGTCA	GTCAATGTCCAGAGGGGTCA
Grin1	glutamate receptor, ionotropic, N-methyl D-aspartate 1 (zeta 1)	Enables calmodulin and cation binding activity.	NM_001177656 .2	AAAATGTGTCCTGTCCATACTCA A	TGATACCGAACCCATGTCTTATCC
Grm3	glutamate receptor, metabotropic 3	Enables group II metabotropic glutamate receptor activity.	NM_181850.2	TTTGCTGAAATCAACTTCACAG	CCCGTCTCCGTAAGTGTCA
Homer 1	homer scaffolding protein 1	Scaffold protein; transmembrane transporter; and type 5 metabotropic glutamate receptor binding activity.	NM_001284189 .2	GATGGAGCTGACCAGTACCC	TGGTGTCAAAGGAGACTGAAGA
Homer 2	homer scaffolding protein 2	Enables actin binding activity and synaptic receptor adaptor activity.	NM_001164086 .1	GTTGGAGCACATTACCGTTAC	GTCAGTACGCACACCCAAA

Gene	Gene name	Putative function	NCBI reference	Forward primer	Reverse primer
Slc17a6	solute carrier family 17 (sodium-dependent inorganic phosphate cotransporter), member 6	Enables L-glutamate transmembrane transporter activity.	NM_001355150 .1	TAGCTTCCTCTGTCCGTGGT	GTCCGAGGGATTTCCAGCA
Slc17a7	solute carrier family 17 (sodium-dependent inorganic phosphate cotransporter), member 7	Enables extracellularly glutamate-gated chloride channel activity.	NM_182993.2	CTTTTGCGCAGTCGTACA	TAGTGCACCAGGGAGGCTAT
Slc32a1	solute carrier family 32 (GABA vesicular transporter), member 1	Enables GABA:proton symporter and glycine transporter activity.	NM_009508	GAGCGTATTAGTGAAGGGTATTT CTG	TCGTTGACAGGAGCCAAAATT
Syn1	synapsin I	Enables identical protein binding activity and protein kinase binding activity.	NM_001110780	TGAGGACATCAGTGTGGGTAA	GGCAATCTGCTCAAGCATAGC
Syn2	synapsin II	Enables identical protein binding activity.	NM_00111015	GGTAGATGCCTGCTCTGAAATGT	TCCATGACCTAAAAATGTAGTCT TT
Syp	Synaptophysin	Enables SH2 domain binding activity and identical protein binding activity.	NM_009305.2	CCTCTGCCCTCCTAACTCT	GGCACTACCAACGTACAGA
Motility					
Astn2	astrotactin 2	Predicted to enable calcium ion binding activity.	NM_019514.3	CCGTGAGGATGAGTTGGTAG	GCTGATTCCCCTTCTTCT
Nefl	neurofilament, light polypeptide	Protein-macromolecule adaptor.	NM_010910	TTTGCCTATCTACAGCTGTGTTGTA CTT	AAATCAACAAACCAAGCAGTTCC T
Nrxn1	neurexin I	Type I membrane protein that belongs to the neurexin family.	NM_020252.3	AAGGTTTGGCTCTGGGATAGTT	GGATACACTTGGAGGCAACGT
Myelin Sheath					
Cadm3	cell adhesion molecule 3	Enables protein homodimerization activity.	NM_053199	CACAGTGGTTCTCAAGTGTCAAGT AA	GATTATCTCGAAGGGCTCTTCT C

Gene	Gene name	Putative function	NCBI reference	Forward primer	Reverse primer
Mbp	myelin basic protein	Myelin sheath constituent of oligodendrocytes and Schwann cells.	NM_001025259	ACAGAGACACGGGCATCCTT	CACCCCTGTCACCGCTAAAG
Mobp	myelin-associated oligodendrocytic basic protein	Structural constituent of myelin sheath.	NM_008614	TCCTCAACTCCAAGCGTGAGA	AAGCAACCGCTTTGAGAT
Mog	myelin oligodendrocyte glycoprotein	Predicted to enable signaling receptor binding activity.	NM_010814	GCAGCTATGCAGGACAATTAG	CTCTGTTCATCCCCAACTAAAG
Myt1	myelin transcription factor 1	Member of the myelin transcription factor 1 gene family.	NM_001171616	TTCCCTTGGGTTCTTTGT	GCAACATGAATCATCCATGAGAA
Plp1	proteolipid protein (myelin) 1	Predicted to enable identical protein binding activity.	NM_001290561	AAAAAAAAGCCCTGATCGAATT	GAATGACAGCACAAATCTACAATGAA
Neurite Growth					
Dclk1	doublecortin-like kinase 1	Encodes a member of the protein kinase superfamily.	NM_001195538	AATAGCAACCACCGCTCTGA	CTTGTACCGGCTCCTCACATC
Stmn1	stathmin 1	Predicted to enable tubulin binding activity.	NM_019641.4	CCTTGCCAGTGGATTGTGTAGA	CCTGAATATCAGAAGATGCCATT
Tln1	talin 1	Enables integrin binding activity.	NM_011602.5	CGCCTGCCGCATGATT	CCCATTCGGAGCATGTAGTAGT
Tmod1	Tropomodulin 1	Enables tropomyosin binding activity.	NM_021883.2	ACAGCCTCACACAATGTCCTACAGA	GCAGGGAGCAGTGCATTATCAGGG
Soluble					
Cadps2	Ca2+-dependent activator protein for secretion 2	Lipid binding activity and metal ion binding activity.	NM_001252105.2	AGGACTCGGACCTAAAGATCAAA TT	CAGGTACCCACTATGCTTCATGTG
Calb1	calbindin 1, intracellular calcium-binding protein belonging to the troponin C superfamily	Regulation of postsynaptic cytosolic calcium ion concentration.	NM_009788.4	TTGGCTCACGTCTTACCCAC	TACAGCTCCCTCCATCCGA
Calb2	calbindin 2, intracellular calcium-binding protein belonging to the troponin C superfamily	Regulation of presynaptic cytosolic calcium ion concentration.	NM_001368293.1	GAGAATGAACGGACGCCCT	GCAGTCACCCCTCCACAGTAG

Gene	Gene name	Putative function	NCBI reference	Forward primer	Reverse primer
Camk4	calcium/calmodulin in-dependent protein kinase IV	Enables calcium-dependent protein serine/threonine kinase activity.	NM_009793	TCCGACATTCAGCTCACT	CAACACCCCCACTATCACCAA
Cbln1	cerebellin 1 precursor protein	Enables identical protein binding activity.	NM_019626.3	TGAGCCGTCGAGATGAGTAAT	GCTGCCTCTGAGTCAAAGTTGT
Gas7	growth arrest specific 7	Enables actin filament binding activity.	NM_001277079	TCCTCACGAAGGGCACATT	CTACGACAGACCCCTGAAGCTACTG
Survival					
Adora1	adenosine A1 receptor	G protein-coupled adenosine receptor.	NM_001008533.3	GTCAAGATCCCTCTCCGTA	CAAGGGAGAGAATCCAGCAG
Akt1	adenylate kinase 1, thymoma viral proto-oncogene 1	Akt serine-threonine protein kinase.	NM_009652.3	TCGTGTGGCAGGATGTGTAT	ACCTGGTGTCACTCAGAGG
Bdnf	brain derived neurotrophic factor	Nerve growth factor.	NM_001048139.1	CGAGAGGTCTGACGACGACAT	GGTCCTCATCCAGCAGCTTT
Ccnd1	Cyclin D1	Cyclin-dependent protein serine/threonine kinase regulator activity.	NM_001379248.1	CTGCTGAAATGGAAC TGCTT	CATCCGCCTCTGGCATT
Neurog2	Neurogenin 2	E-box binding activity.	NM_009718.4	ACGAGAACGACAACACACGA	GTATGGGACGTGGAGTTGG
Pcp2	Purkinje cell protein 2 (L7)	Enables guanyl-nucleotide exchange factor activity.	NM_001129803	GGAGAGGGAGGCTCAGACCTT	GCAGGTTGAAGAAGCCTCCT
Rac1	Rac family small GTPase 1	Enables GTP binding activity; GTP-dependent protein binding activity; and GTPase activity.	NM_001347530.1	GGAGACGGAGCTGTTGGTAAAAC	GGATGTACTCTCCAGGAAATGCA
Sst	somatostatin	Predicted to enable identical protein binding activity.	NM_001417475.1	GACCCAGACTCCGTAGTT	GGGCATCATTCTGTCTGGTT

Gene	Gene name	Putative function	NCBI reference	Forward primer	Reverse primer
Angiogenesis					
Angpt1	angiopoietin 1	Secreted glycoprotein that belongs to the angiopoietin family of vascular growth factors.	NM_001286062.1	GCATTCTCGCTGCCATTCT	TCTCCCTCCGTTTCTGGATT
Angpt2	angiopoietin 2	Endothelial cell-derived regulator of angiogenesis and ligand for endothelial-specific receptor tyrosine kinase.	NM_007426.4	GTCCAACATCAGGATTCACCTTACAG	GGAACACTTGCAGATGCATTG
Anpep	alanyl (membrane) aminopeptidase	Metalloaminopeptidase activity; peptide binding activity; and zinc ion binding activity.	NM_008486.3	GTCGAGAAAAACCAGAGTGCAAA	GTAGCCGGTTACGTTAACATGTTAGT
Serpinf1	serine (or cysteine) peptidase inhibitor, clade F, member 1	Enables serine-type endopeptidase inhibitor activity.	NM_011340.3	AGGACATGAAGCTACAGTCGTTGT	AGCAGCCCTGTGTTCCACTT
Tek	endothelial-specific receptor tyrosine kinase	Enables protein tyrosine kinase activity and signaling receptor activity.	NM_001290549.1	GCTTATTCTGTGAAGGTCGAGTT	GTAGCAGGTAGGAAGGATGCTTGT
Tie1	tyrosine kinase with immunoglobulin-like and EGF-like domains 1	Transmembrane receptor protein tyrosine kinase activity.	NM_011587.2	NA	NA
Cell Adhesion Molecules					
Cdh5	cadherin 5	Member of the cadherin family of calcium-dependent glycoproteins that mediate cell adhesion and regulate many morphogenetic events during development.	NM_009868.4	CAGCGACACTTCTACCACTTCAAG	ATTCGGAAGAATTGGCCTCTGT
Thbs1	thrombospondin 1	Subunit of a disulfide-linked homotrimeric adhesive glycoprotein that mediates cell-to-cell and cell-to-matrix interactions.	NM_011580.4	GCTGACTCGGGACCCATCTA	GCTGATGATTAGGAATCTGACAC
Coagulation cascade					
F3	coagulation factor III	Membrane-bound glycoprotein that forms the primary physiological initiator of the blood coagulation process following vascular damage.	NM_010171.3	TTTACCTTACCGAGACACAAACCTT	GTGAGTCTTTACAACCACGTT

Gene	Gene name	Putative function	NCBI reference	Forward primer	Reverse primer
Serpine1	serine (or cysteine) peptidase inhibitor, clade E, member 1	Enables serine-type endopeptidase inhibitor activity.	NM_008871.2	AGGATCGAGGTAAACGAGAGC	GCGGGCTGAGATGACAAA
Extracellular Matrix					
Col1a1	collagen, type I, alpha 1	Alpha-1 subunit of the fibril-forming type I collagen, the most abundant protein of bone, skin and tendon extracellular matrices.	NM_007742.3	CTGACTGGAAGAGCGGAGAGTC	TGGGGCTGATGTACCAAGTTCT
Mmp2	matrix metallopeptidase 2	Matrix metalloproteinase family of extracellular matrix-degrading enzymes that are involved in tissue remodeling, wound repair, progression of atherosclerosis and tumor invasion.	NM_008610.3	TGGGGGAGATTCTCACTTTG	ACTTTACGCGGACCACTTGT
Mmp9	matrix metallopeptidase 9	Matrix metalloproteinase family of extracellular matrix-degrading enzymes that are involved in tissue remodeling, wound repair, progression of atherosclerosis and tumor invasion.	NM_013599.4	CGTGTCTGGAGATTGACTTGA	TGGTACTGGAAGATGCGTGTGA
Ndp	Norrie disease (pseudoglioma) (human)	Secreted protein that acts a ligand for multiple different receptors and participates in both Wnt and Wnt-independant signalling.	NM_010883.3	ACGCTGCATGAGACACCATTAT	AGCACCATTTGAGCTACATTG
Tim1	tissue inhibitor of metalloproteinas e 1	Cytokine activity; metalloendopeptidase inhibitor activity; and zinc ion binding activity.	NM_011593.2	GCAAAGAGCTTCTCAAAGACC	AGGGATAGATAAACAGGGAAACACT
Growth Factors & Receptors					
Fgf2	fibroblast growth factor 2	Growth factor activity.	NM_008006.2	GACCCACACGTCAAACCTACAAC	TGGCACACACTCCCTTGATAGA
Flk1 (Kdr)	kinase insert domain protein receptor	Growth factor binding activity and vascular endothelial growth factor-activated receptor activity.	NM_001363216.1	TGAATGTCCCACCCAGATC	GCATGTCAATGTCTGCATGGT
Flt1	FMS-like tyrosine kinase 1	Identical protein binding activity and vascular endothelial growth factor-activated receptor activity.	NM_010228.3	ATCGGCAGACCAATACAATCCTA	AGGGTAATTCCAGCTCATTTGC

Gene	Gene name	Putative function	NCBI reference	Forward primer	Reverse primer
Lect1 (Cnmd)	chondromodulin	Endothelial cell morphogenesis; negative regulation of endothelial cell proliferation; and negative regulation of vascular endothelial growth factor receptor signaling pathway.	NM_001310655.1	GAGGAGAGAAGTGCTACATCAAA GC	GATCTGCCTCCAGTTAGAGAT
Nrp1	neuropilin 1	Protein kinase binding activity; transmembrane signaling receptor activity; and vascular endothelial growth factor binding activity.	NM_008737.2	CGCAAGGCTAACGTGTTGA	ATCCTGATGAACCTGTGGAGAGA
Pgf	placental growth factor	Identical protein binding activity; receptor ligand activity; and vascular endothelial growth factor receptor binding activity.	NM_008827.3	TCTCAGGATGTGCTCTGTGAATG	GGTTCCTCAGTCTGTGAGTTCTAC TC
Tgfb1	transforming growth factor, beta 1	Secreted ligand of the TGF-beta (transforming growth factor-beta) superfamily of proteins.	NM_011577.2	TGGAGCAACATGTGGAACTC	CAGCAGCCGGTTACCAAG
Vegfa	vascular endothelial growth factor A	Member of the PDGF/VEGF growth factor family.	NM_009505.4	GCAGCTTGAGTTAACGAACG	GGTTCCGAAACCTGAG

APPENDICES

Appendix 4: Statistical results of the OS panel on the whole cerebellum

Stage	Layer	Gene	Avg DCq (N)	Avg DCq (IH)	Fold Change	Difference [CI95]	t	p.value	Hedge's g [CI95]
P4	Tot	Adcyap1	6.73	6.44	1.22	0.27 [0.04, 0.5]	2.56	0.026 *	1.22 [0.15, 2.26]
P4	Tot	Adh5	3.75	3.98	0.85	-0.23 [-0.37, -0.09]	-3.52	0.005 **	1.61 [0.46, 2.71]
P4	Tot	Aldh1a1	4.82	4.90	0.94	-0.08 [-0.51, 0.34]	-0.44	0.668	0.2 [0.76, 1.15]
P4	Tot	Apc	4.31	4.13	1.13	0.18 [0.02, 0.34]	2.46	0.031 *	1.13 [0.07, 2.15]
P4	Tot	Apex1	5.52	5.44	1.06	0.08 [-0.06, 0.21]	1.26	0.233	0.61 [0.38, 1.58]
P4	Tot	Apoe	0.35	0.10	1.18	0.2 [-0.06, 0.46]	1.71	0.115	0.85 [0.16, 1.83]
P4	Tot	Aqp4	3.23	3.21	1.02	0.03 [-0.25, 0.3]	0.21	0.839	0.09 [0.86, 1.05]
P4	Tot	Aqr	6.14	6.12	1.01	0.03 [-0.14, 0.2]	0.42	0.682	0.12 [0.81, 1.05]
P4	Tot	Atr	7.69	7.67	1.01	0.01 [-0.24, 0.26]	0.10	0.926	0.08 [0.86, 1.01]
P4	Tot	Bax	5.21	5.14	1.05	0.07 [-0.09, 0.22]	0.92	0.375	0.47 [0.49, 1.41]
P4	Tot	Bcl2	6.21	6.34	0.91	-0.14 [-0.27, 0]	-2.24	0.047 *	1.02 [0.02, 2.03]
P4	Tot	Casp3	4.05	3.98	1.05	0.07 [-0.04, 0.18]	1.41	0.187	0.64 [0.34, 1.61]
P4	Tot	Casp9	8.30	8.21	1.07	0.07 [-0.14, 0.29]	0.73	0.480	0.42 [0.54, 1.37]
P4	Tot	Cat	5.06	5.15	0.94	-0.14 [-0.33, 0.06]	-1.51	0.160	0.37 [0.6, 1.33]
P4	Tot	Ccs	6.55	6.52	1.02	0.01 [-0.19, 0.21]	0.15	0.881	0.15 [0.8, 1.1]
P4	Tot	Cox4i1	1.87	1.83	1.02	0.04 [-0.12, 0.19]	0.55	0.594	0.23 [0.73, 1.18]
P4	Tot	Ctsb	3.30	3.22	1.06	0.08 [-0.07, 0.23]	1.18	0.263	0.54 [0.44, 1.5]
P4	Tot	Dnm2	5.58	5.54	1.03	0.04 [-0.17, 0.26]	0.45	0.662	0.2 [0.72, 1.12]
P4	Tot	Ehd2	8.78	8.62	1.12	0.16 [-0.01, 0.34]	2.07	0.062	0.95 [0.07, 1.94]
P4	Tot	Ercc2	6.71	6.36	1.27	0.21 [0, 0.42]	2.17	0.053	0.72 [0.3, 1.7]
P4	Tot	Ercc6	9.84	9.52	1.26	0.29 [-0.05, 0.64]	1.87	0.088	0.91 [0.12, 1.91]
P4	Tot	Fth1	1.60	1.69	0.94	-0.11 [-0.16, -0.05]	-4.23	0.001 **	1.26 [0.17, 2.31]
P4	Tot	Gab1	6.55	6.57	0.99	-0.04 [-0.23, 0.15]	-0.45	0.659	0.08 [0.87, 1.03]
P4	Tot	Gpx1	4.00	3.90	1.08	0.02 [-0.06, 0.11]	0.57	0.581	0.42 [0.55, 1.37]
P4	Tot	Gpx3	6.10	6.16	0.96	-0.03 [-0.17, 0.1]	-0.55	0.591	0.36 [0.61, 1.32]
P4	Tot	Gpx4	5.14	5.03	1.08	0.09 [-0.09, 0.26]	1.10	0.296	0.58 [0.38, 1.5]
P4	Tot	Gpx7	6.94	7.10	0.89	-0.2 [-0.31, -0.09]	-4.10	0.002 **	1.03 [0.01, 2.03]
P4	Tot	Gpx8	6.50	6.51	0.99	-0.09 [-0.34, 0.15]	-0.84	0.417	0.03 [0.9, 0.96]
P4	Tot	Gsr	5.29	5.27	1.01	0.02 [-0.14, 0.18]	0.23	0.824	0.1 [0.83, 1.03]
P4	Tot	Gss	8.78	8.67	1.08	0.09 [-0.07, 0.25]	1.20	0.255	0.63 [0.36, 1.6]
P4	Tot	Gstk1	8.25	8.34	0.94	-0.1 [-0.32, 0.11]	-1.09	0.301	0.4 [0.56, 1.35]
P4	Tot	Gstm1	4.07	3.82	1.19	0.25 [0.05, 0.45]	2.78	0.018 *	1.27 [0.19, 2.32]
P4	Tot	Hadh	6.58	6.60	0.98	-0.11 [-0.28, 0.06]	-1.45	0.175	0.08 [0.87, 1.03]
P4	Tot	Hif1a	5.39	5.35	1.03	0.03 [-0.09, 0.16]	0.58	0.573	0.33 [0.64, 1.28]
P4	Tot	Hmox1	7.52	7.33	1.14	0.17 [0, 0.34]	2.22	0.049 *	1.07 [0.03, 2.08]
P4	Tot	Hspa5	3.54	3.39	1.11	0.14 [0.02, 0.27]	2.55	0.027 *	1.17 [0.11, 2.19]
P4	Tot	Idh1	2.58	2.56	1.01	0.02 [-0.13, 0.16]	0.24	0.815	0.12 [0.83, 1.07]
P4	Tot	Ift172	7.77	7.54	1.17	0.19 [0.01, 0.38]	2.32	0.040 *	1.07 [0.02, 2.09]
P4	Tot	Jak1	4.67	4.72	0.97	-0.07 [-0.18, 0.03]	-1.50	0.162	0.38 [0.58, 1.32]
P4	Tot	Jun	6.49	6.70	0.86	-0.19 [-0.3, -0.08]	-3.81	0.003 **	1.52 [0.33, 2.65]
P4	Tot	Kif9	8.00	7.61	1.31	0.21 [-0.05, 0.47]	1.78	0.102	0.67 [0.33, 1.65]
P4	Tot	Map2k1	7.67	7.40	1.21	0.25 [0.14, 0.36]	5.01	<0.001 ***	2.09 [0.82, 3.32]
P4	Tot	Map2k6	7.25	7.11	1.10	0.13 [0, 0.27]	2.15	0.054	0.99 [0.05, 1.99]
P4	Tot	Mapk1	3.51	3.26	1.19	0.18 [0.07, 0.3]	3.46	0.005 **	1.06 [0.01, 2.09]
P4	Tot	Mapk10	2.67	2.57	1.07	0.05 [-0.06, 0.17]	1.02	0.331	0.55 [0.44, 1.52]
P4	Tot	Mapk14	8.64	8.53	1.08	0.1 [-0.07, 0.28]	1.29	0.224	0.63 [0.36, 1.61]
P4	Tot	Mapk3	4.41	4.22	1.14	0.15 [0.05, 0.26]	3.14	0.009 **	1.25 [0.16, 2.3]

Stage	Layer	Gene	Avg DCq (N)	Avg DCq (IH)	Fold Change	Difference [CI95]	t	p.value	Hedge's g [CI95]
P4	Tot	Mapk8	7.04	7.20	0.90	-0.15 [-0.85, 0.54]	-0.49	0.633	0.22 [0.74, 1.17]
P4	Tot	Mt1	3.82	3.67	1.11	0.13 [-0.11, 0.38]	1.19	0.260	0.6 [0.38, 1.56]
P4	Tot	Mt2	4.67	4.42	1.19	0.25 [0, 0.5]	2.17	0.053	0.99 [0.05, 1.99]
P4	Tot	Ndufv2	2.43	2.57	0.91	-0.14 [-0.23, -0.05]	-3.56	0.004 **	1.57 [0.39, 2.7]
P4	Tot	Nfe2l2	7.46	7.57	0.93	-0.14 [-0.35, 0.08]	-1.39	0.193	0.43 [0.51, 1.35]
P4	Tot	Nfkb1	7.56	7.53	1.02	0.02 [-0.12, 0.15]	0.25	0.806	0.17 [0.79, 1.12]
P4	Tot	Nfkbb1b	6.75	6.64	1.08	0.08 [-0.04, 0.21]	1.46	0.171	0.74 [0.27, 1.72]
P4	Tot	Nos1	7.57	7.41	1.12	0.12 [-0.01, 0.26]	1.96	0.076	0.89 [0.14, 1.88]
P4	Tot	Nqo1	8.81	8.89	0.95	-0.08 [-0.27, 0.11]	-0.95	0.363	0.43 [0.52, 1.37]
P4	Tot	Nudt15	8.45	8.35	1.07	0.08 [-0.02, 0.19]	1.76	0.106	0.85 [0.17, 1.85]
P4	Tot	Park7	4.43	4.25	1.13	0.18 [0.06, 0.3]	3.29	0.007 **	1.51 [0.38, 2.59]
P4	Tot	Parp1	5.69	5.53	1.12	0.13 [-0.02, 0.28]	1.87	0.088	0.88 [0.15, 1.88]
P4	Tot	Por	4.91	4.90	1.01	0.07 [-0.02, 0.16]	1.76	0.107	0.06 [0.88, 0.98]
P4	Tot	Ppp1r15b	5.97	5.95	1.02	0.08 [-0.05, 0.21]	1.38	0.195	0.11 [0.83, 1.05]
P4	Tot	Prdx1	2.10	2.30	0.87	-0.13 [-0.29, 0.02]	-1.85	0.091	0.76 [0.26, 1.75]
P4	Tot	Prdx2	2.61	2.55	1.04	0 [-0.05, 0.05]	0.13	0.902	0.35 [0.62, 1.31]
P4	Tot	Prdx3	5.33	5.34	0.99	-0.01 [-0.1, 0.07]	-0.33	0.744	0.15 [0.81, 1.1]
P4	Tot	Prdx4	5.66	5.73	0.95	-0.11 [-0.27, 0.05]	-1.55	0.151	0.36 [0.61, 1.31]
P4	Tot	Prdx5	3.88	3.81	1.05	0.05 [-0.03, 0.12]	1.27	0.230	0.67 [0.32, 1.62]
P4	Tot	Prdx6	4.64	4.59	1.04	0.05 [-0.15, 0.25]	0.52	0.613	0.27 [0.7, 1.22]
P4	Tot	Psmb5	3.76	3.95	0.88	-0.15 [-0.26, -0.04]	-2.95	0.013 *	1.12 [0.03, 2.17]
P4	Tot	Ptgs1	8.68	8.32	1.28	0.35 [0.12, 0.57]	3.42	0.006 **	1.63 [0.48, 2.74]
P4	Tot	Rela	6.14	6.06	1.06	0.08 [-0.06, 0.22]	1.29	0.223	0.59 [0.4, 1.55]
P4	Tot	Rheb	3.99	4.10	0.93	-0.06 [-0.21, 0.09]	-0.90	0.388	0.53 [0.46, 1.49]
P4	Tot	Slc38a1	5.60	5.53	1.05	0.01 [-0.13, 0.14]	0.11	0.916	0.3 [0.67, 1.26]
P4	Tot	Slc41a3	7.47	7.43	1.03	0.02 [-0.15, 0.19]	0.23	0.820	0.22 [0.74, 1.18]
P4	Tot	Sod1	2.68	2.76	0.95	-0.1 [-0.2, -0.01]	-2.32	0.041 *	0.55 [0.43, 1.52]
P4	Tot	Sod2	5.16	5.04	1.09	0.07 [-0.03, 0.18]	1.53	0.155	0.7 [0.3, 1.66]
P4	Tot	Sod3	8.62	8.57	1.04	0.05 [-0.23, 0.33]	0.40	0.696	0.18 [0.78, 1.13]
P4	Tot	Sp1	6.90	6.78	1.09	0.11 [-0.07, 0.28]	1.33	0.211	0.68 [0.32, 1.65]
P4	Tot	Srxn1	6.47	6.50	0.98	-0.03 [-0.11, 0.05]	-0.79	0.445	0.36 [0.61, 1.32]
P4	Tot	Tmod	10.13	10.02	1.08	0.1 [-0.23, 0.43]	0.68	0.510	0.36 [0.59, 1.3]
P4	Tot	Txnip	5.03	4.63	1.32	0.27 [0.07, 0.46]	3.03	0.011 *	0.93 [0.1, 1.93]
P4	Tot	Txnrd1	5.59	5.48	1.08	0.1 [-0.07, 0.26]	1.24	0.239	0.62 [0.38, 1.59]
P4	Tot	Txnrd3	7.52	7.50	1.01	-0.01 [-0.19, 0.16]	-0.18	0.862	0.1 [0.85, 1.05]
P4	Tot	Xrcc1	7.84	7.60	1.18	0.18 [0.02, 0.33]	2.53	0.028 *	0.98 [0.06, 1.99]
P8	Tot	Adcyap1	7.18	7.24	0.96	-0.06 [-0.22, 0.11]	-0.71	0.492	0.33 [0.61, 1.26]
P8	Tot	Adh5	3.68	3.94	0.83	-0.08 [-0.39, 0.22]	-0.59	0.569	0.92 [0.03, 1.84]
P8	Tot	Aldh1a1	5.50	5.42	1.05	-0.07 [-0.57, 0.43]	-0.30	0.773	0.19 [0.7, 1.07]
P8	Tot	Apc	3.99	4.57	0.67	-0.31 [-0.6, -0.03]	-2.39	0.034 *	1.83 [0.67, 2.95]
P8	Tot	Apex1	5.57	5.74	0.89	0.02 [-0.06, 0.09]	0.54	0.602	1.03 [0.08, 1.94]
P8	Tot	Apoe	-0.02	0.01	0.98	-0.03 [-0.18, 0.12]	-0.43	0.675	0.2 [0.73, 1.12]
P8	Tot	Aqp4	2.49	2.73	0.84	-0.24 [-0.39, -0.1]	-3.66	0.003 **	1.52 [0.29, 2.69]
P8	Tot	Aqr	6.48	6.79	0.80	-0.19 [-0.27, -0.12]	-5.44	<0.001 ***	2.66 [1.3, 3.97]
P8	Tot	Atr	7.95	8.27	0.80	-0.32 [-0.43, -0.2]	-6.01	<0.001 ***	2.88 [1.46, 4.26]
P8	Tot	Bax	5.04	5.11	0.95	-0.04 [-0.2, 0.11]	-0.62	0.549	0.61 [0.36, 1.56]

Stage	Layer	Gene	Avg DCq (N)	Avg DCq (IH)	Fold Change	Difference [CI95]	t	p.value	Hedge's g [CI95]
P8	Tot	Bcl2	6.71	6.98	0.83	-0.17 [-0.32, -0.03]	-2.60	0.023 *	1.9 [0.75, 3.01]
P8	Tot	Casp3	4.79	4.97	0.89	0.01 [-0.1, 0.12]	0.15	0.886	1 [0.04, 1.93]
P8	Tot	Casp9	8.60	8.94	0.79	-0.26 [-0.49, -0.03]	-2.41	0.033 *	1.61 [0.42, 2.74]
P8	Tot	Cat	5.20	5.62	0.75	-0.42 [-0.58, -0.26]	-5.74	<0.001 ***	2.3 [0.77, 3.77]
P8	Tot	Ccs	6.65	7.61	0.51	0.12 [-0.13, 0.38]	1.05	0.315	1.06 [0.1, 1.98]
P8	Tot	Cox4i1	1.32	1.04	1.21	0.17 [-0.26, 0.61]	0.86	0.406	0.85 [0.09, 1.76]
P8	Tot	Ctsb	3.42	3.31	1.08	0.08 [-0.1, 0.26]	0.95	0.361	0.79 [0.22, 1.77]
P8	Tot	Dnm2	5.21	5.63	0.75	-0.42 [-0.55, -0.29]	-6.86	<0.001 ***	3.1 [1.49, 4.66]
P8	Tot	Ehd2	9.06	9.35	0.82	-0.21 [-0.37, -0.06]	-2.94	0.012 *	2.07 [0.88, 3.21]
P8	Tot	Ercc2	7.19	7.55	0.78	-0.3 [-0.44, -0.15]	-4.52	<0.001 ***	2.49 [0.93, 3.98]
P8	Tot	Ercc6	9.80	10.42	0.65	-0.38 [-0.51, -0.25]	-6.24	<0.001 ***	2.75 [1.36, 4.09]
P8	Tot	Fth1	1.56	1.38	1.13	0.02 [-0.1, 0.14]	0.39	0.706	1.09 [0.11, 2.04]
P8	Tot	Gab1	5.87	6.36	0.71	-0.5 [-0.59, -0.4]	-11.44	<0.001 ***	4.94 [2.51, 7.32]
P8	Tot	Gpx1	4.10	3.97	1.09	0.12 [0.02, 0.22]	2.53	0.026 *	1.12 [0.04, 2.15]
P8	Tot	Gpx3	6.27	6.43	0.89	-0.16 [-0.36, 0.04]	-1.75	0.106	0.73 [0.31, 1.72]
P8	Tot	Gpx4	4.47	4.30	1.13	0.02 [-0.12, 0.15]	0.27	0.792	1 [0.03, 1.95]
P8	Tot	Gpx7	6.86	6.85	1.01	0.01 [-0.1, 0.11]	0.17	0.865	0.07 [0.89, 1.02]
P8	Tot	Gpx8	6.81	6.64	1.12	0.06 [-0.07, 0.2]	1.03	0.324	1.17 [0.15, 2.15]
P8	Tot	Gsr	5.59	5.68	0.94	-0.09 [-0.26, 0.09]	-1.04	0.318	0.45 [0.54, 1.4]
P8	Tot	Gss	8.48	8.81	0.80	-0.33 [-0.49, -0.17]	-4.49	<0.001 ***	1.93 [0.61, 3.19]
P8	Tot	Gstk1	7.88	7.91	0.98	-0.03 [-0.15, 0.1]	-0.45	0.659	0.18 [0.78, 1.13]
P8	Tot	Gstm1	4.59	4.51	1.06	0.08 [-0.03, 0.19]	1.57	0.141	0.77 [0.17, 1.69]
P8	Tot	Hadh	6.36	6.76	0.76	-0.2 [-0.36, -0.05]	-2.83	0.015 *	1.81 [0.61, 2.95]
P8	Tot	Hif1a	5.35	5.54	0.88	-0.19 [-0.29, -0.09]	-4.07	0.002 **	1.86 [0.64, 3.03]
P8	Tot	Hmox1	7.63	7.92	0.82	-0.09 [-0.29, 0.1]	-1.04	0.319	1.28 [0.27, 2.26]
P8	Tot	Hspa5	3.85	4.09	0.84	-0.24 [-0.34, -0.14]	-5.30	<0.001 ***	2.42 [1.04, 3.75]
P8	Tot	Idh1	3.64	3.58	1.04	-0.02 [-0.14, 0.11]	-0.32	0.757	0.48 [0.46, 1.4]
P8	Tot	Ift172	7.96	8.23	0.83	-0.4 [-0.48, -0.32]	-10.81	<0.001 ***	2.34 [1.06, 3.58]
P8	Tot	Jak1	5.35	5.28	1.05	-0.09 [-0.22, 0.03]	-1.59	0.137	0.43 [0.43, 1.28]
P8	Tot	Jun	6.82	7.10	0.82	-0.08 [-0.2, 0.04]	-1.46	0.171	1.47 [0.42, 2.47]
P8	Tot	Kif9	8.56	8.79	0.85	-0.23 [-0.38, -0.08]	-3.29	0.006 **	1.63 [0.54, 2.67]
P8	Tot	Map2k1	7.61	7.77	0.89	0.01 [-0.19, 0.21]	0.10	0.923	0.72 [0.24, 1.66]
P8	Tot	Map2k6	7.38	7.61	0.85	-0.23 [-0.34, -0.11]	-4.31	0.001 **	2.15 [0.93, 3.33]
P8	Tot	Mapk1	3.78	3.91	0.92	-0.12 [-0.22, -0.02]	-2.70	0.019 *	1.31 [0.27, 2.31]
P8	Tot	Mapk10	3.30	3.37	0.96	-0.06 [-0.14, 0.01]	-1.80	0.097	0.8 [0.22, 1.78]
P8	Tot	Mapk14	8.51	8.90	0.76	-0.25 [-0.37, -0.12]	-4.28	0.001 **	2.5 [1.15, 3.81]
P8	Tot	Mapk3	4.60	4.79	0.88	-0.13 [-0.24, -0.01]	-2.33	0.038 *	1.62 [0.45, 2.74]
P8	Tot	Mapk8	8.45	8.72	0.83	-0.02 [-0.2, 0.15]	-0.30	0.770	1.09 [0.11, 2.04]
P8	Tot	Mt1	3.65	3.27	1.30	0.37 [0.24, 0.51]	5.94	<0.001 ***	2.5 [0.96, 3.98]
P8	Tot	Mt2	4.53	3.90	1.54	0.62 [0.4, 0.85]	6.10	<0.001 ***	2.43 [0.84, 3.96]
P8	Tot	Ndufv2	2.33	2.26	1.05	0.05 [-0.08, 0.18]	0.77	0.457	0.67 [0.33, 1.64]
P8	Tot	Nfe2l2	7.33	7.70	0.77	-0.24 [-0.36, -0.12]	-4.33	<0.001 ***	2.44 [1.13, 3.7]
P8	Tot	Nfkb1	7.51	7.97	0.72	-0.41 [-0.47, -0.35]	-15.43	<0.001 ***	6.79 [4.13, 9.42]
P8	Tot	Nfkbb	6.71	6.75	0.98	-0.07 [-0.23, 0.09]	-0.98	0.345	0.26 [0.62, 1.14]
P8	Tot	Nos1	7.53	8.00	0.72	-0.29 [-0.46, -0.11]	-3.56	0.004 **	2.21 [0.98, 3.4]
P8	Tot	Nqo1	9.17	9.14	1.02	0.12 [-0.06, 0.3]	1.50	0.159	0.2 [0.74, 1.13]
P8	Tot	Nudt15	8.26	8.53	0.83	-0.14 [-0.27, 0]	-2.15	0.052	1.7 [0.59, 2.76]

Stage	Layer	Gene	Avg DCq (N)	Avg DCq (IH)	Fold Change	Difference [CI95]	t	p.value	Hedge's g [CI95]
P8	Tot	Park7	4.24	4.41	0.89	-0.01 [-0.26, 0.23]	-0.13	0.902	0.73 [0.17, 1.59]
P8	Tot	Parp1	5.62	6.07	0.73	-0.23 [-0.36, -0.09]	-3.69	0.003 **	2.13 [0.89, 3.32]
P8	Tot	Por	5.47	5.45	1.02	-0.12 [-0.2, -0.03]	-3.06	0.010 **	0.19 [0.69, 1.07]
P8	Tot	Ppp1r15b	6.18	6.35	0.89	-0.17 [-0.28, -0.07]	-3.52	0.004 **	1.56 [0.38, 2.69]
P8	Tot	Prdx1	2.12	2.06	1.04	0.06 [-0.05, 0.17]	1.13	0.281	0.44 [0.56, 1.41]
P8	Tot	Prdx2	2.68	2.76	0.95	-0.04 [-0.13, 0.06]	-0.81	0.436	0.93 [0.06, 1.89]
P8	Tot	Prdx3	5.44	5.59	0.90	0 [-0.11, 0.11]	0.00	0.997	0.93 [0.06, 1.89]
P8	Tot	Prdx4	5.58	5.60	0.99	-0.02 [-0.15, 0.11]	-0.30	0.769	0.13 [0.82, 1.07]
P8	Tot	Prdx5	3.55	3.66	0.93	-0.11 [-0.19, -0.02]	-2.63	0.022 *	1.1 [0.01, 2.16]
P8	Tot	Prdx6	4.36	4.56	0.87	-0.15 [-0.27, -0.02]	-2.61	0.023 *	1.8 [0.63, 2.94]
P8	Tot	Psmb5	3.79	3.89	0.93	0 [-0.21, 0.2]	-0.05	0.963	0.57 [0.39, 1.5]
P8	Tot	Ptgs1	8.35	8.53	0.88	-0.19 [-0.41, 0.04]	-1.80	0.097	0.88 [0.09, 1.82]
P8	Tot	Rela	6.30	6.56	0.83	-0.26 [-0.36, -0.17]	-5.97	<0.001 ***	2.88 [1.47, 4.26]
P8	Tot	Rheb	4.35	4.17	1.13	0.14 [0, 0.27]	2.18	0.050 *	1.6 [0.49, 2.66]
P8	Tot	Slc38a1	5.65	5.97	0.80	-0.25 [-0.36, -0.15]	-5.19	<0.001 ***	3.06 [1.58, 4.49]
P8	Tot	Slc41a3	7.61	7.90	0.82	-0.21 [-0.36, -0.06]	-3.06	0.010 **	2.12 [0.92, 3.28]
P8	Tot	Sod1	2.63	2.72	0.94	0.12 [-0.01, 0.25]	1.98	0.072	0.45 [0.43, 1.32]
P8	Tot	Sod2	5.02	5.29	0.83	-0.12 [-0.27, 0.03]	-1.72	0.111	1.54 [0.48, 2.57]
P8	Tot	Sod3	8.11	8.64	0.69	-0.54 [-0.67, -0.4]	-8.67	<0.001 ***	3.55 [1.55, 5.51]
P8	Tot	Sp1	6.93	7.42	0.72	-0.3 [-0.39, -0.21]	-7.10	<0.001 ***	2.91 [1.48, 4.29]
P8	Tot	Srxn1	6.39	6.34	1.03	0.04 [-0.09, 0.17]	0.71	0.494	0.29 [0.68, 1.25]
P8	Tot	Tmod	8.40	9.00	0.66	-0.6 [-0.81, -0.39]	-6.26	<0.001 ***	3.04 [1.58, 4.45]
P8	Tot	Txnip	5.90	5.75	1.11	0.36 [0.18, 0.54]	4.30	0.001 **	0.63 [0.32, 1.55]
P8	Tot	Txnrd1	5.62	5.98	0.78	-0.31 [-0.44, -0.18]	-5.39	<0.001 ***	3.1 [1.49, 4.67]
P8	Tot	Txnrd3	8.57	8.19	1.30	0.09 [-0.03, 0.21]	1.68	0.118	1.49 [0.44, 2.5]
P8	Tot	Xrcc1	8.00	8.08	0.95	-0.29 [-0.39, -0.19]	-6.12	<0.001 ***	0.38 [0.45, 1.2]
P12	Tot	Adcyap1	6.85	6.60	1.18	0.24 [0.05, 0.44]	2.59	0.017 *	0.92 [0.06, 1.76]
P12	Tot	Adh5	3.62	3.95	0.80	-0.41 [-0.54, -0.28]	-6.37	<0.001 ***	1.48 [0.61, 2.33]
P12	Tot	Aldh1a1	4.40	4.62	0.86	-0.28 [-0.45, -0.1]	-3.30	0.003 **	0.56 [0.27, 1.37]
P12	Tot	Apc	4.33	4.29	1.02	0.06 [-0.03, 0.15]	1.43	0.168	0.15 [0.62, 0.92]
P12	Tot	Apex1	5.91	5.86	1.04	0.05 [-0.02, 0.13]	1.43	0.169	0.5 [0.31, 1.3]
P12	Tot	Apoe	-0.29	-0.50	1.16	0.28 [0.12, 0.44]	3.62	0.002 **	0.84 [0.03, 1.63]
P12	Tot	Aqp4	2.06	1.95	1.08	0.11 [-0.01, 0.23]	1.88	0.074	0.73 [0.06, 1.51]
P12	Tot	Aqr	6.22	6.32	0.93	-0.1 [-0.18, -0.02]	-2.74	0.012 *	1.02 [0.17, 1.85]
P12	Tot	Atr	8.01	8.23	0.86	-0.19 [-0.3, -0.08]	-3.68	0.001 **	0.7 [0.14, 1.51]
P12	Tot	Bax	5.02	4.99	1.02	0.1 [-0.04, 0.23]	1.46	0.160	0.11 [0.63, 0.86]
P12	Tot	Bcl2	6.87	7.14	0.83	-0.29 [-0.36, -0.21]	-8.02	<0.001 ***	2.05 [1, 3.06]
P12	Tot	Casp3	5.12	4.83	1.23	0.3 [0.18, 0.41]	5.36	<0.001 ***	1.7 [0.67, 2.69]
P12	Tot	Casp9	8.53	8.31	1.17	0.25 [0.13, 0.38]	4.18	<0.001 ***	0.69 [0.13, 1.49]
P12	Tot	Cat	4.97	5.07	0.93	-0.07 [-0.17, 0.03]	-1.45	0.161	0.69 [0.09, 1.46]
P12	Tot	Ccs	6.05	5.95	1.07	-0.04 [-0.31, 0.23]	-0.32	0.754	0.23 [0.52, 0.97]
P12	Tot	Cox4i1	1.19	1.31	0.91	-0.13 [-0.25, -0.01]	-2.18	0.041 *	0.76 [0.02, 1.52]
P12	Tot	Ctsb	3.43	3.17	1.20	0.26 [0.13, 0.39]	4.16	<0.001 ***	1.61 [0.7, 2.49]
P12	Tot	Dnm2	5.21	5.53	0.80	-0.22 [-0.34, -0.11]	-3.99	<0.001 ***	1.16 [0.31, 1.99]
P12	Tot	Ehd2	8.94	9.01	0.95	-0.07 [-0.19, 0.05]	-1.17	0.255	0.44 [0.36, 1.22]
P12	Tot	Ercc2	7.22	7.05	1.12	0.17 [0.06, 0.29]	3.05	0.006 **	1.15 [0.31, 1.96]

Stage	Layer	Gene	Avg DCq (N)	Avg DCq (IH)	Fold Change	Difference [CI95]	t	p.value	Hedge's g [CI95]
P12	Tot	Ercc6	9.67	9.82	0.90	-0.08 [-0.19, 0.03]	-1.55	0.135	0.84 [0.04, 1.61]
P12	Tot	Fth1	0.85	1.20	0.79	-0.33 [-0.43, -0.23]	-6.85	<0.001 ***	1.9 [0.96, 2.81]
P12	Tot	Gab1	5.22	5.45	0.86	-0.22 [-0.34, -0.11]	-4.03	<0.001 ***	0.6 [0.22, 1.4]
P12	Tot	Gpx1	4.20	4.29	0.94	-0.08 [-0.18, 0.01]	-1.85	0.078	0.61 [0.15, 1.36]
P12	Tot	Gpx3	6.28	6.26	1.02	0.06 [-0.06, 0.18]	1.02	0.319	0.09 [0.65, 0.84]
P12	Tot	Gpx4	4.24	4.35	0.93	-0.11 [-0.21, -0.01]	-2.22	0.037 *	0.86 [0.06, 1.65]
P12	Tot	Gpx7	7.04	7.28	0.85	-0.21 [-0.29, -0.14]	-5.85	<0.001 ***	1.02 [0.14, 1.87]
P12	Tot	Gpx8	7.13	7.26	0.91	-0.09 [-0.2, 0.03]	-1.62	0.120	0.56 [0.27, 1.37]
P12	Tot	Gsr	4.87	4.99	0.92	-0.12 [-0.26, 0.03]	-1.68	0.109	0.65 [0.13, 1.43]
P12	Tot	Gss	7.80	7.74	1.04	0.06 [-0.08, 0.19]	0.87	0.394	0.26 [0.55, 1.06]
P12	Tot	Gstk1	7.93	8.04	0.93	-0.09 [-0.19, 0]	-2.07	0.051	0.91 [0.11, 1.68]
P12	Tot	Gstm1	4.80	4.48	1.25	0.32 [0.21, 0.44]	5.69	<0.001 ***	2.15 [1.13, 3.14]
P12	Tot	Hadh	6.07	6.06	1.00	0.07 [-0.01, 0.15]	1.71	0.101	0.03 [0.69, 0.75]
P12	Tot	Hif1a	4.75	4.70	1.04	0.11 [0.04, 0.18]	3.49	0.002 **	0.36 [0.42, 1.14]
P12	Tot	Hmox1	7.83	7.30	1.45	0.53 [0.1, 0.97]	2.53	0.019 *	0.88 [0.01, 1.73]
P12	Tot	Hspa5	3.78	4.06	0.82	-0.22 [-0.3, -0.14]	-5.67	<0.001 ***	1.93 [0.96, 2.86]
P12	Tot	Idh1	3.46	3.32	1.10	0.12 [0.05, 0.2]	3.45	0.002 **	1.37 [0.49, 2.23]
P12	Tot	Ift172	7.90	8.24	0.79	-0.35 [-0.44, -0.25]	-7.71	<0.001 ***	2.51 [1.44, 3.54]
P12	Tot	Jak1	4.89	4.94	0.97	-0.01 [-0.09, 0.06]	-0.38	0.706	0.42 [0.32, 1.15]
P12	Tot	Jun	6.85	7.12	0.83	-0.27 [-0.35, -0.19]	-6.84	<0.001 ***	1.48 [0.55, 2.38]
P12	Tot	Kif9	8.89	9.01	0.92	-0.07 [-0.2, 0.06]	-1.14	0.268	0.64 [0.13, 1.39]
P12	Tot	Map2k1	7.14	7.11	1.02	0.3 [0.1, 0.5]	3.16	0.005 **	0.05 [0.64, 0.74]
P12	Tot	Map2k6	6.92	7.12	0.87	-0.2 [-0.29, -0.1]	-4.46	<0.001 ***	1.64 [0.69, 2.56]
P12	Tot	Mapk1	3.25	3.01	1.18	0.24 [0.12, 0.36]	4.16	<0.001 ***	1.36 [0.43, 2.25]
P12	Tot	Mapk10	2.97	3.07	0.94	-0.05 [-0.16, 0.06]	-0.99	0.332	0.46 [0.31, 1.21]
P12	Tot	Mapk14	8.01	8.13	0.92	-0.03 [-0.14, 0.07]	-0.65	0.522	0.61 [0.15, 1.37]
P12	Tot	Mapk3	4.28	4.27	1.01	0.04 [-0.05, 0.13]	0.86	0.397	0.09 [0.65, 0.83]
P12	Tot	Mapk8	6.31	6.16	1.11	0.16 [0.03, 0.29]	2.47	0.022 *	0.91 [0.11, 1.68]
P12	Tot	Mt1	3.03	2.58	1.36	0.45 [0.24, 0.65]	4.55	<0.001 ***	1.69 [0.73, 2.62]
P12	Tot	Mt2	4.10	2.99	2.16	1.11 [0.8, 1.42]	7.41	<0.001 ***	2.69 [1.47, 3.88]
P12	Tot	Ndufv2	1.68	1.85	0.89	-0.14 [-0.23, -0.04]	-2.94	0.008 **	1.22 [0.4, 2.03]
P12	Tot	Nfe2l2	6.99	7.18	0.88	-0.13 [-0.2, -0.06]	-3.62	0.002 **	0.8 [0.03, 1.61]
P12	Tot	Nfkb1	7.11	7.18	0.96	-0.06 [-0.16, 0.05]	-1.07	0.296	0.41 [0.38, 1.19]
P12	Tot	Nfkbbib	6.62	6.35	1.20	0.29 [0.14, 0.43]	4.11	<0.001 ***	1.3 [0.47, 2.11]
P12	Tot	Nos1	6.57	6.77	0.87	-0.2 [-0.37, -0.03]	-2.39	0.026 *	0.89 [0.05, 1.7]
P12	Tot	Nqo1	8.95	8.95	1.00	-0.04 [-0.14, 0.07]	-0.71	0.483	0.01 [0.75, 0.77]
P12	Tot	Nudt15	8.11	7.82	1.22	0.29 [0.1, 0.48]	3.22	0.004 **	1.2 [0.32, 2.05]
P12	Tot	Park7	3.96	3.89	1.05	0.1 [0.03, 0.16]	3.07	0.006 **	0.34 [0.44, 1.11]
P12	Tot	Parp1	5.75	6.04	0.82	-0.23 [-0.33, -0.12]	-4.60	<0.001 ***	1.46 [0.54, 2.35]
P12	Tot	Por	5.02	5.02	1.00	0.04 [-0.05, 0.13]	0.95	0.351	0 [0.77, 0.77]
P12	Tot	Ppp1r15b	5.69	5.72	0.98	0.12 [-0.01, 0.24]	1.96	0.063	0.08 [0.69, 0.86]
P12	Tot	Prdx1	1.88	2.11	0.86	-0.18 [-0.28, -0.09]	-4.02	<0.001 ***	1.25 [0.4, 2.08]
P12	Tot	Prdx2	2.79	2.88	0.94	-0.06 [-0.12, 0.01]	-1.86	0.077	0.87 [0.09, 1.64]
P12	Tot	Prdx3	5.10	5.23	0.92	-0.06 [-0.14, 0.02]	-1.48	0.153	0.8 [0.03, 1.56]
P12	Tot	Prdx4	5.51	5.43	1.06	0.1 [-0.01, 0.21]	1.97	0.062	0.39 [0.42, 1.19]
P12	Tot	Prdx5	3.14	3.31	0.89	-0.12 [-0.25, 0]	-2.05	0.053	0.84 [0.07, 1.59]
P12	Tot	Prdx6	4.10	4.14	0.97	0.01 [-0.09, 0.11]	0.23	0.824	0.22 [0.53, 0.97]

Stage	Layer	Gene	Avg DCq (N)	Avg DCq (IH)	Fold Change	Difference [CI95]	t	p.value	Hedge's g [CI95]
P12	Tot	Psmb5	2.89	2.67	1.16	-0.01 [-0.17, 0.14]	-0.18	0.860	0.18 [0.6, 0.95]
P12	Tot	Ptgs1	7.60	7.48	1.09	-0.1 [-0.4, 0.21]	-0.64	0.529	0.14 [0.62, 0.91]
P12	Tot	Rela	5.13	4.90	1.17	0.03 [-0.06, 0.12]	0.77	0.449	0.23 [0.55, 0.99]
P12	Tot	Rheb	3.26	3.27	0.99	-0.12 [-0.23, -0.01]	-2.29	0.033 *	0.02 [0.76, 0.79]
P12	Tot	Slc38a1	4.01	3.85	1.11	-0.01 [-0.09, 0.07]	-0.32	0.755	0.13 [0.65, 0.9]
P12	Tot	Slc41a3	6.46	6.07	1.30	0.26 [0.12, 0.41]	3.75	0.001 **	0.43 [0.37, 1.22]
P12	Tot	Sod1	1.87	1.78	1.06	-0.14 [-0.23, -0.06]	-3.55	0.002 **	0.07 [0.7, 0.84]
P12	Tot	Sod2	3.58	3.25	1.26	0.26 [0.04, 0.48]	2.46	0.023 *	0.35 [0.45, 1.14]
P12	Tot	Sod3	5.29	3.83	2.75	0.78 [0.25, 1.3]	3.07	0.006 **	0.35 [0.44, 1.14]
P12	Tot	Sp1	5.82	5.54	1.21	0.05 [-0.06, 0.16]	1.02	0.320	0.21 [0.57, 0.98]
P12	Tot	Srxn1	5.14	5.33	0.87	-0.28 [-0.38, -0.19]	-6.13	<0.001 ***	0.22 [0.57, 1]
P12	Tot	Tmod	6.79	7.41	0.65	-0.62 [-0.77, -0.47]	-8.70	<0.001 ***	3.08 [1.69, 4.43]
P12	Tot	Txnip	4.83	4.67	1.12	-0.07 [-0.4, 0.26]	-0.43	0.670	0.16 [0.59, 0.91]
P12	Tot	Txnr1d1	4.85	4.57	1.22	0.08 [-0.01, 0.17]	1.91	0.070	0.27 [0.51, 1.03]
P12	Tot	Txnr1d3	7.36	6.32	2.06	0.85 [0.5, 1.19]	5.11	<0.001 ***	0.78 [0.07, 1.61]
P12	Tot	Xrcc1	8.04	8.13	0.94	-0.09 [-0.18, 0]	-2.04	0.054	0.25 [0.54, 1.03]
P21	Tot	Adcyap1	7.71	7.57	1.10	0.14 [-0.09, 0.37]	1.30	0.217	0.57 [0.35, 1.46]
P21	Tot	Adh5	3.87	3.93	0.96	-0.04 [-0.16, 0.07]	-0.83	0.422	0.57 [0.34, 1.46]
P21	Tot	Aldh1a1	2.64	2.61	1.03	0.15 [-0.11, 0.4]	1.26	0.229	0.14 [0.73, 0.99]
P21	Tot	Apc	5.42	5.42	0.99	-0.01 [-0.21, 0.19]	-0.13	0.895	0.04 [0.82, 0.91]
P21	Tot	Apex1	6.44	6.45	0.99	-0.06 [-0.17, 0.05]	-1.09	0.294	0.09 [0.82, 0.99]
P21	Tot	Apoe	-0.03	-0.12	1.07	0.09 [-0.04, 0.23]	1.46	0.169	0.63 [0.3, 1.55]
P21	Tot	Aqp4	2.67	2.70	0.98	-0.04 [-0.22, 0.13]	-0.56	0.584	0.16 [0.74, 1.05]
P21	Tot	Aqr	6.61	6.70	0.94	-0.06 [-0.14, 0.02]	-1.52	0.151	0.43 [0.48, 1.32]
P21	Tot	Atr	8.49	8.48	1.01	-0.02 [-0.15, 0.1]	-0.42	0.684	0.06 [0.84, 0.96]
P21	Tot	Bax	5.20	5.30	0.93	-0.1 [-0.28, 0.07]	-1.25	0.232	0.55 [0.37, 1.45]
P21	Tot	Bcl2	7.27	7.21	1.04	0.05 [-0.05, 0.15]	1.09	0.297	0.46 [0.46, 1.38]
P21	Tot	Casp3	7.02	7.05	0.98	-0.02 [-0.17, 0.12]	-0.34	0.737	0.2 [0.7, 1.1]
P21	Tot	Casp9	8.85	8.76	1.06	0.09 [-0.39, 0.56]	0.40	0.696	0.17 [0.73, 1.08]
P21	Tot	Cat	5.27	5.07	1.15	0.2 [-0.06, 0.46]	1.68	0.118	0.73 [0.22, 1.65]
P21	Tot	Ccs	6.41	6.49	0.95	0.07 [-0.48, 0.62]	0.29	0.776	0.16 [0.75, 1.06]
P21	Tot	Cox4i1	0.00	0.14	0.91	-0.21 [-0.57, 0.16]	-1.22	0.246	0.22 [0.68, 1.12]
P21	Tot	Ctsb	2.62	2.64	0.99	-0.02 [-0.24, 0.2]	-0.19	0.850	0.08 [0.81, 0.98]
P21	Tot	Dnm2	5.27	5.37	0.93	-0.15 [-0.54, 0.24]	-0.82	0.429	0.36 [0.56, 1.27]
P21	Tot	Ehd2	9.34	9.19	1.11	-0.03 [-0.19, 0.12]	-0.46	0.654	0.85 [0.14, 1.8]
P21	Tot	Ercc2	7.11	6.98	1.10	-0.08 [-0.3, 0.15]	-0.75	0.468	0.43 [0.49, 1.34]
P21	Tot	Ercc6	10.20	10.25	0.97	-0.13 [-0.33, 0.06]	-1.52	0.152	0.23 [0.67, 1.12]
P21	Tot	Fth1	-0.01	0.65	0.63	-0.45 [-1.08, 0.18]	-1.55	0.146	0.96 [0.06, 1.94]
P21	Tot	Gab1	5.59	5.61	0.99	-0.07 [-0.29, 0.16]	-0.65	0.530	0.16 [0.75, 1.06]
P21	Tot	Gpx1	4.39	4.13	1.20	0.27 [0.08, 0.45]	3.04	0.010 **	1.32 [0.29, 2.32]
P21	Tot	Gpx3	6.57	6.65	0.95	-0.05 [-0.28, 0.17]	-0.53	0.604	0.27 [0.64, 1.16]
P21	Tot	Gpx4	3.56	3.35	1.16	0.03 [-0.13, 0.2]	0.43	0.674	0.94 [0.07, 1.91]
P21	Tot	Gpx7	8.28	7.75	1.45	0.53 [0.04, 1.02]	2.33	0.036 *	0.92 [0.09, 1.89]
P21	Tot	Gpx8	7.76	7.42	1.27	0.35 [-0.06, 0.75]	1.87	0.085	0.76 [0.21, 1.69]
P21	Tot	Gsr	5.46	5.57	0.93	-0.11 [-0.27, 0.04]	-1.54	0.147	0.67 [0.27, 1.59]
P21	Tot	Gss	7.05	6.99	1.04	-0.04 [-0.32, 0.24]	-0.29	0.778	0.26 [0.65, 1.16]

APPENDICES

Appendix 4: Statistical results of the OS panel on the whole cerebellum

Stage	Layer	Gene	Avg DCq (N)	Avg DCq (IH)	Fold Change	Difference [CI95]	t	p.value	Hedge's g [CI95]
P21	Tot	Gstk1	7.13	7.04	1.07	0.04 [-0.15, 0.24]	0.47	0.644	0.63 [0.3, 1.54]
P21	Tot	Gstm1	4.32	4.70	0.77	-0.23 [-0.94, 0.48]	-0.69	0.500	0.54 [0.39, 1.45]
P21	Tot	Hadh	6.38	6.16	1.16	0.06 [-0.16, 0.27]	0.56	0.582	1.1 [0.07, 2.09]
P21	Tot	Hif1a	4.92	4.92	1.00	0.01 [-0.07, 0.08]	0.14	0.892	0.06 [0.84, 0.96]
P21	Tot	Hmox1	8.25	8.17	1.05	0.08 [-0.06, 0.22]	1.20	0.252	0.51 [0.42, 1.43]
P21	Tot	Hspa5	3.30	3.62	0.80	-0.33 [-0.49, -0.17]	-4.37	<0.001 ***	1.92 [0.77, 3.04]
P21	Tot	Idh1	4.42	4.00	1.34	0.42 [0.1, 0.74]	2.84	0.014 *	1.2 [0.16, 2.2]
P21	Tot	Ift172	7.84	8.00	0.89	-0.17 [-0.48, 0.15]	-1.13	0.279	0.48 [0.45, 1.39]
P21	Tot	Jak1	5.39	5.49	0.94	-0.1 [-0.49, 0.3]	-0.53	0.605	0.23 [0.68, 1.13]
P21	Tot	Jun	6.44	6.61	0.89	0.12 [-0.22, 0.45]	0.76	0.463	0.44 [0.48, 1.34]
P21	Tot	Kif9	8.76	8.46	1.23	0.01 [-0.2, 0.21]	0.08	0.938	1.1 [0.11, 2.07]
P21	Tot	Map2k1	7.05	6.94	1.08	0.08 [-0.02, 0.18]	1.74	0.105	0.57 [0.36, 1.49]
P21	Tot	Map2k6	7.37	7.56	0.88	-0.19 [-0.65, 0.27]	-0.87	0.398	0.4 [0.5, 1.29]
P21	Tot	Mapk1	3.80	3.78	1.01	0.02 [-0.37, 0.4]	0.09	0.929	0.04 [0.87, 0.94]
P21	Tot	Mapk10	2.64	2.84	0.87	-0.14 [-0.79, 0.51]	-0.46	0.656	0.35 [0.56, 1.25]
P21	Tot	Mapk14	8.18	8.55	0.77	-0.37 [-0.84, 0.1]	-1.70	0.113	0.7 [0.26, 1.63]
P21	Tot	Mapk3	4.46	4.65	0.88	-0.14 [-0.59, 0.31]	-0.66	0.519	0.4 [0.52, 1.31]
P21	Tot	Mapk8	9.02	8.33	1.61	0.23 [-0.19, 0.65]	1.19	0.256	0.87 [0.13, 1.82]
P21	Tot	Mt1	0.95	2.25	0.41	-1.01 [-1.96, -0.05]	-2.28	0.040 *	1.17 [0.09, 2.2]
P21	Tot	Mt2	1.53	2.01	0.72	-0.58 [-0.75, -0.4]	-7.02	<0.001 ***	1.91 [0.74, 3.03]
P21	Tot	Ndufv2	1.85	1.99	0.91	0.12 [-0.13, 0.36]	1.03	0.324	0.4 [0.52, 1.3]
P21	Tot	Nfe2l2	7.01	6.84	1.13	0.05 [-0.08, 0.19]	0.83	0.421	0.99 [0.04, 1.96]
P21	Tot	Nfkbb1	7.36	7.55	0.88	-0.19 [-0.64, 0.27]	-0.90	0.387	0.38 [0.54, 1.28]
P21	Tot	Nfkbbib	6.84	7.15	0.81	-0.26 [-0.93, 0.41]	-0.84	0.415	0.48 [0.45, 1.39]
P21	Tot	Nos1	6.54	6.53	1.01	0 [-0.14, 0.15]	0.05	0.957	0.04 [0.85, 0.93]
P21	Tot	Nqo1	8.50	8.69	0.88	-0.26 [-0.4, -0.13]	-4.18	0.001 **	0.8 [0.15, 1.72]
P21	Tot	Nudt15	8.18	8.24	0.96	-0.04 [-0.15, 0.08]	-0.72	0.487	0.41 [0.51, 1.31]
P21	Tot	Park7	4.14	4.05	1.07	0.16 [-0.06, 0.37]	1.59	0.137	0.43 [0.5, 1.34]
P21	Tot	Parp1	5.98	6.00	0.98	-0.09 [-0.2, 0.01]	-1.87	0.084	0.14 [0.75, 1.03]
P21	Tot	Por	5.39	5.72	0.80	-0.32 [-0.85, 0.2]	-1.32	0.210	0.57 [0.37, 1.48]
P21	Tot	Ppp1r15b	5.80	5.97	0.89	-0.16 [-0.3, -0.03]	-2.62	0.021 *	0.94 [0.03, 1.88]
P21	Tot	Prdx1	1.83	1.90	0.95	0 [-0.2, 0.19]	-0.01	0.989	0.42 [0.47, 1.3]
P21	Tot	Prdx2	3.18	3.11	1.05	-0.04 [-0.13, 0.06]	-0.78	0.451	0.38 [0.54, 1.29]
P21	Tot	Prdx3	5.21	5.21	1.00	0 [-0.07, 0.06]	-0.10	0.925	0.04 [0.86, 0.94]
P21	Tot	Prdx4	6.26	6.20	1.05	-0.01 [-0.1, 0.08]	-0.22	0.829	0.43 [0.49, 1.33]
P21	Tot	Prdx5	2.82	2.77	1.03	0.05 [-0.05, 0.14]	1.06	0.307	0.43 [0.49, 1.33]
P21	Tot	Prdx6	3.24	3.23	1.01	0.05 [-0.11, 0.21]	0.66	0.524	0.1 [0.81, 1]
P21	Tot	Psmb5	3.48	3.70	0.86	-0.09 [-0.23, 0.05]	-1.34	0.203	0.88 [0.1, 1.83]
P21	Tot	Ptgs1	8.23	8.19	1.03	0.05 [-0.08, 0.17]	0.78	0.447	0.33 [0.59, 1.24]
P21	Tot	Rela	6.30	6.24	1.05	0.07 [-0.01, 0.15]	1.79	0.097	0.73 [0.23, 1.67]
P21	Tot	Rheb	3.69	3.79	0.93	0 [-0.14, 0.15]	0.01	0.992	0.48 [0.43, 1.36]
P21	Tot	Slc38a1	5.31	5.22	1.07	0 [-0.11, 0.11]	0.08	0.937	0.8 [0.18, 1.74]
P21	Tot	Slc41a3	6.38	6.45	0.95	-0.1 [-0.23, 0.02]	-1.74	0.106	0.44 [0.49, 1.34]
P21	Tot	Sod1	2.68	2.60	1.06	0.05 [-0.02, 0.13]	1.53	0.150	0.99 [0.03, 1.97]
P21	Tot	Sod2	4.62	4.53	1.06	0.05 [-0.08, 0.18]	0.91	0.381	0.74 [0.22, 1.67]
P21	Tot	Sod3	7.21	7.22	0.99	-0.04 [-0.16, 0.09]	-0.61	0.551	0.11 [0.8, 1]
P21	Tot	Sp1	7.05	7.10	0.97	-0.05 [-0.16, 0.07]	-0.88	0.394	0.36 [0.56, 1.27]

Stage	Layer	Gene	Avg DCq (N)	Avg DCq (IH)	Fold Change	Difference [CI95]	t	p.value	Hedge's g [CI95]
P21	Tot	Srxn1	5.15	5.77	0.65	-0.48 [-1.15, 0.19]	-1.54	0.148	0.93 [0.08, 1.89]
P21	Tot	Tmod	6.02	5.92	1.07	-0.03 [-0.18, 0.13]	-0.35	0.731	0.5 [0.43, 1.41]
P21	Tot	Txnip	5.89	6.25	0.78	-0.91 [-1.19, -0.63]	-7.08	<0.001 ***	0.92 [0.07, 1.87]
P21	Tot	Txnr1d1	6.15	6.04	1.08	0.07 [-0.01, 0.15]	1.99	0.068	0.98 [0, 1.94]
P21	Tot	Txnr1d3	8.90	8.68	1.17	0.23 [0.11, 0.35]	4.05	0.001 **	1.77 [0.65, 2.84]
P21	Tot	Xrcc1	8.27	8.03	1.18	0.07 [-0.11, 0.25]	0.83	0.419	1 [0, 1.97]
P70	Tot	Adcyap1	7.36	7.75	0.77	-0.39 [-0.73, -0.04]	-3.10	0.036 *	1.54 [0.06, 3.04]
P70	Tot	Adh5	4.25	4.55	0.81	-0.3 [-0.55, -0.04]	-3.20	0.033 *	1.91 [0.31, 3.44]
P70	Tot	Aldh1a1	2.55	2.19	1.28	0.35 [0.09, 0.61]	3.71	0.021 *	1.2 [0.26, 2.57]
P70	Tot	Apc	5.46	5.31	1.11	0.15 [-0.05, 0.35]	2.04	0.111	0.97 [0.4, 2.25]
P70	Tot	Apex1	6.42	6.51	0.94	-0.1 [-0.31, 0.12]	-1.26	0.276	0.68 [0.59, 1.9]
P70	Tot	Apoe	0.00	-0.29	1.22	0.29 [0.04, 0.54]	3.23	0.032 *	1.89 [0.26, 3.45]
P70	Tot	Aqp4	2.73	2.94	0.87	-0.2 [-0.67, 0.26]	-1.21	0.292	0.65 [0.62, 1.87]
P70	Tot	Aqr	6.34	6.48	0.91	-0.14 [-0.35, 0.07]	-1.89	0.132	1 [0.37, 2.28]
P70	Tot	Atr	8.07	8.10	0.98	-0.03 [-0.29, 0.22]	-0.34	0.751	0.17 [1, 1.32]
P70	Tot	Bax	5.62	5.36	1.20	0.26 [-0.17, 0.68]	1.69	0.167	1 [0.33, 2.25]
P70	Tot	Bcl2	6.74	6.80	0.96	-0.06 [-0.3, 0.18]	-0.69	0.528	0.4 [0.65, 1.41]
P70	Tot	Casp3	7.49	7.53	0.97	-0.04 [-0.37, 0.28]	-0.37	0.729	0.21 [0.99, 1.39]
P70	Tot	Casp9	8.63	8.30	1.25	0.32 [-0.2, 0.85]	1.71	0.163	0.85 [0.47, 2.1]
P70	Tot	Cat	5.70	5.54	1.12	0.16 [-0.14, 0.46]	1.50	0.209	0.79 [0.52, 2.03]
P70	Tot	Ccs	7.87	6.17	3.25	1.7 [0.78, 2.62]	5.15	0.007 **	3.01 [0.93, 5.02]
P70	Tot	Cox4i1	-0.26	-0.79	1.45	0.53 [-0.73, 1.8]	1.17	0.307	0.4 [0.68, 1.41]
P70	Tot	Ctsb	2.17	2.18	1.00	-0.01 [-0.5, 0.49]	-0.04	0.970	0.02 [1.09, 1.13]
P70	Tot	Dnm2	5.37	5.93	0.68	-0.56 [-1.04, -0.07]	-3.19	0.033 *	1.81 [0.2, 3.34]
P70	Tot	Ehd2	8.53	8.71	0.88	-0.18 [-0.48, 0.11]	-1.73	0.158	0.9 [0.44, 2.16]
P70	Tot	Ercc2	6.69	6.63	1.05	0.07 [-0.41, 0.54]	0.38	0.724	0.2 [0.99, 1.36]
P70	Tot	Ercc6	9.57	9.82	0.84	-0.25 [-0.69, 0.19]	-1.60	0.184	0.73 [0.55, 1.92]
P70	Tot	Fth1	-1.04	-0.65	0.76	-0.39 [-0.81, 0.02]	-2.64	0.058	1.29 [0.2, 2.69]
P70	Tot	Gab1	5.75	6.05	0.81	-0.3 [-0.54, -0.06]	-3.43	0.027 *	1.56 [0.08, 3.1]
P70	Tot	Gpx1	3.82	4.21	0.77	-0.38 [-0.54, -0.22]	-6.64	0.003 **	3.94 [1.23, 6.62]
P70	Tot	Gpx3	6.52	6.18	1.26	0.33 [0.1, 0.57]	3.90	0.018 *	1.83 [0.07, 3.5]
P70	Tot	Gpx4	3.16	3.57	0.75	-0.41 [-0.88, 0.06]	-2.40	0.074	1.46 [0.03, 2.8]
P70	Tot	Gpx7	8.54	9.11	0.67	-0.57 [-1.05, -0.09]	-3.28	0.030 *	1.95 [0.32, 3.49]
P70	Tot	Gpx8	7.31	8.07	0.59	-0.77 [-1.55, 0.02]	-2.70	0.054	1.63 [0.14, 3.04]
P70	Tot	Gsr	5.34	5.73	0.76	-0.39 [-0.82, 0.04]	-2.52	0.065	1.34 [0.14, 2.74]
P70	Tot	Gss	7.28	7.54	0.84	-0.26 [-0.54, 0.03]	-2.47	0.069	1.47 [0.02, 2.85]
P70	Tot	Gstk1	6.51	6.77	0.84	-0.25 [-0.62, 0.11]	-1.91	0.129	0.76 [0.51, 1.93]
P70	Tot	Gstm1	2.85	2.93	0.95	-0.08 [-0.58, 0.42]	-0.45	0.678	0.26 [0.94, 1.43]
P70	Tot	Hadh	6.61	6.58	1.03	0.04 [-0.12, 0.19]	0.67	0.542	0.31 [0.86, 1.45]
P70	Tot	Hif1a	4.53	4.73	0.87	-0.2 [-0.55, 0.15]	-1.60	0.185	0.77 [0.53, 1.99]
P70	Tot	Hmox1	8.06	7.88	1.13	0.17 [-0.15, 0.5]	1.51	0.206	0.59 [0.6, 1.7]
P70	Tot	Hspa5	3.81	3.39	1.33	0.42 [-0.02, 0.85]	2.63	0.058	1.06 [0.34, 2.37]
P70	Tot	Idh1	4.53	4.91	0.77	-0.38 [-0.72, -0.05]	-3.17	0.034 *	1.91 [0.31, 3.44]
P70	Tot	Ift172	6.75	7.08	0.80	-0.33 [-0.87, 0.21]	-1.69	0.166	1.01 [0.25, 2.2]
P70	Tot	Jak1	4.63	4.91	0.82	-0.28 [-0.73, 0.16]	-1.79	0.148	0.99 [0.36, 2.27]
P70	Tot	Jun	6.51	6.80	0.82	-0.29 [-0.76, 0.18]	-1.69	0.166	0.99 [0.34, 2.25]

APPENDICES

Appendix 4: Statistical results of the OS panel on the whole cerebellum

Stage	Layer	Gene	Avg DCq (N)	Avg DCq (IH)	Fold Change	Difference [CI95]	t	p.value	Hedge's g [CI95]
P70	Tot	Kif9	8.33	8.03	1.23	0.3 [-0.13, 0.72]	1.94	0.125	1.11 [0.26, 2.41]
P70	Tot	Map2k1	6.61	6.84	0.85	-0.23 [-0.51, 0.05]	-2.32	0.081	1.39 [0.01, 2.7]
P70	Tot	Map2k6	6.87	7.03	0.89	-0.16 [-0.84, 0.51]	-0.67	0.541	0.35 [0.86, 1.52]
P70	Tot	Mapk1	3.19	3.22	0.97	-0.04 [-0.62, 0.54]	-0.18	0.865	0.09 [1.08, 1.26]
P70	Tot	Mapk10	2.12	1.99	1.10	0.14 [-0.25, 0.52]	0.98	0.383	0.45 [0.75, 1.59]
P70	Tot	Mapk14	7.56	7.39	1.12	0.17 [-0.23, 0.56]	1.19	0.299	0.7 [0.43, 1.76]
P70	Tot	Mapk3	4.51	4.48	1.02	0.03 [-0.38, 0.43]	0.19	0.861	0.11 [0.97, 1.19]
P70	Tot	Mapk8	7.46	7.15	1.24	0.31 [-0.17, 0.79]	1.80	0.146	0.59 [0.55, 1.64]
P70	Tot	Mt1	1.32	1.08	1.18	0.24 [-0.1, 0.58]	1.94	0.124	1.14 [0.22, 2.44]
P70	Tot	Mt2	2.28	1.86	1.34	0.42 [0.17, 0.67]	4.60	0.010 *	2.62 [0.67, 4.49]
P70	Tot	Ndufv2	1.79	1.79	1.00	0 [-0.29, 0.29]	0.00	0.999	0 [1.17, 1.17]
P70	Tot	Nfe2l2	6.67	6.70	0.98	-0.03 [-0.22, 0.15]	-0.51	0.639	0.24 [0.93, 1.38]
P70	Tot	Nfkb1	6.85	7.04	0.88	-0.19 [-0.74, 0.37]	-0.92	0.408	0.34 [0.75, 1.38]
P70	Tot	Nfkbb1	6.38	6.50	0.92	-0.12 [-0.95, 0.72]	-0.39	0.720	0.22 [0.98, 1.39]
P70	Tot	Nos1	6.10	6.27	0.89	-0.17 [-0.71, 0.37]	-0.88	0.430	0.41 [0.78, 1.55]
P70	Tot	Nqo1	8.30	8.19	1.08	0.11 [-0.69, 0.91]	0.38	0.722	0.22 [0.98, 1.39]
P70	Tot	Nudt15	8.16	8.03	1.09	0.13 [-0.23, 0.49]	0.99	0.379	0.52 [0.72, 1.71]
P70	Tot	Park7	3.88	3.61	1.20	0.26 [-0.01, 0.54]	2.65	0.057	1.55 [0.06, 2.97]
P70	Tot	Parp1	6.02	5.83	1.15	0.2 [-0.11, 0.5]	1.79	0.148	0.99 [0.36, 2.27]
P70	Tot	Por	4.34	5.02	0.63	-0.67 [-1.03, -0.32]	-5.32	0.006 **	3.04 [0.92, 5.1]
P70	Tot	Ppp1r15b	5.62	5.72	0.93	-0.1 [-0.45, 0.24]	-0.82	0.457	0.35 [0.8, 1.45]
P70	Tot	Prdx1	1.72	1.95	0.86	-0.22 [-0.57, 0.12]	-1.80	0.147	0.97 [0.38, 2.25]
P70	Tot	Prdx2	3.24	3.24	1.00	-0.01 [-0.19, 0.17]	-0.11	0.920	0.06 [1.12, 1.23]
P70	Tot	Prdx3	4.94	4.81	1.09	0.13 [-0.11, 0.36]	1.50	0.208	0.87 [0.43, 2.11]
P70	Tot	Prdx4	6.13	6.28	0.90	-0.16 [-0.39, 0.07]	-1.90	0.130	1.06 [0.31, 2.36]
P70	Tot	Prdx5	2.69	2.75	0.96	-0.06 [-0.31, 0.2]	-0.63	0.565	0.38 [0.81, 1.53]
P70	Tot	Prdx6	3.31	2.70	1.52	0.61 [0.35, 0.87]	6.42	0.003 **	3.37 [0.93, 5.76]
P70	Tot	Psmb5	3.82	3.58	1.18	0.24 [-0.13, 0.61]	1.82	0.143	0.99 [0.37, 2.28]
P70	Tot	Ptgs1	7.49	7.68	0.87	-0.19 [-0.47, 0.08]	-1.98	0.119	1.16 [0.21, 2.46]
P70	Tot	Rela	5.93	6.18	0.84	-0.25 [-0.66, 0.15]	-1.75	0.155	0.61 [0.55, 1.69]
P70	Tot	Rheb	3.59	3.98	0.76	-0.39 [-0.69, -0.08]	-3.53	0.024 *	2.13 [0.44, 3.76]
P70	Tot	Slc38a1	4.53	4.73	0.87	-0.2 [-0.45, 0.06]	-2.15	0.097	1.3 [0.08, 2.61]
P70	Tot	Slc41a3	6.24	6.04	1.15	0.21 [-0.32, 0.73]	1.10	0.334	0.62 [0.64, 1.83]
P70	Tot	Sod1	2.37	2.58	0.86	-0.22 [-0.42, -0.01]	-2.92	0.043 *	1.3 [0.22, 2.71]
P70	Tot	Sod2	4.38	4.31	1.05	0.07 [-0.18, 0.32]	0.76	0.489	0.46 [0.74, 1.62]
P70	Tot	Sod3	6.70	6.53	1.12	0.16 [-0.34, 0.66]	0.91	0.414	0.47 [0.76, 1.65]
P70	Tot	Sp1	6.52	6.57	0.97	-0.04 [-0.38, 0.3]	-0.33	0.760	0.16 [1, 1.29]
P70	Tot	Srxn1	4.75	4.92	0.89	-0.17 [-0.72, 0.38]	-0.86	0.438	0.28 [0.73, 1.23]
P70	Tot	Tmod	5.50	5.91	0.76	-0.4 [-0.82, 0.02]	-2.67	0.056	1.16 [0.29, 2.51]
P70	Tot	Txnip	6.55	6.69	0.90	-0.14 [-0.32, 0.03]	-2.28	0.084	1.36 [0.06, 2.7]
P70	Tot	Txnrd1	5.79	5.78	1.00	0.01 [-0.26, 0.27]	0.05	0.960	0.03 [1.13, 1.18]
P70	Tot	Txnrd3	8.17	8.55	0.77	-0.38 [-0.67, -0.09]	-3.69	0.021 *	1.94 [0.2, 3.59]
P70	Tot	Xrcc1	7.58	8.19	0.66	-0.61 [-1.2, -0.01]	-2.82	0.048 *	1.7 [0.18, 3.14]

Asterisks after p.values indicate the level of statistical significance: one for p < .05, two for p < .01, and three for p < .001

Stage	Layer	Gene	Avg DCq (N)	Avg DCq (IH)	Fold Change	Difference [CI ₉₅]	t	p.value	Hedge's g [CI ₉₅]
P8	PC	Adcyap1	15.06	10.12	30.64	4.94 [-0.13, 10.01]	2.17	0.055	1.04 [0.07, 2.09]
P8	PC	Apex1	5.96	6.13	0.89	-0.17 [-0.65, 0.3]	-0.77	0.453	0.32 [0.61, 1.24]
P8	PC	Casp3	9.14	9.77	0.65	-0.63 [-1.54, 0.28]	-1.51	0.157	0.82 [0.12, 1.73]
P8	PC	Cox4i1	0.88	0.97	0.94	-0.09 [-0.34, 0.15]	-0.83	0.421	0.35 [0.58, 1.27]
P8	PC	Dnm2	10.04	13.19	0.11	-3.15 [-7.36, 1.05]	-1.73	0.122	0.67 [0.5, 1.76]
P8	PC	Fth1	1.41	1.41	1.00	0 [-0.25, 0.25]	-0.01	0.989	0.01 [0.9, 0.92]
P8	PC	Gpx4	3.72	4.35	0.65	-0.63 [-0.94, -0.32]	-4.35	<0.001 ***	1.85 [0.64, 3]
P8	PC	Gpx7	7.50	8.16	0.63	-0.67 [-2.14, 0.8]	-0.99	0.344	0.37 [0.66, 1.36]
P8	PC	Gsr	7.30	10.08	0.15	-2.78 [-4.56, -1]	-3.44	0.006 **	1.67 [0.44, 2.84]
P8	PC	Gss	12.95	9.25	12.97	3.7 [0.56, 6.83]	2.53	0.024 *	0.92 [0.14, 1.94]
P8	PC	Hadh	8.84	8.13	1.64	0.72 [-0.86, 2.29]	0.98	0.346	0.36 [0.58, 1.28]
P8	PC	Hif1a	12.18	13.15	0.51	-0.97 [-5.02, 3.07]	-0.57	0.588	0.34 [0.76, 1.42]
P8	PC	Jun	10.19	9.44	1.68	0.75 [-0.57, 2.07]	1.28	0.232	0.56 [0.55, 1.6]
P8	PC	Mapk1	10.47	9.98	1.41	0.49 [-2.6, 3.58]	0.34	0.737	0.13 [0.79, 1.04]
P8	PC	Mapk14	13.53	14.50	0.51	-0.97 [-2.26, 0.33]	-1.61	0.131	0.72 [0.22, 1.64]
P8	PC	Mapk3	9.35	8.69	1.59	0.67 [-0.91, 2.24]	0.91	0.380	0.36 [0.59, 1.28]
P8	PC	Mt2	6.37	5.39	1.98	0.99 [0.49, 1.48]	4.30	<0.001 ***	1.81 [0.6, 2.96]
P8	PC	Nfkb1	11.22	15.07	0.07	-3.86 [-5.34, -2.38]	-5.59	<0.001 ***	2.2 [0.78, 3.57]
P8	PC	Nfkbib	11.06	8.55	5.71	2.51 [0.92, 4.11]	3.41	0.005 **	1.24 [0.02, 2.39]
P8	PC	Nos1	14.77	19.76	0.03	-4.99 [-7.48, -2.49]	-4.31	<0.001 ***	1.99 [0.78, 3.15]
P8	PC	Parp1	13.23	8.98	18.97	4.25 [1.91, 6.58]	3.89	0.002 **	1.41 [0.19, 2.58]
P8	PC	Por	7.32	6.77	1.46	0.55 [-1.47, 2.57]	0.58	0.568	0.22 [0.71, 1.13]
P8	PC	Prdx2	1.34	2.26	0.53	-0.92 [-1.21, -0.63]	-6.85	<0.001 ***	2.77 [1.19, 4.29]
P8	PC	Prdx3	4.79	5.55	0.59	-0.76 [-1.14, -0.38]	-4.25	<0.001 ***	1.92 [0.78, 3.02]
P8	PC	Prdx5	1.89	2.37	0.72	-0.48 [-0.86, -0.11]	-2.75	0.016 *	1.16 [0.11, 2.17]
P8	PC	Prdx6	5.03	5.69	0.63	-0.66 [-1.01, -0.31]	-4.00	0.001 **	1.66 [0.48, 2.79]
P8	PC	Rheb	4.66	4.48	1.13	0.18 [-0.46, 0.81]	0.60	0.559	0.26 [0.66, 1.17]
P8	PC	Slc41a3	7.51	7.77	0.83	-0.27 [-1.02, 0.49]	-0.76	0.460	0.32 [0.61, 1.24]
P8	PC	Sod2	6.87	6.29	1.50	0.58 [-0.12, 1.29]	1.77	0.099	0.68 [0.31, 1.64]
P8	PC	Srxn1	10.55	8.74	3.53	1.82 [-1.06, 4.7]	1.35	0.197	0.5 [0.47, 1.44]
P12	PC	Adcyap1	11.04	11.79	0.59	-0.75 [-2.31, 0.8]	-1.04	0.315	0.46 [0.5, 1.4]
P12	PC	Aldh1a1	6.94	8.26	0.40	-1.33 [-2.26, -0.39]	-3.11	0.010 **	1.43 [0.27, 2.55]
P12	PC	Apex1	6.66	6.90	0.84	-0.25 [-0.74, 0.25]	-1.04	0.311	0.37 [0.41, 1.13]
P12	PC	Casp3	9.94	10.21	0.83	-0.27 [-0.95, 0.4]	-0.86	0.403	0.32 [0.51, 1.13]
P12	PC	Cox4i1	1.86	1.90	0.98	-0.04 [-0.42, 0.35]	-0.19	0.853	0.07 [0.69, 0.82]
P12	PC	Dnm2	13.39	13.53	0.90	-0.14 [-1.89, 1.61]	-0.17	0.864	0.07 [0.77, 0.9]
P12	PC	Fth1	2.83	2.80	1.02	0.03 [-0.23, 0.3]	0.24	0.814	0.09 [0.68, 0.84]
P12	PC	Gpx4	4.92	4.96	0.98	-0.04 [-0.35, 0.28]	-0.24	0.813	0.09 [0.68, 0.85]
P12	PC	Gpx7	7.63	8.24	0.65	-0.61 [-1.33, 0.1]	-1.78	0.090	0.66 [0.16, 1.47]
P12	PC	Gsr	9.78	9.38	1.32	0.41 [-1, 1.81]	0.60	0.555	0.23 [0.52, 0.96]
P12	PC	Gss	9.44	10.10	0.63	-0.66 [-1.28, -0.03]	-2.19	0.040 *	0.82 [0.02, 1.61]
P12	PC	Hadh	8.05	8.57	0.70	-0.52 [-1.79, 0.74]	-0.85	0.402	0.31 [0.46, 1.07]
P12	PC	Hif1a	13.27	13.20	1.05	0.07 [-1.54, 1.67]	0.09	0.932	0.03 [0.79, 0.86]
P12	PC	Jun	10.68	11.67	0.51	-0.98 [-2.88, 0.91]	-1.08	0.293	0.4 [0.46, 1.24]

Stage	Layer	Gene	Avg DCq (N)	Avg DCq (IH)	Fold Change	Difference [Cl ₉₅]	t	p.value	Hedge's g [Cl ₉₅]
P12	PC	Mapk1	9.73	9.62	1.08	0.11 [-0.72, 0.94]	0.27	0.787	0.1 [0.69, 0.89]
P12	PC	Mapk14	14.63	14.05	1.50	0.59 [-0.87, 2.05]	0.83	0.415	0.29 [0.49, 1.06]
P12	PC	Mapk3	9.13	8.48	1.58	0.66 [-0.07, 1.39]	1.87	0.075	0.66 [0.14, 1.45]
P12	PC	Mt2	6.34	5.40	1.93	0.95 [0.36, 1.53]	3.36	0.003 **	1.19 [0.32, 2.04]
P12	PC	Nfkbia	12.28	12.89	0.66	-0.6 [-2.2, 1]	-0.78	0.444	0.28 [0.48, 1.04]
P12	PC	Nfkbb	8.56	9.68	0.46	-1.12 [-2.41, 0.17]	-1.80	0.085	0.6 [0.22, 1.39]
P12	PC	Parp1	9.18	9.83	0.64	-0.65 [-1.3, 0]	-2.09	0.049 *	0.75 [0.09, 1.56]
P12	PC	Por	7.07	7.17	0.93	-0.11 [-0.83, 0.61]	-0.31	0.763	0.11 [0.63, 0.86]
P12	PC	Ppp1r15b	14.49	13.31	2.26	1.17 [-2.1, 4.45]	0.77	0.455	0.39 [0.44, 1.2]
P12	PC	Prdx2	2.60	2.80	0.87	-0.2 [-0.57, 0.18]	-1.09	0.289	0.38 [0.4, 1.15]
P12	PC	Prdx3	4.94	5.20	0.84	-0.25 [-0.76, 0.26]	-1.03	0.314	0.37 [0.39, 1.13]
P12	PC	Prdx5	2.53	2.72	0.88	-0.19 [-0.37, 0]	-2.10	0.047 *	0.72 [0.1, 1.52]
P12	PC	Prdx6	4.71	4.99	0.82	-0.28 [-0.59, 0.02]	-1.93	0.066	0.69 [0.11, 1.47]
P12	PC	Rheb	3.87	4.32	0.73	-0.46 [-0.82, -0.1]	-2.61	0.016 *	0.93 [0.11, 1.74]
P12	PC	Slc41a3	7.74	8.94	0.43	-1.2 [-2.38, -0.02]	-2.11	0.046 *	0.73 [0.09, 1.53]
P12	PC	Sod2	5.93	6.28	0.78	-0.35 [-0.75, 0.05]	-1.82	0.082	0.66 [0.14, 1.43]
P12	PC	Srxn1	7.60	7.70	0.93	-0.1 [-0.57, 0.37]	-0.44	0.668	0.16 [0.6, 0.91]
P12	PC	Txnip	12.76	12.91	0.90	-0.15 [-1.47, 1.17]	-0.24	0.810	0.1 [0.73, 0.94]
P12	PC	Txnd3	11.64	13.27	0.32	-1.63 [-4.37, 1.11]	-1.26	0.226	0.52 [0.4, 1.42]
P21	PC	Adcyap1	10.70	10.60	1.07	0.09 [-3.41, 3.6]	0.06	0.952	0.03 [0.95, 1.01]
P21	PC	Apex1	6.39	5.31	2.12	1.09 [-0.38, 2.56]	1.60	0.134	0.69 [0.28, 1.62]
P21	PC	Casp3	9.97	10.54	0.68	-0.56 [-4.69, 3.57]	-0.33	0.751	0.14 [0.91, 1.16]
P21	PC	Cox4i1	0.82	0.70	1.08	0.12 [-0.49, 0.72]	0.41	0.687	0.18 [0.71, 1.07]
P21	PC	Dnm2	12.33	10.80	2.88	1.53 [-1.16, 4.22]	1.34	0.222	0.75 [0.4, 1.85]
P21	PC	Fth1	2.15	2.27	0.92	-0.11 [-0.75, 0.52]	-0.39	0.702	0.17 [0.73, 1.07]
P21	PC	Gpx4	3.72	3.17	1.47	0.56 [-0.23, 1.35]	1.51	0.153	0.66 [0.27, 1.57]
P21	PC	Gpx7	7.43	6.92	1.42	0.51 [-1.15, 2.17]	0.69	0.509	0.32 [0.7, 1.34]
P21	PC	Gsr	6.80	7.01	0.87	-0.2 [-1.58, 1.18]	-0.32	0.756	0.14 [0.8, 1.07]
P21	PC	Gss	8.02	7.39	1.55	0.63 [-0.69, 1.95]	1.07	0.311	0.51 [0.53, 1.53]
P21	PC	Hadh	7.81	8.13	0.80	-0.32 [-2.19, 1.55]	-0.37	0.719	0.16 [0.77, 1.09]
P21	PC	Hif1a	11.79	9.12	6.37	2.67 [-0.1, 5.44]	2.28	0.057	0.97 [0.32, 2.18]
P21	PC	Jun	9.80	11.09	0.41	-1.29 [-3.32, 0.74]	-1.40	0.189	0.64 [0.39, 1.65]
P21	PC	Mapk1	8.14	8.05	1.07	0.1 [-1.26, 1.45]	0.16	0.879	0.07 [0.84, 0.97]
P21	PC	Mapk14	13.34	13.08	1.20	0.26 [-1.29, 1.82]	0.36	0.721	0.16 [0.71, 1.02]
P21	PC	Mapk3	9.20	8.42	1.71	0.78 [-0.61, 2.16]	1.20	0.250	0.5 [0.43, 1.42]
P21	PC	Mt2	2.61	2.85	0.84	-0.25 [-1.07, 0.57]	-0.64	0.531	0.28 [0.6, 1.15]
P21	PC	Nfkbia	12.56	12.00	1.48	0.57 [-1.87, 3]	0.50	0.626	0.21 [0.7, 1.12]
P21	PC	Nfkbb	9.52	9.10	1.34	0.43 [-2.95, 3.8]	0.28	0.786	0.13 [0.85, 1.11]
P21	PC	Parp1	6.78	7.18	0.75	-0.41 [-1.66, 0.84]	-0.74	0.481	0.35 [0.7, 1.39]
P21	PC	Por	4.97	6.56	0.33	-1.59 [-4.26, 1.07]	-1.29	0.220	0.55 [0.39, 1.47]
P21	PC	Ppp1r15b	12.05	10.42	3.10	1.63 [-1.33, 4.59]	1.35	0.226	0.71 [0.53, 1.9]
P21	PC	Prdx2	0.96	0.50	1.38	0.46 [-0.37, 1.29]	1.19	0.254	0.51 [0.42, 1.43]
P21	PC	Prdx3	4.31	3.35	1.95	0.96 [-0.63, 2.56]	1.29	0.217	0.56 [0.34, 1.43]

APPENDICES

Appendix 5: Statistical results of the OS panel on Purkinje cells

Stage	Layer	Gene	Avg DCq (N)	Avg DCq (IH)	Fold Change	Difference [CI ₉₅]	t	p.value	Hedge's g [CI ₉₅]
P21	PC	Prdx5	1.76	1.40	1.28	0.36 [-0.3, 1.02]	1.16	0.265	0.51 [0.41, 1.41]
P21	PC	Prdx6	3.10	2.87	1.18	0.24 [-0.36, 0.84]	0.85	0.411	0.37 [0.54, 1.27]
P21	PC	Rheb	3.11	3.43	0.80	-0.32 [-0.86, 0.22]	-1.28	0.222	0.55 [0.35, 1.43]
P21	PC	Slc41a3	6.78	7.39	0.66	-0.61 [-3.46, 2.23]	-0.46	0.652	0.2 [0.71, 1.1]
P21	PC	Sod2	6.34	5.40	1.91	0.94 [-0.84, 2.71]	1.13	0.278	0.49 [0.4, 1.35]
P21	PC	Srxn1	4.62	5.17	0.68	-0.55 [-2.42, 1.32]	-0.63	0.538	0.27 [0.64, 1.18]
P21	PC	Tmod	10.36	8.89	2.77	1.47 [-0.92, 3.85]	1.51	0.182	0.8 [0.46, 2]
P21	PC	Txnip	10.50	11.99	0.36	-1.49 [-3.95, 0.97]	-1.68	0.168	0.95 [0.42, 2.25]
P21	PC	Txnrd3	8.68	11.99	0.10	-3.31 [-6, -0.62]	-3.16	0.025 *	1.88 [0.27, 3.42]
P70	PC	Apex1	1.25	3.76	0.18	-2.51 [-5.8, 0.77]	-2.44	0.093	1.13 [0.35, 2.51]
P70	PC	Cox4i1	-0.18	0.19	0.77	-0.37 [-1.85, 1.1]	-0.81	0.477	0.36 [0.78, 1.44]
P70	PC	Fth1	0.50	0.19	1.24	0.31 [-1.68, 2.3]	0.49	0.658	0.26 [1.04, 1.53]
P70	PC	Gpx4	1.65	2.07	0.75	-0.42 [-2.1, 1.25]	-0.80	0.482	0.4 [0.87, 1.61]
P70	PC	Hadh	1.02	2.04	0.49	-1.02 [-4.15, 2.1]	-1.04	0.374	0.55 [0.8, 1.83]
P70	PC	Hif1a	6.58	5.10	2.79	1.48 [-2.78, 5.74]	1.11	0.350	0.58 [0.77, 1.86]
P70	PC	Mapk14	3.95	5.16	0.43	-1.2 [-3.25, 0.84]	-1.87	0.158	0.91 [0.49, 2.22]
P70	PC	Mapk3	2.12	2.94	0.57	-0.82 [-2.62, 0.97]	-1.46	0.242	0.75 [0.63, 2.05]
P70	PC	Mt2	2.04	2.65	0.65	-0.62 [-1.79, 0.55]	-1.68	0.192	0.84 [0.56, 2.14]
P70	PC	Nfkbia	3.14	3.52	0.77	-0.38 [-1.26, 0.49]	-1.39	0.260	0.6 [0.6, 1.7]
P70	PC	Nfkbb	3.70	5.20	0.35	-1.51 [-3.11, 0.09]	-2.99	0.058	1.37 [0.23, 2.87]

Asterisks after p.values indicate the level of statistical significance: one for $p < .05$, two for $p < .01$, and three for $p < .001$

Stage	Layer	Gene	Avg DCq (N)	Avg DCq (IH)	Fold Change	Difference [CI ₉₅]	t	p.value	Hedge's g [CI ₉₅]
P4	EGL	Akt1	3.85	3.96	0.93	-0.11 [-0.31, 0.09]	-1.22	0.247	0.56 [0.45, 1.55]
P4	EGL	Cacng2	5.44	5.41	1.02	0.04 [-0.28, 0.35]	0.25	0.810	0.11 [0.84, 1.05]
P4	EGL	Cadm3	6.24	6.28	0.98	-0.04 [-0.35, 0.28]	-0.26	0.802	0.12 [0.86, 1.1]
P4	EGL	Calb2	5.80	6.17	0.77	-0.37 [-0.67, -0.07]	-2.72	0.020 *	1.25 [0.13, 2.33]
P4	EGL	Ccnd1	3.24	3.37	0.92	-0.13 [-0.25, 0]	-2.28	0.044 *	1.05 [0.03, 2.1]
P4	EGL	Dclk1	8.57	8.36	1.15	0.21 [-0.35, 0.77]	0.81	0.433	0.38 [0.62, 1.36]
P4	EGL	Gabra1	8.51	8.72	0.87	-0.21 [-0.88, 0.47]	-0.68	0.513	0.31 [0.67, 1.27]
P4	EGL	Gas7	9.15	9.03	1.09	0.12 [-0.51, 0.75]	0.41	0.688	0.19 [0.79, 1.16]
P4	EGL	Gria2	5.73	5.80	0.95	-0.07 [-0.47, 0.34]	-0.36	0.723	0.17 [0.81, 1.13]
P4	EGL	Grm3	8.28	8.24	1.03	0.04 [-0.7, 0.78]	0.12	0.907	0.05 [0.91, 1.02]
P4	EGL	Homer1	7.82	8.23	0.75	-0.41 [-0.73, -0.1]	-2.89	0.015 *	1.28 [0.12, 2.39]
P4	EGL	Homer2	6.40	6.89	0.71	-0.5 [-0.91, -0.08]	-2.64	0.023 *	1.2 [0.07, 2.27]
P4	EGL	Nrxn1	8.35	8.74	0.76	-0.39 [-1.04, 0.25]	-1.34	0.208	0.62 [0.4, 1.62]
P4	EGL	Nxph4	8.52	8.44	1.06	0.08 [-0.52, 0.69]	0.31	0.763	0.14 [0.84, 1.12]
P4	EGL	Pax6	2.85	2.94	0.94	-0.09 [-0.16, -0.01]	-2.46	0.032 *	1.1 [0.01, 2.16]
P4	EGL	Robo1	6.62	6.70	0.95	-0.08 [-0.35, 0.2]	-0.62	0.548	0.28 [0.69, 1.24]
P4	EGL	Slc17a6	7.14	7.62	0.72	-0.48 [-1.07, 0.11]	-1.80	0.100	0.82 [0.23, 1.83]
P4	EGL	Slc17a7	9.42	9.38	1.03	0.04 [-0.46, 0.54]	0.19	0.857	0.09 [0.99, 1.17]
P4	EGL	Stmn1	0.53	0.64	0.93	-0.11 [-0.23, 0.01]	-1.97	0.075	0.89 [0.17, 1.91]
P4	EGL	Syn2	6.15	6.50	0.79	-0.35 [-0.59, -0.1]	-3.16	0.009 **	1.44 [0.26, 2.57]
P4	EGL	Syp	6.71	7.12	0.75	-0.42 [-0.86, 0.02]	-2.09	0.060	0.94 [0.13, 1.96]
P4	EGL	Zic1	2.29	2.50	0.87	-0.21 [-0.3, -0.12]	-5.19	<0.001 ***	2.4 [1.01, 3.75]
P4	IGL	Adora1	7.08	6.46	1.53	0.61 [-0.4, 1.62]	1.48	0.188	0.8 [0.44, 1.99]
P4	IGL	Cadps2	4.38	4.11	1.21	0.27 [-0.03, 0.57]	1.98	0.074	0.9 [0.17, 1.92]
P4	IGL	Calb2	5.47	5.70	0.85	-0.23 [-1.15, 0.69]	-0.56	0.588	0.25 [0.76, 1.24]
P4	IGL	Gabra1	6.67	6.51	1.12	0.16 [-0.67, 1]	0.47	0.653	0.24 [0.89, 1.35]
P4	IGL	Gabrg2	5.09	4.94	1.11	0.15 [-0.33, 0.62]	0.69	0.506	0.32 [0.68, 1.3]
P4	IGL	Grin1	5.35	5.07	1.21	0.28 [-0.2, 0.75]	1.29	0.222	0.6 [0.42, 1.59]
P4	IGL	Grm3	3.07	3.20	0.91	-0.14 [-0.36, 0.09]	-1.35	0.203	0.63 [0.4, 1.62]
P4	IGL	Homer1	6.05	5.40	1.57	0.65 [0.23, 1.07]	3.41	0.006 **	1.58 [0.39, 2.72]
P4	IGL	Homer2	5.83	5.39	1.35	0.43 [-0.02, 0.89]	2.11	0.058	0.97 [0.1, 2.01]
P4	IGL	Nrxn1	4.71	4.63	1.06	0.08 [-0.29, 0.46]	0.49	0.631	0.23 [0.76, 1.2]
P4	IGL	Nxph4	5.32	6.16	0.56	-0.84 [-1.33, -0.36]	-3.84	0.003 **	1.68 [0.37, 2.92]
P4	IGL	Pax6	2.98	2.92	1.04	0.06 [-0.13, 0.25]	0.72	0.486	0.33 [0.66, 1.31]
P4	IGL	Rac1	3.18	3.04	1.10	0.14 [-0.1, 0.37]	1.27	0.231	0.59 [0.43, 1.58]
P4	IGL	Robo1	5.47	5.62	0.90	-0.15 [-0.58, 0.28]	-0.76	0.463	0.33 [0.62, 1.26]
P4	IGL	Slc17a6	5.77	5.99	0.86	-0.22 [-1.08, 0.63]	-0.57	0.580	0.26 [0.73, 1.24]
P4	IGL	Slc17a7	6.59	6.83	0.85	-0.24 [-0.95, 0.47]	-0.79	0.455	0.38 [0.72, 1.46]
P4	IGL	Slc32a1	3.92	4.07	0.90	-0.16 [-0.53, 0.21]	-0.94	0.366	0.44 [0.57, 1.42]
P4	IGL	Sst	6.05	6.52	0.72	-0.47 [-1.14, 0.2]	-1.54	0.151	0.7 [0.32, 1.7]
P4	IGL	Stmn1	1.49	1.45	1.03	0.04 [-0.16, 0.23]	0.41	0.690	0.19 [0.8, 1.17]
P4	IGL	Syn2	3.82	3.75	1.05	0.07 [-0.33, 0.47]	0.37	0.722	0.16 [0.78, 1.09]
P4	IGL	Syp	4.10	4.00	1.08	0.11 [-0.23, 0.44]	0.70	0.500	0.32 [0.67, 1.29]

Stage	Layer	Gene	Avg DCq (N)	Avg DCq (IH)	Fold Change	Difference [CI ₉₅]	t	p.value	Hedge's g [CI ₉₅]
P4	IGL	Tln1	5.20	5.27	0.95	-0.07 [-0.71, 0.57]	-0.24	0.816	0.11 [0.86, 1.08]
P4	IGL	Zic1	0.86	0.84	1.01	0.02 [-0.26, 0.3]	0.16	0.875	0.07 [0.9, 1.05]
P4	MLPC	Astn2	3.24	3.20	1.03	0.04 [-0.21, 0.3]	0.37	0.721	0.17 [0.82, 1.15]
P4	MLPC	Cadm3	4.91	4.92	0.99	-0.02 [-0.51, 0.48]	-0.08	0.940	0.03 [0.93, 1]
P4	MLPC	Cadps2	5.06	5.15	0.94	-0.09 [-0.46, 0.27]	-0.56	0.585	0.25 [0.71, 1.2]
P4	MLPC	Calb1	0.13	0.25	0.92	-0.13 [-0.31, 0.06]	-1.51	0.159	0.7 [0.33, 1.7]
P4	MLPC	Calb2	7.18	6.24	1.92	0.94 [0.05, 1.84]	2.49	0.042 *	1.16 [0.13, 2.38]
P4	MLPC	Camk4	3.64	3.62	1.01	0.02 [-0.41, 0.44]	0.08	0.934	0.04 [0.94, 1.02]
P4	MLPC	Cbln1	4.42	4.78	0.78	-0.35 [-0.73, 0.02]	-2.08	0.061	0.97 [0.1, 2]
P4	MLPC	Gabra1	3.85	4.26	0.75	-0.42 [-0.78, -0.05]	-2.48	0.031 *	1.13 [0.03, 2.19]
P4	MLPC	Gria2	2.83	2.64	1.14	0.19 [-0.09, 0.48]	1.48	0.168	0.68 [0.35, 1.67]
P4	MLPC	Grin1	4.08	4.13	0.97	-0.04 [-0.42, 0.33]	-0.25	0.806	0.12 [0.87, 1.1]
P4	MLPC	Grm3	4.22	4.20	1.01	0.02 [-0.19, 0.23]	0.22	0.827	0.1 [0.87, 1.07]
P4	MLPC	L1cam	3.06	3.06	1.00	0 [-0.25, 0.25]	-0.02	0.987	0.01 [0.97, 0.99]
P4	MLPC	Nefl	1.07	1.28	0.86	-0.21 [-0.47, 0.05]	-1.79	0.101	0.83 [0.22, 1.84]
P4	MLPC	Neurod1	3.73	3.71	1.01	0.02 [-0.18, 0.22]	0.22	0.833	0.1 [0.88, 1.07]
P4	MLPC	Slc32a1	2.30	2.22	1.05	0.08 [-0.21, 0.36]	0.59	0.564	0.27 [0.71, 1.25]
P4	MLPC	Syn1	3.83	3.90	0.95	-0.07 [-0.34, 0.2]	-0.55	0.592	0.25 [0.73, 1.22]
P4	MLPC	Syn2	3.91	4.00	0.94	-0.09 [-0.34, 0.16]	-0.77	0.458	0.35 [0.64, 1.33]
P4	MLPC	Tln1	6.45	6.79	0.79	-0.34 [-0.79, 0.1]	-1.71	0.115	0.78 [0.26, 1.78]
P4	MLPC	Zic1	2.85	2.96	0.93	-0.11 [-0.4, 0.18]	-0.83	0.422	0.39 [0.61, 1.37]
P4	WM	Akt1	3.74	3.19	1.47	0.56 [0.01, 1.1]	2.24	0.046 *	1.04 [0.05, 2.08]
P4	WM	Ascl1	3.14	2.79	1.28	0.35 [-0.02, 0.73]	2.07	0.063	0.95 [0.12, 1.98]
P4	WM	Cacng2	3.98	4.11	0.91	-0.13 [-0.63, 0.36]	-0.66	0.536	0.35 [0.8, 1.48]
P4	WM	Cadps2	4.00	3.90	1.07	0.1 [-0.64, 0.85]	0.31	0.764	0.14 [0.83, 1.1]
P4	WM	Calb2	4.15	4.40	0.84	-0.25 [-1.07, 0.56]	-0.70	0.499	0.34 [0.71, 1.37]
P4	WM	Grm3	3.60	3.48	1.09	0.12 [-0.2, 0.45]	0.84	0.420	0.38 [0.61, 1.35]
P4	WM	Mbp	2.58	2.83	0.84	-0.25 [-1.15, 0.66]	-0.61	0.553	0.29 [0.73, 1.3]
P4	WM	Myt1	5.04	5.01	1.02	0.03 [-1.09, 1.15]	0.10	0.930	0.05 [1.22, 1.32]
P4	WM	Neurog2	4.68	5.03	0.78	-0.35 [-1.35, 0.65]	-0.90	0.409	0.47 [0.76, 1.66]
P4	WM	Nrxn1	3.41	3.49	0.94	-0.08 [-0.79, 0.63]	-0.26	0.803	0.12 [0.86, 1.09]
P4	WM	Nxph4	4.63	3.98	1.57	0.65 [-0.05, 1.36]	2.10	0.066	1.02 [0.14, 2.13]
P4	WM	Plp1	4.07	3.50	1.48	0.57 [-0.24, 1.38]	1.73	0.135	0.89 [0.31, 2.02]
P4	WM	Rac1	2.62	2.25	1.29	0.37 [-0.11, 0.85]	1.69	0.120	0.76 [0.27, 1.77]
P4	WM	Robo1	3.47	2.86	1.53	0.61 [0.06, 1.17]	2.43	0.034 *	1.06 [0.04, 2.12]
P4	WM	Stmn1	1.07	0.40	1.59	0.67 [0.43, 0.9]	6.24	<0.001 ***	2.86 [1.29, 4.38]
P4	WM	Tln1	4.88	3.36	2.86	1.51 [0.48, 2.54]	3.28	0.008 **	1.58 [0.35, 2.75]
P4	WM	Zic1	1.95	1.64	1.24	0.31 [-0.4, 1.01]	0.95	0.360	0.44 [0.56, 1.41]
P8	EGLi	Akt1	3.12	3.53	0.76	-0.4 [-0.56, -0.25]	-5.56	<0.001 ***	2.58 [1.27, 3.85]
P8	EGLi	Cacng2	4.63	5.08	0.73	-0.45 [-0.67, -0.23]	-4.39	<0.001 ***	2.04 [0.87, 3.16]
P8	EGLi	Cadm3	3.09	3.65	0.68	-0.57 [-0.71, -0.42]	-8.25	<0.001 ***	3.62 [1.98, 5.23]
P8	EGLi	Calb2	7.13	7.35	0.86	-0.21 [-0.91, 0.49]	-0.65	0.524	0.29 [0.62, 1.19]
P8	EGLi	Cdh8	7.47	7.47	1.00	0 [-0.54, 0.54]	0.00	0.998	0 [0.97, 0.97]
P8	EGLi	Dclk1	4.38	5.15	0.58	-0.77 [-1.03, -0.52]	-6.62	<0.001 ***	3.08 [1.6, 4.52]

Stage	Layer	Gene	Avg DCq (N)	Avg DCq (IH)	Fold Change	Difference [CI ₉₅]	t	p.value	Hedge's g [CI ₉₅]
P8	EGLi	Gabra1	8.03	8.06	0.98	-0.03 [-0.52, 0.46]	-0.15	0.885	0.07 [0.88, 1.02]
P8	EGLi	Gria2	4.25	4.57	0.80	-0.32 [-0.6, -0.04]	-2.46	0.028 *	1.14 [0.16, 2.08]
P8	EGLi	Grin1	5.63	6.75	0.46	-1.12 [-1.46, -0.77]	-6.96	<0.001 ***	3.02 [1.53, 4.47]
P8	EGLi	Grm3	7.33	7.64	0.81	-0.31 [-0.66, 0.05]	-1.88	0.082	0.86 [0.12, 1.81]
P8	EGLi	Homer1	6.42	6.99	0.67	-0.57 [-0.83, -0.31]	-4.74	<0.001 ***	2.15 [0.92, 3.34]
P8	EGLi	Homer2	6.56	7.31	0.60	-0.75 [-1.29, -0.2]	-2.98	0.011 *	1.34 [0.22, 2.41]
P8	EGLi	Nav3	3.78	3.84	0.96	-0.06 [-0.41, 0.29]	-0.37	0.720	0.17 [0.71, 1.04]
P8	EGLi	Nxph4	4.41	4.83	0.75	-0.42 [-0.61, -0.23]	-4.74	<0.001 ***	2.13 [0.93, 3.28]
P8	EGLi	Pax6	1.73	1.99	0.83	-0.27 [-0.41, -0.13]	-4.22	<0.001 ***	1.96 [0.81, 3.07]
P8	EGLi	Robo1	6.33	6.94	0.65	-0.61 [-0.94, -0.28]	-3.95	0.001 **	1.68 [0.52, 2.79]
P8	EGLi	Slc17a6	5.36	6.14	0.58	-0.78 [-1.12, -0.44]	-4.89	<0.001 ***	2.24 [1.03, 3.41]
P8	EGLi	Slc17a7	5.50	6.51	0.50	-1.01 [-1.3, -0.73]	-7.59	<0.001 ***	3.53 [1.86, 5.17]
P8	EGLi	Stmn1	0.37	0.72	0.79	-0.35 [-0.47, -0.22]	-6.07	<0.001 ***	2.81 [1.44, 4.15]
P8	EGLi	Syn1	3.27	4.01	0.60	-0.74 [-0.93, -0.55]	-8.34	<0.001 ***	3.88 [2.12, 5.62]
P8	EGLi	Syn2	4.58	5.58	0.50	-1 [-1.3, -0.7]	-7.13	<0.001 ***	3.32 [1.71, 4.88]
P8	EGLi	Syp	3.02	3.70	0.62	-0.68 [-0.8, -0.57]	-12.67	<0.001 ***	5.56 [3.28, 7.81]
P8	EGLi	Tln1	8.04	7.92	1.09	0.12 [-0.56, 0.8]	0.38	0.711	0.17 [0.76, 1.09]
P8	EGLi	Zic1	0.13	0.67	0.69	-0.54 [-0.64, -0.43]	-10.88	<0.001 ***	5.01 [2.99, 7]
P8	EGLo	Akt1	3.35	3.59	0.84	-0.24 [-0.42, -0.07]	-3.04	0.009 **	1.4 [0.38, 2.39]
P8	EGLo	Cacng2	5.33	5.68	0.78	-0.35 [-0.5, -0.2]	-4.96	<0.001 ***	2.09 [0.81, 3.32]
P8	EGLo	Ccnd1	4.25	4.54	0.82	-0.29 [-0.52, -0.05]	-2.59	0.021 *	1.21 [0.22, 2.15]
P8	EGLo	Cdh8	7.05	7.15	0.93	-0.1 [-0.52, 0.32]	-0.52	0.613	0.23 [0.69, 1.13]
P8	EGLo	Dclk1	8.44	8.82	0.77	-0.38 [-0.95, 0.19]	-1.42	0.178	0.65 [0.31, 1.58]
P8	EGLo	Grm3	8.81	8.84	0.98	-0.03 [-0.55, 0.48]	-0.14	0.887	0.07 [0.87, 1.01]
P8	EGLo	Homer1	6.90	7.52	0.65	-0.61 [-0.8, -0.42]	-6.90	<0.001 ***	3.18 [1.63, 4.68]
P8	EGLo	Homer2	6.81	7.10	0.82	-0.29 [-0.6, 0.01]	-2.06	0.060	0.88 [0.14, 1.87]
P8	EGLo	Nav3	5.60	5.83	0.86	-0.23 [-0.71, 0.26]	-1.00	0.333	0.46 [0.43, 1.34]
P8	EGLo	Nrxn1	7.37	7.93	0.68	-0.56 [-1.12, 0]	-2.13	0.052	0.99 [0.04, 1.9]
P8	EGLo	Nxph4	6.96	6.68	1.21	0.27 [-0.17, 0.71]	1.33	0.204	0.6 [0.32, 1.51]
P8	EGLo	Pax6	2.30	2.49	0.88	-0.19 [-0.31, -0.06]	-3.22	0.006 **	1.5 [0.45, 2.51]
P8	EGLo	Robo1	6.12	6.65	0.69	-0.53 [-0.82, -0.25]	-4.02	0.001 **	1.72 [0.52, 2.87]
P8	EGLo	Slc17a6	5.70	6.36	0.63	-0.66 [-1.02, -0.31]	-4.05	0.001 **	1.88 [0.72, 3]
P8	EGLo	Slc17a7	8.54	9.01	0.72	-0.47 [-0.87, -0.06]	-2.55	0.027 *	1.17 [0.06, 2.24]
P8	EGLo	Stmn1	0.22	0.50	0.82	-0.28 [-0.41, -0.15]	-4.49	<0.001 ***	2.09 [0.9, 3.23]
P8	EGLo	Syn2	5.90	6.12	0.86	-0.22 [-0.55, 0.11]	-1.42	0.176	0.65 [0.26, 1.55]
P8	EGLo	Syp	5.69	5.81	0.92	-0.13 [-0.32, 0.07]	-1.37	0.193	0.61 [0.32, 1.53]
P8	EGLo	Tln1	5.56	5.97	0.75	-0.41 [-0.8, -0.02]	-2.25	0.041 *	1 [0.02, 1.96]
P8	EGLo	Zic1	1.32	1.67	0.78	-0.35 [-0.46, -0.24]	-7.00	<0.001 ***	3.19 [1.74, 4.61]
P8	IGL	Adora1	5.46	5.95	0.71	-0.49 [-0.83, -0.15]	-3.11	0.008 **	1.39 [0.34, 2.4]
P8	IGL	Cadps2	1.57	2.23	0.64	-0.65 [-0.89, -0.41]	-5.86	<0.001 ***	2.69 [1.37, 3.97]
P8	IGL	Calb2	4.02	4.51	0.71	-0.49 [-0.77, -0.21]	-3.70	0.002 **	1.52 [0.37, 2.63]
P8	IGL	Gabra1	4.82	5.14	0.80	-0.32 [-0.7, 0.07]	-1.78	0.099	0.74 [0.27, 1.71]
P8	IGL	Gabrg2	4.52	4.55	0.98	-0.02 [-0.31, 0.27]	-0.17	0.869	0.07 [0.84, 0.98]

Stage	Layer	Gene	Avg DCq (N)	Avg DCq (IH)	Fold Change	Difference [CI ₉₅]	t	p.value	Hedge's g [CI ₉₅]
P8	IGL	Grin1	2.97	3.64	0.63	-0.67 [-0.86, -0.49]	-7.85	<0.001 ***	3.63 [2.03, 5.19]
P8	IGL	Grm3	4.99	5.11	0.92	-0.12 [-0.36, 0.12]	-1.11	0.287	0.48 [0.46, 1.4]
P8	IGL	Homer1	5.78	6.20	0.75	-0.42 [-0.81, -0.04]	-2.35	0.034 *	1.09 [0.12, 2.02]
P8	IGL	Homer2	4.02	4.80	0.58	-0.78 [-1.05, -0.51]	-6.14	<0.001 ***	2.86 [1.42, 4.25]
P8	IGL	Nrxn1	2.87	3.31	0.74	-0.44 [-0.78, -0.1]	-2.74	0.016 *	1.27 [0.27, 2.23]
P8	IGL	Nxph4	3.99	4.73	0.60	-0.74 [-1.17, -0.31]	-3.72	0.002 **	1.73 [0.63, 2.79]
P8	IGL	Pax6	2.64	2.79	0.90	-0.15 [-0.34, 0.05]	-1.56	0.140	0.72 [0.21, 1.62]
P8	IGL	Pip1	5.60	6.32	0.61	-0.72 [-1.31, -0.13]	-2.63	0.020 *	1.21 [0.22, 2.17]
P8	IGL	Rac1	2.63	2.88	0.84	-0.25 [-0.41, -0.1]	-3.46	0.004 **	1.55 [0.48, 2.59]
P8	IGL	Robo1	5.04	5.60	0.68	-0.55 [-0.84, -0.27]	-4.20	<0.001 ***	1.71 [0.49, 2.88]
P8	IGL	Slc17a6	4.34	4.69	0.78	-0.36 [-0.6, -0.11]	-3.10	0.008 **	1.43 [0.4, 2.42]
P8	IGL	Slc17a7	4.12	4.54	0.74	-0.43 [-0.67, -0.18]	-3.68	0.002 **	1.71 [0.61, 2.78]
P8	IGL	Slc32a1	3.89	4.13	0.85	-0.24 [-0.52, 0.05]	-1.80	0.093	0.8 [0.16, 1.74]
P8	IGL	Sst	6.80	7.09	0.82	-0.29 [-0.86, 0.29]	-1.09	0.298	0.5 [0.48, 1.46]
P8	IGL	Stmn1	1.66	1.99	0.79	-0.33 [-0.5, -0.17]	-4.33	<0.001 ***	1.96 [0.81, 3.07]
P8	IGL	Syn2	2.33	3.11	0.58	-0.78 [-1.01, -0.54]	-7.11	<0.001 ***	3.27 [1.79, 4.71]
P8	IGL	Syp	1.82	2.46	0.64	-0.64 [-0.93, -0.35]	-4.76	<0.001 ***	2.22 [0.96, 3.42]
P8	IGL	Tln1	6.10	6.58	0.71	-0.49 [-0.97, 0]	-2.15	0.050 *	1 [0.05, 1.91]
P8	IGL	Zic1	0.05	0.41	0.78	-0.36 [-0.52, -0.2]	-4.74	<0.001 ***	2.08 [0.86, 3.25]
P8	PC	Akt1	7.43	7.46	0.98	-0.03 [-1.52, 1.46]	-0.04	0.967	0.01 [0.98, 1.01]
P8	PC	Cadps2	7.98	9.68	0.31	-1.7 [-2.99, -0.4]	-3.03	0.016 *	0.87 [0.38, 2.03]
P8	PC	Calb1	-0.19	0.72	0.53	-0.92 [-1.2, -0.63]	-6.85	<0.001 ***	2.68 [1.07, 4.23]
P8	PC	Calb2	6.42	7.83	0.38	-1.41 [-2.72, -0.1]	-2.34	0.037 *	0.97 [0.18, 2.06]
P8	PC	Cbln1	7.32	8.11	0.58	-0.79 [-2.9, 1.33]	-0.84	0.422	0.32 [0.76, 1.35]
P8	PC	Grm3	5.74	6.87	0.46	-1.13 [-2.08, -0.18]	-2.56	0.023 *	0.99 [0.08, 2]
P8	PC	Nefl	2.78	4.21	0.37	-1.43 [-2.04, -0.82]	-5.02	<0.001 ***	1.96 [0.62, 3.25]
P8	PC	Pcp2	5.53	6.61	0.47	-1.08 [-1.86, -0.3]	-3.01	0.011 *	1.28 [0.06, 2.45]
P8	PC	Rac1	8.91	11.28	0.19	-2.37 [-5.96, 1.22]	-1.49	0.170	0.65 [0.49, 1.71]
P8	PC	Slc17a7	10.76	14.79	0.06	-4.04 [-5.33, -2.74]	-7.36	<0.001 ***	3.57 [1.25, 5.84]
P8	PC	Slc32a1	6.02	7.59	0.34	-1.57 [-2.31, -0.84]	-4.60	<0.001 ***	2.06 [0.88, 3.21]
P8	PC	Stmn1	1.47	1.71	0.84	-0.24 [-0.51, 0.02]	-1.95	0.071	0.77 [0.24, 1.74]
P8	PC	Syn1	12.16	12.86	0.62	-0.7 [-2.69, 1.29]	-0.77	0.456	0.37 [0.62, 1.35]
P8	PC	Syn2	4.71	6.96	0.21	-2.25 [-3.17, -1.33]	-5.34	<0.001 ***	2.38 [0.94, 3.77]
P8	PC	Tln1	6.73	8.32	0.33	-1.59 [-2.88, -0.3]	-2.85	0.022 *	1.06 [0.29, 2.31]
P8	PC	Zic1	6.04	7.17	0.45	-1.14 [-1.75, -0.53]	-4.00	0.001 **	1.56 [0.34, 2.72]
P8	WM	Akt1	2.91	3.19	0.83	-0.28 [-0.61, 0.06]	-1.78	0.098	0.83 [0.1, 1.72]
P8	WM	Ascl1	3.50	3.55	0.97	-0.05 [-0.44, 0.35]	-0.26	0.799	0.11 [0.81, 1.02]
P8	WM	Cacng2	4.89	4.80	1.06	0.09 [-0.52, 0.7]	0.31	0.761	0.14 [0.73, 1.01]
P8	WM	Cadps2	5.65	5.26	1.31	0.39 [-0.39, 1.17]	1.15	0.284	0.5 [0.59, 1.55]
P8	WM	Grm3	5.40	4.75	1.56	0.64 [0.11, 1.18]	2.67	0.022 *	1.24 [0.1, 2.33]
P8	WM	Mbp	-0.80	-0.47	0.80	-0.33 [-0.85, 0.19]	-1.36	0.194	0.62 [0.3, 1.52]
P8	WM	Mobp	1.90	2.65	0.59	-0.75 [-1.61, 0.11]	-1.87	0.083	0.87 [0.07, 1.77]
P8	WM	Mog	5.48	5.09	1.31	0.39 [-0.13, 0.91]	1.69	0.125	0.82 [0.3, 1.9]
P8	WM	Myt1	4.92	5.24	0.80	-0.32 [-0.65, 0.01]	-2.10	0.056	0.94 [0.06, 1.91]

Stage	Layer	Gene	Avg DCq (N)	Avg DCq (IH)	Fold Change	Difference [CI ₉₅]	t	p.value	Hedge's g [CI ₉₅]
P8	WM	Neurog2	4.89	5.39	0.71	-0.49 [-0.98, 0]	-2.22	0.049 *	1.03 [0.05, 2.07]
P8	WM	Nrxn1	4.07	4.26	0.88	-0.19 [-0.73, 0.35]	-0.75	0.465	0.33 [0.62, 1.26]
P8	WM	Nxph4	4.33	4.54	0.86	-0.21 [-0.7, 0.27]	-0.95	0.361	0.43 [0.53, 1.39]
P8	WM	Plp1	0.56	1.23	0.63	-0.67 [-1.36, 0.03]	-2.06	0.059	0.96 [0.01, 1.87]
P8	WM	Rac1	2.06	2.17	0.93	-0.11 [-0.32, 0.1]	-1.15	0.271	0.52 [0.4, 1.42]
P8	WM	Robo1	3.95	4.60	0.63	-0.66 [-1.17, -0.14]	-2.74	0.017 *	1.26 [0.22, 2.26]
P8	WM	Stmn1	0.43	0.83	0.76	-0.4 [-0.59, -0.21]	-4.55	<0.001 ***	1.86 [0.6, 3.06]
P8	WM	Tln1	3.67	4.12	0.73	-0.45 [-0.76, -0.14]	-3.11	0.008 **	1.41 [0.37, 2.41]
P8	WM	Zic1	0.94	1.59	0.64	-0.65 [-0.93, -0.37]	-4.98	<0.001 ***	2.3 [1.07, 3.48]
P12	EGL	Akt1	4.02	3.37	1.57	0.65 [-0.03, 1.34]	1.97	0.061	0.74 [0.03, 1.5]
P12	EGL	Cacng2	4.98	5.22	0.84	-0.24 [-0.53, 0.05]	-1.74	0.095	0.65 [0.12, 1.41]
P12	EGL	Cadps2	4.48	4.48	1.00	0.01 [-0.77, 0.78]	0.02	0.988	0.01 [0.74, 0.75]
P12	EGL	Calb1	10.06	9.65	1.33	0.41 [-1.08, 1.89]	0.59	0.566	0.24 [0.66, 1.13]
P12	EGL	Calb2	8.74	7.46	2.43	1.28 [0.54, 2.02]	3.58	0.002 **	1.3 [0.41, 2.16]
P12	EGL	Ccnd1	5.91	5.87	1.03	0.04 [-0.14, 0.22]	0.48	0.634	0.17 [0.6, 0.94]
P12	EGL	Cdh8	8.32	7.69	1.55	0.63 [0.15, 1.11]	2.74	0.012 *	0.99 [0.13, 1.84]
P12	EGL	Dclk1	5.83	6.42	0.67	-0.58 [-0.75, -0.41]	-7.01	<0.001 ***	2.59 [1.38, 3.75]
P12	EGL	Gabra1	8.85	8.78	1.05	0.07 [-0.56, 0.69]	0.22	0.825	0.09 [0.72, 0.9]
P12	EGL	Gas7	8.18	8.36	0.89	-0.17 [-0.78, 0.43]	-0.60	0.553	0.22 [0.6, 1.04]
P12	EGL	Grid2	7.39	7.24	1.11	0.15 [-0.5, 0.8]	0.47	0.644	0.18 [0.61, 0.96]
P12	EGL	Grin1	6.21	6.85	0.64	-0.65 [-1, -0.29]	-3.76	0.001 **	1.38 [0.51, 2.22]
P12	EGL	Grm3	7.89	7.73	1.12	0.17 [-0.29, 0.62]	0.76	0.458	0.29 [0.45, 1.03]
P12	EGL	Homer1	6.72	7.20	0.72	-0.48 [-0.7, -0.26]	-4.59	<0.001 ***	1.64 [0.67, 2.58]
P12	EGL	Homer2	6.98	6.48	1.41	0.5 [0.23, 0.76]	3.92	<0.001 ***	1.48 [0.61, 2.34]
P12	EGL	Nav3	5.03	5.16	0.92	-0.13 [-0.31, 0.06]	-1.40	0.177	0.48 [0.32, 1.27]
P12	EGL	Nxph4	4.63	4.26	1.30	0.37 [0.13, 0.62]	3.12	0.005 **	1.2 [0.39, 1.99]
P12	EGL	Pax6	1.85	1.84	1.00	0.01 [-0.15, 0.17]	0.09	0.926	0.04 [0.7, 0.77]
P12	EGL	Rac1	2.86	2.97	0.92	-0.11 [-0.29, 0.06]	-1.32	0.201	0.5 [0.25, 1.24]
P12	EGL	Robo1	6.67	6.85	0.88	-0.19 [-0.56, 0.19]	-1.03	0.312	0.39 [0.36, 1.13]
P12	EGL	Robo2	6.00	5.93	1.05	0.07 [-0.21, 0.35]	0.52	0.607	0.2 [0.53, 0.92]
P12	EGL	Sema6a	3.11	3.10	1.01	0.01 [-0.2, 0.23]	0.13	0.895	0.05 [0.69, 0.79]
P12	EGL	Slc17a6	5.00	4.77	1.17	0.23 [0.06, 0.39]	2.84	0.009 **	0.95 [0.08, 1.79]
P12	EGL	Slc17a7	6.55	7.25	0.61	-0.71 [-0.97, -0.45]	-5.64	<0.001 ***	2.09 [1.11, 3.04]
P12	EGL	Stmn1	-0.67	-0.44	0.85	-0.23 [-0.43, -0.04]	-2.47	0.022 *	0.95 [0.17, 1.71]
P12	EGL	Syp	3.67	3.77	0.93	-0.1 [-0.27, 0.07]	-1.23	0.231	0.43 [0.36, 1.2]
P12	EGL	Tln1	5.91	6.60	0.62	-0.69 [-1.09, -0.29]	-3.57	0.002 **	1.29 [0.42, 2.13]
P12	EGL	Tmod	7.97	8.37	0.76	-0.4 [-0.96, 0.17]	-1.48	0.156	0.56 [0.29, 1.4]
P12	EGL	Zic1	0.42	0.55	0.92	-0.13 [-0.34, 0.08]	-1.24	0.227	0.48 [0.25, 1.2]
P12	IGL	Adora1	4.76	5.04	0.83	-0.28 [-0.55, 0]	-2.09	0.048 *	0.75 [0.07, 1.55]
P12	IGL	Akt1	3.92	3.90	1.01	0.01 [-0.21, 0.24]	0.13	0.898	0.05 [0.71, 0.8]
P12	IGL	Ascl1	7.22	7.14	1.06	0.08 [-0.9, 1.06]	0.17	0.868	0.07 [0.81, 0.96]
P12	IGL	Cadps2	1.47	1.97	0.71	-0.5 [-0.64, -0.37]	-7.74	<0.001 ***	2.77 [1.58, 3.92]
P12	IGL	Calb1	5.39	6.05	0.63	-0.66 [-1.84, 0.52]	-1.17	0.255	0.46 [0.32, 1.23]

Stage	Layer	Gene	Avg DCq (N)	Avg DCq (IH)	Fold Change	Difference [CI ₉₅]	t	p.value	Hedge's g [CI ₉₅]
P12	IGL	Calb2	2.32	2.69	0.78	-0.37 [-0.73, 0]	-2.07	0.049 *	0.71 [0.11, 1.51]
P12	IGL	Gabra1	2.82	2.83	0.99	-0.01 [-0.32, 0.3]	-0.08	0.938	0.03 [0.71, 0.77]
P12	IGL	Gabrg2	3.76	4.04	0.82	-0.28 [-0.82, 0.25]	-1.08	0.290	0.41 [0.32, 1.15]
P12	IGL	Grid2	4.19	4.17	1.01	0.02 [-0.27, 0.31]	0.14	0.893	0.05 [0.71, 0.81]
P12	IGL	Grin1	2.91	3.29	0.77	-0.38 [-0.55, -0.22]	-4.75	<0.001 ***	1.74 [0.78, 2.67]
P12	IGL	Grm3	6.34	6.16	1.14	0.19 [-0.29, 0.66]	0.81	0.424	0.3 [0.49, 1.09]
P12	IGL	Homer1	5.97	6.12	0.90	-0.15 [-0.44, 0.14]	-1.07	0.297	0.39 [0.4, 1.16]
P12	IGL	Homer2	4.33	4.21	1.09	0.12 [-0.09, 0.33]	1.19	0.246	0.45 [0.29, 1.19]
P12	IGL	Nrxn1	2.61	3.26	0.64	-0.65 [-0.86, -0.45]	-6.52	<0.001 ***	2.49 [1.46, 3.49]
P12	IGL	Nxph4	5.00	5.13	0.92	-0.13 [-0.41, 0.16]	-0.90	0.378	0.34 [0.43, 1.1]
P12	IGL	Pax6	2.77	2.84	0.95	-0.07 [-0.24, 0.1]	-0.85	0.402	0.3 [0.48, 1.07]
P12	IGL	Rac1	2.96	2.84	1.09	0.12 [-0.08, 0.33]	1.24	0.226	0.48 [0.24, 1.19]
P12	IGL	Robo1	5.60	6.00	0.76	-0.4 [-0.64, -0.16]	-3.49	0.002 **	1.28 [0.4, 2.13]
P12	IGL	Robo2	5.79	5.77	1.01	0.01 [-0.25, 0.28]	0.11	0.911	0.04 [0.73, 0.81]
P12	IGL	Sema6a	3.69	3.54	1.11	0.15 [-0.11, 0.41]	1.20	0.244	0.45 [0.3, 1.19]
P12	IGL	Slc17a6	4.84	4.86	0.98	-0.03 [-0.25, 0.2]	-0.23	0.821	0.09 [0.67, 0.84]
P12	IGL	Slc17a7	2.32	2.57	0.84	-0.25 [-0.58, 0.08]	-1.58	0.128	0.56 [0.23, 1.34]
P12	IGL	Slc32a1	4.67	4.50	1.12	0.17 [-0.06, 0.39]	1.55	0.136	0.59 [0.18, 1.35]
P12	IGL	Sst	6.49	6.43	1.05	0.07 [-0.26, 0.39]	0.43	0.672	0.16 [0.61, 0.94]
P12	IGL	Stmn1	2.39	2.35	1.02	0.03 [-0.26, 0.32]	0.23	0.818	0.08 [0.69, 0.85]
P12	IGL	Syn2	1.92	2.39	0.72	-0.47 [-0.66, -0.28]	-5.17	<0.001 ***	1.84 [0.85, 2.79]
P12	IGL	Syp	1.89	1.95	0.96	-0.05 [-0.23, 0.12]	-0.62	0.544	0.24 [0.5, 0.96]
P12	IGL	Tln1	6.53	6.69	0.89	-0.16 [-0.54, 0.22]	-0.88	0.387	0.35 [0.4, 1.1]
P12	IGL	Tmod	5.07	5.64	0.67	-0.58 [-0.83, -0.32]	-4.69	<0.001 ***	1.7 [0.76, 2.61]
P12	IGL	Zic1	0.27	0.16	1.08	0.11 [0.03, 0.18]	2.98	0.007 **	1.1 [0.25, 1.92]
P12	ML	Adora1	5.91	6.11	0.87	-0.2 [-0.77, 0.38]	-0.71	0.485	0.26 [0.52, 1.03]
P12	ML	Akt1	3.11	2.99	1.09	0.12 [-0.1, 0.33]	1.14	0.264	0.44 [0.3, 1.17]
P12	ML	Astn2	2.79	3.14	0.79	-0.35 [-0.55, -0.14]	-3.50	0.002 **	1.32 [0.49, 2.14]
P12	ML	Cadm3	3.32	3.54	0.86	-0.22 [-0.41, -0.02]	-2.29	0.032 *	0.82 [0.01, 1.61]
P12	ML	Cadps2	3.71	4.06	0.79	-0.34 [-0.69, 0]	-2.05	0.052	0.78 [0.02, 1.54]
P12	ML	Calb1	1.80	1.53	1.21	0.27 [-0.07, 0.62]	1.64	0.116	0.59 [0.2, 1.36]
P12	ML	Calb2	5.73	5.28	1.36	0.45 [0.08, 0.82]	2.53	0.019 *	0.97 [0.17, 1.76]
P12	ML	Camk4	3.35	3.77	0.75	-0.42 [-0.69, -0.15]	-3.20	0.004 **	1.2 [0.38, 2.01]
P12	ML	Gabra1	2.65	2.93	0.82	-0.28 [-0.53, -0.03]	-2.29	0.031 *	0.82 [0.01, 1.62]
P12	ML	Grid2	2.20	2.47	0.83	-0.27 [-0.6, 0.07]	-1.65	0.113	0.63 [0.12, 1.37]
P12	ML	Grin1	3.67	3.97	0.81	-0.31 [-0.57, -0.05]	-2.44	0.023 *	0.9 [0.09, 1.68]
P12	ML	Grm3	4.55	4.81	0.83	-0.26 [-0.65, 0.13]	-1.39	0.177	0.53 [0.21, 1.27]
P12	ML	Homer1	5.87	5.87	1.00	0 [-0.44, 0.45]	0.02	0.987	0.01 [0.75, 0.76]
P12	ML	Homer2	5.73	5.72	1.00	0.01 [-0.46, 0.47]	0.02	0.982	0.01 [0.74, 0.75]
P12	ML	L1cam	3.66	4.30	0.64	-0.63 [-0.86, -0.41]	-5.87	<0.001 ***	2.15 [1.14, 3.13]
P12	ML	Neurod1	1.95	2.00	0.97	-0.05 [-0.22, 0.12]	-0.61	0.550	0.22 [0.54, 0.98]
P12	ML	Nxph4	5.89	5.79	1.08	0.11 [-0.22, 0.43]	0.68	0.503	0.25 [0.52, 1]
P12	ML	Pax6	3.96	3.89	1.05	0.07 [-0.19, 0.34]	0.58	0.571	0.2 [0.57, 0.97]
P12	ML	Rac1	3.26	3.33	0.95	-0.07 [-0.2, 0.07]	-1.02	0.318	0.37 [0.39, 1.13]

Stage	Layer	Gene	Avg DCq (N)	Avg DCq (IH)	Fold Change	Difference [CI ₉₅]	t	p.value	Hedge's g [CI ₉₅]
P12	ML	Robo1	6.69	6.87	0.89	-0.17 [-0.68, 0.33]	-0.72	0.480	0.3 [0.54, 1.13]
P12	ML	Robo2	5.49	5.39	1.07	0.1 [-0.19, 0.39]	0.69	0.497	0.25 [0.52, 1.01]
P12	ML	Sema6a	3.82	3.87	0.96	-0.06 [-0.26, 0.15]	-0.56	0.579	0.2 [0.56, 0.96]
P12	ML	Slc17a6	6.14	5.44	1.63	0.71 [0.39, 1.03]	4.64	<0.001 ***	1.75 [0.8, 2.67]
P12	ML	Slc17a7	6.82	7.18	0.78	-0.36 [-0.82, 0.1]	-1.67	0.114	0.71 [0.22, 1.61]
P12	ML	Stmn1	1.88	1.85	1.02	0.02 [-0.16, 0.2]	0.25	0.803	0.09 [0.66, 0.85]
P12	ML	Syp	2.75	2.68	1.05	0.07 [-0.19, 0.33]	0.57	0.572	0.2 [0.56, 0.97]
P12	ML	Tln1	5.88	6.54	0.64	-0.65 [-0.99, -0.32]	-4.04	<0.001 ***	1.62 [0.69, 2.52]
P12	ML	Tmod	6.89	6.89	1.00	0 [-0.67, 0.67]	0.01	0.994	0 [0.89, 0.9]
P12	ML	Zic1	1.85	1.83	1.02	0.02 [-0.15, 0.2]	0.28	0.781	0.11 [0.64, 0.85]
P12	PC	Adora1	11.05	10.23	1.77	0.82 [-0.65, 2.3]	1.17	0.257	0.46 [0.38, 1.29]
P12	PC	Akt1	11.19	9.97	2.33	1.22 [-0.29, 2.74]	1.68	0.108	0.65 [0.15, 1.44]
P12	PC	Cadps2	10.50	11.58	0.47	-1.08 [-2.67, 0.51]	-1.42	0.173	0.51 [0.38, 1.38]
P12	PC	Calb1	0.36	0.36	1.00	-0.01 [-0.54, 0.52]	-0.03	0.979	0.01 [0.75, 0.76]
P12	PC	Calb2	7.94	8.02	0.95	-0.08 [-0.78, 0.63]	-0.22	0.827	0.08 [0.68, 0.84]
P12	PC	Cbln1	9.50	9.38	1.09	0.12 [-0.93, 1.18]	0.24	0.811	0.09 [0.66, 0.84]
P12	PC	Gabra1	5.63	5.80	0.89	-0.17 [-0.59, 0.25]	-0.85	0.403	0.34 [0.39, 1.07]
P12	PC	Gria2	6.08	5.76	1.25	0.32 [-0.09, 0.74]	1.61	0.121	0.6 [0.17, 1.36]
P12	PC	Grid2	3.81	4.41	0.66	-0.61 [-1.13, -0.08]	-2.38	0.026 *	0.8 [0.04, 1.62]
P12	PC	Grin1	9.51	9.34	1.12	0.17 [-1.67, 2.01]	0.19	0.851	0.07 [0.73, 0.87]
P12	PC	Grm3	6.09	6.70	0.66	-0.6 [-1.42, 0.21]	-1.54	0.138	0.54 [0.25, 1.32]
P12	PC	Homer1	9.47	9.50	0.98	-0.03 [-1.52, 1.47]	-0.04	0.967	0.02 [0.87, 0.91]
P12	PC	Homer2	8.62	11.07	0.18	-2.46 [-6.67, 1.76]	-1.43	0.204	0.76 [0.43, 1.89]
P12	PC	Nefl	3.94	3.34	1.52	0.6 [0.3, 0.9]	4.17	<0.001 ***	1.62 [0.69, 2.51]
P12	PC	Nxph4	14.03	13.42	1.52	0.6 [-2, 3.21]	0.51	0.620	0.22 [0.8, 1.22]
P12	PC	Pax6	8.30	8.10	1.15	0.21 [-0.55, 0.96]	0.56	0.578	0.21 [0.57, 0.98]
P12	PC	Pcp2	6.66	6.59	1.05	0.07 [-0.48, 0.62]	0.26	0.794	0.1 [0.66, 0.85]
P12	PC	Rac1	12.20	9.96	4.74	2.24 [0.29, 4.2]	2.41	0.027 *	1.08 [0.23, 1.91]
P12	PC	Robo1	13.70	14.32	0.65	-0.62 [-3.85, 2.61]	-0.44	0.671	0.24 [0.82, 1.29]
P12	PC	Robo2	9.43	8.49	1.91	0.94 [-0.68, 2.56]	1.20	0.243	0.5 [0.3, 1.28]
P12	PC	Sema6a	9.79	9.74	1.04	0.05 [-0.93, 1.03]	0.11	0.917	0.04 [0.74, 0.82]
P12	PC	Slc17a6	10.14	11.27	0.46	-1.13 [-2.82, 0.56]	-1.44	0.172	0.6 [0.38, 1.56]
P12	PC	Slc17a7	13.68	14.88	0.44	-1.2 [-3.46, 1.06]	-1.13	0.277	0.43 [0.56, 1.39]
P12	PC	Slc32a1	6.26	5.86	1.32	0.4 [-0.47, 1.27]	0.96	0.349	0.32 [0.46, 1.1]
P12	PC	Stmn1	2.26	2.35	0.94	-0.09 [-0.68, 0.51]	-0.31	0.761	0.12 [0.59, 0.83]
P12	PC	Syn1	13.09	13.56	0.72	-0.47 [-2.12, 1.18]	-0.60	0.557	0.25 [0.54, 1.03]
P12	PC	Syp	7.55	7.79	0.85	-0.24 [-0.78, 0.3]	-0.91	0.371	0.32 [0.46, 1.09]
P12	PC	Tln1	6.98	6.34	1.55	0.63 [-1.35, 2.62]	0.69	0.504	0.35 [0.46, 1.15]
P12	PC	Tmod	9.72	10.53	0.57	-0.81 [-2.54, 0.93]	-1.02	0.329	0.46 [0.6, 1.47]
P12	PC	Zic1	10.60	10.94	0.79	-0.35 [-3.2, 2.51]	-0.26	0.800	0.11 [0.78, 1]
P12	WM	Adora1	4.33	4.37	0.97	-0.04 [-0.51, 0.43]	-0.17	0.866	0.06 [0.72, 0.84]
P12	WM	Akt1	3.23	3.02	1.16	0.22 [0.06, 0.37]	2.94	0.008 **	1.19 [0.38, 1.98]
P12	WM	Ascl1	5.18	4.91	1.21	0.27 [-0.57, 1.11]	0.76	0.475	0.38 [0.76, 1.5]

Stage	Layer	Gene	Avg DCq (N)	Avg DCq (IH)	Fold Change	Difference [CI ₉₅]	t	p.value	Hedge's g [CI ₉₅]
P12	WM	Cacng2	5.28	5.60	0.80	-0.32 [-0.87, 0.23]	-1.23	0.233	0.44 [0.39, 1.25]
P12	WM	Cadps2	4.31	4.79	0.72	-0.48 [-1.14, 0.18]	-1.52	0.145	0.56 [0.3, 1.39]
P12	WM	Calb1	6.45	6.77	0.80	-0.32 [-1.32, 0.67]	-0.84	0.439	0.4 [0.8, 1.54]
P12	WM	Calb2	4.94	5.16	0.86	-0.21 [-0.88, 0.45]	-0.68	0.507	0.26 [0.56, 1.07]
P12	WM	Gabra1	5.02	5.33	0.81	-0.3 [-0.9, 0.3]	-1.06	0.303	0.45 [0.39, 1.27]
P12	WM	Grid2	3.67	3.70	0.98	-0.03 [-0.17, 0.11]	-0.47	0.644	0.18 [0.62, 0.97]
P12	WM	Grin1	5.08	5.29	0.87	-0.21 [-0.83, 0.42]	-0.69	0.497	0.28 [0.54, 1.1]
P12	WM	Grm3	6.06	5.90	1.12	0.16 [-0.27, 0.6]	0.79	0.443	0.32 [0.54, 1.16]
P12	WM	Homer1	5.48	5.59	0.93	-0.11 [-0.6, 0.38]	-0.47	0.644	0.18 [0.69, 1.04]
P12	WM	Homer2	5.60	5.56	1.03	0.04 [-0.63, 0.7]	0.12	0.903	0.05 [0.8, 0.89]
P12	WM	Mbp	-3.30	-2.43	0.55	-0.86 [-1.53, -0.2]	-2.68	0.013 *	0.94 [0.1, 1.76]
P12	WM	Mobp	-0.84	0.17	0.50	-1.01 [-1.71, -0.31]	-3.00	0.007 **	1.05 [0.16, 1.92]
P12	WM	Mog	2.20	3.09	0.54	-0.89 [-1.58, -0.19]	-2.64	0.015 *	0.92 [0.05, 1.77]
P12	WM	Myt1	5.05	5.19	0.91	-0.14 [-0.62, 0.33]	-0.63	0.538	0.23 [0.58, 1.02]
P12	WM	Nxph4	4.47	4.10	1.30	0.37 [-0.3, 1.04]	1.15	0.261	0.41 [0.4, 1.2]
P12	WM	Pax6	4.01	4.15	0.91	-0.13 [-0.62, 0.35]	-0.57	0.575	0.21 [0.58, 0.99]
P12	WM	Plp1	-1.87	-0.97	0.53	-0.91 [-1.63, -0.18]	-2.59	0.016 *	0.92 [0.08, 1.73]
P12	WM	Rac1	2.10	2.24	0.91	-0.14 [-0.26, -0.02]	-2.41	0.025 *	0.91 [0.09, 1.72]
P12	WM	Robo1	5.24	5.43	0.88	-0.19 [-0.67, 0.28]	-0.84	0.410	0.33 [0.46, 1.1]
P12	WM	Sema6a	1.87	1.81	1.04	0.06 [-0.48, 0.59]	0.22	0.828	0.08 [0.63, 0.8]
P12	WM	Slc17a6	5.74	6.84	0.47	-1.1 [-1.8, -0.4]	-3.57	0.006 **	1.8 [0.48, 3.07]
P12	WM	Slc17a7	5.27	5.72	0.73	-0.45 [-1.11, 0.21]	-1.43	0.170	0.57 [0.29, 1.41]
P12	WM	Stmn1	1.51	1.56	0.97	-0.05 [-0.37, 0.27]	-0.31	0.759	0.11 [0.66, 0.87]
P12	WM	Syp	4.45	4.60	0.90	-0.16 [-0.6, 0.29]	-0.73	0.472	0.28 [0.56, 1.1]
P12	WM	Tln1	3.89	4.25	0.78	-0.36 [-0.65, -0.07]	-2.57	0.017 *	0.99 [0.16, 1.79]
P12	WM	Tmod	5.96	6.58	0.65	-0.62 [-1.19, -0.05]	-2.34	0.034 *	0.99 [0.03, 1.93]
P12	WM	Zic1	2.02	1.78	1.18	0.23 [-0.07, 0.54]	1.60	0.124	0.55 [0.25, 1.33]
P21	IGL	Adora1	2.42	2.55	0.91	-0.14 [-0.27, -0.01]	-2.23	0.042 *	0.97 [0.01, 1.92]
P21	IGL	Cadps2	1.34	1.26	1.06	0.08 [-0.07, 0.23]	1.10	0.291	0.48 [0.45, 1.39]
P21	IGL	Calb2	-0.22	-0.30	1.06	0.08 [-0.05, 0.21]	1.26	0.229	0.54 [0.39, 1.46]
P21	IGL	Gabra1	1.45	1.42	1.02	0.03 [-0.11, 0.17]	0.46	0.652	0.2 [0.71, 1.1]
P21	IGL	Gabrg2	3.19	3.18	1.01	0.01 [-0.24, 0.25]	0.06	0.950	0.03 [0.87, 0.93]
P21	IGL	Grin1	2.01	1.90	1.08	0.11 [-0.04, 0.26]	1.55	0.144	0.67 [0.26, 1.59]
P21	IGL	Grm3	6.79	6.53	1.19	0.25 [-0.05, 0.56]	1.78	0.099	0.79 [0.2, 1.74]
P21	IGL	Homer1	5.84	5.82	1.01	0.01 [-0.23, 0.26]	0.11	0.917	0.05 [0.86, 0.95]
P21	IGL	Homer2	5.91	6.15	0.85	-0.24 [-0.45, -0.02]	-2.39	0.032 *	0.99 [0.02, 1.96]
P21	IGL	Nrxn1	1.63	1.46	1.13	0.18 [-0.08, 0.44]	1.45	0.170	0.63 [0.3, 1.54]
P21	IGL	Nxph4	5.79	6.06	0.83	-0.27 [-0.63, 0.1]	-1.58	0.136	0.66 [0.29, 1.59]
P21	IGL	Pax6	2.46	2.27	1.14	0.19 [0.02, 0.36]	2.38	0.032 *	1.03 [0.04, 1.99]
P21	IGL	Rac1	2.39	2.34	1.03	0.04 [-0.11, 0.2]	0.62	0.545	0.27 [0.62, 1.14]
P21	IGL	Robo1	6.37	6.08	1.22	0.28 [-0.03, 0.6]	1.93	0.075	0.81 [0.16, 1.76]
P21	IGL	Slc17a7	1.03	0.98	1.03	0.05 [-0.12, 0.21]	0.63	0.541	0.27 [0.65, 1.17]
P21	IGL	Slc32a1	4.27	4.14	1.09	0.13 [-0.13, 0.39]	1.07	0.303	0.44 [0.48, 1.34]
P21	IGL	Sst	8.00	7.91	1.06	0.09 [-0.42, 0.59]	0.44	0.676	0.21 [0.9, 1.3]

Stage	Layer	Gene	Avg DCq (N)	Avg DCq (IH)	Fold Change	Difference [CI ₉₅]	t	p.value	Hedge's g [CI ₉₅]
P21	IGL	Stmn1	4.10	3.89	1.16	0.21 [0.04, 0.38]	2.67	0.018 *	1.16 [0.15, 2.13]
P21	IGL	Syn2	1.58	1.57	1.01	0.01 [-0.13, 0.16]	0.22	0.828	0.1 [0.79, 0.98]
P21	IGL	Syp	1.10	1.10	1.00	0 [-0.12, 0.12]	-0.05	0.962	0.02 [0.88, 0.92]
P21	IGL	Tln1	6.72	6.71	1.01	0.01 [-0.39, 0.4]	0.04	0.967	0.02 [0.9, 0.94]
P21	IGL	Tmod	5.38	5.17	1.16	0.21 [-0.06, 0.48]	1.64	0.123	0.72 [0.23, 1.64]
P21	IGL	Zic1	-0.24	-0.43	1.14	0.19 [0.07, 0.32]	3.29	0.005 **	1.42 [0.37, 2.44]
P21	ML	Astn2	2.06	1.97	1.07	0.1 [-0.2, 0.39]	0.71	0.489	0.31 [0.6, 1.21]
P21	ML	Cadm3	3.42	3.56	0.90	-0.14 [-0.43, 0.14]	-1.09	0.294	0.48 [0.47, 1.42]
P21	ML	Cadps2	4.78	5.25	0.72	-0.47 [-1.3, 0.36]	-1.58	0.188	0.76 [0.57, 2.01]
P21	ML	Calb1	2.82	2.81	1.01	0.01 [-0.27, 0.29]	0.07	0.942	0.03 [0.87, 0.93]
P21	ML	Camk4	2.97	3.25	0.82	-0.28 [-0.67, 0.11]	-1.56	0.142	0.68 [0.26, 1.6]
P21	ML	Gabra1	0.62	0.64	0.99	-0.02 [-0.23, 0.19]	-0.20	0.848	0.08 [0.82, 0.98]
P21	ML	Grid2	2.57	2.35	1.16	0.21 [-0.1, 0.53]	1.45	0.169	0.63 [0.3, 1.55]
P21	ML	Grin1	2.68	2.81	0.91	-0.14 [-0.52, 0.25]	-0.76	0.461	0.32 [0.59, 1.23]
P21	ML	Grm3	3.65	3.45	1.15	0.2 [-0.23, 0.63]	1.02	0.326	0.44 [0.48, 1.35]
P21	ML	L1cam	3.78	3.88	0.93	-0.11 [-0.61, 0.4]	-0.45	0.662	0.19 [0.71, 1.1]
P21	ML	Nav3	4.56	3.70	1.82	0.86 [0.26, 1.46]	3.08	0.009 **	1.36 [0.28, 2.39]
P21	ML	Neurod1	3.86	4.22	0.78	-0.35 [-0.8, 0.09]	-1.71	0.110	0.74 [0.21, 1.67]
P21	ML	Nrxn1	3.05	3.12	0.95	-0.07 [-0.51, 0.37]	-0.34	0.742	0.14 [0.76, 1.05]
P21	ML	Sema6a	4.56	4.91	0.78	-0.35 [-0.76, 0.06]	-1.92	0.087	0.85 [0.31, 1.96]
P21	PC	Akt1	8.32	8.42	0.93	-0.1 [-2.17, 1.96]	-0.11	0.915	0.05 [0.94, 1.03]
P21	PC	Cadps2	9.34	11.77	0.18	-2.44 [-7.36, 2.49]	-1.21	0.272	0.51 [0.63, 1.58]
P21	PC	Calb1	-0.97	-0.97	1.00	0.01 [-0.2, 0.22]	0.06	0.952	0.03 [0.88, 0.93]
P21	PC	Calb2	4.89	4.75	1.10	0.13 [-0.49, 0.76]	0.45	0.657	0.19 [0.71, 1.08]
P21	PC	Cbln1	7.31	8.34	0.49	-1.03 [-3.08, 1.02]	-1.11	0.293	0.49 [0.53, 1.49]
P21	PC	Gabra1	3.24	3.70	0.72	-0.46 [-1.17, 0.24]	-1.40	0.182	0.58 [0.36, 1.5]
P21	PC	Gria2	4.52	4.38	1.10	0.14 [-0.76, 1.03]	0.33	0.747	0.14 [0.77, 1.04]
P21	PC	Grid2	3.34	3.14	1.14	0.19 [-0.94, 1.33]	0.37	0.719	0.16 [0.75, 1.06]
P21	PC	Grin1	7.74	6.54	2.29	1.2 [-0.97, 3.37]	1.25	0.244	0.58 [0.48, 1.61]
P21	PC	Grm3	8.56	8.04	1.43	0.52 [-1.3, 2.33]	0.64	0.537	0.29 [0.7, 1.25]
P21	PC	Nefl	3.50	3.66	0.90	-0.16 [-1.23, 0.92]	-0.31	0.758	0.14 [0.75, 1.02]
P21	PC	Pcp2	6.07	7.45	0.38	-1.38 [-3.93, 1.18]	-1.20	0.258	0.48 [0.59, 1.51]
P21	PC	Rac1	9.52	9.70	0.88	-0.18 [-1.84, 1.49]	-0.23	0.823	0.1 [0.84, 1.03]
P21	PC	Slc17a7	12.58	13.38	0.57	-0.8 [-4.09, 2.48]	-0.60	0.571	0.38 [0.7, 1.43]
P21	PC	Slc32a1	4.89	4.50	1.31	0.39 [-1.84, 2.63]	0.38	0.713	0.16 [0.75, 1.06]
P21	PC	Stmn1	3.50	2.99	1.42	0.51 [-0.07, 1.08]	1.87	0.082	0.82 [0.14, 1.75]
P21	PC	Syn1	14.46	11.85	6.09	2.61 [1.3, 3.92]	4.43	0.001 **	2.06 [0.68, 3.4]
P21	PC	Syn2	6.80	6.26	1.46	0.54 [-0.79, 1.88]	0.88	0.394	0.38 [0.55, 1.3]
P21	PC	Syp	5.82	5.53	1.23	0.29 [-0.66, 1.25]	0.66	0.518	0.29 [0.64, 1.21]
P21	PC	Tmod	9.54	7.12	5.35	2.42 [-0.92, 5.76]	1.77	0.127	0.95 [0.31, 2.15]
P21	WM	Akt1	4.04	3.59	1.37	0.46 [-0.02, 0.94]	2.06	0.060	0.89 [0.11, 1.86]
P21	WM	Cadps2	4.83	4.81	1.02	0.03 [-0.87, 0.93]	0.07	0.946	0.03 [0.95, 1.01]
P21	WM	Calb2	4.37	4.03	1.26	0.34 [-0.22, 0.89]	1.33	0.209	0.61 [0.38, 1.57]

Stage	Layer	Gene	Avg DCq (N)	Avg DCq (IH)	Fold Change	Difference [CI ₉₅]	t	p.value	Hedge's g [CI ₉₅]
P21	WM	Grm3	4.30	4.67	0.77	-0.37 [-0.83, 0.09]	-1.74	0.105	0.77 [0.21, 1.73]
P21	WM	Mbp	-5.07	-5.14	1.05	0.07 [-0.2, 0.33]	0.53	0.603	0.23 [0.68, 1.13]
P21	WM	Mobp	-3.09	-3.16	1.05	0.08 [-0.15, 0.3]	0.71	0.491	0.31 [0.61, 1.21]
P21	WM	Mog	0.39	0.23	1.12	0.16 [0, 0.33]	2.09	0.055	0.91 [0.05, 1.85]
P21	WM	Nrxn1	4.77	4.35	1.34	0.43 [-0.2, 1.05]	1.58	0.153	0.79 [0.32, 1.85]
P21	WM	Plp1	-4.14	-4.26	1.09	0.13 [-0.03, 0.29]	1.70	0.112	0.74 [0.2, 1.65]
P21	WM	Rac1	1.60	1.31	1.23	0.29 [0.1, 0.49]	3.27	0.006 **	1.42 [0.37, 2.44]
P21	WM	Stmn1	1.06	1.15	0.94	-0.09 [-0.3, 0.13]	-0.86	0.406	0.37 [0.54, 1.28]
P21	WM	Tln1	3.08	3.05	1.02	0.03 [-0.34, 0.41]	0.19	0.853	0.08 [0.82, 0.98]
P21	WM	Tmod	3.62	3.79	0.89	-0.16 [-0.6, 0.27]	-0.81	0.432	0.36 [0.58, 1.28]
P21	WM	Zic1	3.75	3.26	1.40	0.49 [0.11, 0.86]	2.80	0.014 *	1.17 [0.13, 2.17]
P70	IGL	Adora1	2.33	2.42	0.94	-0.09 [-0.25, 0.08]	-1.34	0.239	0.72 [0.56, 1.95]
P70	IGL	Cadps2	0.74	-0.13	1.83	0.87 [0.43, 1.31]	5.04	0.004 **	2.7 [0.64, 4.7]
P70	IGL	Calb2	-0.59	-0.87	1.22	0.29 [-0.05, 0.62]	2.19	0.080	1.32 [0.07, 2.64]
P70	IGL	Gabra1	1.10	1.27	0.89	-0.16 [-0.53, 0.2]	-1.15	0.303	0.69 [0.53, 1.87]
P70	IGL	Gabrg2	3.66	3.06	1.52	0.61 [-0.13, 1.34]	2.13	0.086	1.29 [0.08, 2.58]
P70	IGL	Grin1	2.10	2.21	0.93	-0.11 [-0.7, 0.48]	-0.48	0.651	0.27 [0.94, 1.44]
P70	IGL	Grm3	6.24	6.14	1.07	0.1 [-0.72, 0.93]	0.35	0.747	0.19 [0.92, 1.27]
P70	IGL	Homer1	5.55	5.23	1.25	0.32 [-0.53, 1.17]	0.96	0.382	0.41 [0.76, 1.52]
P70	IGL	Nrxn1	2.17	1.82	1.27	0.35 [-0.04, 0.73]	2.30	0.070	1.39 [0.01, 2.71]
P70	IGL	Nxph4	5.57	5.29	1.21	0.28 [-0.87, 1.43]	0.68	0.534	0.31 [0.88, 1.45]
P70	IGL	Pax6	2.57	2.30	1.21	0.27 [-0.17, 0.71]	1.60	0.171	0.93 [0.28, 2.06]
P70	IGL	Rac1	2.54	2.28	1.20	0.27 [-0.2, 0.74]	1.47	0.201	0.82 [0.48, 2.06]
P70	IGL	Robo1	5.50	5.36	1.10	0.14 [-0.85, 1.13]	0.36	0.732	0.14 [0.92, 1.18]
P70	IGL	Slc17a7	0.87	1.00	0.92	-0.13 [-0.44, 0.19]	-1.05	0.343	0.63 [0.57, 1.78]
P70	IGL	Slc32a1	3.85	3.73	1.09	0.13 [-0.22, 0.48]	0.93	0.396	0.53 [0.71, 1.72]
P70	IGL	Stmn1	1.93	2.03	0.93	-0.11 [-0.49, 0.28]	-0.70	0.514	0.37 [0.84, 1.55]
P70	IGL	Syn2	1.51	1.24	1.21	0.27 [-0.12, 0.66]	1.78	0.135	0.8 [0.5, 2.01]
P70	IGL	Syp	1.10	1.07	1.02	0.03 [-0.22, 0.28]	0.32	0.763	0.14 [0.98, 1.24]
P70	IGL	Tln1	5.25	5.64	0.76	-0.39 [-1.15, 0.37]	-1.31	0.246	0.71 [0.57, 1.93]
P70	IGL	Tmod	4.47	4.92	0.73	-0.45 [-0.91, 0.01]	-2.53	0.052	1.48 [0.01, 2.88]
P70	IGL	Zic1	0.12	-1.09	2.31	1.21 [-0.28, 2.7]	2.09	0.091	1.22 [0.17, 2.54]
P70	ML	Astn2	2.79	2.09	1.62	0.69 [-0.13, 1.51]	2.17	0.082	0.76 [0.47, 1.9]
P70	ML	Calb1	2.73	3.02	0.82	-0.29 [-0.86, 0.29]	-1.29	0.254	0.76 [0.4, 1.86]
P70	ML	Gabra1	0.44	0.76	0.80	-0.32 [-0.86, 0.21]	-1.56	0.180	0.65 [0.58, 1.8]
P70	ML	Grid2	3.02	2.50	1.44	0.52 [-0.25, 1.29]	1.75	0.141	0.74 [0.53, 1.92]
P70	ML	Grin1	2.53	2.14	1.31	0.39 [-0.25, 1.02]	1.56	0.180	0.67 [0.58, 1.83]
P70	ML	Tln1	4.76	3.70	2.09	1.06 [-0.65, 2.78]	1.97	0.143	0.94 [0.46, 2.23]
P70	PC	Calb1	0.38	1.22	0.56	-0.83 [-1.72, 0.06]	-2.98	0.059	1.36 [0.23, 2.86]
P70	PC	Gabra1	0.30	1.07	0.59	-0.77 [-1.41, -0.12]	-3.78	0.032 *	1.75 [0.06, 3.48]
P70	WM	Grm3	3.09	2.02	2.10	1.07 [0.02, 2.12]	3.26	0.047 *	1.24 [0.23, 2.64]
P70	WM	Mbp	-3.69	-4.01	1.25	0.32 [-0.16, 0.79]	1.71	0.148	1.04 [0.26, 2.26]
P70	WM	Mobp	-2.34	-2.50	1.12	0.16 [-0.14, 0.47]	1.37	0.230	0.8 [0.49, 2.02]
P70	WM	Mog	1.11	1.41	0.81	-0.3 [-1.19, 0.58]	-0.88	0.419	0.51 [0.72, 1.7]

Stage	Layer	Gene	Avg DCq (N)	Avg DCq (IH)	Fold Change	Difference [CI ₉₅]	t	p.value	Hedge's g [CI ₉₅]
P70	WM	Plp1	-2.52	-3.04	1.44	0.52 [0.05, 0.99]	2.84	0.036 *	1.52 [0.02, 2.98]
P70	WM	Stmn1	1.13	0.21	1.89	0.92 [0.37, 1.47]	4.28	0.008 **	1.66 [0.07, 3.31]
P70	WM	Tln1	2.57	1.45	2.18	1.12 [0.76, 1.49]	7.86	<0.001 ***	3.89 [1.04, 6.71]

Asterisks after p.values indicate the level of statistical significance: one for p < .05, two for p < .01, and three for p < .001

Stage	Layer	Gene	Avg DCq (N)	Avg DCq (IH)	Fold Change	Difference [Cl ₉₅]	t	p.value	Hedge's g [Cl ₉₅]
P4	Tot	Angpt1	5.65	5.55	1.07	0.1 [-0.14, 0.35]	0.92	0.380	0.44 [0.59, 1.45]
P4	Tot	Angpt2	9.00	8.73	1.20	0.27 [0.07, 0.46]	3.00	0.013 *	1.45 [0.25, 2.59]
P4	Tot	Anpep	8.42	8.39	1.02	0.03 [-0.21, 0.28]	0.31	0.767	0.14 [0.87, 1.15]
P4	Tot	Cdh5	7.42	7.37	1.04	0.05 [-0.1, 0.2]	0.77	0.460	0.34 [0.68, 1.33]
P4	Tot	Col1a1	3.84	3.82	1.02	0.03 [-0.18, 0.24]	0.28	0.787	0.12 [0.87, 1.1]
P4	Tot	F3	6.43	6.21	1.16	0.22 [0.04, 0.39]	2.74	0.021 *	1.26 [0.07, 2.39]
P4	Tot	Fgf2	10.26	10.17	1.06	0.09 [-0.13, 0.31]	0.93	0.373	0.45 [0.58, 1.46]
P4	Tot	Flk1	6.17	5.86	1.24	0.31 [0.08, 0.54]	3.06	0.012 *	1.47 [0.27, 2.62]
P4	Tot	Flt1	7.71	7.39	1.25	0.33 [0.14, 0.51]	3.90	0.003 **	1.85 [0.54, 3.1]
P4	Tot	Lect1	10.37	10.29	1.06	0.08 [-0.19, 0.34]	0.65	0.528	0.3 [0.72, 1.31]
P4	Tot	Mmp2	8.15	8.17	0.99	-0.02 [-0.18, 0.14]	-0.30	0.769	0.13 [0.87, 1.13]
P4	Tot	Mmp9	9.16	9.02	1.10	0.14 [-0.04, 0.31]	1.77	0.107	0.76 [0.33, 1.8]
P4	Tot	Ndp	8.90	8.87	1.02	0.03 [-0.16, 0.21]	0.36	0.729	0.17 [0.81, 1.14]
P4	Tot	Nrp1	5.47	5.33	1.10	0.14 [-0.08, 0.35]	1.43	0.183	0.66 [0.41, 1.69]
P4	Tot	Pgf	8.36	8.35	1.00	0.01 [-0.23, 0.24]	0.06	0.951	0.03 [0.98, 1.04]
P4	Tot	Serpine1	11.18	11.18	1.00	0 [-0.19, 0.2]	0.04	0.969	0.02 [0.95, 0.99]
P4	Tot	Serpinf1	7.06	7.20	0.91	-0.14 [-0.32, 0.03]	-1.81	0.100	0.86 [0.24, 1.91]
P4	Tot	Tek	8.39	8.33	1.04	0.06 [-0.07, 0.19]	1.00	0.339	0.47 [0.58, 1.49]
P4	Tot	Tgfb1	8.38	8.18	1.14	0.19 [0.02, 0.36]	2.50	0.032 *	1.18 [0.03, 2.29]
P4	Tot	Thbs1	6.84	6.69	1.11	0.15 [0.02, 0.27]	2.61	0.026 *	1.23 [0.06, 2.34]
P4	Tot	Tie1	7.96	8.10	0.90	-0.14 [-0.35, 0.06]	-1.60	0.141	0.77 [0.3, 1.8]
P4	Tot	Timp1	10.16	10.31	0.90	-0.15 [-0.38, 0.08]	-1.45	0.177	0.68 [0.39, 1.72]
P4	Tot	Vegfa	7.01	6.38	1.54	0.63 [0.45, 0.8]	7.96	<0.001 ***	3.74 [1.81, 5.61]
P8	Tot	Angpt1	5.15	5.37	0.85	-0.23 [-0.39, -0.07]	-3.04	0.009 **	1.35 [0.22, 2.43]
P8	Tot	Angpt2	9.03	9.10	0.95	-0.07 [-0.28, 0.13]	-0.81	0.434	0.4 [0.47, 1.26]
P8	Tot	Anpep	9.23	9.89	0.63	-0.66 [-0.97, -0.35]	-4.66	<0.001 ***	2.05 [0.73, 3.32]
P8	Tot	Cdh5	7.84	8.54	0.61	-0.7 [-0.93, -0.47]	-6.61	<0.001 ***	2.86 [1.24, 4.42]
P8	Tot	Col1a1	4.24	4.19	1.03	0.05 [-0.21, 0.31]	0.38	0.709	0.18 [0.74, 1.1]
P8	Tot	F3	6.26	6.23	1.02	0.03 [-0.28, 0.33]	0.19	0.855	0.09 [0.84, 1.01]
P8	Tot	Fgf2	10.34	10.95	0.65	-0.61 [-0.77, -0.45]	-8.35	<0.001 ***	3.42 [1.47, 5.32]
P8	Tot	Flk1	6.42	6.84	0.74	-0.43 [-0.62, -0.23]	-4.68	<0.001 ***	2.1 [0.79, 3.36]
P8	Tot	Flt1	7.69	8.59	0.54	-0.9 [-1.17, -0.63]	-7.17	<0.001 ***	3.25 [1.6, 4.85]
P8	Tot	Lect1	10.14	10.77	0.64	-0.64 [-0.86, -0.41]	-6.00	<0.001 ***	2.95 [1.53, 4.33]
P8	Tot	Mmp2	8.81	9.60	0.58	-0.79 [-0.94, -0.63]	-10.84	<0.001 ***	4.9 [2.66, 7.11]
P8	Tot	Mmp9	9.36	9.21	1.10	0.14 [-0.28, 0.57]	0.73	0.478	0.37 [0.49, 1.21]
P8	Tot	Ndp	8.90	8.79	1.08	0.11 [-0.01, 0.23]	2.02	0.064	0.95 [0.06, 1.92]
P8	Tot	Nrp1	6.53	6.84	0.81	-0.31 [-0.47, -0.14]	-4.06	0.001 **	1.7 [0.43, 2.92]
P8	Tot	Pgf	8.87	9.24	0.78	-0.37 [-0.67, -0.07]	-2.63	0.021 *	1.32 [0.3, 2.29]
P8	Tot	Serpine1	11.58	12.38	0.57	-0.8 [-1.03, -0.58]	-7.66	<0.001 ***	3.49 [1.78, 5.17]
P8	Tot	Serpinf1	6.94	7.20	0.83	-0.26 [-0.34, -0.18]	-6.91	<0.001 ***	3.06 [1.43, 4.65]
P8	Tot	Tek	8.70	9.16	0.73	-0.45 [-0.61, -0.3]	-6.41	<0.001 ***	2.57 [0.94, 4.16]
P8	Tot	Tgfb1	8.35	8.97	0.65	-0.62 [-0.82, -0.41]	-6.56	<0.001 ***	2.55 [0.87, 4.17]
P8	Tot	Thbs1	7.52	8.25	0.60	-0.73 [-0.98, -0.48]	-6.30	<0.001 ***	3.1 [1.64, 4.53]
P8	Tot	Tie1	7.97	8.84	0.55	-0.88 [-1.11, -0.64]	-8.04	<0.001 ***	3.05 [1.12, 4.94]

Stage	Layer	Gene	Avg DCq (N)	Avg DCq (IH)	Fold Change	Difference [CI ₉₅]	t	p.value	Hedge's g [CI ₉₅]
P8	Tot	<i>Timp1</i>	10.24	10.44	0.87	-0.2 [-0.4, 0.01]	-2.06	0.060	1.01 [0.02, 1.96]
P8	Tot	Vegfa	6.92	7.41	0.71	-0.5 [-0.68, -0.31]	-5.76	<0.001 ***	2.85 [1.45, 4.2]
P12	Tot	<i>Angpt1</i>	5.29	5.36	0.95	-0.07 [-0.26, 0.12]	-0.77	0.451	0.26 [0.55, 1.05]
P12	Tot	Angpt2	9.60	9.40	1.14	0.19 [0.05, 0.34]	2.76	0.011 *	1.07 [0.24, 1.88]
P12	Tot	Anpep	9.15	9.46	0.81	-0.31 [-0.48, -0.14]	-3.82	<0.001 ***	1.38 [0.44, 2.28]
P12	Tot	<i>Cdh5</i>	7.89	7.99	0.94	-0.09 [-0.29, 0.11]	-0.98	0.338	0.38 [0.38, 1.14]
P12	Tot	<i>Col1a1</i>	4.77	4.61	1.12	0.16 [-0.05, 0.37]	1.61	0.122	0.64 [0.11, 1.39]
P12	Tot	<i>F3</i>	5.66	5.84	0.88	-0.18 [-0.37, 0.01]	-1.97	0.061	0.71 [0.12, 1.52]
P12	Tot	Fgf2	10.31	10.01	1.23	0.3 [0.1, 0.49]	3.18	0.004 **	1.2 [0.33, 2.04]
P12	Tot	<i>Flk1</i>	6.01	5.95	1.04	0.06 [-0.08, 0.2]	0.88	0.388	0.32 [0.47, 1.1]
P12	Tot	<i>Flt1</i>	7.15	7.04	1.08	0.12 [-0.03, 0.26]	1.64	0.115	0.65 [0.13, 1.41]
P12	Tot	Lect1	9.88	10.40	0.70	-0.52 [-0.79, -0.26]	-4.08	<0.001 ***	1.58 [0.68, 2.45]
P12	Tot	Mmp2	8.54	8.28	1.20	0.26 [0.02, 0.5]	2.25	0.035 *	0.86 [0.05, 1.65]
P12	Tot	Mmp9	9.54	9.26	1.21	0.28 [0.06, 0.49]	2.68	0.014 *	1.06 [0.25, 1.85]
P12	Tot	Ndp	8.69	9.11	0.75	-0.42 [-0.51, -0.32]	-9.26	<0.001 ***	3.3 [1.86, 4.7]
P12	Tot	<i>Nrp1</i>	6.42	6.49	0.96	-0.07 [-0.22, 0.09]	-0.85	0.406	0.29 [0.52, 1.08]
P12	Tot	Pgf	9.46	9.08	1.30	0.38 [0.13, 0.63]	3.12	0.005 **	1.25 [0.43, 2.05]
P12	Tot	SerpinE1	11.59	11.92	0.80	-0.33 [-0.56, -0.1]	-2.97	0.007 **	1.19 [0.37, 1.98]
P12	Tot	SerpinF1	6.74	7.00	0.84	-0.26 [-0.43, -0.09]	-3.13	0.005 **	1.2 [0.35, 2.03]
P12	Tot	Tek	8.23	8.50	0.83	-0.27 [-0.45, -0.09]	-3.18	0.004 **	1.25 [0.41, 2.07]
P12	Tot	Tgfb1	7.96	7.74	1.17	0.22 [0.05, 0.39]	2.71	0.013 *	0.97 [0.11, 1.81]
P12	Tot	Thbs1	8.06	7.83	1.17	0.23 [0.01, 0.46]	2.12	0.045 *	0.79 [0.04, 1.59]
P12	Tot	<i>Tie1</i>	7.79	7.82	0.98	-0.03 [-0.27, 0.22]	-0.22	0.827	0.09 [0.66, 0.83]
P12	Tot	<i>Timp1</i>	10.19	10.42	0.85	-0.23 [-0.58, 0.11]	-1.38	0.180	0.48 [0.34, 1.28]
P12	Tot	Vegfa	6.31	6.54	0.85	-0.23 [-0.36, -0.1]	-3.74	0.001 **	1.44 [0.55, 2.3]
P21	Tot	Angpt1	5.59	6.37	0.58	-0.78 [-1, -0.56]	-7.46	<0.001 ***	3.23 [1.74, 4.67]
P21	Tot	Angpt2	9.68	10.21	0.69	-0.53 [-0.72, -0.33]	-5.84	<0.001 ***	2.53 [1.24, 3.78]
P21	Tot	<i>Anpep</i>	10.00	9.98	1.02	0.02 [-0.11, 0.16]	0.38	0.708	0.17 [0.71, 1.04]
P21	Tot	<i>Cdh5</i>	9.41	9.43	0.99	-0.02 [-0.14, 0.1]	-0.37	0.717	0.16 [0.75, 1.06]
P21	Tot	<i>Col1a1</i>	5.71	5.70	1.01	0.01 [-0.31, 0.33]	0.07	0.946	0.03 [0.87, 0.93]
P21	Tot	F3	4.77	5.27	0.71	-0.5 [-0.61, -0.39]	-9.87	<0.001 ***	4.3 [2.51, 6.05]
P21	Tot	Fgf2	10.83	11.01	0.88	-0.19 [-0.34, -0.03]	-2.54	0.024 *	1.1 [0.09, 2.07]
P21	Tot	Flk1	7.13	7.56	0.74	-0.43 [-0.73, -0.12]	-3.01	0.009 **	1.3 [0.27, 2.3]
P21	Tot	Flt1	7.93	8.15	0.86	-0.22 [-0.36, -0.08]	-3.33	0.005 **	1.41 [0.34, 2.45]
P21	Tot	<i>Lect1</i>	9.21	9.32	0.93	-0.1 [-0.3, 0.09]	-1.14	0.275	0.48 [0.45, 1.39]
P21	Tot	<i>Mmp2</i>	9.83	9.91	0.95	-0.07 [-0.17, 0.03]	-1.58	0.136	0.69 [0.25, 1.61]
P21	Tot	<i>Mmp9</i>	10.34	10.50	0.90	-0.16 [-0.37, 0.06]	-1.58	0.136	0.69 [0.26, 1.61]
P21	Tot	<i>Ndp</i>	7.94	8.22	0.82	-0.29 [-0.58, 0.01]	-2.08	0.056	0.89 [0.07, 1.81]
P21	Tot	<i>Nrp1</i>	7.90	7.95	0.97	-0.05 [-0.19, 0.09]	-0.73	0.479	0.31 [0.61, 1.21]
P21	Tot	Pgf	8.94	9.15	0.86	-0.22 [-0.4, -0.03]	-2.51	0.025 *	1.06 [0.05, 2.04]
P21	Tot	<i>SerpinE1</i>	12.36	12.44	0.94	-0.09 [-0.33, 0.16]	-0.75	0.466	0.33 [0.56, 1.2]
P21	Tot	<i>SerpinF1</i>	6.70	6.66	1.03	0.04 [-0.05, 0.13]	0.92	0.375	0.4 [0.51, 1.3]
P21	Tot	Tek	9.07	9.48	0.75	-0.41 [-0.56, -0.26]	-5.79	<0.001 ***	2.34 [0.92, 3.72]

APPENDICES

Appendix 7: Statistical results of the vascularization panel on the whole cerebellum

Stage	Layer	Gene	Avg DCq (N)	Avg DCq (IH)	Fold Change	Difference [Cl ₉₅]	t	p.value	Hedge's g [Cl ₉₅]
P21	Tot	Tgfb1	8.81	8.83	0.99	-0.02 [-0.18, 0.14]	-0.25	0.809	0.11 [0.8, 1.01]
P21	Tot	Thbs1	8.49	8.60	0.93	-0.11 [-0.29, 0.07]	-1.30	0.213	0.56 [0.38, 1.47]
P21	Tot	Tie1	8.86	8.76	1.07	0.1 [-0.08, 0.27]	1.21	0.246	0.53 [0.4, 1.44]
P21	Tot	Timp1	10.67	10.84	0.89	-0.17 [-0.35, 0.01]	-2.04	0.061	0.89 [0.08, 1.83]
P21	Tot	Vegfa	6.84	6.98	0.90	-0.14 [-0.22, -0.07]	-4.29	<0.001 ***	1.87 [0.73, 2.96]
P70	Tot	Angpt1	5.33	5.44	0.93	-0.11 [-0.62, 0.4]	-0.55	0.605	0.32 [0.87, 1.49]
P70	Tot	Angpt2	9.89	10.34	0.73	-0.45 [-0.77, -0.12]	-3.57	0.016 *	2.04 [0.34, 3.66]
P70	Tot	Anpep	9.29	9.47	0.88	-0.18 [-0.52, 0.16]	-1.38	0.225	0.8 [0.48, 2.03]
P70	Tot	Cdh5	8.10	8.48	0.77	-0.38 [-0.61, -0.15]	-4.25	0.008 **	2.12 [0.26, 3.9]
P70	Tot	Col1a1	6.68	7.04	0.78	-0.35 [-0.83, 0.13]	-1.89	0.118	0.71 [0.52, 1.84]
P70	Tot	F3	3.81	3.96	0.90	-0.16 [-0.44, 0.13]	-1.41	0.218	0.74 [0.55, 1.97]
P70	Tot	Fgf2	9.36	9.54	0.88	-0.18 [-0.36, 0]	-2.59	0.049 *	1.45 [0.04, 2.86]
P70	Tot	Flk1	7.21	7.82	0.66	-0.61 [-1.07, -0.15]	-3.41	0.019 *	1.11 [0.3, 2.42]
P70	Tot	Flt1	5.81	6.29	0.72	-0.48 [-0.68, -0.28]	-6.22	0.002 **	2.69 [0.39, 4.96]
P70	Tot	Lect1	9.74	10.03	0.82	-0.29 [-0.71, 0.12]	-1.81	0.130	0.82 [0.49, 2.04]
P70	Tot	Mmp2	9.66	9.93	0.83	-0.26 [-0.79, 0.26]	-1.29	0.253	0.66 [0.61, 1.87]
P70	Tot	Mmp9	9.27	9.59	0.80	-0.32 [-0.7, 0.07]	-2.12	0.087	1.26 [0.13, 2.58]
P70	Tot	Ndp	7.48	7.51	0.98	-0.03 [-0.38, 0.32]	-0.23	0.831	0.12 [1.06, 1.28]
P70	Tot	Nrp1	7.05	7.44	0.77	-0.38 [-0.69, -0.07]	-3.17	0.025 *	1.47 [0.12, 2.96]
P70	Tot	Pgf	8.48	8.48	1.00	0 [-0.17, 0.16]	-0.06	0.956	0.03 [1.14, 1.2]
P70	Tot	SerpinE1	11.61	12.08	0.72	-0.47 [-0.85, -0.09]	-3.16	0.025 *	1.09 [0.31, 2.41]
P70	Tot	SerpinF1	6.29	6.56	0.82	-0.28 [-0.67, 0.12]	-1.80	0.131	1.08 [0.26, 2.34]
P70	Tot	Tek	8.09	8.45	0.78	-0.36 [-0.57, -0.15]	-4.41	0.007 **	2.3 [0.39, 4.13]
P70	Tot	Tgfb1	8.23	8.43	0.87	-0.2 [-0.4, 0]	-2.51	0.054	1.05 [0.35, 2.34]
P70	Tot	Thbs1	8.10	8.26	0.90	-0.16 [-0.51, 0.19]	-1.18	0.292	0.53 [0.69, 1.67]
P70	Tot	Tie1	8.03	8.37	0.79	-0.35 [-0.57, -0.13]	-4.05	0.010 **	2.45 [0.62, 4.21]
P70	Tot	Timp1	11.08	11.79	0.61	-0.71 [-1.49, 0.08]	-2.31	0.069	0.72 [0.46, 1.81]
P70	Tot	Vegfa	5.61	5.93	0.80	-0.32 [-0.6, -0.05]	-3.06	0.028 *	1.83 [0.25, 3.34]

Asterisks after p.values indicate the level of statistical significance: one for p < .05, two for p < .01, and three for p < .001

Etude des altérations moléculaires, cellulaires et vasculaires induites par l'apnée du prématuré dans le cervelet de la souris

Le cervelet est impliqué dans diverses fonctions, du contrôle moteur jusqu'aux émotions. À la naissance, le cortex cérébelleux humain est encore immature, ce qui le rend vulnérable aux événements périnataux tels que l'hypoxie. L'apnée du prématuré (ADP) est l'une des principales causes d'hypoxie périnatale, puisqu'elle survient chez plus de 50 % des enfants prématurés. Or, plusieurs relations entre les fonctions cérébelleuses et les déficits observés chez les enfants ayant souffert d'ADP ont été démontrées, mais les mécanismes physio-pathologiques par lesquels l'ADP affecte le cervelet restent mal compris. Ce travail vise à mettre en lumière les mécanismes sous-jacents aux lésions hypoxiques cérébelleuses. A cette fin, nous avons développé un protocole d'hypoxie intermittente (HI), consistant en des cycles répétés de 2 minutes d'hypoxie-reoxygénéation (dont 20 secondes à 5% d'O₂), entre P2 et P12, 6 heures par jour, qui constitue un modèle murin valide de l'ADP. Dans un premier temps, nous montrons que le cervelet est effectivement sensible à l'HI, et présente un retard de maturation significatif à la fin de notre protocole. De plus, l'hypoxie semble induire une surexpression de gènes impliqués dans la production d'espèces réactives de l'oxygène (ROS), qui s'accumulent dans le cervelet. A l'inverse, les gènes codant pour les enzymes antioxydantes sont sous-exprimés après l'HI, ce qui suggère une défaillance du système de défense contre les ROS. L'HI induit également des dommages à long terme, sous la forme de déficits d'apprentissage et de motricité, qui sont associés à la sur-innervation des cellules de Purkinje par les fibres grimpantes. Nous avons complété ces résultats par une étude transcriptomique des gènes impliqués dans la différenciation et la migration cellulaire. Nous avons analysé l'expression de ces gènes par RT-qPCR, à différents stades de développement et dans différents types de cellules, en utilisant la microdissection par capture laser pour séparer les couches cérébelleuses. Ceci nous a permis de déterminer que la période la plus vulnérable à l'HI est le stade P8 chez la souris, au cours duquel un nombre significatif de gènes sont dérégulés dans toutes les couches corticales cérébelleuses. De plus, il semble que les processus impliqués dans le développement du cervelet soient affectés, y compris la prolifération, la différenciation, la connectivité synaptique et la myélinisation. Plusieurs mécanismes compensatoires et neuroprotecteurs sont mis en place pendant et après l'HI, mais ils ne semblent pas suffisamment efficaces compte tenu de la persistance des déficits à l'âge adulte. Enfin, étant donné le lien établi entre l'hypoxie et la vascularisation, nous avons testé un panel de gènes axés sur ces processus et avons trouvé des régulations significatives des facteurs angiogéniques et de croissance. En outre, les résultats préliminaires d'imagerie suggèrent que le cervelet HI a un réseau vasculaire plus lâche et moins volumineux, un facteur qui pourrait participer à la physiopathologie de l'ADP. Nous avons l'intention de poursuivre cet axe de recherche avec des études immunohistochimiques et de transparisation supplémentaires. Dans l'ensemble, les données présentées ici démontrent que le cervelet est affecté par l'HI, et qu'une lésion cérébelleuse est, au moins en partie, responsable des symptômes observés chez les enfants ayant subi une ADP. Ce projet fournit des éléments pour mieux comprendre l'ADP, en reliant les altérations comportementales et histologiques à des mécanismes cellulaires et moléculaires sous-jacents plausibles. À long terme, il pourrait conduire à l'identification de nouvelles cibles thérapeutiques afin d'améliorer la prise en charge clinique actuelle de cette pathologie très prévalente.

Mots clés : cervelet, développement, hypoxie intermittente, périnatal, apnée du prématuré, histologie, apoptose, stress oxydatif, transcriptome, différenciation

Study of molecular, cellular, and vascular alterations induced by apnea of prematurity in the mouse cerebellum

The cerebellum is involved in diverse functions, from motor control and equilibrium to spatial learning and emotion. At birth, the human cerebellar cortex is still immature, making it vulnerable to perinatal events such as hypoxia. Apnea of prematurity (AOP) is a main cause of perinatal hypoxia, as it occurs in over 50% of preterm infants. Several relationships between cerebellar functions and the deficits observed in children having suffered from AOP have been demonstrated, but the physio-pathological mechanisms by which AOP affects the cerebellum remain poorly understood. This work aims at shedding light on the mechanisms underlying cerebellar hypoxic injury. To this end, we developed an intermittent hypoxia (IH) protocol, consisting of repeated 2-minute cycles of hypoxia-reoxygenation (including 20 seconds at 5% O₂), applied between P2 and P12, 6 hours per day, which constitutes a valid murine model of AOP. In a first study, we show that the cerebellum is indeed sensitive to IH, and presents a significant delay in maturation at the end of our IH protocol. In addition, hypoxia seems to induce an overexpression of genes involved in reactive oxygen species (ROS) production, which accumulate in the cerebellum. Conversely, genes coding for antioxidant enzymes are underexpressed after IH, suggesting a failure of the defense system against ROS. IH also induces long-term damage, in the form of learning and motor deficits, which are associated with the over-innervation of Purkinje cells by climbing fibers. We followed these results with a transcriptomic study of genes involved in cell differentiation and migration. We analyzed the expression of these genes by RT-qPCR, in different developmental stages and in different cell types, using laser capture microdissection to separate cerebellar layers. This allowed us to determine that the period most vulnerable to IH is the P8 stage in mice, during which a significant number of genes are dysregulated in all cerebellar cortical layers. Moreover, it seems that all processes involved in cerebellar development are impacted, including proliferation, differentiation, synaptic connectivity, and myelination. Several compensatory and neuroprotective mechanisms are put in place during and after IH, but they do not seem to be sufficiently effective considering the persistence of deficits through adulthood. Finally, given the established connection between hypoxia and vascularization, we tested a gene panel focused on these processes and found significant regulations of angiogenic and growth factors. In addition, preliminary imaging results suggest that IH cerebella have a looser and less voluminous vascular network, a factor that could participate in the pathophysiology of AOP. We aim to pursue this line of inquiry with additional immunohistochemical and clearing studies. Overall, the data presented here demonstrate that the cerebellum is affected by IH, and that its injury is, at least in part, responsible for the symptoms observed in children having experienced AOP. This project provides elements to better understand AOP, by connecting behavioral and histological alterations to plausible underlying cellular and molecular mechanisms. In the long term, it could lead to the identification of novel therapeutic targets to improve the current clinical management of this highly prevalent pathology.

Keywords: cerebellum, development, intermittent hypoxia, perinatal, apnea of prematurity, histology, apoptosis, oxidative stress, transcriptome, differentiation